

**MASARYK UNIVERSITY**

**FACULTY OF SCIENCE**

**DEPARTMENT OF GEOGRAPHY**

**M U N I**

**ACTIVE LAYER THERMAL REGIME AND  
THICKNESS IN ANTARCTICA**

**HABILITATION THESIS**

**FILIP HRBÁČEK**

**BRNO 2025**



## **Acknowledgements**

Over the past decade, I have met many great people who have supported and shaped my scientific career. First, I would like to thank my PhD supervisor, Kamil Láska, for giving me the opportunity to work on this unique topic; Daniel Nývlt for broadening my perspectives in geomorphological research; and Marc Oliva for introducing me to the international research community.

I am also grateful to Petr Dobrovolný and Petr Kubíček for creating the conditions at the Department of Geography that have allowed me to continue my work in academia. I appreciate all the co-authors of the papers I have led or contributed to. My thanks also go to the crew members of the Johann Gregor Mendel station, who assisted me with my research.

Funding for this work was provided by various programs of the Ministry of Education, Youth and Sports of the Czech Republic supporting the operation of Czech Antarctic Research Infrastructure and Czech Antarctic Research Programme. In 2017, I received the fellowship award of the Scientific Committee on Antarctic Research for one year research activities. My current research is funded by Czech Science Foundation project Juniorstar (GM22-28659M)

Last but not least, I would like to thank my partner, Michaela, for her support, assistance in the field, and collaboration on the research, as well as my parents, Iva and Pavel, for their encouragement and for taking care of our dog during expeditions to Antarctica, conferences, and other travels.

## List of contents

|  |    |
|--|----|
| Preface .....  | 5  |
| 1 Introduction .....   | 8  |
| 2 Motivation and research objectives .....   | 12 |
| 3 Study area .....   | 13 |
| 4 Data and methods .....   | 15 |
| 4.1 Air and ground temperatures .....  | 15 |
| 4.2 Active layer thickness .....   | 16 |
| 4.3 Soil physical properties .....   | 17 |
| 5 Results and discussion.....  | 18 |
| 5.1 Objective 1: Active layer thermal regime and thickness on James Ross Island .....                        | 18 |
| 5.1.1 Spatio-temporal changes of active layer thermal regime and thickness .....                             | 18 |
| 5.1.2 The effect of local conditions on active layer variability.....  | 21 |
| 5.1.3 Circumpolar active layer monitoring on James Ross Island .....   | 26 |
| 5.2 Objective 2: Modelling of active layer thickness and temperature .....                                   | 29 |
| 5.2.1 Active layer thickness modelling .....   | 29 |
| 5.2.2 Modelling of temperature on the top of permafrost .....  | 30 |
| 5.3 Objective 3: Spatiotemporal variability of active layer thermal regime and thickness in Antarctica ..... | 32 |
| 6 Summary .....  | 34 |
| 7 Research perspectives and conclusions.....   | 35 |
| 8 References .....   | 37 |
| 9 Supplements .....  | 45 |

## Preface

This thesis summarizes my research activities on topic of active layer thermal regime and thickness which I conducted over past decade on James Ross Island and other regions of Antarctica. My research activities on James Ross Island can be divided into two phases. The initial stage of my research (2015-2020) was focused on identifying the interactions between the active layer and factors like climate conditions (air temperature, snow cover), lithology, and vegetation. These findings were published as a set of case studies (*Papers 1-6*), which provided the foundation for further research directions. Since 2020, our research has shifted to focus more on long-term data evaluation, modelling, and a complex understanding of the effects of soil physics on the active layer thermal regimes (*Papers 7-12*). Thanks to international collaboration with scientists working in other parts of Antarctica, we were able to utilize our results from James Ross Island and interpret them more thoroughly, drawing from data and knowledge from other Antarctic regions (*Papers 13-16*). The aim of this thesis is to provide comprehensive summary of following 16 scientific papers which documents the best my research on active layer thermal regime and dynamics in Antarctica

### Paper 1:

**Hrbáček, F.,** Láska, K., Engel, Z., (2016): Effect of snow cover on the active-layer thermal regime – a case study from James Ross Island, Antarctic Peninsula. *Permafrost and Periglacial Processes*, 27(3), 307–315. <https://doi.org/10.1002/ppp.1871>

*Author contribution: 60 % (writing, data analysis)*

### Paper 2:

**Hrbáček, F.,** Oliva, M., Laska, K., Ruiz-Fernández, J., de Pablo, M. A., Vieira, G., Ramos, M., & Nývlt, D. (2016). Active layer thermal regime in two climatically contrasted sites of the Antarctic Peninsula region. *Cuadernos de Investigación Geográfica*, 42(2), 457–474. <https://doi.org/10.18172/cig.2915>.

*Author contribution: 70 % (writing, concept, data analysis)*

### Paper 3:

**Hrbáček, F.,** Nývlt, D., Láska, K., (2017): Active Layer Thermal Dynamics at Two lithologically Different Sites on James Ross Island, Eastern Antarctic Peninsula. *Catena*, 149(2), 592–602. <https://doi.org/10.1016/j.catena.2016.06.020>

*Author contribution: 75 % (writing, concept, data analysis, fieldwork)*

### Paper 4:

**Hrbáček, F.,** Kňázková, M., Nývlt, D., Láska, K., Mueller, C.W., Ondruch, J., (2017): Active layer monitoring at CALM-S site near J.G. Mendel Station, James Ross Island, eastern Antarctic Peninsula. *Science of the Total Environment*, 601, 987-997. <http://dx.doi.org/10.1016/j.scitotenv.2017.05.266>

*Author contribution: 70 % (writing, concept, data analysis, fieldwork)*

**Paper 5:**

Kňázková, M., **Hrbáček, F.**, Kavan, J., & Nývlt, D. (2020). Effect of hyaloclastite breccia boulders on meso-scale periglacial-aeolian landsystem in semi-arid Antarctic environment, James Ross Island, Antarctic Peninsula. *Cuadernos de Investigación Geográfica*, 46(1), 7–31. <https://doi.org/10.18172/cig.3800>

*Author contribution: 20 % (concept, writing, fieldwork)*

**Paper 6:**

**Hrbáček, F.**, Cannone, N., Kňázková, M., Malfasi, F., Convey, P., Guglielmin, M., (2020): Effect of climate and moss vegetation on ground surface temperature and the active layer among different biogeographical regions in Antarctica. *Catena*, 190, 104562. <https://doi.org/10.1016/j.catena.2020.104562>

*Author contribution: 50 % (concept, writing, data analysis, fieldwork)*

**Paper 7:**

**Hrbáček, F.**, Uxa, T., 2020. The evolution of a near-surface ground thermal regime and modeled active-layer thickness on James Ross Island, Eastern Antarctic Peninsula, in 2006–2016. *Permafrost and Periglacial Processes*, 31(1), 141–155. <https://doi.org/10.1002/ppp.2018A>

*uthor contribution: 50 % (concept, writing, fieldwork, data analysis)*

**Paper 8:**

**Hrbáček, F.**, Engel, Z., Kňázková, M., Smolíková, J. (2021). Effect of summer snow cover on the active layer thermal regime and thickness on CALM-S JGM site, James Ross Island, eastern Antarctic Peninsula. *Catena*, 207, 105608. <https://doi.org/10.1016/j.catena.2021.105608>

*Author contribution: 45 % (writing, concept, data analysis, fieldwork)*

**Paper 9:**

**Hrbáček, F.**, Kňázková, M., Farzamian, M., Baptista, J. (2023). Variability of soil moisture on three sites in the Northern Antarctic Peninsula in 2022/23. *Czech Polar Reports*, 13 (1), 10 – 23. <https://doi.org/10.5817/CPR2023-1-2>

*Author contribution: 60 % (writing, concept, data analysis, fieldwork)*

**Paper 10:**

Kňázková, M., **Hrbáček, F.** (2024). Interannual variability of soil thermal conductivity and moisture on the Abernethy Flats (James Ross Island) during thawing seasons 2015–2023. *Catena*, 234, 107640, <https://doi.org/10.1016/j.catena.2023.107640>

*Author contribution: 20 % (concept, fieldwork, supervision)*

**Paper 11:**

Kaplan Pastříková, L., **Hrbáček, F.**, Uxa, T., Láska, K. (2023). Permafrost table temperature and active layer thickness variability on James Ross Island, Antarctic Peninsula, in 2004–2021. *Science of the Total Environment*, 869, 161690. <http://dx.doi.org/10.1016/j.scitotenv.2023.161690>

*Author contribution: 20 % (concept, supervision, fieldwork, data analysis)*

**Paper 12:**

**Hrbáček, F.**, Kňázková, M., Láska, K., Kaplan Pastířiková, L., (*accepted*). Active layer warming and thickening on CALM-S JGM, James Ross Island, in the period 2013/14–2022/23. Permafrost and Periglacial Processes. <https://doi.org/10.1002/ppp.2274>  
*Author contribution: 70 % (writing, concept, data analysis, fieldwork).*

**Paper 13:**

**Hrbáček, F.**, Oliva, M., Ruiz-Fernández, J., Kňázková, M., de Pablo, M.A. et al., (2020). Modelling ground thermal regime in bordering (dis)continuous permafrost environments. Environmental Research, 181, 108901. <https://doi.org/10.1016/j.envres.2019.108901>  
*Author contribution: 70 % (writing, concept, data analysis)*

**Paper 14:**

Obu, J., Westermann, S., Vieira, G., Abramov, A., Balks, M.R., Bartsch, A., **Hrbáček, F.**, Kaab, A., Ramos, M., (2020): Pan-Antarctic map of near-surface permafrost temperatures at 1 km(2) scale. The Cryosphere, 14(2), 497 - 519. <https://doi.org/10.5194/tc-14-497-2020>  
*Author contribution: <10 % (methods, data analysis)*

**Paper 15:**

**Hrbáček, F.**, Vieira, G., Oliva, M., Balks, M., Guglielmin, M., de Pablo, M.A., Molina, A., Ramos, M., Goyanes, G., Meiklejohn, I., Abramov, A., Demidov, N., Fedorov-Davydov, D., Lupachev, A., Rivkina, E., Láska, K., Kňázková, M., Nývlt, D., Raffi, R., Strelin, J., Sone, T., Fukui, K., Dolgikh, A., Zazovskaya, E., Mergelov, N., Osokin, N., Miamin, V., 2021. Active layer monitoring in Antarctica: an overview of results from 2006 to 2015. Polar Geography, 44 (3), 217–231. <https://doi.org/10.1080/1088937X.2017.1420105>  
*Author contribution: 60 % (writing, concept, data analysis)*

**Paper 16:**

**Hrbáček, F.**, Oliva, M., Hansen, C., Balks, M., O'Neill, T.A., de Pablo, M.A., Ponti, S., Ramos, M., Vieira, G., Abramov, A., Kaplan Pastířiková, L., Guglielmin, M., Goyanes, G., Francellino, M.R., Schaefer, C., Lacelle, D., 2023. Active layer and permafrost thermal regimes in the ice-free areas of Antarctica. Earth Science Reviews, 242, 104458. <https://doi.org/10.1016/j.earscirev.2023.104458>  
*Author contribution: 50 % (writing, concept, data analysis).*

# 1 Introduction

The active layer and permafrost are crucial components of periglacial environments in the ice-free areas of Antarctica (e.g., Guglielmin, 2012; López-Martínez et al., 2012). Changes in parameters such as permafrost temperature and active layer thickness (ALT) serve as important indicators of climate change, as these parameters are highly sensitive to climate variability (e.g., Anisimov et al., 1997; Romanovsky et al., 2010; Vieira et al., 2010; Guglielmin and Cannone, 2012). Moreover, permafrost temperature and ALT are considered among the Essential Climate Variables proposed by the World Meteorological Organization to track climate change's impacts on permafrost systems. Thus, investigating these parameters is crucial for assessing how climate change affects the Antarctic ice-free environments. The potential sensitivity of active layer stability could result in significant changes to Antarctic terrestrial ecosystems, leading to permafrost degradation, soil alteration, and shifts in vegetation patterns.

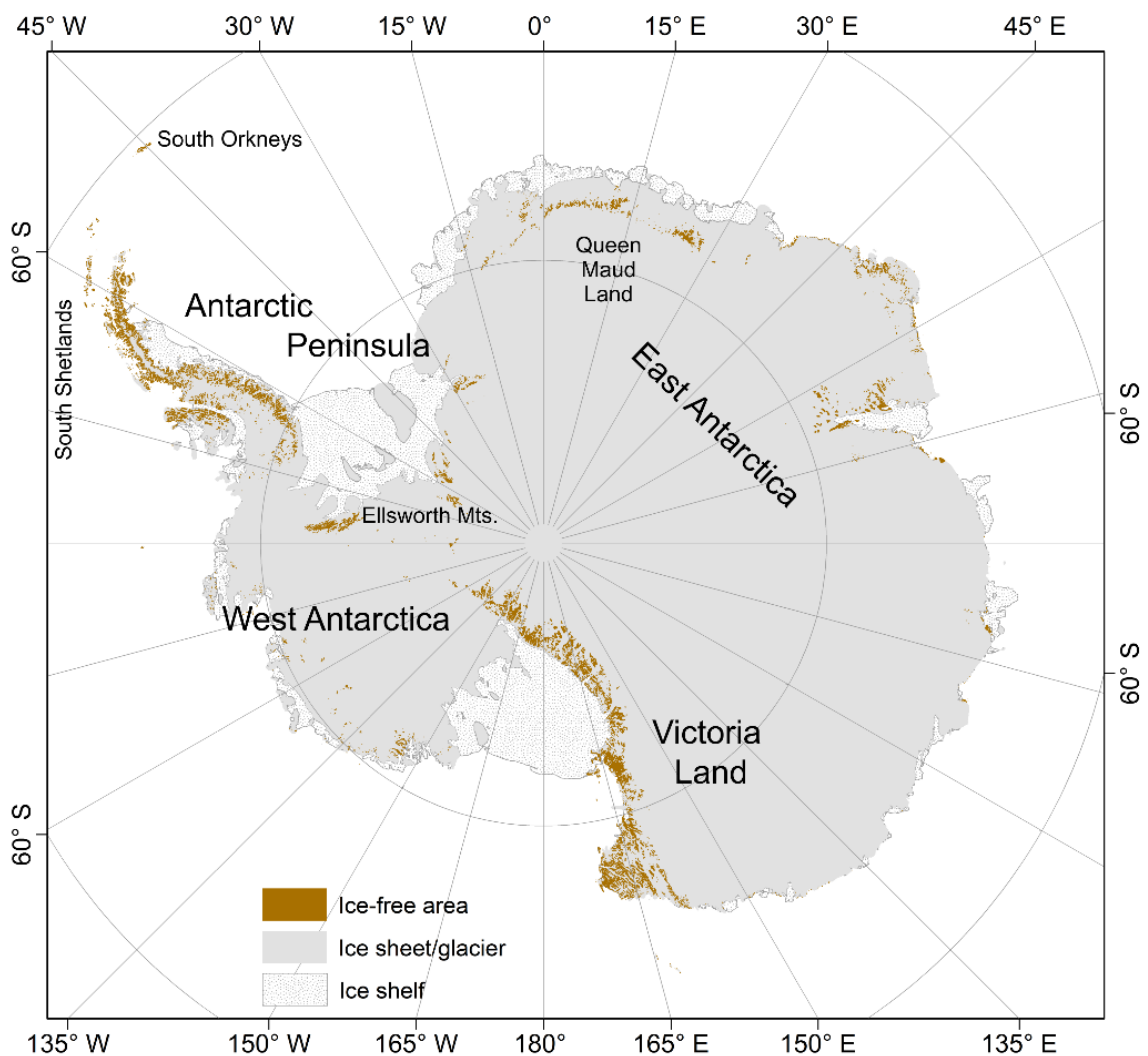


Figure 1. Extension of ice-free areas in Antarctica. Data source: Antarctic Digital Database (2024), rock outcrop polygon was used in medium resolution.

In Antarctica, ice-free areas are fragmented into small, separate oases, covering approximately 45,000 to 55,000 km<sup>2</sup>, or around 0.2% of the entire Antarctic continent (e.g., Brooks et al., 2019; Hrbáček et al., 2023a, Figure 1). These oases create a heterogeneous environment, ranging from small rock outcrops or nunataks smaller than 0.1 km<sup>2</sup> to relatively large oases extending over 100 km<sup>2</sup>. The ice-free landscapes are strongly influenced by a variety of periglacial, paraglacial, and glacial processes, which operate on timescales from just a few years in newly exposed areas to millions of years on the oldest ice-free surfaces, such as those in the McMurdo region (e.g., Marchant et al., 2002). Notably, these ice-free areas are the only locations in Antarctica where the active layer can be found. Traditionally, the active layer is thermally defined as the soil layer with temperatures above 0°C, subject to annual cycles of thawing and refreezing (Figure 2). The active layer thickness (ALT) in Antarctica varies widely, from less than 5 cm in the high-elevation sites of the McMurdo Dry Valleys to over 500 cm in bedrock-formed sites of the Antarctic Peninsula (Vieira et al., 2010; Bockheim et al., 2013).

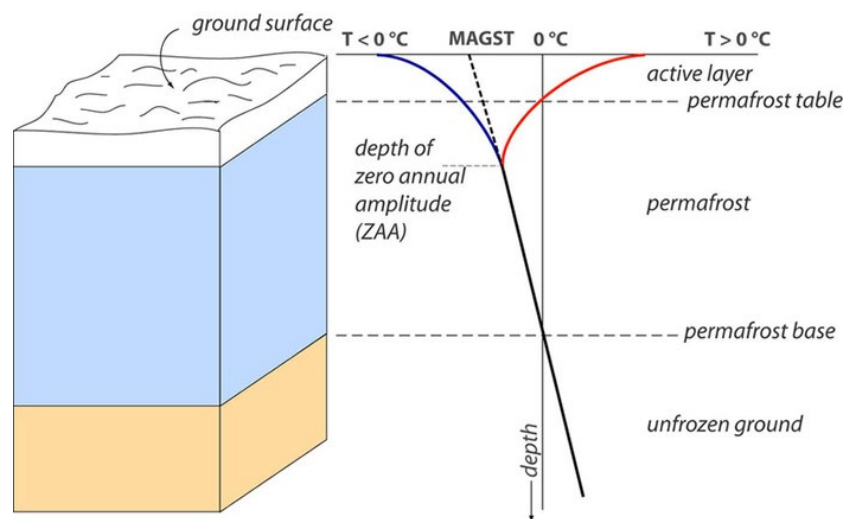


Figure 2. Thermal profile of the active layer and permafrost (Noetzli and Gruber, 2005).

Unlike the distribution of the active layer, the presence of permafrost in Antarctica remains a somewhat debated topic. According to the classical definition, permafrost is “a material with a temperature below 0°C for at least two consecutive years” (Muller, 1943), and based on this, permafrost is widespread across nearly all of Antarctica, including areas beneath the ice sheet. From a physical perspective, the ground beneath glaciers can be either frozen or unfrozen, depending on the thermal regime of the glacier. Below cold-based glaciers, the ground remains frozen, while beneath warm-based glaciers, it is unfrozen. However, even in these cases, the temperature at the base of warm glaciers often remains below 0°C, and this is referred to as “cryotic ground” (van Everdingen, 1976). To date, detailed information about the thermal state of the ground beneath glaciers is limited, with most available data derived from geophysical surveys and modelling, primarily conducted as part of glaciological studies (e.g., Burton-Johnson et al., 2020). In the ice-free areas, permafrost typically has a thickness of less than 5 m in the South Shetlands, up to more than 1000 m in Victoria Land. The only regions where

permafrost is considered to be discontinuous or sporadic are the low-elevation parts of the South Shetland Islands and the western Antarctic Peninsula. These findings are based on modelling the temperature at the top of the permafrost (Ferreira et al., 2017) and geophysical surveying (Correia et al., 2017).

The thermal dynamics of the active layer are a key indicator of how terrestrial environments respond to climate change. Over the past few decades, numerous case studies have explored various aspects of the active layer thermal regime, ALT, and permafrost temperatures in different parts of Antarctica. These studies have provided insights into general patterns of the active layer and examined the role of factors such as general climate conditions (e.g., Adlam et al., 2010, Kotze and Meiklejohn, 2017), snow cover (Guglielmin et al., 2014a,b; de Pablo et al., 2017; Tarca et al., 2022), and vegetation (Cannone and Guglielmin, 2009; Cannone et al., 2006, 2021). However, soil moisture has received relatively less attention, despite being considered one of the key parameters shaping terrestrial ecosystems, particularly in terms of vegetation abundance (Kennedy, 1993; Ugolini and Bockheim, 2009; Guglielmin et al., 2014a). Soil moisture is also crucial as an agent driving factors such as the intensity of freeze-thaw cycles, soil thermal properties variability, geomorphological processes, and pedogenesis. The notable exceptions to this include the McMurdo area in Victoria Land, where soil moisture research has been ongoing for several decades (e.g., Seybold et al., 2010; Levy et al., 2011; Ball and Levy, 2015). Recently, there has been a greater focus on soil moisture in research conducted on James Ross Island (Hrbáček et al., 2023b; Kňázková and Hrbáček, 2024).

From the perspective of general understanding of the active layer thermal regime in Antarctica, most of the studies published so far have been limited in both spatial and temporal scale, which has resulted in findings that are somewhat scattered. The first comprehensive summary of fragmented results from Antarctica was published by Vieira et al. (2010), who analyzed advancements in active layer research during the International Polar Year (IPY) 2007–08 and provided the first continental overview on the variability of active layer thickness (ALT) and near-surface ground temperature in Antarctica. In the Antarctic Peninsula, the results regarding the active layer and permafrost thermal regime were further summarized by Bockheim et al. (2013), who also proposed the boundaries of permafrost presence.

The first assessment of longer continuous datasets of the active layer thermal regime from multiple locations was provided by Hrbáček et al., (2021). In this work, the authors evaluated results from active layer thickness and near-surface ground temperature monitoring conducted at Circumpolar Active Layer Sites in Antarctica (CALM-S). Our most recent synthesis (Hrbáček et al., 2023a), which summarizes results from over 80 studies post-IPY, provides the current baseline knowledge of the active layer thermal regime in Antarctica. In this work, we defined the spatial and temporal variability of near-surface ground temperature and ALT, identified the major factors influencing the active layer thermal regime, and proposed possible

future research directions for the active layer in Antarctica. The findings of this work are part of this thesis and will be discussed in more detail in the following sections.

In contrast to the active layer, relatively little is known about permafrost temperatures. Permafrost temperature is defined as the temperature at a depth of zero annual amplitude (ZAA), typically located between 10 and 20 meters below the surface. The long-term change in permafrost temperature is a reliable indicator of climate variability in sub-surface temperatures. Measuring temperatures at this depth requires deep boreholes, making research technically and logistically challenging. Currently, only a few operational boreholes exist in Antarctica. The findings from these sites were included in a global synthesis of the thermal state of permafrost by Biskaborn et al. (2019). Antarctic sites exhibited a strong warming trend; however, the results were not statistically significant due to the limited number of monitoring sites across the continent.

## 2 Motivation and research objectives

The core area of my work is James Ross Island, located in the northeastern Antarctic Peninsula region, which has provided a natural laboratory for testing different hypotheses and methods in active layer research. The baseline for our research was set by the works of Vieira et al. (2010) and Bockheim et al. (2013), which, however, provided very limited results from James Ross Island. It became a significant research challenge to fill the gap in the map with our findings. Another challenge was testing various hypotheses regarding the quantification of the effects of a wide range of factors - such as climate, snowpack, vegetation, lithology, and geomorphology - on the active layer thermal regime and thickness. The research hypothesis was often framed using insights from regions such as the Arctic, South Shetlands, and McMurdo.

The thesis summarizes the findings on the topic of active layer thermal regime and thickness on key study sites of James Ross Island as well as our research conducted in other parts of Antarctica. I structured the work around three major objectives, each focused on addressing key research questions:

**Objective 1:** To assess the variability of the active layer thermal regime and thickness on James Ross Island.

- **Research question:** How do the thermal regime and thickness of the active layer vary across different sites on James Ross Island, and what are the key factors influencing this variability?

**Objective 2:** To develop and apply models for active layer thickness and permafrost temperature prediction.

- **Research question:** What is the reliability and performance of the models used for predicting active layer thickness and temperature on the top of permafrost in Antarctica?

**Objective 3:** To analyse the spatiotemporal variability of the active layer thermal regime across Antarctica.

- **Research question:** What are the spatial variability and temporal trends in the active layer thermal regime and thickness in Antarctica?

### 3 Study area

The primary area of research presented in this thesis is James Ross Island, situated in the northeastern part of the Antarctic Peninsula. The northern part of the Ulu Peninsula is the largest ice-free area (approximately 310 km<sup>2</sup>) in the Antarctic Peninsula region (Figure 3, 4). This relatively large ice-free area, which has been gradually extending throughout the Holocene (e.g. Roman et al., 2024), combined with its diverse lithological and topographical conditions (e.g. Mlčoch et al., 2020; Jennings et al., 2021), offers unique opportunities to investigate various aspects of the active layer thermal regime and its spatial and temporal variability. In addition to the research conducted on James Ross Island, several studies were also carried out using data from sites on the South Shetlands (Figure 3).

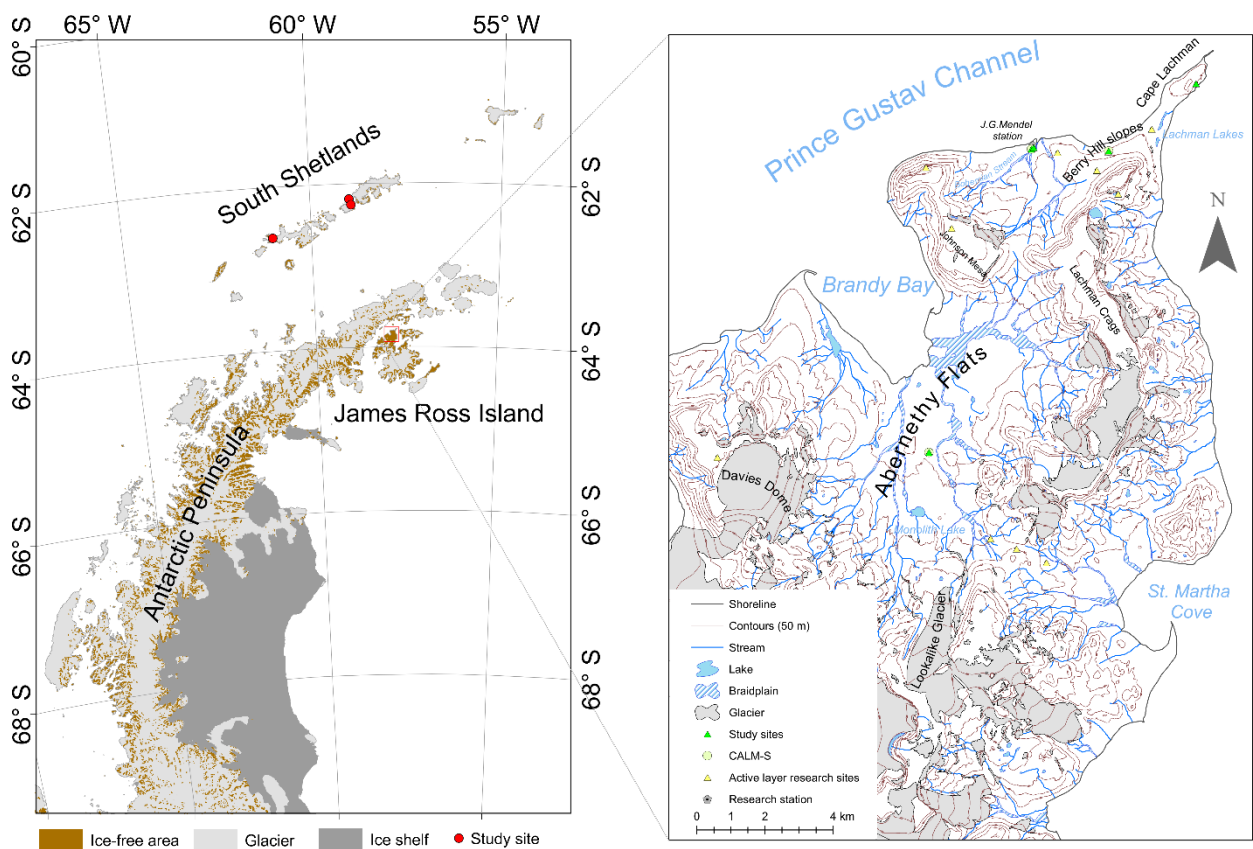


Figure 3. Regional setting of the northern Antarctic Peninsula (left) and James Ross Island (right)

The climate of James Ross Island lies between cold oceanic and cold polar continental types (King and Comiso, 2003). The mean annual air temperature (MAAT) near the JGM station was  $-6.7^{\circ}\text{C}$  from 2004 to 2020 (Kaplan Pastřiková et al., 2023). Precipitation is influenced by the orographic barrier of the Antarctic Peninsula and is estimated to range between 300 and 700 mm of water equivalent per year. Most of the precipitation falls as snow and is usually unevenly distributed due to the effects of wind (Kavan et al., 2020). In comparison to other Antarctic sites covered in this thesis, James Ross Island experiences a border climate. It is situated between the oceanic climate of the South Shetlands (with a MAAT around  $-2.0^{\circ}\text{C}$ ) and the

cold polar continental climate of Victoria Land (with a MAAT of less than  $-15\text{ }^{\circ}\text{C}$ ). The climate conditions at sites along the East Antarctica coastal area tend to be slightly colder, with a MAAT around  $-10\text{ }^{\circ}\text{C}$ .

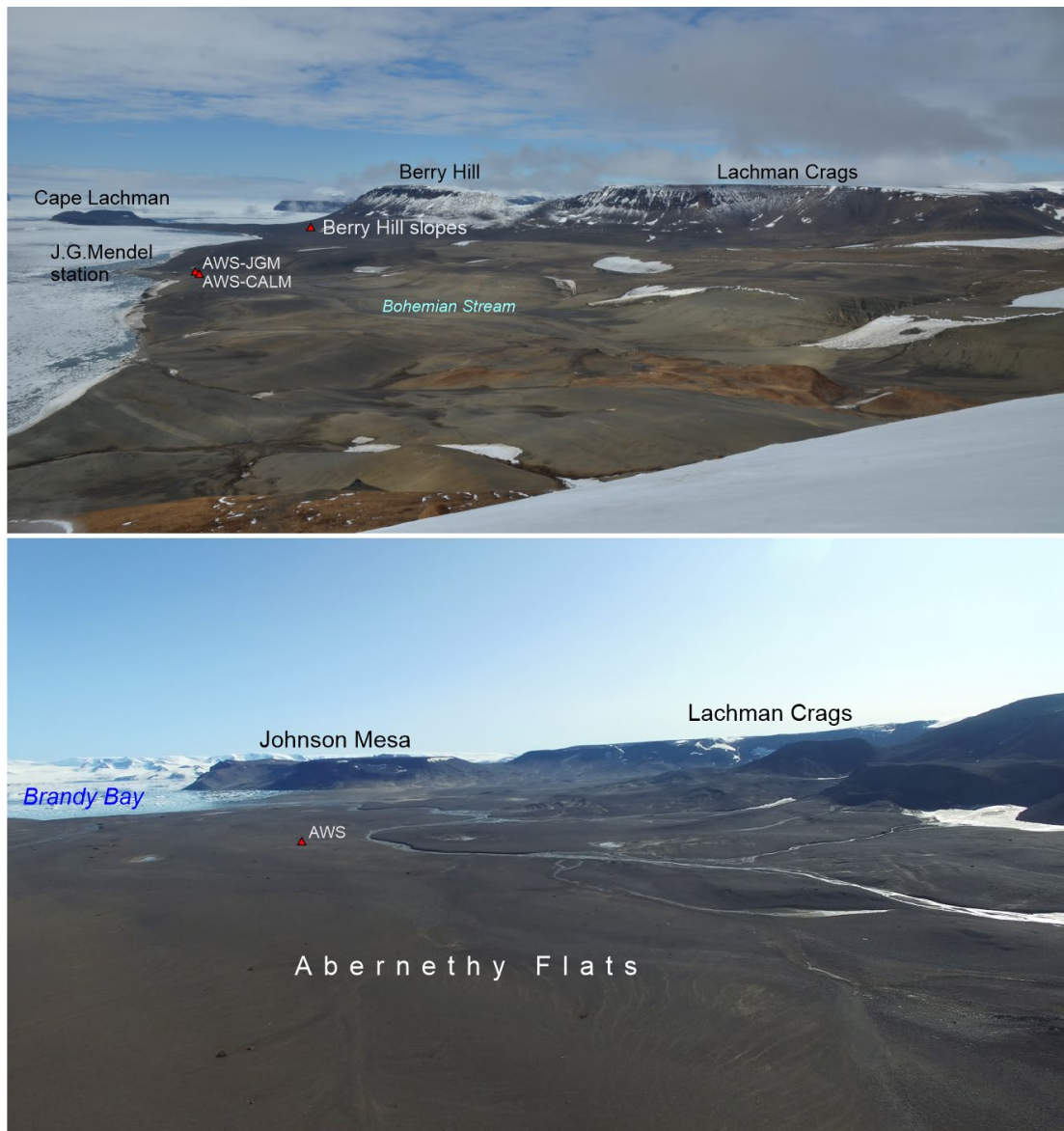


Figure 4. Landscape of Ulu Peninsula, the red triangles indicate the position of the key study sites.

The research activities of Czech scientists focusing on the active layer in the Ulu Peninsula began in 2005 with the installation of the first temporary stations for soil temperature monitoring. In 2006, continuous measurements of active layer temperature were initiated near the Johann Gregor Mendel station (AWS-JGM) and at the site at Abernethy Flats (Figures 3, 4, 5). Currently, the network includes  $> 10$  stations located in various parts of the Ulu Peninsula, alongside three CALM-S sites providing spatial data on active layer thaw depth (Figures 3, 4, 5). Since 2016, several research papers have been published detailing the results on the spatial-temporal variability of the active layer thermal regime and thickness on James Ross Island.

## 4 Data and methods

The thesis incorporates a range of field, analytical, and laboratory techniques that are well-established and widely used in active layer and permafrost research. In general, most data were collected from automatic weather stations, which provided continuous measurements of various atmospheric and soil parameters. Given the differing study sites, methods, and datasets used across the studies, I summarize the research methods and datasets for each paper in Table 1.

Table 1. Summary of the methods used in the presented papers.

| Paper                                      | Study area            |                    |                   | Method      |                       |        |                    | Datasets            |                       |                  |                        |                 |      |           |              |               |                         |
|--|-----------------------|--------------------|-------------------|-------------|-----------------------|--------|--------------------|---------------------|-----------------------|------------------|------------------------|-----------------|------|-----------|--------------|---------------|-------------------------|
|  | Number of study sites | Larger scale study | James Ross Island | Other areas | Continuous monitoring | CALM-S | ALT/TTOP Modelling | Laboratory analysis | Geophysical surveying | Soil temperature | Active layer thickness | Air temperature | Snow | Radiation | Soil texture | Soil moisture | Soil thermal properties |
| Paper 1 (Hrbáček et al., 2016a)            | 1                     |                    |                   |             |                       |        |                    |                     |                       |                  |                        |                 |      |           |              |               |                         |
| Paper 2 (Hrbáček et al., 2016b)            | 2                     |                    |                   |             |                       |        |                    |                     |                       |                  |                        |                 |      |           |              |               |                         |
| Paper 3 (Hrbáček et al., 2017a)            | 2                     |                    |                   |             |                       |        |                    |                     |                       |                  |                        |                 |      |           |              |               |                         |
| Paper 4 (Hrbáček et al., 2017b)            | 2                     |                    |                   |             |                       |        |                    |                     |                       |                  |                        |                 |      |           |              |               |                         |
| Paper 5 (Kňázková et al., 2020)            | 3                     |                    |                   |             |                       |        |                    |                     |                       |                  |                        |                 |      |           |              |               |                         |
| Paper 6 (Hrbáček et al., 2020a)            | 6                     |                    |                   |             |                       |        |                    |                     |                       |                  |                        |                 |      |           |              |               |                         |
| Paper 7 (Hrbáček and Uxa, 2020)            | 1                     |                    |                   |             |                       |        |                    |                     |                       |                  |                        |                 |      |           |              |               |                         |
| Paper 8 (Hrbáček et al., 2021a)            | 2                     |                    |                   |             |                       |        |                    |                     |                       |                  |                        |                 |      |           |              |               |                         |
| Paper 9 (Hrbáček et al., 2023b)            | 3                     |                    |                   |             |                       |        |                    |                     |                       |                  |                        |                 |      |           |              |               |                         |
| Paper 10 (Kňázková and Hrbáček, 2024)      | 1                     |                    |                   |             |                       |        |                    |                     |                       |                  |                        |                 |      |           |              |               |                         |
| Paper 11 (Kaplan Pastířiková et al., 2023) | 1                     |                    |                   |             |                       |        |                    |                     |                       |                  |                        |                 |      |           |              |               |                         |
| Paper 12 (Hrbáček et al., 2025)            | 2                     |                    |                   |             |                       |        |                    |                     |                       |                  |                        |                 |      |           |              |               |                         |
| Paper 13 (Hrbáček et al., 2020b)           | 8                     |                    |                   |             |                       |        |                    |                     |                       |                  |                        |                 |      |           |              |               |                         |
| Paper 14 (Obu et al., 2020)                | -                     |                    |                   |             |                       |        |                    |                     |                       |                  |                        |                 |      |           |              |               |                         |
| Paper 15 (Hrbáček et al., 2021b)           | 11                    |                    |                   |             |                       |        |                    |                     |                       |                  |                        |                 |      |           |              |               |                         |
| Paper 16 (Hrbáček et al., 2023a)           | > 20                  |                    |                   |             |                       |        |                    |                     |                       |                  |                        |                 |      |           |              |               |                         |

### 4.1 Air and ground temperatures

In all studies, we used datasets of soil and air temperature, primarily measured with resistance thermometers featuring a high accuracy of  $\pm 0.15$  °C. On James Ross Island, this monitoring is standardized to measure air temperature at 2 m above the ground and soil temperature at depths of 5, 10, 20, 30, 50, and 75 cm, with additional measurements at 100, 150, and 200 cm at several sites (Figure 5).

Temperatures were most often analysed at various temporal scales, ranging from 30-minute records to annual data. Daily mean temperature values were used to calculate Thawing Degree Days (TDD) and Freezing Degree Days (FDD), which summarize cumulative positive and negative temperatures of air and ground over the summer and winter seasons, respectively (e.g., Riseborough, 2003). These indices are among the most commonly used metrics in active layer and permafrost research. Additionally, TDD and FDD served as key temperature inputs for the models used to predict active layer thickness (ALT) and temperature at the top of the permafrost table.

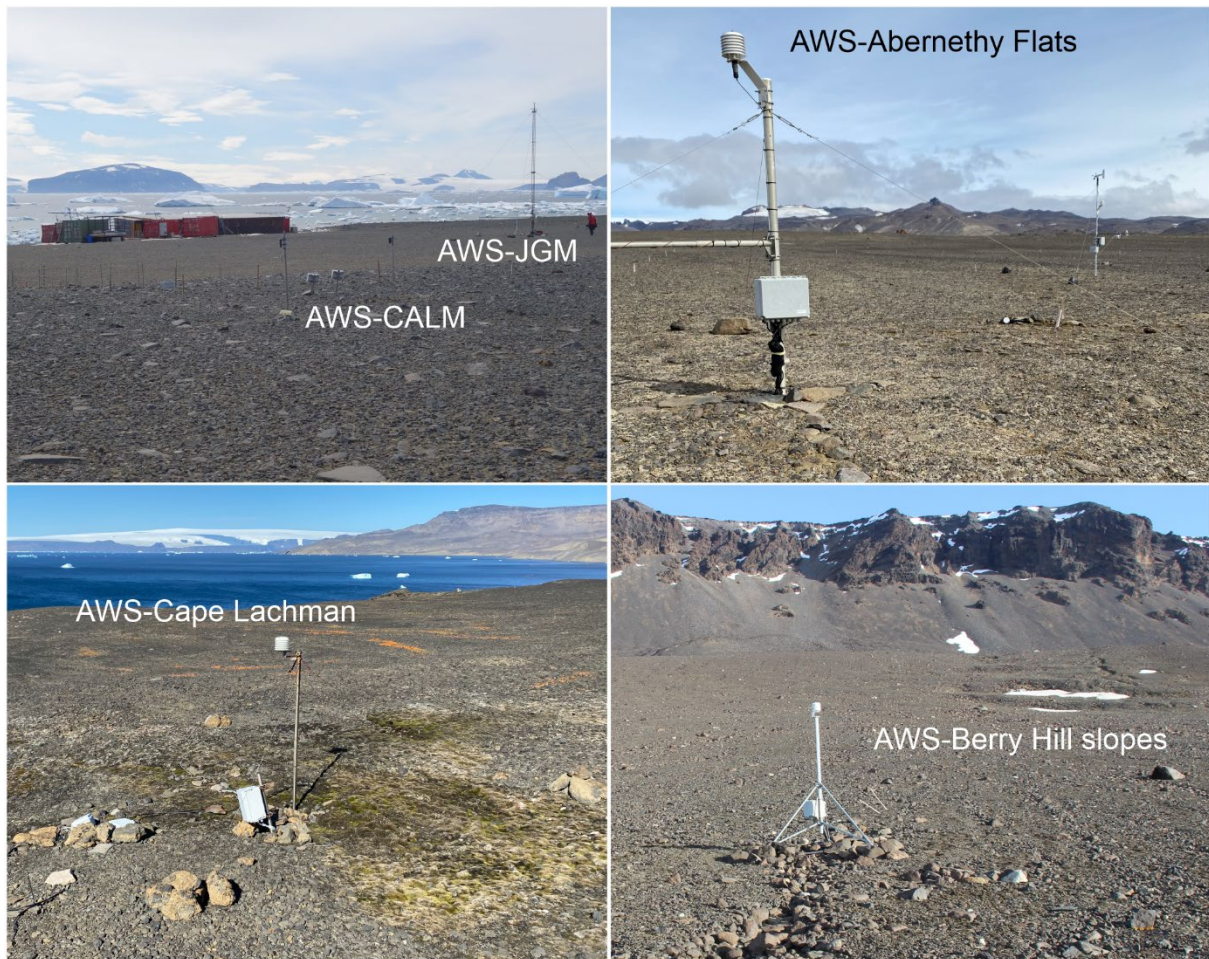


Figure 5. Detailed picture of the key study sites on James Ross Island.

#### 4.2 Active layer thickness

Soil temperature data were also used to determine the depth of the 0 °C isotherm, representing the annual maximum ALT for each year (Figure 2). This calculation was performed using linear interpolation between the maximum annual temperature recorded at the deepest sensor with a temperature > 0 °C and the next sensor with a maximum temperature < 0 °C. In cases where thermometers were not installed in the permafrost table, ALT was extrapolated using a logarithmic fit based on at least three of the deepest sensors within the active layer.

Mechanical probing of thaw depth was the second approach used to determine the annual ALT. Probing is one of the primary monitoring methods employed at Circumpolar Active Layer Monitoring (CALM) sites. The CALM protocol provides standardized guidelines for measuring ALT (Brown et al., 2000). In Antarctica, this protocol was adapted into CALM-S to account for specific local conditions, such as coarse ground that may hinder mechanical probing, logistical constraints, and challenges in timing measurements to capture the seasonal maximum (Guglielmin, 2006).

### **4.3 Soil physical properties**

Beyond climatological variables, we analysed soil physical properties (including texture, moisture, and thermal properties) in several studies. These data provide essential insights into the lithological differences between study sites and help clarify the distinct effects of various factors.

#### **a) Soil texture:**

We used soil texture data from study sites on James Ross Island, analysed in laboratories at the Technical University of Munich. Fractions  $> 0.063$  mm were assessed using analytical sieves, while the finest fraction ( $< 0.063$  mm) was measured using a Sedigraph.

#### **b) Soil moisture:**

We measured soil moisture using three different approaches:

Gravimetric Soil Moisture: Determined by drying soil samples (100 cm<sup>3</sup> volume) for 48 hours at 105 °C.

Continuous Measurement of Volumetric Water Content (VWC): Conducted using TDR sensors (CS655, Campbell Scientific) with a 12 cm probe length, installed at three or four depths between 5 and 75 cm, depending on site-specific conditions.

Surficial VWC: Measured at the CALM-S JGM site using a Hydrosense II device with a TDR CS659 sensor (Campbell Scientific).

#### **c) Soil thermal Properties:**

Laboratory measurements of soil thermal conductivity, heat capacity, and thermal diffusivity were performed using the ISOMET 2114 device (Applied Precision, Slovakia). Both intact and bulk samples, with a minimum volume of 750 cm<sup>3</sup>, were collected from the surficial part (0–10 cm) and the middle part (approximately 30 cm) of the active layer.

Additionally, we modelled soil thermal conductivity using soil heat flux measurements (HFP01 plate by Hukseflux, installed at 5 and 20 cm) combined with soil temperature data from the same depths. The Least Squares Method trend-fitting was applied as a numerical solution to Fourier's Law of Heat Conduction. This approach was used to calculate soil thermal conductivity for the summer seasons from 2015/16 to 2022/23 at AWS-Abernethy Flats (Kňázková and Hrbáček, 2024).

## 5 Results and discussion

The results of our research are further presented according to the main objectives mentioned in Section 2.

### 5.1 Objective 1: Active layer thermal regime and thickness on James Ross Island

We used the Ulu Peninsula on James Ross Island as a natural laboratory, enabling a detailed study of various aspects of active layer thermal dynamics and thickness variability. This thesis summarizes 12 studies conducted at four sites on James Ross Island (Figure 3), covering the period from 2004 to 2023 and addressing five key research topics (Table 2). The results provide essential insights into how the active layer responds to local environmental conditions. Furthermore, they offer valuable contributions to the broader understanding of active layer changes on a continental scale in Antarctica.

Table 2. Summary and timeline of the papers from James Ross Island used in this thesis

| Study site           | 2004 | 2005 | 2006 | 2007 | 2008 | 2009 | 2010 | 2011    | 2012     | 2013     | 2014    | 2015 | 2016 | 2017    | 2018    | 2019 | 2020 | 2021 | 2022 | 2023 |
|----------------------|------|------|------|------|------|------|------|---------|----------|----------|---------|------|------|---------|---------|------|------|------|------|------|
| AWS-JGM and AWS-CALM |      |      |      |      |      |      |      | Paper 1 |          |          | Paper 4 |      |      |         | Paper 8 |      |      |      |      |      |
|                      |      |      |      |      |      |      |      |         |          | Paper 15 |         |      |      |         |         |      |      |      |      |      |
|                      |      |      |      |      |      |      |      |         | Paper 11 |          |         |      |      |         |         |      |      |      |      |      |
|                      |      |      |      |      |      |      |      |         |          |          |         |      |      |         |         |      |      |      |      |      |
|                      |      |      |      |      |      |      |      |         |          |          |         |      |      |         |         |      |      |      |      |      |
| Abernethy Flats      |      |      |      |      |      |      |      |         |          |          | Paper 2 |      |      |         |         |      |      |      |      |      |
|                      |      |      |      |      |      |      |      |         | Paper 3  |          |         |      |      |         |         |      |      |      |      |      |
|                      |      |      |      |      |      |      |      |         |          |          |         |      |      |         |         |      |      |      |      |      |
| Berry Hill slopes    |      |      |      |      |      |      |      |         |          | Paper 3  |         |      |      |         |         |      |      |      |      |      |
| Cape Lachman         |      |      |      |      |      |      |      |         |          |          |         |      |      | Paper 6 |         |      |      |      |      |      |

Considering the diverse range of topics addressed on James Ross Island, I divided Objective 1 into the following sub-chapters:

- Spatio-temporal changes in the active layer thermal regime and thickness on James Ross Island
- The effect of local conditions on the active layer
- Active layer thickness variability at CALM-S JGM

#### 5.1.1 Spatio-temporal changes of active layer thermal regime and thickness

This section summarizes findings on air and ground temperatures, as well as active layer thickness, based on individual case studies (Table 2). Since 2006, we have observed substantial variability in mean annual air temperature (MAAT) and mean annual ground temperature (MAGT) on James Ross Island. At low-elevation sites (< 60 m a.s.l.), MAAT ranged from  $-3.0^{\circ}\text{C}$  to  $-9.5^{\circ}\text{C}$ . Similarly, MAGT exhibited significant variability, ranging from  $-2.5^{\circ}\text{C}$  to  $-9.0^{\circ}\text{C}$  at 5 cm depth and  $-3.5^{\circ}\text{C}$  to  $-8.5^{\circ}\text{C}$  at 50 cm depth (summary of *Papers 1–12*). This high interannual variability is characteristic of the northeastern Antarctic Peninsula, as

documented by long-term monitoring records from Marambio and Esperanza stations (Turner et al., 2020).

The longest MAGT dataset comes from Abernethy Flats (45 m a.s.l.), a representative site for the lowlands in the central Ulu Peninsula (Figure 4, 5). Between 2006 and 2023, the site recorded a MAAT of  $-6.0^{\circ}\text{C}$ , while MAGT ranged from  $-5.7^{\circ}\text{C}$  (5 cm) to  $-6.0^{\circ}\text{C}$  (50 cm) (*Papers 7, 10*, Figure 6). The mean daily air and ground temperatures varied annually between  $-25^{\circ}\text{C}$  and  $+5^{\circ}\text{C}$ , with extreme values dropping below  $-30^{\circ}\text{C}$  and exceeding  $+10^{\circ}\text{C}$  (Figure 6). We observed an increasing trend between  $1.43^{\circ}\text{C/decade}$  (MAGT at 50 cm) and  $1.93^{\circ}\text{C/decade}$  (MAAT). Such a warming air temperature trend is higher than we observed on AWS-JGM ( $+0.6^{\circ}\text{C/decade}$ ) in the period 2004-2020 (*Paper 11*).

Compared to other monitoring sites on James Ross Island, MAAT and MAGT at Abernethy Flats closely resembled values at AWS-JGM, AWS-CALM (*Paper 11,12*) and AWS-Cape Lachman (*Paper 6*). but was slightly lower (by a few tenths of a degree) than at AWS Berry Hill slopes (*Paper 3*).

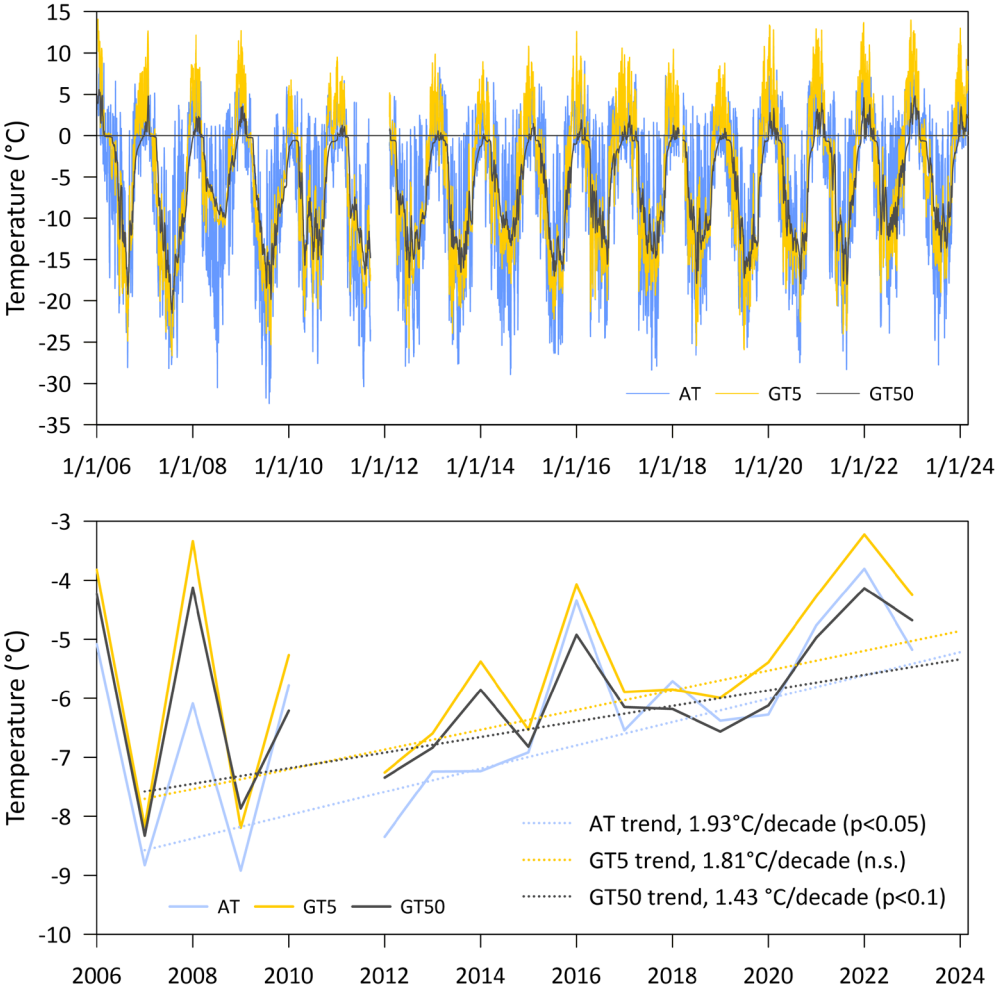


Figure 6. Variability of mean daily (top) and mean annual (bottom) air temperature (AT) and ground temperature at depths of 5 cm (GT5) and 50 cm (GT50) on AWS-Abernethy Flats from 2006 to 2023. Results from *Papers 7 and 10*.

Despite the relatively similar MAAT and MAGT across sites, we observed distinct differences in ALT. The thickest active layers were found at AWS Berry Hill slope and AWS-CALM, where ALT typically ranged from 85 to 95 cm (Figure 7). In contrast, much thinner active layer was recorded at AWS-JGM, with a long-term (2011–2023) ALT mean of 60 cm (*Papers 11, 12*). The lowest ALT were observed on moss-covered part of AWS-Cape Lachman (*Paper 6*; see more in section 5.1.2). The interannual variability in active layer temperatures and ALT exhibited a strong correlation ( $r > 0.8$ ) with mean summer air temperatures. However, the relationship between ALT and mean annual air temperatures was only moderate ( $r < 0.7$ ) and statistically non-significant (*Papers 7, 11, 12*).

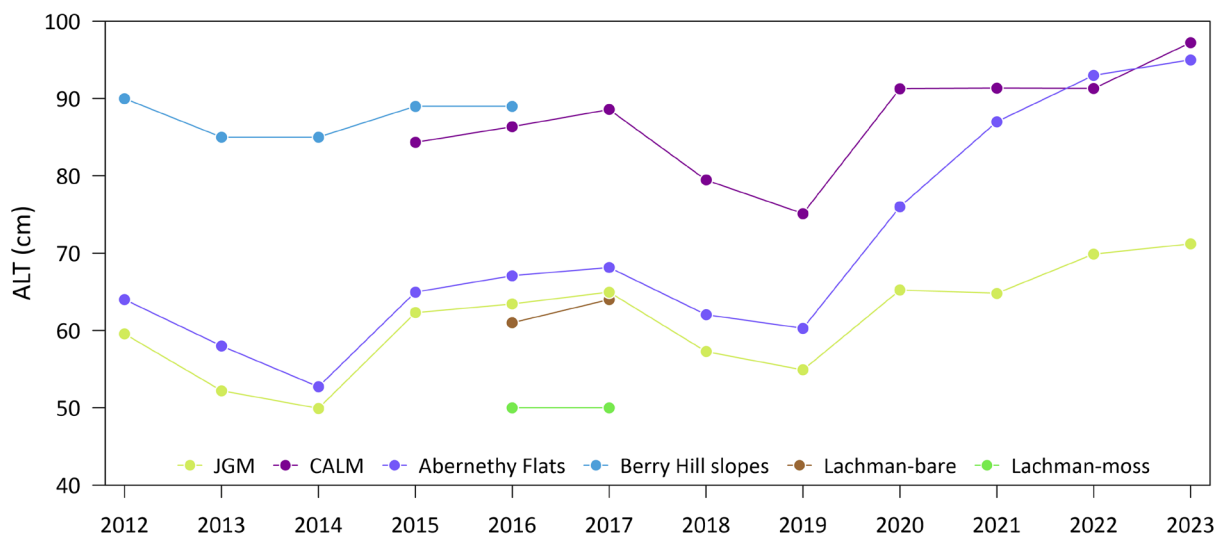


Figure 7. Variability of ALT on selected study sites of James Ross Island. Composition of results published in *Papers 1-12*

In the initial phase of our research, MAGTs and ALTs were strongly influenced by the short-term cooling period that occurred in the Antarctic Peninsula between 2000 and 2015 (Turner et al., 2016; Oliva et al., 2017a; Bozkurt et al., 2020). This atmospheric cooling led to the thinning and cooling of the active layer, a trend observed at multiple sites across the Antarctic Peninsula (Oliva et al., 2017; Ramos et al., 2017). The cooling peaked around 2011 on James Ross Island (*Paper 11*). Although temperatures have risen since then, the MAAT from 2011 to 2015 remained below the long-term average. The warming trend persisted until 2022, the warmest year on record for James Ross Island (*Papers 10, 11, 12*; Dunn et al., 2023).

The gradual increase in air temperatures during the summer months led to significant thickening and warming of the active layer between 2016 and 2023 at Abernethy Flats (*Paper 10*, Figure 7). Similarly, an ALT increase of 15 cm/decade at AWS-JGM and 11 cm/decade at AWS-CALM was observed from 2014 to 2023 (*Paper 12*). During the summer of 2022/23, the deepest active layer was recorded at the major study sites (*Papers 11,12*; Figure 7). These results support the hypothesis that ALT is highly sensitive to climate variability, reinforcing its role as an indicator of regional climate change in the Antarctic Peninsula (Bockheim et al., 2013)

### 5.1.2 The effect of local conditions on active layer variability

The differences in ALT at sites with similar air and near-surface temperatures clearly highlight the role of site-specific conditions. The assessment of factors influencing the active layer thermal regime and thickness was a key objective of *Paper 16*. In this study, the major groups of factors affecting the active layer thermal regime were identified as follows:

- Climate conditions
- Lithology and geomorphology
- Biota
- Hydric regime

This chapter summarizes findings from case studies conducted on James Ross Island and the South Shetland Islands, providing insights into the specific characteristics of these regions. Additionally, it discusses how these studies have contributed to the broader understanding of surface–active layer interactions across Antarctica.

#### 5.1.2.1 Climate conditions

Climate conditions are naturally the most critical factor influencing soil temperatures. In particular, near-surface temperatures exhibit a strong interaction with atmospheric conditions and can be moderated by snow cover. In our research, we focused on evaluating the effects of air temperature, solar radiation, and snow cover on the thermal regime and thickness of the active layer. However, the role of precipitation and wind speed has not yet been analysed in detail.

##### 1) Air temperature

Air temperature is generally the dominant factor influencing ground thermal regime variability worldwide (Lembrechts et al., 2022). In many Antarctic sites, a strong correlation ( $r > 0.7$ ) has been observed between daily air and ground temperatures (Guglielmin, 2006; Kotze and Meiklejohn, 2017; Carshalton et al., 2022; *Paper 3*). This correlation is particularly evident in areas with bare-ground surfaces and irregular snowpack occurrence. In contrast, moderate to weak correlations ( $r < 0.7$ ) are primarily influenced by snow cover (*Papers 1,2*) or vegetation (*Paper 7*, Cannone et al., 2006). These elements act as insulating layers due to their low thermal conductivity, reducing direct heat transfer between air and ground.

Additionally, in *Papers 7, 10, 11 and 12*, we analyzed the relationship between ALT and air temperature at seasonal (summer/winter) and annual levels. Our findings revealed a) very strong correlation ( $r > 0.8$ ) between ALT and summer air temperatures, b) moderate correlation ( $r \approx 0.5$ ) between ALT and winter or annual air temperatures. This highlights that summer air temperature plays a critical role in controlling active layer thickness, while winter and annual temperatures have a less direct influence.

## 2) Solar radiation

Solar radiation plays a pronounced role in high-polar regions, particularly in areas like Victoria Land, where near-surface ground temperatures often show a very high correlation ( $> 0.9$ ) with solar radiation. In these regions, solar radiation can significantly contribute to maximum surficial temperatures, which can sometimes exceed  $30\text{ }^{\circ}\text{C}$  (Guglielmin and Cannone, 2012). The seasonal rates of TDDg (ground) can even surpass  $600\text{ }^{\circ}\text{C.days}$ , despite the TDDa (air) being below  $50\text{ }^{\circ}\text{C.days}$  (*Paper 6*, Cannone and Guglielmin, 2009). However, the effect of solar radiation in other parts of Antarctica decreases and typically exhibits moderate (0.5 to 0.6) or weak (0.3 to 0.5) correlations. The strength of this correlation often depends on cloudiness in the region or the surface type (*Paper 6*).

## 3) Snow cover

Snow cover is a highly effective insulator due to its low thermal conductivity. It is generally assumed that a snow thickness of about 40 cm is sufficient to fully insulate the ground from the atmosphere (Zhang, 2005). Our initial research on James Ross Island focused on assessing the effect of snow cover on the active layer thermal regime and thickness (*Paper 1*). We hypothesized that, similar to observations in the Arctic (Zhang et al., 1997) and Antarctic (de Pablo et al., 2014), snow would significantly affect the active layer thermal regime.

We found that the snow cover on James Ross Island was relatively thin during winter, reaching about 30 cm in height on AWS-JGM (*Paper 1*). This observation serves as a basis for the hypothesis that the snow-cover effect is negligible in general on James Ross Island. These findings further supported the observation of high freezing n-factor values exceeding 0.9, indicating good heat transfer between air and ground (Lunardini, 1978; Karunaratne and Burn, 2003). The freezing n-factor is a key indicator, suggesting that snow cover do not play a significant role in this region, which was confirmed also on other sites of James Ross Island where the n-factor value was usually  $> 0.9$  (*Papers 3 and 7*).

The pronounced effect of snow was only observed under topographically induced conditions, where winter warming of the ground occurred in areas with snow depths exceeding 50 cm (*Paper 5*). In the summer of 2018, we also determined that a snowpack of about 30 cm, lasting for 10 days during the high summer season, could reduce the ALT by approximately 10 cm (*Paper 8*). However, this was a unique case observed only once in over a decade of monitoring on James Ross Island. In the context of the Antarctic continent, the snow effect on active layer variability can be summarized as follows (*Paper 16*):

### a) Warming effect of snow:

This effect is typically observed in areas with relatively high MAAT and where snow cover during the winter months is between 40 to 100 cm. Such conditions are common in the South Shetlands area, where high snow accumulation is frequent (de Pablo et al., 2014, 2017; Ramos et al., 2020). Our findings confirmed that near-surface ground temperatures at sites covered by snow were, on average, about  $0.7^{\circ}\text{C}$  higher than at snow-free areas (*Paper 16*). Further, in Oliva

et al., 2017b, we observed thicker active layers in areas with greater snow depth, suggesting a warming effect driven by snow.

*b) Cooling effect of snow:*

The cooling effect is typically observed at sites where long-lasting winter snow cover exceeds 100 cm, such as in Rothera on the Western Antarctic Peninsula (Guglielmin et al., 2014a). In extreme cases, persistent snow patches can prevent the summer thawing of the active layer, potentially leading to permafrost cooling and aggradation (Ramos et al., 2020). Additionally, snow presence in the summer can also reduce ALT, as previously described in **Paper 8**.

**5.1.2.2 Lithology and geomorphology**

The evaluation of lithology and geomorphology effects on the active layer thermal regime was a key aspect of our initial research on James Ross Island. We hypothesized that the variability of soil texture and geochemistry parameters would significantly affect the soil thermal properties and soil water holding capacity, which in turn would influence the variability of the active layer thickness (ALT) and thermal regime in deeper parts of the active layer or topmost permafrost. This hypothesis was first explored in **Paper 3**, where we compared conditions at two sites: AWS-Berry Hill slopes and AWS-Abernethy Flats. The observed differences in ALT were primarily attributed to variations in water content and calcite content, which resulted in differences in soil thermal conductivity between these sites. A more pronounced response to lithological differences was observed at the CALM-S JGM site, where the ALT varied by more than 50 cm along the lithological gradient. This variability was quantified by measuring the differences in thermal conductivity between the two dominant types of soil in the area (more details in section 5.1.3).

Table 3. Soil physical properties on selected study sites of James Ross Island

| Site                  | Lithology   | Texture (%) |      |      | $\omega$<br>(%) | $\lambda$<br>(Wm <sup>-1</sup> K <sup>-1</sup> ) | Reference                              |
|-----------------------|---|-------------|------|------|-----------------|--|--|
|                       |   | Sand        | Silt | Clay |                 |  |  |
| AWS-JGM               | Holocene marine terrace; sandy soil   | 75          | 15   | 10   | 10 – 20         | 0.3 – 0.6  | Hrbáček et al., 2019; Papers 4, 11, 12 |
| AWS-CALM              | Cretaceous sedimentary rocks (Whisky Bay Fm.)                               | 50          | 23   | 27   | 20 – 30         | 0.7 - 0.9  |  |
| AWS-Abernethy Flats   | Cretaceous sedimentary rocks (Alpha Member, Santa Marta Fm.)                | 53          | 22   | 25   | 15 – 25         | 0.5 - 0.8  | Hrbáček et al., 2019; Papers 6,7       |
| AWS-Berry Hill slopes | Neogene glaciogenic, glaciomarine and marine sedimentary rocks (Mendel Fm.) | 62          | 22   | 16   | 25              | 0.9  | Hrbáček et al., 2019                   |

To quantify the differences in lithology on James Ross Island, we focused on analyzing and modelling key soil physical parameters (such as thermal conductivity, moisture, and texture) which are summarized in Table 3. This data allowed us to clearly distinguish between the specific study sites, highlighting notable differences in ALT. Specifically, ALT was found to

be lowest at AWS-JGM, while it was deepest at AWS-CALM and on the AWS-Berry Hill slopes.

The first detailed study on soil thermal properties (*Paper 10*) revealed the significant role of soil moisture variability during the thawing season. Using laboratory and modelling approaches, we observed a natural increase in soil thermal conductivity with rising soil moisture (Figure 8). However, this increase in moisture and thermal conductivity led to a decrease in ALT. This behaviour can be explained by the increased latent heat of fusion required for the phase change of water, which influences the thermal dynamics of the soil.

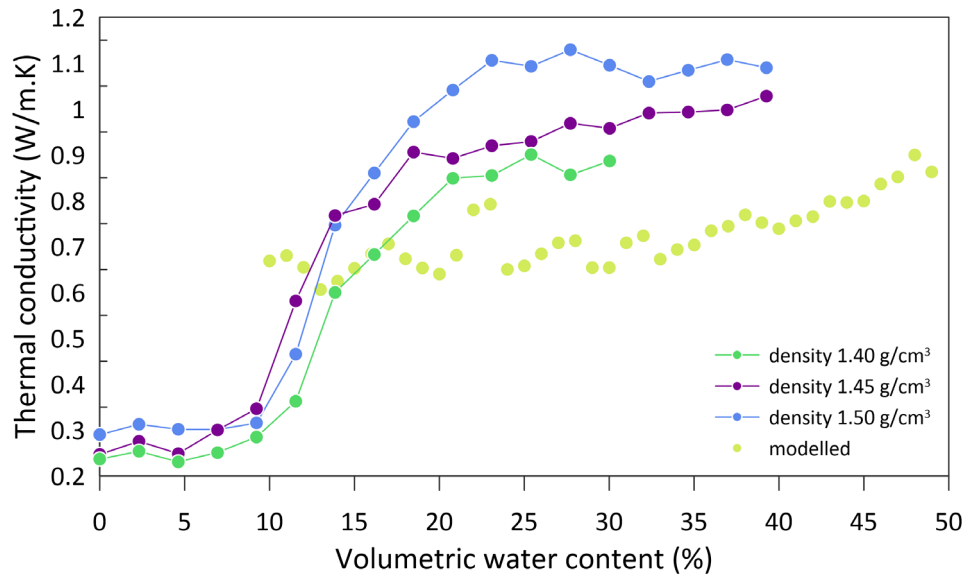


Figure 8. The relationship between volumetric water content and soil thermal conductivity a) measured for different soil densities and b) modelled from heat flux and temperature data. Adapted from *Paper 10*.

In Antarctica, the effect of lithology on the active layer remains relatively understudied, although analogies to James Ross Island can be drawn from other studies. In the South Shetlands, the influence of lithology is often overshadowed by other factors, such as snow cover. However, a clear lithological effect can be observed at the Crater Lake site, formed by coarse, low-conductive pyroclastic material. There, the ALT ranged from 30 to 50 cm (Ramos et al., 2017), while at other sites in the region, ALT often exceeds 100 cm (e.g., *Paper 2*; Oliva et al., 2017b; de Pablo et al., 2017; Ferreira et al., 2017). The thickest active layers were detected in bedrock sites, where they can reach several meters (summary in *Paper 16*).

This significant difference can be attributed to the much higher thermal conductivities of solid bedrock, which reach values of 2.6 and 4.3  $\text{Wm}^{-1}\text{K}^{-1}$  in some of the investigated sites in Antarctica (Guglielmin et al., 2011; Correia et al., 2012; Wilhelm et al., 2015). In contrast, soil thermal conductivities typically range below 1.0  $\text{Wm}^{-1}\text{K}^{-1}$  and can even decrease to less than 0.3  $\text{Wm}^{-1}\text{K}^{-1}$  in very dry material (e.g., Liu et al., 2018), explaining the variations in ALT between these different environments. The significance of geomorphological settings is often linked to snow cover distribution and the formation of surficial water tracks. On James Ross

Island (*Paper 5*) and in the South Shetlands (Oliva et al., 2017b), we observed how different topographical features either promote accumulation or deflation of the snowpack, influencing the ALT.

Certain landscape features, such as ice-cored moraines, can facilitate the development of a permafrost layer, even at sea level in the SSI, where permafrost is generally absent at low altitudes (e.g. Correia et al., 2017; Ferreira et al., 2017). In hyper-arid areas like McMurdo, the ALT variations can be driven by the formation of water tracks in the depressions, which play a critical role in the distribution and depth of permafrost (e.g., Levy et al. 2011).

### **5.1.2.3 Vegetation**

Overall, vegetation in Antarctica is quite scarce, covering only a small fraction of the ice-free areas. For example, the total area of vegetation patches in the Antarctic Peninsula is estimated to be only 12 km<sup>2</sup> (Roland et al., 2024). James Ross Island is no exception, with limited vegetation abundance. In our study area on the northern Ulu Peninsula, only a few compact moss patches are found (Barták et al., 2015). Therefore, research on the interactions between vegetation and the active layer provides valuable site-specific characteristics and ecological insights, helping to explain broader patterns across larger regions. At our experimental site, AWS Cape Lachman, we observed that the active layer was 9 to 14 cm thinner, and the mean annual ground temperature (MAGT) was 0.9 to 1.2°C lower beneath the moss patch compared to the bare-ground profile. Notably, the distance between the active layer measurement profiles was approximately 5 meters (*Paper 6*). These results are consistent with findings from other Antarctic sites, where areas covered by vegetation patches tend to have lower ground temperatures and thinner active layers than bare ground areas (Cannone and Guglielmin, 2009; Michel et al., 2012; *Paper 6*).

A more pronounced effect of moss carpets has been observed on Signy Island in sub-Antarctica, where the moss communities form thicker carpets, acting as effective insulators. In such conditions, the active layer can be more than 100 cm thicker under bare ground than under mosses (*Paper 6*). We can anticipate that the predicted "greening" of the warmest parts of the Antarctic Peninsula will lead to the expansion of new vegetation communities (e.g., Siegert et al., 2019), which may further insulate the ground, potentially mitigating the impact of warming air temperatures on the soil thermal regime.

### **5.1.2.4 Soil hydric regime**

Despite being one of the most crucial parameters affecting the Antarctic environment in terms of biological (e.g. Convey and Peck, 2019), geomorphological (Levy et al., 2011), or soil evolution (e.g. Kennedy, 1993; Ugolini and Bockheim, 2008), the knowledge on soil moisture in Antarctica remains limited. The only exception to this is the McMurdo Dry Valleys region, where systematic soil research has been conducted for several decades (Seybold et al., 2010).

In this region, soil moisture has been studied as a physical parameter related to permafrost ice (e.g. Bockheim et al., 2007; Linhardt et al., 2019) or as a factor affecting vegetation and

microorganisms' abundance (e.g. Wlostowski et al., 2017). In particular, water tracks, which have higher amounts of liquid water, are essential for the local environment. These areas form specific thermal regime patterns and influence active layer thickness. However, these findings are not easily transferable to other parts of Antarctica, as McMurdo represents a specific hyper-arid, cold polar environment with very low, almost undetectable, soil moisture contents. In the Antarctic Peninsula, soil moisture data have been presented, but interpretations on how it affects the environment remain limited (e.g. Michel et al., 2012; Almeida et al., 2017; Thomazini et al., 2020).

On James Ross Island, we primarily monitored gravimetric soil moisture to establish the general differences between the study sites (Table 3). We conducted the first analysis of one-year variability from January 2022 to February 2023, using data from AWS-JGM and two other sites in the South Shetlands (Stansbury Peninsula, Nelson Island, and Barton Peninsula, King George Island) as described in *Paper 9*. This study examined general soil moisture patterns, finding similar trends of increasing moisture with depth. It also identified the freeze-thaw behaviour with a well-defined hysteresis loop between the freezing and thawing phases. Additionally, we observed relatively high unfrozen soil moisture content during winter (approximately 0.1 cm<sup>3</sup>/cm<sup>3</sup>).

In *Paper 10*, we analysed the summer variability of near-surface soil moisture from 2017 to 2023 at Abernethy Flats. We observed high values (> 0.4 cm<sup>3</sup>/cm<sup>3</sup>) in the beginning of the summer period which was followed by decrease to 0.15 to 0.25 cm<sup>3</sup>/cm<sup>3</sup> in the high summer. Such a seasonal variability is important from the perspective of moisture effect on thermal conductivity (Figure 8). On the seasonal level we observed a strong negative correlation between moisture content and TDDg and ALT, which suggest that surficial drying may promote active layer thickening in this site. Similar results were reported from CALM-S JGM (*Paper 12*), but in this case the medium correlation lack statistical significance (see more in Section 5.1.3).

### **5.1.3 Circumpolar active layer monitoring on James Ross Island**

The CALM-S JGM is the first site established according to the CALM protocol in the eastern part of the Antarctic Peninsula. The site measures 80 x 70 meters, and the first measurement was carried out in February 2014. The relatively small size of the grid was specifically chosen to ensure the sustainability of measurements in conditions generally unfavourable for thaw depth probing, while also avoiding direct interference from the Johann Gregor Mendel Station facility. The site is situated at an elevation between 8 and 12 meters above sea level, with a gentle inclination of 1-5° towards the sea to the north. The CALM-S JGM grid consists of two distinct areas formed by different lithologies, which influence ALT variability. The northern approximately 75% of the grid is composed of gravelly to sandy sediments of a Holocene marine terrace. The remaining 25% in the southern part is made up of silt-loam sediments of the Cretaceous Whisky Bay Formation (*Paper 4*, Figure 9).

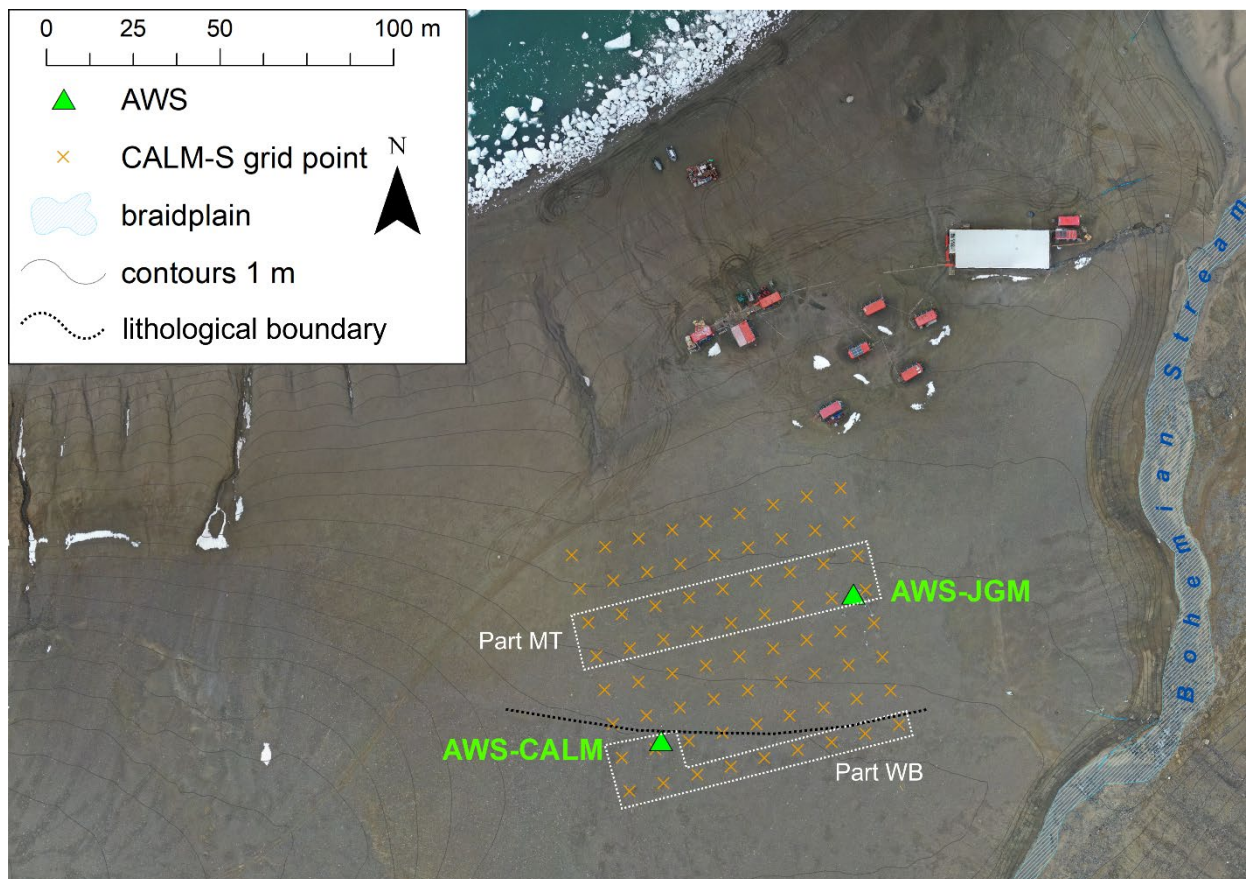


Figure 9. Aerial view on the area of vicinity of Johann Gregor Mendel station, CALM-S JGM and study profiles AWS-JGM and AWS-CALM. Adapted from *Paper 12*.

The first analysis of three years of monitoring at CALM-S JGM revealed a clear lithological effect on thaw depth (*Paper 4*). The thaw depth ranged between 50 and 75 cm in the sandy soils, whereas it exceeded 100 cm in the finer material of Whisky Bay Fm. Laboratory analysis showed that the Whisky Bay Fm. sediments had a three times higher soil thermal conductivity (ca.  $0.7\text{-}0.9\text{ Wm}^{-1}\text{K}^{-1}$ ) compared to the Holocene marine terrace sediments (ca.  $0.3\text{-}0.6\text{ Wm}^{-1}\text{K}^{-1}$ ). This was confirmed by a study in *Paper 12*, which analysed 10 years of monitoring at CALM-S JGM (Figure 8). The study found that, on average, the ALT was 24 cm thicker at AWS-CALM located on Whisky Bay Fm. sediments than at AWS-JGM, located on Holocene marine terrace sediments. Between 2014 and 2023, ALT thickened by 1.3 to 2.2 cm/year in the two sediment types, with a maximum thaw depth of 130 cm recorded in 2023. The study also examined the relationship between surficial soil moisture and thaw depth. The moisture content followed a similar distribution to thaw depth, with values between 25 and 35% in Whisky Bay Fm. sediments (Figure 8). A moderate negative correlation ( $r = -0.52$ ) was found between soil moisture and thaw depth, suggesting that ALT might increase with surficial drying. However, the results were not statistically significant due to the relatively short 7-year dataset.

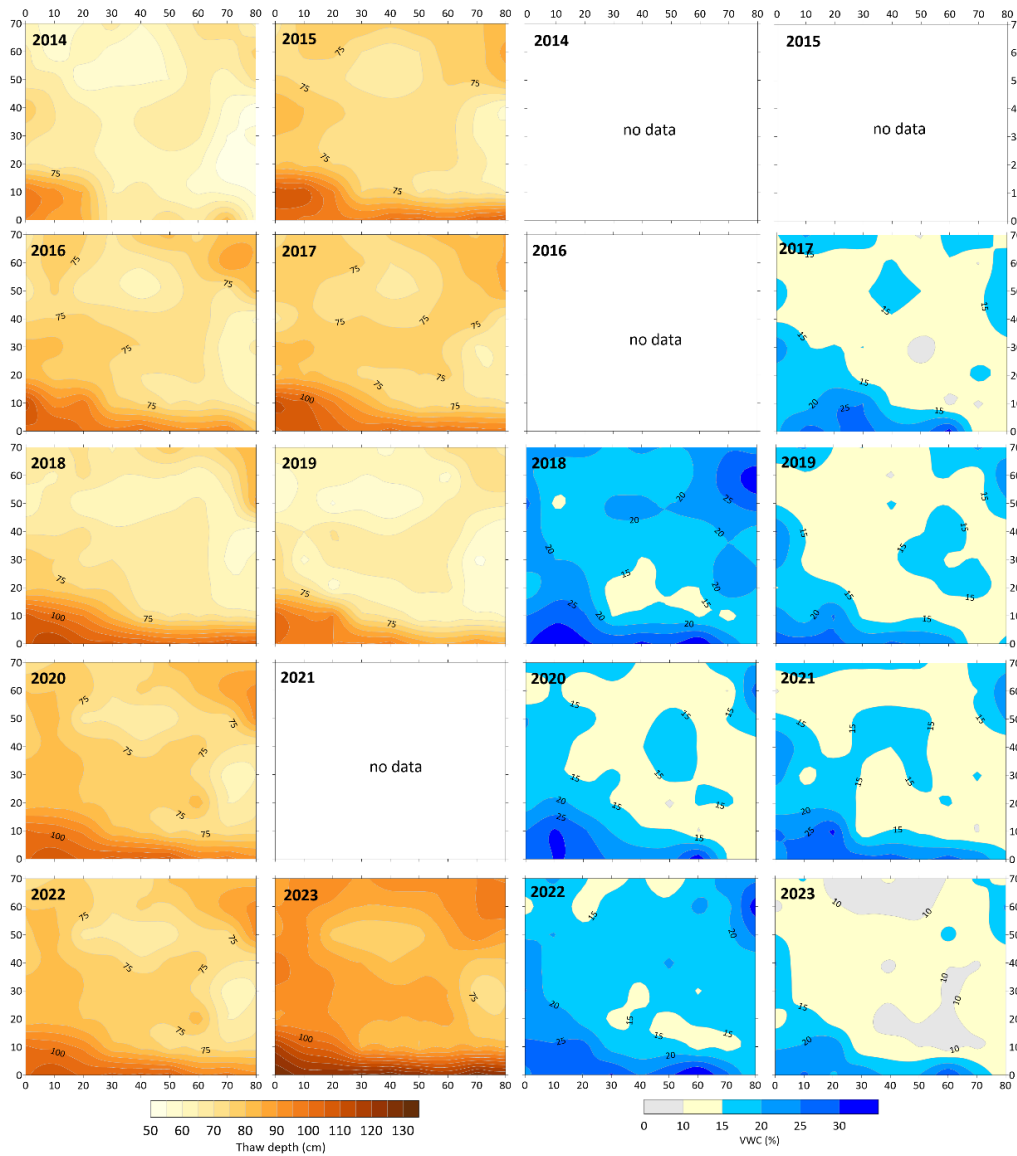


Figure 10. Variability of active layer thaw depth and surficial soil moisture on CALM-S JGM in the period 2014 to 2023 (*Paper 12*).

Compared to other CALM-S sites, where ALT distribution was primarily influenced by factors like snow presence (e.g. de Pablo et al., 2017; Guglielmin et al., 2014), vegetation (Guglielmin et al., 2014), or was relatively homogeneous (Ramos et al., 2017), the ALT variability at CALM-S JGM was attributed to the lithological pattern. A key advantage of CALM-S JGM is the ability to perform probing measurements around the date of maximum ALT occurrence, which is an issue at some sites, such as in the South Shetlands, where the ALT maximum occurs in late March, while the field season is in February (de Pablo et al., 2014).

## 5.2 Objective 2: Modelling of active layer thickness and temperature

The limitations of direct observations of ALT and temperature in Antarctica emphasize the importance of modelling approaches. One of the most widely used models for ALT estimation is based on the numerical solutions proposed by Stefan (1891) and Kudryavtsev et al. (1977). The temperature at the top of the permafrost table, or the base of the active layer, is modelled using the TTOP model (Smith and Riseborough, 1996). The key advantages of these models are their simplicity, relatively low requirements for input data, and strong performance (e.g. Riseborough et al., 2008).

However, the application of these models, and similar ones, was limited in Antarctica before 2020. The TTOP model was used by Ferreira et al. (2017) to model temperatures and probability of permafrost presence on Livingston Island. Both Stefan and Kudryavtsev models were employed by Wilhelm et al. (2015) to model ALT on Amsler Island in the Western Antarctic Peninsula, though their results were contradictory due to a lack of validation and clarity, as discussed by Uxa (2016). The model of Gold and Lachenbruch (1973) provided relatively good predictions using data from Victoria Land (Guglielmin et al., 2012). Building on these models, our collection of studies (*Papers 7, 11, 13, 14*) contributes significantly to advancing the understanding of ALT and temperature modelling in Antarctica. In addition to being used for reconstructing decadal datasets, we also provided thorough validation, strengthening the credibility of these approaches.

### 5.2.1 Active layer thickness modelling

In our initial modelling study, we tested the Stefan and Kudryavtsev models on a dataset from the Abernethy Flats site (*Paper 7*). We used modified versions of the models proposed by Kurylyk and Hayashi (2016) and Riseborough (2003). Both models were driven by near-surface (5 cm) ground temperature datasets from 2006-2015. We used soil thermal properties parameters obtained from laboratory treatments of soil samples taken from the surficial part (0-10 cm) and approximately middle part (20-30 cm) of the active layer. We observed slightly better accuracy in the models when using the soil physical properties dataset from the middle part of the profile (30 cm) than surficial (10 cm). Overall, the model errors were 2.6 cm (5.0 %) and 3.4 cm (5.9 %) for the Stefan model and the Kudryavtsev model, respectively. We attribute the high accuracy to the relatively low heterogeneity of physical properties in the Antarctic soil, making the parameterization highly representative for the studied profile.

In *Paper 11*, we applied the modified Stefan model to a dataset from AWS-JGM. Unlike the first study, the model was driven by air temperature data from 2004-2020 and validated against ALT measurements available from 2011-2020. The soil thermal properties parameterization used data from 30 cm depth, derived from five years of measurements. Similar to the Abernethy Flats results (*Paper 7*), we found that the model provided high accuracy 2.7 cm (4.7 %).

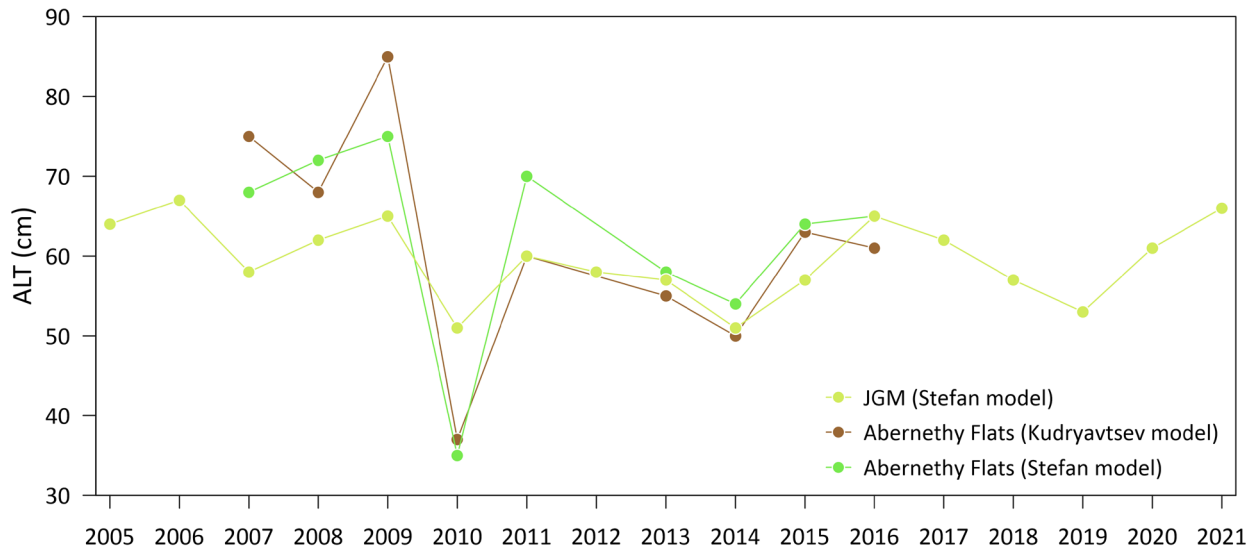


Figure 11. Active layer thickness variability on James Ross Island in the period 2004 to 2020 modelled by Stefan Model (SM) and Kudryavtsev Model (KM) on Abernethy Flats and JGM site. Results from *Papers 7 and 11*.

These two studies provided ALT data covering the periods 2006-2015 (*Paper 7*) and 2004-2020 (*Paper 11*). We concluded that the models are suitable tools for retrieving long-term ALT data, which can be accurately modelled using air temperature data alone. The models predicted ALT thinning by 16 cm/decade during 2006-2015 (Figure 9), which aligns with the overall climate conditions in the Antarctic Peninsula (Turner et al., 2016; Oliva et al., 2017). The modelling from AWS-JGM suggested ALT thinning in the period 2004-2020 by 1.6 cm/decade. Much lower trend value point to active layer thickening which was initiated in 2011 (Figure 10; *Paper 11*).

### 5.2.2 Modelling of temperature on the top of permafrost

The TTOP model is widely used for estimating the temperature at the top of the permafrost, marking the interface between the base of the active layer and the permafrost table. This model has been further developed into several versions, such as the Cryogrid model (e.g., Gissnas et al., 2014; Westerman et al., 2022), which enables spatial reconstruction of permafrost temperatures. For instance, the Cryogrid-1 model was applied to predict TTOP in the ice-free areas of Antarctica (*Paper 14*), using ERA-Interim reanalysis data. This model provided a 1 km<sup>2</sup> resolution TTOP reconstruction for the ice-free regions of Antarctica, though it only reflected spatial variability without accounting for trends, as it utilized data from 2000-2017. From the perspective of James Ross Island, results of *Paper 14* suggest whole area in the continuous permafrost zone.

In the application of TTOP in specific case studies, the model was first tested on ground temperature data from 2017-2019 collected from Byers Peninsula, Livingston Island (*Paper 13*). The results suggested that Byers Peninsula is situated in a marginal zone between continuous and discontinuous permafrost, which aligned with previous geophysical surveys

(Correia, et al., 2017). The model revealed that areas with long-term winter snow cover had a higher probability of permafrost absence, where the modelled temperature was greater than 0 °C. Different soil moisture scenarios were used to adjust the  $r_k$  factor, which determines the ratio between the thermal conductivity of thawed and frozen ground (Smith and Riseborough, 1996), but the differences in predictions between dry and wet scenarios were minimal, suggesting the model performed well overall.

The TTOP model was also applied to data from AWS-JGM (*Paper 11*). It used the same air temperature dataset as the Stefan model. The model provided excellent results for air temperature-based permafrost temperature reconstructions. The mean absolute error was 0.36 °C, and the RMSE was 0.52 °C. The model predicted a permafrost table cooling of 0.1 °C/decade from 2004 to 2020. Notably, the study period was divided into two phases: cooling from 2004-2010/11 ( $-0.13^{\circ}\text{C}/\text{year}$ ) and warming from 2011/12-2020 ( $0.19^{\circ}\text{C}/\text{year}$ ). The overall 2004-2020 trend was found as  $-0.12^{\circ}\text{C}/\text{decade}$ .

### 5.3 Objective 3: Spatiotemporal variability of active layer thermal regime and thickness in Antarctica

Even though the first measurements of soil temperature in Antarctica were initiated in the 1960s, the first overview providing basic knowledge on ALT or thermal regime variability for the whole continent was provided by Vieira et al. (2010), who summarized the research activities during the International Polar Year. This work primarily focused on identifying the number of monitoring sites and providing a general description of the active layer thermal regime and thickness characteristics in Antarctica. We contributed to the improvement of the overall knowledge of the Antarctic active layer through two subsequent studies:

*Paper 15* summarizes the measurements from the Antarctic CALM-S site between 2006 and 2015. We included 16 sites, providing data on thermally defined ALT (8 sites) and manually probed thaw depth (8 sites). The studied sites were spread across three major regions (Antarctic Peninsula, Victoria Land, and East Antarctica coast), covering MAAT between approximately  $-2\text{ }^{\circ}\text{C}$  and  $24\text{ }^{\circ}\text{C}$ . We observed ALTs ranging from 7 cm in the coldest areas of Victoria Land to more than 130 cm in the Antarctic Peninsula region. Year-to-year variability of ALT was pronounced in the Antarctic Peninsula and coastal East Antarctica, but relatively stable in the East Antarctica mountains and Victoria Land. In the Antarctic Peninsula, the data reflected the impact of regional cooling (Turner et al., 2016; Oliva et al., 2017), which led to thaw depth reductions with minimums in 2013 and 2014. Despite analyzing 10 years of data, no statistically significant trends were detected.

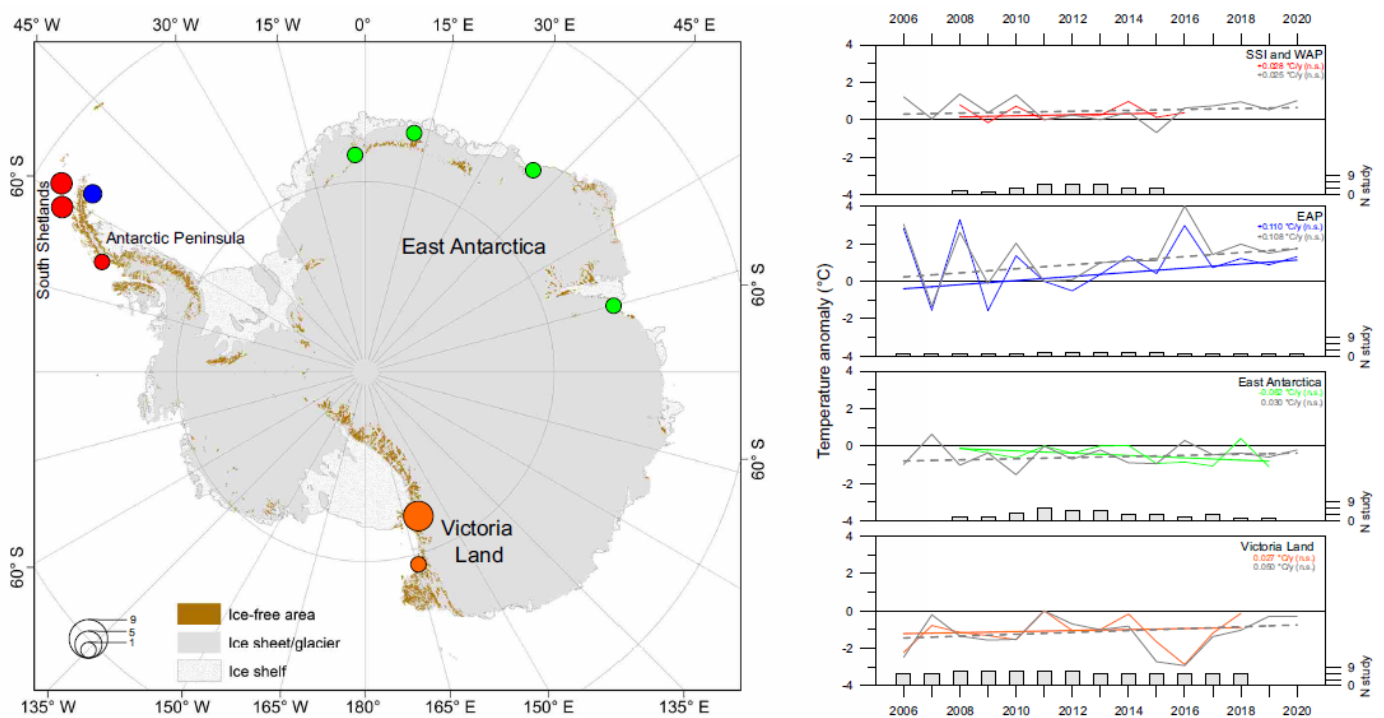


Figure 12. Variability of mean annual air temperature and near-surface ground temperature anomalies in Antarctica in the period 2006 to 2020 (*Paper 16*).

**Paper 16** provides a comprehensive overview of the scientific literature published from Antarctic sites after the International Polar Year. We synthesized data from more than 80 papers, including our own works involved in this thesis, and conducted a thorough spatiotemporal analysis of active layer thermal regime and ALT variability from 2006 to 2020. In total, we identified approximately 80 sites with soil temperature measurements in profiles deeper than 50 cm across five regions of Antarctica (Antarctic Peninsula, East Antarctica, Victoria Land, Transantarctic Mountains, and West Antarctica) and sub-Antarctic Islands.

Despite the extension of datasets to the period 2006-2020, we did not detect any statistically significant cooling or warming trends for air and near-surface ground temperature. However, data from the Antarctic Peninsula region exhibited a strong warming tendency, especially in the northeastern part where James Ross Island is located (Figure 11). These findings suggest that the regional cooling at the beginning of the 21st century was only a short-term event. The lowest trend values in East Antarctica and Victoria Land are consistent with the overall stable climate conditions in these regions, which, from a long-term perspective, have even exhibited cooling trends (Turner et al., 2020).

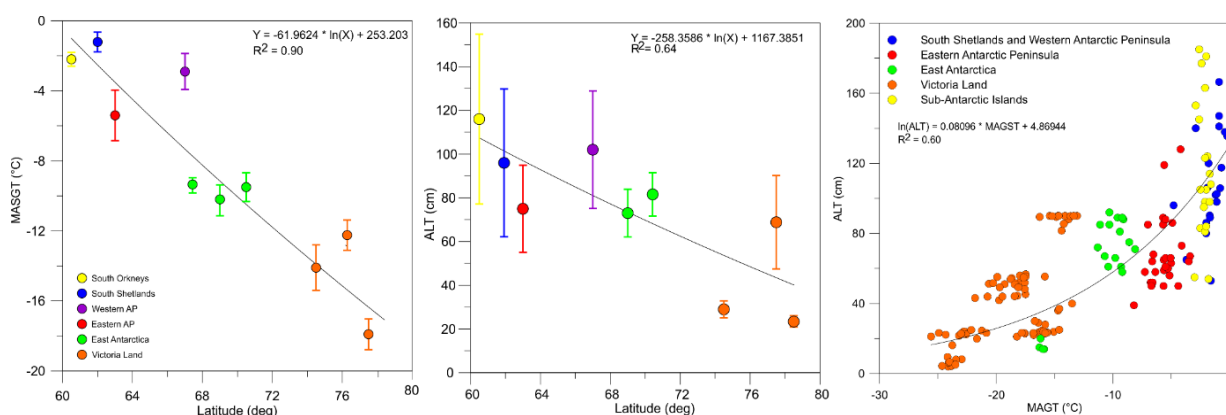


Figure 13. Mutual relationships between mean annual near-surface ground temperature (MASGT), active layer thickness (ALT) and latitude in Antarctica (**Paper 16**).

The compilation of the published data allowed us to determine the relationship between near-surface MAGT, ALT, and the latitudinal gradient (Figure 12). We found that the temperatures varied within a relatively narrow range at each study region and followed a latitudinal trend of  $-0.9\text{ }^{\circ}\text{C}/\text{deg}$ . In contrast, the variability of ALT was in the tens of centimetres and was highest in the warmest region of the sub-Antarctic Islands and South Shetlands. Notably, this analysis excluded bedrock sites where ALT was reported to exceed 5 m at sites in the South Shetlands. The ALT latitudinal trend was set at  $-3.4\text{ cm}/\text{deg}$ .

## 6 Summary

Our research systematically built upon initial case studies (*Papers 1–6*), which allowed us to better understand the general characteristics, properties, thermal regime, and thickness of the active layer on James Ross Island. Thanks to the dense and reliable monitoring network on James Ross Island, we were able to analyze active layer changes using datasets exceeding 10 years (*Papers 7, 10, 11, 12*). Long-term datasets are crucial for validating our original hypothesis, which was primarily based on short-term datasets (typically 2–3 years) published in earlier case studies.

The initial results from James Ross Island were influenced by a period of cooling in air temperatures that occurred on the Antarctic Peninsula between 2000 and 2015 (e.g., Turner et al., 2016; Oliva et al., 2017). However, this cooling peaked around 2011 on James Ross Island, and since then, we have observed a significant increase in both air and ground temperatures, culminating in 2022, which was the warmest year recorded. In summer of 2022/23, the greatest thickness of the active layer was also observed. The findings on year-to-year variability align with the general climate pattern observed in the northeastern Antarctic Peninsula (e.g., Turner et al., 2020; Bozkurt et al., 2020).

Our studies on modelling ALT and TTOP have significantly contributed to the state of the art in this field in Antarctica. Both the Stefan and Kudryavtsev models demonstrated high reliability and potential for predicting ALT using near-surface ground or air temperature data (*Papers 7 and 11*). The models benefit from the parameterization of soil physical properties based on data obtained from in-situ collected samples. Furthermore, the application of the Cryogrid-1 and TTOP models provided unique insights into the continental distribution of permafrost top temperatures (*Paper 14*) and demonstrated their applicability for temporal reconstructions and defining the limits of permafrost presence (*Paper 13*).

Beyond these contributions, our work on James Ross Island raised several important topics, such as the role of lithology, soil moisture, and the variability of soil thermal parameters—factors that have been investigated to a very limited extent in Antarctica. These factors are particularly important in dry, bare-ground conditions, which constitute a significant portion of ice-free areas and likely play a key role in active layer formation. Comparisons of our findings with studies from other sites in Antarctica allowed us to provide a comprehensive assessment of these factors at the continental level (*Paper 16*). Furthermore, this study offered an overview of the current knowledge on the spatial and temporal variability of the near-surface active layer’s thermal regime and thickness.

## 7 Research perspectives and conclusions

The intensive international collaboration allowed us to incorporate the results from James Ross Island into a large dataset with data from other Antarctic regions and create a more complete picture of active layer properties in Antarctica. A major output of these activities is *Paper 16*, which provides a detailed analysis of the results from the entire continent. Beyond this, we have identified key perspectives for upcoming research on the Antarctic active layer, summarised as follows:

### **a) Increasing density of measurements, including deep boreholes**

From the perspective of our major study area on James Ross Island, installing deeper boreholes is highly valuable. Data on permafrost temperature at depths with zero annual amplitude offer valuable insights into the long-term variability and stability of permafrost. Furthermore, this data is considered one of the essential climate variables for the cryosphere. However, logistical challenges present major limits to this effort.

### **b) Implementation of standardised soil moisture monitoring**

Our results have already highlighted the critical role of soil moisture in influencing soil thermal properties on James Ross Island. In 2022, through the Czech Science Foundation Juniorstar project, I initiated a soil moisture monitoring network across the Antarctic Peninsula region. Currently, the network includes 20 sites. We aim to analyse freeze-thaw characteristics and examine the differences or specificities of individual sites. A key question that soil moisture data can help answer is: What is the role of unfrozen water content during winter in permafrost stability? Our initial data, published in *Paper 9*, reveal that unfrozen water content can exceed 20%, potentially accelerating summer thawing and permafrost degradation. Changes in soil water content could also significantly affect local vegetation conditions (e.g., Robinson et al., 2017; Colesie et al., 2023).

### **c) Modelling of the current and future state of the Antarctic active layer and permafrost**

Given the spatiotemporal limitations of direct active layer and permafrost observations, modelling plays a crucial role in understanding past, present, and future conditions. So far, the only continental-scale map of TTOP (Top of Permafrost) is *Paper 14* which used the ERA5-Interim reanalysis dataset for the period 2000-2015. Considering ongoing climate change, it is essential to understand the potential future changes in the active layer and permafrost, including predictions for newly exposed surfaces, which are expected to double in the Antarctic Peninsula region by 2100 (e.g., Lee et al., 2017).

### **d) Geophysical surveying applied to identify the limits of permafrost presence**

Until recently, evidence of permafrost absence in Antarctica has primarily been based on geophysical surveys. In recent years, an initial network of Automatic Electrical Resistivity Tomography (A-ERT) was installed as part of an international effort (Farzamian et al., 2023). This system can provide more spatially extensive data on the freeze-thaw characteristics of the

ground. In the long term, it can be a valuable tool for detecting permafrost degradation. Notably, one of the sites is located at CALM-S JGM on James Ross Island.

In addition to these research tasks for the upcoming years, another urgent focus is the multidisciplinary study of the Antarctic terrestrial environment, merging earth sciences and biological disciplines. As proposed by Convey and Peck, 2019 and more recently by Colesie et al., 2023, the physio-chemical properties of soils are key to understanding the interactions between vegetation and abiotic components of the environment. For example, Robinson et al., (2018) reported that environmental drying over a relatively short period (13 years) had a significant impact on vegetation health and activity. Our recent unpublished observations of declining moss vitality associated with the dry summer of 2016/17 on James Ross Island (eastern Antarctic Peninsula) suggest that such a scenario could likely occur in other, potentially drier areas of the Antarctic Peninsula. As the active layer deepens, it may exacerbate surficial drying, making this a potential concern for other parts of Antarctica. The implementation of our datasets and findings on active layer properties can significantly contribute to a broader understanding of Antarctic ice-free environments and the possible scenarios for their future evolution under ongoing global climate change.

In conclusion, the compilation of studies presented in this work has significantly advanced our understanding of the thermal regime and thickness of the active layer in Antarctica. Although our research is based on nearly two decades of monitoring, the high climate variability in the northeastern Antarctic Peninsula region has allowed us to analyse the active layer's response to both warm and cold conditions. Alongside providing a basic description of the current state of the active layer at individual study sites, we have gained valuable insights into its spatial variability and sensitivity to various environmental factors. The findings presented here offer a solid foundation for further research into the complex environmental conditions of Antarctica's ice-free areas.

## 8 References

- Adlam, L.S., Balks, M.R., Seybold, C.A., & Campbell, D.I. (2010). Temporal and spatial variation in active layer depth in the McMurdo Sound Region, Antarctica. *Antarctic Science*, 22(1), 45–52. doi:10.1017/S0954102009990460
- Almeida, I.C.C., Schaefer, C.E.G.R., Michel, R.F.M., Fernandes, R.B.A., Pereira, T.T.C., DE Andrade, A.M., Francelino, M.R., Elpidio, J., Filho, F. & Bockheim, J.G. (2017). Long term active layer monitoring at a warm-based glacier front from maritime Antarctica. *Catena*, 149(2), 572-581.
- Anisimov, O.A., Shiklomanov, N., & Nelson, F.E. (1997). Global warming and active-layer thickness: Results from transient general circulation models. *Global and Planetary Change*, 15, 61–77.
- Ball, B.A., & Levy, J. (2015). The role of water tracks in altering biotic and abiotic soil properties and processes in a polar desert in Antarctica. *Journal of Geophysical Research: Biogeosciences*, 120, 270–279. <https://doi.org/10.1002/2014JG002856>
- Barták, M., Váczi, P., Stachoň, Z., & Kubešová, S. (2015). Vegetation mapping of moss-dominated areas of the northern part of James Ross Island (Antarctica) and a suggestion of protective measures. *Czech Polar Reports*, 5(1), 47–56. <https://doi.org/10.5817/CPR2015-1-8>
- Biskaborn, B.K., Smith, S.L., Noetzli, J., Matthes, H., Vieira, G., Streletskiy, D.A., Schoeneich, P., Romanovsky, V.E., Lewkowicz, A.G., Abramov, A., Allard, M., Boike, J., Cable, W.L., Christiansen, H.H., Delaloye, R., Diekmann, B., Drozdov, D., Etzelmüller, B., Grosse, G., Guglielmin, M., Ingeman-Nielsen, T., Isaksen, K., Ishikawa, M., Johansson, M., Johannsson, H., Joo, A., Kaverin, D., Kholodov, A., Konstantinov, P., Kröger, T., Lambiel, C., Lanckman, J.P., Luo, D., Malkova, G., Meiklejohn, I., Moskalenko, N., Oliva, M., Phillips, M., Ramos, M., Sannel, A.B.K., Sergeev, D., Seybold, C., Skryabin, P., Vasiliev, A., Wu, Q., Yoshikawa, K., Zheleznyak, M., & Lantuit, H. (2019). Permafrost is warming at a global scale. *Nature Communication*. 10, 1–11. <https://doi.org/10.1038/s41467-018-08240-4>.
- Bockheim, J. G., Campbell, I. B., & McLeod, M. (2007). Permafrost distribution and active-layer depths in the McMurdo Dry Valleys, Antarctica. *Permafrost and Periglacial Processes*, 18(3), 217–227. <https://doi.org/10.1002/ppp.588>
- Bockheim, J., Vieira, G., Ramos, M., López-Martínez, J., Serrano, E., Guglielmin, M., Wilhelm, K., & Nieuwendam, A. (2013). Climate warming and permafrost dynamics in the Antarctic Peninsula region, *Global and Planetary Change*, 100, 215–223. doi:10.1016/j.gloplacha.2012.10.018.
- Bozkurt, D., Bromwich, D.H., Carrasco, J., Hines, K.M., Maureira, J.C., & Ronadanelli, R., (2020). Recent Near-surface Temperature Trends in the Antarctic Peninsula from Observed, Reanalysis and Regional Climate Model Data. *Advances in Atmospheric Science*, 37, 477–493 <https://doi.org/10.1007/s00376-020-9183-x>

- Brooks, S. T., Jabour, J., van den Hoff, J., & Bergstrom, D. M. (2019). Our footprint on Antarctica competes with nature for rare ice-free land. *Nature Sustainability*, 2(3), 185–190. <https://doi.org/10.1038/s41893-019-0237-y>
- Brown J., Hinkel K.M., & Nelson F.E. (2000). The Circumpolar Active Layer Monitoring (CALM) program: historical perspectives and initial results. *Polar Geography* 24(3): 165-258.
- Burton-Johnson, A., Dziadek, R., & Martin, C. (2020). Review article: Geothermal heat flow in Antarctica: Current and future directions. *The Cryosphere*, 14, 3843–3873. <https://doi.org/10.5194/tc-14-3843-2020>
- Cannone, N., & Guglielmin, M. (2009). Influence of vegetation on the ground thermal regime in continental Antarctica. *Geoderma*, 151(3–4), 215–223. <https://doi.org/10.1016/j.geoderma.2009.04.007>
- Cannone, N., Guglielmin, M., Malfasi, F., Hubberten, H.W., & Wagner, D. (2021). Rapid soil and vegetation changes at regional scale in continental Antarctica. *Geoderma*, 394, 115017. <https://doi.org/10.1016/j.geoderma.2021.115017>
- Cannone, N., Ellis Evans, J.C., Strachan, R., & Guglielmin, M. (2006). Interactions between climate, vegetation, and active layer in Maritime Antarctica. *Antarctic Science*, 18, 323–333.
- Carshalton, A.G., Balks, M.R., O’Neill, T.A., Bryan, K.R., & Seybold, C.A. (2022). Climatic influences on active layer depth between 2000 and 2018 in the McMurdo Dry Valleys, Ross Sea Region, Antarctica. *Geoderma Regional*, 29, e00497. <https://doi.org/10.1016/j.geodrs.2022.e00497>
- Colesie, C., Walshaw, C. V., Sancho, L. G., Davey, M. P., & Gray, A. (2023). Antarctica's vegetation in a changing climate. *WIREs Climate Change*, 14(1), e810. <https://doi.org/10.1002/wcc.810>
- Convey, P., & Peck, L. S., (2019). Antarctic environmental change and biological responses. *Science Advances*, 5(11), eaaz0888.
- Correia, A., Vieira, G., & Ramos, M. (2012). Thermal conductivity and thermal diffusivity of cores from a 26-meter deep borehole drilled in Livingston Island, Maritime Antarctic. *Geomorphology*, 155-156, 7–11. <https://doi.org/10.1016/j.geomorph.2011.12.012>
- Correia, A., Oliva, M., & Ruiz-Fernández, J. (2017). Evaluation of frozen ground conditions along a coastal topographic gradient at Byers Peninsula (Livingston Island, Antarctica) by geophysical and geoecological methods. *Catena*, 149, 529–537. <https://doi.org/10.1016/j.catena.2016.08.006>
- de Pablo, M. A., Ramos, M., & Molina, A. (2014). Thermal characterisation of the active layer at the Limnopolar Lake CALM-S site on Byers Peninsula (Livingston Island), Antarctica. *Solid Earth*, 5(2), 721–739. <https://doi.org/10.5194/se-5-721-2014>

- de Pablo, M. A., Ramos, M., & Molina, A. (2017). Snow cover evolution, on 2009-2014, at the Limnopolar Lake CALM-S site on Byers Peninsula, Livingston Island, Antarctica. *CATENA*, 149, 538–547. <https://doi.org/10.1016/j.catena.2016.06.002>
- Dunn, R. J. H., Blannin, J., Gobron, N., et al., (2024). Global climate. *Bulletin of the American Meteorological Society*, 105(8), S12–S155.
- Dunn, R. J. H., Miller, J. B., Willett, K. M., et al., (2023). Global climate. *Bulletin of the American Meteorological Society*, 104(9), S11–S145.
- Dunn, R. J. H., Aldred, F., Gobron, N., et al., (2022). Global climate. *Bulletin of the American Meteorological Society*, 103(8), S11–S142.
- Ferreira, A., Vieira, G., Ramos, M., & Nieuwendam, A. (2017). *CATENA*, 149, 560–571. <https://doi.org/10.1016/j.catena.2016.08.027>
- Gisnås, K., Etzelmüller, B., Farbrøt, H., Schuler, T.V., & Westermann, S. (2013). CryoGRID 1.0: Permafrost distribution in Norway estimated by a spatial numerical model. *Permafrost and Periglacial Processes*, 24(1), 2–19. <https://doi.org/10.1002/ppp.1765>
- Gold, L.W., & Lachenbruch, A.H. (1973). Thermal conditions in permafrost: A review of North American literature. In *Proceedings of the 2nd International Permafrost Conference* (pp. 3–25). National Academy of Sciences. North American contribution.
- Guglielmin, M., & Cannone, N. (2012). A permafrost warming in a cooling Antarctica? *Climate Change*, 111(2), 177–195. <https://doi.org/10.1007/s10584-011-0137-2>
- Guglielmin, M., Balks, M.R., Adlam, L.S., Baio, F. (2011). Permafrost Thermal Regime from Two 30-m Deep Boreholes in Southern Victoria Land, Antarctica. *Permafrost and Periglacial Processes*, 22, 129–139. <https://doi.org/10.1002/ppp.715>
- Guglielmin, M., Dalle Fratte, M., & Cannone, N. (2014a). Permafrost warming and vegetation changes in continental Antarctica. *Environmental Research Letters*, 9(4), 045001.
- Guglielmin, M., Worland, M. R., Baio, F., & Convey, P. (2014b). Permafrost and snow monitoring at Rothera Point (Adelaide Island, Maritime Antarctica): Implications for rock weathering in cryotic conditions. *Geomorphology*, 225, 47-56."
- Guglielmin, M., (2006). Ground surface temperature (GST), active layer, and permafrost monitoring in continental Antarctica. *Permafrost and Periglacial Processes*, 17, 133–143. DOI: 10.1002/ppp.553
- Guglielmin, M. (2012). Advances in permafrost and periglacial research in Antarctica: A review. *Geomorphology*, 155–156, 1–6. <https://doi.org/10.1016/j.geomorph.2011.12.008>
- Hrbáček, F., Nývlt, D., Láska, K., Kňázková, M., Kampová, B., Engel, Z., Oliva, M., & Mueller, C. W. (2019). Permafrost and active layer research on James Ross Island: An overview. *Czech Polar Reports*, 9(1), 20–36. <https://doi.org/10.5817/CPR2019-1-3>

- Hrbáček, F., Vieira, G., Oliva, M., Balks, M., Guglielmin, M., de Pablo, M.A., Molina, A., Ramos, M., Goyanes, G., Meiklejohn, I., Abramov, A., Demidov, N., Fedorov- Davydov, D., Lupachev, A., Rivkina, E., Láska, K., Kňazková, M., Nývlt, D., Raffi, R., Strelin, J., Sone, T., Fukui, K., Dolgikh, A., Zazovskaya, E., Mergelov, N., Osokin, N., & Miamin, V., (2021). *Polar Geography*, 44(3), 217–231, <https://doi.org/10.1080/1088937X.2017.1420105>
- Hrbáček, F., Oliva, M., Hansen, C., Balks, M., O'Neill, T.A., de Pablo, M.A., Ponti, S., Ramos, M., Vieira, G., Abramov, A., Kaplan Pastíriková, L., Guglielmin, M., Goyanes, G., Francellino, M.R., Schaefer, C., & Lacelle, D. (2023a). Active layer and permafrost thermal regimes in the ice-free areas of Antarctica. *Earth Science Reviews*, 242, 104458. <https://doi.org/10.1016/j.earscirev.2023.104458>
- Hrbáček, F., Kňazková, M., Farzamian, M., & Baptista, J. (2023b). Variability of soil moisture on three sites in the Northern Antarctic Peninsula in 2022/23. *Czech Polar Reports*, 13(1), 10–23.
- Jennings, S.J.A., Davies, B.J., Nývlt, D., Glasser, N.F., Engel, Z., Hrbáček, F., Carrivick, J.L., Mlčoch, B., & Hambrey, M.J. (2021). Geomorphology of Ulu Peninsula, James Ross Island, Antarctica. *Journal of Maps*, 17(2), 125–139. <https://doi.org/10.1080/17445647.2021.1893232>
- Kaplan Pastíriková, L., Hrbáček, F., Uxa, T., & Láska, K. (2023). Permafrost table temperature and active layer thickness variability on James Ross Island, Antarctic Peninsula, in 2004–2021. *Science of the Total Environment*, 869, 161690. <https://doi.org/10.1016/j.scitotenv.2023.161690>
- Karunaratne, K.C., & Burn, C.R. (2003). Freezing n-factors in discontinuous permafrost terrain, Takhini River, Yukon Territory, Canada. In *Proceedings of the Eighth International Conference on Permafrost* (pp. 645–650). Zurich, Switzerland.
- Kavan, J., Nývlt, D., Láska, K., Engel, Z., & Kňazková, M. (2020) High-latitude dust deposition in snow on the glaciers of James Ross Island, Antarctica. *Earth Surf. Process. Landforms*, 45: 1569– 1578. <https://doi.org/10.1002/esp.4831>.
- Kennedy, A.D. (1993). Water as a limiting factor in the Antarctic terrestrial environment: A biogeographical synthesis. *Arctic and Alpine Research*, 25(4), 308–315.
- Kňazková, M., & Hrbáček, F. (2024). Interannual variability of soil thermal conductivity and moisture on the Abernethy Flats (James Ross Island) during thawing seasons 2015–2023. *Catena*, 234, 107640. <https://doi.org/10.1016/j.catena.2023.107640>
- Kotzé, C., & Meiklejohn, I. (2017). Temporal variability of ground thermal regimes on the northern buttress of the Vesleskarvet nunatak, western Dronning Maud Land, Antarctica. *Antarctic Science*, 29(1), 73–81. <https://doi.org/10.1017/S095410201600047X>
- Kudryavtsev, V.A., Garagulya, L.S., Kondrat'yeva, K.A., & Melamed, V.G. (1977). *Fundamentals of frost forecasting in geological engineering investigations (Draft Translation 606)*. U.S. Army Cold Regions Research and Engineering Laboratory.

- Kurylyk, B.L., & Hayashi, M. (2016). Improved Stefan equation correction factors to accommodate sensible heat storage during soil freezing or thawing. *Permafrost and Periglacial Processes*, 27(2), 189–203.
- Lee, J.R., Raymond, B., Bracegirdle, T.J., Chadés, I., Fuller, R.A., Shawn, J.D., & Terauds, A. (2017). Climate change drives expansion of Antarctic ice-free habitat. *Nature*, 547, 49–54. doi:10.1038/nature22996
- Lembrechts, J., van den Hoogen, Lenoir, J., et al., (2022). Global maps of soil temperature. *Global Change Biology*, 28 (9), 3110–3144. DOI10.1111/gcb.16060
- Levy, J.S., Fountain, A.G., Gooseff, M.N., Welch, K.A., & Lyons, W.B. (2011). Water tracks and permafrost in Taylor Valley, Antarctica: Extensive and shallow groundwater connectivity in a cold desert ecosystem. *GSA Bulletin*, 123(11-12), 2295–2311. <https://doi.org/10.1130/B30436.1>
- Linhardt, T., Levy, J. S., & Thomas, C. K. (2019). Water tracks intensify surface energy and mass exchange in the Antarctic McMurdo Dry Valleys, *The Cryosphere*, 13, 2203–2219, <https://doi.org/10.5194/tc-13-2203-2019>.
- Liu, L., Sletten, R. S., Hallet, B., & Waddington, E. D. (2018). Thermal Regime and Properties of Soils and Ice-Rich Permafrost in Beacon Valley, Antarctica. *Journal of Geophysical Research: Earth Surface*, 123(8), 1797–1810. <https://doi.org/10.1029/2017JF004535>
- López-Martínez, J., Serrano, E., Schmid, T., Mink, S., & Linés, C. (2012). Periglacial processes and landforms in the South Shetland Islands (northern Antarctic Peninsula region). *Geomorphology*, 155–156, 62–79. <https://doi.org/10.1016/j.geomorph.2011.12.018>
- Lunardini, V.J. (1978). Theory of N-factors and correlation of data. In *Proceedings of the Third International Conference on Permafrost* (Vol. 1, pp. 40–46). National Council of Canada.
- Marchant, D.R., Lewis, A., Philips, W.C., Moore, E.J., Souchez, R., & Landis, G.P. (2002). Formation of patterned-ground and sublimation till over Miocene glacier ice in Beacon Valley, Antarctica. *Geological Society of America Bulletin*, 114, 718–730.
- Michel, R.F.M., Schaefer, C.E.G.R., Poelking, E.L., Simas, F.N.B., Filho, E.I.F., & Bockheim, J.G. (2012). Active layer temperature in two Cryosols from King George Island, Maritime Antarctica. *Geomorphology* 155-156, 12–19. doi:10.1016/j.geomorph.2011.12.013
- Mlčoch, B., Nývlt, D., Mixa, P., et al. (2020). Geological map of James Ross Island – Northern part 1:25,000. Czech Geological Survey.
- Muller, S. W. (1943). Permafrost or permanently frozen ground and related engineering problems. Special Report, Strategic Engineering Study, Intelligence Branch, Office, Chief of Engineers, no. 62, 136 pp. Second printing, 1945, 230 pp. (Reprinted in 1947, J. W. Edwards, Ann Arbor, Michigan, 231 pp.)
- Noetzli, J., & Gruber, S. (2005). Alpiner Permafrost – ein Überblick. *Jahrbuch des Vereins zum Schutz der Bergwelt*, 70, 111–122.

- Oliva, M., Navarro, F., Hrbáček, F., Hernández, A., Nývlt, D., Perreira, P., Ruiz-Fernández, J., & Trigo, R., (2017a). Recent regional climate cooling on the Antarctic Peninsula and associated impacts on the cryosphere. *Science of the Total Environment*, 580, 210–223. <http://dx.doi.org/10.1016/j.scitotenv.2016.12.030>
- Oliva, M., Hrbacek, F., Ruiz-Fernández, J., de Pablo, M. Á., Vieira, G., Ramos, M., & Antoniades, D. (2017b). Active layer dynamics in three topographically distinct lake catchments in Byers Peninsula (Livingston Island, Antarctica). *CATENA*, 149, 548–559. <https://doi.org/10.1016/j.catena.2016.07.011>
- Ramos, M., Vieira, G., de Pablo, M.A., Molina, A., Abramov, A., & Goyanes, G. (2017). Recent shallowing of the thaw depth at Crater Lake, Deception Island, Antarctica (2006–2014). *Catena* 149 (2), 519–528. <https://doi.org/10.1016/j.catena.2016.07.019>.
- Ramos, M., Vieira, G., de Pablo, M.A., Molina, A., & Jimenez, J.J. (2020). Transition from a Subaerial to a Subnival Permafrost Temperature Regime Following Increased Snow Cover (Livingston Island, Maritime Antarctic). *Atmosphere* 11, 1332. <https://doi.org/10.3390/atmos11121332>.
- Riseborough, D.W. (2003). Thawing and freezing indices in the active layer. In *Proceedings of the 8th International Conference on Permafrost* (pp. 953–958). AA Balkema Rotterdam.
- Riseborough, D., Shiklomanov, N., Etzelmüller, B., Gruber, S., & Marchenko, S. (2008). Recent advances in permafrost modelling. *Permafrost and Periglacial Processes*, 19(2), 137–156. <https://doi.org/10.1002/ppp.615>
- Roman, M., Nývlt, D., Davies, B.J., Braucher, R., Jennings, S.J.A., Břežný, M., Glasser, N.F., Hambrey, M.J., Lirio, J.M., Rodés, Á., & ASTER Team. (2024). Accelerated retreat of northern James Ross Island ice streams (Antarctic Peninsula) in the Early-Middle Holocene induced by buoyancy response to postglacial sea level rise. *Earth and Planetary Science Letters*, 641, 118803. <https://doi.org/10.1016/j.epsl.2024.118803>
- Robinson, S.A., King, D.H., Bramley-Alves, J., Waterman, M.J., Ashcroft, M.B., Wasley, J., Turnbull, J.D., Miller, R.E., Ryan-Colton, E., Benny, T., Mullany, K., Clarke, L.J., Barry, L.A., & Hua, Q. (2018). Rapid change in East Antarctic terrestrial vegetation in response to regional drying. *Nature Climate Change*, 8(10), 879–884. <https://doi.org/10.1038/s41558-018-0280-0>
- Romanovsky, V.E., Smith, S.L., & Christiansen, H.H. (2010). Permafrost thermal state in the polar Northern Hemisphere during the international polar year 2007–2009: A synthesis. *Permafrost and Periglacial Processes*, 21(2), 106–116.
- Roland, T.P., Bartlett, O.T., Charman, D.J., Anderson, K., Hodgson, D.A., Amesbury, M.J., Maclean, I., Fretwell, P.T., & Fleming, A. (2024). Sustained greening of the Antarctic Peninsula observed from satellites. *Nature Geoscience*, 17, 1121–1126. <https://doi.org/10.1038/s41561-024-01564-5>

- Ruiz-Fernández, J., Oliva, M., Nývlt, D., Cannone, N., García-Hernández, C., Guglielmin, M., Hrbáček, F., Roman, M., Fernández, S., López-Martínez, J., & Antoniades, D. (2019). Patterns of spatio-temporal paraglacial response in the Antarctic Peninsula region and associated ecological implications. *Earth Science Reviews*, 192, 379–402. <https://doi.org/10.1016/j.earscirev.2019.03.014>.
- Seybold, C. A., Balks, M. R., & Harms, D. S. (2010). Characterisation of active layer water contents in the McMurdo Sound region, Antarctica. *Antarctic Science*, 22(6), 633–645. <https://doi.org/10.1017/S0954102010000696>
- Siegert, M., Atkinson, A., Banwell, A., Brandon, M., Convey, P., Davies, B., Downie, R., Edwards, T., Hubbard, B., Marshall, G., Rogelj, J., Rumble, J., Stroeve, J. & Vaughan, D. (2019) The Antarctic Peninsula Under a 1.5°C Global Warming Scenario. *Frontier in Environmental Science*, 7 (102). doi: 10.3389/fenvs.2019.00102
- Smith, M.W., & Riseborough, D.W. (1996). Permafrost monitoring and detection of climate change. *Permafrost and Periglacial Processes*, 7(4), 301–309. [https://doi.org/10.1002/\(SICI\)1099-1530\(199610\)7:4<301::AID-PPP231>3.0.CO;2-R](https://doi.org/10.1002/(SICI)1099-1530(199610)7:4<301::AID-PPP231>3.0.CO;2-R)
- Stefan, J. (1891). Über die Theorie der Eisbildung, insbesondere über die Eisbildung im Polarmee. *Annalen der Physik*, 278(2), 269–286. <https://doi.org/10.1002/andp.18912780206>
- Tarca, G., Guglielmin, M., Convey, P., Worland, M. R., & Cannone, N. (2022). Small-scale spatial–temporal variability in snow cover and relationships with vegetation and climate in maritime Antarctica. *Catena*, 208, 105739. <https://doi.org/10.1016/j.catena.2021.105739>
- Thomazini, A., Francelino, M.R., Pereira, A.B., Schünemann, A.L., Mendonca, E.S., Michel, R.F.M., Schaefer, C.E.G.R. (2020). The current response of soil thermal regime and carbon exchange of a paraglacial coastal land system in maritime Antarctica. *Land Degradation and Development*, 31: 655–666. DOI: 10.1002/ldr.3479
- Turner, J., Lu, H., White, I., King, J.C., Phillips, T., Scott Hosking, J., Bracegirdle, T.J., Marshall, G.J., Mulvaney, R., & Deb, P., (2016). Absence of 21st century warming on Antarctic Peninsula consistent with natural variability. *Nature* 535. <http://dx.doi.org/10.1038/nature18645>.
- Turner, J., Marshall, G., Clem, K., Colwell, S., Phillips, T. & Lu, H., 2020. Antarctic temperature variability and change from station data. *International Journal of Climatology*, 40 (6), 2986 – 3007. <https://doi.org/10.1002/joc.6378>.
- Ugolini, F.C., & Bockheim, J.G. (2008). Antarctic soils and soil formation in a changing environment: A review. *Geoderma*, 144 (1-2), 1–8. <https://doi.org/10.1016/j.geoderma.2007.10.005>
- Uxa T., (2016). Discussion on, 'active layer thickness prediction on the Western Antarctic peninsula' by Wilhelm et al. 2015. *Permafrost and Periglacial Processes*, 28, 493–498.

van Everdingen, R.O., 1976. "Geocryological terminology." *Canadian Journal of Earth Sciences*, 13 (6), 862–867.

Vieira, G., Bockheim, J., Guglielmin, M., Balks, M., Abramov, A.A., Boelhouwers, J., Cannone, N., Ganzert, L., Gilichinsky, D., Goryachkin, S., López-Martínez, J., Raffi, R., Ramos, M., Schaefer, C., Serrano, E., Simas, F., Sletten, R., & Wagner, D., (2010). Thermal state of permafrost and active-layer monitoring in the Antarctic: advances during the international polar year 2007–2008. *Permafrost and Periglacial Processes*, 21, 182–197.

Westermann, S., Ingeman-Nielsen, T., Scheer, J., Aalstad, K., Aga, J., Chaudhary, N., Etzelmüller, B., Filhol, S., Kääh, A., Renette, C., Schmidt, L. S., Schuler, T. V., Zweigel, R. B., Martin, L., Morard, S., Ben-Asher, M., Angelopoulos, M., Boike, J., Groenke, B., Miesner, F., Nitzbon, J., Overduin, P., Stuenzi, S. M., & Langer, M. (2023). The CryoGrid community model (version 1.0) – a multi-physics toolbox for climate-driven simulations in the terrestrial cryosphere. *Geoscientific Model Development*, 16, 2607–2647. <https://doi.org/10.5194/gmd-16-2607-2023>

Wilhelm, K. R., Bockheim, J. G., & Kung, S. (2015). Active Layer Thickness Prediction on the Western Antarctic Peninsula. *Permafrost and Periglacial Processes*, 26(2), 188–199. <https://doi.org/10.1002/ppp.1845>

Wlostowski, A. N., Gooseff, M. N., McKnight, D. M., & Lyons, W. B. (2018). Transit Times and Rapid Chemical Equilibrium Explain Chemostasis in Glacial Meltwater Streams in the McMurdo Dry Valleys, Antarctica. *Geophysical Research Letters*, 45(24). <https://doi.org/10.1029/2018GL080369>

Zhang, T., Osterkamp, T.E., & K. Stamnes (1997), Effects of climate on the active layer and permafrost on the North Slope of Alaska, U.S.A., *Permafrost Periglacial Processes*, 8, 45–67.

Zhang, T. (2005). Influence of the seasonal snow cover on the ground thermal regime: An overview. *Reviews of Geophysics*, 43 (4), RG4002, doi:10.1029/2004RG000157

## 9 Supplements

The list of attached publications:

### **Paper 1:**

**Hrbáček, F.,** Láska, K., Engel, Z., (2016): Effect of snow cover on the active-layer thermal regime – a case study from James Ross Island, Antarctic Peninsula. *Permafrost and Periglacial Processes*, 27(3), 307–315. (IF 2.0, Q2).

### **Abstract:**

The response of active-layer thickness and the ground thermal regime to climatic conditions on the Ulu Peninsula (James Ross Island, northeastern Antarctic Peninsula) in 2011–13 is presented. The mean air temperature over this period was  $-8.0^{\circ}\text{C}$  and ground temperature at 5 cm depth varied from  $-6.4^{\circ}\text{C}$  (2011–12) to  $-6.7^{\circ}\text{C}$  (2012–13). The active-layer thickness ranged between 58 cm (January 2012) and 52 cm (February 2013). Correlation analyses indicate that air temperature affects ground temperature more significantly on snow-free days ( $R^2 = 0.82$ ) than on snow cover days ( $R^2 = 0.53$ ). Although the effect of snow cover on the daily amplitude of ground temperature was observable to 20 cm depth, the overall influence of snow depth on ground temperature was negligible (freezing n-factor of 0.95–0.97).

### **Paper 2:**

**Hrbáček, F.,** Oliva, M., Laska, K., Ruiz-Fernández, J., de Pablo, M. A., Vieira, G., Ramos, M., & Nývlt, D. (2016). Active layer thermal regime in two climatically contrasted sites of the Antarctic Peninsula region. *Cuadernos de Investigación Geográfica*, 42(2), 457–474. (ESCI, Q3)

### **Abstract:**

Permafrost controls geomorphic processes in ice-free areas of the Antarctic Peninsula (AP) region. Future climate trends will promote significant changes of the active layer regime and permafrost distribution, and therefore a better characterization of present-day state is needed. With this purpose, this research focuses on Ulu Peninsula (James Ross Island) and Byers Peninsula (Livingston Island), located in the area of continuous and discontinuous permafrost in the eastern and western sides of the AP, respectively. Air and ground temperatures in as low as 80 cm below surface of the ground were monitored between January and December 2014. There is a high correlation between air temperatures on both sites ( $r=0.74$ ). The mean annual temperature in Ulu Peninsula was  $-7.9^{\circ}\text{C}$ , while in Byers Peninsula was  $-2.6^{\circ}\text{C}$ . The lower air temperatures in Ulu Peninsula are also reflected in ground temperatures, which were between  $4.9$  (5 cm) and  $5.9^{\circ}\text{C}$  (75/80 cm) lower. The maximum active layer thickness observed during the study period was 52 cm in Ulu Peninsula and 85 cm in Byers Peninsula. Besides climate, soil characteristics, topography and snow cover are the main factors controlling the ground thermal regime in both areas.

**Paper 3:**

**Hrbáček, F.,** Nývlt, D., Láška, K., (2017): Active Layer Thermal Dynamics at Two lithologically Different Sites on James Ross Island, Eastern Antarctic Peninsula. *Catena*, 149(2), 592–602. (IF 3.19, Q1).

**Abstract:**

The active layer thermal regime was studied at two sites with different lithological properties located on James Ross Island, eastern Antarctic Peninsula, to assess the main driving factors. The Abernethy Flats site (41 m a.s.l.) is located in Cretaceous calcareous sandstones and siltstones of the Santa Marta Formation. In contrast, the Berry Hill slopes site (56 m) is composed of muddy to intermediate diamictites, tuffaceous siltstones to fine-grained sandstones of the Mendel Formation. The data of air temperature at 2 m and ground temperature at two 75-cm-deep profiles were analysed for the period 1 January 2012, to 31 December 2014. Small differences were found when comparing mean air temperatures and ground temperatures at 5, 50 and 75 cm depths, in the period 2012–2014. While the mean air temperatures varied between  $-7.7\text{ }^{\circ}\text{C}$  and  $-7.0\text{ }^{\circ}\text{C}$ , the average ground temperatures oscillated between  $-6.6\text{ }^{\circ}\text{C}$  and  $-6.1\text{ }^{\circ}\text{C}$  at 5 cm;  $-6.7\text{ }^{\circ}\text{C}$  and  $-6.0\text{ }^{\circ}\text{C}$  at 50 cm; and  $-6.9\text{ }^{\circ}\text{C}$  and  $-6.0\text{ }^{\circ}\text{C}$  at 75 cm at Abernethy Flats and Berry Hill slopes, respectively. The increasing difference of ground temperature with depth, and a significant difference in active layer thickness – 52 to 64 cm at Abernethy Flats and 85 to 90 cm at Berry Hill slopes, respectively – suggests the significant effect of lithology. The higher proportion of fine particles and more thermally conductive minerals, together with higher water saturation, has been found to be fundamental for higher active layer thickness documented at Berry Hill slopes.

**Paper 4:**

**Hrbáček, F.,** Kňázková, M., Nývlt, D., Láška, K., Mueller, C.W., Ondruch, J., (2017): Active layer monitoring at CALM-S site near J.G. Mendel Station, James Ross Island, eastern Antarctic Peninsula. *Science of the Total Environment*, 601, 987-997. (IF 4.90; D1).

**Abstract:**

The Circumpolar Active Layer Monitoring – South (CALM-S) site was established in February 2014 on James Ross Island as the first CALM-S site in the eastern Antarctic Peninsula region. The site, located near Johann Gregor Mendel Station, is labelled CALM-S JGM. The grid area is gently sloped ( $b3^{\circ}$ ) and has an elevation of between 8 and 11 m a.s.l. The lithology of the site consists of the muddy sediments of Holocene marine terrace and clayey sandy Cretaceous sedimentary rocks, which significantly affect the texture, moisture content, and physical parameters of the ground within the grid. Our objective was to study seasonal and interannual variability of the active layer depth and thermal regime at the CALM-S site, and at two ground temperature measurement profiles, AWS-JGM and AWS-CALM, located in the grid. The mean air temperature in the period March 2013 to February 2016 reached  $-7.2\text{ }^{\circ}\text{C}$ . The mean ground temperature decreased with depth from  $-5.3\text{ }^{\circ}\text{C}$  to  $-5.4\text{ }^{\circ}\text{C}$  at 5 cm, to  $-5.5\text{ }^{\circ}\text{C}$  to  $-5.9\text{ }^{\circ}\text{C}$  at 200 cm. Active layer thickness was significantly higher at AWS-CALM and ranged between 86 cm

(2014/15) and 87 cm(2015/16), while at AWS-JGM it reached only 51 cm(2013/14) to 65 cm (2015/16). The mean probed active layer depth increased from 66.4 cm in 2013/14 to 78.0 cm in 2014/15. Large differences were observed when comparing the minimum (51 cm to 59 cm) and maximum (100 cm to 113 cm) probed depths. The distribution of the active layer depth and differences in the thermal regime of the uppermost layer of permafrost at CALM-S JGM clearly show the effect of different lithological properties on the two lithologically distinct parts of the grid.

**Paper 5:**

Kňázková, M., **Hrbáček, F.**, Kavan, J., & Nývlt, D. (2020). Effect of hyaloclastite breccia boulders on meso-scale periglacial-aeolian landsystem in semi-arid Antarctic environment, James Ross Island, Antarctic Peninsula. *Cuadernos de Investigación Geográfica*, 46(1), 7–31. (ESCI, Q3).

**Abstract:**

In this study we aim to describe the processes leading to the creation of a specific periglacial and aeolian landsystem, which evolves around the hyaloclastite breccia boulders on James Ross Island, north-eastern Antarctic Peninsula. These boulders were deposited as a result of the Late Holocene advance of Whisky Glacier, forming a well-developed boulder train approximately 5-km long, stretching front Whisky Glacier moraine to Brandy Bay. The combination of ground temperature monitoring, snow cover measurements, grain size analysis and field survey were used to quantify and understand the interplay of periglacial and aeolian processes leading to the formation of the specific meso-scale landsystems around the boulders. The ground temperature probes were installed during January 2017 in the vicinity of two selected boulders. The two study sites, at Monolith Lake (large boulder) and Keller Stream (smaller boulder), were also fitted with snow stakes and trail cameras. An automatic weather station (AWS) on the Abernethy Flats, located approximately two kilometres to the north-west, was used as a reference site for ground temperature and snow cover thickness. The hyaloclastite breccia boulders act as obstacles to wind and trap wind-blown snow, resulting in the formation of snow accumulations on their windward and lee sides. These accumulations affect ground thermal regime and lead to the transport of fine particles by meltwater from the snow during the summer season. The snow cover also traps wind-blown fine sand resulting in the formation of finegrained rims on the windward and lee sides of the boulders after the snow has melted. Furthermore, the meltwater affects ground moisture content, creating favourable, but spatially limited conditions for colonisation by mosses and lichens.

**Paper 6:**

**Hrbáček, F.,** Cannone, N., Křažková, M., Malfasi, F., Convey, P., Guglielmin, M., (2020): Effect of climate and moss vegetation on ground surface temperature and the active layer among different biogeographical regions in Antarctica. *Catena*, 190, 104562. (IF 4.333; D1).

**Abstract:**

Ground surface temperature (GST) and active layer thickness (ALT) are key indicators of climate change (CC) in permafrost regions, with their relationships with climate and vegetation being crucial for the understanding of future climate change scenarios, as well as of CC feedbacks on the carbon cycle and water balance. Antarctic ice free-areas host simplified ecosystems with vegetation dominated by mosses and lichens, and an almost negligible anthropogenic impact, providing a good template of ecosystem responses to CC. At three different Antarctic Conservation Biogeographical Regions (ACBR) sites in Antarctica located between 74 degrees and 60 degrees S, we compared barren ground and moss vegetated sites to understand and quantify the effects of climate (air temperature and incoming radiation) and of vegetation on GST and ALT. Our data show that incoming radiation is the most important driver of summer GST at the southernmost site, while in the other sites air temperature is the main driver of GST. Our data indicate that there is a decoupling between ALT and summer GST, because the highest GST values correspond with the thinnest ALT. Moreover, our data confirm the importance of the buffering effect of moss vegetation on GST in Antarctica. The intensity of the effect of moss cover on GST and ALT mainly depends on the species-specific moss water retention capacity and on their structure. These results highlight that the correct assessment of the moss type and of its water retention can be of great importance in the accurate modelling of ALT variation and its feedback on CC.

**Paper 7:**

**Hrbáček, F.,** Uxa, T., 2020. The evolution of a near-surface ground thermal regime and modeled active-layer thickness on James Ross Island, Eastern Antarctic Peninsula, in 2006-2016. *Permafrost and Periglacial Processes*, 31(1), 141–155. (IF 2.701; Q1).

**Abstract:**

Thermal regime and thickness of the active layer respond rapidly to climate variations, and thus they are important measures of cryosphere changes in polar environments. We monitored air temperature and ground temperature at a depth of 5 cm and modeled active-layer thickness using the Stefan and Kudryavtsev models at the Abernethy Flats site, James Ross Island, Eastern Antarctic Peninsula, in the period March 2006 to February 2016. The decadal average of air and ground temperature was -7.3 and -6.1 degrees C, respectively, and the average modeled active-layer thickness reached 60 cm. Mean annual air temperature increased by 0.10 degrees C  $y^{-1}$  over the study period, while mean annual ground temperature showed the opposite tendency of -0.05 degrees C  $y^{-1}$ . The cooling took place mainly in summer and caused thawing season shortening and active-layer thinning of 1.6 cm  $y^{-1}$ . However, these trends need to be taken carefully because all were non-significant at  $p < 0.05$ . The Stefan and

Kudryavtsev models reproduced the active-layer thickness with mean absolute errors of 2.6 cm (5.0%) and 3.4 cm (5.9%), respectively, which is better than in most previous studies, making them promising tools for active-layer modelling over Antarctica.

**Paper 8:**

**Hrbáček, F.,** Engel, Z., Kňázková, M., Smolíková, J. (2021). Effect of summer snow cover on the active layer thermal regime and thickness on CALM-S JGM site, James Ross Island, eastern Antarctic Peninsula. *Catena*, 207, 105608. (IF 5.198; D1).

**Abstract:**

This study aims to assess the role of ephemeral snow cover on ground thermal regime and active layer thickness in two ground temperature measurement profiles on the Circumpolar Active Layer Monitoring Network - South (CALM-S) JGM site on James Ross Island, eastern Antarctic Peninsula during the high austral summer 2018. The snowstorm of 13-14 January created a snowpack of recorded depth of up to 38 cm. The snowpack remained on the study site for 12 days in total and covered 46% of its area six days after the snowfall. It directly affected ground thermal regime as indicates temperature record at snow-covered profile AWS-JGM which subsurface section was nearly 5 degrees C colder compared to the snow-free AWS-CALM profile. The thermal insulation effect of snow cover is also reflected in the mean monthly (January) and summer (DJF) ground temperatures on AWS-JGM that decreased by ca 1.1 and 0.7 degrees C, respectively. Summer thawing degree days at a depth of 5 cm decreased by ca 10% and active layer was ca 5-10 cm thinner when compared to previous snow-free summer seasons. Surveying by ground penetrating radar revealed a general active layer thinning of up to 20% in those parts of the CALM-S which were covered by snow of >20 cm depth for at least six days.

**Paper 9:**

**Hrbáček, F.,** Kňázková, M., Farzadian, M., Baptista, J. (2023). Variability of soil moisture on three sites in the Northern Antarctic Peninsula in 2022/23. *Czech Polar Reports*, 13 (1), 10 – 23. (IF 1.0; Q4).

**Abstract:**

Soil moisture represents one of the crucial parameters of the terrestrial environments in Antarctica. It affects the biological abundance and also the thermal state of the soils. In this study, we present one year of volumetric water content and soil temperature measured at all sites increased with depth. The mean summer values were between 0.24 and 0.37 cm<sup>3</sup>/cm<sup>3</sup> (James Ross Island), 0.30 and 0.40 cm<sup>3</sup>/cm<sup>3</sup> (Nelson Island) and 0.11 and 0.36 cm<sup>3</sup>/cm<sup>3</sup> (King George Island). We found that the freezing point of the soils was close to 0 °C on Nelson Island and King George Island. We attributed the lower temperature of soil freezing around -0.5°C on James Ross Island to the site location close to the sea. Even though the sites are located in the distinctive climate zones and comprise of contrasting soil types, the only differences of moisture regime were observed the surficial layer of the studied sites.

**Paper 10:**

Kňažková, M., **Hrbáček, F.** (2024). Interannual variability of soil thermal conductivity and moisture on the Abernethy Flats (James Ross Island) during thawing seasons 2015-2023. *Catena*, 234, 107640. (IF 5.4, D1).

**Abstract:**

The knowledge of soil thermal properties is important for determining how a soil will behave under changing climate conditions, especially in the sensitive environment of permafrost affected soils. This paper represents the first complex study of the interplay between the different parameters affecting soil thermal conductivity of soils in Antarctica. Antarctic Peninsula is currently the most rapidly warming region of the whole Antarctica, with predictions of this warming to continue in the upcoming decades. This study focuses on James Ross Island, where the Abernethy Flats automatic weather station is located in a lowland area with semi-arid climate. Air and ground temperature, soil heat flux and soil moisture during the thawing season were monitored on this site from 2015 to 2023. Moreover, two approaches to determining soil thermal conductivity were compared - laboratory measurements and calculation from field data. During this period, mean annual temperatures have increased dramatically for both air (from -6.9 degrees C in 2015/2016 to -3.8 degrees C in 2022/2023) and ground (from -6.5 degrees C to -3.2 degrees C), same as active layer thickness (from 68 cm to 95 cm). Average soil thermal conductivity for the thawing period reached values between 0.49 and 0.74 W/m.K-1 based on field data. Statistically significant relationships were found between the seasonal means of volumetric water content and several other parameters - soil thermal conductivity ( $r = 0.91$ ), thawing degree days ( $r = -0.87$ ) and active layer thickness ( $r = -0.88$ ). Although wetter soils generally have a higher conductivity, the increase in temperature exhibits a much stronger control over the active layer thickening, also contributing to the overall drying of the upper part of the soil profile.

**Paper 11:**

Kaplan Pastříková, L., **Hrbáček, F.**, Uxa, T., Láska, K. (2023). Permafrost table temperature and active layer thickness variability on James Ross Island, Antarctic Peninsula, in 2004–2021. *Science of the Total Environment*, 869, 161690. (IF 9.8; D1).

**Abstract:**

Climate change and its impacts on sensitive polar ecosystems are relatively little studied in Antarctic regions. Permafrost and active layer changes over time in periglacial regions of the world are important indicators of climate variability. These changes (e. g. permafrost degradation, increasing of the active layer thickness) can have a significant impact on Antarctic terrestrial ecosystems. The study site (AWS-JGM) is located on the Ulu Peninsula in the north of James Ross Island. Ground temperatures at depths of 5, 50, and 75 cm have been measured at the site since 2011, while air temperature began to be measured in 2004. The main objective is to evaluate the year-to-year variability of the reconstructed temperature of the top of the permafrost table and the active layer thickness (ALT) since 2004 based on air temperature data

using TTOP and Stefan models, respectively. The models were verified against direct observations from a reference period 2011/12-2020/21 showing a strong correlation of 0.95 (RMSE = 0.52) and 0.84 (RMSE = 3.54) for TTOP and Stefan models, respectively. The reconstructed average temperature of the permafrost table for the period 2004/05-2020/21 was -5.8 degrees C with a trend of -0.1 degrees C/decade, while the average air temperature reached -6.6 degrees C with a trend of 0.6 degrees C/decade. Air temperatures did not have an increasing trend throughout the period, but in the first part of the period (2004/05-2010/11) showed a decreasing tendency (-1.3 degrees C/decade). In the period 2011/ 12-2020/21, it was a warming of 1.9 degrees C/decade. The average modelled ALT for the period 2004/05-2020/21 reached a value of 60cm with a trend of -1.6 cm/decade. Both models were found to provide reliable results, and thus they significantly expand the information about the permafrost and ALT, which is necessary for a better understanding of their spatiotemporal variability and the impact of climate change on the cryosphere.

**Paper 12:**

**Hrbáček, F.,** Kňázková, M., Láska, K., Kaplan Pastřířková, L., (*accepted*). Active layer warming and thickening on CALM-S JGM, James Ross Island, in the period 2013/14–2022/23. Permafrost and Periglacial Processes. (IF 3.0, D1)

**Abstract:**

The Circumpolar Active Layer Monitoring – South (CALM-S) site was established near the Johann Gregor Mendel (JGM) research station on James Ross Island in February 2014. The CALM-S JGM grid, measuring 80 × 70 m, encompasses two distinct lithological units: a Holocene marine terrace (covering approximately 75% of the grid) and Cretaceous sediments of the Whisky Bay Formation (covering the remaining 25%). Within each lithology, a monitoring profile was established to track the active layer thermal regime and thickness. Additionally, active layer thaw depth probing has been conducted annually around mid-February. Since 2017, the dataset has been further supplemented by surficial soil water content measurements. During the study period (2013/14–2022/23), air temperature increased at a rate of 0.2 °C per year. Consequently, the active layer thickness, defined by the 0 °C isotherm, increased by an average of 1.5 cm per year, while mechanically probed thaw depths showed an annual increase of 1.9 cm. This study confirms that local lithology strongly influences active layer thermal regime. On average, the active layer thickness was 24 cm greater on AWS-CALM (Cretaceous sediments) than on AWS-JGM (marine terrace). The thaw depth was 28 cm greater in the Cretaceous sediment part of CALM-S compared to the marine terrace part. A strong correlation ( $r = 0.82$  to  $r = 0.91$ ) was found between active layer thickness and thaw depth with thawing degree days of air and near-surface ground temperature in both lithologies.

**Paper 13:**

**Hrbáček, F.**, Oliva, M., Ruiz-Fernández, J., Kňázková, M., de Pablo, M.A. et al., (2020). Modelling ground thermal regime in bordering (dis)continuous permafrost environments. *Environmental Research*, 181, 108901. (IF 5.715; Q1)

**Abstract:**

Permafrost controls geomorphological dynamics in maritime Antarctic ecosystems. Here, we analyze and model ground thermal regime in bordering conditions between continuous and discontinuous permafrost to better understand its relationship with the timing of glacial retreat. In February 2017, a transect including 10 sites for monitoring ground temperatures was installed in the eastern fringe of Byers Peninsula (Livingston Island, northern Antarctic Peninsula), together with one station recording air temperatures and snow thickness. The sites were selected following the Mid-Late Holocene deglaciation of the area at a distance ranging from 0.30 to 3.15 km from the current Rotch Dome glacier front. The transect provided data on the effects of topography, snow cover and the timing of ice-free exposure, on the ground thermal regime. From February 2017 to February 2019, the mean annual air temperature was - 2.0 degrees C, which was > 0.5 degrees C higher than 1986-2015 average in the Western Antarctic Peninsula region. Mean annual ground temperature at 10 cm depth varied between 0.3 and -1.1 degrees C, similar to the modelled Temperatures on the Top of the Permafrost (TTOP) that ranged from 0.06 +/- 0.08 degrees C to -1.33 +/- 0.07 degrees C. The positive average temperatures at the warmest site were related to the long-lasting presence of snow which favoured warmer ground temperatures and may trigger permafrost degradation. The role of other factors (topography, and timing of the deglaciation) explained intersite differences, but the overall effect was not as strong as snow cover.

**Paper 14:**

Obu, J., Westermann, S., Vieira, G., Abramov, A., Balks, M.R., Bartsch, A., **Hrbáček, F.**, Kaab, A., Ramos, M., (2020): Pan-Antarctic map of near-surface permafrost temperatures at 1 km(2) scale. *The Cryosphere*, 14(2), 497 - 519. (IF 4.713; D1).

**Abstract:**

Permafrost is present within almost all of the Antarctic's ice-free areas, but little is known about spatial variations in permafrost temperatures except for a few areas with established ground temperature measurements. We modelled a temperature at the top of the permafrost (TTOP) for all the ice-free areas of the Antarctic mainland and Antarctic islands at 1 km(2) resolution during 2000-2017. The model was driven by remotely sensed land surface temperatures and downscaled ERA-Interim climate reanalysis data, and subgrid permafrost variability was simulated by variable snow cover. The results were validated against in situ-measured ground temperatures from 40 permafrost boreholes, and the resulting root-mean-square error was 1.9 degrees C. The lowest near-surface permafrost temperature of -36 degrees C was modelled at Mount Markham in the Queen Elizabeth Range in the Transantarctic Mountains. This is the lowest permafrost temperature on Earth, according to global-scale modelling results. The

temperatures were most commonly modelled between -23 and -18 degrees C for mountainous areas rising above the Antarctic Ice Sheet and between -14 and -8 degrees C for coastal areas. The model performance was good where snow conditions were modelled realistically, but errors of up to 4 degrees C occurred at sites with strong wind-driven redistribution of snow.

**Paper 15:**

**Hrbáček, F.**, Vieira, G., Oliva, M., Balks, M., Guglielmin, M., de Pablo, M.A., Molina, A., Ramos, M., Goyanes, G., Meiklejohn, I., Abramov, A., Demidov, N., Fedorov-Davydov, D., Lupachev, A., Rivkina, E., Láska, K., Kňázková, M., Nývlt, D., Raffi, R., Strelin, J., Sone, T., Fukui, K., Dolgikh, A., Zazovskaya, E., Mergelov, N., Osokin, N., Miamin, V., 2021. Active layer monitoring in Antarctica: an overview of results from 2006 to 2015. *Polar Geography*, 44 (3), 217–231. (IF 2.6, Q2).

**Abstract:**

Monitoring of active layer thawing depth and active layer thickness (ALT), using mechanical pronging and continuous temperature data logging, has been undertaken under the Circumpolar Active Layer Monitoring - South (CALM-S) program at a range of sites across Antarctica. The objective of this study was to summarize key data from sites in different Antarctic regions from 2006 to 2015 to review the state of the active layer in Antarctica and the effectiveness of the CALM-S program. The data from 16 sites involving 8 CALM-S and another 8 boreholes across the Antarctic have been used in the study. Probing for thaw depth, while giving information on local spatial variability, often underestimates the maximum ALT of Antarctic soils compared to that determined using continuous temperature monitoring. The differences are likely to be caused by stones limiting probe penetration and the timing of probing not coinciding with the timing of maximum thaw, which varies between seasons. The information on the active layer depth is still sparse in many regions and the monitoring needs to be extended and continued to provide a better understanding of both spatial and temporal variability in Antarctic soil thermal properties.

**Paper 16:**

**Hrbáček, F.**, Oliva, M., Hansen, C., Balks, M., O'Neill, T.A., de Pablo, M.A., Ponti, S., Ramos, M., Vieira, G., Abramov, A., Kaplan Pastíriková, L., Guglielmin, M., Goyanes, G., Francellino, M.R., Schaefer, C., Lacelle, D., 2023. Active layer and permafrost thermal regimes in the ice-free areas of Antarctica. *Earth Science Reviews*, 242, 104458. (IF 12.1, D1).

**Abstract:**

Ice-free areas occupy <0.5% of Antarctica and are unevenly distributed across the continent. Terrestrial ecosystem dynamics in ice free areas are strongly influenced by permafrost and the associated active layer. These features are the least studied component of the cryosphere in Antarctica, with sparse data from permanent study sites mainly providing information related to the ground thermal regime and active layer thickness (ALT). One of the most important results of the International Polar Year (IPY, 2007/08) was an increase in ground thermal regime monitoring sites, and consequently our knowledge of Antarctic permafrost dynamics. Now, 15 years after the IPY, we provide the first comprehensive summary of the state of permafrost across Antarctica, including the sub-Antarctic Islands, with analyses of spatial and temporal patterns of the dominant external factors (climate, lithology, biota, and hydric regime) on the ground thermal regime and active layer thickness. The mean annual ground temperatures of the active layer and uppermost part of the permafrost in Antarctica remain just below 0 C in the warmest parts of the Antarctic Peninsula, and were below -20 degrees C in mountainous regions of the continent. The ALT varies between a few cm in the coldest, mountainous, parts of the Transantarctic Mountains up to >5 m in bedrock sites in the Antarctic Peninsula. The deepest and most variable ALTs (ca. 40 to >500 cm) were found in the Antarctic Peninsula, whereas the maximum ALT generally did not exceed 90 cm in Victoria Land and East Antarctica. Notably, found that the mean annual near-surface temperature follows the latitudinal gradient of -0.9 degrees C/deg. ( $R^2 = 0.9$ ) and the active layer thickness 3.7 cm/deg. ( $R^2 = 0.64$ ). The continuous permafrost occurs in the vast majority of the ice-free areas in Antarctica. The modelling of temperature on the top of the permafrost indicates also the permafrost presence in South Orkneys and South Georgia. The only areas where deep boreholes and geophysical surveys indicates discontinuous or sporadic permafrost are South Shet-lands and Western Antarctic Peninsula.

## Short Communication

# Effect of Snow Cover on the Active-Layer Thermal Regime – A Case Study from James Ross Island, Antarctic Peninsula

Filip Hrbáček,<sup>1\*</sup> Kamil Láška<sup>1</sup> and Zbyněk Engel<sup>2</sup>

<sup>1</sup> Masaryk University, Faculty of Science, Department of Geography, Brno, Czech Republic

<sup>2</sup> Charles University in Prague, Department of Physical Geography and Geocology, Praha, Czech Republic

### ABSTRACT

The response of active-layer thickness and the ground thermal regime to climatic conditions on the Ulu Peninsula (James Ross Island, northeastern Antarctic Peninsula) in 2011–13 is presented. The mean air temperature over this period was  $-8.0^{\circ}\text{C}$  and ground temperature at 5 cm depth varied from  $-6.4^{\circ}\text{C}$  (2011–12) to  $-6.7^{\circ}\text{C}$  (2012–13). The active-layer thickness ranged between 58 cm (January 2012) and 52 cm (February 2013). Correlation analyses indicate that air temperature affects ground temperature more significantly on snow-free days ( $R^2=0.82$ ) than on snow cover days ( $R^2=0.53$ ). Although the effect of snow cover on the daily amplitude of ground temperature was observable to 20 cm depth, the overall influence of snow depth on ground temperature was negligible (freezing  $n$ -factor of 0.95–0.97). Copyright © 2015 John Wiley & Sons, Ltd.

KEY WORDS: active-layer; ground temperature; snow cover; air temperature; Antarctic Peninsula; active layer thickness

### INTRODUCTION

The Antarctic Peninsula (AP) has experienced the largest atmospheric warming of all regions on Earth over the last 50 years (Turner *et al.*, 2002), with the temperature increase accelerating downwasting of ice sheets on the AP (Vaughan, 2006) and causing the collapse of ice shelves along its eastern coast (Cook and Vaughan, 2010). The response of regional permafrost to this warming remains unknown and represents one of the most important topics in climate modelling, because numerical models suggest that permafrost may become the dominant contributor of  $\text{CO}_2$  and  $\text{CH}_4$  into the atmosphere in the 21<sup>st</sup> century (Schaefer *et al.*, 2011). Despite the increasing number of periglacial studies focusing on the AP in the last decade (Vieira *et al.*, 2010; Guglielmin *et al.*, 2014; Bockheim *et al.*, 2013; De Pablo *et al.*, 2014; Almeida *et al.*, 2014; Goyanes *et al.*, 2014), thermal conditions in the active layer and its interaction with meteorological factors are not well known. In particular, the influence of snow on active-layer thickness (ALT) and the thermal regime is relatively poorly understood, despite being a major modulating factor to the atmosphere (Boike *et al.*, 2008; Vieira

*et al.*, 2014). In this paper, we evaluate the effect of air temperature and snow cover on active-layer temperature in the northern part of James Ross Island (JRI) from March 2011 to April 2013, one of the largest permafrost regions in the northeastern AP.

### REGIONAL SETTINGS

The study site ( $63^{\circ}48'S$   $57^{\circ}52'W$ ) is located in the Ulu Peninsula, northern JRI (Figure 1), approximately 100 m south of the Johann Gregor Mendel Station at 10 m asl. Glaciers started to retreat from the Ulu Peninsula before 12.9 ka (Nývlt *et al.*, 2014), leaving low-lying areas ice-free at the beginning of the Holocene. At present, small glaciers persist only on high-altitude volcanic plateaus and in valley heads (Engel *et al.*, 2012). Permafrost in the northern part of JRI can approach 95 m in thickness and the ALT is highly variable, ranging from 22 to 150 cm (Borzotta and Trombotto, 2004; Engel *et al.*, 2010; Bockheim *et al.*, 2013). The study site is located on a Holocene marine terrace (Figure 2) formed by beach deposits composed of gravelly sand (Stachoň *et al.*, 2014).

The climate of JRI is dominated by the advection of air masses, which are strongly influenced by the position of the AP relative to the circumpolar trough of low pressure

\*Correspondence to: F. Hrbáček, Masaryk University, Faculty of Science, Department of Geography, Kotlářská 2, 611 37 Brno, Czech Republic. E-mail: hrbacekfilip@gmail.com

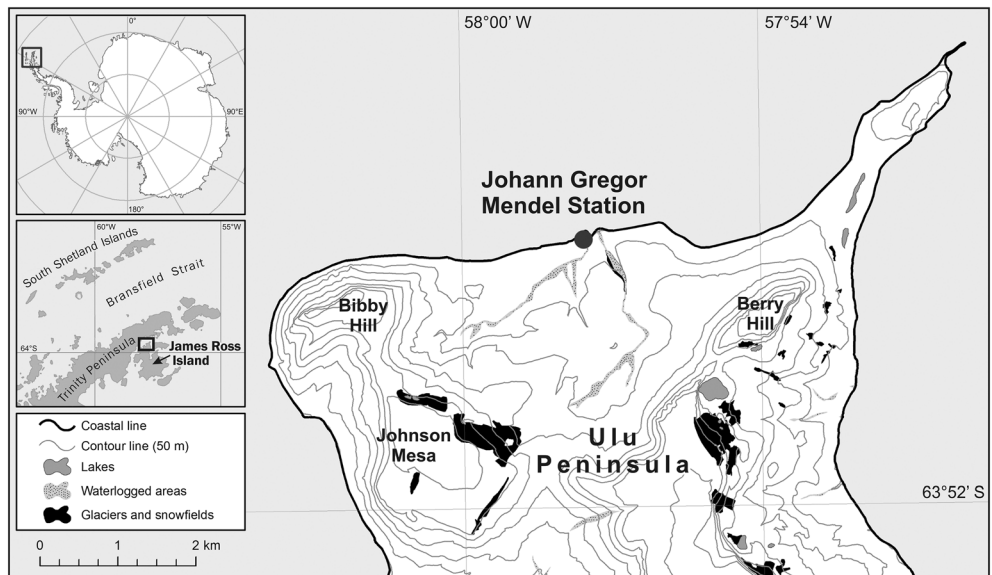


Figure 1 Location of the study site in the northern part of James Ross Island, close to the eastern coast of the Antarctic Peninsula.

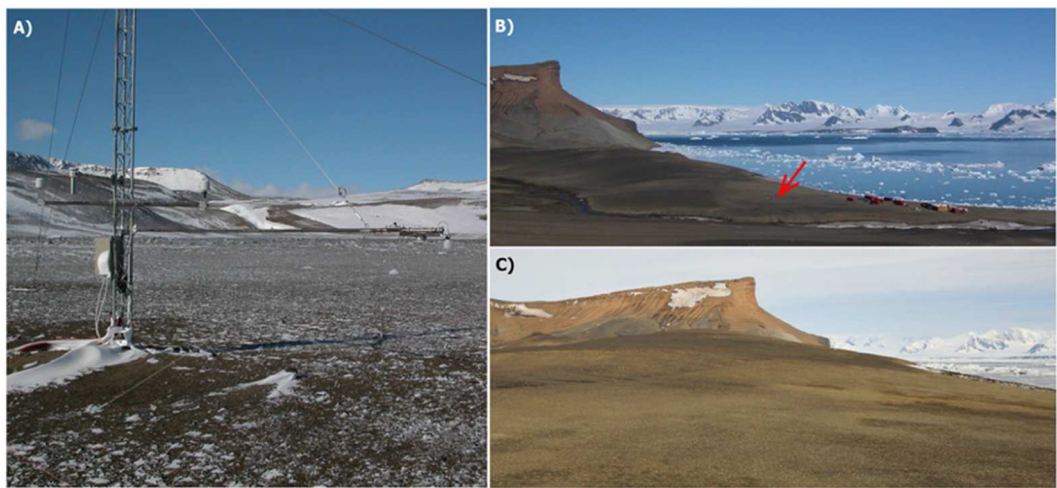


Figure 2 (A) Detailed view of the study site and (B, C) its geomorphological position on the northern coast of the Ulu Peninsula. The red arrow marks the study site near Mendel Station. This figure is available in colour online at [wileyonlinelibrary.com/journal/ppp](http://wileyonlinelibrary.com/journal/ppp)

(Domack *et al.*, 2003). A complex orography causes frequent variation between two main advection patterns: (1) cold and dry southerly winds blowing along the eastern coast of the AP, and (2) westerly winds bringing relatively warm maritime air masses across the peninsula to northern JRI (King *et al.*, 2003; Zvěřina *et al.*, 2014). The mean annual air temperature (MAAT) at Mendel Station is  $-6.8^{\circ}\text{C}$  (2006–11) and the extremes of mean daily air temperatures vary between around  $8^{\circ}\text{C}$  in January and  $-30^{\circ}\text{C}$  in July/August (Láska *et al.*, 2012). Mean daily temperatures above  $0^{\circ}\text{C}$  typically occur only for 2 months each summer (December–January), with hourly maximum and minimum values of  $10^{\circ}\text{C}$  and  $-5^{\circ}\text{C}$ , respectively (Láska *et al.*, 2011). According to data from Esperanza, the nearest station making

long-term observations on the northern AP, the temperature was  $0.2^{\circ}\text{C}$  colder in 2011–13 than over the reference period of 1961–2000, with a MAAT of  $-5.2^{\circ}\text{C}$  (Turner *et al.*, 2004). Precipitation is mostly snow and estimated to range from 300 to 500 mm water equivalent per year (Van Lipzig *et al.*, 2004).

## METHODS

Temperature in the active layer was measured at depths of 5, 10, 20, 30, 50 and 75 cm using Pt100/Class A platinum resistance thermometers (EMS, Brno, Czech Republic). Air temperature was measured 2 m above ground level using

an EMS33 sensor (EMS Brno) with a Pt100/Class A platinum resistance thermometer placed inside a solar radiation shield. Both ground and air temperatures were measured with an accuracy of  $\pm 0.15^\circ\text{C}$  and data were recorded at 30 min intervals with an EdgeBox V12 datalogger (EMS Brno). We then calculated mean daily air temperatures, the cumulative sum of mean daily air temperatures above  $0^\circ\text{C}$  (the thawing-degree days – TDD<sub>a</sub>) and the cumulative sum of mean daily air temperatures below  $0^\circ\text{C}$  (the freezing-degree days – FDD<sub>a</sub>), according to Guglielmin *et al.* (2008) and De Pablo *et al.* (2014). Incoming and reflected shortwave radiation (used to estimate albedo) were measured using EMS-11 (EMS Brno) and CM6B (Kipp & Zonen, Delft, The Netherlands) pyranometers, respectively, at 10 s time intervals and stored as 30 min average values. Snow depth was recorded every 2 h using an ultrasonic depth sensor (Judd Communication, Salt Lake City, UT, USA) with an accuracy of  $\pm 1$  cm. All meteorological parameters and ground temperature data were analysed during the period from 1 March 2011 to 30 April 2013. MAAT and mean annual ground temperature (MAGT) were also calculated for a period of 2 years from March 2011 to February 2013, referred to in the text as the 2011–12 and 2012–13 periods.

The ground thermal regime for the period of 2011–13 was evaluated in accordance with recent studies investigating Maritime Antarctic (Guglielmin *et al.*, 2008; Michel *et al.*, 2012; De Pablo *et al.*, 2014), using the following parameters: (1) mean annual and monthly ground temperatures; (2) the cumulative sum of mean daily ground temperatures above  $0^\circ\text{C}$  (the thawing-degree days – TDD<sub>g</sub>); (3) the cumulative sum of mean daily ground temperatures below  $0^\circ\text{C}$  (the freezing-degree days – FDD<sub>g</sub>); and (4) the ALT, interpolated as the  $0^\circ\text{C}$  isotherm depth and derived from contours of the daily mean ground temperature interpolated using kriging algorithms in the Surfer® software program (Golden Software, Golden, CO, USA).

Freezing and thawing *n*-factors (Karunaratne and Burn, 2003) were calculated in order to evaluate the buffering effects of the snow layer on heat transmission between air and the ground surface (De Pablo *et al.*, 2014), with the effect of air temperature on the ground analysed at 5 cm depth (e.g. Zhang *et al.*, 1997).

Snow cover duration was estimated using a combination of ultrasonic depth sensors and the radiometric albedo. The criteria for snow occurrence were a depth  $> 2$  cm (from the ultrasonic sensors) and albedo  $> 0.4$  (which corresponds to old snow; Warner, 2004). Snow depth records were available for the period from 1 March 2011 to 11 June 2012, while radiometric albedo data were available for the periods from 20 February to 16 May 2011 and 5 March 2012 to 30 April 2013. Despite the presence of gaps in the records due to sensor malfunctions, we were able to analyse an insulation effect of snow cover on the ground temperature regime at 5 cm depth using (1) correlation analysis between mean daily air and ground temperatures during the surface snow-free and snow cover periods, and (2) comparison of the snow cover records with ground temperature daily amplitudes (Zhang *et al.*, 1997).

## RESULTS

### Air and Ground Temperatures

The MAAT over the whole 2 year study period was  $-8.0^\circ\text{C}$ ; although the individual MAAT values for the 2 years were equal, the temperature range differed from  $44.0^\circ\text{C}$  (2011–12) to  $42.3^\circ\text{C}$  (2012–13). The larger temperature extreme in 2011–12 was documented by a lower mean temperature of the coldest month (July 2011,  $-18.5^\circ\text{C}$ ) and a higher mean temperature of the warmest month (December 2011,  $2.0^\circ\text{C}$ ) compared to those for 2012–13 ( $-15.0^\circ\text{C}$  and  $0.2^\circ\text{C}$ , respectively). The maximum air temperature recorded during the entire study period was  $11.6^\circ\text{C}$  on 23 February 2013; the minimum recorded was  $-34.1^\circ\text{C}$  on 26 July 2011.

The MAGT at 5 cm depth was  $-6.4^\circ\text{C}$  in 2011–12 and  $-6.7^\circ\text{C}$  in 2012–13. The mean monthly ground temperature at 5 cm depth varied between  $-16.3^\circ\text{C}$  (July 2011) and  $6.1^\circ\text{C}$  (December 2011). Minimum ( $-26.3^\circ\text{C}$ ) and maximum ( $16.0^\circ\text{C}$ ) 5 cm ground temperatures over the study period were recorded on 1 August 2011 and 18 December 2012, respectively. The MAGT at 50 cm depth, which represents active-layer conditions close to the permafrost table, ranged between  $-6.1^\circ\text{C}$  in 2011–12 and  $-6.0^\circ\text{C}$  in 2012–13. Minimum ( $-16.3^\circ\text{C}$ ) and maximum ( $1.3^\circ\text{C}$ ) ground temperatures at 50 cm were recorded on 5 August 2011 and 26 January 2012, respectively. The MAGT at 75 cm depth, which represents the uppermost part of the permafrost zone, reached  $-5.8^\circ\text{C}$ , while maximum and minimum temperatures for the greatest depth were  $-1.0^\circ\text{C}$  and  $-14.4^\circ\text{C}$ , respectively.

### Thawing and Freezing Seasons

The duration of the thawing season as defined by the thermal regime at 5 cm depth differed significantly between the two periods (Table 1). In 2011–12, the thawing season started on 9 October 2011 and terminated on 27 March 2012, lasting for 170 days. In 2012–13, the thawing season both started and ended later (13 December 2012 and 20 April 2013, respectively) and its duration was considerably shorter (128 days). The mean ground temperature at 5 cm depth was lower during the longer thawing season of 2011–2012 ( $2.3^\circ\text{C}$ ) than during the shorter thawing season of 2012–13 ( $4.3^\circ\text{C}$ ). TDD<sub>g</sub> calculated for the thawing season, however, was much higher in 2011–12 ( $496.1^\circ\text{C day}$ ) than in 2012–13 ( $358.3^\circ\text{C day}$ ). The active layer thawed slowly in 2011–12, reaching its maximum on 26 January 2012 (58 cm). In contrast, active-layer thaw was more rapid in 2012–13, reaching its maximum on 13 February 2013 (52 cm).

The freezing season at 5 cm depth lasted for 203 days in 2011 and 259 days in 2012. The mean ground temperature at 5 cm varied from  $-13.4^\circ\text{C}$  in the freezing season of 2011 to  $-10.6^\circ\text{C}$  in that of 2012. Despite the lower mean temperature recorded in 2011, a small difference in total FDD<sub>g</sub> was observed between the two freezing seasons, at

Table 1 Quantitative characteristics of freezing and thawing seasons at Mendel Station during the period 2011–13.

|                              | Freezing season        |                         | Thawing season         |                         |
|------------------------------|------------------------|-------------------------|------------------------|-------------------------|
|                              | 2011                   | 2012                    | 2011–12                | 2012–13                 |
| Period                       | 19/3/2011<br>8/10/2011 | 28/3/2012<br>12/12/2012 | 9/10/2011<br>27/3/2012 | 13/12/2012<br>20/4/2013 |
| Duration (days)              | 203                    | 259                     | 170                    | 128                     |
| Mean air temperature (°C)    | −13.7                  | −11.0                   | −1.0                   | −0.5                    |
| Mean GT <sub>5 cm</sub> (°C) | −13.4                  | −10.6                   | 2.3                    | 4.3                     |
| Min air temperature (°C)     | −34.1                  | −30.7                   | −17.2                  | −14.6                   |
| Max air temperature (°C)     | 5.7                    | 7.1                     | 9.9                    | 11.6                    |
| Min GT <sub>5 cm</sub> (°C)  | −26.0                  | −23.5                   | −12.3                  | −11.4                   |
| Max GT <sub>5 cm</sub> (°C)  | −0.4                   | −0.3                    | 15.3                   | 16.0                    |
| Min GT <sub>75 cm</sub> (°C) | −14.4                  | −12.0                   | −9.0                   | −3.3                    |
| Max GT <sub>75 cm</sub> (°C) | −1.2                   | −1.0                    | −1.0                   | −1.1                    |
| FDD <sub>a</sub> (°C day)    | −2814.1                | −2878.9                 | −330.4                 | −195.8                  |
| FDD <sub>g</sub> (°C day)    | −2735.5                | −2748.5                 | −100.6                 | −77.6                   |
| <i>n</i> -factor             | 0.97                   | 0.95                    | 3.03                   | 2.27                    |
| TDD <sub>a</sub> (°C day)    | 22.0                   | 28.9                    | 163.8                  | 157.7                   |
| TDD <sub>g</sub> (°C day)    | 0.0                    | 0.0                     | 496.1                  | 358.3                   |

GT<sub>5 cm</sub> = Ground temperature at 5 cm depth. See text for other abbreviations.

−2735.5°C day in 2011 and −2748.5°C day in 2012. Although positive air temperatures were recorded on several days during both the freezing seasons (Table 1), there were no signs of ground thaw at 5 cm depth.

### Effect of Snow Cover on Ground Temperature

The temporal distribution and duration of snow cover on JRI varied significantly over the study period (Figure 3). In 2011–12, snow covered the study site for 167 days, with the period of continuous snow cover lasting from 22 March to 20 September (67 days). The period of maximum snow depth (21 to 34 cm) persisted from 29 June to 23 July. In 2012–13, continuous snow cover occurred between 8 May and 12 December. The maximum snow depth of 15 cm was observed on 8 May, with relatively thick snow cover (up to 10 cm) lasting until at least 6 June. The continuous period of fresh snow cover was registered between 21 June and 10 December, based on an albedo > 0.80 (Warner, 2004).

Figure 4 shows the relationship between air temperature and ground temperature at 5 cm depth for all days (Figure 4A, D), snow-free days (Figure 4B, E) and snow cover days (Figure 4C, F) during 2011–12 (Figure 4A–C) and 2012–13 (Figure 4D–F). The correlation patterns reveal a significant relationship between the air and ground temperatures (coefficient of determination  $R^2=0.80$ ) in 2011–12. Moreover, a closer correlation between these temperatures was found for snow-free days ( $R^2=0.82$ ) than for snow cover days ( $R^2=0.53$ ). In contrast, a less significant relationship ( $R^2=0.67$ ) between air and ground temperatures at 5 cm depth, as well as a very small difference between snow-free days ( $R^2=0.56$ ) and snow cover days ( $R^2=0.52$ ), was observed in 2012–13.

The effect of snow cover on the active-layer thermal regime was also indicated by a reduction in the daily amplitude of ground temperature. Although the influence of snow cover on amplitude values was detected to a depth of 20 cm, the most significant temperature changes were recorded at 5 cm depth (Figure 5). Mean daily ground temperature amplitudes during snow-free days in thawing seasons ranged between 5.8°C at 5 cm and 1.5°C at 20 cm. The maximum daily ground temperature amplitude was recorded between 6 and 9 March 2012, when values ranged from 15°C at 5 cm to 5°C at 20 cm. The effects of snow cover on daily ground temperature amplitudes were more significant during freezing seasons, with the longer duration of snow cover in 2012 resulting in lower amplitude values (1.9°C at 5 cm and 0.9°C at 20 cm) than those recorded in 2011 (3.7°C and 1.2°C). Diurnal amplitudes of ground temperature rarely decreased to 0.1°C during freezing seasons. The longest period of very low diurnal amplitudes at depths from 5 to 20 cm (0.1 to 0.4°C) was observed between 1 and 11 November 2012.

The overall influence of snow on the ground thermal regime at 5 cm depth during the freezing seasons can be seen in the obtained values of the freezing *n*-factors (Table 1; Figure 6). Total freezing *n*-factors varied between 0.97 (2011) and 0.95 (2012), with values ranging from 0.85 to 0.95 on snow cover days. Differences in freezing *n*-factor development were observed between the respective freezing seasons of 2011 and 2012. The slower increase in the *n*-factor during the period from the end of March 2011 to the end of May 2011 indicates a more significant effect of snow cover during this early winter than in 2012. The observed freezing *n*-factor regime indicates periods with thicker snow cover, which caused a slight decrease from values > 0.95 to approx. 0.90 in both study years.

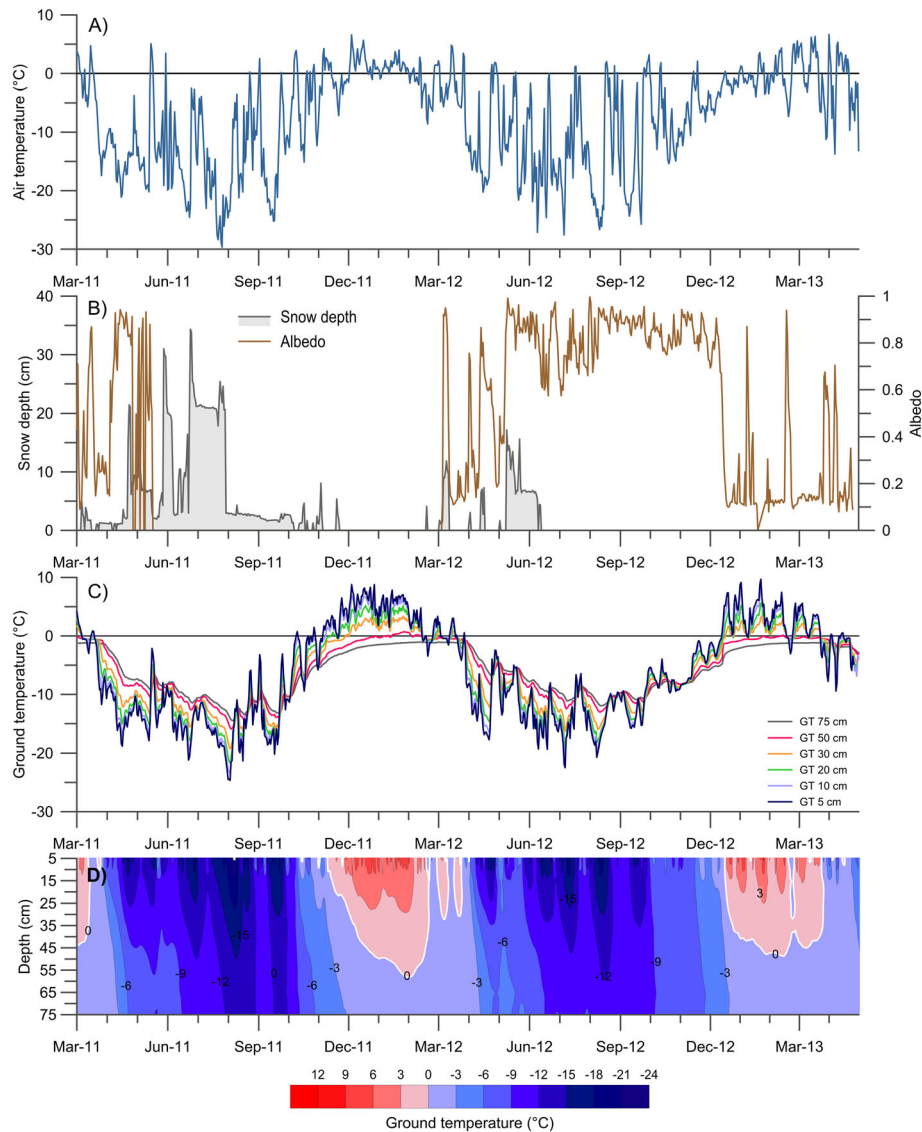


Figure 3 (A) Daily mean air temperature, (B) albedo and snow depth, (C) ground temperature (GT) at 5, 10, 20, 30, 50 and 75 cm depths and (D) GT isopleths at the study site for the period between 1 March 2011 and 30 April 2013. This figure is available in colour online at [wileyonlinelibrary.com/journal/ppp](http://wileyonlinelibrary.com/journal/ppp)

## DISCUSSION

### Active-Layer Conditions

The annual variability of air and ground temperatures at Mendel Station, compared to similar data from the South Shetland Islands and South Orkney Islands, suggests that considerably colder climatic conditions occur on JRI (see Table 2). This is also indicated by the significantly lower FDD<sub>g</sub> values (-2735.5 to -2748.5°C day) calculated for Mendel Station compared to those of -500 and -900 to -1200°C day reported from the South Shetland Islands and South Orkney Islands, respectively (Michel *et al.*, 2012; Guglielmin *et al.*, 2012; Almeida *et al.*, 2014; De Pablo *et al.*, 2014).

Although winters are generally much colder on JRI than in the northern AP, we detected that subsurface conditions can potentially be warmer during thawing seasons on JRI than on South Shetland or South Orkney. TDD<sub>g</sub> values calculated for JRI (496.1°C day in 2011–12 and 358.3°C day in 2012–13) are significantly higher than those for Livingston Island (98 to 257°C day; De Pablo *et al.*, 2014) and Signy Island (2 cm TDD<sub>g</sub> ranged between 260.5 and 378.0°C day for the period 2006–09; Guglielmin *et al.*, 2012). An even higher TDD<sub>g</sub> value of 618°C day has been recorded at Rothera Point, Adelaide Island (Guglielmin *et al.*, 2014).

The active layer is generally thinner and less variable on JRI (22 to 150 cm according to Borzotta and Trombotto, 2004; Engel *et al.*, 2010) than on the South Orkney Islands

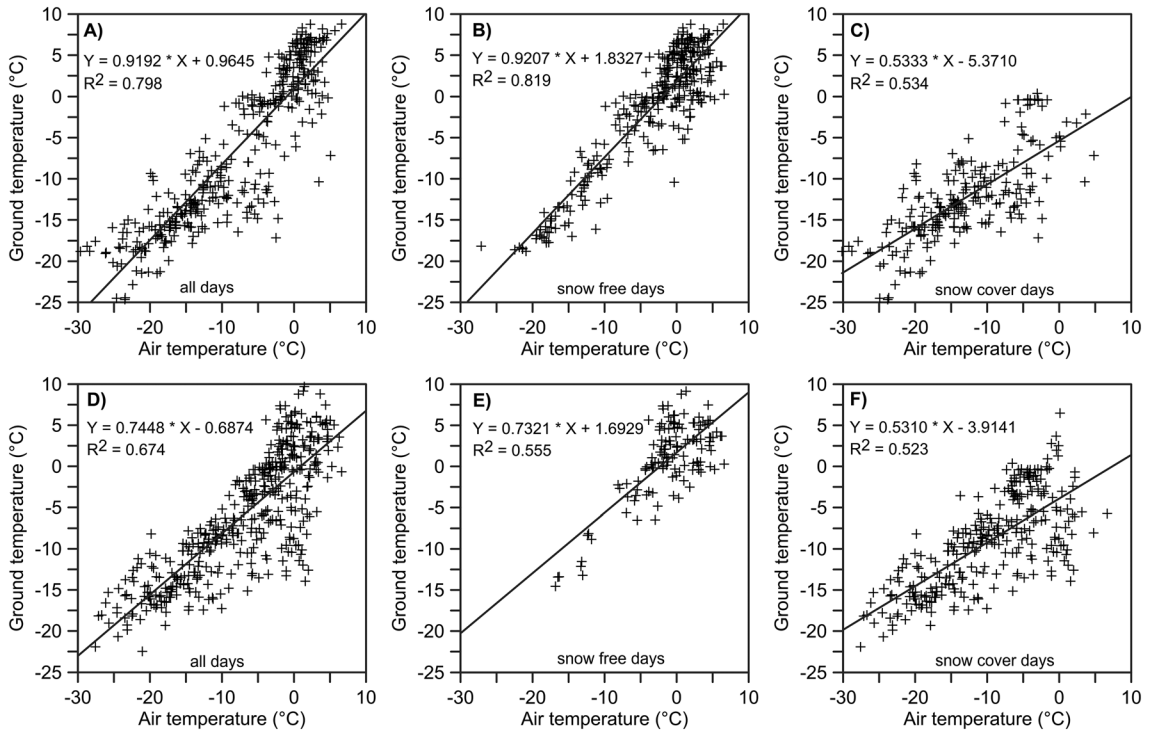


Figure 4 Relationship between air and ground temperatures at 5 cm depth for the periods (A–C) 2011–12 and (D–F) 2012–13 for (A, D) all days, (B, E) under snow-free conditions and (C, F) under snow cover. Coefficients of determination  $R^2$  for a simple linear regression model are given in the plots.

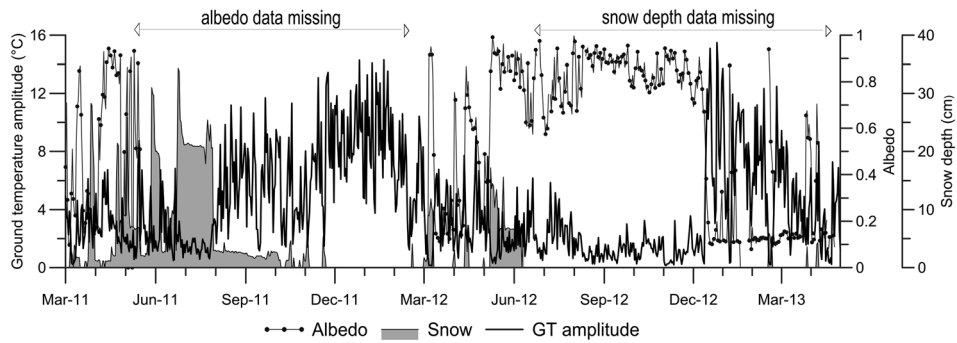


Figure 5 Variation in ground temperature (GT) daily amplitude, snow depth and albedo for the period from 1 March 2011 to 30 April 2013.

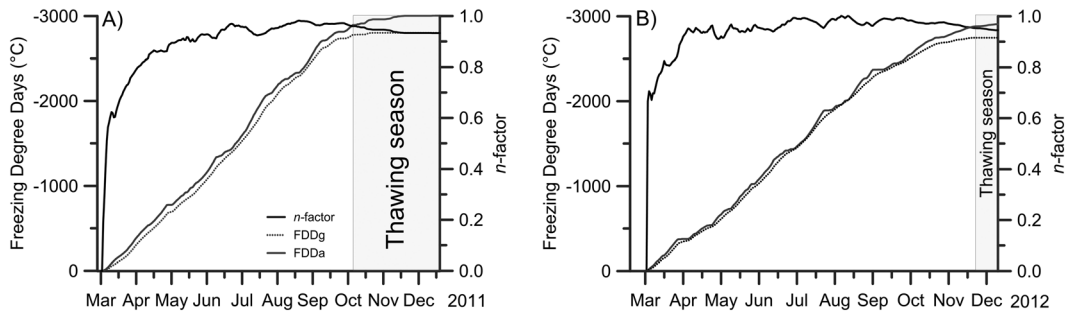


Figure 6 Cumulative sums of  $n$ -factors and freezing-degree days for air temperature ( $FDD_a$ ) and ground temperature at 5 cm depth ( $FDD_g$ ) during the freezing seasons of (A) 2011 and (B) 2012.

Table 2 Climatic conditions and active-layer depths at reported sites in the northern Antarctic Peninsula.

| Region                 | Study area         | Elevation (m asl) | Period     | MAAT (°C) | MAGT (°C)         | Ground temperature measurement depth (cm) | ALT (cm) | Reference                       |
|------------------------|--------------------|-------------------|------------|-----------|-------------------|---|----------|---------------------------------|
| South Orkney Islands   | Signy Island       | 80                | 1/06–12/09 | −3.7      | −2.4              | 2   | 112–158  | Guglielmin <i>et al.</i> (2012) |
|                        |                    |                   |            |           | −2.0 <sup>a</sup> | 2   | 101      |                                 |
| South Shetland Islands | King George Island | 65–70             | 2/08–1/09  | NA        | −0.8              | 8.5                                       | 89–92    | Michel <i>et al.</i> (2012)     |
|                        |                    |                   |            |           |                   |   |          |                                 |
|                        | Deception Island   | 105               | 2/09–2/13  | −2.5      | −0.8              | 2.5                                       | 99–105   | De Pablo <i>et al.</i> (2014)   |
|                        |                    |                   |            |           |                   |   |          |                                 |
| 130                    | 1/10–12/10         | −2.3              | −1.5       | 2         | 46–67             | Goyanes <i>et al.</i> (2014)              |          |                                 |

<sup>a</sup>Data for site covered by vegetation. NA = Data not available. See text for other abbreviations.

(80 to 220 cm according to Guglielmin *et al.*, 2008, 2012; Bockheim *et al.*, 2013) and South Shetland Islands (30 to > 500 cm; Vieira *et al.*, 2010; Michel *et al.*, 2012; Bockheim *et al.*, 2013; De Pablo *et al.*, 2014; Almeida *et al.*, 2014; Goyanes *et al.*, 2014). The ALT of 52 to 58 cm recorded at Mendel Station during the period 2011–13 is significantly lower than that observed in other low-elevation parts of JRI and the AP region over the last decade (Borzotta and Trombotto, 2004; Engel *et al.*, 2010; Bockheim *et al.*, 2013).

### Effects of Air Temperature and Snow Cover on the Ground Thermal Regime

The data obtained in northern JRI between March 2011 and April 2013 reveal the impacts of air temperature and snow cover on the ground thermal regime. The correlation between air and ground temperatures indicates a close relationship between these two variables during snow-free days, with diurnal ground temperature changes on these days directly reflecting air temperature variation (Figure 3A, C). Such changes in air temperature also control the duration of the freezing and thawing seasons, as indicated by the seasonal differences observed between 2011–12 and 2012–13. Mean monthly air temperatures from October to December 2011 (−5.3 to 2.0°C) were significantly higher than those in 2012 (−8.8 to −2.7°C), resulting in an extended thawing period in 2011–12. The colder climatic conditions at the end of the 2012 freezing season also prolonged the presence of snow cover (see below), which in turn prevented the ground from thawing on days with high solar radiation.

A number of studies have suggested that the effect of air temperature on ground temperature is highly variable in the AP region (Cannone *et al.*, 2006; Guglielmin *et al.*, 2014). Whereas a relatively weak correlation ( $r=0.58$  to  $0.82$ )

between air and ground temperatures was reported from King George Island and Signy Island (Cannone *et al.*, 2006) in areas covered by different types of vegetation, a stronger relationship ( $r > 0.90$ ) was described in areas of bare ground at Rothera Point (Guglielmin *et al.*, 2014). This difference in effect may be attributed to the variable ground surface conditions at the various study sites. The ground surface at the site on JRI investigated in the present study is free of vegetation, which is, by contrast, well developed on Signy Island, where a significant influence of vegetation cover on ground temperatures was found (Cannone *et al.*, 2006). We also observed greater variability in ground temperature at 5 cm depth during winters with thinner snow cover, in contrast to the South Shetland Islands where a snow depth greater than 40 cm had a significant effect on the active-layer thermal regime (De Pablo *et al.*, 2014). The minor effect of a thin snow cover on the ground thermal regime during the freezing season at the study site is also indicated by the high freezing  $n$ -factor values (0.95 to 0.97). Lower  $n$ -factor values (0.2 to 0.7) have been reported from Maritime Antarctica (De Pablo *et al.*, 2014; Almeida *et al.*, 2014), reflecting the deeper winter snow cover at sites on Livingston Island (De Pablo *et al.*, 2014) and King George Island (Almeida *et al.*, 2014).

Our conclusions regarding the effect of snow cover on active-layer conditions, however, should be treated with caution, as snow cover depth and distribution are highly variable and our field data cover only a brief time period. The irregular pattern of snow cover results from a combination of local climatic conditions, wind structure and orographic effects on precipitation (e.g. Turner *et al.*, 2002). Moreover, Van Lipzig *et al.* (2004) confirmed an orographic effect of the AP on the spatial distribution and irregular accumulation of snow along the AP coast. On the Ulu Peninsula, the relationship between snow drift and prevailing wind direction was reported by

Zvěřina *et al.* (2014), suggesting a redistribution of snow deposits in areas of low elevation in the Abernethy Flats (6 km south of Mendel Station). Clearly, more work is needed regarding the snow cover distribution across JRI, using both ground-based and remote sensing observations.

## CONCLUSIONS

Based on 2 years of meteorological observations and active-layer ground temperature monitoring at Mendel Station on JRI, we draw the following conclusions:

1. ALTs were observed between the end of January and the middle of February. Thicknesses of 58 and 52 cm measured in 2012 and 2013, respectively, are significantly lower than the ALT reported from low-elevation sites on the South Shetland Islands and South Orkney Islands.
2. Correlation analysis indicates a significant effect of air temperature on the ground thermal regime. This effect is especially apparent under snow-free conditions and during the advection of relatively warm air masses that cause large day-to-day changes in air temperature during winter.

## REFERENCES

Almeida ICC, Schaefer CEGR, Fernandes RBA, Pereira TTC, Nieuwendam A, Pereira AB. 2014. Active layer thermal regime at different vegetation covers at Lion Rumps, King George Island, Maritime Antarctica. *Geomorphology* **225**: 36–46.

Bockheim J, Vieira G, Ramos M, Lopez-Martinez J, Serrano E, Guglielmin M, Wilhelm K, Nieuwendam A. 2013. Climate warming and permafrost dynamics in the Antarctic Peninsula region. *Global and Planetary Change* **100**: 215–223.

Boike J, Hagedorn B, Roth K. 2008. Heat and water transfer processes in permafrost affected soils: A review of field-and modeling-based studies for the Arctic and Antarctic. In *Proceeding of the Ninth International Conference on Permafrost*, Douglas LK, Kenneth MH (eds). University of Alaska: Fairbanks; Vol. **1**: 149–154.

Borzotta E, Trombotto D. 2004. Correlation between frozen ground thickness measured in Antarctica and permafrost thickness estimated on the basis of the heat flow obtained from magnetotelluric soundings. *Cold Region Science and Technology* **40**: 81–96.

Cannone N, Evans JCE, Strachan R, Guglielmin M. 2006. Interactions between climate, vegetation and the active layer at two Maritime Antarctica sites. *Antarctic Science* **18**: 323–333.

Cook AJ, Vaughan DG. 2010. Overview of areal changes of the ice shelves on the Antarctic

Peninsula over the past 50 years. *The Cryosphere* **4**: 77–98.

De Pablo MA, Ramos M, Molina A. 2014. Thermal characterization of the active layer at the Limnopol Lake CALM-S site on Byers Peninsula (Livingston Island), Antarctica. *Solid Earth* **5**: 721–739.

Domack EW, Burnett A, Leventer A. 2003. Environmental setting of the Antarctic Peninsula. In *Antarctic Peninsula Climate Variability: Historical and Paleoenvironmental Perspectives*, Domack E, Leventer A, Burnett A, Bindshadler R, Convey P, Kirby M (eds). American Geophysical Union: Washington, DC; Vol. **79**: 1–13.

Engel Z, Láska K, Franta T, Máčka Z, Marvánek O. 2010. Recent changes of permafrost active layer on the James Ross Island, Maritime Antarctic. In *Abstracts from the Third European Conference on Permafrost*, Mertes JR, Christiansen HH, Eitzelmüller B (eds). UNIS: Longyearbyen; 129.

Engel Z, Nývlt D, Láska K. 2012. Ice thickness, bed topography and glacier volume changes on James Ross Island, Antarctic Peninsula. *Journal of Glaciology* **58**: 904–914.

Goyanes G, Vieira G, Caselli A, Cardoso M, Marmy A, Bernardo I, Hauck C. 2014. Geothermal anomalies, permafrost and geomorphological dynamics (Deception Island, Antarctica). *Geomorphology* **225**: 57–68.

Guglielmin M, Evans CJE, Cannone N. 2008. Active layer thermal regime under different vegetation conditions in permafrost areas. A case study at Signy Island (Maritime Antarctica). *Geoderma* **144**: 73–85.

3. The effect of snow cover depth on the ground thermal regime is indicated not only by the reduction in the daily ground temperature amplitude, but also by the total freezing *n*-factor values that were higher than 0.9. The overall influence of snow depth on ground temperature seems therefore to be negligible regarding the high values of the *n*-factor, associated with a thin and irregularly distributed snow cover.

## ACKNOWLEDGEMENTS

We thank the personnel at the Johann Gregor Mendel Station for their hospitality and logistical support. We are also very grateful to the members of the summer expeditions in 2011–14 for their field assistance on JRI. The work of F. Hrbáček and K. Láska was supported by the Masaryk University project MUNI/A/0952/2013: Analysis, evaluation and visualisation of global environmental changes in the landscape sphere. Finally, we would like to thank two anonymous reviewers for their comments and suggestions which improved the manuscript.

Guglielmin M, Worland MR, Cannone N. 2012. Spatial and temporal variability of ground surface temperature and active layer thickness at the margin of maritime Antarctica, Signy Island. *Geomorphology* **155–156**: 20–33.

Guglielmin M, Worland MR, Baio F, Convey P. 2014. Permafrost and snow monitoring at Rothera Point (Adelaide Island, Maritime Antarctica): Implications for rock weathering in cryotic conditions. *Geomorphology* **225**: 47–56.

Karunaratne KC, Burn CR. 2003. Freezing *n*-factors in discontinuous permafrost terrain, Takhini River, Yukon Territory, Canada. In *Proceedings of the 8th International Conference on Permafrost*, Phillips M, Springman SM, Arenson LU (eds). University of Alaska: Fairbanks; 519–524.

King JC, Turner J, Marshall GJ, Connelly WM, Lachlan-Cope TA. 2003. Antarctic Peninsula climate variability and its causes as revealed by analysis of instrumental records. In *Antarctic Peninsula Climate Variability: Historical and Palaeoenvironmental Perspectives*, Domack EW, Leventer A, Burnett A, Bindshadler R, Convey P, Kirby M (eds). American Geophysical Union: Washington DC; Vol. **79**: 17–30.

Láska K, Barták M, Hájek J, Prošek P, Bohuslavová O. 2011. Climatic and ecological characteristics of deglaciated area of James Ross Island, Antarctica, with a special respect to vegetation cover. *Czech Polar Reports* **1**: 49–62.

Láska K, Nývlt D, Engel Z, Budík L. 2012. Seasonal variation of meteorological variables

- and recent surface ablation / accumulation rates on Davies Dome and Whisky Glacier, James Ross Island, Antarctica. *Geophysical Research Abstracts* **14**: EGU2012–5545.
- Michel RFM, Schaefer CEGR, Poelking EL, Simas FNB, Filho EIF, Bockheim JG. 2012. Active layer temperature in two Cryosols from King George Island, Maritime Antarctica. *Geomorphology* **155–156**: 12–19.
- Nývlt D, Braucher R, Engel Z, Mlčoch B, AS-TER team. 2014. Timing of the Northern Prince Gustav Ice Stream retreat and the deglaciation of northern James Ross Island, Antarctic Peninsula during the last glacial–interglacial transition. *Quaternary Research* **82**: 441–449.
- Schaefer K, Zhang T, Brujwiler L, Barrett AP. 2011. Amount and timing of permafrost carbon release in response to climate warming. *Tellus* **63**: 165–180.
- Stachoň Z, Rusznák J, Nývlt D, Hrbáček F. 2014. Stabilization of geodetic points in the surrounding of Johann Gregor Mendel Station, James Ross Island, Antarctica. *Czech Polar Reports* **4**(1): 80–89.
- Turner J, Lachlan-Cope TA, Marshall GJ, Morris EM, Mulvaney R, Winter W. 2002. Spatial variability of Antarctic Peninsula net surface mass balance. *Journal of Geophysical Research* **107**: 4173.
- Turner J, Colwell SR, Marshall GJ, Lachlan-Cope TA, Carleton AM, Jones PD, Lagun V, Reid PA, Iagovkina S. 2004. The SCAR READER project: towards a high-quality database of mean Antarctic meteorological observations. *Journal of Climate* **17**: 2890–2898.
- Van Lipzig NPM, King JC, Lachlan-Cope TA, van der Broeke MR. 2004. Precipitation, sublimation and snow drift in the Antarctic Peninsula region from a regional atmospheric model. *Journal of Geophysical Research* **109**: D24106.
- Vaughan DG. 2006. Recent trends in melting conditions on the Antarctic Peninsula and their implications for ice-sheet mass balance. *Arctic, Antarctic, and Alpine Research* **38**: 147–152.
- Vieira G, Bockheim J, Guglielmin M, Balks M, Abramov AA, Boelhouwers J, Cannone N, Ganzert L, Gilichinsky DA, Goryachkin S, López-Martínez J, Meiklejohn I, Raffi R, Ramos M, Schaefer C, Serrano E, Simas F, Sletten R, Wagner D. 2010. Thermal State of permafrost and active-layer monitoring in the Antarctic: advances during the International Polar Year 2007–09. *Permafrost and Periglacial Processes* **21**: 182–197. DOI: 10.1002/ppp.685.
- Vieira G, Mora C, Pina P, Schaefer C. 2014. A proxy for snow cover and winter ground surface cooling: mapping *Usnea* sp communities using high resolution remote sensing imagery (Maritime Antarctica). *Geomorphology* **225**(15): 69–75.
- Warner TT. 2004. *Desert Meteorology*. Cambridge University Press: Cambridge, UK.
- Zhang T, Osterkamp TE, Stamnes K. 1997. Effects of climate on the active layer and permafrost on the North Slope of Alaska, U.S.A. *Permafrost and Periglacial Processes* **8**: 45–67. 10.1002/(SICI)1099-1530(199701)8:<45::AID-PPP240>3.0.CO;2-K.
- Zvěřina O, Láška K, Červenka R, Kuta J, Coufalík P, Komárek J. 2014. Analysis of mercury and other heavy metals accumulated in lichen *Usnea antarctica* from James Ross Island, Antarctica. *Environmental Monitoring and Assessment* **186**: 9089–9100.

## ACTIVE LAYER THERMAL REGIME IN TWO CLIMATICALLY CONTRASTED SITES OF THE ANTARCTIC PENINSULA REGION

F. HRBÁČEK<sup>1</sup>, M. OLIVA<sup>2\*</sup>, K. LÁŠKA<sup>2</sup>, J. RUIZ-FERNÁNDEZ<sup>3</sup>, M. Á. DE PABLO<sup>4</sup>, G. VIEIRA<sup>2</sup>, M. RAMOS<sup>5</sup>, D. NÝVLT<sup>1</sup>

<sup>1</sup>Department of Geography, Masaryk University, Brno, Czech Republic.

<sup>2</sup>Centre for Geographical Studies – IGOT, University of Lisboa, Portugal.

<sup>3</sup>Department of Geography, University of Oviedo, Oviedo, Spain.

<sup>4</sup>Department of Geology, Geography and Environment, University of Alcalá, Madrid, Spain.

<sup>5</sup>Department of Physics and Mathematics, University of Alcalá, Madrid, Spain.

**ABSTRACT.** Permafrost controls geomorphic processes in ice-free areas of the Antarctic Peninsula (AP) region. Future climate trends will promote significant changes of the active layer regime and permafrost distribution, and therefore a better characterization of present-day state is needed. With this purpose, this research focuses on Ulu Peninsula (James Ross Island) and Byers Peninsula (Livingston Island), located in the area of continuous and discontinuous permafrost in the eastern and western sides of the AP, respectively. Air and ground temperatures in as low as 80 cm below surface of the ground were monitored between January and December 2014. There is a high correlation between air temperatures on both sites ( $r=0.74$ ). The mean annual temperature in Ulu Peninsula was  $-7.9^{\circ}\text{C}$ , while in Byers Peninsula was  $-2.6^{\circ}\text{C}$ . The lower air temperatures in Ulu Peninsula are also reflected in ground temperatures, which were between  $4.9$  (5 cm) and  $5.9^{\circ}\text{C}$  (75/80 cm) lower. The maximum active layer thickness observed during the study period was 52 cm in Ulu Peninsula and 85 cm in Byers Peninsula. Besides climate, soil characteristics, topography and snow cover are the main factors controlling the ground thermal regime in both areas.

### **Régimen termal de la capa activa en dos áreas climáticamente contrastadas de la Península Antártica**

**RESUMEN.** El permafrost controla los procesos geomorfológicos en las regiones libres de hielo de la Península Antártica (AP). Las tendencias climáticas futuras conllevarán cambios significativos en el régimen térmico de la capa activa y en la distribución del permafrost, y por ello, se necesita una mejor caracterización de su estado actual. Con este objetivo, esta investigación se centra en la Península Ulu (isla James Ross) y la Península Byers (isla Livingston), áreas emplazadas en zonas de permafrost continuo y discontinuo del este y oeste de la AP, respectivamente. Las temperaturas del aire y de suelo hasta 80 cm fueron monitorizadas

*entre enero y diciembre de 2014. Existe una alta correlación entre la temperatura del aire en ambos sitios ( $r = 0,74$ ). La temperatura media anual en la Península Ulu fue de  $-7,9^{\circ}\text{C}$ , mientras que en la Península Byers fue  $-2,6^{\circ}\text{C}$ . Las temperaturas del aire más frías registradas en la Península Ulu también se detectaron en las temperaturas del suelo, que fueron entre  $4,9$  (5 cm) y  $5,9^{\circ}\text{C}$  (75/80 cm) más frías. El espesor máximo de la capa activa durante el período de estudio fue de 52 cm de la Península Ulu y 85 cm en la Península Byers. Además del clima, las características del suelo, la topografía y la cubierta de nieve, son los principales factores que controlan el régimen térmico del suelo en ambas regiones.*

**Key words:** Antarctic Peninsula, James Ross Island, Livingston Island, active layer, air and ground temperatures.

**Palabras clave:** Península Antártica, isla James Ross, isla Livingston, capa activa, temperaturas de suelo y de aire.

Received: December, 13, 2015

Accepted: January, 22, 2016

\*Corresponding author: Marc Oliva, Centre for Geographical Studies – IGOT, Universidade de Lisboa, Alameda da Universidade, 1600-214, Lisboa, Portugal. E-mail: oliva\_marc@yahoo.com.

## 1. Introduction

The air temperature in the Antarctic Peninsula region (AP) increased locally by ca.  $2.5^{\circ}\text{C}$  since the mid-20th century (Turner *et al.*, 2005) with one of the fastest warming rates on Earth. In the ice-free areas of the AP region, this warming has had a significant impact on terrestrial and aquatic ecosystems (Bockheim *et al.*, 2013). Since the International Polar Year (2007-2009), an increasing interest of the cryospheric community has been directed towards understanding the active layer dynamics and permafrost distribution in the Antarctic Peninsula region. Most of the studies have focused on the western part of AP, mainly on the South Shetlands region (Ramos and Vieira, 2003; Ramos *et al.*, 2008; de Pablo *et al.*, 2013, 2014; Goyanes *et al.*, 2014), while only a few studies examined the state and characteristics of permafrost in the eastern part of AP (e.g. Hrbáček *et al.*, 2015). Over the last few years some studies provided a brief comparison between active layer conditions on the western and eastern sides of the AP summarizing primary information such as permafrost temperatures or maximum active layer thickness (ALT) (e.g. Vieira *et al.*, 2010; Bockheim *et al.*, 2013). However, these studies have not compared active layer thermal regimes in both regions.

This research focuses on two sites located on James Ross Island (eastern AP) and Livingston Island (western AP). While permafrost distribution is known to be continuous on James Ross Island (Davies *et al.*, 2013), it is discontinuous in the lowlands of the Livingston Island turning to continuous in elevations above 150 m (Vieira *et al.*, 2010). The main purpose of this study is the comparative examination of the ground thermal

regime on both sites in order to better understand the factors controlling active layer dynamics in the AP region.

## 2. Study sites

This work focuses on two large ice-free areas located on islands on both sides of the AP region: (a) Ulu Peninsula (ca. 180 km<sup>2</sup>), James Ross Island, eastern AP, and (b) Byers Peninsula (ca. 60 km<sup>2</sup>), Livingston Island, western AP (Figs. 1 and 2).

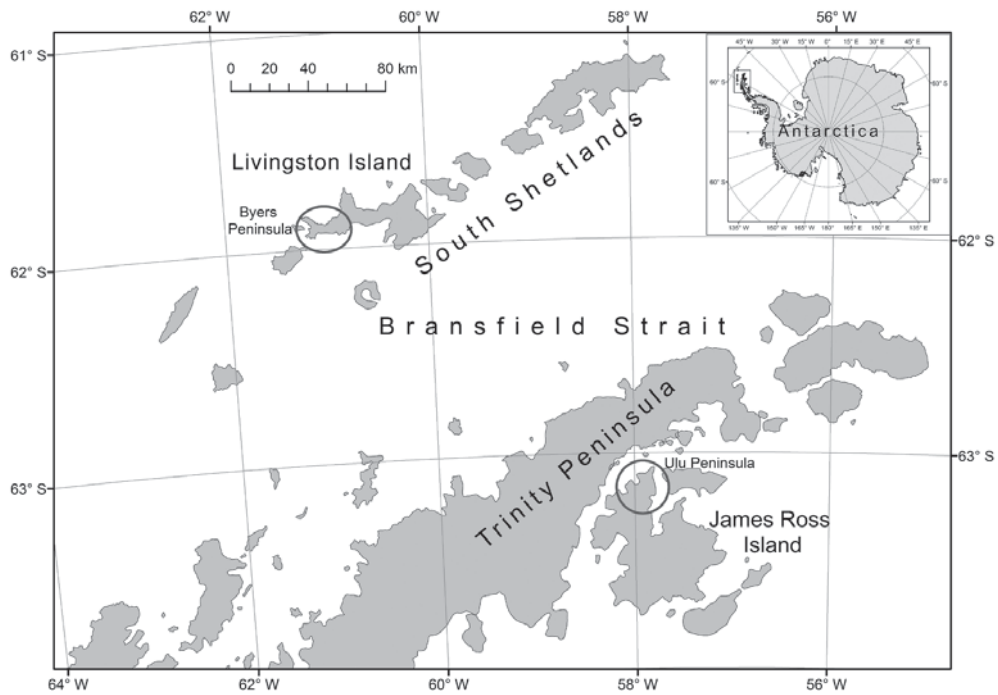


Figure 1. Location of Ulu Peninsula (James Ross Island) and Byers Peninsula (Livingston Island) in northern Antarctic Peninsula region.

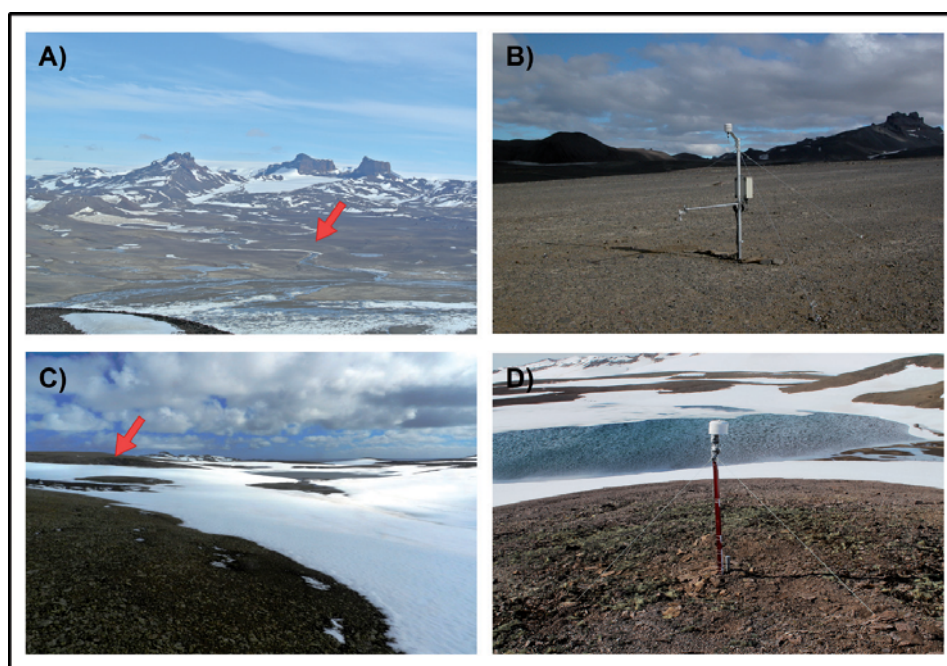


Figure 2. View to study sites and its vicinity at Ulu Peninsula (A, B) and Byers Peninsula (C, D).

### 2.1. James Ross Island - Ulu Peninsula

Climate of the Ulu Peninsula corresponds to semi-arid polar continental regime (Martin and Peel, 1978) with mean annual air temperature (MAAT) at sea level of  $-6.8^{\circ}\text{C}$  for the period 2006-2011 (Láska *et al.*, 2012). The annual amplitude of air temperatures exceeds  $40^{\circ}\text{C}$  with summer maxima  $>10^{\circ}\text{C}$  and winter minima  $<-30^{\circ}\text{C}$ . Precipitation shadow effect caused by Trinity Peninsula (Davies *et al.*, 2013) significantly affects precipitation, mainly in the form of snow during the winter season. The estimated annual precipitation is 400–500 mm (van Lipzig *et al.*, 2004), although high wind speeds cause irregular deposition and significant snow removal from the landscape (Nývlt *et al.*, 2016) and therefore the maximum thickness of snow layer does not exceed 0.3 m in flat areas (Zvěřina *et al.*, 2014; Hrbáček *et al.*, 2015).

The deglaciation of the lowermost parts of the Ulu Peninsula started around 12.9 ka (Nývlt *et al.*, 2014) and only small glaciers remained here until present days (Engel *et al.*, 2012). The landscape of the Ulu Peninsula has been, besides glacial erosion and accumulation, sculpted by paraglacial and periglacial processes (Davies *et al.*, 2013). Permafrost on Ulu Peninsula is continuous (Bockheim *et al.*, 2013) with an approximate thickness of 67 m according to geoelectrical measurements (Borzotta and Trombotto, 2004). ALT is strongly influenced by local lithology and varied between 52 and 85 cm on three sites during the period 2012-2015 (Hrbáček *et al.*, submitted). The study site on James Ross Island is located in the central flat part of Ulu Peninsula, at Abernethy Flats, 41 m a. s. l. on a flat terrain ( $<2^{\circ}$ ). (Table 1). Fine-grained calcareous sandstones and siltstones of the Alpha Member and Santa Marta Formation of Late Cretaceous age (Olivero *et al.*, 1986; Crame *et al.*, 1991) form study

site. The superficial part is generally weathered to form loose sandy regolith with occasional gravel clasts mostly of James Ross Island Volcanic Group basalts; finer fraction is generally blown away (Davies *et al.*, 2013). Vegetation cover is very scarce with concentration spots mostly along streams, or around seal carcasses (Nývlt *et al.*, 2016).

Table 1. Geographical characteristics of the study sites.

| Site                                      | Locality          | Latitude<br>Longitude      | Altitude<br>(m a. s. l.) | Slope |
|---|-------------------|----------------------------|--------------------------|-------|
| <b>Abernethy Flats,<br/>Ulu Peninsula</b> | James Ross Island | 63°52'30" S<br>58°57'10" W | 41                       | 0-2°  |
| <b>Domo, Byers<br/>Peninsula</b>          | Livingston Island | 62°37'19" S<br>60°58'33" W | 45                       | 0-2°  |

## 2.2. Livingston Island - Byers Peninsula

Byers Peninsula shows a cold and wet oceanic climate with MAAT of  $-2.8^{\circ}\text{C}$  at 70 m a. s. l. for the period 2002-2010. The maximum daily air temperature does not exceed  $10^{\circ}\text{C}$  with mean summer maximum of  $2.7^{\circ}\text{C}$ , while the minimum temperature during the winter rarely drops below  $-25^{\circ}\text{C}$ , with a mean winter daily minimum of  $-9.8^{\circ}\text{C}$  (Bañón *et al.*, 2013). Estimated precipitation is ca. 500-800 mm in the form of both rain and snow in the summer and snow in winter, resulting in snow cover for 8 to 9 months per year (Bañón *et al.*, 2013, Navarro *et al.*, 2013).

The Byers Peninsula is composed mainly of mudstone, sandstone, conglomerate and volcanic and volcanoclastic rocks of the Late Jurassic to Early Cretaceous age, intruded by igneous bodies (López-Martínez *et al.*, 1996). Vegetation cover is very scarce and mostly concentrated on the marine terraces surrounding the main plateau. Byers Peninsula constitutes the largest ice-free area of the South Shetland Islands (SSI), with ca.  $60\text{ km}^2$ . The area has been deglaciated during the Holocene following the eastward retreat of the Rotch Dome glacier (Oliva *et al.*, accepted). The relief of Byers is organized around a central plateau (70-100 m) surrounded by Holocene marine terraces and the present-day beaches, with a few isolated hills exceeding an elevation of 140 m rising above the plateau (López-Martínez *et al.*, 2012). A wide range of periglacial processes and landforms are distributed across the ice-free landscape of Byers Peninsula. The study site is located near Domo Lake, at 45 m a. s. l., on a flat hilltop above the lake with an inclination of 0-2° (Table 1). Soils have a very low organic matter content and are composed of coarse-grained sediments, with abundant gravels in a sandy-silty matrix, which conditions water circulation through the soil in summer (Navas *et al.*, 2008). The area is continuously affected by very strong winds that effectively redistribute snow cover.

## 3. Material and Methods

This study analyses the data obtained during the period from 29 January 2014 to 5 January 2015 on the two aforementioned sites. The study period was constrained by the availability of data from Byers Peninsula. Two sets of devices were used to monitor ground and air temperatures on each site (Table 2).

Table 2. Main characteristics of the devices used in this research.

| Locality                           | Type            | Sensor            | Height/depth (m)      | Resolution (°C) | Accuracy (°C) |
|------------------------------------|-----------------|-------------------|-----------------------|-----------------|---------------|
| James Ross Island, Ulu Peninsula   | Air temperature | EMS 33            | 2.0                   | 0.01            | 0.15          |
|                                    | Soil profile    | Pt100             | 5, 10, 20, 40, 50, 75 | 0.01            | 0.15          |
| Livingston Island, Byers Peninsula | Air temperature | Tynitag           | 1.5                   | 0.02            | 0.25          |
|                                    | Borehole        | Ibutton (DS1922L) | 5, 10, 20, 40, 60, 80 | 0.0625          | 0.5           |

Air temperature in Ulu Peninsula was measured at 2.0 m above ground using EMS 33 sensor and ground temperature was measured using platinum resistance probes Pt100/8 installed along a profile at depths of 5, 10, 20, 30, 40, 50 and 75 cm. Sensors were connected to a V12 data logger (EMS Brno) recording data every 30 minutes. In Byers Peninsula, air temperature was measured at 1.5 m above ground using Tynitag (Plus 2) sensor and ground temperatures were monitored with a chain of iButtons DS1922L thermometers at depths of 5, 10, 20, 40, 60 and 80 cm placed inside a sealed PVC-cased borehole. Air and ground temperatures were measured every 120 minutes.

Raw data was used for the calculation of daily mean, maximum and minimum temperatures and amplitude values. Ground temperatures were plotted as isopleths using the kriging interpolation approach in Surfer 11 software (Golden Software), which allowed comparison between sites. Small differences for deeper level temperatures on the two sites are because the lowest loggers are set up at 75 and 80 cm at Ulu Peninsula and Byers Peninsula respectively (referred to 75/80 cm throughout the text). Ground thermal dynamics for each depth was described using following thermal parameters commonly used in recent studies on active layer properties in the AP (e.g. Guglielmin *et al.*, 2008; de Pablo *et al.*, 2013; Hrbáček *et al.*, submitted; Oliva *et al.*, submitted).

1. The thawing and freezing seasons were defined from the daily thermal regime at 5 cm. Our data was limited to the end of thawing season 2013/14 and beginning of thawing season 2014/15.
2. The active layer thickness was determined using the deepest position of the 0°C isotherm by interpolation (Ulu Peninsula) and extrapolation (Byers Peninsula), respectively.
3. Thawing degree-days (TDD) and freezing degree-days (FDD) were calculated as sums of mean daily temperatures above 0°C and below 0°C, respectively for both air temperature (TDD<sub>A</sub>/FDD<sub>A</sub>) and ground temperature (TDD<sub>G</sub>/FDD<sub>G</sub>).
4. Thawing days are days with minimum temperature above 0.5°C; freezing days are days with maximum temperature below -0.5°C; freeze-thaw days show both maximum above 0.5°C and minimum below -0.5°C; and isothermal days show daily temperatures between 0.5°C and -0.5°C.

The freezing n-factor is a ratio between  $FDD_G$  and  $FDD_A$  at 5 cm for indirect determination of snow cover effect on ground temperature during freezing season (Karunaranth and Burn, 2003). The thawing n-factor was calculated separately for the period before 29 January to 31 October 2014, which represents the end of thawing seasons 2013/14 and for the period 1 November 2014 to 5 January 2015 representing the early beginnings of thawing season 2014/15. TDD during freezing season was found as negligible, therefore this period was added to thawing seasons 2013/14.

Finally, correlation analysis to compare daily means for both air and ground temperature at 5 cm between Ulu Peninsula and Byers Peninsula has been undertaken to determine the relationship of these factors. All results showed significant relationship in level of significance 0.01.

## 4. Results

### 4.1. Ulu Peninsula

The main characteristics of both air and ground temperatures at Ulu Peninsula for 29 January 2014 to 5 January 2015 are presented in Table 3 and Fig. 3a, 3b. Mean air temperatures averaged  $-7.9^{\circ}\text{C}$ , with a maximum of  $12.3^{\circ}\text{C}$  (1 November) and a minimum of  $-32.9^{\circ}\text{C}$  (18 August). Consequently, the annual amplitude of air temperatures reached  $45.2^{\circ}\text{C}$ . The warmest month was December, with a mean air temperature of  $-1.0^{\circ}\text{C}$  and the coldest one was August ( $-16.0^{\circ}\text{C}$ ). During the entire study period  $TDD_A$  reached  $140^{\circ}\text{Cday}$ , from which  $TDD_A$   $37^{\circ}\text{Cday}$  (29 January to 7 March) and  $21^{\circ}\text{Cday}$  (26 November to 5 January) while  $TTD_A$   $82^{\circ}\text{Cday}$  were observed during freezing seasons (8 March to 25 November).  $FDD_A$  reached  $-2528^{\circ}\text{Cday}$ , from which  $-2385^{\circ}\text{Cday}$  were recorded during the freezing season (Fig. 4).

Table 3. Basic statistics of air temperature (AT) and ground temperature (GT) at Ulu Peninsula and Byers Peninsula in period 29 January 2014 to 5 January 2015.

| Parameter | Ulu Peninsula |      |       | Byers Peninsula |      |       |
|-----------|---------------|------|-------|-----------------|------|-------|
|           | Mean          | Max  | Min   | Mean            | Max  | Min   |
| AT        | -7.9          | 12.3 | -32.9 | -2.6            | 6.1  | -13.5 |
| GT 5 cm   | -6.2          | 21.1 | -18.6 | -1.3            | 17.9 | -9.9  |
| GT 10 cm  | -6.5          | 12.7 | -17.5 | -1.2            | 7.0  | -7.7  |
| GT 20 cm  | -6.3          | 7.7  | -15.9 | -1.1            | 4.6  | -5.5  |
| GT 40 cm  | -6.3          | 2.6  | -14.2 | -0.9            | 3.8  | -3.7  |
| GT 50 cm  | -6.4          | 0.3  | -13.4 | --              | --   | --    |
| GT 60 cm  | --            | --   | --    | -0.8            | 2.5  | -2.9  |
| GT 75 cm  | -6.6          | -0.9 | -12.4 | --              | --   | --    |
| GT 80 cm  | --            | --   | --    | -0.7            | 0.2  | -2.4  |

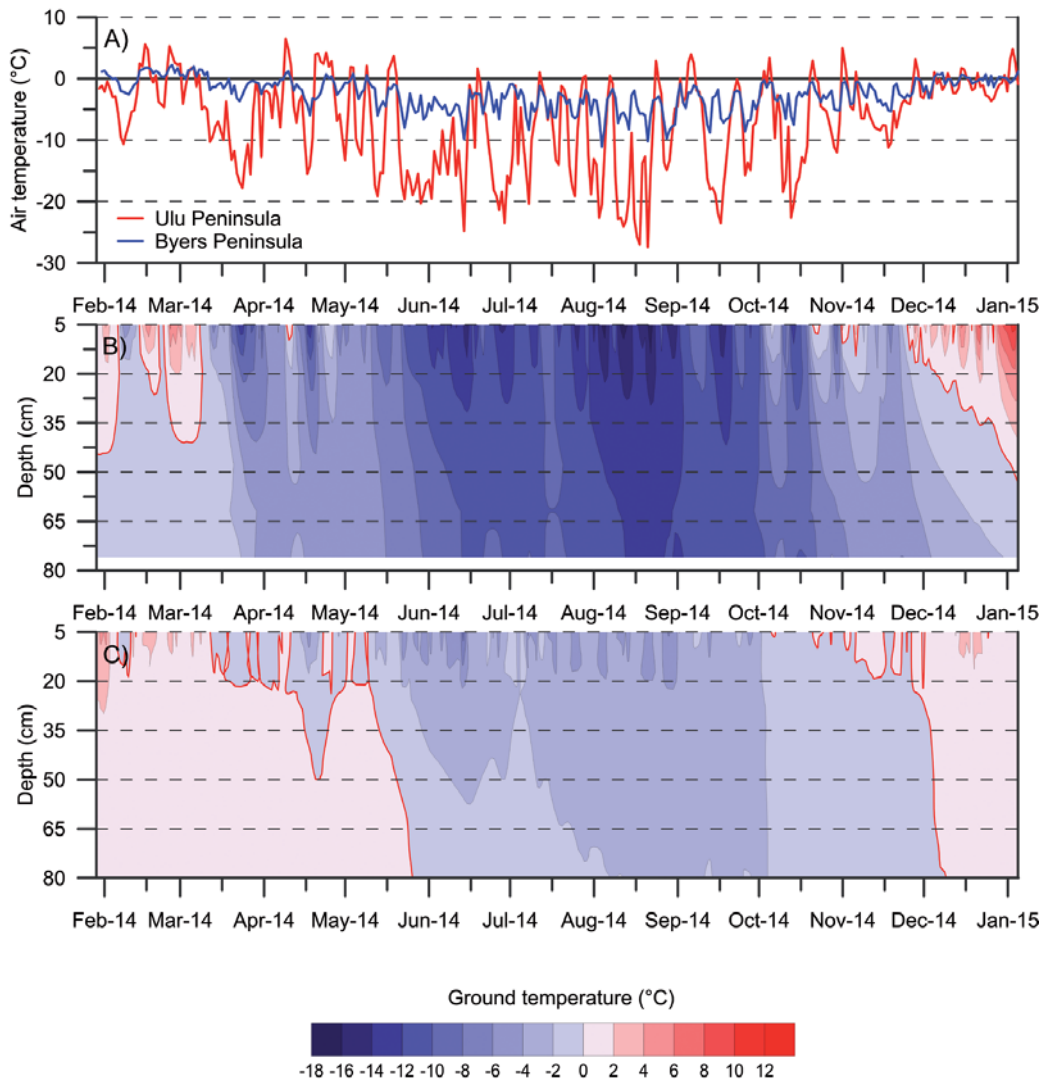


Figure 3. Variability of mean daily air temperature (a) and ground temperature at Ulu Peninsula (b) and Byers Peninsula (c) in period 29 January 2014 to 5 January 2015. Red lines in (b) and (c) plots represent 0°C isotherm.

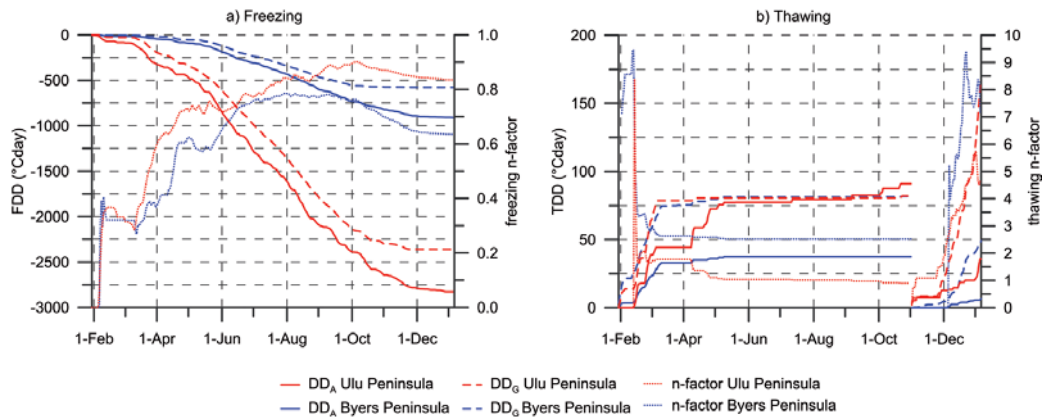


Figure 4. Seasonal evolution of freezing ( $FDD$ ) and thawing ( $TDD$ ) degree days ( $DD$ ) of air temperature ( $AT$ ) and ground temperature ( $GT$ ) and freezing and thawing  $n$ -factor at Ulu Peninsula and Byers Peninsula in 2014.

Mean ground temperatures during the study period gradually decreased with depth from  $-6.2^{\circ}\text{C}$  (5 cm) to  $-6.6^{\circ}\text{C}$  (75 cm) (Table 3, Fig. 5a). Similarly, maximum ground temperatures decreased from  $21.1^{\circ}\text{C}$  at 5 cm (3 January) to  $-0.9^{\circ}\text{C}$  at 75 cm (13 March), as well as minimum ground temperature, which ranged between  $-18.6^{\circ}\text{C}$  at 5 cm (22 August) and  $-12.4^{\circ}\text{C}$  at 75 cm (25 August). The highest mean monthly ground temperature from 5 to 40 cm depth was observed in December ( $3.3^{\circ}\text{C}$  at 5 cm to  $-0.3^{\circ}\text{C}$  at 40 cm) while at 50 cm ( $-0.6^{\circ}\text{C}$ ) and 75 cm ( $-1.4^{\circ}\text{C}$ ) was in February.

The end of the thawing season 2013/14 occurred between 29 January and 7 March 2014 while the beginning of the thawing season 2014/15 encompassed period from 26 November 2014 to 5 January 2015. There was only one day between refreezing at depths 5-10 cm (7 March) and 20-30 cm (8 March), while the active layer at lower depths (40 to 75 cm) was already frozen by the end of thawing season 2013/14. The thawing of the active layer started in 26 November and reached 50 cm until 3 January 2015.

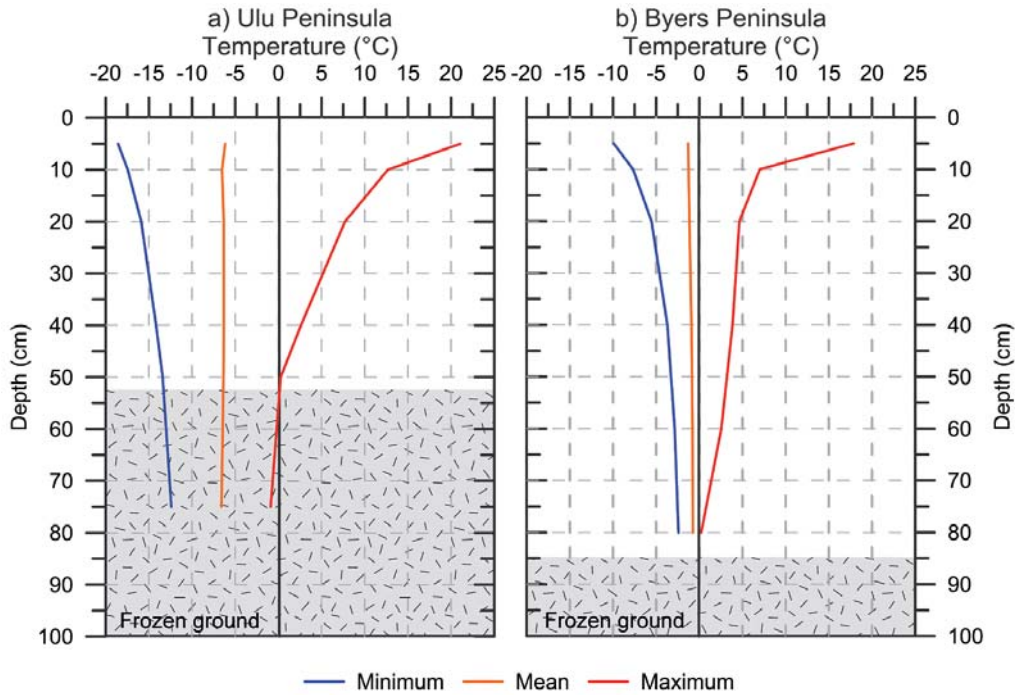


Figure 5. Vertical profiles of ground temperature at Ulu Peninsula (a) and Byers Peninsula (b) in 2014.

ALT reached 52 cm during the thawing season 2014/15 (5 January 2015), and only 45 cm during the thawing season 2013/14 (29 January 2014). Active layer remained frozen during the freezing season (8 March to 25 November), with only several days in March and November during which a thin near-surface layer up to 5 cm thawed.

The main thermal parameters for Ulu Peninsula are summarized in Table 4, showing large variability with depth.  $TDD_G$  rapidly decreased from 5 cm (251.1°Cday) to 40 cm (13°Cday) and was not observed at 75 cm. The regime of  $TDD_G$  at 5 cm was similar to  $TDD_A$ . In total,  $TDD_G$  at 5 cm reached 81°Cday before 7 March while 159°Cday after 26 November. Thawing n-factor varied between 1.77 (end of thawing season 2014/15) and 4.65 (beginning of thawing seasons 2014/15) (Fig. 4b).  $TDD_G$  at 5 cm reached only 12°Cday during freezing season. Although the  $TDD_G$  were highest at 5 cm, the number of thawing days was maximum at 20 cm with 25 days observed. (Table 4).

Table 4. Thermal characteristics of active layer at Ulu Peninsula and Byers Peninsula in period 29 January 2014 to 5 January 2015.

| Site            | Depth | TDD | TD | FDD   | FD  | FT-D | IT-D |
|-----------------|-------|-----|----|-------|-----|------|------|
| Ulu Peninsula   | 5 cm  | 251 | 11 | -2361 | 223 | 35   | 0    |
|                 | 10 cm | 144 | 16 | -2378 | 267 | 24   | 0    |
|                 | 20 cm | 85  | 25 | -2250 | 268 | 0    | 5    |
|                 | 40 cm | 13  | 5  | -2176 | 277 | 0    | 25   |
|                 | 50 cm | 0   | 0  | -2176 | 318 | 0    | 9    |
|                 | 75 cm | 0   | 0  | -2257 | 342 | 0    | 0    |
| Byers Peninsula | 5 cm  | 134 | 22 | -577  | 147 | 48   | 37   |
|                 | 10 cm | 82  | 33 | -507  | 153 | 6    | 88   |
|                 | 20 cm | 61  | 30 | -453  | 160 | 0    | 123  |
|                 | 40 cm | 55  | 35 | -366  | 161 | 0    | 135  |
|                 | 60 cm | 42  | 8  | -312  | 178 | 0    | 151  |
|                 | 80 cm | 27  | 0  | -280  | 182 | 0    | 159  |

TD – number of thawing days

FD – number of freezing days

FT-D – number of freeze-thawing days

IT-D – number of isothermal days

Contrary to  $TDD_G$ ,  $FDD_G$  increased with depth from 5 cm (-2361°Cday) to 40 cm (-2176°Cday) and decreased down to 75 cm (-2257°Cday). Freezing n-factor reached 0.82 in December, though the value ranged between 0.70 and 0.90 during the winter months (Fig. 4a). The total number of freezing days gradually increased from 5 cm (223 days) to 75 cm (342 days). Isothermal days characterized by low amplitude of ground temperature around 0°C were observed between 20 and 50 cm, with the maximum at 40 cm (25 days). On the other hand, freeze-thawing days were detected at near-surface layer, only at 5 and 10 cm depths. The scatter of freeze-thawing days was very small comparing the end of the thawing season 2013/14 from February to April (17 freeze-thawing days) and the early beginning of the thawing season 2014/15 from October to December (18 freeze-thawing days). Freeze-thawing days occurred most frequently in November (9 days), while in April and October only 4 days were recorded (Fig. 6a).

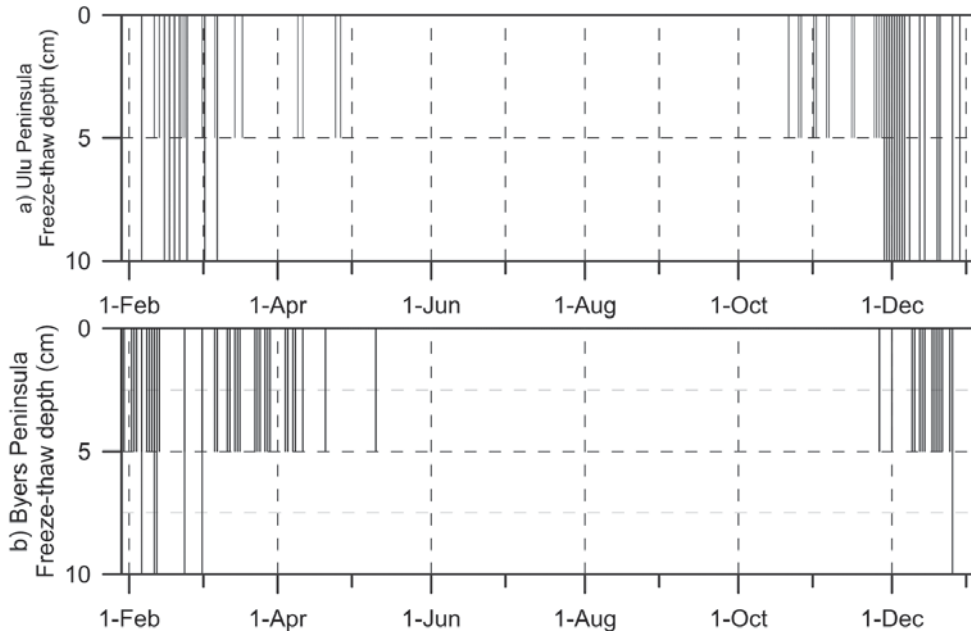


Figure 6. Freezing-thawing days calendar at depths 5 and 10 cm at Ulu Peninsula (a) and Byers Peninsula (a) in 2014.

#### 4.2. Byers Peninsula

The main thermal characteristics recorded during the study period in Byers Peninsula are presented in Table 3 and Fig. 3a, 3c. The mean air temperature during study period reached  $-2.6^{\circ}\text{C}$ . The maximum air temperature reached  $6.5^{\circ}\text{C}$  (24 December), while the minimum dropped to  $-13.5^{\circ}\text{C}$  (4 August) making thus an annual amplitude of only  $20.0^{\circ}\text{C}$ . The highest mean monthly air temperature was recorded in February ( $0.3^{\circ}\text{C}$ ), while the coldest month was August ( $-5.6^{\circ}\text{C}$ ). The  $\text{TDD}_A$  reached only  $44^{\circ}\text{Cday}$ , with an irregular distribution between the thawing periods 2013/14 from 29 January to 12 March ( $33^{\circ}\text{Cday}$ ) and from 2 November to 5 January ( $7^{\circ}\text{Cday}$ ). The total sum of  $\text{FDD}_A$  reached  $-909^{\circ}\text{Cday}$ , from which  $-808^{\circ}\text{Cday}$  was calculated for the freezing season (13 March to 1 November).

The average ground temperatures during the study period slightly increased with depth from  $-1.3^{\circ}\text{C}$  at 5 cm to  $-0.7^{\circ}\text{C}$  at 80 cm (Table 3, Fig. 5b). The maximum ground temperatures reached  $17.9^{\circ}\text{C}$  at 5 cm (20 December) and decreased with depth to  $0.2^{\circ}\text{C}$  at 80 cm (from 29 January to 22 May). The minimum ground temperature of  $-9.9^{\circ}\text{C}$  was recorded at 5 cm (14 June), while the minimum at 80 cm was  $-2.4^{\circ}\text{C}$  (1-3 September). The highest mean monthly ground temperature was recorded in February at depths from 5 cm ( $1.6^{\circ}\text{C}$ ) to 60 cm ( $0.5^{\circ}\text{C}$ ), while at 80 cm mean monthly ground temperature reached  $0.2^{\circ}\text{C}$ , same value as maximum, due to constant ground temperature from February to April.

The thawing season 2013/14 ended on 12 March, though the active layer re-thawed at 5 cm depth during several events until 5 May. The deeper layers of the profile remained thawed until 26 May, when the active layer at 80 cm frozen. The beginning of the thawing season 2014/15 occurred on 2 November; however, there was not sharp boundary between freezing and thawing seasons similarly as the end of thawing seasons 2013/14. Active layer thawing events were observed since 6 October. ALT reached 85 cm during the thawing season 2013/14 and 82 cm during the beginning of the thawing season 2014/15.

The  $TDD_G$  gradually decreased with depth from  $134^{\circ}\text{Cday}$  (5 cm) to  $27^{\circ}\text{Cday}$  (80 cm). Most of the  $TDD_G$  were detected before 12 March ( $78^{\circ}\text{Cday}$ ), while only  $49.0^{\circ}\text{Cday}$  after 2 November. Thawing n-factor varied between 2.63 (end of thawing season 2014/15) and 7.15 (beginning of thawing seasons 2014/15). The  $TDD_G$  at 5 cm reached  $7.0^{\circ}\text{Cday}$  only during freezing season (Fig. 4b). The number of thawing days gently increased from 5 cm (22 days) to 40 cm (35 days), decreasing to only 8 days at 60 cm (Table 4).

The  $FDD_G$  increased with depth from 5 cm ( $-577^{\circ}\text{Cday}$ ) to 80 cm ( $-280^{\circ}\text{Cday}$ ). The freezing n-factor reached 0.64 in December, while it ranged from 0.75 to 0.78 during the winter season from June to September (Fig. 4b). Similarly, the total number of freezing days ( $FDD_G$ ) increased from 147 days at 5 cm to 182 days at 80 cm. The highest occurrence of isothermal days (159) was observed at 80 cm and gradually decreased to 37 days at 5 cm (Table 4). The freeze-thawing days were only detected at 5 and 10 cm (Fig. 6b). In total, up to 48 freeze-thaw days were recorded at 5 cm unevenly distributed between the period before mid-May (34 days) and the period from November to December (14 days). The total number of freeze-thaw days at 10 cm was significantly lower, with only 6 days: 5 in February and only 1 day in December.

## 5. Discussion

The studied sites at Ulu Peninsula and Byers Peninsula have similar topography, but are located in different climate settings, which make them suitable for ground thermal regime inter-comparison.

### 5.1. Air temperature differences

The air temperature over period February 2014 to January 2015 ( $-2.6^{\circ}\text{C}$ ) in Byers Peninsula was similar as MAAT ( $-2.6^{\circ}\text{C}$ ) in the period 2007 to 2012, during which MAAT ranged between  $-1.7^{\circ}\text{C}$  and  $-3.3^{\circ}\text{C}$  (Bañón *et al.*, 2013; de Pablo *et al.*, 2014). Generally, the interannual differences of air temperatures on Livingston Island are lower than on Ulu Peninsula. Here, mean air temperature during the study period ( $-7.9^{\circ}\text{C}$ ) was slightly lower than MAAT at Abernethy Flats over the period of 2006-2014 ( $-7.5^{\circ}\text{C}$ ), however the MAAT varied between  $-5.0^{\circ}\text{C}$  and  $-10.3^{\circ}\text{C}$  (Hrbáček *et al.*, submitted, unpublished data). From this point of view, air temperatures at both sites were very close to average thermal conditions during last several years.

The differences in the regime of air temperatures between both sites are shown in Fig. 3a and Table 3. The mean period air temperature was 4.4°C higher in Byers Peninsula, though the absolute maximum air temperature was 6.2°C higher at Ulu Peninsula. Remarkably, the minimum air temperature was 19.4°C lower at Ulu Peninsula. In general, the air temperature regime at Ulu Peninsula corresponds to a more continental climate pattern, with high oscillations of mean daily temperatures ranging between -25°C and 5°C during winter, while in Byers Peninsula daily temperatures during this season typically ranged between -10°C and 0°C (Fig. 3). The different climate resulted in substantial differences in daily mean air temperatures between Ulu Peninsula and Byers Peninsula, which varied between -21.2°C to 7.4°C (Fig. 7).

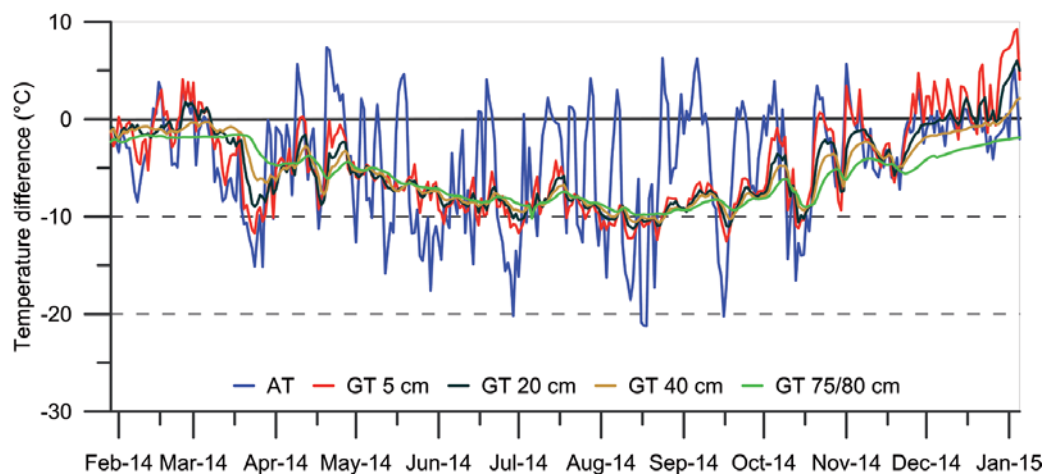


Figure 7. Differences of mean daily air temperature (AT) and ground temperature (GT) at 5, 20, 40 and 75/80 cm between Ulu Peninsula and Byers Peninsula in 2014.

The different climate conditions were well documented by the  $TDD_A$  and  $FDD_A$ .  $TDD_A$  was higher by 96°Cday at Ulu Peninsula during the study period. The main differences were observed during freezing seasons ( $TDD$  higher by 78°Cday at Ulu Peninsula) and between 1 November and 5 January ( $TDD$  higher by 14°Cday). On the other hand,  $FDD_A$  was -1920°Cday lower in Ulu Peninsula.

Despite significant differences observed in the variability of air temperatures, the correlation between mean daily temperatures at Ulu Peninsula and Byers Peninsula resulted in  $r=0.74$ , without any time-lag (Fig. 8c). This partly confirms the modelled results of King and Comiso (2003) which suggested a correlation of  $r>0.75$  between James Ross Island and the South Shetland Islands during the winter months.

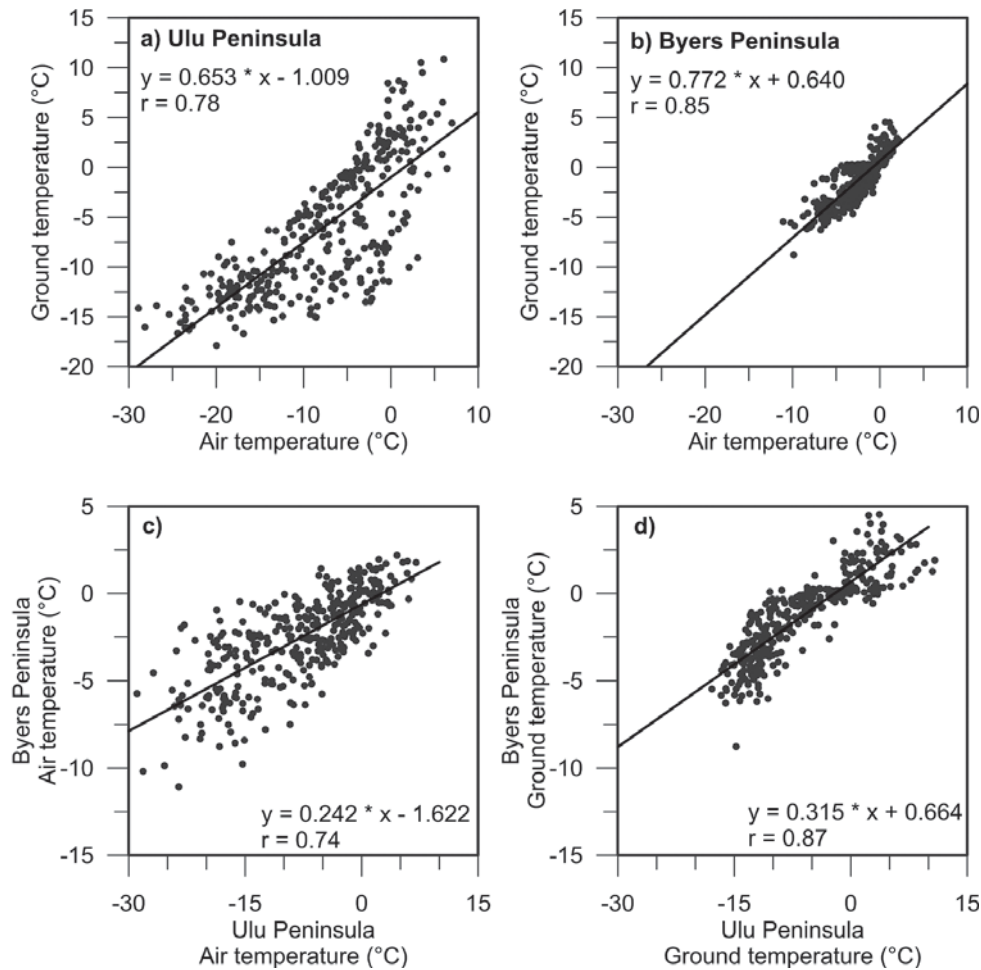


Figure 8. Correlation analysis of mean daily air temperature vs mean daily ground temperature 5 cm at Ulu Peninsula (a) and Byers Peninsula (b); mean daily air temperatures (c) and mean daily ground temperatures (d) at Ulu Peninsula vs Byers Peninsula in 2014.

## 5.2. Ground temperature

Two very different active layer thermal regimes were observed in Ulu Peninsula and Byers Peninsula. The mean period ground temperature was lower at Ulu Peninsula ( $-4.9^{\circ}\text{C}$  at 5 cm and  $-5.9^{\circ}\text{C}$  at 75/80 cm), showing warmer ground in Byers Peninsula. The ground temperature at 5 and 20 cm was  $12.5^{\circ}\text{C}$  higher in Byers Peninsula between 11 April and 22 October, but in December was  $9.3^{\circ}\text{C}$  higher in Ulu Peninsula. Ground temperatures at 40 cm depth were up to  $10.5^{\circ}\text{C}$  higher during the period 29 January to 30 December at Byers Peninsula and the difference at 75/80 cm depth was between 1.6 and  $10.2^{\circ}\text{C}$ , always warmer in Byers Peninsula (Fig. 7).

Despite the lower mean period ground temperature, maximum ground temperatures and  $TDD_G$  were higher in the upper 20 cm in Ulu Peninsula, while the maximum and TDD at lower depths, were higher in Byers Peninsula. The most pronounced differences were observed in the development of  $TDD_G$  at 5 cm. Its total sum in Ulu Peninsula ( $251^\circ\text{Cday}$ ) was almost twice higher than Byers Peninsula ( $134^\circ\text{Cday}$ ). During the period from 1 November 2014 to 5 January 2015 the TDD reached more than three times higher values in Ulu Peninsula ( $167^\circ\text{Cday}$ ) than in Byers Peninsula ( $49^\circ\text{Cday}$ ). However, the lower levels were significantly warmer in Byers Peninsula, where the total sum of the  $TDD_G$  decreased gently with depth up to  $27^\circ\text{Cday}$  at 80 cm, while the  $TDD_G$  decreased very rapidly to  $0^\circ\text{Cday}$  only at 50 cm depth in Ulu Peninsula. Similarly, the total number of thawing days increased with depth up to 40 cm (with 8 days observed at 60 cm in Byers Peninsula), while the increment of thawing days was observed up to 20 cm (with 5 days only at 40 cm in Ulu Peninsula).

The most significant differences between both sites are related to the thawing seasons 2013/14 and 2014/15. Although the thawing season 2013/14 at 5 cm ended in 12 March, the active layer in the deeper parts of the profile remained unfrozen until 26 May, with a maximum thickness estimated at 85 cm in Byers Peninsula. In contrast, in Ulu Peninsula active layer, completely froze between 7 (5-10 cm) and 8 (20-30 cm) March and reached maximum ALT (45 cm) in 29 January. The thawing season 2014/15 started between 2 November (Byers Peninsula) and 26 November (Ulu Peninsula). Despite higher temperatures and rapidly increasing TDD at near-surfaces depths was observed at Ulu Peninsula, active layer thawed much more quickly in Byers Peninsula, and a thickness of ca. 82 cm was detected at the beginning of December, while only 52 cm was observed at Ulu Peninsula in 5 January 2015.

The mean daily temperature could drop below  $-14^\circ\text{C}$  at 40 cm depth in Ulu Peninsula, while ground temperature did not drop below  $-4^\circ\text{C}$  at the same depths in Byers Peninsula. Very intensive active layer freezing was observed in Ulu Peninsula as suggested by the  $FDD_G$ , about four times lower at 5 cm and even eight times lower at 75/80 cm comparing to Byers Peninsula. Similarly, the number of freezing days was significantly higher in Ulu Peninsula with respect to Byers Peninsula: 223 vs. 147 (5 cm) to 342 vs. 182 (75/80 cm) days.

### 5.3. Factors affecting the active layer thermal regime

The data confirms earlier results and conclusions suggesting significant differences both in air temperatures and in active layer thermal dynamics between ice-free areas in the eastern and western sides of the AP (Bockheim *et al.*, 2013; Hrbáček *et al.*, 2015). However, this study is the first comparison between ground thermal regimes on two sites within these regions.

The differences of the active layer thermal regime between both sites were highly affected by differences of air temperatures. In both sites a close relationship was found between air temperature and ground temperatures, reaching  $r=0.78$  and  $r=0.85$  at Ulu Peninsula and Byers Peninsula, respectively (Fig. 8a, b). This suggests air temperature

as very important driver affecting daily regime of ground temperature during the whole year. The flattening of scatter plots around 0°C, which is typical for snowy conditions, was only limited in case of Byers Peninsula (Fig. 8b). Analysing the relationship between mean daily ground temperatures at 5 cm in Ulu Peninsula and Byers Peninsula showed even a closer correlation of  $r=0.87$  than was determined for air temperature, which reveals similar patterns of near-surface thermal regime in both sites (Fig. 8d).

Snow cover, thickness and duration, is of paramount importance for the ground thermal regime. Although snow cover data were not available for both sites, freezing n-factors were used as indicators of the presence of snow. The freezing n-factor around 0.90 during the winter months showed a very limited insulating effect of snow in Ulu Peninsula, which is typical for this area (Hrbáček *et al.*, 2015). Lower value of freezing n-factor, around 0.60, suggests a more significant effect of snow as thermal insulator in Byers Peninsula. However, other studies in Byers Peninsula showed even lower n-factors, around 0.30, typical for sites or seasons with longer persistence of snow cover thicker than 60 cm (de Pablo *et al.*, 2013). While there were no studies describing the active layer thermal regime under significantly different snow conditions on James Ross Island, the active layer was found thicker (ca. 130 to 150 cm) on sites with more persistent snow cover with thickness more than 60 cm at South Shetlands (de Pablo *et al.*, 2014; Oliva *et al.*, submitted).

An important but still very little known factor affecting active layer thermal regime is local lithology. A preliminary study suggests lithological and physical properties are the most important factors causing local differences in active layer thermal regime and its thickness on James Ross Island (Hrbáček *et al.*, submitted). Similarly, the lithology was found very important factor affecting active layer thermal regime and its thickness on Livingston Island. In different sites of Livingston Island, Hurd Peninsula, Ramos and Vieira (2009) modelled ALT in bedrock ranging even between 2 and 5 m.

## 6. Conclusions

This study presents a preliminary analysis of air and ground temperatures during 2014 in two sites of the western (Byers Peninsula, Livingston Island) and eastern part (Ulu Peninsula, James Ross Island) of the Antarctic Peninsula. The comparison provides a better understanding of the main patterns of active layer thermal regime in both regions and gives insights about the factors controlling ground temperatures, which can be summarized as follows:

1. Both areas are affected by different type of climate regimes. Higher mean air temperatures were recorded in Livingston Island (-2.6°C), with lower temperature amplitude (20°C), while in James Ross Island mean annual air temperatures were significantly lower (-7.9°C), although with a higher amplitude (45.2°C).
2. The mean ground temperatures at 5 cm were significantly higher in Livingston Island (-1.3°C) than in James Ross Island (-6.2°C), while the TDD<sub>G</sub> at 5 cm

was much higher at James Ross Island (251 °Cday) than at Livingston Island (134°Cday).

3. In Livingston Island, thaw depth varied between 82 (15 December 2014 to 5 January 2015) and 85 cm (29 January 2014 to 24 May 2014). In James Ross Island, the active layer thickness ranged between 45 cm (29 January 2014) and 52 cm (2015).

This preliminary work will be complemented during the coming years with more intensive collaboration and coordination between research teams working on South Shetlands and James Ross Island on active layer characteristics in the AP region. Although we found that the active layer thermal regime at near-surface depths in both sites was strongly affected by air temperature (high correlations between mean daily temperatures on Livingston Island and James Ross Island have been found), other parameters such as lithology, moisture, snow cover thickness and persistence probably have a major effect on the variability of the active layer dynamics. These preliminary findings will be complemented in future studies for a better understanding of the active layer dynamics across the AP region.

### Acknowledgements

We acknowledge the Johann Gregor Mendel Station for logistical support. We are very grateful to the members of the summer expeditions in 2014 and 2015 for their company and field assistance on JRI. The work was supported by the Masaryk University project MUNI/A/561 1370/2014: Global environmental changes in time and space; research project HOLOANTAR (Holocene environmental change in the Maritime Antarctic. Interactions Between permafrost and the lacustrine environment) and the Portuguese Polar Program (PROPOLAR), both funded by the Portuguese Science Foundation. M. Oliva acknowledges the AXA Research Fund for sponsoring his research activities in Antarctica.

### References

- Bañón, M., Justel, A., Velázquez, A., Quesada, A. 2013. Regional weather survey in Byers Peninsula, Livingston Island, South Shetland Islands, Antarctica. *Antarctic Science* 25, 146-156.
- Bockheim, J., Vieira, G., Ramos, M., López-Martínez, J., Serrano, E., Guglielmin, M., Wilhelm, K., Nieuwendam, A. 2013. Climate warming and permafrost dynamics in the Antarctic Peninsula region. *Global and Planetary Change* 100, 215-223.
- Borzotta, E., Trombotto, D. 2004. Correlation between frozen ground thickness measured in Antarctica and permafrost thickness estimated on the basis of the heat flow obtained from magnetotelluric soundings. *Cold Region Science and Technology* 40, 81-96.
- Crame, J.A., Pirrie, D., Riding, J.B., Thomson, M.R.A. 1991. Campanian–Maastrichtian (Cretaceous) stratigraphy of the James Ross Island area, Antarctica. *Journal of the Geological Society of London* 148, 1125-1140.
- Davies, B.J., Glasser, N.F., Carrivick, J.L., Hambrey, M.J., Smellie, J.L., Nývlt, D. 2013. Landscape evolution and ice-sheet behaviour in a semi-arid polar environment: James Ross Island, NE

- Antarctic Peninsula. In Hambrey, M.J., Barker, P.F., Barrett, P.J., Bowman, V.C., Davies, B.J., Smellie, J.L., Tranter, M. (eds.), *Antarctic palaeoenvironments and earth surface processes*. Geological Society Special Publication 381, Geological Society of London, London, 353-395.
- De Pablo, M.A., Blanco, J.J., Molina, A., Ramos, M., Quesada, A., Vieira, G. 2013. Interannual active layer variability at the Limnopolar Lake CALM site on Byers Peninsula, Livingston Island, Antarctica. *Antarctic Science* 25, 167-180.
- De Pablo, M.A., Ramos, M., Molina, A. 2014. Thermal characterization of the active layer at the Limnopolar Lake CALM-S site on Byers Peninsula (Livingston Island), Antarctica. *Solid Earth* 5, 721-739.
- Engel, Z., Nývlt, D., Láska, K. 2012. Ice thickness, bed topography and glacier volume changes on James Ross Island, Antarctic Peninsula. *Journal of Glaciology* 58, 904-914.
- Guglielmin, M., Evans, C.J.E., Cannone, N. 2008. Active layer thermal regime under different vegetation conditions in permafrost areas. A case study at Signy Island (Maritime Antarctica). *Geoderma* 144, 73-85.
- Goyanes, G., Vieira, G., Caselli, A., Mora, C., Ramos, M., de Pablo, M.A., Neves, M., Santos, F., Bernardo, I., Gilichinsky, D., Abramov, A., Batista, V., Melo, R., Nieuwendam, A., Ferreira, A., Oliva, M. 2014. Régimen térmico y variabilidad espacial de la capa activa en isla Decepción, Antártida. *Revista de la Asociación Geológica Argentina* 71 (1), 112-124.
- Hrbáček, F., Láska, K., Engel, Z. (early view). Effect of snow cover on active-layer thermal regime – a case study from James Ross Island, Antarctic Peninsula. *Permafrost and Periglacial Processes*. Doi: 10.1002/ppp.1871.
- Hrbáček, F., Nývlt, D., Láska, K. (submitted). Active layer thermal dynamics at two lithologically different sites on James Ross Island, Eastern Antarctic Peninsula. *Catena*.
- Karunaratne, K.C., Burn, C.R. 2003. Freezing n-factors in discontinuous permafrost terrain, Takhini River, Yukon Territory, Canada. In M. Phillips, S.M. Springman, L.U. Arenson (eds.), *Proceedings of the 8th International Conference on Permafrost*, University of Alaska, Fairbanks, pp. 519-524.
- King, J.C., Comiso, J.C. 2003. The spatial coherence of interannual temperature variation in the Antarctic Peninsula. *Geophysical Research Letters* 30 (2), 1040. Doi:10.1029/2002GL015580.
- Láska, K., Nývlt, D., Engel, Z., Budík, L. 2012. Seasonal variation of meteorological variables and recent surface ablation / accumulation rates on Davies Dome and Whisky Glacier, James Ross Island, Antarctica. *Geophysical Research Abstracts* 14, EGU2012–5545.
- López-Martínez, J., Martínez de Pisón, E., Serrano, E., Arche, A. 1996. Geomorphological map of Byers Peninsula, Livingston Island. Cambridge (UK). *British Antarctic Survey, Geomap Series* Sheet 5-A.
- López-Martínez, J., Serrano, E., Schmid, T., Mink, S., Linés, C. 2012. Periglacial processes and landforms in the South Shetland Islands (northern Antarctic Peninsula region). *Geomorphology* 155, 62-79.
- Martin, P.J., Peel, D.A. 1978. The spatial distribution of 10m temperatures in the Antarctic Peninsula. *Journal of Glaciology* 20, 311-317.
- Navarro, F., Jonsell, U., Corcuera, M.I., Martín Español, A. 2013. Decelerated mass loss of Hurd and Johnsons Glaciers, Livingston Island, Antarctic Peninsula. *Journal of Glaciology* 59 (213), 115–128.
- Navas, A., López-Martínez, J., Casas, J., Machín, J., Durán, J.J., Serrano, E., Cuchi, J.A., Mink, S. 2008. Soil characteristics on varying lithological substrates in the South Shetland Islands, maritime Antarctica. *Geoderma* 144, 123-139.

- Nývlt, D., Braucher, R., Engel, Z., Mlčoch, B., ASTER Team, 2014. Timing of the Northern Prince Gustav Ice Stream retreat and the deglaciation of northern James Ross Island, Antarctic Peninsula during the last glacial–interglacial transition. *Quaternary Research* 82, 441-449.
- Nývlt, D., Nývltová Fišáková, M., Barták, M., Stachoň, Z., Pavel, V., Mlčoch, B., Láska, K. 2016. Death age, seasonality, taphonomy and colonization of seal carcasses from Ulu Peninsula, James Ross Island, Antarctic Peninsula. *Antarctic Science* 28, 3-16.
- Oliva, M., Antoniades, D., Giralt, S., Granados, I., Pla, S., Toro, M., Sanjurjo, J., Liu, E.J., Vieira, G. (accepted). The Holocene deglaciation of the Byers Peninsula (Livingston Island, Antarctica) based on the dating of lake sedimentary records. *Geomorphology*.
- Oliva, M., Hrbáček, F., Ruiz-Fernández, J., De Pablo, M.A., Vieira, G., Ramos, M. (submitted). Active layer dynamics in three topographically contrasted lake catchments in Byers Peninsula (Livingston Island, Antarctica). *Catena*.
- Olivero, E., Scasso, R.A., Rinaldi, C.A. 1986. Revision of the Marambio Group, James Ross Island, Antarctica. *Instituto Antártico Argentino, Contribución* 331, 28 pp.
- Ramos, M., Vieira, G. 2003. Active layer and permafrost monitoring in Livingston Island, Antarctic. First results from 2000 and 2001. In M. Phillips, S.M. Springman, L.U. Arenson (eds.), *Proceedings of the Eight International Conference on Permafrost*, Balkema – Swets & Zeitlinger, Zurich, Switzerland, pp. 929-933.
- Ramos, M., Vieira, G., Blanco, J.J., Gruber, S., Hauck, C., Hidalgo, M.A., Tomé, D. 2008. Active layer temperature monitoring in two boreholes in Livingston Island, Maritime Antarctic: first results for 2000-2006. In Kane, D., Hinkel, K. (eds.), *Proceedings of the 9th International Conference on Permafrost*, University of Alaska Press, Fairbanks, United States, pp. 1463-1467.
- Ramos, M., Vieira, G. 2009. Evaluation of the ground surface Enthalpy balance from bedrock temperatures (Livingston Island, Maritime Antarctic). *The Cryosphere* 3, 133-145
- Turner, J., Colwell, S.R., Marshall, G.J., Lachlan-Cope, T.A., Carleton, A.M., Jones, P.D., Lagun, V., Reid, P.A., Iagovkina, S. 2005. Antarctic climate change during last 50 years. *International Journal of Climatology* 25, 279-294.
- Van Lipzig, N.P.M., King, J.C., Lachlan-Cope, T.A., van der Broeke, M.R. 2004. Precipitation, sublimation and snow drift in the Antarctic Peninsula region from a regional atmospheric model. *Journal of Geophysical Research* 109, D24106.
- Vieira, G., Bockheim, J., Guglielmin, M., Balks, M., Abramov, A.A., Boelhouwers, J., Cannone, N., Ganzert, L., Gilichinsky, D., Goryachkin, S., López-Martínez, J., Meiklejohn, I., Raffi, R., Ramos, M., Schaefer, C., Serrano, E., Simas, F., Sletten, R., Wagner, D. 2010. Thermal state of permafrost and active-layer monitoring in the Antarctic: advances during the International Polar Year 2007-2008. *Permafrost and Periglacial Processes* 21, 182-197.
- Zvěřina, O., Láska, K., Červenka, R., Kuta, J., Coufalík, P., Komárek, J. 2014. Analysis of mercury and other heavy metals accumulated in lichen *Usnea antarctica* from James Ross Island, Antarctica. *Environmental Monitoring and Assessment* 186, 9089-9100.



# Active layer thermal dynamics at two lithologically different sites on James Ross Island, Eastern Antarctic Peninsula



Filip Hrbáček<sup>a,\*</sup>, Daniel Nývlt<sup>a,b</sup>, Kamil Láska<sup>a</sup>

<sup>a</sup> Masaryk University, Faculty of Science, Department of Geography, Kotlářská 2, 611 37 Brno, Czech Republic

<sup>b</sup> Czech Geological Survey, Brno Branch, Leitnerova 22, 658 69 Brno, Czech Republic

## ARTICLE INFO

### Article history:

Received 6 October 2015

Received in revised form 8 June 2016

Accepted 12 June 2016

Available online 12 July 2016

### Keywords:

Active layer thermal regime

Ground temperature

Lithological properties

Active layer thickness

Air temperature

Antarctic Peninsula

## ABSTRACT

The active layer thermal regime was studied at two sites with different lithological properties located on James Ross Island, eastern Antarctic Peninsula, to assess the main driving factors. The Abernethy Flats site (41 m a.s.l.) is located in Cretaceous calcareous sandstones and siltstones of the Santa Marta Formation. In contrast, the Berry Hill slopes site (56 m) is composed of muddy to intermediate diamictites, tuffaceous siltstones to fine-grained sandstones of the Mendel Formation. The data of air temperature at 2 m and ground temperature at two 75-cm-deep profiles were analysed for the period 1 January 2012, to 31 December 2014. Small differences were found when comparing mean air temperatures and ground temperatures at 5, 50 and 75 cm depths, in the period 2012–2014. While the mean air temperatures varied between  $-7.7$  °C and  $-7.0$  °C, the average ground temperatures oscillated between  $-6.6$  °C and  $-6.1$  °C at 5 cm;  $-6.7$  °C and  $-6.0$  °C at 50 cm; and  $-6.9$  °C and  $-6.0$  °C at 75 cm at Abernethy Flats and Berry Hill slopes, respectively. The increasing difference of ground temperature with depth, and a significant difference in active layer thickness – 52 to 64 cm at Abernethy Flats and 85 to 90 cm at Berry Hill slopes, respectively – suggests the significant effect of lithology. The higher proportion of fine particles and more thermally conductive minerals, together with higher water saturation, has been found to be fundamental for higher active layer thickness documented at Berry Hill slopes.

© 2016 Elsevier B.V. All rights reserved.

## 1. Introduction

Permafrost represents one of the key indicators of climate change as its superficial part reacts sensitively to climate variations and global temperature rise (e.g.; Romanovsky and Osterkamp, 1997; Guglielmin, 2006; Turner and Marshall, 2011). It is therefore crucial to fully understand the response of permafrost and the active layer particularly to undergoing climate change in Polar regions. The largest annual surface air warming on the Earth over the last 50 years was reported on the western side of the Antarctic Peninsula (AP): the mean air temperature increased at a rate of  $0.56$  °C/decade at the Faraday/Vernadsky Station (Turner et al., 2005). The mean annual air temperatures rose substantially along the eastern coast of Antarctic Peninsula as well, accelerating glacier retreats, ice-shelf breakups and permafrost temperature increase (e.g.; Cook and Vaughan, 2010; Turner and Marshall, 2011; Davies et al., 2012; Bockheim et al., 2013). At the same time, a positive trend in precipitation and snow accumulation has been observed and/or modelled on the western AP since 1950, as a result of changes in the atmospheric circulation, and its regional variability and patterns (Van den Broeke et al., 2006; Thomas et al., 2008).

High sensitivity of the active layer thickness (ALT) to climate fluctuations was found to be an important indicator of air and ground temperature increase. However, active layer thermal properties and thickness are not only related to the local air temperature and precipitations, but are also influenced by other variables and factors, such as incoming solar radiation, or ground surface lithology and moisture content (e.g.; Romanovsky and Osterkamp, 1997; Guglielmin et al., 2012).

A general overview of permafrost and active layer thermal dynamics in the AP region by Bockheim et al. (2013) showed that most of the studies have been conducted in areas of the western AP and the sub-Antarctic islands. Still, the overall knowledge about the active layer thermal regime and its dependence on climate factors, the local comprehension of air temperature, snow thickness and the geological conditions controlling active layer dynamics in the AP is still less than that known about the Arctic, or the Dry Valleys region in Antarctica (Vieira et al., 2010).

Results bringing a wider spectrum of information describing different patterns of active layer have been published mainly in the past few years. The main subjects were studies on the general characteristics of the active layer thermal regime (e.g.; Guglielmin et al., 2012; Michel et al., 2012; Almeida et al., 2014; De Pablo et al., 2014), physical thermal properties (e.g.; Correia et al., 2012; Goyanes et al., 2014), snow effect on ground temperature (e.g.; De Pablo et al., 2013; Guglielmin et al., 2014), or the effect of air temperature and vegetation cover

\* Corresponding author.

E-mail address: [hrbackefilip@gmail.com](mailto:hrbackefilip@gmail.com) (F. Hrbáček).

(e.g.; Cannone et al., 2006) in the western AP region. Although large ice-free areas are also located along the eastern coast of the AP – e.g. on James Ross Island (JRI), Vega Island or Seymour Island – very little information is available about the active layer thermal regime, which suggests significant differences when compared to the western side of the AP (Bockheim et al., 2013). The active layer thermal regime and its relationship to air temperature and snow cover near the Johann Gregor Mendel Station (JGM Station) on JRI was recently described in detail by Hrbáček et al. (2016), while earlier works from the eastern part of the AP bring only limited information on the state of the permafrost and active layer (e.g.; Fukuda et al., 1992; Borzotta and Trombotto, 2004; Ermolin et al., 2004).

The completion of local knowledge about the active layer thermal regime, its variability in different lithological conditions, its physical properties and relationship with climate factors above the JRI, which forms one of the largest ice-free areas in the AP region, represents a further challenge for the future work of the Czech Antarctic geoscientific research team that has been working at the JGM Station since 2006.

The main aims of this study are: 1) to describe the current state and thermal dynamics of the active layer at two distinct sites on James Ross Island in the period 2012–2014; 2) to assess the influence of different lithological conditions on active layer thermal dynamics; and 3) to determine the air temperature effect on the active layer thermal regime.

## 2. Study area

The study sites are located in the northern part of JRI, which is one of the largest islands located in Antarctic Peninsula region (Nedbalová

et al., 2013). The northern tip of JRI, called the Ulu Peninsula (Fig. 1), is considered one of the largest ice-free areas in the region (Nedbalová et al., 2013; Kavan et al., in review), with only small glaciers remaining in the present landscape (Engel et al., 2012), where the deglaciation process of low-lying areas (<60 m) started  $12.9 \pm 1.2$  ka ago (Nývlt et al., 2014).

The climate on JRI is a semi-arid Polar-continental, influenced by an orographic barrier of the Trinity Peninsula mountains (Martin and Peel, 1978; Davies et al., 2013). The mean annual air temperature (MAAT) at the JGM Station was  $-6.8$  °C in the period 2006–2011 (Láska et al., 2012). The maximum air temperatures during summer can exceed  $+10$  °C, while winter minima drop below  $-30$  °C (Láska et al., 2011). The precipitation falls mainly as snow in the winter season. However, the high wind speed causes snow drifting and irregular snow deposition (Zvěřina et al., 2014; Hrbáček et al., 2016), making standard rain gauge measurement inapplicable (Nývlt et al., 2016). Hence, estimates of precipitation range from 400 to 500 mm of water equivalent per year (Van Lipzig et al., 2004). The snow cover thickness measured near the JGM Station during the winter seasons is highly variable, with a maximum thickness not exceeding 30 cm (Hrbáček et al., 2016).

For the purpose of studying the active layer thermal dynamics, the Abernethy Flats and Berry Hill slopes sites were chosen. The study sites are located at similar altitudes, are not covered by vegetation but have different topographic and lithological properties (Table 1). The northern part of the Ulu Peninsula (Fig. 1) is formed of four Cretaceous formations of James Ross Basin marine sediments (Ineson et al., 1986; Olivero et al., 1986; Whitham et al., 2006), Neogene volcanic rocks of the James Ross Island Volcanic Group (Nelson, 1975; Smellie et al.,

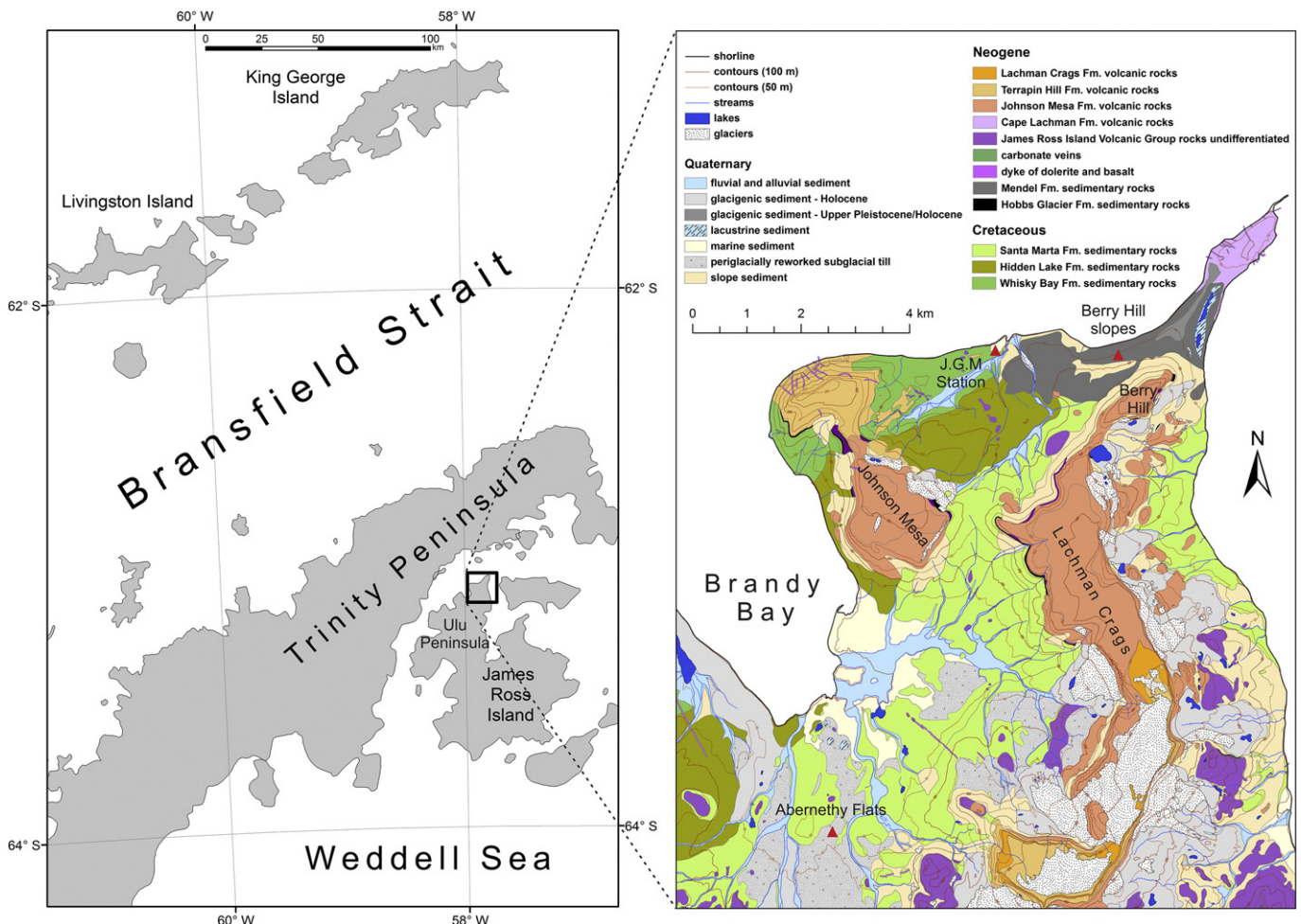


Fig. 1. Regional settings and geological characteristics of Ulu Peninsula, James Ross Island (adopted from Mlčoch et al., 2015).

**Table 1**  
Topographic and physical characteristics of the studied sites.

| Site              | Coordinates                  | Altitude    | Slope | Aspect     | Gravimetric water content <sup>a</sup> |
|-------------------|------------------------------|-------------|-------|------------|--|
| Abernethy Flats   | S63°52'52.9"<br>W57°56'53.7" | 41 m a.s.l. | 1–3°  | North-east | ~17%                                   |
| Berry Hill slopes | S63°48'09.5"<br>W57°50'19.4" | 56 m a.s.l. | 7°    | North-west | ~22%                                   |

<sup>a</sup> Water content was measured at 5 cm depth in January 2015.

2013) and associated siliciclastic and volcanoclastic sediments (Nelson et al., 2009; Nývlt et al., 2011; Nehyba and Nývlt, 2014, 2015). The Abernethy Flats area (Fig. 2A, B) is composed of fine-grained calcareous sandstones and siltstones of the Alpha Member, Santa Marta Formation (Olivero et al., 1986; Crame et al., 1991), covered by hyaloclastite breccia and basalt boulders valley train from the advance of the Whisky Glacier (Davies et al., 2013), while the Berry Hill slopes area (Fig. 2C, D) is composed of muddy to intermediate diamictites, tuffaceous siltstones to fine-grained sandstones of the Mendel Formation (Nývlt et al., 2011).

Rather diverse geology significantly influences the thermal conditions and the moisture of the active layer. Past studies on permafrost have focused mostly on glacial and periglacial processes and landforms (e.g.; Strelin et al., 2007; Carrivick et al., 2012; Davies et al., 2013; Nývlt et al., 2014), while permafrost and active layer thermal or physical properties on JRI are very poorly known. The primary findings report the thickness of permafrost estimated at 67 m in the low-lying areas (Borzotta and Trombotto, 2004), and variable ALT between 40 and 107 cm in the northern part of JRI (Bockheim et al., 2013).

### 3. Material and methods

The ground temperature was measured with identical devices at both sites using platinum resistance probes Pt100/8 (accuracy  $\pm 0.15$  °C), which were installed directly to the vertical profile in the ground at depths of 5, 10, 20, 30, 50 and 75 cm, and connected to an EdgeBox V12 datalogger (EMS, Czech Republic). The air temperature was measured at a height of 2 m above ground level using an EMS 33 sensor (EMS, Czech Republic) at the Abernethy Flats site, and a Minikin TH datalogger (EMS, Czech Republic) at the Berry Hill slopes site; both with an accuracy  $\pm 0.15$  °C. All parameters were measured and recorded every 30 min at the Abernethy Flats, and every 60 min at the Berry Hill slopes, owing to the different technical parameters of the used dataloggers. The data were analysed and compared for the period 1 January 2012 to 31 December 2014. Missing data from the Abernethy Flats in the period 1 January 2012 to 6 February 2012 were replaced by a regression equation ( $R^2 > 95\%$  in all cases), determined between the Abernethy Flats and Berry Hill slopes for the mean daily values. All

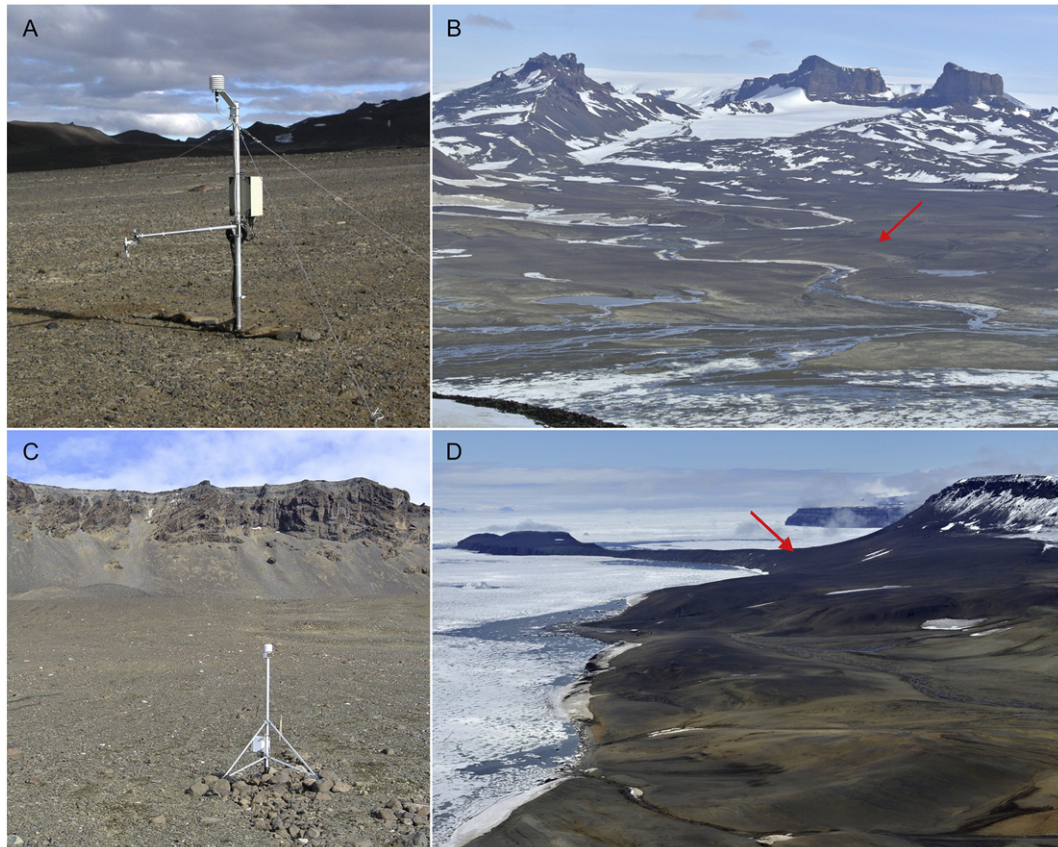


**Fig. 2.** Pictures of the study site Abernethy Flats (A, B) and Berry Hill slopes (C, D). The position of sites is marked by red arrows.

processed data were used for the creation of line and contour plots using Grapher® 9 and Surfer® 11 software (Golden Software, LLC). Furthermore, we used Statistica® 10 software for correlation analysis to determine the effect of the mean daily air temperature on the ground temperature at depths of 5 and 50 cm, representing near-surface and lower parts of the active layer, where time lags between air temperature and ground temperature variables were expected.

The raw data were used for the calculation of mean daily temperatures, the determination of maximum and minimum temperatures for both air and ground, and the calculation and assessment of different characteristics, describing the active layer thermal regime proposed by Guglielmin et al. (2008), and were used in several other studies from the AP region (e.g.; Michel et al., 2012; De Pablo et al., 2014; Guglielmin et al., 2014; Hrbáček et al., 2016):

- Freezing degree days (FDD) were calculated as the sum of negative temperatures and thawing degree days (TDD) were calculated as the sum of positive temperatures, both for air and ground.
- Freezing and thawing  $n$ -factors were determined for air temperature at 2 m, and ground temperature at 5 cm.
- Thermally defined ALT was determined as the maximum depth of the 0 °C isotherm, the position of which was interpolated for the Abernethy Flats site, and extrapolated according to the fitting curve for the maximum ground temperature at each depth for Berry Hill slopes.
- The total sum of freeze-thaw days with temperatures both below  $-0.5$  °C and above  $+0.5$  °C were calculated.

Thermal characteristics of active layer were calculated for the whole period from 1 January 2012 to 31 December 2014 at Berry Hill slopes, while the missing ground temperature data between 1 January 2012 and 6 February 2012 limited the calculation of all characteristics for the Abernethy Flats site.

The thawing season was defined for periods 2012/13 and 2013/14, according to De Pablo et al. (2014), based on the mean daily temperature regime at 5 cm as a period with ground temperature above 0 °C, during which the active layer at 5 cm stayed almost constantly unfrozen with only a few freezing degree days.

## 4. Results

### 4.1. Air temperature regime

The MAAT showed important differences at both stations for the period 2012–2014 (Table 2, Fig. 3). Slightly higher air temperatures were

observed at Berry Hill slopes, where MAAT varied between  $-7.6$  °C (2012) and  $-6.6$  °C (2014). MAAT at Abernethy Flats was a little lower, ranging between  $-8.6$  °C (2012) and  $-7.1$  °C (2013). Significantly lower MAAT in 2012 was caused by pronounced seasonal differences. The mean air temperature at Abernethy Flats during austral autumn (March to May) 2012 was  $-9.1$  °C, which was  $3.6$  °C and  $1.5$  °C lower than that in 2013 and 2014, respectively. Similarly, mean autumn air temperature in 2012 ( $-7.8$  °C) at Berry Hill slopes was lower by  $2.6$  °C and  $1.5$  °C in 2013 and 2014, respectively. The mean spring (September to November) air temperature in 2012 was lower by  $2.2$  °C and  $2.0$  °C in 2013 and 2014 at Abernethy Flats, respectively, while it was lower by  $1.7$  °C and  $1.5$  °C in 2013 and 2014 at Berry Hill slopes, respectively.

Both maximum ( $15.2$  °C in 24 February 2013) and minimum ( $-33.9$  °C in 18 August 2014) temperatures were recorded at Abernethy Flats, while temperature extremes at Berry Hill slopes ranged between  $13.0$  °C (24 February 2013) and  $-31.2$  °C (20 June 2013).

### 4.2. Active layer thermal conditions

#### 4.2.1. Abernethy Flats

Mean annual ground temperature (MAGT) at Abernethy Flats has shown different development along the vertical profile in individual years (Table 2, Fig. 3). Whereas the MAGT increased slightly from  $-7.5$  °C (5 cm) to  $-7.3$  °C (75 cm) in 2012, a gradual decrease of the MAGT, from  $-6.6$  °C (5 cm) to  $-7.1$  °C (75 cm) and from  $-5.6$  °C (5 cm) to  $-6.3$  °C (75 cm), was found in 2013 and 2014, respectively (Fig. 4). The maximum ground temperatures ranged from  $-0.6$  °C at 75 cm (8 February 2012) to  $19.3$  °C at 5 cm (22 December 2014) during the study period. The minimum ground temperatures ranged from  $-15.7$  °C at 75 cm (8 June 2012) to  $-26.9$  °C at 5 cm (7 June 2012). The effect of air temperature on ground temperature was analysed for 5 and 50 cm depths for each year of observation. The correlation analysis showed a high relationship between the air temperature and ground temperature at 5 cm, with  $r = 0.78$  (2012) to  $r = 0.85$  (2013), whereas the cross-correlation showed a smaller relationship of air temperature and ground temperature at 50 cm;  $r = 0.67$  (2014) to  $r = 0.78$  (2013) with a 4–6 day time lag (Table 4).

The thawing season duration ranged from 99 (2012/13) to 110 days (2013/14), with the warmest phase in January and February (Table 3). The mean ground temperature during the thawing season (MSGT) at 5 cm was higher in 2012/13 ( $2.9$  °C) than in 2013/14 ( $2.6$  °C). The other characteristics indicating active layer thawing intensity showed that the 2012/13 thawing season was warmer than 2013/14. In the 2012/13 thawing season, TDDg at 5 cm reached  $310.8$  °C·day ( $269.9$  °C·day in 2013/14), and TDDg at 50 cm reached  $2.7$  °C·day ( $0.2$  °C·day in 2013/14). The ALT reached 64 cm at the end of the 2011/12 thawing season, while 58 and 52 cm was determined for the 2012/13 and 2013/14 thawing seasons, respectively.

The thawing  $n$ -factor at the end of thawing seasons varied between 2.1 (2012/13) and 3.2 (2013/14) (Fig. 5a). Thawing  $n$ -factor reached its highest values  $>7.0$  in the first few weeks of each thawing season. Two maximum peaks were observed approximately in the period mid-December to mid-January in both thawing seasons. The thawing  $n$ -factor decreased slightly in the second part of thawing seasons. The duration of the freezing seasons showed higher variability than the duration of the thawing seasons. The length of freezing seasons varied between 246 days (2013) and 301 days (2012). The active layer remained almost constantly frozen from the end of April to the beginning of November in each freezing season. The FDDg at 5 cm varied between  $-2924.9$  °C·day (2012) and  $-2359.9$  °C·day (2014) (Fig. 6a), when only a few days with positive temperature were observed. Seasonal freezing  $n$ -factors varied between 0.96 in 2013 and 0.84 in 2014, suggesting a more pronounced insulation effect of the snow cover during July to September 2014, when it varied by around 0.80 (Fig. 6a).

**Table 2**  
Mean annual temperatures (in °C) of the air (AT) and the ground (GT) at different depths.

|                          | 2012 | 2013 | 2014 | 2012–2014 |
|--------------------------|------|------|------|-----------|
| <b>Abernethy Flats</b>   |      |      |      |           |
| AT                       | −8.6 | −7.1 | −7.4 | −7.7      |
| GT 5 cm                  | −7.5 | −6.6 | −5.6 | −6.6      |
| GT 10 cm                 | −7.9 | −7.0 | −6.0 | −6.9      |
| GT 20 cm                 | −7.6 | −6.8 | −5.8 | −6.7      |
| GT 30 cm                 | −7.6 | −6.9 | −6.0 | −6.9      |
| GT 50 cm                 | −7.3 | −6.8 | −6.0 | −6.7      |
| GT 75 cm                 | −7.4 | −7.1 | −6.3 | −6.9      |
| <b>Berry Hill slopes</b> |      |      |      |           |
| AT                       | −7.6 | −6.9 | −6.6 | −7.0      |
| GT 5 cm                  | −7.0 | −5.7 | −5.7 | −6.1      |
| GT 10 cm                 | −7.0 | −5.7 | −5.7 | −6.1      |
| GT 20 cm                 | −6.8 | −5.7 | −5.6 | −6.1      |
| GT 30 cm                 | −6.6 | −5.6 | −5.5 | −5.9      |
| GT 50 cm                 | −6.6 | −5.7 | −5.6 | −6.0      |
| GT 75 cm                 | −6.5 | −5.8 | −5.6 | −6.0      |

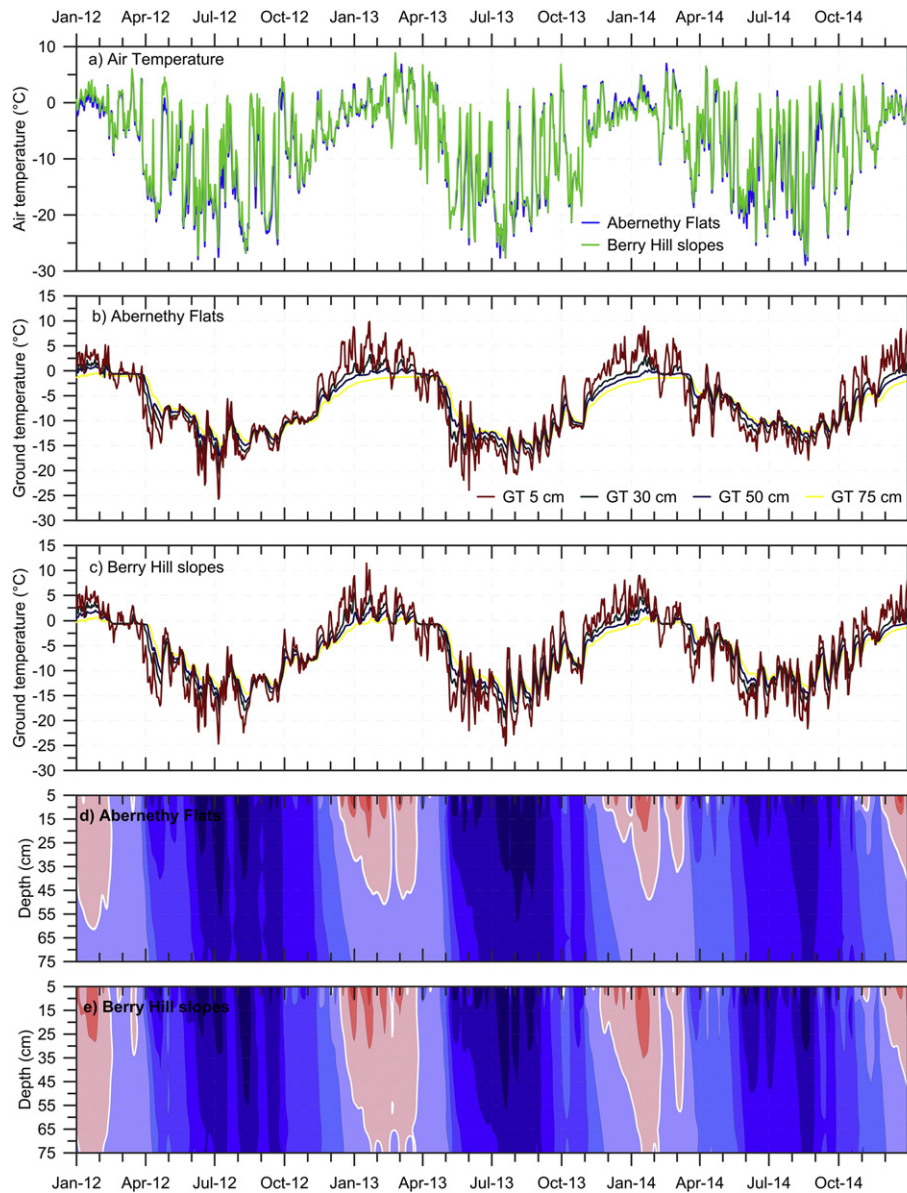


**Fig. 3.** Variability of a) mean daily air temperature (AT), ground temperature (GT) at 5, 20, 50 and 75 cm at b) Abernethy Flats and c) Berry Hill slopes and GT isopleths at d) Abernethy Flats and e) Berry Hill slopes in the period January 2012 to December 2014.

Freeze-thawing days occurred rather evenly between the freezing and thawing seasons. The frequency of freeze-thawing days at Abernethy Flats decreased rapidly with depth (Table 3): 37 days (2013) and 60 days (2014) were observed at 5 cm depth, but only one freeze-thawing day was found at 20 cm and at 30 cm depth in 2013 and 2012, respectively.

#### 4.2.2. Berry Hill slopes

Some differences in MAGT along the vertical profile (Fig. 4) at the Berry Hill slopes were found between the year 2012 and the years 2013 and 2014. While the MAGT decreased more significantly with depth, from  $-7.0$  °C (5 cm) to  $-6.5$  °C (75 cm) in 2012, only small MAGT differences between  $-5.7$  °C (5 cm) and  $-5.8$  °C (75 cm) were found in 2013, and were between  $-5.7$  °C (5 cm) and  $-5.6$  °C (75 cm) in 2014. The maximum ground temperatures in the study profile varied between  $0.6$  °C at 75 cm (27–28 January 2014) and  $19.5$  °C at 5 cm (10 January 2014). The minimum ground temperatures ranged between  $-15.8$  °C at 75 cm (21 June 2012) and  $-27.7$  °C at 5 cm (20 June 2012). Correlation analysis showed a close relationship between air temperature and ground temperature at 5 cm ( $r = 0.81$  in 2012 to

$r = 0.89$  in 2013), while the cross-correlation showed a smaller relationship between air temperature and ground temperature at 50 cm ( $r = 0.68$  in 2014 to  $r = 0.79$  in 2013), with a 3-day time lag (Table 4).

The duration of the thawing season at Berry Hill slopes ranged from 100 (2012/13) to 103 days (2013/14) (Table 3). The MSGT at 5 cm reached  $3.1$  °C (2012/13) and  $2.4$  °C (2013/14). TDDg at 5 cm ranged from  $323.8$  °C·day (2012/13) to  $296.6$  °C·day (2013/14), and decreased significantly at a depth of 50 cm to  $62.2$  °C·day (2012/13) and  $42.3$  °C·day (2013/14). Finally, TDDg at 75 cm reached  $6.4$  °C·day (2012/13) and  $5.1$  °C·day (2013/14). ALT reached 90 cm in the 2011/12 thawing season, while a slightly lower ALT of 85 cm was observed in both the 2012/13 and 2013/14 thawing seasons. The thawing  $n$ -factor at the end of the thawing seasons reached 2.4 (2012/13) and 4.4 (2013/14) (Fig. 5b). However, the maximum  $n$ -factor values exceeded 12.0 during both thawing seasons. Very high values were typical for the beginning of the thawing seasons. However, a different development of the thawing  $n$ -factor with two maximum peaks was observed in 2012/13 compared to one maximum peak in 2013/14 (Fig. 5b).

The duration of the freezing seasons showed high variability, between 239 days (2013) and 302 days (2012). The FDDg at 5 cm reached

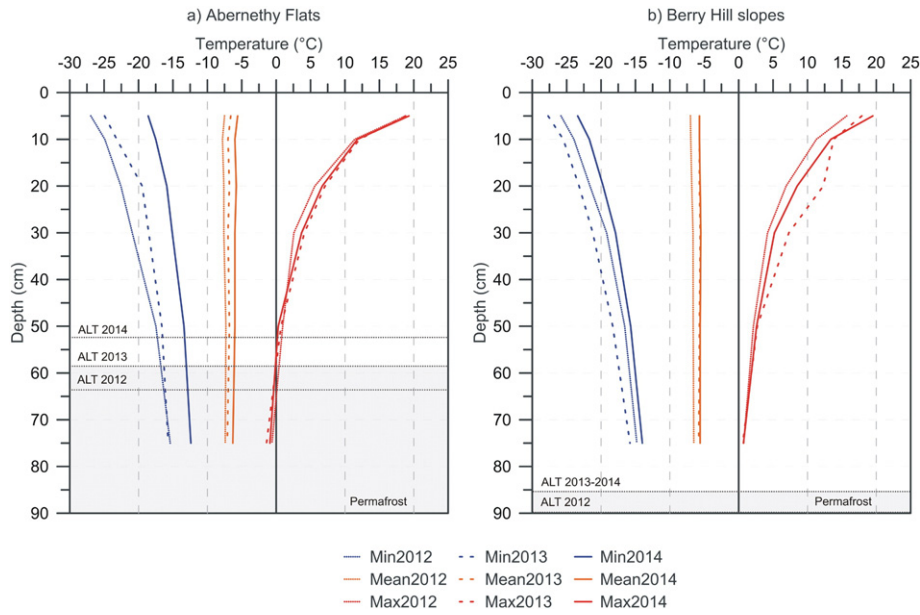


**Fig. 4.** Interannual development of minimum (Min) mean and maximum (Max) ground temperature at profile in years 2012 to 2014 at the a) Abernethy Flats and b) Berry Hill slopes. The ALT is maximum depth of active layer thickness in each year, the grey zone indicate position of permafrost.

–2444.3 °C·day in 2013 to –2810.7 °C·day in 2012 (Fig. 6b), while the active layer only refroze for several days during the freezing seasons. The seasonal freezing *n*-factors varied between 0.91 in 2013 and 0.97 in 2012, with a maximum reaching 1.01 in September 2012 and 2014, which suggests a very limited insulating effect of snow cover on the ground thermal regime (Fig. 6b).

The total number of freeze-thaw days at 5 cm depth in 2013 (74 days) and 2014 (75 days) were very similar, while the number of freeze-thaw days in 2012 (43 days) was significantly lower. A similar annual difference of the number of freeze-thawing days was observed

at 10 and 20 cm depths (Table 5). Freeze-thaw days were not detected at depths below 20 cm.

### 5. Interpretation and discussion

The results presented above indicated important differences in the air and ground thermal regimes between the Abernethy Flats and Berry Hill slopes sites in the period January 2012 to December 2014.

#### 5.1. Controls on air temperature

The air temperature data showed that the Abernethy Flats were generally colder by 0.7 °C than the Berry Hill slopes, despite their slightly higher elevation. Differences of MAAT, ranging from 0.2 °C (2013) to 1.0 °C (2012), indicate warmer climate conditions at Berry Hill slopes in contrast to the Abernethy Flats. The largest differences were found when comparing MAAT between the years 2013 and 2014, when MAAT increased by 0.3 °C at Berry Hill slopes, from the former to the latter year, but decreased by 0.3 °C at Abernethy Flats. Moreover, significantly higher variability in the mean daily air temperatures was found at Abernethy Flats (Fig. 3). The fact that both maximum and minimum air temperatures were registered at Abernethy Flats suggests that the study site's distance from the coast (effect of continentality) could play an important role in forming inverse temperature events at more inland sites, such as the Abernethy Flats. These observations are also supported by the mean seasonal air temperatures, which were higher by 0.1 °C (2013) to 0.8 °C (2014) during austral summer (December–February) at Abernethy Flats, whereas the observed mean seasonal air temperatures were 0.9 °C (2013) to 2.0 °C (2014) higher at Berry Hill slopes during austral winter (June–August).

#### 5.2. Lithological and hydrological characteristics

The active layer monitoring profiles at Berry Hill slopes and the Abernethy Flats have a different lithological composition. The sandstones predominating in the wider area of the Abernethy Flats (Pirrie, 1989) are generally poorly sorted, very fine to medium-grained sandstones, or silty sandstones with common concretions. They are variably calcareous: the average measured content of Ca by the means of X-Ray fluorescence measurements is ~3.3% (unpublished data of D. Nývlt),

**Table 3**  
Characteristics of active layer thermal regime during thawing seasons 2012/13 and 2013/14.

| Site                             | Abernethy Flats |              | Berry Hill slopes |              |
|----------------------------------|-----------------|--------------|-------------------|--------------|
|                                  | 2012/13         | 2013/14      | 2012/13           | 2013/14      |
| Beginning 5 cm                   | 11 Dec. 2012    | 24 Nov. 2013 | 12 Dec. 2012      | 17 Nov. 2013 |
| End 5 cm                         | 21 Mar. 2013    | 7 Mar. 2014  | 21 Mar. 2013      | 7 Mar. 2014  |
| Duration 5 cm (days)             | 100             | 103          | 99                | 110          |
| ALT (cm)                         | 58              | 52           | 85                | 85           |
| Mean AT (°C)                     | 0.4             | –0.8         | 0.2               | –1.2         |
| Mean GT5 (°C)                    | 2.9             | 2.3          | 3.1               | 2.4          |
| Mean GT30 (°C)                   | 0.4             | –0.2         | 1.5               | 0.8          |
| Mean GT50 (°C)                   | –0.7            | –1.2         | 0.3               | –0.2         |
| Mean GT75 (°C)                   | –2.1            | –2.3         | –0.7              | –1.1         |
| Max AT (°C)                      | 15.2            | 10.8         | 13                | 8.8          |
| Max GT5 (°C)                     | 18.8            | 19.2         | 17.9              | 19.5         |
| Max GT30 (°C)                    | 4.1             | 3.7          | 7.3               | 5.2          |
| Max GT50 (°C)                    | 0.7             | 0.3          | 2.7               | 2.6          |
| Max GT75 (°C)                    | –1.3            | –1.3         | 0.6               | 0.7          |
| TDDa (°C days)                   | 144.6           | 84           | 134.1             | 66.7         |
| TDDg5 (°C days)                  | 310.8           | 269.9        | 323.8             | 299.6        |
| TDDg30 (°C days)                 | 68.1            | 38.2         | 160.5             | 117.0        |
| TDDg50 (°C days)                 | 2.7             | 0.2          | 62.2              | 42.4         |
| TDDg75 (°C days)                 | 0.0             | 0.0          | 6.4               | 5.1          |
| FDDa (°C days)                   | –106.4          | –162.1       | –110.8            | –196.6       |
| FDDg5 (°C days)                  | –13.0           | –32.1        | –15.9             | –35.4        |
| FDDg30 (°C days)                 | –31.8           | –60.2        | –13.1             | –28.1        |
| FDDg50 (°C days)                 | –78.0           | –126.9       | –33.9             | –66.1        |
| FDDg75 (°C days)                 | –207.8          | –238.5       | –74               | –124.3       |
| Freeze-thawing 5 cm <sup>a</sup> | 2 + 7           | 9 + 10       | 11 + 19           | 45 + 21      |

<sup>a</sup> Number of freeze-thawing day at the beginning of thawing season (before 31 December) + at the end of thawing season (after 1 January). See text for abbreviations.

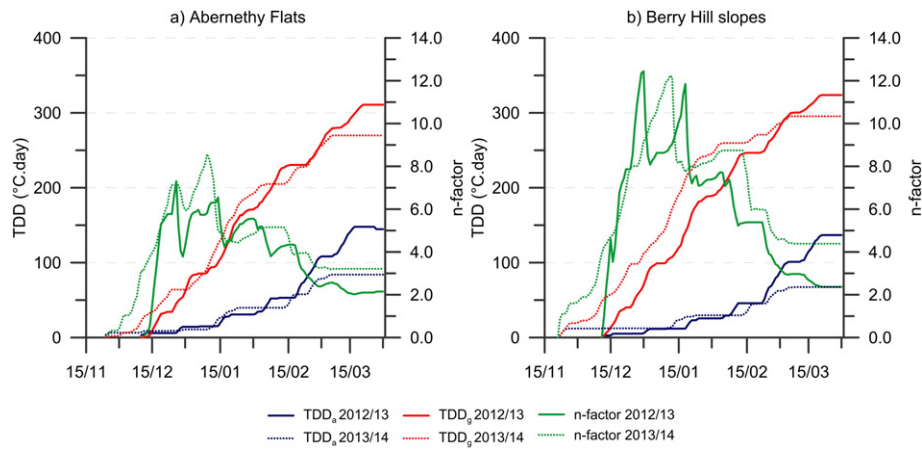


**Fig. 5.** Seasonal variability of thawing degree days for air temperature (TDDa) and ground temperature (TDDg) and  $n$ -factors ( $n$ -fac) at a) Abernethy Flats and b) Berry Hill slopes in 2012/13 and 2013/14.

corresponding to the average calcium carbonate (calcite) content of 8.2%. They appear in planar sheets usually a few dm thick, however Pirrie (1989) describes their maximum bed thickness up to 7.5 m. The sedimentary facies show mostly on high-energy sediment gravity flow processes of the mid-shelf depositional environment (Pirrie, 1989), implying the removal of fine silt and clay. The surface part is generally unconsolidated, as the result of periglacial action and weather, to form a loose friable sandy regolith. On the other hand, the facies cropping out on the surface of Berry Hill slopes are represented mostly by intermediate diamictite units of the Mendel Formation, deposited either as subglacial tills, proximal to intermediate glaciomarine diamictites, or glaciomarine debris flows (Nývlt et al., 2011), which imply direct glacial or glaciomarine deposition without significant winnowing of fine particles. The measured content of Ca in Mendel Formation diamictite units averages at ~1.9% (unpublished data of D. Nývlt), which corresponds to the average calcite content of ~4.7%.

The different content of fine particles (especially clay) in studied active layer profiles implies diverse porosity and permeability of the substrate, and thus distinct moisture and thermal properties of the active layer at the two sites. Substrates with a higher content of finer particles may keep a higher proportion of water owing to capillary and adhesive waters in the pore space (e.g.; Putkonen, 1998). This is reflected in the higher water saturation of the active layer at Berry Hill slopes, where the substrate could retain ~22% of water (see Table 1 for measured gravimetric water content), although it is located on a steeper slope, which triggers gradual water percolation and its concentration either above the permafrost table, or its rise to the surface. The measured

gravimetric water content at the Abernethy Flats site is ~5% lower compared to the Berry Hill slopes. Generally, the sandy regolith of the Abernethy Flats prevents the creation of adhesive water and limits capillary water, thus having most of the water in larger voids of the unsaturated zone of the active layer as it is gravitational and only partly capillary. Larger void spaces, however, increase the removal of fine particles from the active layer profile by water gravitational percolation, and their concentration near the permafrost table (Stachoň et al., 2014), leading to a decreasing ability to retain water.

Importantly, a higher water content increases the heat transfer in the active layer profile, owing to pore fluid migration (e.g.; Hinzman et al., 1991; Putkonen, 1998). Nearly half of the calcite content was found in the diamictites building the Berry Hill slopes site, when compared to the sandstones at the Abernethy Flats site. Calcite has nearly half the thermal conductivity in comparison to quartz (e.g.; Berman and Brown, 1985), which predominates the lithologies at both studied sites. Both the effect of higher water content and a lower share of calcite increases the thermal conductivity at Berry Hill slopes. This is well expressed both in faster spring thawing at this site, and especially in the deeper part of the active layer thermal properties, which leads to a 20–30 cm higher maximum ALT at Berry Hill slope than at the Abernethy Flats (see Fig. 3 and the discussion below).

### 5.3. Active layer thermal regime

Different thermal regimes of the active layer were observed at both sites during the study period. Besides the particular analysis of the

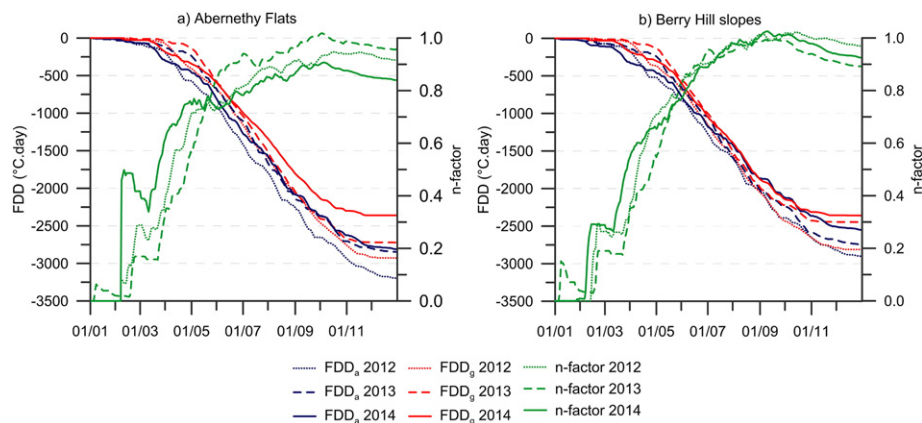


**Fig. 6.** Annual variability of freezing degree days for air temperature (FDDa) and ground temperature (FDDg) and  $n$ -factors at a) Abernethy Flats and b) Berry Hill slopes in 2012 to 2014.

**Table 4**

Correlation matrix showing relationship between air temperature (AT) and ground temperature (GT) at 5 and 50 cm depths and time-lag of ground temperature at 50 cm to air temperature in 2012–2014.

| Year | Abernethy Flats          |                           |                           | Berry Hill slopes        |                           |                           |
|------|--------------------------|---------------------------|---------------------------|--------------------------|---------------------------|---------------------------|
|      | AT vs GT <sub>5 cm</sub> | AT vs GT <sub>50 cm</sub> | Time-lag <sub>50 cm</sub> | AT vs GT <sub>5 cm</sub> | AT vs GT <sub>50 cm</sub> | Time-lag <sub>50 cm</sub> |
| 2012 | 0.78                     | 0.70                      | 6 days                    | 0.81                     | 0.70                      | 4 days                    |
| 2013 | 0.85                     | 0.78                      | 4 days                    | 0.89                     | 0.79                      | 2 days                    |
| 2014 | 0.79                     | 0.67                      | 4 days                    | 0.82                     | 0.68                      | 3 days                    |

active layer thermal regime our data showed the position of the permafrost table, which lies below the active layer at depths of 64 cm at Abernethy Flats and approx. 85 cm at Berry Hill slopes.

Our data suggested that higher variability of the ground thermal regime was found at Abernethy Flats, where MAGT at 5 cm varied between  $-5.6$  °C and  $-7.5$  °C, compared to Berry Hill slopes ( $-5.7$  °C to  $-7.0$  °C). More significant differences of MAGT were found at the lowest level of the profile (75 cm depth), where MAGT varied between  $-6.3$  °C and  $-7.4$  °C at Abernethy Flats, while MAGT between  $-5.6$  °C and  $-6.5$  °C was observed at Berry Hill slopes (Table 2).

The thawing seasons had an essential role in the active layer development at the study sites. Only small differences in their length were found according to the definition based on the thermal regime at 5 cm depth. The thawing season started 1 day earlier at Abernethy Flats in 2012/13 compared to 2013/14 when it started 7 days earlier at Berry Hill slopes. The end of the thawing season was on the same date in both years. Although the mean seasonal air temperature was 0.2 to 0.4 °C higher at Abernethy Flats, the MSGT was higher by 0.1–0.2 °C (5 cm) to 0.9–2.0 °C (75 cm) at Berry Hill slopes. Differences in MSGT are also reflected in TDDg at 5 cm, which was higher by 13.0 °C·day to 29.7 °C·day at Berry Hill slopes.

The active layer thawed much faster at the beginning of the thawing seasons at Berry Hill slopes. The upper 50 cm of the active layer thawed by  $1.6 \text{ cm} \cdot \text{day}^{-1}$  (2013/14) to  $2.5 \text{ cm} \cdot \text{day}^{-1}$  (2012/13) at Berry Hill slopes, while thawing of  $0.9 \text{ cm} \cdot \text{day}^{-1}$  (2013/14) to  $1.2 \text{ cm} \cdot \text{day}^{-1}$  (2012/13) was observed at Abernethy Flats. Significantly, the rapid progress of the active layer thawing front was affected by a higher thawing  $n$ -factor at Berry Hill slopes with values exceeding 12.0 at maximum, while a thawing  $n$ -factor of only 7.0 was reached at Abernethy Flats. As a result of the different progress of the thawing front, the MSGT at 50 cm was higher by 1.0 °C and MSGT at 75 cm was higher by 1.2–1.4 °C, at Berry Hill slopes. Similarly, TDDg at 50 cm reached only 0.2 to 2.7 °C·day at Abernethy Flats, while TDDg at 75 cm was even higher (5.1 °C·day to 6.4 °C·day) at Berry Hill slopes. These differences in active layer thawing and thermal regime resulted in a deeper ALT observed at Berry Hill slopes (85 to 90 cm) than at Abernethy Flats (52 to 64 cm).

Our data allowed both direct analysis of the air temperature effect and the indirect assessment of snow cover effect on the ground temperature regime. We found close correlations, which showed a similar relationship between air and near-surface ground temperature, as already reported for the AP region for the sites without vegetation cover (e.g.; Cannone et al., 2006; Guglielmin et al., 2014; or Hrbáček et al., 2016). Overall, a less close relationship was found between the air temperature

and the ground temperature at 50 cm depth. Despite a very small difference in correlation coefficients, differences in time lag between air temperature and ground temperature at 50 cm were more pronounced. The ground temperature at 50 cm correlates best with a 2–4-day delay at Berry Hill slopes, while a 4–6-day delay was found at Abernethy Flats. The shorter time lag suggests a better heat exchange through the active layer profile at Berry Hill slopes than at Abernethy Flats, owing to higher water content and lower shares of thermally less conductive minerals, such as calcite (see the discussion above).

The study sites are not covered by any vegetation such as moss carpet, which generally has an insulation effect and low thermal conductivity when compared to clastic sediments, or regolith (e.g.; Romanovsky and Osterkamp, 1997; Brouchkov et al., 2005). In addition, the snow cover is considered a very important factor affecting the ground thermal regime (e.g.; Goodrich, 1982; Zhang, 2005). The effect and distribution of snow cover on ground temperatures in northern JRI near to the JGM Station were found to be negligible in the previous study (Hrbáček et al., 2016). As the result of a missing measurement of snow thickness or albedo at both sites, the freezing  $n$ -factors and daily amplitude of the ground temperature at 5 cm were used to evaluate the effect of snow cover.

We assumed a slightly higher effect of snow cover at Abernethy Flats in general, as shown by lower values of freezing  $n$ -factor (0.80 to 0.90), and lower daily amplitude of the ground temperature at 5 cm during the freezing season, while a freezing  $n$ -factor  $> 1.00$  and daily amplitudes higher than  $\sim 3$  °C at Berry Hill slopes exclude a significant effect of snow cover on the ground thermal regime (Figs. 6, 7). The evolution of the freezing  $n$ -factor suggests the regular presence of snow cover at both sites at the beginning of the freezing season in March. These periods were typical for a low  $n$ -factor (0.2 to 0.4), but its duration did not exceed 20 days. During the freezing season, periods with developed snow cover could be delimited according to the decreasing freezing  $n$ -factor. However, these events were very scarce at Abernethy Flats (e.g., in July 2013, or August 2014), and were not detected at Berry Hill slopes (Fig. 6). The decrease in the freezing  $n$ -factor at the end of the freezing seasons (October to December) was caused by a more intense warming of the ground temperature compared to the air temperature, with a probable contribution of increasing global radiation. The presence of snow was not very probable during this period, as shown by the regime of daily amplitude of the ground temperature at 5 cm, with relatively high variability (1.5 °C to 10.0 °C) during the winter months, whereas only a few periods with low daily amplitude ( $< 1.5$  °C) suggesting snow conditions were observed (Fig. 7).

#### 5.4. Comparison of ground thermal regime with other localities

This study extends the time series of air and ground temperature monitoring in the northern part of JRI near the JGM Station in the period 2011 to 2012, published by Hrbáček et al. (2016). We found climate conditions slightly warmer in 2012–2014, when the mean air temperature reached  $-7.0$  °C and  $-7.7$  °C at Berry Hill slopes and Abernethy Flats, respectively, compared to the period 2011–2012, when the mean annual air temperature at the JGM Station reached  $-8.0$  °C.

Although different sites were studied in this work, many similarities were found when comparing the results of the active layer thermal regime and the effect of air temperature and snow cover described in this study, and by Hrbáček et al. (2016), from the site at the JGM Station. The active layer monitoring site at the JGM Station is located in a gravelly sand of a Holocene marine terrace (Davies et al., 2013), which is formed by permeable material with larger void spaces, which imply a lower thermal conductivity (Stachoň et al., 2014). This corresponds to similar ALT at the JGM Station when compared to Abernethy Flats, but is lower when compared to Berry Hill slopes. Likewise, the air temperature: only small differences in the mean ground temperature in 2011–2012 and 2012–2014 were found at the three sites monitored on the northern JRI (Table 5). Even though the mean ground temperature at depths of

**Table 5**

Frequency of freeze-thawing days at the studied sites in 2012–2014.

| Year | Abernethy Flats |                |                |                | Berry Hill slopes |       |       |       |
|------|-----------------|----------------|----------------|----------------|-------------------|-------|-------|-------|
|      | 5 cm            | 10 cm          | 20 cm          | 30 cm          | 5 cm              | 10 cm | 20 cm | 30 cm |
| 2012 | 32 <sup>a</sup> | 6 <sup>a</sup> | 0 <sup>a</sup> | 1 <sup>a</sup> | 43                | 22    | 5     | 0     |
| 2013 | 37              | 23             | 1              | 0              | 75                | 34    | 10    | 0     |
| 2014 | 60              | 25             | 0              | 0              | 74                | 34    | 15    | 0     |

<sup>a</sup> Calculated for the period 7 February to 31 December 2012.

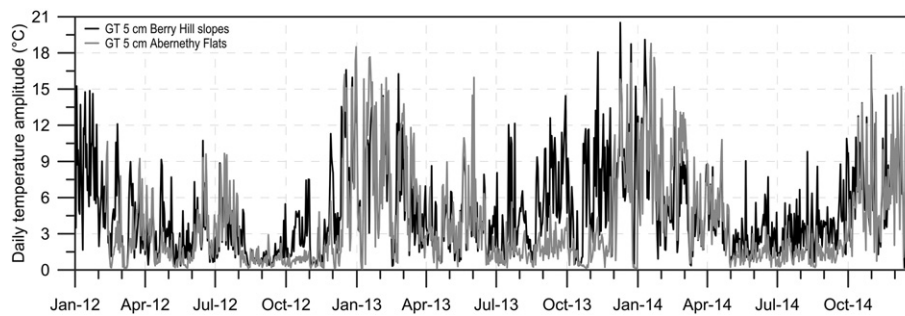


Fig. 7. Regime of daily temperature amplitude at 5 cm at Abernethy Flats and Berry Hill slopes in period January 2012 to December 2014.

50 to 75 cm near the JGM Station was 0.6–0.7 °C higher than at Abernethy Flats, and only 0.1–0.2 °C lower than at Berry Hill slopes, the ALT reached 52 to 58 cm at JGM Station in 2011 and 2012, respectively; similar values to those observed at Abernethy Flats (this study).

When comparing results from JRI with studies from several localities on the western AP, many differences were found. Generally, the MAAT and MAGT are about 3 to 5 °C lower on JRI, eastern AP, than in areas in the western AP (Bockheim et al., 2013). More detailed comparison suggests very similar or even warmer conditions during the thawing seasons between JRI and some areas of South Shetlands (western AP).

Longer and more intensive thawing seasons on JRI were observed when compared to different sites on Livingston Island (South Shetlands), where several localities were studied in 2009–2014 (e.g.; De Pablo et al., 2013, 2014; Oliva et al., in this issue). In general, the duration of the thawing season on Livingston Island were found to be slightly shorter, as described by De Pablo et al. (2014) at the Limnopolar Lake site. The length of the thawing seasons did not exceed 96 days (in period 2009–2012), while >100 days long thawing seasons were observed at the northern JRI (this study). Similarly, TDD<sub>g</sub> at 5 cm at different sites on Livingston Island reached a maximum of around 250 °C·day in the period 2009–2014 (De Pablo et al., 2014; Oliva et al., in this issue), while TDD<sub>g</sub>, which could exceed 300 °C·day, were observed on JRI in 2011–2014 (Hrbáček et al., 2016). On the other hand, freezing seasons were significantly warmer on Livingston Island, where FDD<sub>g</sub> did not drop below –600 °C·day (De Pablo et al., 2014; Oliva et al., in this issue) compared to values lower than –2300 °C·day on JRI.

The similar patterns of the ground thermal regime to Livingston Island have been described in diverse studies based on ground temperature measurements before 2012, at some sites on King George Island in the western AP (Michel et al., 2012; Almeida et al., 2014), or the South Orkney Islands (Guglielmin et al., 2012). Generally, the observations at these sites showed the TDD<sub>g</sub> during the thawing seasons reached around 200–400 °C·day, which is comparable to JRI, while the FDD<sub>g</sub> during freezing seasons did not drop below –1000 °C·day.

A very important factor affecting the active layer thermal regime in AP region is snow cover (Vieira et al., 2010). However, snow cover presence on JRI was found to be rather irregular over time, with a maximum thickness rarely reaching 30 cm (Hrbáček et al., 2016), whereas it could persist for 7–8 months and reach a maximum thickness of >60 cm in the areas of western AP (e.g.; De Pablo et al., 2013; Guglielmin et al., 2014; Oliva et al., in this issue). The only exception with a limited snow cover was observed on volcanic Deception Island, where the snow thickness rarely exceeded 20 cm (Goyanes et al., 2014). Areas with higher snow thickness in the AP region were typical, with a very low freezing *n*-factor between 0.30 and 0.60 (e.g.; De Pablo et al., 2014; Oliva et al., in this issue), compared to a freezing *n*-factor > 0.85 observed under snow-free conditions on JRI (Hrbáček et al., 2016).

Snow cover works as a very effective insulator, and has a significant effect on the ground thermal regime. It leads to an almost isothermal regime of ground temperature when the snow thickness exceeds ~40 cm (Zhang, 2005). This effect has been demonstrated by the results of very

low daily ground temperature amplitudes at 5 cm (0.0–0.1 °C) under 20 to 40 cm of snow, on Livingston Island, by Oliva et al. (in this issue), while on JRI the snow thickness reached a max. 30 cm, which caused a reduction in the ground temperature daily amplitude by 0.1–0.5 °C (Hrbáček et al., 2016). According to these findings, the daily amplitude of the ground temperature (Fig. 7) and the freezing *n*-factor confirm the previous results of Hrbáček et al. (2016) who suggest the overall effect of snow on the ground thermal regime is negligible on JRI.

Considering all the differences observed in the ground thermal regime, as well as the role of snow, significant differences between the eastern AP (JRI) and western AP could be expected. However, in general, the ALT showed very large spatial variability (Bockheim et al., 2013); that is, ALT reached 85 to >130 cm at different sites on Livingston Island (De Pablo et al., 2014; Oliva et al., in this issue), whereas ALT between 81 and 185 cm was observed at Signy Island in 2006–2009 (Guglielmin et al., 2012). At different sites on King George Island ALT varied between ca. 90 cm in 2008 (Michel et al., 2012) and 120 to 147 cm in 2009–2010 (Almeida et al., 2014). Similarly, ALT between 30 and 100 cm was measured at Deception Island (Vieira et al., 2010; Goyanes et al., 2014).

Despite the fact that data from different years were presented in these studies, the very high spatial variability of ALT suggests that local conditions, especially lithological factors or moisture, should be another very important factor affecting ground thermal regime. However, a general comparison of ALT between JRI and other localities in the western AP seems to be difficult, owing to an important interannual variability of ALT and the inconsistency of datasets, as only one season is published mostly.

While the studies presented above described the results of measurement in soils or regoliths on unconsolidated ground, several works described ALT measurement in solid bedrock where ALT could reach several metres thickness (Ramos and Vieira, 2009). A large difference in the thermal conductivity between unconsolidated material and solid bedrock has been documented on the western AP. Correia et al. (2012) showed from their measurements on Livingston Island that the thermal conductivity in solid quartz sandstone is larger than in looser siltstone, and much larger than for unconsolidated material, such as soil or regolith. This corresponds to larger ALT in solid bedrock rather than in unconsolidated material, which has been reported by Guglielmin et al. (2014) at Rothera Point, Adelaide Island, or by Ramos and Vieira (2009) on Livingston Island.

## 6. Conclusions

In this contribution we studied the thermal properties of the active layer at two lithologically contrasting sites at the northern part of the Ulu Peninsula, James Ross Island. Our data showed variances in air temperature and ground thermal regime that were significantly different at both sites. A contrasting regime of air temperature was observed when comparing winter (higher air temperature at Berry Hill slopes) and summer (higher air temperature at Abernethy Flats) months. Despite similar a thermal regime at the near-surface 5 cm depth during the

thawing seasons, the active layer thawed significantly faster at Berry Hill slopes owing to a higher thermal conductivity caused by local lithology. The active layer thickness reached 85 to 90 cm at Berry Hill slopes, which was 26 to 33 cm deeper than at Abernethy Flats.

Moreover, our results confirmed some observations found in a previous study from James Ross Island. Significant differences in the ground thermal regime between James Ross Island and localities on the western part of the Antarctic Peninsula are caused by a more continental climate, with a warmer summer and a colder winter on James Ross Island. The freezing  $n$ -factors and the daily amplitude of ground temperature at 5 cm suggest a limited effect of snow cover on the ground thermal regime at the northern James Ross Island sites.

From a lithological point of view, the share of fine particles and less conductive minerals (such as calcite) has been found to be fundamental for the thermal conductivity and the active layer thickness documented at the sites with unconsolidated material. Therefore, a higher active layer thickness has been documented in the diamictites of the Mendel Formation (Berry Hill slopes) than in calcareous Cretaceous marine strata (Abernethy Flats), or in the Holocene marine terrace sediments (Johann Gregor Mendel Station). Furthermore, considerable shares of fine particles trigger higher water saturation of the active layer as long as it is available from the previous snow-cover thawing. However, we consider a better understanding of the lithological and physical properties of studied sites to be challenging for further research on the ground thermal regime on James Ross Island.

## Acknowledgements

We thank the Johann Gregor Mendel Station infrastructure for logistical support. We are very grateful to the members of the summer expeditions in 2011–2015 for their company and field assistance on JRI. The work was supported by the Masaryk University project MUNI/A/1315/2015. The work of DN on this paper has been supported by the project, “Employment of Best Young Scientists for International Cooperation Empowerment” (CZ.1.07/2.3.00/30.0037) co-financed from European Social Fund and the state budget of the Czech Republic. We also acknowledge the suggestions and comments on earlier drafts of the manuscript provided by Marc Oliva and constructive comments of both journal reviewers.

## Appendix A. Supplementary data

Supplementary data associated with this article can be found in the online version, at doi: <http://dx.doi.org/10.1016/j.catena.2016.06.020>. These data include the Google maps of the most important areas described in this article.

## References

- Almeida, I.C.C., Schaefer, C.E.G.R., Fernandes, R.B.A., Pereira, T.T.C., Nieuwendam, A., Pereira, A.B., 2014. Active layer thermal regime at different vegetation covers at Lion Rumps, King George Island, Maritime Antarctica. *Geomorphology* 225, 36–46.
- Berman, R.G., Brown, T.H., 1985. Heat Capacity of Minerals in the System  $\text{Na}_2\text{O}-\text{K}_2\text{O}-\text{CaO}-\text{MgO}-\text{FeO}-\text{Fe}_2\text{O}_3-\text{Al}_2\text{O}_3-\text{SiO}_2-\text{TiO}_2-\text{H}_2\text{O}-\text{CO}_2$ : Representation, Estimation and High Temperature Extrapolation. *Contrib. Mineral. Petrol.* 89, 168–183.
- Bockheim, J., Vieira, G., Ramos, M., López-Martínez, J., Serrano, E., Guglielmin, M., Wilhelm, K., Nieuwendam, A., 2013. Climate warming and permafrost dynamics in the Antarctic Peninsula region. *Glob. Planet. Chang.* 100, 215–223.
- Borzotta, E., Trombotto, D., 2004. Correlation between frozen ground thickness measured in Antarctica and permafrost thickness estimated on the basis of the heat flow obtained from magnetotelluric soundings. *Cold Reg. Sci. Technol.* 40, 81–96.
- Brouchkov, A., Fukuda, M., Iwahana, G., Kobayashi, Y., Konstantinov, P., 2005. Thermal Conductivity of Soils in the Active Layer of Eastern Siberia. *Permafrost. Periglacial.* 16, 217–222.
- Cannone, N., Evans, J.C.E., Strachan, R., Guglielmin, M., 2006. Interactions between climate, vegetation and the active layer at two Maritime Antarctica sites. *Antarct. Sci.* 18, 323–333.
- Carrivick, J.L., Davies, B.J., Glasser, N.F., Nývlt, D., Hambrey, M.J., 2012. Late Holocene changes in character and behaviour of land-terminating glaciers on James Ross Island, Antarctica. *J. Glaciol.* 58, 1176–1190.
- Cook, A.J., Vaughan, D.G., 2010. Overview of areal changes of the ice shelves on the Antarctic Peninsula over the past 50 years. *Cryosphere* 4, 77–98.
- Correia, A., Vieira, G., Ramos, M., 2012. Thermal conductivity and thermal diffusivity of cores from a 26 meter deep borehole drilled in Livingston Island, Maritime Antarctic. *Geomorphology* 155–156, 7–11.
- Crame, J.A., Pirrie, D., Riding, J.B., Thomson, M.R.A., 1991. Campanian–Maastrichtian (Cretaceous) stratigraphy of the James Ross Island area, Antarctica. *J. Geol. Soc. Lond.* 148, 1125–1140.
- Davies, B.J., Carrivick, J.L., Glaser, N.F., Hambrey, M.J., Smellie, J.L., 2012. Variable glacier response to atmospheric warming, northern Antarctic Peninsula, 1988–2009. *Cryosphere* 6, 1031–1048.
- Davies, B.J., Glasser, N.F., Carrivick, J.L., Hambrey, M.J., Smellie, J.L., Nývlt, D., 2013. Landscape evolution and ice-sheet behaviour in a semi-arid polar environment: James Ross Island, NE Antarctic Peninsula. In: Hambrey, M.J., Barker, P.F., Barrett, P.J., Bowman, V., Davies, B., Smellie, J.L., Tranter, M. (Eds.), *Antarctic Palaeoenvironments and Earth-Surface Processes*. Geological Society, London, Special Publications 381, pp. 353–395.
- De Pablo, M.A., Blanco, J.J., Molina, A., Ramos, M., Quesada, A., Vieira, G., 2013. Interannual active layer variability at the Limnopolar Lake CALM site on Byers Peninsula, Livingston Island, Antarctica. *Antarct. Sci.* 25, 167–180.
- De Pablo, M.A., Ramos, M., Molina, A., 2014. Thermal characterization of the active layer at the Limnopolar Lake CALM-S site on Byers Peninsula (Livingston Island), Antarctica. *Solid Earth* 5, 721–739.
- Engel, Z., Nývlt, D., Láška, K., 2012. Ice thickness, bed topography and glacier volume changes on James Ross Island, Antarctic Peninsula. *J. Glaciol.* 58, 904–914.
- Ermolin, E., De Angelis, H., Skvarca, P., Rau, F., 2004. Ground ice in permafrost on Seymour (Marambio) and Vega Islands, Antarctic Peninsula. *Ann. Glaciol.* 39, 373–378.
- Fukuda, M., Shimokawa, K., Takahashi, N., Sone, T., 1992. Permafrost in Seymour Island and James Ross Island, Antarctic Peninsula region. *Geogr. Rev. Jpn. Ser. A* 65 (2), 124–131.
- Goodrich, L.E., 1982. The influence of snow cover on the ground thermal regime. *Can. Geotech. J.* 19, 421–432.
- Goyanes, G., Vieira, G., Caselli, A., Cardoso, M., Marmy, A., Bernardo, I., Hauck, C., 2014. Geothermal anomalies, permafrost and geomorphological dynamics (Deception Island, Antarctica). *Geomorphology* 225, 57–68.
- Guglielmin, M., 2006. Ground surface temperature (GST), active layer, and permafrost monitoring in continental Antarctica. *Permafrost. Periglacial.* 17, 133–143.
- Guglielmin, M., Worland, M.R., Baio, F., Convey, P., 2014. Permafrost and snow monitoring at Rothera Point (Adelaide Island, Maritime Antarctica): Implications for rock weathering in cryotic conditions. *Geomorphology* 225, 47–56.
- Guglielmin, M., Evans, J.C.E., Cannone, N., 2008. Active layer thermal regime under different vegetation conditions in permafrost areas. A case study at Signy Island (Maritime Antarctica). *Geoderma* 144, 73–85.
- Guglielmin, M., Worland, M.R., Cannone, N., 2012. Spatial and temporal variability of ground surface temperature and active layer thickness at the margin of Maritime Antarctica, Signy Island. *Geomorphology* 155, 20–33.
- Hinzman, L.D., Kane, D.L., Gieck, R.E., Everett, K.R., 1991. Hydrologic and thermal properties of the active layer in the Alaskan Arctic. *Cold Reg. Sci. Technol.* 19, 95–110.
- Hrbáček, F., Láška, K., Engel, Z., 2016. Effect of snow cover on active-layer thermal regime – a case study from James Ross Island, Antarctic Peninsula. *Permafrost. Periglacial.* <http://dx.doi.org/10.1002/ppp.1871>.
- Ineson, J.R., Crame, J.A., Thomson, M.R.A., 1986. Lithostratigraphy of the Cretaceous strata of west James Ross Island, Antarctica. *Cretac. Res.* 7, 141–159.
- Kavan, J., Ondruch, J., Nývlt, D., Hrbáček, F., Carrivick, J.L., Láška, K., 2016. Seasonal hydrological and suspended sediment transport dynamics in proglacial streams, James Ross Island, Antarctica. *Geogr. Ann. A* (in review).
- Láška, K., Barták, M., Hájek, J., Prošek, P., Bohuslavová, O., 2011. Climatic and ecological characteristics of deglaciated area of James Ross Island, Antarctica, with a special respect to vegetation cover. *Czech Polar Rep.* 1, 49–62.
- Láška, K., Nývlt, D., Engel, Z., Budík, L., 2012. Seasonal variation of meteorological variables and recent surface ablation/accumulation rates on Davies Dome and Whisky Glacier, James Ross Island, Antarctica. *Geophys. Res. Abstr.* 14, EGU2012–EGU5545.
- Martin, P.J., Peel, D.A., 1978. The spatial distribution of 10 m temperatures in the Antarctic Peninsula. *J. Glaciol.* 20, 311–317.
- Michel, R.F.M., Schaefer, C.E.G.R., Poelking, E.L., Simas, F.N.B., Filho, E.I.F., Bockheim, J.G., 2012. Active layer temperature in two Cryosols from King George Island, Maritime Antarctica. *Geomorphology* 155–156, 12–19.
- Mlčoch, B., Nývlt, D., Míxa, P. (Eds.), 2015. James Ross Island. Geological Map of the Northern Part. 1: 25 000. Czech Geological Survey, Praha Unpublished manuscript.
- Nedbalová, L., Nývlt, D., Kopáček, J., Šobr, M., Elster, J., 2013. Freshwater lakes of Ulu Peninsula, James Ross Island, northeast Antarctic Peninsula: origin, geomorphology and physical and chemical limnology. *Antarct. Sci.* 25, 358–372.
- Nehyba, S., Nývlt, D., 2014. Deposits of pyroclastic mass flows at Bibby Hill (Pliocene, James Ross Island, Antarctica). *Czech Polar Rep.* 4, 103–122.
- Nehyba, S., Nývlt, D., 2015. “Bottomsets” of the lava-fed delta of James Ross Island Volcanic Group, Ulu Peninsula, James Ross Island, Antarctica. *Pol. Polar Res.* 36, 1–24.
- Nelson, P.H.H., 1975. The James Ross Island Volcanic Group of North-East Graham Land. *Brit. Antarct. Surv. Sci. Rep.* 54 (62 pp.).
- Nelson, A.E., Smellie, J.L., Hambrey, M.J., Williams, M., Vautravers, M., Salzmann, U., McArthur, J.M., Regulous, M., 2009. Neogene glacial debris flows on James Ross Island, northern Antarctic Peninsula, and their implications for regional climate history. *Quat. Sci. Rev.* 28, 3138–3160.
- Nývlt, D., Braucher, R., Engel, Z., Mlčoch, B., ASTER Team, 2014. Timing of the Northern Prince Gustav Ice Stream retreat and the deglaciation of northern James Ross Island,

- Antarctic Peninsula during the last glacial–interglacial transition. *Quat. Res.* 82, 441–449.
- Nývlt, D., Košler, J., Mlčoch, B., Mixa, P., Lisá, L., Bubík, M., Hendriks, B.W.H., 2011. The Mendel Formation: Evidence for Late Miocene climatic cyclicity at the northern tip of the Antarctic Peninsula. *Palaeogeogr. Palaeoecol.* 299, 363–384.
- Nývlt, D., Nývtová Fišáková, M., Barták, M., Stachoň, Z., Pavel, V., Mlčoch, B., Láška, K., 2016. Death age, seasonality, taphonomy and colonization of seal carcasses from Ulu Peninsula, James Ross Island, Antarctic Peninsula. *Antarct. Sci.* 28, 3–16.
- Oliva, M., Ruiz-Fernandez, J., Hrbáček, F., Vieira, G., De Pablo, M.A., Ramos, M., 2016. The role of topography controlling active layer dynamics in three contrasted sites in the Byers Peninsula (Livingston Island, Antarctica). *Catena* (in revision, in this issue).
- Olivero, E., Scasso, R.A., Rinaldi, C.A., 1986. Revision of the Marambio Group, James Ross Island, Antarctica. Instituto Antártico Argentino, Contribución 331 (28 pp.).
- Pirrie, D., 1989. Shallow marine sedimentation within an active margin basin, James Ross Island, Antarctica. *Sediment. Geol.* 63, 61–82.
- Putkonen, J., 1998. Soil thermal properties and heat transfer processes near Ny-Ålesund, northwestern Spitsbergen, Svalbard. *Polar Res.* 17, 165–179.
- Ramos, M., Vieira, G., 2009. Evaluation of the ground surface Enthalpy balance from bedrock temperatures (Livingston Island, Maritime Antarctic). *The Cryosphere* 3, 133–145.
- Romanovsky, V.E., Osterkamp, T.E., 1997. Thawing of the Active Layer on the Coastal Plain of the Alaskan Arctic. *Permafrost. Periglac.* 8, 1–22.
- Smellie, J.L., Johnson, J.S., Nelson, A.E., 2013. Geological map of James Ross Island. I. James Ross Island Volcanic Group (1:125 000 Scale). BAS GEOMAP 2 Series, Sheet 5 British Antarctic Survey, Cambridge.
- Stachoň, Z., Russnák, J., Nývlt, D., Hrbáček, F., 2014. Stabilisation of geodetic points in the surroundings of Johann Gregor Mendel Station, James Ross Island, Antarctica. *Czech Polar Rep.* 4, 81–90.
- Strelin, J.A., Torielli, C.A., Sone, T., Fukui, K., Mori, J., 2007. Particularidades genéticas de glaciares de roca en la Isla James Ross, Península Antártica. *Rev. Asoc. Geol. Argent.* 62, 627–634.
- Thomas, E.R., Marshall, G.J., McConnell, J.R., 2008. A doubling in snow accumulation in the western Antarctic Peninsula since 1850. *Geophys. Res. Lett.* 35, L01706.
- Turner, J., Marshall, G.J., 2011. *Climate Change in the Polar Regions*. Cambridge University Press, Cambridge (ISBN 978-0-521-85010-0, 448 pp.).
- Turner, J., Colwell, S., Marshall, G.J., Lachlan-Cope, T.A., Carleton, A.M., Jones, P.D., Lagun, V., Reid, P.A., Iagovkina, S., 2005. Antarctic climate change during the last 50 years. *Int. J. Climatol.* 25, 279–294.
- Van den Broeke, M.R., van de Berg, W., von Meijgaard, E., 2006. Snowfall in coastal West Antarctica much greater than previously assumed. *Geophys. Res. Lett.* 33, L02505.
- Van Lipzig, N.P.M., King, J.C., Lachlan-Cope, T.A., van der Broeke, M.R., 2004. Precipitation, sublimation and snow drift in the Antarctic Peninsula region from a regional atmospheric model. *J. Geophys. Res.* 109, D24106.
- Vieira, G., Bockheim, J., Guglielmin, M., Balks, M., Abramov, A.A., Boelhouwers, J., Cannone, N., Ganzert, L., Gilichinsky, D., Goryachkin, S., López-Martínez, J., Meiklejohn, I., Raffi, R., Ramos, M., Schaefer, C., Serrano, E., Simas, F., Sletten, R., Wagner, D., 2010. Thermal state of permafrost and active-layer monitoring in the Antarctic: advances during the International Polar Year 2007–2008. *Permafrost. Periglac.* 21, 182–197.
- Whitham, A.G., Ineson, J.R., Pirrie, D., 2006. Marine volcanoclastics of the Hidden Lake Formation (Coniacian) of James Ross Island, Antarctica: an enigmatic element in the history of a back-arc basin. In: Francis, J.E., Pirrie, D., Crame, J.A. (Eds.), *Cretaceous–Tertiary High-Latitude Palaeoenvironments, James Ross Basin, Antarctica*. Geological Society, London, Special Publications 258, pp. 21–47.
- Zhang, T., 2005. Influence of the seasonal snow cover on the ground thermal regime: an overview. *Rev. Geophys.* 43. <http://dx.doi.org/10.1029/2004RG000157>.
- Zvěřina, O., Láška, K., Červenka, R., Kuta, J., Coufalík, P., Komárek, J., 2014. Analysis of mercury and other heavy metals accumulated in lichen *Usnea Antarctica* from James Ross Island, Antarctica. *Environ. Monit. Assess.* 186, 9089–9100.



## Active layer monitoring at CALM-S site near J.G.Mendel Station, James Ross Island, eastern Antarctic Peninsula



Filip Hrbáček<sup>a,\*</sup>, Michaela Kňazková<sup>a</sup>, Daniel Nývlt<sup>a</sup>, Kamil Láška<sup>a</sup>, Carsten W. Mueller<sup>b</sup>, Jakub Ondruch<sup>a</sup>

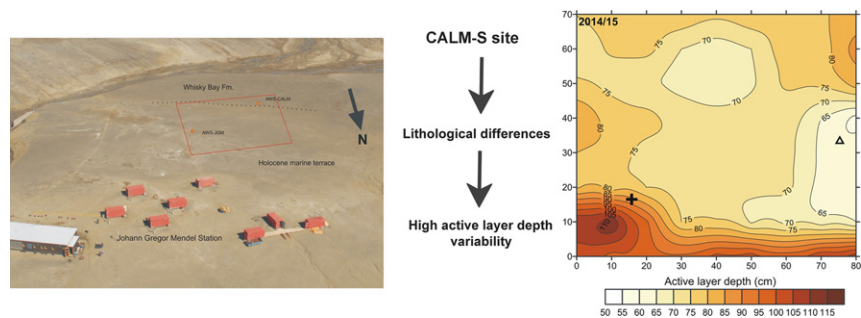
<sup>a</sup> Department of Geography, Masaryk University, Brno, Czech Republic

<sup>b</sup> Lehrstuhl für Bodenkunde, TU Munchen, Freising-Weihenstephan 85356, Germany

### HIGHLIGHTS

- Active layer depth was measured on the CALM-S site in eastern Antarctic Peninsula.
- Mean seasonal active layer depth varied between 66.4 cm and 78.0 cm.
- Maximum active layer depth reached >110 cm.
- Ground physical properties had essential role for active layer development.

### GRAPHICAL ABSTRACT



### ARTICLE INFO

#### Article history:

Received 3 January 2017

Received in revised form 7 May 2017

Accepted 29 May 2017

Available online 3 June 2017

#### Keywords:

Active layer thickness  
Ground thermal regime  
Permafrost  
CALM-S  
Antarctic Peninsula  
Climate

### ABSTRACT

The Circumpolar Active Layer Monitoring – South (CALM-S) site was established in February 2014 on James Ross Island as the first CALM-S site in the eastern Antarctic Peninsula region. The site, located near Johann Gregor Mendel Station, is labelled CALM-S JGM. The grid area is gently sloped (<3°) and has an elevation of between 8 and 11 m a.s.l. The lithology of the site consists of the muddy sediments of Holocene marine terrace and clayey-sandy Cretaceous sedimentary rocks, which significantly affect the texture, moisture content, and physical parameters of the ground within the grid. Our objective was to study seasonal and interannual variability of the active layer depth and thermal regime at the CALM-S site, and at two ground temperature measurement profiles, AWS-JGM and AWS-CALM, located in the grid. The mean air temperature in the period March 2013 to February 2016 reached –7.2 °C. The mean ground temperature decreased with depth from –5.3 °C to –5.4 °C at 5 cm, to –5.5 °C to –5.9 °C at 200 cm. Active layer thickness was significantly higher at AWS-CALM and ranged between 86 cm (2014/15) and 87 cm (2015/16), while at AWS-JGM it reached only 51 cm (2013/14) to 65 cm (2015/16). The mean probed active layer depth increased from 66.4 cm in 2013/14 to 78.0 cm in 2014/15. Large differences were observed when comparing the minimum (51 cm to 59 cm) and maximum (100 cm to 113 cm) probed depths. The distribution of the active layer depth and differences in the thermal regime of the uppermost layer of permafrost at CALM-S JGM clearly show the effect of different lithological properties on the two lithologically distinct parts of the grid.

© 2017 Elsevier B.V. All rights reserved.

\* Corresponding author.

E-mail address: [hrbacekfilip@gmail.com](mailto:hrbacekfilip@gmail.com) (F. Hrbáček).

## 1. Introduction

The active layer and permafrost are components of the cryosphere, which are very sensitive to climate variability. One of the most important characteristics of the active layer is its thickness, whose variability is considered to be a potential indicator of regional climate change (e.g. Anisimov et al., 1997; Romanovsky et al., 2010; Guglielmin and Cannone, 2012). It is thought that global warming before the end of 21st century may cause a significant increase in active layer thickness, which may exceed 3.5 m in ca. 35 to 81% of permafrost areas, mainly in the northern hemisphere (IPCC, 2013). In marginal parts of Antarctica, the changing of the environment in connection with present and future climate change will lead to changes in soil hydric regime, biota, and active layer thickness (RCP models for 2100 CE; IPCC, 2013).

Permafrost is thought to occupy >20% of Antarctica (ca. 2.5 mil km<sup>2</sup>; Bockheim, 1995), however the majority consists of sub-glacial permafrost, while the ice-free areas comprise around 44,900 km<sup>2</sup>, of which about 3500 km<sup>2</sup> are in the areas of Antarctic Peninsula north of 70°S (Antarctic Digital Database, 2017). From the perspective of terrestrial ecosystems in Antarctica, any changes in the active layer dynamics are very important, since the temporal extent of seasonal thawing or moisture content levels could significantly affect the distribution and variability of biota and soil nutrients (e.g.; Strauss et al., 2009; Boy et al., 2016).

The most important progress in active layer research in the Antarctic Peninsula region has been carried out during International Polar Year, when the number of study sites increased significantly (Vieira et al., 2010). Most of the studies conducted on newly-founded sites were focused on analysing the effect of snow cover (e.g.; Hrbáček et al., 2016a; Ferreira et al., 2017; de Pablo et al., 2017; Oliva et al., 2017b; Ramos et al., 2017), the insulation effect of vegetation (e.g. Cannone et al., 2006; Guglielmin et al., 2012; Almeida et al., 2017), or the effect of lithological properties (e.g. Guglielmin et al., 2014a; Hrbáček et al., 2017) on active layer thermal regimes. Individual effects of these factors were found to be more important triggers of active layer seasonal thawing than changes in the regional climate setting between different climate zones of the Antarctic Peninsula (Hrbáček et al., 2016b). However, all these studies were focused on one or two sites only, and did not consider the spatial variability of active layer thickness, unlike some works in Victoria Land (e.g. Adlam et al., 2010; Seybold et al., 2010).

In order to better understand the local variability of active layer thickness, the original Circumpolar Active Layer Monitoring protocol (CALM) of Brown et al. (2000) was implemented in its southern form (CALM-S), taking into account conditions in Antarctica, especially coarse ground texture, which is very hard to probe (Guglielmin, 2006; Vieira et al., 2010). Until 2010, a total of 28 CALM-S sites had been established across the Antarctic continent (Vieira et al., 2010). Initial results showed quite high variability in active layer depth over areas of 50 × 50 to 100 × 100 m. However, these results are still very sparse and limited to areas of the South Shetlands in the western Antarctic Peninsula (de Pablo et al., 2013; Ramos et al., 2017), sub-Antarctica (Guglielmin et al., 2012), and continental eastern Antarctica (Guglielmin, 2006; Guglielmin et al., 2014b), while the results from CALM-S sites in other parts of Antarctica involved in the CALM-S overview (Vieira et al., 2010) have not yet been individually published.

The CALM-S Johann Gregor Mendel (JGM) was established as the first CALM-S site in the eastern Antarctic Peninsula region in February 2014. In this study, results of active layer depth measurements carried out during the summers of 2014 to 2016 are presented. The analysis of the effects of ground physical and lithological properties on the active layer thermal regime and thickness was conducted using data from two study profiles within the CALM-S, located in different lithological conditions. Furthermore, the paper focuses on:

- 1) Presentation of the first data concerning ground physical properties (thermal conductivity, capacity and diffusivity, water content, dry bulk density, texture).
- 2) Evaluation of the seasonal and interannual variability of the active layer thermal regime and depth at the CALM-S JGM site.
- 3) Comparison of the permafrost temperatures from two 200-cm-deep profiles located in different lithology, from the perspective of lithological effect on the thermal stability of permafrost.

## 2. Regional setting

With an area of over 2400 km<sup>2</sup>, James Ross Island is the largest island in the northern Antarctic Peninsula region (Fig. 1). It is situated off the south-eastern coast of the peninsula and separated from the mainland by Prince Gustav Channel, which is 12–20 km wide. Approximately 600 km<sup>2</sup> (ca. 25%) of the total area of James Ross Island is ice-free

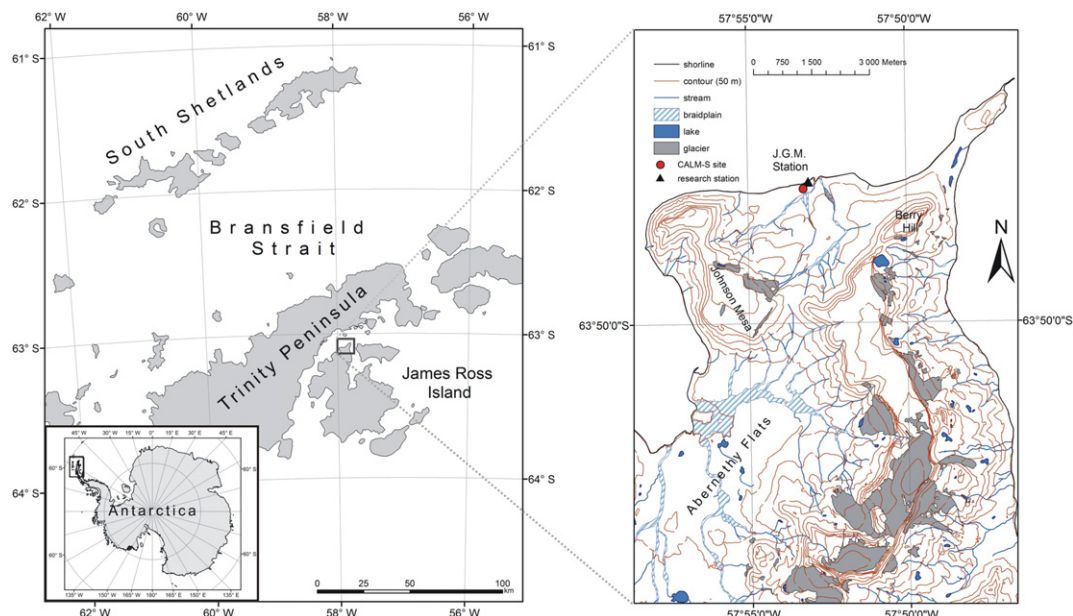


Fig. 1. Regional setting and topographical map of northern James Ross Island.

(Davies et al., 2013), composed of several separate ice-free areas. Deglaciation of the northern part of James Ross Island, called the Ulu Peninsula, started  $12.9 \pm 1.2$  ka ago (Nývlt et al., 2014). Until recently,  $>300$  km<sup>2</sup> of lowland were exposed (Kavan et al., 2017). Small glaciers preserved until the present day cover the high-altitude plateaus and heads of valleys (Engel et al., 2012). The environment of the Ulu Peninsula is unique, because this region is the largest individual ice-free area in the region, forming around 8% of all the deglaciated area in the northern Antarctic Peninsula region.

The climate of James Ross Island is cold polar-continental. The mean annual air temperature at sea level in the vicinity of Johann Gregor Mendel Station was  $-7.0$  °C in the period 2006–2015 (Hrbáček et al., 2016c). Mean daily air temperatures in summer can reach up to  $+5$  °C, while it can drop below  $-30$  °C during winter (Láska et al., 2011). The orographic barrier of the Trinity Peninsula Mountains to the west influences the amount of precipitation, which is predominantly in the form of snow (Martin and Peel, 1978). Estimates of precipitation range from 300 to 500 mm water-equivalent per year (van Lipzig et al., 2004). However, due to the strong effect of wind drift, the snow accumulates unevenly with thicknesses not exceeding 30 cm in the flat areas (Hrbáček et al., 2016a).

The ice-free surfaces of James Ross Island are underlain by continuous permafrost (Bockheim et al., 2013). The thickness of the permafrost was estimated, using geothermal flux, to be approximately 6 to 67 m in lowland areas near the sea (Fukuda et al., 1992; Borzotta and Trombotto, 2004). The active layer thickness strongly depends on the local lithology (Hrbáček et al., 2017) and varies approximately between 50 cm and 90 cm (Hrbáček et al., 2016b, 2017).

### 3. Measuring methods and equipment

#### 3.1. CALM-S JGM site description

The monitoring area of CALM-S Johann Gregor Mendel (JGM) involved in the GTN-P database was delimited in February 2014, to the south of Johann Gregor Mendel Station (Fig. 2) at an elevation of between 8 and 11 m, in accordance with the protocol proposed by Guglielmin (2006). Due to the morphological conditions of the terrain it was necessary to limit the size of the monitoring area to  $70 \times 80$  m, as opposed to the  $100 \times 100$  m standard (Brown et al., 2000). The active layer depth was measured during the first week of February using a

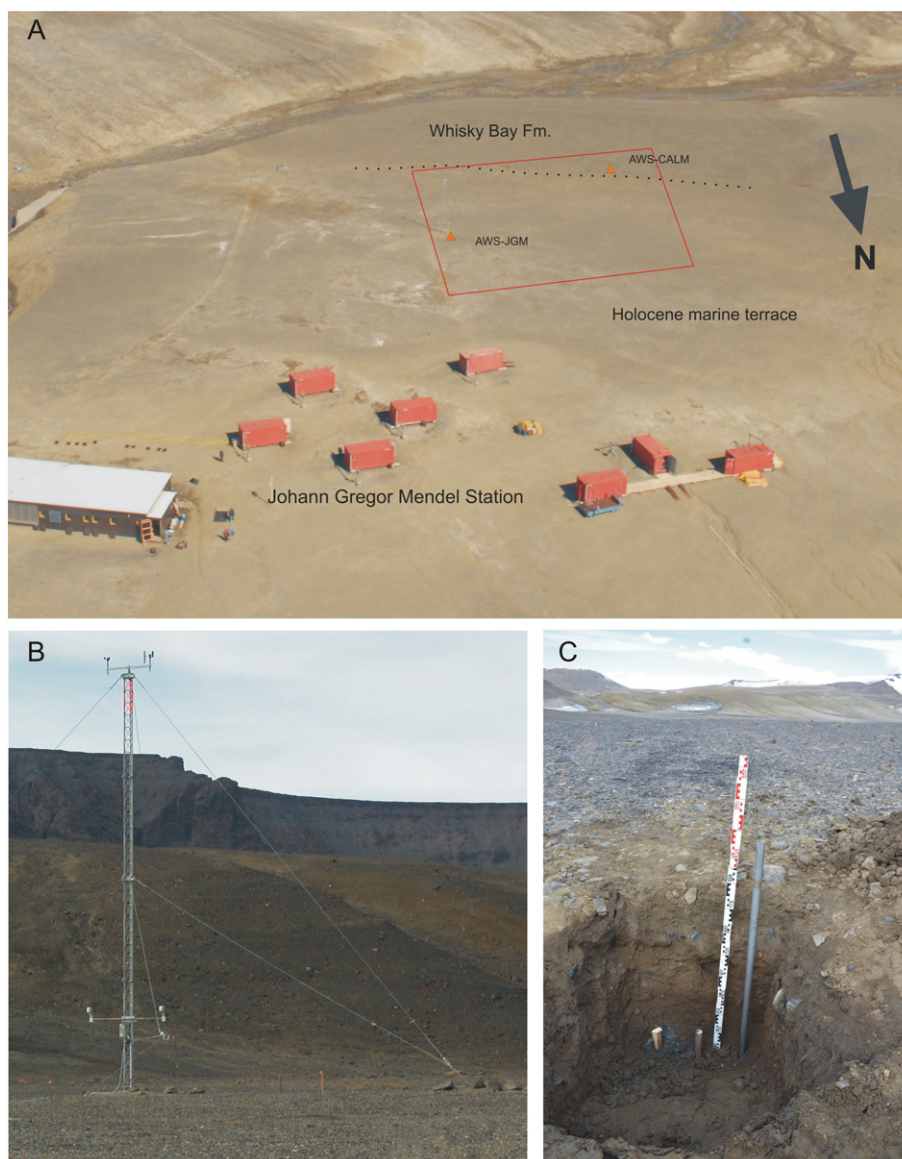


**Fig. 2.** Pictures of study site; (A) aerial image of CALM-S JGM site; (B) detailed image of AWS-JGM; (C) ground profile near to AWS-CALM. The dotted line indicates the lithological boundary between Holocene marine terrace sediments and Cretaceous sediments.

probing rod with a diameter of 10 mm, at a total of 72 points within a 10-meter grid. The spatial variability of the active layer depth was visualised and evaluated in Surfer 11 software, using kriging interpolation. The probing was limited in seasons 2015/16 by logistical conditions, which prevented measurements during the days of maximum thaw, which is one of main issues for CALM-S (Guglielmin, 2006).

The entire area of CALM-S is flat, with an average slope of  $<3^\circ$ . The surface is bare ground, non-vegetated, and stabilised by a pebble-boulder hamada-like pavement with common desert varnish on large basaltic stones (Stachoň et al., 2014). It features a Holocene marine terrace, the sediments of which transition in the northern part of CALM-S JGM to a Cretaceous Whisky Bay Formation (Fig. 2) composed of weathered sedimentary rocks (Crame et al., 2006; Nývlt et al., 2011; Mlčoch et al., 2016).

To confirm local differences in lithology, samples from two 70-cm-deep profiles located near the two monitoring sites were collected, each 10 cm long, for texture analysis. For particle dispersion, a 0.025 M  $\text{Na}_4\text{P}_2\text{O}_7$  solution was used. The fractions  $> 63 \mu\text{m}$  were determined via wet sieving and weighing, according to the DIN grade scale (630  $\mu\text{m}$  to 2000  $\mu\text{m}$ , 200  $\mu\text{m}$  to 630  $\mu\text{m}$ , and 63  $\mu\text{m}$  to 200  $\mu\text{m}$ ). The fractions  $< 63 \mu\text{m}$  (20  $\mu\text{m}$  to 63  $\mu\text{m}$ , 6.3  $\mu\text{m}$  to 20  $\mu\text{m}$ , 2  $\mu\text{m}$  to 6.3  $\mu\text{m}$ , and  $< 2 \mu\text{m}$ ) were determined according to the DIN grade scale using the X-ray attenuation method (Micromeritics, Sedigraph III Plus). Due to the very low carbon content, no destruction of organic matter was needed to disperse the bulk samples prior to the analysis. The lack of macro aggregation was tested before texture analysis using ultrasonic soil disruption. Ground samples used for the analysis of physical soil properties and water content were collected in February 2014, to represent both lithologically different parts of CALM-S. Intact samples from 10 and 30 cm depths were taken using 500  $\text{cm}^2$  steel cylinders. Ground

thermal properties were analysed in a laboratory using an ISOMET 104 analyser (Applied Precision, Bratislava). For each parameter, the resulting value was calculated as an average from 10 measurements. Then, the samples were air-dried at  $105^\circ\text{C}$  for 24 h to determine the total water content in the samples, and dry bulk density was calculated (Table 1).

### 3.2. Data acquisition and processing

The CALM-S JGM grid was established around an already functioning measurement site, AWS-JGM (marine terrace), that provides air temperature data and ground temperature data from a 200-cm-deep profile (Hrbáček et al., 2016a). In this study, data from a 37-month-long period from 1 March 2013 to 31 March 2016 were used. As a reference site for Whisky Bay Fm., part of CALM-S JGM, a new study profile, AWS-CALM, was established on 15 February 2014. At both sites, ground temperature was measured using Pt100/8 resistance thermometers (accuracy  $\pm 0.15^\circ\text{C}$ ). The thermistors were placed directly in the vertical soil profiles at depths of 5, 10, 20, 30, 50, 75, 100, 150, and 200 cm. An EMS 33 air temperature sensor with a Pt100/A thermometer (accuracy  $\pm 0.15^\circ\text{C}$ ) was placed at 200 cm above ground into the radiation protective shield. All sensors were connected to EMS V12 dataloggers (EMS Brno) set to record temperature at 30 min intervals.

The collected data were used to calculate the mean, maximum, and minimum daily values. Annual means were calculated for the period from March to February to cover a 12-month period containing complete freezing and thawing seasons. The ground thermal regime was evaluated using a common approach for Antarctic active layer research (e.g. Guglielmin, 2006). Mean daily values were further used for the definition of thawing and freezing seasons using the 5 cm depth data (e.g.

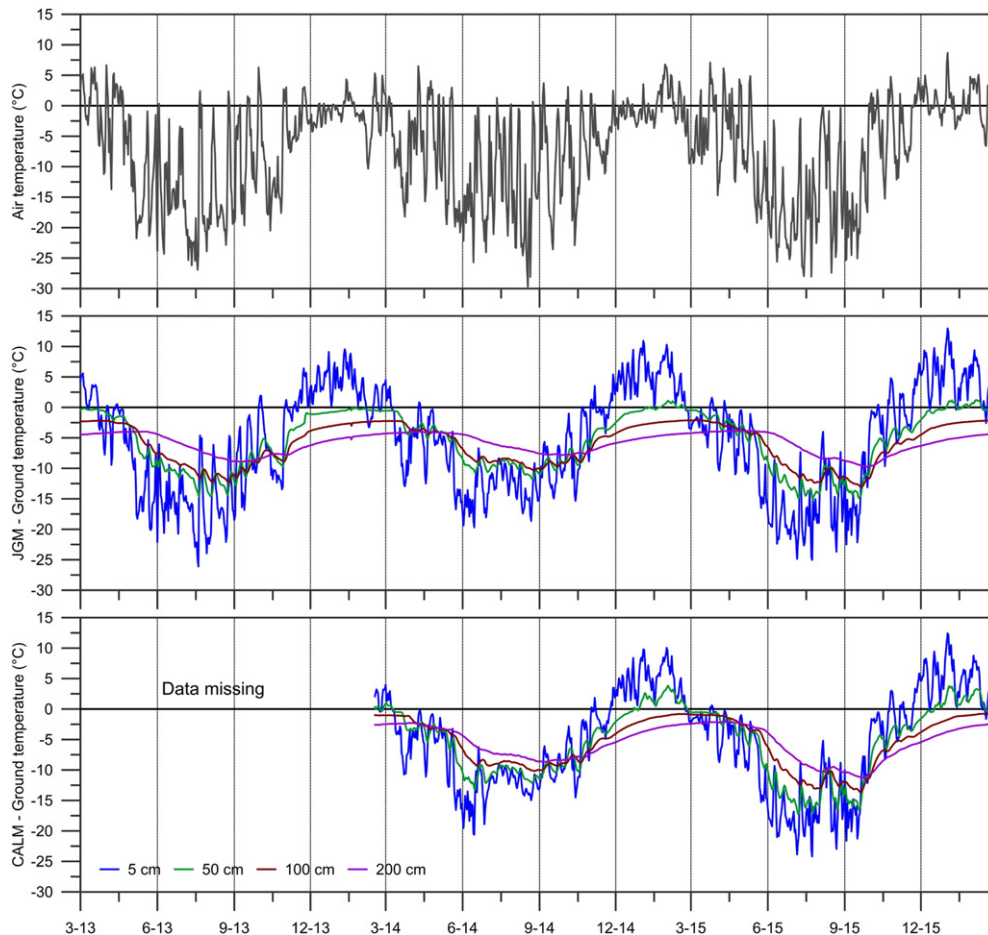


Fig. 3. Variability of air temperature and ground temperature at 5, 50, 100, and 200 cm at the AWS-JGM and AWS-CALM sites in the period 1 March 2013 to 29 February 2016.

**Table 1**  
Ground physical properties of Holocene marine terrace (Terrace) and Whisky Bay Formation (WB Fm.)

| Depth (cm) | Conductivity ( $W\ m^{-1}\ K^{-1}$ ) |             | Capacity ( $MJ\ m^{-3}\ K^{-1}$ ) |             | Diffusivity ( $m^2\ s^{-1}$ ) |             | Water content |        | Dry bulk density ( $g\cdot cm^{-3}$ ) |             |
|------------|--------------------------------------|-------------|-----------------------------------|-------------|-------------------------------|-------------|---------------|--------|---------------------------------------|-------------|
|            | Terrace                              | WB Fm.      | Terrace                           | WB Fm.      | Terrace                       | WB Fm.      | Terrace       | WB Fm. | Terrace                               | Wb. Fm.     |
| 10         | 0.38 ± 0.08                          | 0.70 ± 0.22 | 1.17 ± 0.29                       | 1.85 ± 0.47 | 0.32 ± 0.08                   | 0.37 ± 0.03 | 9%            | 17%    | 1.45 ± 0.03                           | 1.42 ± 0.03 |
| 30         | 0.17 ± 0.06                          | 0.72 ± 0.17 | 0.46 ± 0.18                       | 1.95 ± 0.41 | 0.39 ± 0.06                   | 0.36 ± 0.01 | 11%           | 19%    | 1.47 ± 0.03                           | 1.42 ± 0.03 |

de Pablo et al., 2013; Hrbáček et al., 2017). The thawing degree days (TDD) were calculated as a sum of positive mean daily temperatures, the freezing degree days (FDD) were calculated as a sum of negative mean daily temperatures (Lunardini, 1981). The n-factors both for thawing and freezing seasons were calculated as a ratio between thawing/freezing days of air temperature and thawing/freezing days of ground temperature at 5 cm (Lunardini, 1978). Maximum daily values of ground temperature were used for the interpolation of the daily position of the 0 °C isotherm and the calculation of the mean daily propagation rate of the active layer depth. Seasonal development of the active layer depth was observed during the period from October to March, which allowed for precise determination of the date of the maximum depth of the active layer.

**4. Results**

**4.1. Annual thermal regime**

**4.1.1. Air temperature**

The mean air temperature for the whole studied period (March 2013 to February 2016) was -7.2 °C, which was identical for all three years (Table 2). The most significant differences in air temperature were observed in its seasonal regime. The mean seasonal air temperature was highest during the summer months (December to February) when it reached -0.8 °C (2013/14) to 0.0 °C (2015/16), while the lowest mean seasonal air temperature was observed in the winter months (June to August) when it decreased to -15.9 °C (2015/16) to -13.4 °C (2014/15). The air temperature annual regime was typical, with a very high amplitude (Fig. 3) between 41.3 °C (2013/14) and 45.2 °C (2014/15). The maximum air temperature reached 13.3 °C (March 2015), while the minimum air temperature decreased to -34.2 °C (August 2014).

**4.2. Ground thermal regime**

**4.2.1. Site 1: AWS-JGM**

The mean annual ground temperature (MAGT) at AWS-JGM during the study period March 2013 to February 2016 gradually decreased with depth from -5.4 °C at 5 cm to -6.0 °C at 100 cm, while at 200 cm it increased very gently to -5.9 °C (Table 2, Fig. 4). Interannual differences in ground temperature were very small, reaching only 0.4 °C to 0.7 °C in the study profile. The warmest period was 2014/15, when MAGT varied between -5.0 °C at 5 cm and -5.7 °C at 100 cm, while

in the coldest period in both 2013/14 and 2015/16 the MAGT ranged from -5.6 °C at 5 cm to -6.0 °C at 100 cm.

The highest seasonal temperatures in the superficial 1 m were during the summer months from December to February, when the mean ground temperature ranged from 3.3 °C (2013/14) to 4.7 °C (2014/15 and 2015/16) at 5 cm to -2.7 °C (2014/15 and 2015/16) to -2.8 °C (2013/14) at 100 cm (Fig. 3, Table 2). The warmest seasons at 200 cm depth occurred in the autumn months from March to May, when the ground temperature reached from -4.0 °C (2015/16) to -4.2 °C (2014/15). The lowest seasonal temperatures were observed during winter at depths of from 5 cm (-12.9 °C in 2014/15 to -15.6 °C in 2015/16) to 100 cm (-8.8 °C in 2014/15 to -10.4 °C in 2015/16), while at 200 cm the lowest temperatures were detected in spring (-7.3 °C in 2014/15 to -8.3 °C in 2015/16) (Table 2).

The maximum ground temperature at AWS-JGM at 5 cm varied between 19.6 °C (2015/16) and 18.5 °C (2013/14) and decreased with depth to 200 cm, where it ranged from -3.7 °C (2014/15) to -4.5 °C (2015/16). The minimum ground temperature at AWS-JGM at 5 cm ranged from -20.8 °C (2014/15) to -27.9 °C (2015/16), and gradually increased to 200 cm, where it reached -7.9 °C (2014/15) to -9.8 °C (2015/16) (Fig. 4).

**4.2.2. Site 2 AWS-CALM**

The mean ground temperature at AWS-CALM during the period from March 2014 to February 2016 decreased slightly with depth from -5.3 °C at 5 cm, to -5.5 °C at 200 cm. The warmer season occurred in 2014/15, when MAGT ranged from -4.9 °C, at 5 cm to -5.2 °C at 200 cm. In 2015/16, ground temperatures varied between -5.6 °C at 5 cm, and -5.8 °C at 50 and 100 cm. (Fig. 3, Table 2). The warmest season in the superficial 1 m of the profile was summer from December to February (Table 2). The mean seasonal ground temperature ranged from 4.4 °C (2014/15) to 4.6 °C (2015/16) at 5 cm, to -1.7 °C (2014/15) to -1.6 °C (2015/16) at 100 cm, while the warmest months at 200 cm occurred in autumn (March to May) with mean seasonal ground temperatures between -2.8 °C (2014/15) and -2.5 °C (2015/16). Similarly, the lowest temperatures were observed during winter in the superficial 1 m only (Table 2). The seasonal ground temperature reached -12.7 °C (2014/15) to -16.4 °C (2015/16) at 5 cm, and -8.9 °C (2014/15) to -11.0 °C (2015/16) at 100 cm. The coldest seasons at 200 cm occurred during the spring months, when the mean ground temperature varied between -7.6 °C (2014/15) and -8.6 °C (2015/16).

The maximum ground temperature at AWS-CALM varied between 17.7 °C (2015/16) and 15.3 °C (2014/15) at 5 cm, and gradually

**Table 2**  
Mean seasonal air (AT) and ground (GT) temperature at different depths on AWS-JGM and AWS-CALM sites.

| Parameter | 2013/14 |         |       |        | 2014/15 |         |       |        | 2015/16 |         |       |        | 2013/14 | 2014/15 | 2015/16 | 2013-16 |
|-----------|---------|---------|-------|--------|---------|---------|-------|--------|---------|---------|-------|--------|---------|---------|---------|---------|
|           | III-V   | VI-VIII | IX-XI | XII-II | III-V   | VI-VIII | IX-XI | XII-II | III-V   | VI-VIII | IX-XI | XII-II |         |         |         |         |
| AT        | -5.1    | -15.1   | -7.1  | -1.2   | -7.1    | -13.4   | -7.5  | -0.5   | -5.6    | -15.9   | -7.4  | 0.0    | -7.2    | -7.2    | -7.2    | -7.2    |
| JGM       |         |         |       |        |         |         |       |        |         |         |       |        |         |         |         |         |
| GT 5 cm   | -5.2    | -15.7   | -4.9  | 3.3    | -5.9    | -13.3   | -5.5  | 4.7    | -5.2    | -16.7   | -5.3  | 4.7    | -5.6    | -5.0    | -5.6    | -5.4    |
| GT 50 cm  | -3.1    | -11.5   | -6.8  | -0.6   | -3.6    | -9.8    | -6.9  | -0.3   | -3.2    | -12.3   | -7.5  | -0.1   | -5.5    | -5.1    | -5.8    | -5.5    |
| GT 100 cm | -3.4    | -10.1   | -7.8  | -2.8   | -3.7    | -8.8    | -7.6  | -2.7   | -3.3    | -10.4   | -8.6  | -2.7   | -6.0    | -5.7    | -6.3    | -6.0    |
| GT 200 cm | -4.2    | -6.8    | -7.9  | -5.0   | -4.2    | -6.1    | -7.3  | -4.9   | -4.0    | -6.8    | -8.3  | -5.1   | -6.0    | -5.6    | -6.0    | -5.9    |
| CALM      |         |         |       |        |         |         |       |        |         |         |       |        |         |         |         |         |
| GT 5 cm   | -       | -       | -     | -      | -5.4    | -12.7   | -5.9  | 4.4    | -4.7    | -16.4   | -5.7  | 4.6    | -       | -4.9    | -5.6    | -5.3    |
| GT 50 cm  | -       | -       | -     | -      | -3.3    | -10.8   | -7.0  | 0.9    | -2.9    | -13.8   | -7.4  | 1.1    | -       | -5.0    | -5.8    | -5.4    |
| GT 100 cm | -       | -       | -     | -      | -2.6    | -8.9    | -7.5  | -1.7   | -2.1    | -11.0   | -8.3  | -1.6   | -       | -5.2    | -5.8    | -5.5    |
| GT 200 cm | -       | -       | -     | -      | -2.8    | -7.1    | -7.6  | -3.5   | -2.5    | -8.3    | -8.6  | -3.5   | -       | -5.2    | -5.7    | -5.5    |

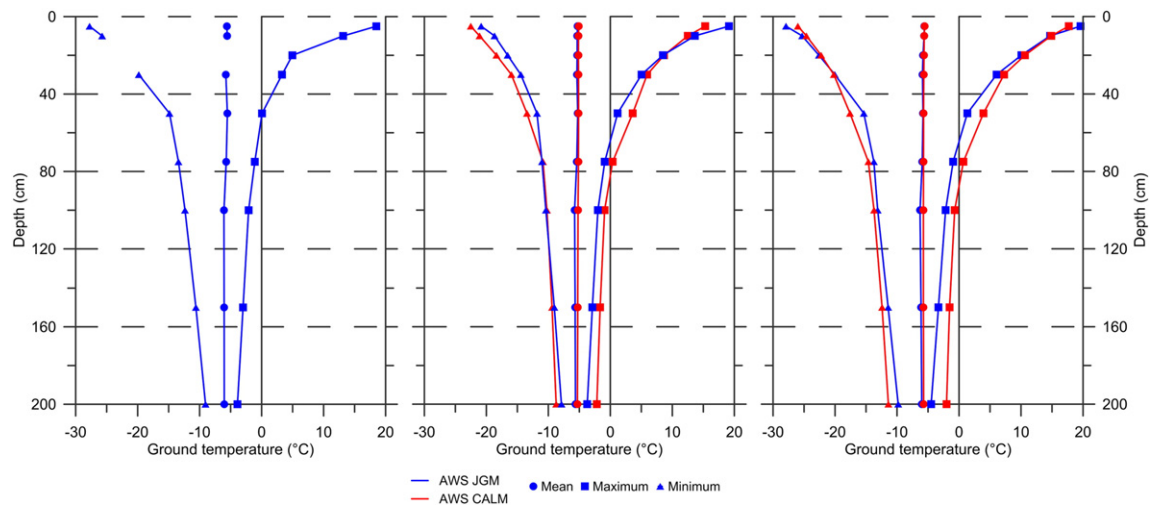


Fig. 4. Vertical temperature profiles of the active layer and permafrost at AWS-JGM and AWS-CALM in the seasons 2013/14 to 2015/16.

decreased with depth to 200 cm, where it reached  $-2.0$  °C (2015/16) and  $-2.2$  °C (2014/15). The minimum ground temperature dropped to  $-22.5$  °C (2014/15) and  $-26.0$  °C (2015/16) at 5 cm, while at 200 cm the minimum temperature reached  $-8.7$  °C (2014/15) and  $-11.4$  °C (2015/16) (Fig. 4).

#### 4.3. Freezing seasons

Freezing seasons lasted between 240 days (2013) and 272 days (2015) (Table 3). The difference between the AWS-JGM and AWS-CALM sites was 1 day in both the seasons of 2014 and 2015. The mean air temperature during freezing seasons ranged from  $-9.8$  °C (2014) to  $-10.6$  °C (2013). FDDa varied between  $-2492$  °C·day (2014) and  $-2684$  °C·day (2015). The mean freezing season ground temperature at 5 cm at AWS-JGM decreased to  $-8.7$  °C (2014) and  $-10.4$  °C (2013). FDDg at 5 cm depth ranged from  $-2301$  °C·day (2014) to  $-2579$  °C·day (2015). The freezing n-factor varied within a small interval between 0.88 (2014) and 0.95 (2013). A slightly higher mean freezing season ground temperature at 5 cm was observed at the AWS-CALM site (Table 3). It varied between  $-8.5$  °C (2014) and  $-9.2$  °C (2015). Consequently, FDDg at 5 cm decreased to  $-2231$  °C·day (2014) and  $-2510$  °C·day (2015). The freezing n-factor at AWS-CALM reached 0.85 (2014) and 0.90 (2015).

#### 4.4. Thawing seasons

The dates of the beginnings and ends of thawing seasons were almost identical for both profiles within the CALM-SJGM area (Table 4). All thawing seasons begun between 17 and 24 November, while the end date varied significantly between 23 February (2014/15) and 8 March (2013/14). The duration of thawing seasons ranged from 92/93 days (2014/15) to 111 days (2013/14). The maximum active layer thickness determined from the  $0$  °C isotherm occurred within the span of more than two weeks between 24 January in 2013/14, and 8 February both in 2014/15 and 2015/16 (Fig. 5).

The mean air temperature during thawing seasons increased from  $-1.1$  °C (2013/14) to  $0.5$  °C (2015/16). Similarly, TDDa rose from  $61$  °C·day (2013/14) to  $134$  °C·day (2015/16). The mean thawing season ground temperature at 5 cm at AWS-JGM varied between  $5.0$  °C in 2014/15 and  $3.3$  °C in 2013/14, while it did not exceed  $0$  °C during any season at 50 cm, where it ranged from  $-0.3$  °C in 2015/16 to  $-0.8$  °C in 2013/14 (Table 4). TDDg at 5 cm followed the pattern of MSGT and varied between  $506$  °C·day (2015/16) and  $380$  °C·day (2013/14). TDDg at 50 cm was not detected in 2013/14, but it reached  $13$  °C·day

(2014/15) and  $26$  °C·day (2015/16). High values of thawing n-factor were observed when it reached  $6.22$  (2013/14) to  $3.77$  (2015/16).

A slightly lower mean thawing season ground temperature at 5 cm was observed at AWS-CALM (Table 4), where it reached  $4.6$  °C (2014/15) to  $4.4$  °C (2015/16). TDDg at 5 cm reached values between  $478$  °C·day (2015/16) and  $418$  °C·day (2014/15). The mean thawing season ground temperature at 50 cm was positive, and varied between  $0.8$  °C (2015/16) and  $0.7$  °C (2014/15). TDDg at 50 cm reached  $122$  °C·day (2014/15) and  $96$  °C·day (2015/16).

#### 4.5. Thawing depth propagation

Initial short-term active layer thawing started several weeks before the beginning of the thawing season in every year and similarly, several episodes of shallow thawing were observed after the end of the thawing season (Fig. 5). Data from AWS-JGM shows that the date of the first active layer thawing event took place between 1 October (2013/14) and 21 October (2014/15). During several episodes of shallow thawing, the active layer depth reached up to 18 cm (2014/15) and 23 cm (2015/16). With the starts of all thawing seasons, the thawing depth propagated at an approximate rate of  $1.2$  cm day<sup>-1</sup> (2013/14) to  $1.5$  cm day<sup>-1</sup> (2014/15 and 2015/16) during the first 30 days of thawing, until mid-December (Fig. 5). Around this time, the thawing propagation rate started to slow down to ca.  $0.3$  cm day<sup>-1</sup> (2013/14 and 2014/15) and  $0.4$  cm day<sup>-1</sup> (2015/16), with several episodes of active layer depth decrease. A maximum active layer thickness of 51 cm occurred at the end of January 2013/14, while it exceeded 60 cm in February 2014/15 (63 cm) and 2015/16 (65 cm).

Pre-thawing events at the AWS-CALM site started between 11 October (2015/16) and 1 November (2014/15), and there were fewer

Table 3  
Thermal characteristics of freezing seasons at AWS-JGM and AWS-CALM sites.

| Parameter            | 2013     |      | 2014     |          | 2015     |          |
|----------------------|----------|------|----------|----------|----------|----------|
|                      | JGM      | CALM | JGM      | CALM     | JGM      | CALM     |
| Beginning            | 23/03/13 | -    | 08/03/14 | 09/03/14 | 23/02/15 | 24/02/15 |
| End                  | 16/11/13 | -    | 24/11/14 | 24/11/14 | 21/11/15 | 21/11/15 |
| Duration             | 240      | -    | 262      | 261      | 272      | 271      |
| AT <sup>a</sup>      | $-10.6$  | -    | $-9.8$   | -        | $-9.8$   | -        |
| FDDa                 | $-2614$  | -    | $-2615$  | -        | $-2786$  | -        |
| GT <sup>b</sup> 5 cm | $-10.4$  | -    | $-8.7$   | $-8.5$   | $-9.4$   | $-9.2$   |
| FDDg 5 cm            | $-2480$  | -    | $-2301$  | $-2231$  | $-2579$  | $-2510$  |
| n-Factor             | 0.95     | -    | 0.88     | 0.85     | 0.93     | 0.90     |

<sup>a</sup> AT is mean seasonal air temperature in °C.

<sup>b</sup> GT is mean seasonal ground temperature in °C.

**Table 4**  
Thermal characteristics of thawing seasons at AWS-JGM and AWS-CALM sites.

| Parameter             | 2013/14  |          | 2014/15  |          | 2015/16  |          |
|-----------------------|----------|----------|----------|----------|----------|----------|
|                       | JGM      | CALM     | JGM      | CALM     | JGM      | CALM     |
| Beginning             | 17/11/13 | –        | 24/11/14 | 24/11/14 | 22/11/15 | 22/11/15 |
| End                   | 07/03/14 | 08/03/14 | 23/02/15 | 24/02/15 | 06/03/16 | 06/03/16 |
| Duration              | 111      | –        | 92       | 93       | 101      | 78       |
| AT <sup>a</sup>       | –1.1     | –        | –0.3     | –        | 0.5      | –        |
| TDDa                  | 61       | –        | 86       | –        | 134      | –        |
| GT <sup>b</sup> 5 cm  | 3.3      | –        | 5        | 4.6      | 4.7      | 4.4      |
| GT <sup>b</sup> 50 cm | –0.8     | –        | –0.5     | 0.7      | –0.3     | 0.8      |
| TDD 5 cm – JGM        | 380      | –        | 456      | 418      | 506      | 478      |
| TDD 50 cm – JGM       | 0        | –        | 13       | 107      | 26       | 122      |
| n-factor              | 6.22     | –        | 5.30     | 4.86     | 3.77     | 3.57     |

<sup>a</sup> AT is mean seasonal air temperature in °C.

<sup>b</sup> GT is mean seasonal ground temperature in °C.

thawing events identified in total (Fig. 6). Calculated thawing depths during the pre-thawing events were between 14 cm (2014/15) and 18 cm (2015/16). The thawing propagation rate in both thawing seasons followed the same pattern. It reached approximately  $1.5 \text{ cm day}^{-1}$  until mid-December, when it started to slow down to ca.  $0.7 \text{ cm day}^{-1}$ . The active layer depth > 80 cm was reached for two weeks at the turn of January and February, with the maximum depth of 86 cm (2014/15) and 87 cm (2015/16) observed on 8 February in both seasons (Table 5, Fig. 5).

#### 4.6. CALM-S JGM probing

The mean probed active layer depth varied between  $66.4 \pm 9.8 \text{ cm}$  (2013/14) and  $78.4 \pm 12.2 \text{ cm}$  (2014/15). Standard deviation values showed lower variability of the active layer depth during 2013/14, and higher variability during the 2014/15 and 2015/16 seasons (Table 5). The differences between the maximum and minimum depths were similar, being between 49 cm (2013/14) and 54 cm (2014/15). The maximum active layer depth varied between 100 cm (2013/14) and 113 cm (2015/16). Values exceeding 100 cm were observed at only one grid point in 2013/14 (Fig. 6), but appeared more frequently during 2014/15 (7 values) and 2015/16 (5 values). In all cases, the deepest active layer was found in the south-western grid corner (Fig. 6). The minimum active layer depth ranged from 51 cm in 2013/14 to 59 cm in 2015/16. Measurements < 60 cm appeared to be abundant during the season 2013/14, with 20 values located in the north-western and eastern grid sectors. However, during 2014/15 and 2015/16 values < 60 cm were observed sporadically (1 value in 2014/15 and 2

values in 2015/16) and were restricted to the eastern grid sector around AWS-JGM only.

#### 4.7. Ground texture and physical properties

Sediments of the Holocene marine terrace are generally represented by silty to gravelly sand, with 69–80% of sand fraction and the highest admixture of gravel and fine sized soil particle fractions in the superficial part (Fig. 7). The proportion of silt is generally higher than that of clay, except for in the lowermost part of the profile, where the clay fraction proportion rises significantly. Whisky Bay Formation is in its superficial part weathered to loose regolith, which has a typical bimodal composition of clayey fine sand, with 45–57% of sand and 24–31% of clay (Fig. 7). The highest sand proportion (>50%) is found in the middle part of the profile (30–50 cm), which is connected with the depletion of finer particles. Sediments of the Holocene marine terrace are generally better sorted due to prevailing shallow marine and beach sorting during their deposition. In contrast, the Whisky Bay Fm. clayey sandstones were deposited in a submarine fan, or slope apron environment (Crame et al., 2006) with changing sedimentation from turbidite flows and suspension causing the bimodal grain-size composition.

### 5. Discussion

#### 5.1. Climate background

The Antarctic Peninsula region had, until recently, been considered one of the most rapidly warming parts of the Earth, with a significant effect of air temperature warming on the active layer and permafrost thermal state and properties (e.g. Guglielmin, 2006; Vieira et al., 2010; Bockheim et al., 2013). In fact, the air temperature cooling in the region started around 1998–2000 in the north-eastern Antarctic Peninsula (Turner et al., 2016). From an air temperature point of view, the study period of 2013 to 2015 was  $0.2 \text{ °C}$  colder than the average mean annual air temperature in 2006–2015, which was  $-7.0 \text{ °C}$  (Hrbáček et al., 2016c). Nevertheless, for the active layer development, summer temperatures reflected also as TDD indices are more important than annual temperatures, which are significantly affected by temperature during the winter months (e.g. Zhang and Stames, 1998). The air temperature decrease was most pronounced during the summer months (Turner et al., 2016), which has caused the active layer thinning and decrease of ground temperatures in the Antarctic Peninsula region (Oliva et al., 2017a). However, between summer 2013/14 and 2015/16 the air temperature increased by  $1.2 \text{ °C}$  and the ground temperature at 5 cm by  $2.2 \text{ °C}$  on James Ross Island, which resulted in a significant increase of the active layer thickness on AWS-JGM from 51 to 65 cm.

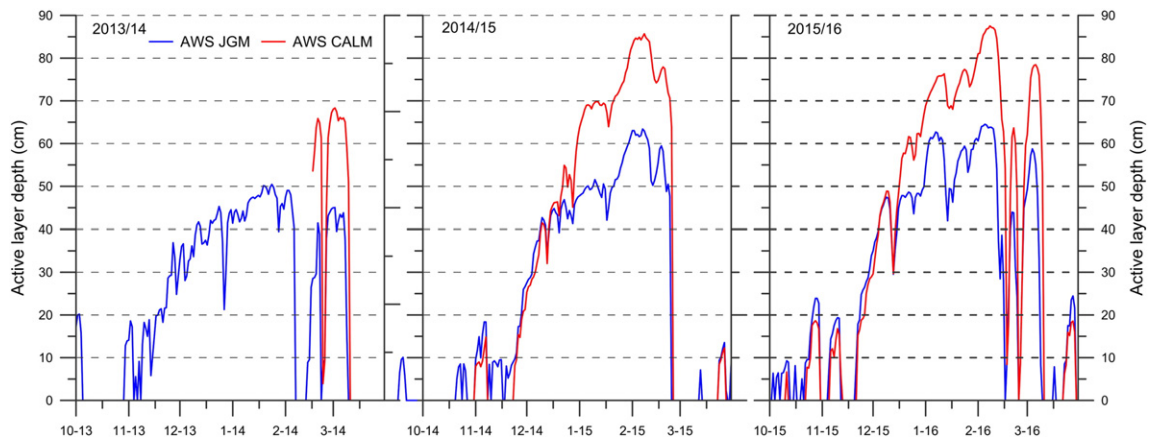


**Fig. 5.** Seasonal development of active layer depth at AWS-JGM and AWS-CALM in thawing seasons 2013/14 to 2015/16.

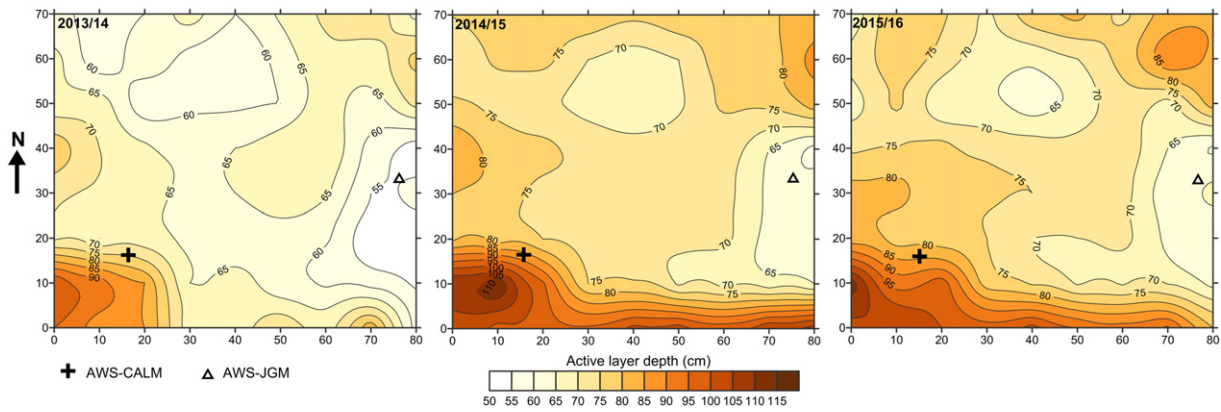


Fig. 6. Variability of probed active layer depth in CALM-S sites in thawing seasons 2013/14 to 2015/16.

### 5.2. Effect of lithology on active layer depth and the permafrost thermal regime

The most important factors affecting the active layer thermal regime and thickness are considered to be climate, snow, vegetation, and ground physical properties (e.g. Brown et al., 2000; Frauenfeld et al., 2004; Zhang, 2005), the effects of which were discussed in the case of James Ross Island by Hrbáček et al. (2016b). From the perspective of the active layer thermal and depth variability on CALM-S JGM, the only important factors considered here are the ground physical properties, which strongly depend on lithology. The possible effects of the other above-mentioned factors were neglected because a) the climate conditions can be considered uniform for such a small area; b) the effect of snow cover and its insulation capability on the ground thermal regime was found to be negligible in previous studies (e.g. Hrbáček et al., 2016a), which was also confirmed by very high values of freezing n-factors ( $>0.85$ ) at both sites. According to the empirical measurements of Goodrich (1982), or Riseborough and Smith (1998) such high values suggest prevailing snow-free conditions during the winter; c) the vegetation on James Ross Island is limited only to specific, small areas (Barták et al., 2015; Nývlt et al., 2016), which are not present on CALM-S JGM.

Ground physical properties are conditioned by lithology, especially by grain-size characteristics of the material. They are fundamental for moisture content, and ground thermal conductivity. The significantly higher content of clay in the north-western part of CALM-S JGM (Fig. 7) allows the ground to retain more liquid water (c.f. Putkonen, 1998), which resulted in ca. 8% higher water content in the northern part of CALM-S JGM located in Whisky Bay Fm. sediments. Only small differences in dry bulk density between both lithology suggest, that the texture and water content differences are the most important factor causing 2–4  $\times$  higher soil thermal conductivity, and significantly higher soil thermal capacity in Whisky Bay Fm. sediments (c.f. Farouki, 1981; Abu-Hamdeh and Reeder, 2000). Another consequence of the different moisture contents between AWS-CALM and AWS-JGM was the later beginning of the initial thawing of the active layer at AWS-CALM (Fig. 5). Despite a higher thermal conductivity and capacity at AWS-CALM, a

larger amount of heat was necessary for the phase change of water. Therefore, active layer thawing started earlier and reached greater depths at AWS-JGM.

Despite significant differences in thermal and moisture properties, no signs of any “zero-curtain” phenomena have been observed in the ground thermal regime typical of the beginnings and endings of thawing seasons, during which phase change occurs (Outcalt et al., 1990). This was not detected even in the deeper parts of both profiles, which is in contrast with observations from other parts of the Antarctic Peninsula (e.g. de Pablo et al., 2014), or continental Antarctica (e.g. Guglielmin and Cannone, 2012).

Different lithological properties caused diverse heat transport to deeper parts of the active layer and the uppermost part of the permafrost. Despite relatively low differences (0.4 to 0.5  $^{\circ}\text{C}$ ) between the mean annual temperatures of permafrost at 100 and 200 cm depths between AWS-CALM and AWS-JGM, the maximum mean seasonal temperature of permafrost on AWS-CALM was higher by 1.0  $^{\circ}\text{C}$  (100 cm) to 1.5  $^{\circ}\text{C}$  (200 cm), than on AWS-JGM. The predicted warming in Eastern Antarctica during the 21st century (RCP model; IPCC, 2013) could therefore cause faster degradation of the uppermost part of the permafrost, as well as thickening of the active layer in areas with higher ground thermal conductivity and capacity. Furthermore, models predict pronounced drying (reduction of moisture content in the surficial part of the active layer) of the ice-free areas of James Ross Island due to ongoing glacial shrinkage and enhanced active layer thawing (ATCM, 2015). It can be assumed that such a change of hydric regime would affect the biological activity of soils, material transport, and erosion in coastal areas of James Ross Island.

### 5.3. Active layer depth variability

Active layer depth probing showed that this simple method could be very useful for gaining a better understanding of its local variability (Bonnaventure and Lamoreaux, 2013). Despite the smaller area of the CALM-S JGM site, very large differences of around 50 cm were observed between the minimum and maximum active layer depths. The distribution of active layer depths clearly distinguishes between the parts of

Table 5  
Summary of active layer depth (ALD) measurement and active layer thickness (ALT) on CALM-S JGM.

| Season  | Date of maximum thickness | ALD probing | ALD mean (cm) | ALD max (cm) | ALD min (cm) | Sd. <sup>a</sup> | ALT JGM (cm) | ALT CALM (cm) |
|---------|---------------------------|-------------|---------------|--------------|--------------|------------------|--------------|---------------|
| 2013/14 | 24 January                | 5 February  | 66.4          | 100          | 51           | 9.8              | 51           | –             |
| 2014/15 | 8 February                | 6 February  | 78.4          | 110          | 58           | 12.2             | 63           | 86            |
| 2015/16 | 8 February                | 29 January  | 77.0          | 113          | 59           | 11.6             | 65           | 87            |

<sup>a</sup> Standard deviation.

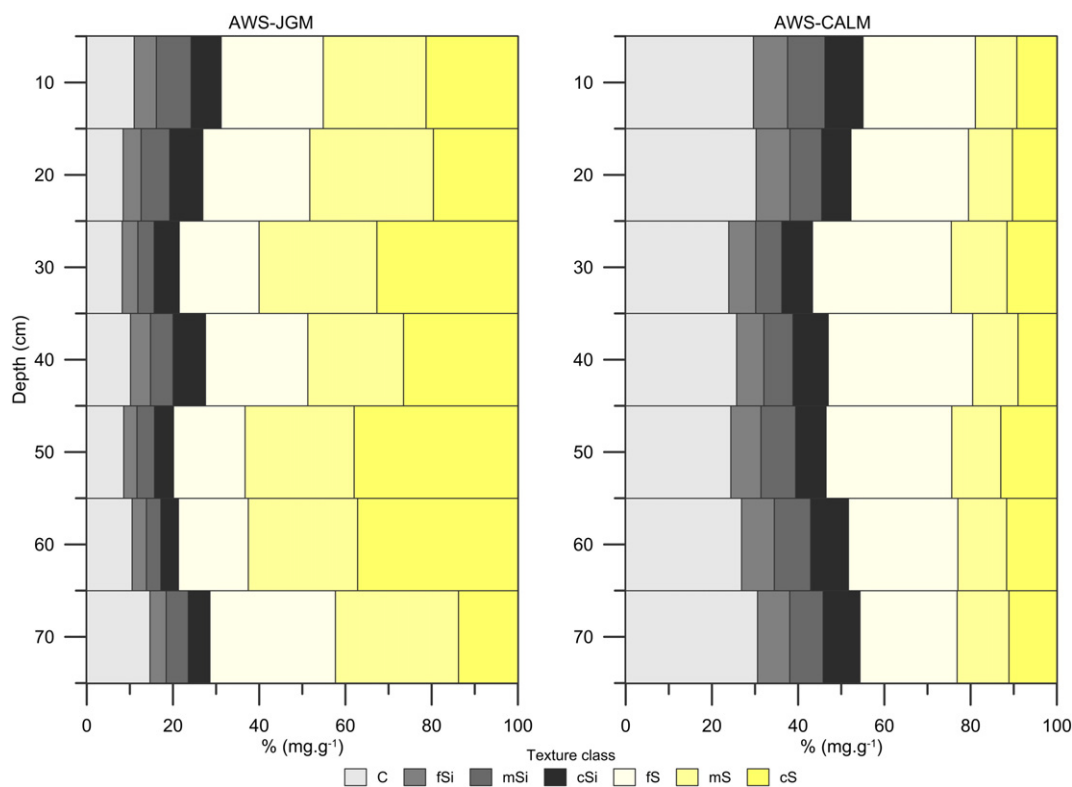


Fig. 7. Ground texture characteristics. C represents clay; fSi – fine silt; mSi – medium silt; cSi – coarse silt; fS – fine sand; mS – medium sand; cS – coarse sand.

CALM-S formed by marine terrace sediments (60–70 cm) and Cretaceous sediments (80–100 cm) (Figs. 2 and 6). Such a clear effect of lithology has not yet been described on any other CALM-S sites in Antarctica. The spatial distribution of the active layer depth has usually been driven by snow cover distribution influenced by local mesotopography (Guglielmin, 2006; de Pablo et al., 2013; Ramos et al., 2017) and spots of vegetation cover (Guglielmin et al., 2014b).

The maximum probed active layer depth within the grid exceeded by about 25 cm the active layer thickness determined by the 0 °C isotherm at AWS-CALM. To calculate the maximum possible active layer depth in 2015/16, when probing was not undertaken at the end of the season, the correction according to the 0 °C isotherm development was applied (Brown et al., 2000). At first, the temporal change in active layer depth between 18 and 29 January 2016 (Table 6) was analysed. The mean active layer depth increased by 6 cm (from 71 cm to 77 cm). In 60% of the grid, the increment to the active layer depth was between 3 cm and 9 cm (Fig. 8), while the active layer thickness at AWS-JGM and AWS-CALM increased by 7 cm and 4 cm, respectively. A more rapid increase of active layer thickness by 12 cm was observed at AWS-CALM between 29 January and 8 February, but the active layer thickness increased by 4 cm only at AWS-JGM (Table 6 and Fig. 5). Considering the part of CALM-S with the deepest active layer located close to AWS-CALM, the maximum active layer depth may have reached almost 125 cm in February 2016. Moreover, using the mean value of the active layer thickness increment (8 cm) at AWS-JGM and AWS-CALM, the mean active layer depth within the CALM-S may have reached 85 cm. From the perspective of active layer depth variability on James Ross Island, both the lowest and highest active layer depths were observed within the CALM-S site when compared with other localities on James Ross Island (e.g. Engel et al., 2010; Hrbáček et al., 2016a, 2017).

Even though the mean annual air temperature on James Ross Island is about 4–5 °C lower than on the South Shetlands in the western Antarctic Peninsula region, the thawing seasons during summer are generally warmer with higher TDD indices (Hrbáček et al., 2016b). Comparing the results of mean active layer depths from CALM-S sites

in Deception Island (Ramos et al., 2017) and Livingston Island (de Pablo et al., 2013), the mean active layer depth in the CALM-S grid has been about 30–50 cm higher on James Ross Island. This difference is caused by snow cover, which has persisted on the ground in the South Shetlands during the summer season, impeding deep active layer thawing (de Pablo et al., 2017), while snow-free conditions and an equally developed active layer depth are typical for CALM-S on James Ross Island. Nevertheless, the active layer thicknesses at different sites formed by loose material in the western Antarctic Peninsula region reach higher values than on James Ross Island, varying usually between 100 and 120 cm (e.g. Vieira et al., 2010; Bockheim et al., 2013; de Pablo et al., 2014; Oliva et al., 2017b; Almeida et al., 2017). At solid bedrock sites the active layer thickness could even reach from 150 cm up to 500 cm, due to the higher thermal conductivity of solid rocks (>3.0 W m K<sup>-1</sup>; Ramos and Vieira, 2009; Correia et al., 2012; Guglielmin et al., 2014a).

## 6. Conclusions

In this study, the first results of CALM-S monitoring from a study site in the eastern Antarctic Peninsula region are presented. James Ross Island offers a unique opportunity to study the active layer thermal regime and its thickness, because it contains the largest ice-free area in the whole Antarctic Peninsula region, and active layer thermal regime

Table 6

Active layer thickness (ALT) and depth (ALD) development on CALM-S between 18 January 2016 and 8 February 2016. Numbers in brackets indicate increment of active layer depth and thickness.

| Date       | Mean ALD (cm)   | Max ALD (cm)     | Min ALD (cm)    | ALT JGM (cm) | ALT CALM (cm) |
|------------|-----------------|------------------|-----------------|--------------|---------------|
| 18 January | 71              | 100              | 53              | 52           | 71            |
| 29 January | 77 (+6)         | 113 (+13)        | 59 (+6)         | 59 (+7)      | 75 (+4)       |
| 8 February | 85 <sup>a</sup> | 125 <sup>a</sup> | 63 <sup>a</sup> | 63 (+4)      | 87 (+12)      |

<sup>a</sup> Recalculated value of ALD according to ALT increment.

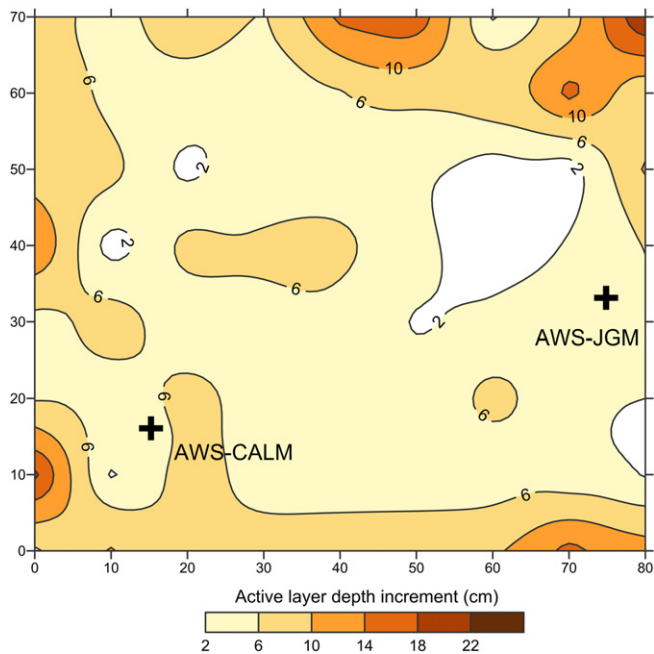


Fig. 8. Differences in probed active layer depth between 18 January and 29 January 2016.

could be studied under different lithological, geomorphological, hydrological, ecological, and meteorological conditions. With respect to local conditions, which neglect the effects of snow cover or vegetation on the active layer thermal regime and thawing depth, this study focused on the effects of differences in lithology.

The study site established near the Johann Gregor Mendel Station encompassed contrasting lithological settings of Holocene marine terrace and Cretaceous sedimentary rocks, which resulted in significant differences in the active layer depth. It reached around 60–70 cm in the marine terrace part, while it reached 80–100 cm in the Cretaceous sediments. The difference between maximum and minimum depths was >50 cm. This variability explains primarily different soil texture and soil moisture which significantly affect ground thermal properties in both parts of CALM-S. The lithology further significantly affects the ground thermal regime in the permafrost. During the summer and autumn seasons, a temperature of >1.0 °C higher at 200 cm was found in the area of CALM-S with higher heat permeability, which may cause higher vulnerability of the permafrost to thawing in the case of future climate changes in this area.

The probing at the CALM-S site highlighted this approach as a very useful method for active layer research. It was possible to identify very large differences in the active layer depth over a small area. These were not possible to detect with ground temperature monitoring only. However, one of the main issues in the first year of monitoring at CALM-S JGM was the timing of the final measurements, which was inconsistent with the date of the maximum active layer depth. Therefore, recalculation was used according to the CALM protocol, taking into account the propagation of the 0 °C isotherm. The maximum recalculated active layer depth may have reached around 125 cm, and the mean active layer depth within the grid may have reached 85 cm in 2015/16. These observations therefore suggest that at least two active layer depth probing and continuous ground temperature measurements from at least two profiles at CALM-S grid are necessary for active layer depth recalculation in seasons when the measurement of the maximum active layer depth is not possible.

#### Acknowledgement

This work was supported by the Masaryk University project MUNI/A/1315/2015: Integrated research of environmental changes in the

landscape sphere. The work was also supported by the Ministry of Education, Youth, and Sports (MEYS) large infrastructure project LM2015078 “Czech Polar Research Infrastructure”. Carsten W. Mueller’s work was supported by the German Research Foundation DFG for funding in the frame of the priority program SPP1158 (MU 3021/8-1). The authors thank Petr Dědeček from Institute of Geophysics of the Czech Academy of Science for help with laboratory analysis of ground samples. Finally, we are grateful to two anonymous referees and the handling editor for their beneficial comments, which significantly improved the final version of manuscript.

#### References

- Abu-Hamdeh, N.H., Reeder, R., 2000. Soil thermal conductivity: Effects of density, moisture, salt concentration, and organic matter. *Soil Sci. Soc. Am. J.* 64, 1285–1290.
- Adlam, L.S., Balks, M.R., Seybold, C.A., Campbell, D.I., 2010. Temporal and spatial variation in active layer depth in the McMurdo Sound Region, Antarctica. *Antarct. Sci.* 22 (1), 45–52.
- Almeida, I.C.C., Schaefer, C.E.G.R., Michel, R.F.M., Fernandes, R.B.A., Pereira, T.T.C., de Andrade, A.M., Francelino, M.R., Elpidio, I., Filho, F., Bockheim, J.G., 2017. Long term active layer monitoring at a warm-based glacier front from maritime Antarctica. *Catena* 149 (2), 572–581.
- Anisimov, O.A., Shiklomanov, N., Nelson, F.E., 1997. Global warming and active-layer thickness: results from transient general circulation models. *Glob. Planet. Chang.* 15, 61–77.
- Antarctic Digital Database, 2017. <http://www.add.scar.org/> (accessed 01.05.17).
- ATCM, 2015. Information Paper 034. Antarctic Trial of WWF’s Rapid Assessment of Circum-Arctic Ecosystem Resilience (RACER) Conservation Planning Tool: Results of RACER Workshop Focused on James Ross Island. Information paper by Great Britain and Czechia, 38th Antarctic Treaty Consultative Meeting, Sofia.
- Barták, M., Václav, P., Stachoň, Z., Kubešová, S., 2015. Vegetation mapping of moss-dominated areas of northern part of James Ross Island (Antarctica) and a suggestion of protective measures. *Czech Polar Rep.* 5 (1), 75–87.
- Bockheim, J., 1995. Permafrost Distribution in the Southern Circumpolar Region and its Relation to the Environment: a Review and Recommendations for Further Research. *Permafrost. Periglac.* 6, 27–45.
- Bockheim, J., Vieira, G., Ramos, M., López-Martínez, J., Serrano, E., Guglielmin, M., Wilhelm, K., Nieuwendam, A., 2013. Climate warming and permafrost dynamics in the Antarctic Peninsula region. *Glob. Planet. Chang.* 100, 215–223.
- Bonnaventure, P.P., Lamoreaux, S.F., 2013. The active layer: a conceptual review of monitoring, modelling techniques and changes in a warming climate. *Prog. Phys. Geogr.* 37 (3), 352–376.
- Borzotta, E., Trombotto, D., 2004. Correlation between frozen ground thickness measured in Antarctica and permafrost thickness estimated on the basis of the heat flow obtained from magnetotelluric soundings. *Cold Reg. Sci. Technol.* 40, 81–96.
- Boy, J., Godoy, R., Shubitsova, O., Boy, D., McCulloch, R., Andrino de la Fuente, A., Morales, M.A., Mikutta, R., Guggenberger, G., 2016. Successional patterns along soil development gradients formed by glacier retreat in the maritime Antarctic, King George Island. *Rev. Chil. Hist. Nat.* 89 (6). <http://dx.doi.org/10.1186/s40693-016-0056-8>.
- Brown, J., Hinkel, K.M., Nelson, F.E., 2000. The circumpolar active layer monitoring (CALM) program: research designs and initial results. *Polar Geogr.* 24 (3), 165–258.
- Cannone, N., Ellis Evans, J.C., Strachan, R., Guglielmin, M., 2006. Interactions between climate, vegetation and the active layer in soils at two Maritime Antarctic sites. *Antarct. Sci.* 18 (3), 323–333.
- Correia, A., Vieira, G., Ramos, M., 2012. Thermal conductivity and thermal diffusivity of cores from 26 meter deep borehole drilled in Livingston Island, Maritime Antarctic. *Geomorphology* 155–156, 7–11.
- Crame, J.A., Pirrie, D., Riding, J.B., 2006. Mid-Cretaceous stratigraphy of the James Ross Basin, Antarctica. In: Francis, J.E., Pirrie, D., Crame, J.A. (Eds.), *Cretaceous-Tertiary High-Latitude Palaeoenvironments, James Ross Basin, Antarctica*. Geological Society, London, Special Publications 258, pp. 7–19.
- Davies, B.J., Glasser, N.F., Carrivick, J.L., Hambrey, M.J., Smellie, J.L., Nývlt, D., 2013. Landscape evolution and ice-sheet behaviour in a semi-arid polar environment: James Ross Island, NE Antarctic Peninsula. In: Hambrey, M.J., Barker, P.F., Barrett, P.J., Bowman, V., Davies, B., Smellie, J.L., Tranter, M. (Eds.), *Antarctic Palaeoenvironments and Earth-Surface Processes*. Geological Society, London, Special Publications Vol. 381, pp. 353–395.
- De Pablo, M.A., Blanco, J.J., Molina, A., Ramos, M., Quesada, A., Vieira, G., 2013. Interannual active layer variability at the Limnopolar Lake CALM site on Byers Peninsula, Livingston Island, Antarctica. *Antarct. Sci.* 25, 167–180.
- De Pablo, M.A., Ramos, M., Molina, A., 2014. Thermal characterization of the active layer at the Limnopolar Lake CALM-S site on Byers Peninsula (Livingston Island), Antarctica. *Solid Earth* 5, 721–739.
- De Pablo, M.A., Ramos, M., Molina, A., 2017. Snow cover evolution, on 2009–2014, at the Limnopolar Lake CALM-S site on Byers Peninsula, Livingston Island, Antarctica. *Catena* 149 (2), 538–547.
- Engel, Z., Láška, K., Franta, T., Máčka, Z., Marvánek, O., 2010. Recent changes of permafrost active layer on the James Ross Island, maritime Antarctic. In: Mertes, J.R., Christiansen, H.H., Eitzelmüller, B. (Eds.), *In Abstracts from the Third European Conference on Permafrost*. 129. UNIS, Longyearbyen.
- Engel, Z., Nývlt, D., Láška, K., 2012. Ice thickness, bed topography and glacier volume changes on James Ross Island, Antarctic Peninsula. *J. Glaciol.* 58, 904–914.
- Farouki, O.T., 1981. *Thermal Properties of Soils*. U.S. Army Cold Regions Research and Engineering Laboratory Monograph (81-1).

- Ferreira, A., Vieira, G., Ramos, M., Nieuwendam, A., 2017. Ground temperature and permafrost distribution in Hurd Peninsula (Livingston Island, Maritime Antarctic): An assessment using freezing indexes and TTOP modelling. *Catena* 149 (2), 560–571.
- Frauenfeld, O.W., Zhang, T., Barry, R.G., Gilichinsky, D., 2004. Interdecadal changes in seasonal freeze and thaw depths in Russia. *J. Geophys. Res.* 109, D05101. <http://dx.doi.org/10.1029/2003JD004245>.
- Fukuda, M., Shimokawa, K., Takahashi, N., Sone, T., 1992. Permafrost in Seymour Island and James Ross Island, Antarctic Peninsula region. *Geogr. Rev. Jpn Ser. A* 65 (2), 124–131.
- Goodrich, L.E., 1982. The influence of snow cover on the ground thermal regime. *Can. Geotech. J.* 19, 421–432.
- Guglielmin, M., 2006. Ground surface temperature (GST), active layer, and permafrost monitoring in continental Antarctica. *Permafr. Periglac.* 17, 133–143.
- Guglielmin, M., Cannone, N., 2012. A permafrost warming in a cooling Antarctica? *Clim. Chang.* 111:177. <http://dx.doi.org/10.1007/s10584-011-0137-2>.
- Guglielmin, M., Worland, M.R., Cannone, N., 2012. Spatial and temporal variability of ground surface temperature and active layer thickness at the margin of Maritime Antarctica. *Signy Island. Geomorphology* 155, 20–33.
- Guglielmin, M., Worland, M.R., Baio, F., Convey, P., 2014a. Permafrost and snow monitoring at Rothera Point (Adelaide Island, Maritime Antarctica): Implications for rock weathering in cryotic conditions. *Geomorphology* 225, 47–56.
- Guglielmin, M., Dalle Fratte, M., Cannone, N., 2014b. Permafrost warming and vegetation changes in continental Antarctica. *Environ. Res. Lett.* 9. <http://dx.doi.org/10.1088/1748-9326/9/4/045001>.
- Hrbáček, F., Láška, K., Engel, Z., 2016a. Effect of snow cover on the active-layer thermal regime – a case study from James Ross Island, Antarctic Peninsula. *Permafr. Periglac. Process.* 27 (3), 307–315.
- Hrbáček, F., Oliva, M., Láška, K., Ruiz-Fernández, J., de Pablo, M.A., Vieira, G., Ramos, M., Nývlt, D., 2016b. Active layer thermal regime in two climatically contrasted sites of the Antarctic Peninsula region. *Cuad. Investig. Geogr.* 42 (2), 457–474.
- Hrbáček, F., Láška, K., Nývlt, D., Engel, Z., Oliva, M., 2016c. Active layer thickness variability on James Ross Island, eastern Antarctic Peninsula. In: Gunther, F., Morgenstern, A. (Eds.), XI. International Conference on Permafrost Exploring Permafrost in a Future Earth, Potsdam, Germany, Bibliothek Wissenschaftspark Albert Einstein, 2016: p. p125 <http://dx.doi.org/10.2312/GFZ.LIS.2016.001>.
- Hrbáček, F., Nývlt, D., Láška, K., 2017. Active layer thermal dynamics at two lithologically different sites on James Ross Island, Eastern Antarctic Peninsula. *Catena* 149 (2), 592–602.
- IPCC Climate Change, 2013. 2013. The Physical Science Basis. Contribution of Working Group I to the Fifth Assessment Report of the Intergovernmental Panel on Climate Change. Cambridge University Press, Cambridge (1535 pp).
- Kavan, J., Ondruch, J., Nývlt, D., Hrbáček, F., Carrivick, J.L., Láška, K., 2017. Seasonal hydrological and suspended sediment transport dynamics in proglacial streams, James Ross Island, Antarctica. *Geogr. Ann.* A 97 (1), 38–55.
- Láška, K., Barták, M., Hájek, J., Prošek, P., Bohuslavová, O., 2011. Climatic and ecological characteristics of deglaciated area of James Ross Island, Antarctica, with a special respect to vegetation cover. *Czech Polar Rep.* 1, 49–62.
- Lunardini, V.J., 1978. Theory of N-factors and correlation of data. In *Proceedings of the Third International Conference on Permafrost*, Vol. 1. National Council of Canada: Ottawa, pp. 40–46.
- Lunardini, V.J., 1981. Heat Transfer in Cold Climate. Chapter 4. Van Nostrand Reinhold, New York.
- Martin, P.J., Peel, D.A., 1978. The spatial distribution of 10 m temperatures in the Antarctic Peninsula. *J. Glaciol.* 20, 311–317.
- Mlčoch, B., Nývlt, D., Mixa, P. (Eds.), 2016. James Ross Island. Geological Map of the Northern Part. 1:25 000. Czech Geological Survey, Praha (Unpublished manuscript).
- Nývlt, D., Košler, J., Mlčoch, B., Mixa, P., Lisá, L., Bubík, M., Hendriks, B.W.H., 2011. The Mendel formation: evidence for late Miocene climatic cyclicity at the northern tip of the Antarctic Peninsula. *Palaeogeogr. Palaeoclimatol. Palaeoecol.* 299, 363–384.
- Nývlt, D., Braucher, R., Engel, Z., Mlčoch, B., Team, A.S.T.E.R., 2014. Timing of the Northern Prince Gustav Ice Stream retreat and the deglaciation of northern James Ross Island, Antarctic Peninsula during the last glacial–interglacial transition. *Quat. Res.* 82, 441–449.
- Nývlt, D., Nývltová Fišáková, M., Barták, M., Stachoň, Z., Pavel, V., Mlčoch, B., Láška, K., 2016. Death age, seasonality, taphonomy and colonization of seal carcasses from Ulu Peninsula, James Ross Island, Antarctic Peninsula. *Antarct. Sci.* 28, 3–16.
- Oliva, M., Navarro, F., Hrbáček, F., Hernández, A., Nývlt, D., Perreira, P., Ruiz-Fernández, J., Trigo, R., 2017a. Recent regional climate cooling on the Antarctic Peninsula and associated impacts on the cryosphere. *Sci. Total Environ.* 580, 210–223.
- Oliva, M., Hrbáček, F., Ruiz-Fernández, J., de Pablo, M.A., Vieira, G., Ramos, M., Antoniadou, D., 2017b. Active layer dynamics in three topographically distinct lake catchments in Byers Peninsula (Livingston Island, Antarctica). *Catena* 149 (2), 548–559.
- Outcalt, S.I., Nelson, F.E., Hinkel, K.M., 1990. The zero-curtain effect: heat and mass transfer across an isothermal region in freezing soil. *J. Water Resour. Res.* 26, 1509–1516.
- Putkonen, J., 1998. Soil thermal properties and heat transfer processes near Ny-Ålesund, northwestern Spitsbergen, Svalbard. *Polar Res.* 17, 165–179.
- Ramos, M., Vieira, G., 2009. Evaluation of the ground surface Enthalpy balance from bedrock temperatures (Livingston Island, Maritime Antarctic). *Cryosphere* 3, 133–145.
- Ramos, M., Vieira, G., de Pablo, M.A., Molina, A., Abramov, A., Goyanes, G., 2017. Recent shallowing of the thaw depth at Crater Lake, Deception Island, Antarctica (2006–2014). *Catena* 149 (2), 519–528.
- Riseborough, D., Smith, S., 1998. Exploring the limits of permafrost. Seventh International Conference on Permafrost (Proceedings), Yellowknife (Canada). Collection Nordicana. 55, pp. 935–941.
- Romanovsky, V.E., Smith, S.L., Christiansen, H.H., 2010. Permafrost thermal state in the polar Northern Hemisphere during the international polar year 2007–2009: a synthesis. *Permafr. Periglac.* 21 (2), 106–116.
- Seybold, C.A., Balks, M.R., Harms, D.S., 2010. Characterization of active layer water contents in the McMurdo Sound region, Antarctica. *Antarct. Sci.* 22 (6), 633–645.
- Stachoň, Z., Russnák, J., Nývlt, D., Hrbáček, F., 2014. Stabilisation of geodetic points in the surroundings of Johann Gregor Mendel Station, James Ross Island, Antarctica. *Czech Polar Rep.* 4, 81–90.
- Strauss, S.L., Ruhland, C.T., Day, T.A., 2009. Trends in soil characteristics along a recently deglaciated foreland on Anvers Island, Antarctic Peninsula. *Polar Biol.* 32 (12), 1779–1788.
- Turner, J., Lu, H., White, I., King, J.C., Phillips, T., Scott Hosking, J., Bracegirdle, T.J., Marshall, G.J., Mulvaney, R., Deb, P., 2016. Absence of 21st century warming on Antarctic Peninsula consistent with natural variability. *Nature* 535, 411–415.
- Van Lipzig, N.P.M., King, J.C., Lachlan-Cope, T.A., van der Broeke, M.R., 2004. Precipitation, sublimation and snow drift in the Antarctic Peninsula region from a regional atmospheric model. *J. Geophys. Res.* 109, D24106.
- Vieira, G., Bockheim, J., Guglielmin, M., Balks, M., Abramov, A.A., Boelhouwers, J., Cannone, N., Ganzert, L., Gilichinsky, D., Goryachkin, S., López-Martínez, J., Meiklejohn, I., Raffi, R., Ramos, M., Schaefer, C., Serrano, E., Simas, F., Sletten, R., Wagner, D., 2010. Thermal state of permafrost and active-layer monitoring in the Antarctic: advances during the International Polar Year 2007–2008. *Permafr. Periglac.* 21, 182–197.
- Zhang, T., 2005. Influence of the seasonal snow cover on the ground thermal regime: an overview. *Rev. Geophys.* 43. <http://dx.doi.org/10.1029/2004RG000157>.
- Zhang, T., Stames, K., 1998. Impact of climatic factors on the active layer and permafrost at Barrow, Alaska. *Permafr. Periglac.* 9, 229–246.

# EFFECT OF HYALOCLASTITE BRECCIA BOULDERS ON MESO-SCALE PERIGLACIAL-AEOLIAN LANDSYSTEM IN SEMI-ARID ANTARCTIC ENVIRONMENT, JAMES ROSS ISLAND, ANTARCTIC PENINSULA<sup>1</sup>

M. KŇAŽKOVÁ\*, F. HRBÁČEK, J. KAVAN, D. NÝVL

Department of Geography, Masaryk University, Brno, Czech Republic

**ABSTRACT.** *In this study we aim to describe the processes leading to the creation of a specific periglacial and aeolian landsystem, which evolves around the hyaloclastite breccia boulders on James Ross Island, north-eastern Antarctic Peninsula. These boulders were deposited as a result of the Late Holocene advance of Whisky Glacier, forming a well-developed boulder train approximately 5-km long, stretching from Whisky Glacier moraine to Brandy Bay. The combination of ground temperature monitoring, snow cover measurements, grain size analysis and field survey were used to quantify and understand the interplay of periglacial and aeolian processes leading to the formation of the specific meso-scale landsystem around the boulders. The ground temperature probes were installed during January 2017 in the vicinity of two selected boulders. The two study sites, at Monolith Lake (large boulder) and Keller Stream (smaller boulder), were also fitted with snow stakes and trail cameras. An automatic weather station (AWS) on the Abernethy Flats, located approximately two kilometres to the north-west, was used as a reference site for ground temperature and snow cover thickness. The hyaloclastite breccia boulders act as obstacles to wind and trap wind-blown snow, resulting in the formation of snow accumulations on their windward and lee sides. These accumulations affect ground thermal regime and lead to the transport of fine particles by meltwater from the snow during the summer season. The snow cover also traps wind-blown fine sand resulting in the formation of fine-grained rims on the windward and lee sides of the boulders after the snow has melted. Furthermore, the meltwater affects ground moisture content, creating favourable, but spatially limited conditions for colonisation by mosses and lichens.*

---

<sup>1</sup> This paper has received the First Prize and Honorable Mention (shared) from the Young Researcher Innovation Award on Cryosphere Science, granted by the Research Group on Physical Geography in High Mountains, Complutense University of Madrid (Department of Geography), Spain.

***Importancia de los bloques de hialoclastita en la morfogénesis periglacial y eólica a escala media en ambiente semiárido antártico, Isla James Ross, Península Antártica***

**RESUMEN.** En este trabajo tratamos de describir los procesos que conducen a la creación de un sistema específico periglacial y eólico, que evoluciona alrededor de bloques de hialoclastita en la Isla James Ross, nordeste de la Península Antártica. Estos bloques fueron depositados como resultado del avance a finales del Holoceno del Glaciar Whisky, formando un cordón de bloques de unos 5 km de longitud, desde la morrena del Glaciar Whisky hasta la Bahía Brandy. La combinación del seguimiento de la temperatura del suelo, medidas de la cubierta nival, análisis granulométricos y trabajo de campo permitieron cuantificar y entender las interacciones de los procesos periglaciares y eólicos que conducen a la formación de un sistema específico a mediana escala alrededor de los bloques. Se instalaron sondas de temperatura del suelo en enero de 2017 en la proximidad de dos bloques seleccionados. Los dos lugares de estudio, en el Lago Monolith (bloque mayor) y el río Keller (bloque menor), fueron también controlados con estacas de nieve y cámaras de seguimiento. Una estación meteorológica automática en los Abernethy Flats, localizada aproximadamente 3 km al nordeste, fue utilizada como lugar de referencia para la temperatura del suelo y el espesor de la cubierta nival. Los bloques brechosos de hialoclastita actúan como obstáculos y atrapan la nieve desplazada por el viento, dando lugar a la formación de acumulaciones de nieve a sotavento y barlovento. Estas acumulaciones afectan al régimen termal del suelo y conducen al transporte de partículas finas por el agua de fusión durante el verano. La cubierta nival también atrapa arena fina transportada por el viento, dando lugar a la formación de anillos de arena fina en los lados de sotavento y barlovento de los bloques, una vez que la nieve ha fundido. Además, el agua de fusión afecta al contenido de humedad del suelo, creando condiciones favorables, aunque espacialmente limitadas, para la colonización por musgos y líquenes.

**Key words:** Ground sorting, periglacial environment, Antarctica, wind accumulation, snowmelt.

**Palabras clave:** ordenación de suelos, ambiente periglacial, Antártida, acumulación eólica, fusión nival.

Received: 30 October 2018

Accepted: 25 January 2019

\*Corresponding author: Michaela Kňažková, Department of Geography, Masaryk University, Brno, Czech Republic. E-mail address: michaelaknazkova@gmail.com

## **1. Introduction**

Ice-free areas in Antarctica, in which periglacial processes dominate, form less than 0.5% of the continent (Burton-Johnson *et al.*, 2016; Hrbáček *et al.*, 2019). Moreover, significant parts of the ice-free areas are formed by rock outcrops or nunataks, which prevent the development of soils. Nevertheless, sorted ground can be found covering the whole range of deglaciated surfaces in Antarctica, regardless of age. The oldest sorted ground can be found in Victoria Land, and are estimated to be in excess of 8.1 Ma (Marchant *et al.*, 2002). In the Antarctic Peninsula region, the origin of sorted ground is related to the Late Pleistocene-Holocene deglaciation of the area (Ó Cofaigh *et al.*, 2014); however, sorted ground in the early stage of development have also been observed in areas that have become deglaciated during the last few decades (e.g. Oliva and Ruiz-Fernández, 2015). Mapping of periglacial landforms in the South Shetland Islands suggests that sorted ground form about 20% of all ice-free surfaces in this region (López-Martínez *et al.*, 2012).

Wind is an important geomorphic agent in both hot and cold desert environments (e.g. Koster and Dijkmans, 1988; McKenna Neuman, 1993; Seppälä, 2004), mainly resulting from the absence of ground-protective vegetation. Analogies can therefore be drawn between some of the features commonly observed in the hot deserts of the world and the ice-free areas of Antarctica (McKenna Neuman, 2004). Wind derived landforms are especially common in the Antarctic regions with an abundance of source material and sufficient wind velocities. Ripples reaching a height of several decimetres have been reported from Marion Island (Hedding *et al.*, 2015), as well as dunes located near Canada Glacier in Taylor Valleys (Šabacká *et al.*, 2012). The largest Antarctic dune field, Packard Sand Dunes, covers an area of approximately 1.5 km<sup>2</sup> near Lake Victoria in the McMurdo Dry Valleys (McGowan *et al.*, 2014).

One of the most important group of processes acting in periglacial environments are aeolian and niveo-aeolian processes (French, 2017). In the polar regions, comparatively little research has been conducted on this topic until present (Hedding *et al.*, 2015). Traditionally, the majority of the studies dealing with these processes and their dynamics in cold regions were focused on sedimentation rates (e.g. Koster and Dijkmans, 1988; McKenna Neuman, 1993; Brookfield, 2011), a situation which was similar for research conducted on niveo-aeolian processes in Antarctica (e.g. Lancaster, 2004; Ayling and McGowan, 2006; Atkins and Dunbar, 2009; Gillies *et al.*, 2013). Consequently, studies in to landform evolution (e.g. Speirs *et al.*, 2008; Bourke *et al.*, 2009), as well as the role that niveo-aeolian erosion plays in rock weathering (e.g. Matsuoka *et al.*, 1996; Hedding *et al.*, 2015) are limited to a few pioneering investigations.

In this paper, we present the findings of a study investigating the interplay between periglacial and aeolian processes forming a specific landsystem around hyaloclastite breccia boulders on James Ross Island, Eastern Antarctic Peninsula. Landsystem approach includes the range of processes and forms; and their relationships associated with the past and present geographic setting of the area (Eyles, 1983; Benn and Evans, 2010). Mostly glacial, periglacial, or paraglacial landsystems and associated sediment-landform assemblages were defined in the literature (Evans, 2003; Davies *et al.*, 2013; Kovanan and Slaymaker, 2015). The assemblages can be recognised at a range

of scales, from the site to the continent scale. The hierarchical approach is a powerful means of describing how sediments and landforms fit together, and determining how organisation in the landscape reflects the depositional processes and external controls in the environment. In our case, we intent to describe the processes and forms at the site and its surroundings, which is referred to as the meso-scale level. However, it is probably the first time when such a periglacial-aeolian landsystem at the meso-scale was described from Antarctica. The main objectives of this study are: (i) to describe the processes leading to the formation of snow accumulation and its geometry around the boulders, (ii) to quantify the effect of snow on ground thermal regime, and 3) to discuss the role of hyaloclastite breccia boulders on the formation of specific meso-scale landforms in the periglacial environment of semi-arid maritime Antarctica.

## 2. Study area

James Ross Island lies off the northeastern coast of the Antarctic Peninsula (Fig. 1). It covers an area of approximately 2500 km<sup>2</sup> in the altitudinal range of 0-1630 m, of which approximately 25% is ice-free. The largest ice-free area on James Ross Island is the Ulu Peninsula, which covers approximately 300 km<sup>2</sup>, and is also the largest ice-free area within the Antarctic Peninsula region.

The climate of James Ross Island is classified as semi-arid polar as it lies in the precipitation shadow of the Antarctic Peninsula mountain range. Estimates of average annual precipitation range between 200-500 mm, most of which falls in the form of snow (van Lipzig *et al.*, 2004). However, snow accumulation distribution across James Ross Island is spatially heterogeneous as a result of strong winds.

The geological composition of James Ross Island comprises Jurassic to Cretaceous sedimentary rocks of the James Ross Basin (del Valle *et al.*, 1992), which crop out mostly in the low-lying areas of James Ross Island (Mlčoch *et al.*, 2018). The Mesozoic strata are protruded and overlain by Neogene to Quaternary rocks of the James Ross Island Volcanic Group (Nelson, 1975; Smellie *et al.*, 2013), which consists of various types of hyaloclastites, basaltic lavas, dykes and subordinate pyroclastic rocks (Košler *et al.*, 2009; Altunkaynak *et al.*, 2018) that predominantly originate in a subglacial setting (Smellie *et al.*, 2008). At the Abernethy Flats, siltstones and sandstones of the Alpha Member of the Santa Marta Formation (Olivero *et al.*, 1986; Crame *et al.*, 1991) are covered by boulders of hyaloclastite breccia brought to the area from the Stickle Ridge and Smellie Peak volcanic elevations during the Holocene advance of Whisky Glacier, forming well-developed boulder trains (Hjort *et al.*, 1997; Davies *et al.*, 2013).

The deglaciation of Ulu Peninsula is altitude-dependent, with the low-lying areas (< 50 m a.s.l.) having become deglaciated during the late Pleistocene ( $12.9 \pm 1.2$  ka; Nývlt *et al.*, 2014); however, areas of mid-altitudes (200-400 m a.s.l.) remained ice-covered throughout the early Holocene (Johnson *et al.*, 2011). During the mid-Holocene, glacier extent was broadly similar to present glacial coverage (Glasser *et al.*, 2014). The mid-late Holocene is characterised by Neoglacial advances of local glaciers that have been recognised from Ulu Peninsula based on sedimentary sequences

of glacial landforms (Hjort *et al.*, 1997) and associated lacustrine records (Björck *et al.*, 1996). Modelling experiments suggest that glaciers on Ulu Peninsula remained stable during the mid-late Holocene, and that the Neoglacial re-advance took place in the last millennium, or during the local Little Ice Age (Davies *et al.*, 2014). Current glacier systems include ice aprons, cirque, piedmont and land-terminating valley glacier, as well as small ice caps located on volcanic mesas (Carrivick *et al.*, 2012; Engel *et al.*, 2012). To the south, the ice-free area of Ulu Peninsula is bounded by the Dobson Dome and Mt. Haddington Ice Caps (Davies *et al.*, 2012). All of these glaciers have experienced a pronounced amount of mass loss during the previous few decades (Davies *et al.*, 2012; Engel *et al.*, 2012; Seehaus *et al.*, 2018); however, positive mass balances have been observed between 2009 and 2015 (Engel *et al.*, 2018).

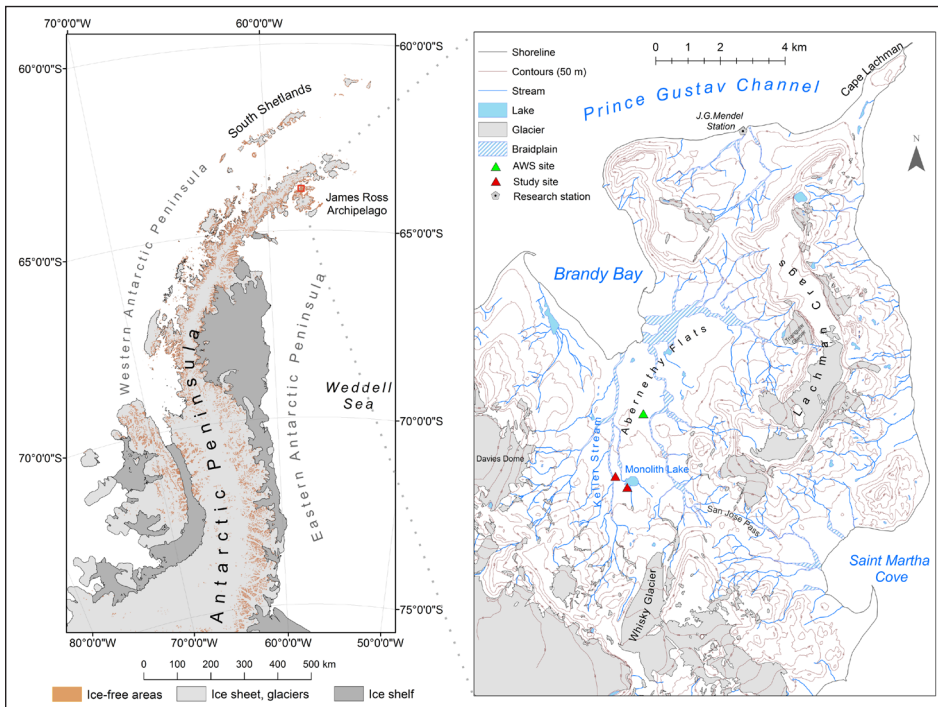


Figure 1. Regional setting and the location of study area on James Ross Island.

### 3. Methods

#### 3.1. Ground temperature monitoring

Automatic systems for ground temperature monitoring were installed in January 2017 in close proximity to the two selected boulders of hyaloclastite breccia. The two monitored boulders vary in size. The larger boulder is located close to Monolith Lake,

with the smaller boulder lying approximately 500 m to the west of Monument Lake, next to Keller Stream. Both boulders were selected based on their location, as they were located in relatively flat areas with no other boulders shielding them from the prevailing wind direction. The boulder on the Monument Lake site is approximately 5 m high and measures 46.7 m in circumference. The smaller boulder on the Keller Stream site measures approximately 1.8 m in height and is 8 m in circumference. The scheme of ground temperature probe positions can be seen in (Table 1) and (Fig. 2).

Table 1. Distance of the ground temperature probe from the boulder for Monument Lake and Keller Stream sites in cm.

|    | Z1 | Z2  | Z3  | Z4  |
|----|----|-----|-----|-----|
| M1 | 75 | 175 | 385 | 600 |
| M2 | 75 | 175 | 385 | 600 |
| K1 | 40 | 150 | 380 | -   |
| K2 | 40 | 150 | 420 | -   |

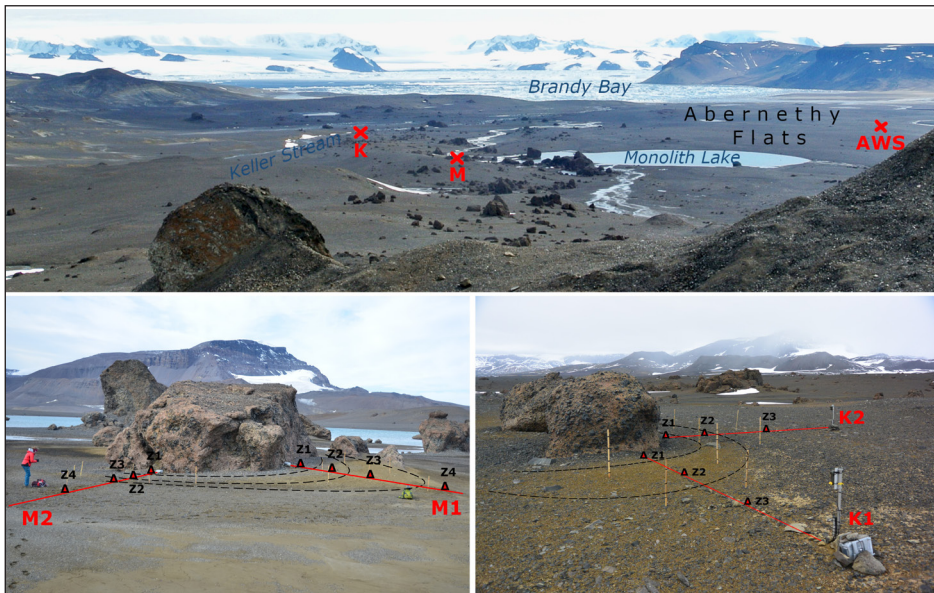


Figure 2. Study area. A panoramic view from the Whisky Glacier moraine towards the hyaloclastite breccia boulder train with Abernethy Flats and Brandy Bay (A), the study sites at the Monument Lake (B) and Keller Stream (C).

The ground temperature measuring equipment consists of two dataloggers at both the Monument Lake site (V12 EMS) and at the Keller Stream site (Fiedler MiniLog). Pt100 temperature probes (accuracy  $\pm 0.15$  °C) were installed across transects at various depths

(2 cm, 5 cm and 15 cm for Monolith Lake site; 5 cm and 15 cm for Keller Stream site and at various distances from the boulder, see Table 1). The orientation of the primary transect (dataloggers M1 and K1) corresponds to the prevailing local wind direction (azimuth 205°), with the secondary transect (dataloggers M2 and K2) orientated perpendicular to the primary transect (azimuth 295°). The temperature was measured and recorded every 30 minutes. The data were used for the calculation of mean, maximum and minimum daily temperatures. Additionally, the daily amplitude was used as a marker of snow presence on the site (e.g. Hrbáček *et al.*, 2016; Oliva *et al.*, 2017).

In order to describe ground thermal properties, the thermal indices were calculated, which are commonly used in other studies in both the Arctic and Antarctic (e.g. Frauenfeld *et al.*, 2007). The thermal indices used in this study are:

- a) Freezing degree days (FDD) as a sum of mean daily temperatures  $< 0\text{ }^{\circ}\text{C}$  of air (FDDa) and 5 cm depth (FDDg)
- b) Thawing degree days (TDD) as a sum of mean daily temperatures  $> 0\text{ }^{\circ}\text{C}$  of air (TDDa) and 5 cm depth (TDDg)
- c) The freeze-thaw days with the maximum daily temperature  $> 0.15\text{ }^{\circ}\text{C}$  and the minimum daily temperature  $< -0.15\text{ }^{\circ}\text{C}$
- d) Isothermal days as days with the daily amplitude  $< 0.3\text{ }^{\circ}\text{C}$

The freeze-thaw and isothermal days were defined with a respect to the accuracy of the temperature sensors.

### *3.2. Snow cover monitoring*

Both sites have been fitted with trail cameras (LTL Acorn 6310 MCW), one at the end of each transect, facing towards the boulder. Stakes marked with snow height indicators were placed between the camera and the boulder.

At the Keller Stream site, both trail cameras functioned for the whole year from January 2017 to January 2018, taking photos approximately every 3 hours. At the Monolith Lake site, one of the trail cameras installed on the main transect malfunctioned in mid-June as a result of being buried in a snow drift. The second camera also ceased working for the same reason at the end of June.

### *3.3. Field survey*

During January 2017, a field survey was undertaken in the vicinity of the hyaloclastite breccia boulder train. Approximately 50 boulders were selected with the aim of determining their dimensions in relation to the width of the sorted area around the boulder. For each boulder, the following characteristics were recorded using the specified equipment:

- GPS coordinates (Garmin GPSMap 62s handheld GPS device)
- height (Nikon 550 AS distance meter, accuracy 0.1 m)
- circumference (measuring tape)

- width of the sorted area (measuring tape)
- geometry of snow accumulations and sorted zones around the boulders (Garmin GPSMap 62s handheld GPS device)

### 3.4. Grain size analysis

Regolith samples were collected from both sites along the main transects, with samples being collected from the surface as well as from a depth of 10 cm at different distances from the boulder. At the Monolith Lake site, samples were collected from 4 zones (Z1-Z4), and at the Keller Stream site samples were collected from 3 zones.

As a result of logistical reasons, it was not possible to transport large samples of regolith from Antarctica to Europe. Therefore, each sample was dry sieved on site, and only the fraction below 2 mm was transported for further analysis. Once transported to the laboratory, the samples were processed using a combined laser and camera Bettersize S3 Plus particle size analyser at Polar-Geo-Lab, Department of Geography, Masaryk University in Brno.

For a better overall representation of the sorting processes occurring around the boulders, we also calculated fine-to-coarse sand index, which shows the relative proportion of the two most commonly found fractions.

### 3.5. Reference weather station

The reference automatic weather station (AWS) is located on the Abernethy Flats and provides data for the wider area (Hrbáček *et al.*, 2017). In this study, the data from 01 February 2017 to 31 January 2018 was processed for analysis. The surrounding area of the automatic weather station is formed of an approximately flat surface with slope angles of  $< 3^\circ$ , therefore the meteorological parameters measured were not affected by topography and are lithologically analogical to the surroundings of the studied boulders. Air temperature data was measured at 2 m above the ground by a EMS 33 sensor (accuracy  $\pm 0.15^\circ\text{C}$ ) mounted in a radiation shield, with the ground temperature at 5 cm depth measured by Pt100 (accuracy  $\pm 0.15^\circ\text{C}$ ). Wind speed and direction was measured at 3 m above the ground by a Young Wind Monitor-HD 05108 (wind speed accuracy  $\pm 0.3\text{ m s}^{-1}$ ; wind direction accuracy  $\pm 3$  degrees), and the snow thickness was measured using a Depth Sensor manufactured by Judd Communication (accuracy  $\pm 1\text{ cm}$ ).

The temperature data were evaluated in an identical way as those from the Monolith Lake and Keller Stream sites. Wind speed, wind direction, and snow thickness data provided information necessary for the evaluation of the boulder's effect on snow accumulation and ground sorting.

## 4. Results

In the following section the results of the ground temperature monitoring, as well as the snow and wind conditions are presented for the study period. For comparison, data from the reference AWS on the Abernethy Flats is used. Data collected from environmental monitoring is supplemented with field survey, mapping, and laboratory analyses.

### 4.1. Ground thermal characteristics

The mean annual air temperature at the reference site on Abernethy Flats was  $-6.6\text{ }^{\circ}\text{C}$  (Table 2), while the mean daily air temperature varied between  $7.4\text{ }^{\circ}\text{C}$  and  $-28.9\text{ }^{\circ}\text{C}$  (Fig. 3). The warmest month was December 2017 (mean temperature  $0.6\text{ }^{\circ}\text{C}$ ), while the coldest month was June 2017 ( $-15.3\text{ }^{\circ}\text{C}$ ). TDDa reached  $244\text{ }^{\circ}\text{C}\cdot\text{days}$ , FDDa was  $-2653\text{ }^{\circ}\text{C}\cdot\text{days}$ . The number of air temperature defined freeze-thawing days was 142. Mean annual ground temperature at 5 cm at the Abernethy Flats site was  $-5.9\text{ }^{\circ}\text{C}$ . The mean daily ground temperature varied between  $10.5\text{ }^{\circ}\text{C}$  and  $-19.4\text{ }^{\circ}\text{C}$ . TDDg was  $480\text{ }^{\circ}\text{C}\cdot\text{days}$ , FDDg dropped to  $-2638\text{ }^{\circ}\text{C}\cdot\text{days}$ . The total number of freeze-thawing days at 5 cm was 81, while the number of isothermal days at 5 cm was 35.

Table 2. Air and ground thermal characteristics at the Abernethy Flats AWS.

| Parameter                                  | Value |
|--|-------|
| MAAT ( $^{\circ}\text{C}$ )                | -6.6  |
| MAGT 5 cm ( $^{\circ}\text{C}$ )           | -5.9  |
| TDDa ( $^{\circ}\text{C}\cdot\text{day}$ ) | 244   |
| TDDg ( $^{\circ}\text{C}\cdot\text{day}$ ) | 480   |
| FDDa ( $^{\circ}\text{C}\cdot\text{day}$ ) | -2653 |
| FDDg ( $^{\circ}\text{C}\cdot\text{day}$ ) | -2638 |
| F-T days air                               | 142   |
| F-T days 5 cm                              | 81    |
| IT days 5 cm                               | 35    |

The mean annual ground temperature at the Monolith Lake site varied between  $-6.7$  and  $-5.4\text{ }^{\circ}\text{C}$  within the main transect (M1), and between  $-6.5$  and  $-5.5\text{ }^{\circ}\text{C}$  within the secondary transect (Fig. 3). There were only very slight differences in mean ground temperature between the three monitored depths (Table 3). In the main transect, the lowest mean annual ground temperatures occurred closest to the boulder in Z1, increased towards Z2, and then decreased slightly in Z3 and Z4. In the secondary transect, the lowest temperatures occurred at the furthest distance from the boulder and increased in the direction towards the boulder. The mean daily ground temperature amplitude in M1 decreased away from the boulder and also with depth. The maximum and minimum

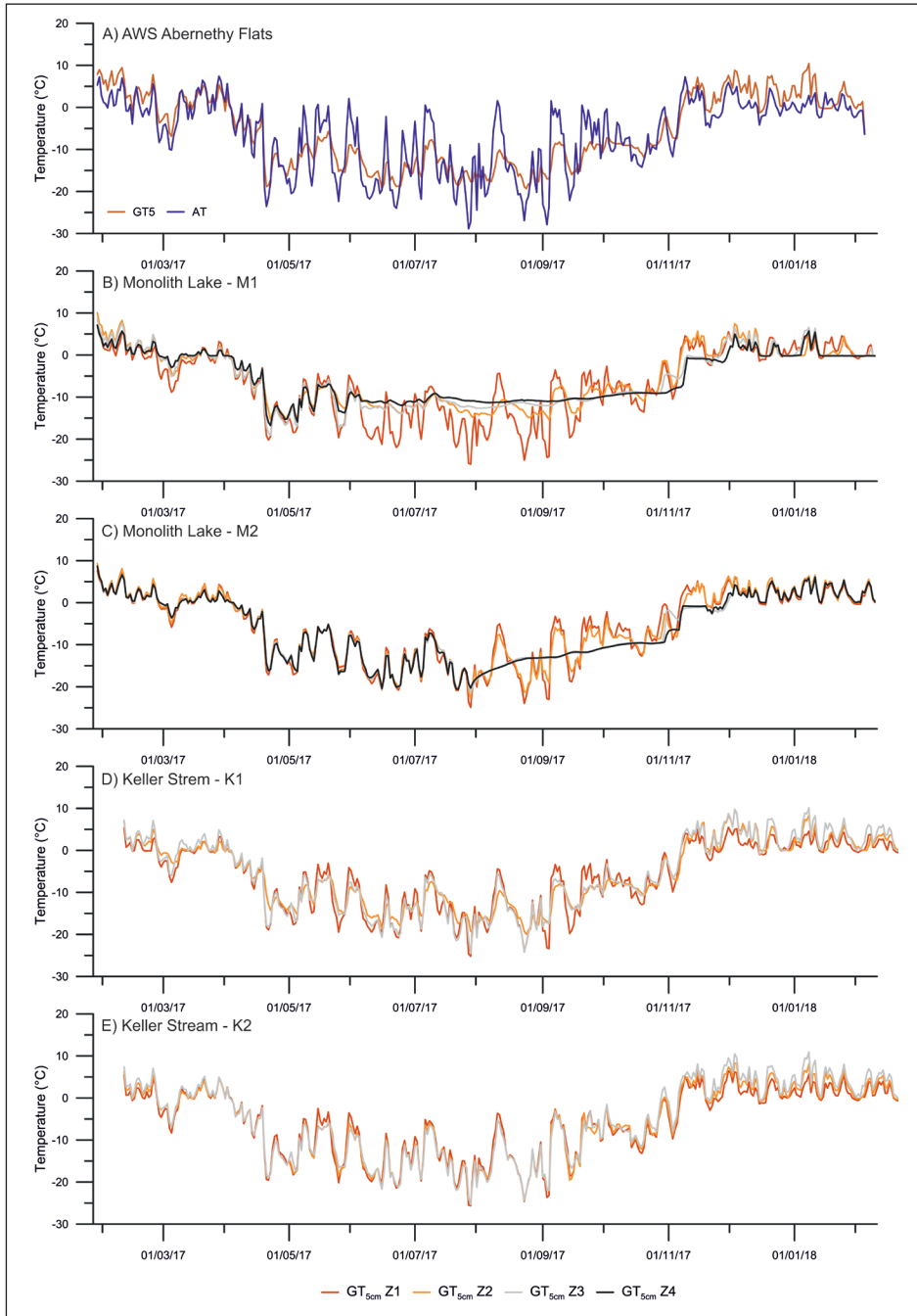


Figure 3. Variability of air temperature (AT) and ground temperature (GT) at selected depths at the Abernethy Flats reference site and Monolith Lake and Keller Stream study sites in the zones 1-4 (Z1-Z4).

Table 3. Ground thermal characteristics at the Monolith Lake site.

| Parameter       | Monolith Lake 1 |       |       |       | Monolith Lake 2 |       |       |       |
|-----------------|-----------------|-------|-------|-------|-----------------|-------|-------|-------|
|                 | Z1              | Z2    | Z3    | Z4    | Z1              | Z2    | Z3    | Z4    |
| MAGT 2 cm (°C)  | -6.6            | -5.4  | -5.9  | -5.7  | -5.5            | -6.2  | -6.2  | -6.5  |
| MAGT 5 cm (°C)  | -6.7            | -5.4  | -5.7  | -5.6  | -5.8            | -5.7  | -6.2  | -6.3  |
| MAGT 15 cm (°C) | -6.5            | -5.4  | -5.7  | -5.5  | -5.6            | -5.7  | -6.3  | -6.3  |
| GTA 2 (°C)      | 6.1             | 4.0   | 4.4   | 3.5   | 7.1             | 7.9   | 4.3   | 3.8   |
| GTA 5 (°C)      | 4.8             | 2.6   | 2.4   | 1.5   | 4.5             | 4.3   | 2.6   | 2.6   |
| GTA 15 (°C)     | 2.7             | 1.5   | 1.1   | 0.9   | 2.7             | 2.4   | 1.8   | 1.6   |
| TDD 5 (°C·day)  | 240             | 288   | 232   | 152   | 348             | 397   | 292   | 289   |
| FDD 5 (°C·day)  | -2768           | -2313 | -2391 | -2259 | -2521           | -2546 | -2611 | -2648 |
| IT days 2       | 2               | 63    | 139   | 163   | 0               | 0     | 46    | 56    |
| IT days 5       | 2               | 73    | 149   | 186   | 0               | 0     | 51    | 69    |
| IT days 15      | 21              | 97    | 184   | 205   | 4               | 6     | 54    | 64    |
| F-T days 2      | 115             | 72    | 89    | 82    | 118             | 138   | 68    | 99    |
| F-T days 5      | 77              | 22    | 24    | 31    | 73              | 24    | 33    | 56    |
| F-T days 15     | 30              | 11    | 8     | 11    | 35              | 6     | 18    | 50    |

amplitudes were 6.1 °C and 3.5 °C in Z1 and Z4, respectively. A similar pattern was observed also in M2, with amplitudes reaching slightly higher than in M1, with the maximum and minimum amplitudes being 7.9 °C (Z2) and 1.6 °C (Z4), respectively. The number of isothermal days increased away from the boulder. There were only 2 isothermal days observed in the main transect in Z1 close to the ground surface, in contrast to 163 such days in Z4. The number of isothermal days also increased greatly with depth. Approximately one third of the total amount of isothermal days were observed in Z3 and Z4 on the secondary transect; however, in Z1 and Z2 no isothermal days at 2 and 5 cm depths were detected. The number of freeze-thaw days in Z1 was similar in both transects. The frequency of freeze-thaw cycles decreased with depth. The maximum number of freeze-thaw days (138) was observed in Z2 in the secondary transect, closest to ground surface. The minimum (6) was within the same zone, at 15 cm below ground surface (Fig. 4). TDDg was between 152 and 288 °C·days within the primary transect, and between 289 and 397 °C·days in the secondary transect. FDDg dropped to between -2259 and -2768 °C·days (primary transect) and -2521 and -2648 °C·days (secondary transect).

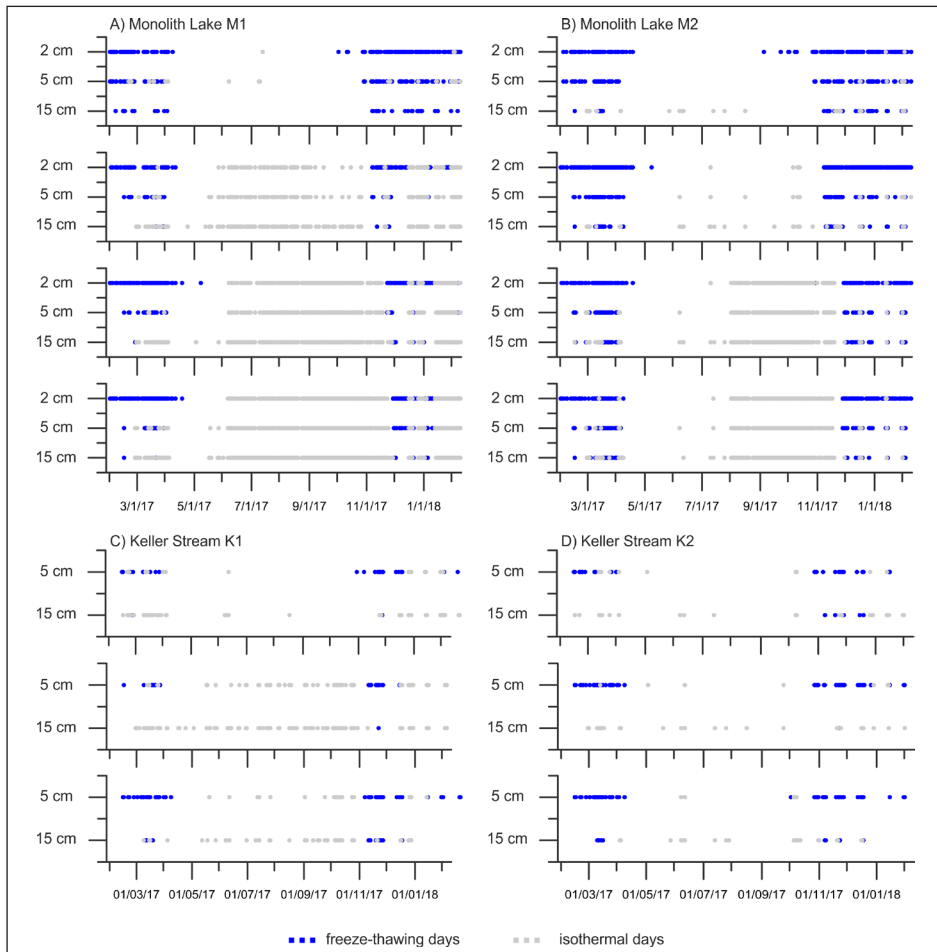


Figure 4. Calendar of freeze-thaw days and isothermal days at the Monolith Lake and Keller Stream sites.

At the Keller Stream site, mean annual ground temperature decreased away from the boulder in both transects. Overall, in the comparison between the two transects, there were very similar averages for all zones, with the maximum difference being only 0.2 °C in Z2 (Table 4 and Fig. 3). Greater differences between the two transects can be seen in mean daily ground temperature amplitude. This is slightly higher in all zones of K2. The amplitude in K2 increases away from the boulder; however, in K1, the minimum amplitude is observed in Z2. The number of isothermal days is higher in K1, where most such days occur in Z2. The number of isothermal days increases with depth. The occurrence of freeze-thaw days is higher in the secondary transect, especially in Z2, where 55 freeze-thaw days were observed at a depth of 5 cm, in comparison to only 19 freeze-thawing days in the main transect. In Z1 and Z3, the total number of freeze-thawing days is similar for both

Table 4. Ground thermal characteristics at the Keller Stream site.

| Parameter         | Keller Stream 1 |       |       | Keller Stream 2 |       |       |
|-------------------|-----------------|-------|-------|-----------------|-------|-------|
|                   | Z1              | Z2    | Z3    | Z1              | Z2    | Z3    |
| MAGT 5 cm (°C)    | -5.4            | -5.6  | -6.2  | -5.3            | -5.8  | -6.1  |
| MAGT 15 cm (°C)   | -5.4            | -5.6  | -6.1  | -5.4            | -5.7  | -6.1  |
| GTA 5 cm (°C)     | 4.1             | 3.1   | 5.4   | 4.8             | 5.5   | 6.1   |
| GTA 15 cm (°C)    | 2.3             | 1.7   | 2.8   | 2.7             | 2.8   | 3.0   |
| TDD 5 cm (°C·day) | 197             | 332   | 435   | 235             | 360   | 508   |
| FDD 5 cm (°C·day) | -2575           | -2490 | -2553 | -2575           | -2662 | -2588 |
| IT days 5         | 8               | 34    | 14    | 5               | 4     | 10    |
| IT days 15        | 34              | 60    | 27    | 20              | 20    | 18    |
| F-T days 5        | 24              | 19    | 45    | 27              | 55    | 51    |
| F-T days 15       | 3               | 1     | 13    | 5               | 1     | 10    |

transects. However, fewer freeze-thawing days were observed at a depth of 15 cm than were observed at a depth of 5 cm (Fig. 4). TDDg on the Keller Stream site was between 197 and 435 °C·days within the primary transect, and between 235 and 508 °C·days in the secondary transect, with FDDg dropping to between -2490 and -2575 °C·days (primary transect) and -2575 and -2662 °C·days (secondary transect).

#### 4.2. Snow accumulation

Continuous snow cover at the reference site on the Abernethy Flats occurred between the beginning of May and the beginning of November 2017 (Fig. 5). The mean thickness of the snow was 19 cm, with the maximum thickness in mid-October reaching 50 cm. The data from the time-lapse camera at the Monolith Lake site showed a rapid snow accumulation between mid-May and the beginning of June, during which time the maximum snow thickness around the boulder increased from 20 to 70 cm (Fig. 5). The minimum thickness at the margin of the snow accumulation corresponds with the snow thickness measured at the Abernethy Flats site. At the Keller Stream site, the snow accumulation starts to develop in early March. At this site, the snow thickness corresponds to those observed at the Abernethy Flats site; however, there were more peaks indicating the snow accumulation forming. Unlike the Monolith Lake site, the snow thickness at the Keller Stream site never exceeded 50 cm (Fig. 5).

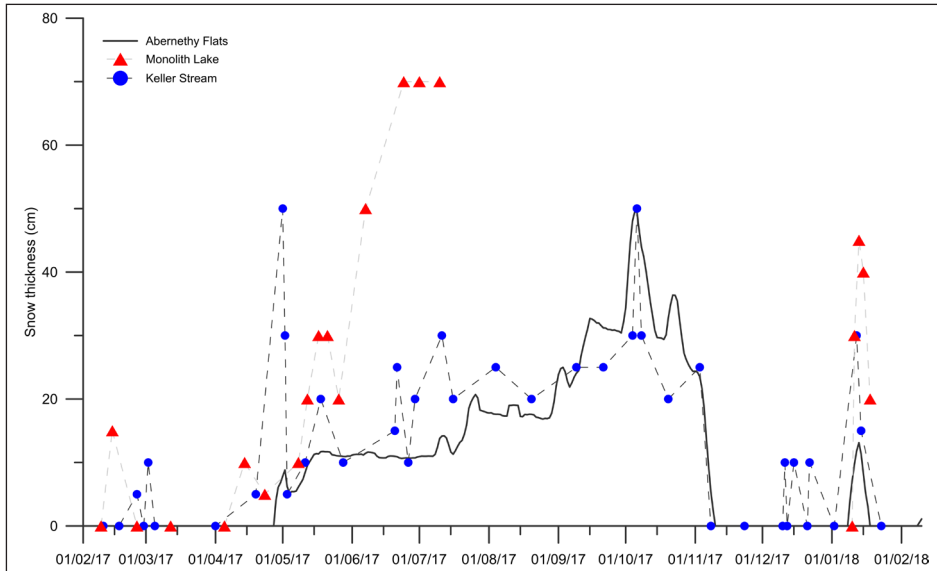


Figure 5. Evolution of snow cover at the Abernethy Flats reference site, Monolith Lake and Keller Stream sites.

#### 4.3. Wind conditions

The most common wind direction azimuths at the reference weather station were between 210° and 240° (25.5%) and between 240° and 270° (12.6%), which account for 38.1% of the total wind directions for 60° span (Fig. 6). The mean wind speed was 5.3 m s<sup>-2</sup>, however it varied significantly with the wind direction. The highest wind speeds which exceeded 20 ms<sup>-2</sup> were observed for the azimuth 210° to 240°, while the lowest wind speeds that rarely exceeded 5 ms<sup>-2</sup> were from 150° to 210° (Fig. 6).

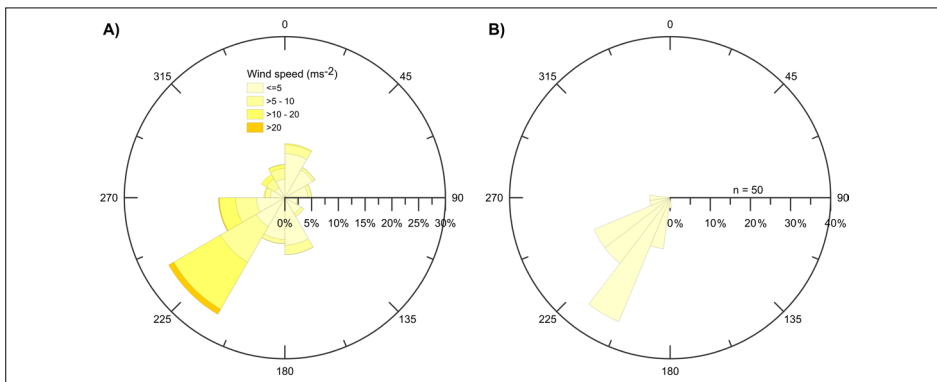


Figure 6. Variability of wind speed and wind direction at Abernethy Flats (A) and the azimuths of the sorted rims around the boulders (B).

#### 4.4. Geometry of sorted zone around the boulders

The prevailing wind direction in the area was assumed from the geometry of the snow accumulations created on windward sides of the boulders. The sorted zones around the boulders also have slightly elongated geometries, with the main axis orientated towards the prevailing wind direction. The most frequent azimuths were observed between 210° and 225° (33.3%), with all the azimuths of the monitored boulders orientated between 180° and 270° (Fig. 6).

A close relationship was discovered between boulder morphometry and the width of the longest axis of the sorted zone. Strong logarithmical correlation ( $r = 0.88$ ) significant at  $p < 0.01$  (Fig. 7) was observed between the circumference of the boulder and the width of the sorted rim. The logarithmical correlation between the boulder height and the width of the sorted zone was slightly weaker ( $r = 0.81$ ), but also significant at  $p < 0.01$  (Fig. 7).

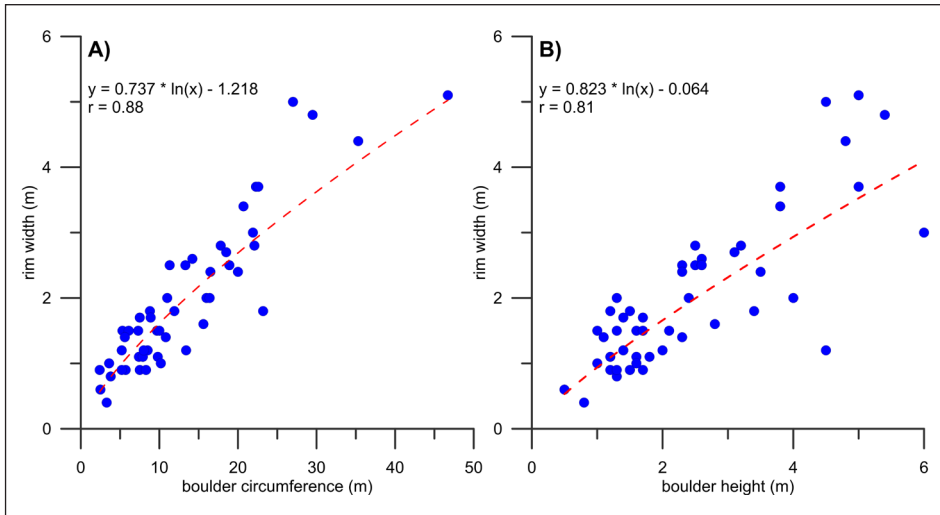


Figure 7. Relationship of sorted rim width to boulder circumference (A) and to boulder height (B).

#### 4.5. Grain size analysis

Grain size analyses of samples from the Monolith Lake site show very low and relatively stable distributions of clay and silt within the whole transect. The most significant differences between the individual zones can be seen in the fine sand fraction, the share of which increases significantly with distance from the boulder, peaking in Z3 and subsequently decreasing again towards Z4. The maximum share of the fine sand fraction reaches almost 65% in Z3 at a depth of 10 cm (Fig. 8). Subsequently, the amount of coarse sand decreases outwards from its maximum in Z1 towards Z3, then increases again in Z4. The share of fine fractions up to medium sand is higher at 10 cm below the surface than at the surface in all the zones. However, this

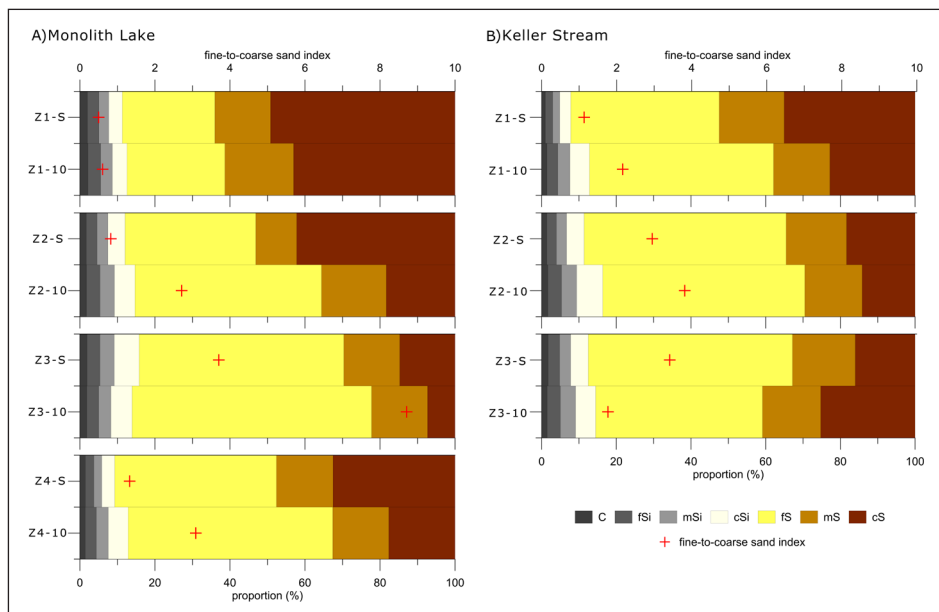


Figure 8. Grain size analysis results for the Monolith Lake (A) and Keller Stream (B) sites.

difference is most pronounced in Z2. The fine-to-coarse sand index increases from Z1 to Z3, where there is almost 9x higher proportion of fine sand when compared to coarse sand. In Z4, the fine-to-coarse sand index decreases to approximately 3 at a depth of 10 cm (Fig. 8).

The Keller Stream site shows a similar pattern to that of the Monolith Lake site (Fig. 8). The most abundant fraction, comprising > 50% in Z2, is fine sand, but its increase is not as pronounced as at the Monolith Lake site. The proportion of clay is very low overall, accounting for less than 2% (Fig. 8). Similarly, the silt share is also negligible. The differences between the two depths also show slightly coarser material composition on the surface in Z1 and Z2; however, this is not the case in Z3, where the deeper sample is coarser. The fine-to-coarse sand index is lower compared to the Monolith Lake site and it reaches the highest values in Z2 (Fig. 8).

## 5. Discussion

The breccia boulders represent unique landforms in the central flats of the Ulu Peninsula, James Ross Island. As natural obstacles to wind-transported material, such as snow and sand, they strongly affect wind flow and the accumulation of material around themselves. Therefore, they represent important geomorphological features, which significantly change the formation of micro- to meso-scale landforms in semi-arid periglacial environments.

### *5.1. Ground thermal effect on material sorting*

Ground thermal conditions are one of the most important parameters studied in periglacial environments (e.g. Frauenfeld *et al.*, 2007). The ground temperature monitoring around the breccia boulders and its comparison with the reference AWS site at the Abernethy Flats is therefore important for understanding the specific physical processes associated with the meso-scale periglacial landsystems found around the boulders.

The ground thermal conditions around the breccia boulders differ in some parameters when compared to the AWS at the Abernethy Flats. The main impact that the boulders had on ground thermal regime was caused by the shadowing effect of the boulders that prevented some of the summer incoming radiation reaching the ground, reducing an important input for ground thermal balance (e.g. Smith and Riseborough, 1996), as well as inducing increased snow accumulation around them. Unlike flat areas on James Ross Island, where snow thickness is usually less than 30 cm and its effect on ground thermal regime is not very significant (Hrbáček *et al.*, 2016), snow accumulation around breccia boulders can exceed 40 cm for longer periods of time. Such thickness is considered sufficient to cause the isothermal regime of the ground (Zhang *et al.*, 2005).

The effect of the above-mentioned factors is well demonstrated in thawing and freezing degree day indices. The shadowing effect of the boulders was most pronounced in the primary transects and zones closest to the breccia boulders, where TDDg reached the lowest values of approximately 40-50% lower than at the reference AWS on the Abernethy Flats. In the marginal zones, low values of TDDg were affected by snow accumulation, which caused a shorter thawing period (e.g. Zhang *et al.*, 2005; Oliva *et al.*, 2017). Conversely, in the Z3 zone of both transects from the Keller Stream site, TDDg were very close (K1) or even higher (K2) than on the Abernethy Flats (Table 2). This suggests that these parts of transects were not affected by either the boulder shadowing or the snow accumulation.

The most pronounced effect of the snow was observed in the primary transects, particularly at Z3 and Z4 zones of the Monolith Lake site. Despite the hiatus in snow data for the majority of the winter, the available measurements demonstrate that the snow thickness reached at least 70 cm, and that snow cover exceeding 40 cm, which corresponds to the occurrence of isothermal days, persisted for more than 150 days (Fig. 4).

During the summer months when the area is snow-free, the thermal regime is typical, with high occurrence of freeze-thawing days, which are most frequent at the surficial 2 cm depth in all transects. Areas with this type of thermal regime that have high moisture contents from the thawing of snow, creates suitable conditions for ground sorting. As a result, sorted rims are commonly found around the breccia boulders.

### *5.2. Wind-conditioned snow and sand accumulation*

In cold semi-arid climates, such as that found in the ice-free areas of James Ross Island, frost and snow are very important factors affecting landscape-forming processes.

Snowfall is generally redistributed by strong winds (e.g. Nývlt *et al.*, 2016). This leads to snow filling topographic depressions; however, a substantial portion of snow also accumulates on the windward and lee sides of obstacles in the form of large drifts. The remaining snow is blown towards the lowest altitudes and commonly accumulates on sea-ice during the winter, or is deposited into the open sea during the summer. The drift surfaces may also bear sastrugi that resemble similar shapes as sand dunes. Tsoar (2001) describes the types of dunes controlled by topographical obstacles such as cliff faces, boulders etc. The airflow streamlines are forced to separate when they hit the front of the obstacle. The front and sides of the obstacle are therefore the most heavily eroded parts. On the windward side, an echo dune is formed of either sand or, in this case, wind-blown snow. Shaped as a semicircle in plan view, its windward slope has a convex profile, with a steep lee slope. Furthermore, a lee dune is created on the lee side of the obstacle.

The shape of the echo dune and, subsequently, the sorted zone around the boulder, is not perfectly circular, but is slightly elongated along the main axis pointing in the prevailing wind direction (Fig. 9). The prevailing azimuths of the sorted rims around the boulders (Fig. 6), which also represent the azimuths of the snow accumulations, corresponds well with prevailing wind direction on the northern Ulu Peninsula (Kavan *et al.*, 2018). Prevailing south-southwestern wind directions are deviated by up to 90° as a result of comparatively large-scale topography (for example, in the San Jose Pass, or near to Triangular Glacier). In a similar way, the wind direction varies around the boulders, especially where the boulders are clustered in a small area, which therefore affects the airflow direction between them. The direction from which the material is transported by wind in the Abernethy Flats corresponds well ( $r^2 = 0.55$ ;  $p < 0.01$ ) with prevailing wind direction (Fig. 6).

The most common fraction in the sorted rim around the hyaloclastite breccia boulders is fine sand (0.063-0.250 mm). This fraction is most easily entrained by wind, as it is not as

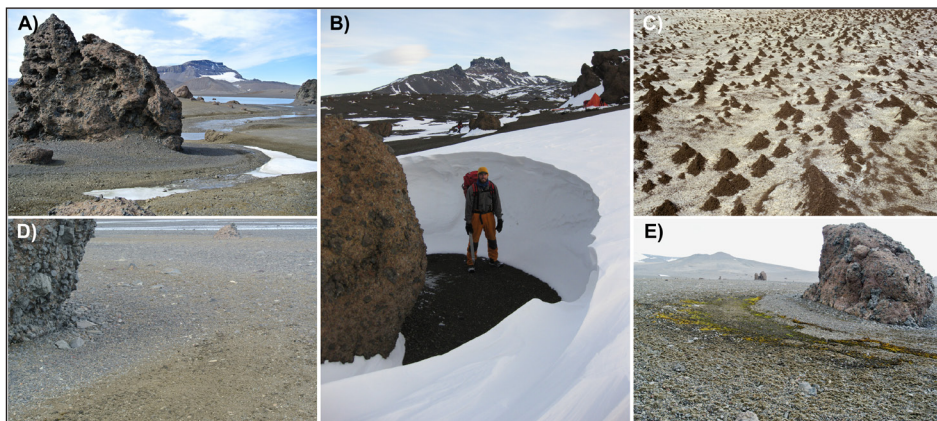


Figure 9. Periglacial-aeolian landsystem evolution. Hyaloclastite breccia boulder during the summer with the remnants of an oval-shaped snow accumulation (A), large snow accumulation with standing person for scale (B), detail of wind-blown sand on the surface of the snow (C), detail of ground sorting around the boulder (D), vegetation cover in the proximity of the boulder (E).

electrostatically and molecularly cohesive as clay or silt particles, but is still light enough compared to coarser fractions to be entrained and transported by the wind in suspension. Saltation induced by bombardment of already wind-transported particles, represents the other important process of sand grain entrainment by the wind (Thomas, 1997).

The limiting factors of aeolian sediment transport are usually sediment supply, to a lesser extent wind speed (Lancaster, 2002), and also surface moisture (McKenna Neuman, 2004; Wiggs, 2004). Surface moisture was reported as an important factor limiting the amount of fine-grained material entrainment by wind and its subsequent transport on James Ross Island, with a higher probability of aeolian transport at the end of summer season when surface moisture is at its minimum (Kavan *et al.*, 2018). Accumulation of snow as a result of the presence of boulders, plays an important role in the subsequent deposition of fine sandy material on the windward and lee sides of the boulders. The adhesion of a wet surface of snow (or later melt-water) is certainly greater than of the surrounding relatively dry surface, thus leading to higher accumulation rates on snow surfaces (Fig. 9).

Apart from the depositional processes on the windward and lee side of boulders, the effect of melting snow on local microecosystems is directly connected to the boulder surface and its immediate vicinity (Fig. 9). The boulders are often inhabited by lichens or algal/cyanobacterial crusts where conditions are favourable and the communities are protected from the wind (Balks and O'Neill, 2016). Also, ground moisture is substantially higher on the windward and lee sides of the boulders, as a result of meltwater originating from the accumulated snow. This results in a greater abundance of mosses and lichens, and presumably also algae and cyanobacteria. This localised nature of colonisation resembles colonisation around seal carcasses that are spread around the ice-free area of Ulu Peninsula (Nývlt *et al.*, 2016).

### *5.3. Meso-scale periglacial-aeolian landsystem around the hyaloclastite breccia boulders*

The origin of specific meso-scale landsystems driven by periglacial and aeolian processes that evolved around the boulders of hyaloclastite breccia, can be presented in a three-step development model (Fig. 10).

- a) Hyaloclastite breccia boulder train deposition. The boulders were transported to their present position by the Late-Holocene advance of Whisky Glacier (Davies *et al.*, 2013, 2014) and deposited when the glacier receded. The boulders must have been supraglacially transported as the hyaloclastite breccia would have easily disintegrated if transported subglacially or englacially. This phase represents the only stage where glacial processes dominate the landscape formation. Physical weathering including freeze-thaw induced disintegration of the boulder surfaces produced coarse-grained weathering rims around the boulders (Fig. 10).
- b) Snow and sand accumulations around the breccia boulders. The hyaloclastite breccia boulders act as natural obstacles for the prevailing south to southwestern

winds, allowing snow to accumulate in elongated shapes around the boulders with the echo and lee dunes being the highest (Fig. 10). Subsequently, dry winds transporting loose material from the ice-free surface of the Abernethy Flats (Kavan *et al.*, in prep.) deposit fine sand on the surface of snow accumulations (cf. Fig. 10). The snow cover around the boulders effectively insulates the

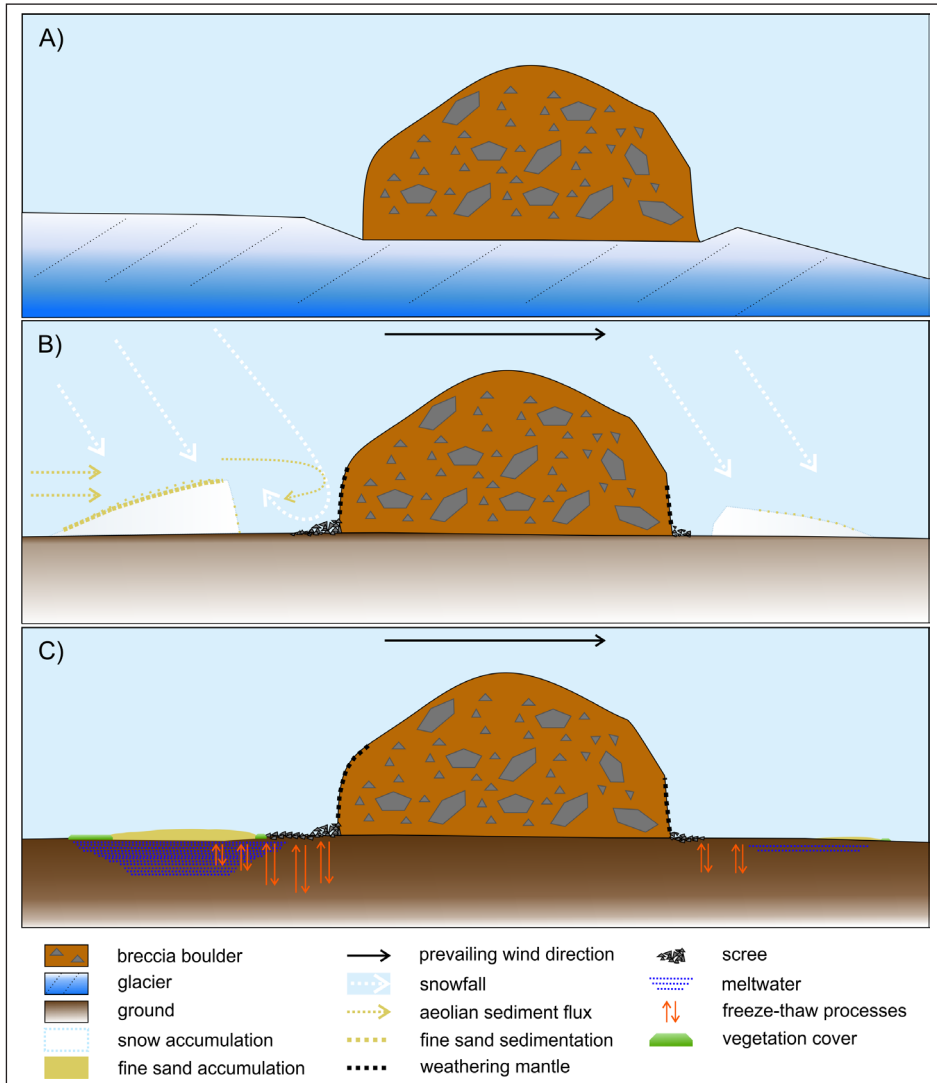


Figure 10. Three-step development model of a meso-scale periglacial and aeolian landsystem around the hyaloclastite breccia boulder. The boulder is transported supraglacially (A), the winter situation with snow accumulation forming on the windward side (B), the summer situation with fine sand accumulation and vegetation cover (C).

active layer, inducing an isothermal ground regime (Zhang *et al.*, 2005). This is important as snow accumulation in the flat areas of James Ross Island is generally limited (Hrbáček *et al.*, 2016), and therefore isothermal ground regimes do not widely occur.

- c) Snow melting and formation of sorted rims around breccia boulders. After the melting of snow accumulations around the hyaloclastite breccia boulders, the fine sand released from the snow deposits in the windward sector of the boulders making a well-developed rim of sorted fine material (Fig. 10). This is further enhanced by freeze-thaw processes associated with increased moisture in the surrounding of boulders. The width and distance of the sorted rim from the hyaloclastite boulder corresponds with the width of the boulder (represented in our case by the measured circumference) and less importantly with the height of the boulder (Fig. 7). Continuous melting of accumulated snow also develops specific niches for colonisation by mosses and lichens (Fig. 10).

## **6. Conclusions**

In this paper, a three-step development model of a meso-scale periglacial and aeolian landsystem, which is specific for the arid to semi-arid environment within the Antarctic Peninsula region, has been presented. The hyaloclastite breccia boulder train located in the central part of Ulu Peninsula presents a unique opportunity to study periglacial and aeolian processes at a micro- to meso-scale. The hundreds of large and small boulders, forming a 5-km long belt, mainly act as obstacles to the prevailing wind, causing snow to accumulate in dune-like drifts on their windward and lee sides. Normally, the snow is blown away from the flat surfaces of James Ross Island, and limited snow thickness has generally been observed on such surfaces. The snow accumulations are well-developed in the south to southwestern sector of the boulders, aligned with the direction of the snow-bringing winds that come during the winter. The presence of snow significantly affects the thermal and hydric regime of the underlying permafrost and active layer. Thick layers of snow decrease the ground temperature and increase the number of isothermal days, while the number of freeze-thaw cycles is reduced. The adhesive surface of snow also acts as a trap for the particles of wind-blown fine sand, producing fine-grained rims around the windward and lee sides of the boulders. Water content of the ground is often a limiting factor for biota development in the otherwise semi-arid climate of James Ross Island. Meltwater from the accumulated snow presents a unique source of moisture, and enables moss and lichen colonization in the vicinity of the boulders. The hyaloclastite breccia boulders can therefore be considered a significant agent for the creation of localised favourable biotic conditions.

## **Acknowledgements**

Research was supported by Ministry of Education, Youth and Sports of the Czech Republic projects LM2015078 and Z.02.1.01/0.0/0.0/16\_013/0001708 and by the Masaryk University project MUNI/A/1251/2017. We thank Stephen J.A. Jennings for his contribution regarding proofreading of the manuscript.

## References

- Altunkaynak, Ş., Aldanmaz, E., Güraslan, I.N., Çalışkanoğlu, A.Z., Ünal, A., Nývlt, D. 2018. Lithostratigraphy and petrology of Lachman Crags and Cape Lachman lava-fed deltas, Ulu Peninsula, James Ross Island, north-eastern Antarctic Peninsula: Preliminary results. *Czech Polar Reports* 8 (1), 60-83.
- Atkins, C.B., Dunbar, G.B. 2009. Aeolian sediment flux from sea ice into Southern McMurdo Sound, Antarctica. *Global and Planetary Change* 69 (3), 133-141. <https://doi.org/10.1016/j.gloplacha.2009.04.006>.
- Ayling, B.F., McGowan, H.A. 2006. Niveo-eolian sediment deposits in coastal South Victoria Land, Antarctica: Indicators of regional variability in weather and climate. *Arctic, Antarctic and Alpine Research* 38 (3), 313-324. [https://doi.org/10.1657/1523-0430\(2006\)38\[313:NSDICS\]2.0.CO;2](https://doi.org/10.1657/1523-0430(2006)38[313:NSDICS]2.0.CO;2).
- Balks, M.R., O'Neill, T.A. 2016. Soil and permafrost in the Ross Sea region of Antarctica: stable or dynamic? *Cuadernos de Investigación Geográfica* 42 (2), 415-434. <https://doi.org/10.18172/cig.2923>.
- Benn, D.I., Evans, D.J.A. 2010. *Glaciers and Glaciation*. 2<sup>nd</sup> Edition. 802 pp., Hodder Arnold Publication, London.
- Björck, S., Olsson, S., Ellis-Evans, C., Håkansson, H., Humlum, O., de Lirio, J.M. 1996. Late Holocene palaeoclimatic records from lake sediments on James Ross Island, Antarctica. *Palaeogeography, Palaeoclimatology, Palaeoecology* 121 (3-4), 195-220. [https://doi.org/10.1016/0031-0182\(95\)00086-0](https://doi.org/10.1016/0031-0182(95)00086-0).
- Bourke, M.C., Ewing, R.C., Finnegan, D., McGowan, H.A. 2009. Sand dune movement in the Victoria Valley, Antarctica. *Geomorphology* 109, 14-160. <https://doi.org/10.1016/j.geomorph/2009.02.028>.
- Brookfield, M.E. 2011. Aeolian processes and features in cool climates. In: Martini, I.P., French, H.M., Pérez Alberti, A. (Eds.), *Ice-marginal and periglacial processes and sediments*. Geological Society of London, Special Publication, 354, pp. 241-258. <https://doi.org/10.1144/SP354.16>.
- Burton-Johnson, A., Black, M., Fretwell, P.T., Kaluza-Gilbert, J. 2016. An automated methodology for differentiating rock from snow, clouds and sea in Antarctica from Landsat 8 imagery: a new rock outcrop map and area estimation for the entire Antarctic continent. *Cryosphere* 10 (4), 1665-1677. <https://doi.org/10.5194/tc-101665-2016>.
- Carrivick, J.L., Davies, B.J., Glasser, N.F., Nývlt, D., Hambrey, M.J. 2012. Late-Holocene changes in character and behaviour of land-terminating glaciers on James Ross Island, Antarctica. *Journal of Glaciology* 58 (212), 1176-1190. <https://doi.org/10.3189/2012JoG11J148>.
- Crame, J.A., Pirrie, D., Riding, J.B., Thomson, M.R.A. 1991. Campanian–Maastrichtian (Cretaceous) stratigraphy of the James Ross Island area, Antarctica. *Journal of the Geological Society, London* 148, 1125-1140. <https://doi.org/10.1144/gsjgs.148.6.1125>.
- Davies, B.J., Hambrey, M.J., Smellie, J.L., Carrivick, J.L., Glasser, N.F. 2012. Antarctic Peninsula Ice Sheet evolution during the Cenozoic Era. *Quaternary Science Reviews* 31, 30-66. <https://doi.org/10.1016/j.quascirev.2011.10.012>.
- Davies, B.J., Glasser, N.F., Carrivick, J.L., Hambrey, M.J., Smellie, J.L., Nývlt, D. 2013. Landscape evolution and ice-sheet behaviour in a semi-arid polar environment: James Ross Island, NE Antarctic Peninsula. In: Hambrey, M.J., Barker, P.F., Barrett, P.J., Bownam, V., Davies, B., Smellie, J.L., Tranter, M. (Eds.), *Antarctic Palaeoenvironments and Earth-Surface Processes*. Geological Society of London, Special Publication, 381, pp. 353-395. <https://doi.org/10.1144/SP381.1>.
- Davies, B.J., Gollidge, N.R., Glasser, N.F., Carrivick, J.L., Ligtenberg, S.R.M., Barrand, N.E., van den Broeke, M., Hambrey, M.J., Smellie, J.L. 2014. Modelled glacier response to centennial

- temperature and precipitation trends on the Antarctic Peninsula. *Nature Climate Change* 4 (11), 993-998. <https://doi.org/10.1038/nclimate2369>.
- Del Valle, R.A., Elliot, D.H., Macdonald, D.I.M. 1992. Sedimentary basins on the east flank of the Antarctic Peninsula: proposed nomenclature. *Antarctic Science* 4, 477-478. <https://doi.org/10.1017/S0954102092000695>.
- Engel, Z., Nývlt, D., Láska, K. 2012. Ice thickness, areal and volumetric changes of Davies Dome and Whisky Glacier (James Ross Island, Antarctic Peninsula) in 1979-2006. *Journal of Glaciology* 58 (211), 904-914. <https://doi.org/10.3189/2012JoG11J156>.
- Engel, Z., Láska, K., Nývlt, D., Stachoň, Z. 2018. Surface mass balance of small glaciers on James Ross Island, north-eastern Antarctic Peninsula, during 2009-2015. *Journal of Glaciology* 64 (245), 349-361. <https://doi.org/10.1017/jog.2018.17>.
- Evans, D.J.A., Ed. 2003. *Glacial Landsystems*. 532 pp., Arnold, London.
- Eyles, N. 1983. Glacial geology: a landsystem approach. In: N. Eyles (Ed.), *Glacial Geology: An Introduction for Engineers and Earth Scientists*. Pergamon Press, Oxford, pp. 1-18. <https://doi.org/10.1016/B978-0-08-030263-8.50007-5>.
- Frauenfeld, O.W., Zhang, T., McCreight, J.L., 2007. Northern hemisphere freezing/thawing index variations over the twentieth century. *International Journal of Climatology* 27, 47-63. <https://doi.org/10.1002/joc1372>.
- French, H.M. 2017. *The Periglacial Environment*. 4<sup>th</sup> Edition. Wiley-Blackwell, Oxford, 515 pp.
- Gillies, J.A., Nickling, W.G., Tilson, M. 2013. Frequency, magnitude, and characteristics of aeolian sediment transport: McMurdo Dry Valleys, Antarctica. *Journal of Geophysical Research-Earth Surface* 118 (2), 461-479. <https://doi.org/10.1002/jgrf.20007>.
- Glasser, N.F., Davies, B.J., Carrivick, J.L., Rodés, A., Hambrey, M.J., Smellie, J.L., Domack, E. 2014. Ice-stream initiation, duration and thinning on James Ross Island, northern Antarctic Peninsula. *Quaternary Science Reviews* 86, 78-88. <https://doi.org/10.1016/j.quascirev.2013.11.012>.
- Hedding, D.W., Nel, W., Anderson, R.L. 2015. Aeolian processes and landforms in the sub-Antarctic: preliminary observations from Marion Island. *Polar Research* 34 (1), 26365. <https://dx.doi.org/10.3402/polar.v34.26365>.
- Hjort, C., Ingólfsson, Ó., Möller, P., Lirio, J.M. 1997. Holocene glacial history and sea-level changes on James Ross Island, Antarctic Peninsula. *Journal of Quaternary Science* 12, 259-273. [https://doi.org/10.1002/\(SICI\)1099-1417\(199707/08\)12:4<259::AID-JQS307>3.3.CO;2-Y](https://doi.org/10.1002/(SICI)1099-1417(199707/08)12:4<259::AID-JQS307>3.3.CO;2-Y).
- Hrbáček, F., Láska, K., Engel, Z. 2016. Effect of Snow Cover on the Active-Layer Thermal Regime – A Case Study from James Ross Island, Antarctic Peninsula. *Permafrost and Periglacial Processes* 27, 307-315. <https://doi.org/10.1002/ppp.1871>.
- Hrbáček, F., Nývlt, D., Láska, K. 2017. Active layer thermal dynamics at two lithologically different sites on James Ross Island, Eastern Antarctic Peninsula. *Catena*, 149, 592-602. <https://doi.org/10.1016/j.catena.2016.06.020>.
- Hrbáček, F., Vieira, G., Oliva, M., Balks, M., Guglielmin, M., de Pablo, M.A., Molina, A., Ramos, M., Goyanes, G., Meiklejohn, I., Abramov, A., Demidov, N., Fedorov-Davydov, D., Lupachev, A., Rivkina, E., Láska, K., Kňázková, M., Nývlt, D., Raffi, R., Strelin, J., Sone, T., Fukui, K., Dolgikh, A., Zazovskaya, E., Mergelov, N., Osokin, N., Miamin, V., 2019. Active layer monitoring in Antarctica: an overview of results from 2006 to 2015. *Polar Geography*, in press. <https://doi.org/10.1080/1088937X.2017.1420105>.
- Johnson, J.S., Bentley, M.J., Roberts, S.J., Binnie, S.A., Freeman, S.P.H.T. 2011. Holocene deglacial history of the northeast Antarctic Peninsula - A review and new chronological constraints. *Quaternary Science Reviews* 30, 3791-3802. <https://doi.org/10.1016/j.quascirev.2011.10.011>.
- Kavan, J., Dagsson-Waldhauserova, P., Renard, J.B., Láska, K., Ambrožová, K. 2018. Aerosol concentrations in relationship to local atmospheric conditions on James Ross Island,

- Antarctica. *Frontiers in Earth Science-Atmospheric Science* 6, 207. <https://doi.org/10.3389/feart.2018.00207>.
- Košler, J., Magna, T., Mlčoch, B., Mixa, P., Nývlt, D., Holub, F.V. 2009. Combined Sr, Nd, Pb and Li isotope geochemistry of alkaline lavas from northern James Ross Island (Antarctic Peninsula) and implications for back-arc magma formation. *Chemical Geology* 258, 207-218. <https://doi.org/10.1016/j.chemgeo.2008.10.006>.
- Koster, E.A., Dijkmans, J.W.A. 1988. Niveo-aeolian deposits and denivation forms, with special reference to the Great Kobuk sand dunes, northwestern Alaska. *Earth Surface Processes and Landforms* 13 (2), 153-170. <https://doi.org/10.1002/esp.3290130206>.
- Kovanan, D., Slaymaker, O. 2015. The paraglacial geomorphology of the Fraser Lowland, southwest British Columbia and northwest Washington. *Geomorphology* 232, 78-93. <https://doi.org/10.1016/j.geomorph.2014.12.021>.
- Lancaster, N. 2002. Flux of eolian sediment in the McMurdo Dry Valleys, Antarctica: a preliminary assessment. *Arctic, Antarctic, and Alpine Research* 34 (3), 318-323. <https://doi.org/10.1080/15230430.2002.12003500>.
- Lancaster, N. 2004. Relations between aerodynamic and surface roughness in a hyper-arid cold desert: McMurdo Dry Valleys, Antarctica. *Earth Surface Processes and Landforms* 29 (7), 853-867. <https://doi.org/10.1002/esp.1073>.
- López-Martínez, J., Serrano, E., Schmid, T., Mink, S., Linés, C. 2012. Periglacial processes and landforms in the South Shetland Islands (northern Antarctic Peninsula region). *Geomorphology* 155, 62-79. <https://doi.org/10.1016/j.geomorph.2011.12.018>.
- Marchant, D.R., Lewis, A.R., Phillips, W.M., Moore, E.J., Souchez, R.A., Denton, G.H., Sugden, D.E., Potter, N., Landis, G.P. 2002. Formation of patterned ground and sublimation till over Miocene glacier ice in Beacon Valley, southern Victoria Land, Antarctica. *Geological Society of America Bulletin* 114 (6), 718-730. [https://doi.org/10.1130/0016-7606\(2002\)114<0718:FOPGAS>3.3.CO;2](https://doi.org/10.1130/0016-7606(2002)114<0718:FOPGAS>3.3.CO;2).
- Matsuoka, N., Moriwaki, K., Hirakawa, K. 1996. Field experiments on physical weathering and wind erosion in an Antarctic cold desert. *Earth Surface Processes and Landforms* 21, 687-699. [https://doi.org/10.1002/\(SICI\)1096-9837\(199608\)21:8<687::AID-ESP614>3.3.CO;2-A](https://doi.org/10.1002/(SICI)1096-9837(199608)21:8<687::AID-ESP614>3.3.CO;2-A).
- McGowan, H.A., Neil, D.T., Speirs, J.C. 2014. A reinterpretation of geomorphological evidence for Glacial Lake Victoria, McMurdo Dry Valleys, Antarctica. *Geomorphology* 208, 200-206. <https://doi.org/10.1016/j.geomorph.2013.12.005>.
- McKenna Neuman, C. 1993. A review of aeolian transport processes in cold environments. *Progress in Physical Geography: Earth and Environment* 17 (2), 137-155. <https://doi.org/10.1177/030913339301700203>.
- McKenna Neuman, C. 2004. Effects of temperature and humidity upon the transport of sedimentary particles by wind. *Sedimentology* 51, 1-17. <https://doi.org/10.1046/j.1365-3091.2003.00604.x>.
- Mlčoch, B., Nývlt, D., Mixa, P., (Eds.) 2018. *Geological map of James Ross Island – Northern part 1: 25,000*. Czech Geological Survey, Praha.
- Nelson, P.H.H. 1975. *The James Ross Island Volcanic Group of North-East Graham Land*. British Antarctic Survey Scientific Report 54, 62 pp.
- Nývlt, D., Braucher, R., Engel, Z., Mlčoch, B., ASTER Team 2014. Timing of the Northern Prince Gustav Ice Stream retreat and the deglaciation of northern James Ross Island, Antarctic Peninsula during the last glacial-interglacial transition. *Quaternary Research* 82, 441-449. <https://doi.org/10.1016/j.yqres.2014.05.003>.
- Nývlt, D., Nývltová Fišáková, M., Barták, M., Stachoň, Z., Pavel, V., Mlčoch, B., Láška, K. 2016. Death age, seasonality, taphonomy and colonization of seal carcasses from Ulu Peninsula,

- James Ross Island, Antarctic Peninsula. *Antarctic Science* 28, 3-16. <https://doi.org/10.1017/S095410201500036X>.
- Ó Cofaigh, C., Davies, B.J., Livingstone, S.J., Smith, J.A., Johnson, J.S., Hocking, E.P., Hodgson, D.A., Anderson, J.B., Bentley, M.J., Canals, M., Domack, E., Dowdeswell, J.A., Evans, J., Glasser, N.F., Hillenbrand, C.D., Larter, R.D., Roberts, S.J., Simms, A.R. 2014. Reconstruction of ice-sheet changes in the Antarctic Peninsula since the Last Glacial Maximum. *Quaternary Science Reviews* 100, 87-110. <https://doi.org/10.1016/j.quascirev.2014.06.023>.
- Oliva, M., Ruiz-Fernández, J. 2015. Coupling patterns between para-glacial and permafrost degradation responses in Antarctica. *Earth Surface Processes and Landforms* 40 (9), 1227-1238. <https://doi.org/10.1002/esp.3716>.
- Oliva, M., Hrbáček, F., Ruiz-Fernández, J., de Pablo, M.A., Vieira, G., Ramos, M., Antoniadis, D. 2017. Active layer dynamics in three topographically distinct lake catchments in Byers Peninsula (Livingston Island, Antarctica). *Catena* 149 (2), 548-559. <https://doi.org/10.1016/j.catena.2016.07.011>.
- Olivero, E., Scasso, R.A., Rinaldi, C.A. 1986. *Revision of the Marambio Group, James Ross Island, Antarctica*. Instituto Antártico Argentino, Contribución 331, 28 pp.
- Šabacká, M., Priscu, J.C., Basagic, H.J., Fountain, A.G., Wall, D.H., Virginia R.A., Greenwood, M.C. 2012. Aeolian flux of biotic and abiotic material in Taylor Valley, Antarctica. *Geomorphology* 155-156, 102-111. <https://doi.org/10.1016/j.geomorph.2011.12.009>.
- Seehaus, T., Cook, A.J., Silva, A.B., Braun, M. 2018. Changes in glacier dynamics in the northern Antarctic Peninsula since 1985. *Cryosphere* 12 (2), 577-594. <https://doi.org/10.5194/tc-12577-2018>.
- Seppälä, M. 2004. *Wind as a geomorphic agent*. Cambridge University Press, Cambridge, 368 pp.
- Smellie, J.L., Johnson, J.S., McIntosh, W.C., Esser, R., Gudmundsson, M.T., Hambrey, M.J., Van Wyk De Vries, B. 2008. Six million years of glacial history recorded in volcanic lithofacies of the James Ross Island Volcanic Group, Antarctic Peninsula. *Palaeogeography, Palaeoclimatology, Palaeoecology* 260, 122-148. <https://doi.org/10.1016/j.palaeo.2007.08.011>.
- Smellie, J.L., Johnson, J.S., Nelson, A.E. 2013. *Geological map of James Ross Island. 1. James Ross Island Volcanic Group (1:125 000 Scale)*. BAS GEOMAP 2 Series, Sheet 5, British Antarctic Survey, Cambridge.
- Smith, M.W., Riseborough, D.W. 1996. Permafrost Monitoring and Detection of Climate Change. *Permafrost and Periglacial Processes* 7, 301-309. [https://doi.org/10.1002/\(SICI\)1099-1530\(199610\)7:4<301::AID-PPP231>3.0.CO;2R](https://doi.org/10.1002/(SICI)1099-1530(199610)7:4<301::AID-PPP231>3.0.CO;2R).
- Speirs, J.C., McGowan, H.A., Neil, D.T. 2008. Meteorological controls on sand transport and dune morphology in a polar-desert: Victoria Valley, Antarctica. *Earth Surface Processes and Landforms* 33 (12), 1875-1891. <https://doi.org/10.1002/esp.1739>.
- Thomas, D.S.G. 1997. *Arid Zone Geomorphology*. 2<sup>nd</sup> Edition. John Wiley & Sons, 624 pp.
- Tsoar, H. 2001. Types of Aeolian Sand Dunes and Their Formation. In: N.J. Balmforth, A. Provenzale (Eds.) *Geomorphological Fluid Mechanics*. Lecture Notes in Physics, vol. 582. Springer, Berlin, Heidelberg.
- Van Lipzig, N.P.M., King, J.C., Lachlan-Cope, T.A., van der Broeke, M.R. 2004. Precipitation, sublimation and snow drift in the Antarctic Peninsula region from a regional atmospheric model. *Journal of Geophysical Research-Atmosphere* 109, D24106. <https://doi.org/10.1029/2004JD004701>.
- Wiggs, G., Baird, A., Atherton, R. 2004. The dynamic effects of moisture on the entrainment and transport of sand by wind. *Geomorphology* 59, 13-30. <https://doi.org/10.1016/j.geomorph.2003.09.002>.
- Zhang, T. 2005. Influence of the seasonal snow cover on the ground thermal regime: an overview. *Reviews of Geophysics* 43 (4). <https://doi.org/10.1029/2004RG000157>.





# Effect of climate and moss vegetation on ground surface temperature and the active layer among different biogeographical regions in Antarctica

Filip Hrbáček<sup>a</sup>, Nicoletta Cannone<sup>b</sup>, Michaela Kňázková<sup>a</sup>, Francesco Malfasi<sup>c</sup>, Peter Convey<sup>d</sup>, Mauro Guglielmin<sup>c,\*</sup>

<sup>a</sup> Masaryk University, Faculty of Science, Department of Geography, Brno, Czech Republic

<sup>b</sup> Department of Science and High Technology, Insubria University, Como, Italy

<sup>c</sup> Department Theoretical and Applied Sciences, Insubria University, Varese, Italy

<sup>d</sup> British Antarctic Survey, NERC, High Cross, Madingley Road, Cambridge CB3 0ET, United Kingdom



## ARTICLE INFO

### Keywords:

Active layer thickness  
Antarctica  
Mosses  
Climate change  
Ecosystems  
Soil thermal regime

## ABSTRACT

Ground surface temperature (GST) and active layer thickness (ALT) are key indicators of climate change (CC) in permafrost regions, with their relationships with climate and vegetation being crucial for the understanding of future climate change scenarios, as well as of CC feedbacks on the carbon cycle and water balance.

Antarctic ice free-areas host simplified ecosystems with vegetation dominated by mosses and lichens, and an almost negligible anthropogenic impact, providing a good template of ecosystem responses to CC. At three different Antarctic Conservation Biogeographical Regions (ACBR) sites in Antarctica located between 74° and 60°S, we compared barren ground and moss vegetated sites to understand and quantify the effects of climate (air temperature and incoming radiation) and of vegetation on GST and ALT. Our data show that incoming radiation is the most important driver of summer GST at the southernmost site, while in the other sites air temperature is the main driver of GST. Our data indicate that there is a decoupling between ALT and summer GST, because the highest GST values correspond with the thinnest ALT. Moreover, our data confirm the importance of the buffering effect of moss vegetation on GST in Antarctica. The intensity of the effect of moss cover on GST and ALT mainly depends on the species-specific moss water retention capacity and on their structure. These results highlight that the correct assessment of the moss type and of its water retention can be of great importance in the accurate modelling of ALT variation and its feedback on CC.

## 1. Introduction

Ground surface temperature and active layer thickness (ALT) are the key indicators of climate change (CC) in permafrost regions (e.g. Romanovsky et al., 2002, Guglielmin, 2006), indeed the former is determined by the energy balance of the surface and therefore reflects not only air temperature but also radiation and the effect of the snow and vegetation cover while the second is a seasonal response to the changes of the former. Relationships between ALT, climate and vegetation, and their feedbacks with CO<sub>2</sub> and CH<sub>4</sub> emissions and water balance changes are crucial for the understanding of future climate change scenarios.

Despite less than 0.5% of Antarctica being ice-free, such areas include a range of very variable environments in terms of topography, geology and, above all, climate. The ice-free areas of Antarctica occur

over a wide geographical and climatic gradient, spanning areas suffering amongst the strongest trends of regional air warming in recent decades (i.e. the Antarctic Peninsula) to areas in which air temperature remains stable, such as Victoria Land (Turner et al., 2009, 2013).

Antarctic ice-free areas have two distinctive features with respect to those of the Arctic, allowing their use as a template of ecosystem responses to CC: i) Antarctic vegetation is dominated by mosses and lichens, with only two vascular plants occurring in the Antarctic Peninsula, providing simplified ecosystems, and ii) Antarctic ice free areas are generally pristine, with almost negligible anthropogenic impact.

With this background, a number of active layer studies have been developed over the last 10 years in Antarctica, although a minority of these have focused on the relationships between CC, active layer and

*Abbreviations:* ALT, Active Layer Thickness; GST, Ground Surface Temperature; DJF, Summer Temperature; MAM, Autumn Temperature; JJA, Winter Temperature; SON, Spring Temperature

\* Corresponding author.

E-mail address: [mauro.guglielmin@uninsubria.it](mailto:mauro.guglielmin@uninsubria.it) (M. Guglielmin).

<https://doi.org/10.1016/j.catena.2020.104562>

Received 9 September 2019; Received in revised form 11 February 2020; Accepted 13 March 2020

Available online 18 March 2020

0341-8162/ © 2020 Elsevier B.V. All rights reserved.

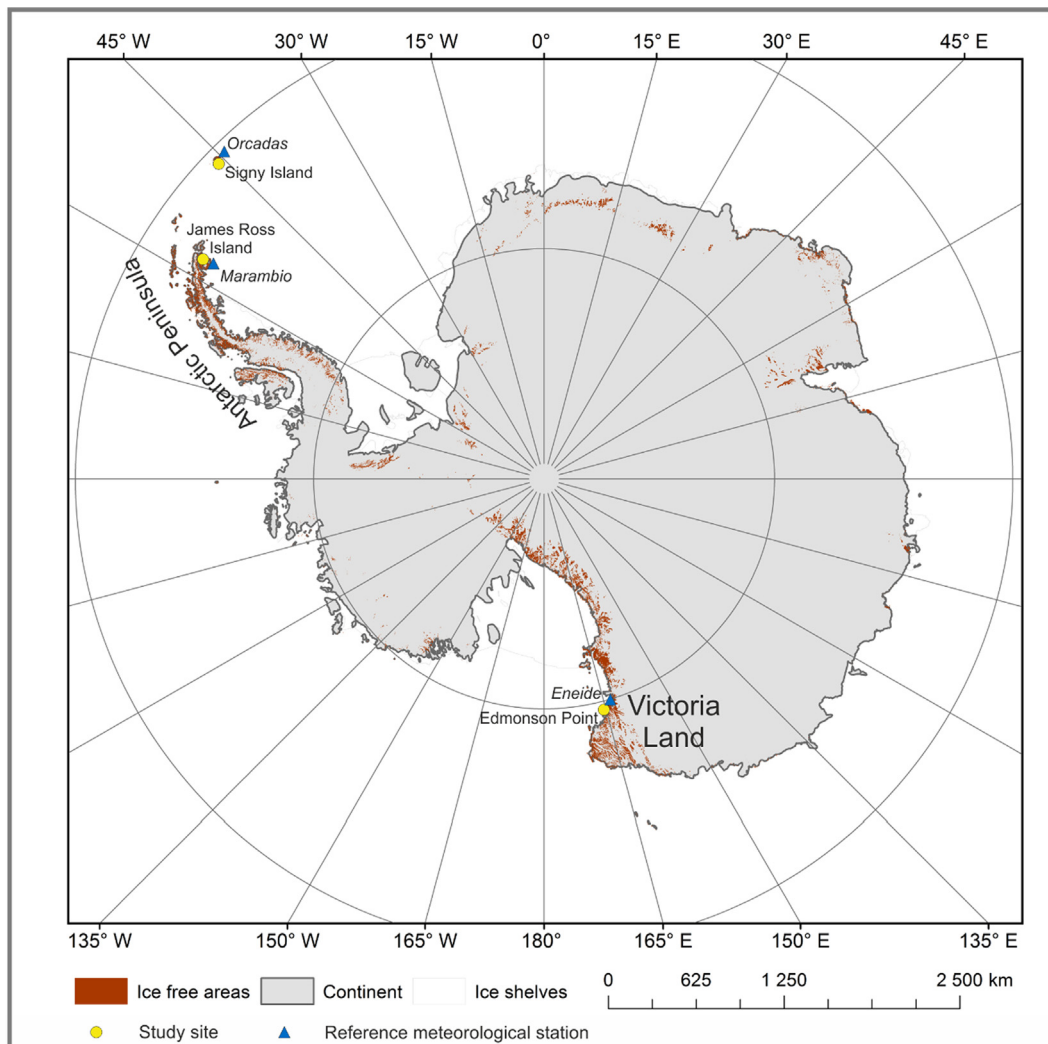


Fig. 1. Location of the study sites and the reference meteorological stations.

vegetation changes. In particular, studies have addressed the role of vegetation (e.g. Michel et al., 2012; Guglielmin et al., 2014a), snow cover (e.g., Guglielmin et al., 2014b; Hrbáček et al., 2016; De Pablo et al., 2017; Ferreira et al., 2017; Oliva et al., 2017) or climate control (e.g., Guglielmin and Cannone, 2012; Lacelle et al., 2016). However, in spite of the recent increase in scientific interest, most of these studies were performed at a local scale, analysing only one or two study sites. Thus there are few available publications providing a regional perspective on the variability of active layer properties across Antarctica or across latitudinal transects, including different regions, such as the Antarctic Peninsula (e.g., Bockheim et al., 2013; Wilhelm and Bockheim, 2017), the McMurdo Dry Valleys (e.g., Adlam et al., 2010), or general overviews of the whole continent (e.g., Vieira et al., 2010; Hrbáček et al., 2019).

Mosses are an important component of the cryptogamic Antarctic tundra vegetation occurring in ice-free areas in Antarctica (Convey, 2017). They are also an important component of Arctic vegetation, where they are considered to play an important role in critical tundra ecosystem processes involved in water and energy exchange, as they exert a strong insulating effect on soil temperature (Blok et al., 2011; Soudzilovskaia et al., 2013). Laboratory experiments indicate that mosses may exert strong controls on understory water and heat fluxes, with impacts on permafrost thaw (Blok et al., 2011). In particular, bryophyte functional traits relating to water economy strategies are crucial (Blok et al., 2011; Soudzilovskaia et al., 2013) because species

may differ considerably in water retention capacity (Elumeeva et al., 2011). Therefore, important traits of moss include water content at field capacity, volume and density ( $\text{mg cm}^{-3}$ ) of water saturated and oven-dried patches (Elumeeva et al., 2011). Indeed, field moisture content may affect bryophyte thermal conductivity (Soudzilovskaia et al., 2013).

Some field studies on Antarctic mosses suggest that the control exerted by mosses on soil temperature differs between moss species and their ecological requirements (e.g., Cannone et al., 2006; Cannone and Guglielmin, 2009). On the other hand, field and laboratory experiments on sub-Arctic mosses suggest that moss control was not defined at the species level but rather depended mainly on the thickness (and density) of the moss mat and its moisture content (e.g., Soudzilovskaia et al., 2013). Therefore, despite the insulating effect of moss being widely recognized, the buffering effect of different moss species on soil temperature still needs further investigation. Moreover, despite a net cooling effect of mosses on soil temperature observed in different environments, ranging from tundra to boreal forest (e.g. Cannone and Guglielmin, 2009; Blok et al., 2011; Guglielmin et al., 2012; Fisher et al., 2016), Soudzilovskaia et al. (2013) reported that mosses did not influence the mean soil temperature, but only reduced the amplitude of soil temperature fluctuations and freeze–thaw cycle frequency. These data highlight the discrepancies deriving from comparisons of laboratory or model predictions with the results of *in situ* observations, revealing biases (e.g. Park et al., 2018). Future changes in moss or

vegetation cover triggered by climate change may have important consequences for permafrost thaw and concomitant soil carbon release in Arctic tundra ecosystems (Blok et al., 2011). Therefore, it is extremely important to provide a quantitative assessment of moss influence on soil temperature and ALT, and include it in models focusing on the impacts of climate warming in permafrost regions (e.g. Porada et al., 2016, 2017; Park et al., 2018).

Antarctic ice-free regions are ideal for analysing the effect of mosses on ground temperature and ALT, while quantifying changes in this influence across gradients characterized by different climate change magnitude and direction.

In this study we took a comparative approach across a wide geographic region, encompassing three different biogeographic regions of Antarctica (Ochyra et al., 2008; Convey, 2017): i) Victoria Land (continental Antarctica), where the southernmost extensive moss vegetation development is found at Edmonson Point (74°S); ii) the north-eastern tip of the Antarctic Peninsula at Cape Lachman (James Ross Island, 63°S); iii) the northern part of the maritime Antarctic (Signy Island, 60°S). Moreover, these sites also correspond to three different Antarctic Conservation Biogeographical Regions (ACBR) (Terauds et al., 2012; Terauds and Lee, 2016).

Here we aim to evaluate:

- i) the ground surface temperature (GST) and ALT across the geographic and climatic range, hypothesizing that the main climatic drivers of GST may change among the different ACBR, while ALT was influenced also by other surface factors (including vegetation);
- ii) how different moss species affect the GST and ALT under natural field conditions, hypothesizing that mosses decrease the mean GST with respect to barren grounds, and that their buffering effect is species specific and depends on specific traits including moss density, water content (minimum vs maximum).

## 2. Study area

The study sites are located between latitudes 74°S and 60°S (Fig. 1) in three contrasting climatic regions and different biogeographic regions (Ochyra et al., 2008; Terauds et al., 2012; Terauds and Lee, 2016; Convey, 2017) and can be used as templates of their respective ACBR that, from South to North, are: North Victoria Land (Edmonson Point, 74°S); North-East Antarctic peninsula (James Ross Island, 63°S) and South Orkneys Islands (Signy Island, 60°S).

### 2.1. Edmonson Point

Edmonson Point is located in continental Antarctica, in the North Victoria Land ACBR. The climate is cold polar continental with MAAT around  $-16\text{ }^{\circ}\text{C}$  (Cannone and Guglielmin, 2009). The precipitation, as snow, is estimated to be 100–200 mm water equivalent (Bromwich et al., 2011). The ice free area of about  $1.8\text{ km}^2$  is formed by rock outcrops, debris and alluvial deposits of volcanic origin (Cannone, 2006) with continuous permafrost where ALT ranges between 40 and 50 cm (Cannone and Guglielmin, 2009). The vegetation of Victoria Land is the Antarctic non-vascular cryptogamic tundra, which is composed exclusively of mosses and lichens, includes the lowest number of species compared to the other two study sites (Cannone and Seppelt, 2008).

### 2.2. James Ross Island

This is the largest island in the North-East Antarctic Peninsula ACBR. The study site is located at Cape Lachman, which is the north-eastern tip of James Ross Island. The climate is semi-arid polar continental with MAAT around  $-7\text{ }^{\circ}\text{C}$  (Hrbáček et al., 2019). Annual precipitation is estimated between 200 and 500 mm water equivalent, largely as snow during the winter (van Lipzig et al., 2004). The

lithologies of the study site are weathered vesicular agglomerate and scoria (Mlčoch et al., 2018). Permafrost is continuous with an ALT from 50 to 125 cm (Hrbáček et al., 2017a). The vegetation is composed of the non-vascular cryptogamic tundra vegetation similarly to that of Signy Island, although with fewer species of mosses and lichens.

### 2.3. Signy Island

Signy Island (South Orkney Islands) is located in northern maritime Antarctica, south of Coronation Island, which is the largest island in the archipelago. It lies in the South Orkney Islands ACBR. The MAAT in Signy Island is around  $-3.5\text{ }^{\circ}\text{C}$  with precipitation of about 400 mm formed primarily by summer rain (Cannone et al., 2017). The ice-free area of the island covers about  $10\text{ km}^2$  and it is composed by bedrock of quartz-mica-schist, morainic deposits, scree slopes, beaches and alluvial deposits (Matthews and Maling, 1967). Permafrost is continuous with an ALT variable between 40 cm to  $> 3\text{ m}$  (Guglielmin et al., 2008; Guglielmin and Cannone, 2012). The vegetation includes both the Antarctic vascular herb tundra, (with the occurrence of the two native vascular plant species, *Deschampsia antarctica* Desv. and *Colobanthus quitensis* Bartl) and of the Antarctic non-vascular cryptogam tundra, dominated by mosses and lichens.

## 3. Material and methods

The study sites in each ACBR were selected in order to have comparable conditions with respect to altitude, topography, and distance from the sea (Table 1).

All the monitored plots are located on almost flat areas ( $3\text{--}5^{\circ}$ ) and the vegetation of the sites was dominated by different species of mosses, with coverage greater than 90% at all sites (Table 1, Fig. 2), and different thickness (between 1 cm at Edmonson Point to 5 cm at Signy Island) (Table 1). In the close vicinity of each moss site, a control site for the ground temperature measurement was installed in bare ground conditions.

In detail, the monitored plots are flat areas characterized by basalt regolith on bare ground plot and alluvial deposits composed almost completely by basalt clasts at Edmonson Point, while at James Ross Island are on flat terrace composed by debris derived by the vesicular agglomerate and scoria, and at Signy on a flat area characterised by thin glacial deposits.

Air temperature was measured between 160 and 200 cm above the ground surface into the radiation protective shield. Ground surface temperature (GST) was measured at 2 cm depth both in moss-covered and bare-ground areas and, additionally, across profiles with depth which varied from 20 to 250 cm. Both air and ground temperatures were measured with thermometers (accuracy of  $\pm 0.1$  to  $\pm 0.2\text{ }^{\circ}\text{C}$ ) (Table 2). Incoming radiation was also measured at each location (Table 2). All data were recorded every 60 min along two complete hydrological years (1st March 2015–28th February 2017).

The raw data were used for the calculation of mean daily values of temperature and incoming radiation, and the assessment of daily maximum and minimum temperatures, which were used to compute the daily amplitude. Mean daily values were further used for the calculation of the mean seasonal temperature and incoming radiation (autumn - MAM, winter - JJA, spring - SON, summer - DJF) and the annual temperatures for the period March to February. The mean monthly air temperatures over the period 1997 to 2016 were obtained from the closest permanent meteorological stations located in the vicinity to our study sites. In particular, data from Orcadas and Marambio were extracted from the READER database (<https://legacy.bas.ac.uk/met/READER/data.html>), and data from Eneide were obtained from the Meteorological Observatory of PNRA ([www.climantartide.it](http://www.climantartide.it)).

Air and near surface ground thermal indices were calculated based on mean daily temperatures following the protocol described by Guglielmin et al. (2008), and widely used in other studies in the

**Table 1**  
Topographical and climatic characteristics of the sites and lithological and vegetational characteristics of the monitored plots.

| Site              | Coordinates          | Elevation(m a.s.l.) | Distance from sea (m) | MAAT (°C) | Precipitation (mm y <sup>-1</sup> ) | Slope (°) | Aspect (°) | Lithology   | Dominated vegetation   | Average vegetation thickness | Study site coverage | Moss thermal Conductivity (W m <sup>-1</sup> K <sup>-1</sup> ) |
|-------------------|----------------------|---------------------|-----------------------|-----------|-------------------------------------|-----------|------------|---|--|------------------------------|---------------------|--|
| Edmonson Point    | 74°20' S<br>165°08'W | 40*                 | 500                   | -14       | 100-200                             | 3         | 90         | Alluvial deposits*<br>Basalt regolith**                                 | <i>Schistidium antarctici</i>  | 1 cm                         | 90%                 | 0.359-0.455  |
| James Ross Island | 63° 47'S<br>57° 47'W | 50                  | 200                   | -7        | 200-500                             | 5         | 135        | Debris (derived by scoria and vesicular agglomerate)<br>Glacial deposit | <i>Distichium inclinatum</i> (dominant), <i>Hypnum revolutum</i> ,<br><i>Chorisodontium aciphyllum</i> ,<br><i>Sanionia uncinata</i> | 2 cm                         | 100%                | 0.438-0.478<br>0.45-0.516                                      |
| Signy Island      | 60°43'S<br>45°38'W   | 85                  | 200                   | -3        | 400                                 | 3         | 340        |   |  | 5 cm                         | 100%                | 0.389-0.523<br>0.363-0.496                                     |

\* Moss site.

\*\* Bare ground site.

Antarctic Peninsula region (e.g. Michel et al., 2012; Hrbáček et al., 2016; Oliva et al., 2017), hence allowing to generate data comparable with other studies. For each year we calculated: a) the thawing degree days (TDD) as a sum of positive daily mean air (TDD<sub>A</sub>) and ground temperature (TDD<sub>G</sub>), b) the freezing degree days (FDD) as a sum of negative daily mean air (FDD<sub>A</sub>) and ground temperature (FDD<sub>G</sub>), and c) the thawing (n<sub>t</sub>) and freezing (n<sub>f</sub>) n-factors calculated as the ratio between TDD and FDD of the air and ground, respectively.

Lacking snow thickness data in all the sites some GST elaborations were used to estimate the effect of snow. In particular the previous literature (e.g. Gadek and Leszkiewicz, 2010; Gubler et al., 2011; Schmid et al., 2012) was taken account and adapted to the Antarctic conditions. In detail, we consider as proxies for the days in which snow occurs the following conditions:

- I) days in which the GST is around 0 °C (± 0.2 °C = ISTD): as it suggests melting/freezing at the surface;
- II) among the days in which the GST is < 0 °C (GST<sup>0</sup>): when GST<sup>0</sup> is lower than air temperature it is due to the cooling effect of snow (please note that this effect has been documented only with a thin snow cover, e.g. Gubler et al., 2011; Guglielmin et al., 2014a, 2014b)
- III) among the days in which the GST is < 0 °C (GST<sup>0</sup>): when the incoming radiation is negligible (< 20 W m<sup>-2</sup>) and GST<sup>0</sup> is warmer than the air temperature (GST<sup>0</sup> > AT\*), the snow exerts a warming effect because its thickness is enough to insulate the ground from air temperature.

It is important to remind that when radiation exceeds 20 W m<sup>-2</sup> and GST<sup>0</sup> is warmer than the air temperature, it is not possible to say if this is due to the insulating effect of the snow or to the radiation heating. In addition, the seasonal development of the depth of the permafrost table (0 °C isotherm) was calculated according to the best fitting curve between the deepest sensors with positive temperature and the next deeper sensor with negative temperature (Hrbáček et al., 2017a).

Laboratory analyses were carried out to quantify for each single moss species (*Chorisodontium aciphyllum* (Hook. f. & Wils.) Broth., CA; *Distichium inclinatum* (Hedw.) Bruch, Schimp. & W. Guembel, DI; *Hypnum revolutum* (Mitt.) Lindb., HR; *Schistidium antarctici* (Cardot) L.I. Savicz & Smirnova, SA; *Sanionia uncinata* (Hedw.) Loeske, SU) the following functional traits (according to Elumeeva et al., 2011): moss density, minimum and maximum water retention capacity. The thermal conductivity of dry moss as well as of mosses with different water retention capacity (minimum and maximum) have been calculated according to Williams and Smith (1989).

Moreover, we applied the Stefan equation (Nelson et al., 1997), used to simulate the ALT of soils with the different moss species assuming that the thickness of the moss was infinite and compare the result with the ALT effectively estimated *in situ* as maximum depth of 0 °C isotherm.

$$\text{Stefan Equation ALT} = \sqrt{2 * K * IT / Q}$$

where ALT is the active layer thickness, K is the thermal conductivity of the unfrozen bryophyte, IT is the thawing index for the analysed surfaces, Q is the volumetric latent heat of fusion, which is given by the following equation:

$$Q = L \times D \times W$$

where L is the latent heat of ice, D is the dry moss density, and W is the total moisture content.

As water content changes largely influence the bryophyte thermal conductivity, the equations were computed twice for each bryophyte species: i) with minimum water content; ii) with maximum water content.

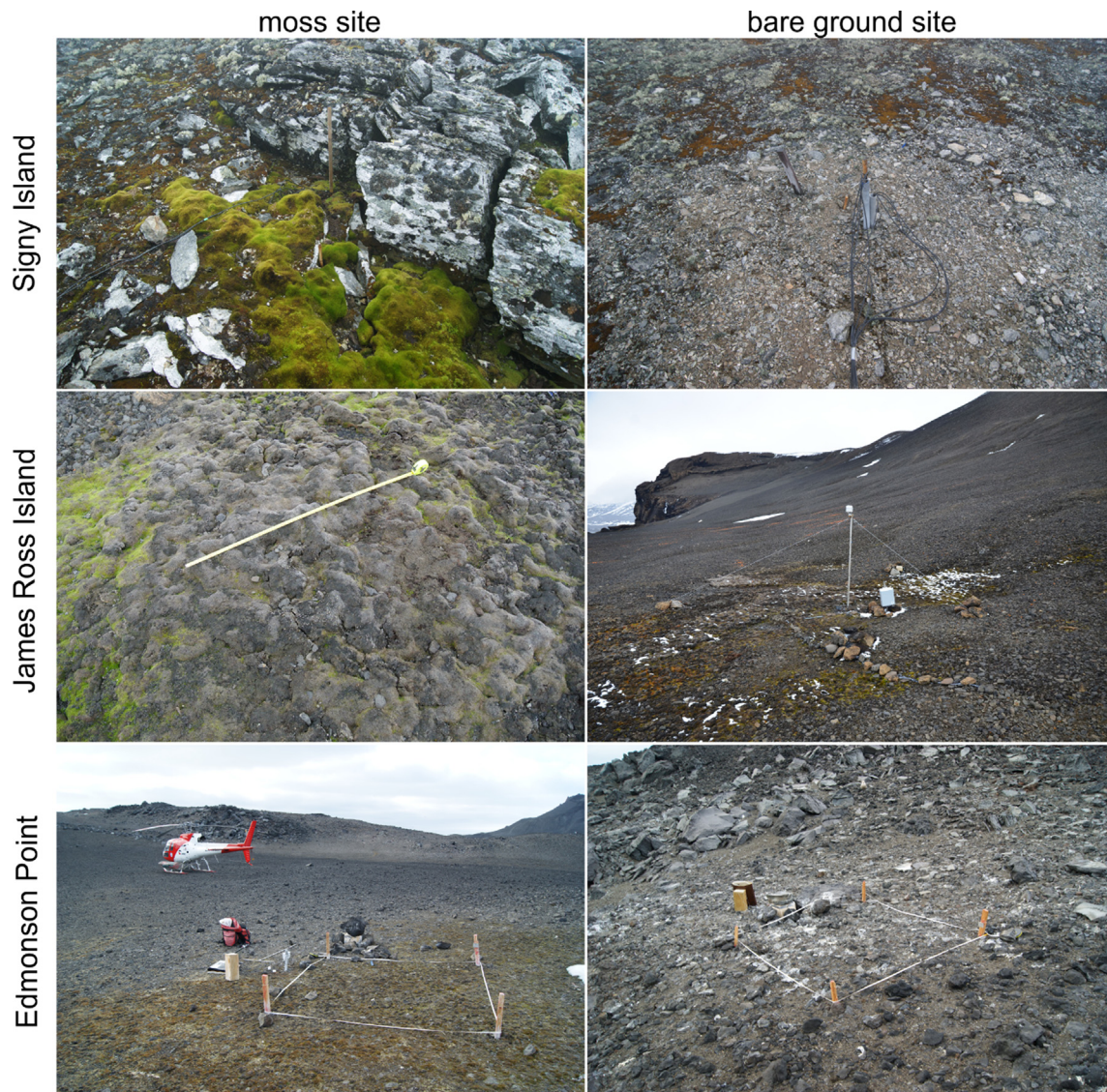


Fig. 2. Detailed images of the moss and bare ground study sites at Signy Island, James Ross Island and Edmonson Point.

## 4. Results

### 4.1. Climate

The two studied years were representative of the average climatic conditions of the selected sites in the last two decades, considering the monthly means of the air temperature of the available closest automatic weather stations (AWS) (Fig. 3).

#### 4.1.1. Edmonson Point

The mean annual air temperature at Edmonson Point was  $-16.6\text{ }^{\circ}\text{C}$  in 2015/16 and  $-16.4\text{ }^{\circ}\text{C}$  in 2016/17. Summer was the warmest period

in both seasons, with mean temperatures  $-2.3\text{ }^{\circ}\text{C}$  and  $-2.0\text{ }^{\circ}\text{C}$  during 2015/16 and 2016/17, respectively (Fig. 4a, Table 3). The lowest mean air temperatures occurred during the winter, as low as  $-27.2\text{ }^{\circ}\text{C}$  in 2016/17 (Fig. 4a, Table 3). Mean incoming radiation was similar during both seasons (slightly higher in 2015/16,  $102.7\text{ W m}^{-2}$ ) (Fig. 5). The maxima during the summer reached 240.2 to  $244.7\text{ W m}^{-2}$ , while during the winter incoming radiation was zero for 85 days between early May and early August (Fig. 5, Table 3).

#### 4.1.2. James Ross Island

On James Ross Island, mean annual air temperature was  $-7.2\text{ }^{\circ}\text{C}$  in 2015/16, while 2016/17 was warmer at  $-4.3\text{ }^{\circ}\text{C}$  (Fig. 4b, Table 3). The

Table 2

Technical specification of the measurement sensors.

| Site              | Air temperature | Profile depth/sensor numbers | Temperature sensor accuracy        | Manufacture | Incoming radiation |
|-------------------|-----------------|------------------------------|------------------------------------|-------------|--------------------|
| Edmonson Point    | 160 cm          | 100 cm/5                     | $\pm 0.2\text{ }^{\circ}\text{C}$  | Onset       | S-LIB sensor       |
| James Ross Island | 200 cm          | 50 cm/6                      | $\pm 0.15\text{ }^{\circ}\text{C}$ | EMS Brno    | EMS11 sensor       |
| Signy Island      | 160 cm          | 20* cm/2<br>250** cm/9       | $\pm 0.1\text{ }^{\circ}\text{C}$  | Campbell    | Kipp & Zonen CNR1  |

\* Moss site.

\*\* Bare ground site.

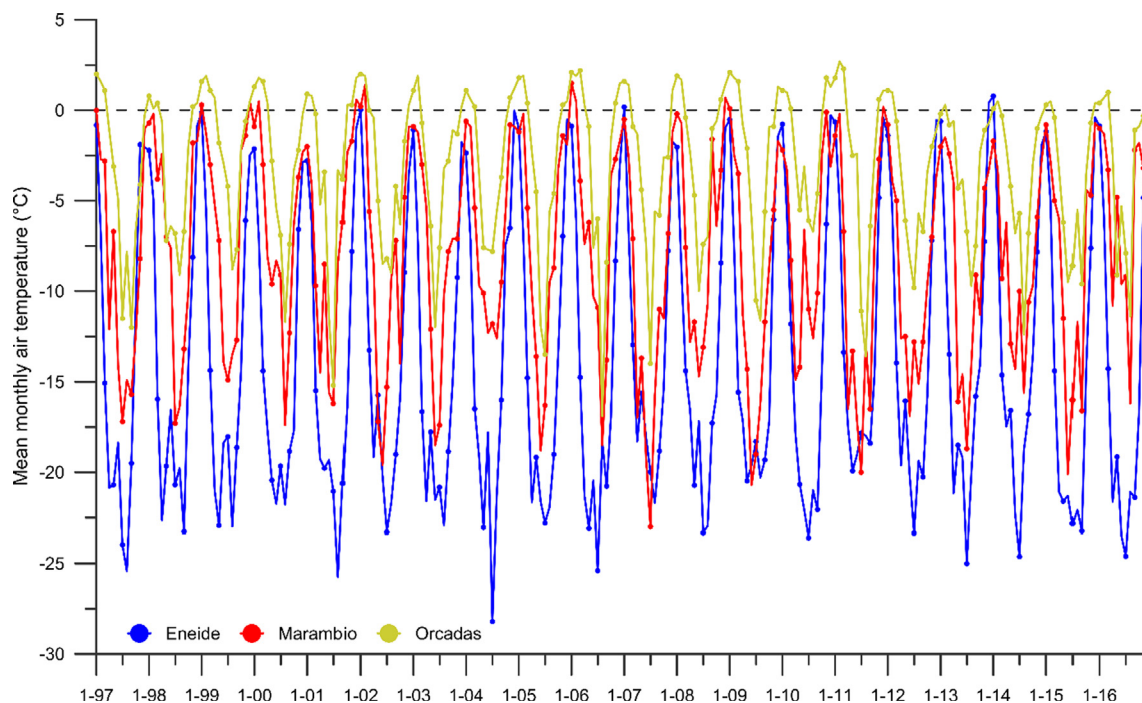


**Fig. 3.** Monthly mean air temperatures between 1996 and 2016 in the three closest automatic weather stations available for the three study sites, respectively Eneide for Edmonson Point; Marambio for James Ross Island and Orcadas for Signy Island (see the locations of the AWS and the sites in Fig. 1a).

summers reached  $+0.2$  °C in the former and  $-0.5$  °C in the latter year, while the coldest mean temperatures were  $-15.5$  °C during winter in 2015/16 (Fig. 4b, Table 3). Mean incoming radiation was higher during 2015/16 at  $116.6$   $W\ m^{-2}$ , while maxima were recorded during the summer ( $229.4$  and  $206.7$   $W\ m^{-2}$ ) and, as expected, minima during the winter months ( $16.1$  and  $16.2$   $W\ m^{-2}$ ) (Fig. 5, Table 3).

#### 4.1.3. Signy Island

Signy Island is the warmest and most northern of the three sites, with mean annual air temperatures  $-4.2$  °C and  $-3.4$  °C in 2015/16 and 2016/17, respectively (Fig. 4c, Table 3). The difference between mean summer and winter temperatures was lower, with winter temperatures dropping to  $-8.5$  °C and rising to  $+0.4$  °C during the summer in 2016/17 (Fig. 4c, Table 3). Mean incoming radiation, in contrast, was the lowest of the three sites, with only  $78.3$   $W\ m^{-2}$  in 2016/17. Signy Island received maximum incoming radiation during the summer ( $140.9$  and  $140.8$   $W\ m^{-2}$ ) and minimum during the winter ( $21.7$  and  $20.8$   $W\ m^{-2}$ ), but the difference between summer and winter was less pronounced than on James Ross Island or Edmonson Point (Fig. 5, Table 3).

Comparing the sites, as expected the southernmost location (Edmonson Point) experienced the coldest annual, summer and winter mean air temperatures (Table 3; Fig. 4), while the northernmost location (Signy Island) presented a closely similar summer mean and, in 2016/17, was colder than the intermediate location (James Ross Island). Inter-annual variability was higher for James Ross Island (especially during the winter) than the other two sites.

All three sites recorded large, sudden and short-lived fluctuations in air temperature in the middle of the dark winter period, even reaching positive values, likely due to the occurrence of the episodes known as “coreless winter” (Van Loon, 1967; King and Turner, 1997; Guglielmin and Dramis, 1997; Guglielmin and Cannone, 2012) mainly due to cyclonic circulation coming from the sea. While these episodes initiated at temperatures above  $-20$  °C at James Ross Island and Signy Island (Fig. 4), at Edmonson Point they initiated from lower temperatures and were less frequent. At all sites these fluctuations were of similar amplitude.

Mean incoming radiation during the summer (DJF) showed an opposite trend, with the lowest mean values at the lowest latitude site (Signy), roughly 50% of that recorded at Edmonson Point (Table 3, Fig. 5).

## 4.2. Ground surface temperature (GST) and ALT

### 4.2.1. Edmonson Point

The mean annual GST was  $-13.5$  °C in 2015/16 and  $-14.7$  °C in 2016/17 for the bare ground site, and slightly cooler in the moss site showing an insulating effect respect to air temperature ( $-14.6$  °C and  $-15.8$  °C in 2015/16 and 2016/17, respectively) (Table 3). The seasonal GST exhibited greater differences (up to  $6.9$  °C) during the summer, when the bare GST reached up to  $5.3$  °C versus  $-1.6$  °C under the mosses. During the winter, the mean GST dropped to  $-29.2$  °C for bare ground and  $-25.5$  °C under mosses (Fig. 4a, Table 3).

The effect of moss cover was appreciable mainly during the summer season, when the  $TDD_G$  of the moss covered site was 3–5 times lower than that measured in bare ground, both in 2015/16 and in 2016/17 (Table 4). During the winter these differences were minimal, as testified by the similar  $FDD_G$  between bare ground and moss sites (differences  $\leq 10\%$ ) (Table 4). The buffering effect of moss vegetation was also confirmed by the  $n_t$  values (Table 4).

Lacking direct measurements, the role of the snow has been estimated through the GST analyses. Table 5 showed that less than one third of the summer days (DJF) are still snow covered. On the contrary during the spring more than 20 days are snow free, having GST higher than  $0$  °C. Moreover, the days with snow cooling effect ( $GST^0 < AT$ ) are more frequent than those with the snow warming effect ( $GST^0 > AT^*$ ).

The active layer initial thawing was delayed by 39 days (2015/16) and 43 days (2016/17) at the moss site (Fig. 6) with respect to the bare ground. The maximum ALT was recorded in mid-January and reached 40 cm (2015/16) and 36 cm (2016/17) in bare ground, while it was thinner, reaching 36 cm (2015/16) and 23 cm, at the moss site, with a slight delay of ca. 7 days. The refreezing of the active layer occurred around the same date in both bare and moss covered ground in 2015/

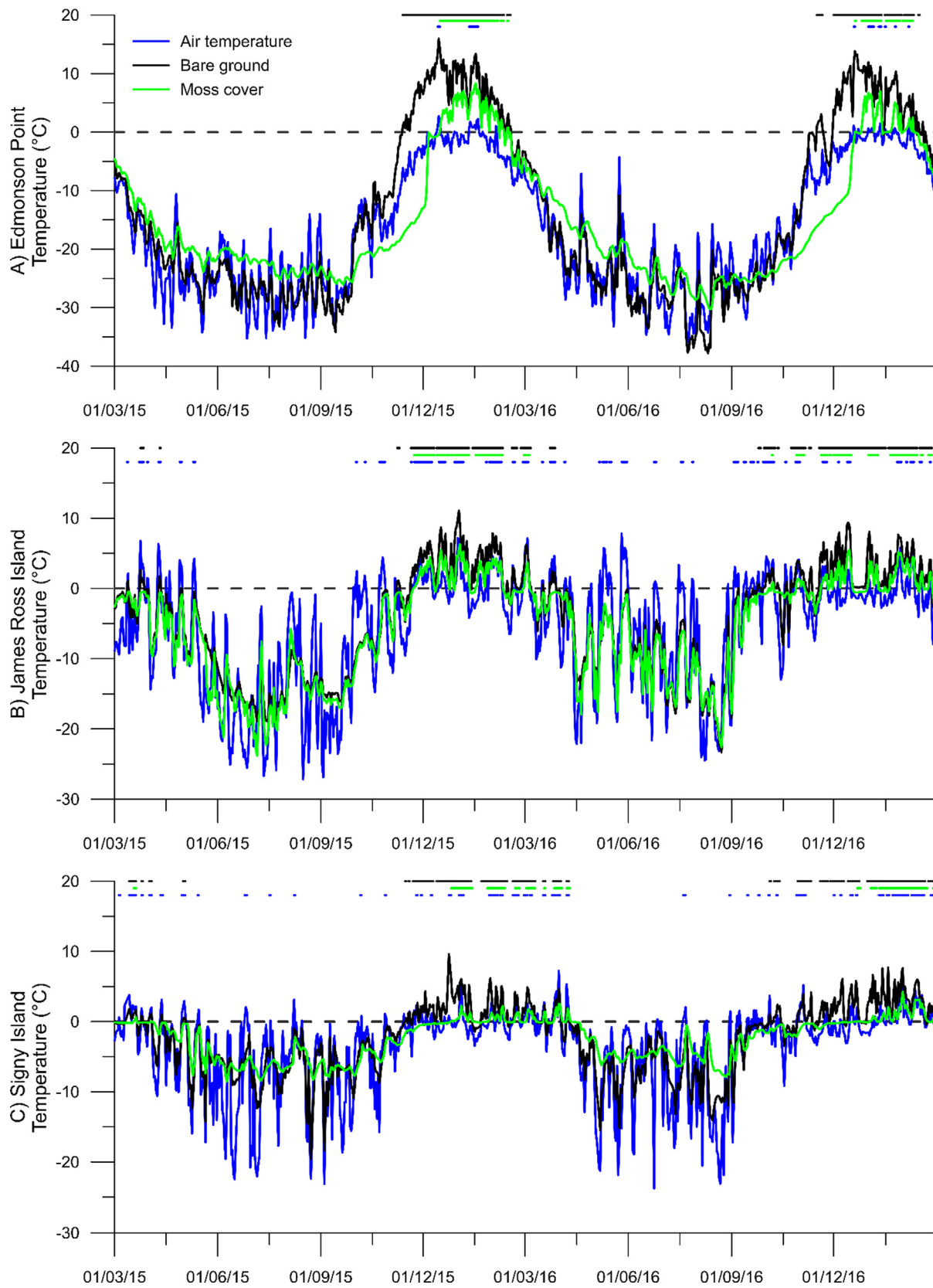


Fig. 4. Daily variability of air temperature and near-surface ground temperature in bare ground and moss sites. The horizontal lines indicates the positive mean daily temperature of air (blues), bare ground site (black) and moss site (green). (For interpretation of the references to colour in this figure legend, the reader is referred to the web version of this article.)

**Table 3**

Annual and seasonal averages of air temperature (AirT), ground-surface temperature (GST) at bare-ground site (BG) and moss site (M) and incoming radiation (IR) on the study sites.

| Site              | Parameter               | 2015/16 |       |       |       | 2016/17 |       |       |       | 2015/16 | 2016/17 |
|-------------------|-------------------------|---------|-------|-------|-------|---------|-------|-------|-------|---------|---------|
|                   |                         | MAM     | JJA   | SON   | DJF   | MAM     | JJA   | SON   | DJF   |         |         |
| Edmonson Point    | AirT (°C)               | -21.2   | -26.3 | -16.7 | -2.3  | -19.4   | -27.2 | -17.0 | -2.0  | -16.6   | -16.4   |
|                   | GST BG (°C)             | -19.3   | -26.9 | -14.1 | 6.2   | -18.8   | -29.2 | -16.2 | 5.3   | -13.5   | -14.7   |
|                   | GST M (°C)              | -16.3   | -22.6 | -20.9 | 1.2   | -14.9   | -25.4 | -21.4 | -1.6  | -14.6   | -15.8   |
|                   | IR (W m <sup>-2</sup> ) | 19.8    | 1.2   | 145.1 | 244.7 | 18.5    | 1.1   | 146.9 | 240.2 | 102.7   | 101.7   |
| James Ross Island | AirT (°C)               | -5.9    | -15.6 | -7.6  | 0.2   | -4.7    | -10.6 | -1.4  | -0.5  | -7.2    | -4.3    |
|                   | GST BG (°C)             | -4.4    | -14.4 | -7.1  | 3.7   | -4.7    | -12.1 | -0.5  | 3.1   | -5.5    | -3.5    |
|                   | GST M (°C)              | -5.4    | -15.5 | -7.9  | 1.8   | -5.2    | -12.4 | -1.5  | 1.4   | -6.7    | -4.4    |
|                   | IR (W m <sup>-2</sup> ) | 50.9    | 16.2  | 169.9 | 229.4 | 51.6    | 16.1  | 161.4 | 206.7 | 116.6   | 109.0   |
| Signy Island      | AirT (°C)               | -3.4    | -8.2  | -5.2  | -0.2  | -4.0    | -8.5  | -1.6  | 0.4   | -4.2    | -3.4    |
|                   | GST BG (°C)             | -2.5    | -6.9  | -4.1  | 2.1   | -3.1    | -7.3  | -0.5  | 2.9   | -2.9    | -2.0    |
|                   | GST M (°C)              | -1.7    | -6.1  | -4.4  | 0.2   | -1.6    | -5.0  | -1.5  | 0.7   | -3.0    | -1.8    |
|                   | IR (W m <sup>-2</sup> ) | 44.7    | 21.7  | 137.3 | 140.9 | 38.8    | 20.8  | 112.9 | 140.8 | 86.1    | 78.3    |

16 and 6 days earlier in 2016/17 in the moss-covered ground (Fig. 6).

4.2.2. James Ross Island

The mean annual GST at this site was -5.5 °C in 2015/16 and -3.5 °C in 2016/17 for bare ground and slightly lower for the moss-covered site (-6.7 °C in 2015/16 and -4.4 °C in 2016/17) (Table 3). Notably, during the winter the differences between bare ground and the moss site were around 1.1 °C (maximum), with the former being always colder than the latter (Fig. 4b).

The effect of moss cover was strong: the TDD<sub>G</sub> as well as the n<sub>t</sub> in the moss site was half that measured in the bare ground, while during the winter the difference in FDD<sub>G</sub> was similar (Table 4).

Table 5 showed that during the summer James Ross Island is the site showing the minimum number of snow covered days (14), while snow cooling effect here is much stronger than the warming one, recording in 2016/17 the maximum value (154 days) among all sites.

The active layer thawing of the bare ground site started 3 days earlier than in the moss site in 2015/16, while the beginning of active layer thawing in 2016/17 was interrupted by two short-term periods of refreezing for the bare ground site (Fig. 6). The ALT at both bare ground and moss sites was observed in mid-February (one month later than in continental Antarctica), with ALT reaching 61 cm (2015/16) and 64 cm (2016/17) in the bare ground profile, but only 50 cm the moss site in both years (Fig. 6).

4.2.3. Signy Island

The mean annual GST values were very similar for bare and moss ground (-2.9 vs. -3.0 °C in 2015/16 and -2.0 vs. -1.8 °C in 2016/

17, respectively) (Fig. 4c, Table 3). The bare ground GST was higher during the summer and lower in winter when compared to the moss site, with the maximum difference observed during the summer (around 2 °C). The winter at Signy Island was milder than at the other two sites, with a mean GST around -7°C for the bare ground and slightly warmer for moss site.

The largest buffering effect of mosses was detected in summer, with the TDD<sub>G</sub> in the bare ground being between 4 and 8 times higher than that recorded in moss site, again supported by the very low n<sub>t</sub> in the moss site (0.29 and 0.55) in comparison with n<sub>t</sub> of more than 2 in the bare ground (Table 4).

As in the two other locations, active layer thawing started 27 to 50 days earlier in the bare ground. The maximum ALT was observed in mid-March, ca. one month later than on James Ross Island. ALT in bare ground reached 153 cm (2015/16) and 181 cm (2016/17), while in the moss site ALT was much less, 55 cm (2015/16) and 54 cm (2016/17). ALT remained thawed until early-May.

Comparing the sites, the summer GST (DJF) and the TDD of the bare ground exhibited an opposite trend respect to latitude, with the highest values recorded at Edmonson Point, in agreement with the trend of the incoming radiation. In moss sites the GST did not follow the same trend of the bare ground, indeed, unexpectedly, the warmest site was James Ross (Table 4). Moreover, differently from the bare ground, in the moss sites the TDD did not have the same GST trend, as the warmest sites were James Ross or Edmonson Point, depending on the selected year.

Table 5 showed that snow cover in summer is more variable at Signy (20 days in 2015/16 and 13 days in 2016/17) than in James Ross Island or Edmonson Point, while it is less variable during the rest of the year.

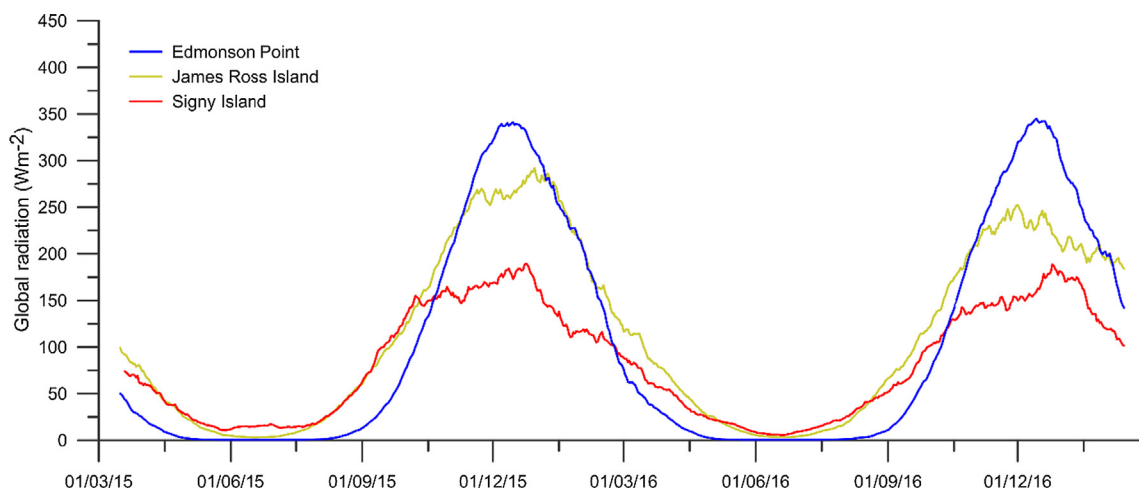


Fig. 5. Incoming global radiation at the three study sites. The daily values was smoothed by 7 days moving average.

**Table 4**

Annual values of thawing (TDD) and freezing (FDD) degree days, thawing ( $n_t$ ) and freezing ( $n_f$ ) n-factor of air (A), bare ground (BG) and moss (M) and the active layer thickness (ALT) on study sites.

|                     | Signy Island |         | James Ross Island |         | Edmonson Point |         |
|---------------------|--------------|---------|-------------------|---------|----------------|---------|
|                     | 2015/16      | 2016/17 | 2015/16           | 2016/17 | 2015/16        | 2016/17 |
| TDD <sub>A</sub>    | 101.1        | 168.4   | 206.7             | 249.3   | 17.4           | 10.2    |
| TDD <sub>G</sub> BG | 231.2        | 364.5   | 395.5             | 408.7   | 702.6          | 534.4   |
| TDD <sub>G</sub> M  | 29.2         | 93.1    | 195.3             | 172.1   | 238.0          | 110.8   |
| FDD <sub>A</sub>    | -1628.2      | -1426.7 | -2850.1           | -1834.0 | -6105.4        | -6018.5 |
| FDD <sub>G</sub> BG | -1260.5      | -1112.8 | -2424.5           | -1718.0 | -5665.8        | -5940.2 |
| FDD <sub>G</sub> M  | -1116.8      | -770.3  | -2664.1           | -1806.6 | -5164.5        | -5314.0 |
| $n_t$ BG            | 2.29         | 2.16    | 1.91              | 1.64    | 40.44          | 52.23   |
| $n_t$ M             | 0.29         | 0.55    | 0.95              | 0.69    | 13.70          | 10.83   |
| $n_f$ BG            | 0.77         | 0.78    | 0.85              | 0.94    | 0.93           | 0.99    |
| $n_f$ M             | 0.69         | 0.54    | 0.93              | 0.99    | 0.92           | 0.98    |
| ALT BG (cm)         | 153          | 181     | 61                | 64      | 40             | 36      |
| ALT M (cm)          | 55           | 54      | 50                | 50      | 37             | 23      |

**Table 5**

Role of the snow cover on bare ground plots derived by GST and air temperature (AT). Legend: ISTD = days in which the GST daily mean is between +0.2 and -0.2 °C independently by the air temperature; GST<sup>0</sup> = Days in which the GST daily mean is lower than 0 °C; SSD = summer (DJF) snow days determined by the sum of the days of ISTD and GST<sup>0</sup> during DJF; AT\* = days in which radiation is lower than 10 Wm<sup>-2</sup>; in bold between parenthesis are reported the values for the winter (JJA).

| Site                   | EP15/16  | EP16/17 | S15/16  | S16/17  | JRI15/16 | JRI16/17 |
|------------------------|----------|---------|---------|---------|----------|----------|
| GST > 0                | 91       | 72      | 103     | 130     | 95       | 130      |
| GST <sup>0</sup>       | 273      | 286     | 247     | 212     | 257      | 210      |
| ISTD                   | 2        | 7       | 16      | 23      | 14       | 25       |
| GST <sup>0</sup> < AT  | 109 (52) | 146(65) | 104(49) | 105(50) | 154(33)  | 117(61)  |
| GST <sup>0</sup> > AT* | 70(40)   | 48(27)  | 32(26)  | 17(11)  | 57(42)   | 14(14)   |
| SSD                    | 17       | 22      | 20      | 13      | 14       | 14       |

The ALT of the bare ground followed an opposite trend with latitude, with the thinnest ALT recorded at the southernmost location (Edmonson Point) and more similar ALT between this location and James Ross.

In all moss sites ALT was thinner compared to bare grounds, with the largest differences between moss and bare ground ALT detected in the northernmost site.

4.3. Bryophyte functional traits, GST and ALT

The bryophyte species occurring in our study sites exhibited large variations of their dry density (from almost 400 mgcm<sup>-3</sup> of *S. antarctici* to the 4 times less dense *C. aciphyllum*, Fig. 7A). Important differences among moss species concerned also the minimum and maximum water retention capacity, as measured in laboratory (Fig. 7B). Comparing moss water retention capacity and their dry density, there wasn't any apparent relationship.

Interestingly, our data show that the intensity of the moss buffering effect during summer (and also in spring) was not proportional to the moss layer thickness, as the highest effect detected at Edmonson Point corresponded to the thinnest moss layer (1 cm) (Table 3 and 4).

The simulated ALT (computed using the traits of each single species and assuming that the moss thickness was infinite) exhibited a range of variation for each species depending on the moss water retention capacity (Fig. 8). At all sites the ALT computed with the minimum water content retention capacity exhibited higher similarity with the ALT values measured *in situ*, allowing to hypothesize that at all sites xeric environmental conditions prevailed. The only apparent exception was *H. revolutum* at James Ross Island, but this species was not dominant in the moss community.

5. Discussion

5.1. Climate among different ACBRs

The data obtained in this study demonstrated, as expected, decreasing air temperature (annual and seasonal) with increasing latitude. The incoming radiation exhibited the opposite trend, with the northernmost site experiencing the lowest mean incoming radiation during the summer, complicating the interpretation of the GST patterns obtained. However, the patterns of incoming radiation can be easily explained. Indeed, it is well known that the prevailing westerly winds bring a very high level of cloud cover at Signy Island, but also to the Western Antarctic Peninsula region more generally (WAP; e.g. Thomas et al., 2015). On the other hand, it is also known that in Victoria Land the effect of the westerly winds is negligible. Very recently on Victoria Land the incoming radiation variability (with a high increase between 1990 and 2012; e.g. Guglielmin et al., 2014a, 2014b) has been related to stratospheric sulfur dioxide (Obryk et al., 2018).

Despite the lack of direct measurements of the snow cover at all sites, the GST analyses of the bare ground shows that the role of the snow cover is highly variable among the different sites, as well as in the different years (Table 5). However, it seems that the cooling effect of the snow is more important than the warming one (higher number of GST<sup>0</sup> < AT than GST > AT\* + ISTD) in all sites.

5.2. Effect of climate on GST

At Signy Island and James Ross Island permafrost is continuous, including also areas close to the shoreline (Bockheim et al., 2013).

The selected ACBRs have great climatic differences although summer air temperature was very similar between James Ross Island and Signy Island, while both these sites differed from Edmonson Point by 2.1–2.4 °C. The summer GST measured in bare ground showed an apparent paradox, with the highest values (5.3–6.2 °C) at the southernmost site (Edmonson Point) and the lowest (2.1–2.9 °C) at the northernmost site (Signy Island), as also confirmed by the TDD<sub>G</sub> and by the  $n_f$  (Table 3). This apparent paradox is related to the incoming radiation, as shown in Fig. 5. Indeed, at Signy Island, likely due to the effect of the westerly winds, the radiation reached an average daily value in the summer that was < 60% of that received at Edmonson Point. The interannual variation (2015/16 and 2016/17) of the GST in both sites (6.2 °C vs 5.3 °C at Edmonson Point; while 2.1 °C vs 2.9 °C at Signy Island) is probably related to the air temperature (see Table 3), but also to the different snow cover. Indeed, despite at each site the incoming radiation does not show any appreciable interannual variation (Table 3), GST is higher when the summer snow days (SSD) are lower (17 vs 22 at Edmonson Point and 20 vs 17 at Signy Island,

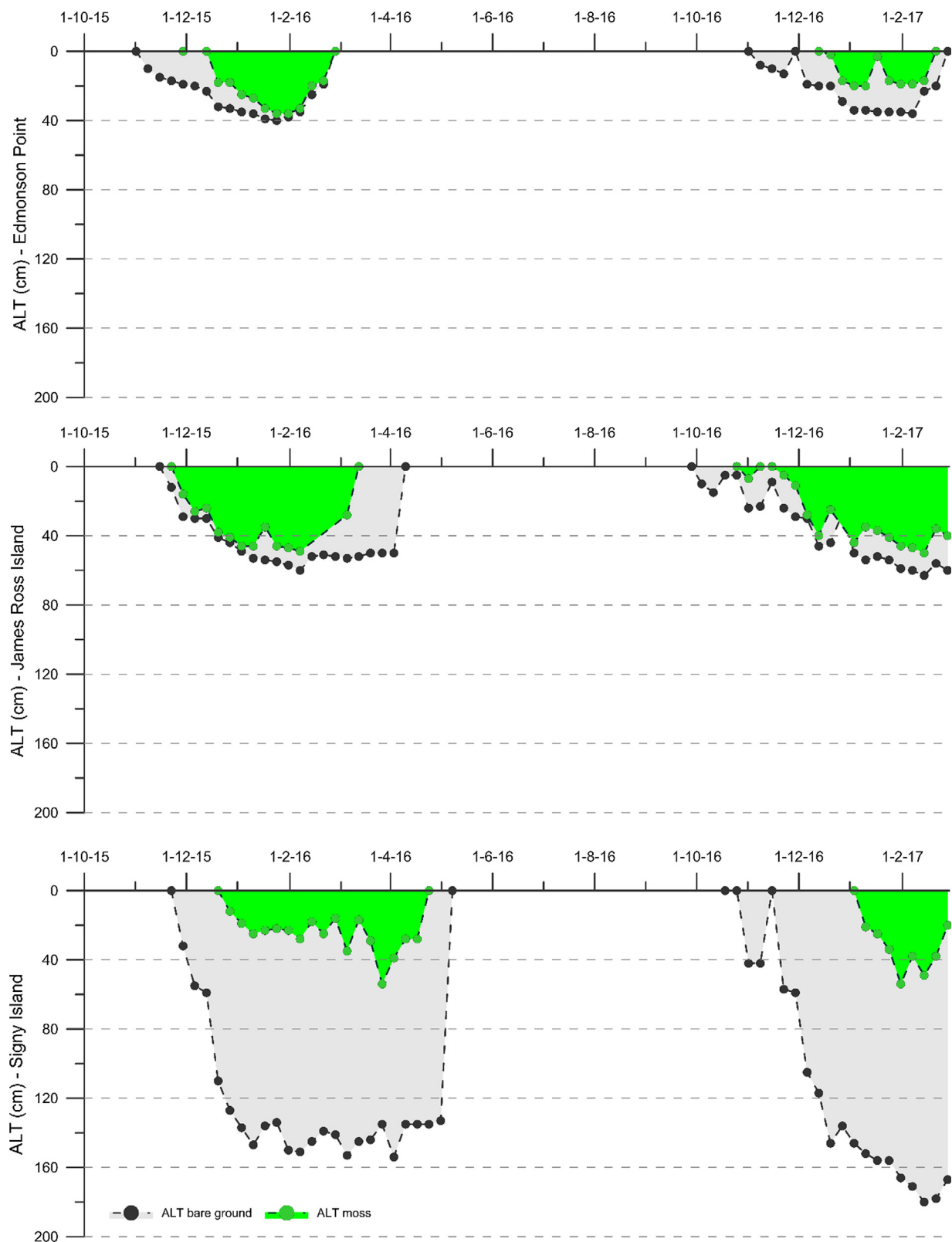


Fig. 6. Seasonal evolution of active layer thickness at moss (green area) and bare-ground sites (grey area). (For interpretation of the references to colour in this figure legend, the reader is referred to the web version of this article.)

Table 5).

During the winter air temperature was the main driver of the GST (Table 6), as testified by the FDD, the  $n_f$  and the winter mean GST (Table 3 and 4), because the net effect of snow cover was not pronounced, and was also variable between years. Considering the

$GST^0 < AT$  and the  $GST^0 > AT^*$  for the winter, as reported in Table 5, the cooling effect of the snow on the ground surface is clearly prevalent at Edmonson Point in both years. Indeed, in both cases the GST is lower than the air temperature, with the greatest cooling occurring in the season 2016/17 when the GST of the bare ground was

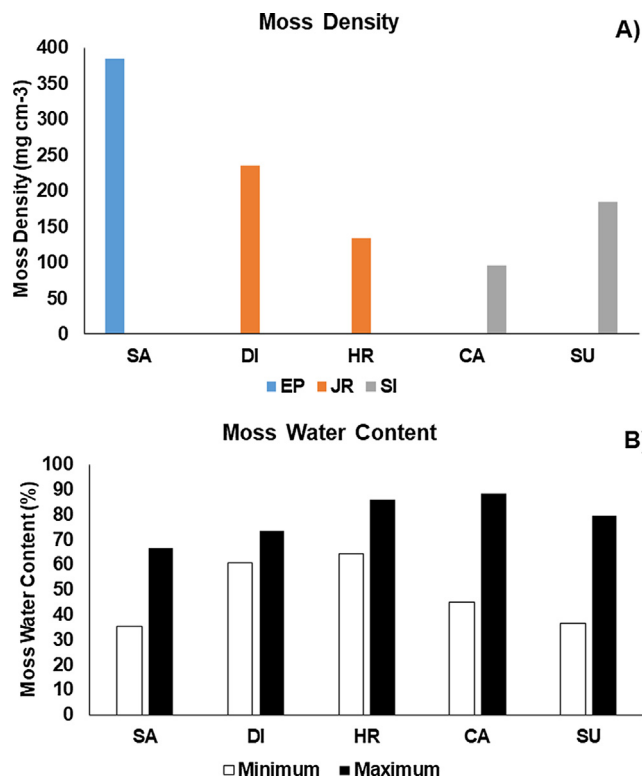


Fig. 7. (A) Density of the investigated moss species ( $\text{g cm}^{-3}$ ) compared with, (B) the water content (minimum, maximum) (%) of the investigated moss species. Legend: SA = *S. antarctici*; DI = *D. inclinatum*; HR = *H. revolutum*; CA = *C. aciphyllum*; SU = *S. uncinata*; EP = Edmonson Point; JR = James Ross Island; SI = Signy Island.

2 °C lower than the air. Moreover, the days in which  $\text{GST}^0 < \text{AT}$  were 65, while in the previous season (2015/16) the GST was lower only of 0.6 °C and the days with  $\text{GST}^0 < \text{AT}$  were 52.

Also at James Ross Island in 2016/2017 the winter GST of the bare ground resulted 1.5 °C lower than the air temperature: also in this case

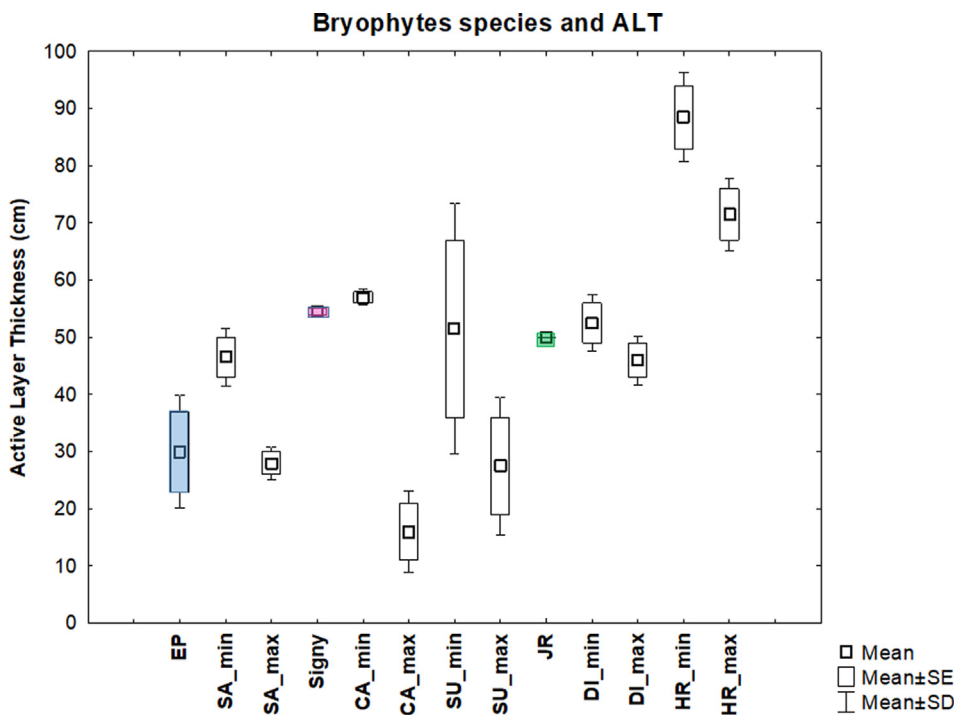


Fig. 8. Comparison of measured ALT (colored boxes: blue = Edmonson Point; pink = James Ross Island; green = Signy Island) and calculated ALT according to the Stefan equation for the different bryophytes species with minimum and maximum bryophyte water content. Legend: SA = *S. antarctici*; CA = *C. aciphyllum*; SU = *S. uncinata*; DI = *D. inclinatum*; HR = *H. revolutum*. (For interpretation of the references to colour in this figure legend, the reader is referred to the web version of this article.)

**Table 6**  
Relationship between mean daily ground temperature at bare ground sites (BG) and moss sites (M) with mean daily air temperature (AirT) and incoming radiation (IR).

| Site              |    | MAM  |      | JJA  |    | SON  |      | DJF  |       |
|-------------------|----|------|------|------|----|------|------|------|-------|
|                   |    | AirT | IR   | AirT | IR | AirT | GR   | AirT | IR    |
| Edmonson Point    | BG | 0.89 | 0.78 | 0.76 | -  | 0.95 | 0.92 | 0.78 | 0.90  |
|                   | M  | 0.77 | 0.81 | 0.17 | -  | 0.90 | 0.93 | 0.56 | 0.13  |
| James Ross Island | BG | 0.76 | 0.54 | 0.75 | -  | 0.78 | 0.54 | 0.76 | 0.63  |
|                   | M  | 0.73 | 0.55 | 0.76 | -  | 0.76 | 0.52 | 0.74 | 0.47  |
| Signy Island      | BG | 0.90 | 0.48 | 0.71 | -  | 0.83 | 0.20 | 0.63 | 0.09  |
|                   | M  | 0.67 | 0.54 | 0.22 | -  | 0.64 | 0.18 | 0.70 | -0.22 |

it is possible to see how the  $\text{GST}^0 < \text{AT}$  were almost the double of the previous season. This cooling effect was already described in Antarctica for Rothera area by Guglielmin et al. (2014b), comparing snow thickness measurements and GST. Although continuous data documenting snow conditions are not available for all three sites, snow thickness rarely exceeds 30 cm, and is generally thinner than 10 cm (e.g. as demonstrated by similar values of snow and  $n_f$  by Smith and Riseborough (2002) in the Arctic) or even less, allowing the net cooling of the ground surface.

5.3. Moss effect on GST and on active layer

Our data confirm the buffering effect of moss cover resulting in a GST cooling during summer (Fig. 4, Table 3), which was observed at all study sites in both years. This is in agreement with other studies in the Arctic and sub-Arctic, as well as in Antarctic locations (e.g., Gornall et al., 2007; Cannone and Guglielmin 2009; Blok et al., 2011; Turetsky et al., 2012; Almeida et al., 2014). The cooling effect of moss cover in summer was more pronounced in the southernmost location (Edmonson Point), where it decreased the mean soil temperature by 5.0–6.9 °C, while in the other two sites the cooling effect on GST was limited to 1.7–2.2 °C. Our data confirm the observations of Gornall et al. (2007) showing in the high Arctic that mosses had an immediate impact on soil temperature in terms of both average temperatures and amplitude of

fluctuations. However, our data contradict those of Soudzilovskaia et al. (2013) who reported that mosses reduced only soil temperature fluctuations, but not mean soil temperature. Our data confirm that even a thin moss cover (1 cm) is able to influence the GST on a seasonal level (Table 1).

We observed a similar cooling effect of moss cover during spring (Table 3), with the same patterns across study sites, although the intensity of cooling was reduced to ca. 1 °C at James Ross Island and Signy Island compared to the summer season. As highlighted in the results, unexpectedly, we show that the intensity of the moss buffering effect during summer (and also in spring) was not proportional to the moss layer thickness. A potential explanation of this evidence could be related to the minimum moss water retention, which is characterized by the lowest values for *S. antarctici* (occurring at Edmonson Point) (Fig. 7B). Indeed, it is known that the insulating capacity of mosses increases when they are dry (O'Donnell et al., 2009; Blok et al., 2011; Turetsky et al., 2012). The lowest water retention exhibited by *S. antarctici* could depend on its highest density (compared to the other moss species) (Fig. 7A) allowing to retain a lower amount of water compared to the other species. The wetter conditions normally recorded during the summer in maritime Antarctica than in continental Antarctica are further enhanced by occurrence of liquid precipitation, increasing the moisture content of both soils and mosses and decreasing the insulating capacity of the latter.

The buffering effect of moss cover includes also a warming of soil temperature during winter (e.g. Park et al., 2018), but we observed this pattern only at Edmonson Point and Signy Island, while at James Ross Island the moss soil was cooler than the bare ground both during winter as well as in autumn (Table 3). The winter warming in the moss sites at Edmonson Point and Signy Island could be also due to the snow cover that is slightly thicker where mosses occurred (data not shown). In the case of James Ross Island the results of  $n_f$  (Table 4) and correlation analysis (Table 6) suggest that the low effect of snow cover and the cooler GST recorded at the moss site could be related to an extremely thin snow cover, not enough to insulate the ground. Indeed, when short wave radiation is minimum, a thin snow cover (< 2 cm) can exceed the balance of the long wave radiation, as reported at Rothera in the western Antarctic Peninsula (e.g. Guglielmin et al., 2014b). The higher emissivity of snow cover than snow free surfaces (0.96–0.98 vs 0.91–0.92 according to Zhang, 2005) results in a surface cooling with respect to air temperature, as observed at James Ross Island. Therefore, the patterns of winter GST at James Ross Island likely are not influenced by the moss cover but, rather, by the thin snow cover causing its cooling.

The more pronounced warming effect detected at Edmonson Point than at Signy Island both in winter and autumn (Table 3), despite the thinner moss layer of the former, could be explained again by the different moss hydration characteristics (and density). A less dense and wet moss (such as *C. aciphyllum*) can freeze more easily than a dry and dense moss (such as *S. antarctici*), thus increasing its thermal conductivity (Burn and Smith, 1988) and decreasing its insulation effect (Porada et al., 2016, 2017; Park et al., 2018). Therefore, the higher water retention measured for the mosses at Signy Island (Fig. 7B) suggest a higher thermal conductivity in autumn and winter, resulting in a lower moss buffering effect than at Edmonson Point, despite the fivefold greater thickness of mosses at Signy Island.

One of the most important traits involved in heat transfer processes and, hence, potentially able to provide a physical explanation of the observed ALT differences, is the water retention capacity of mosses, because field moisture content may affect bryophyte thermal conductivity (Soudzilovskaia et al., 2013). Our data show that, when comparing the simulated ALT of moss sites with the ALT estimated *in situ*, the highest similarity was provided when the simulation was performed using the minimum water retention capacity of each moss species (Fig. 8). At all three sites we observed an ALT reduction in moss sites in comparison with bare ground, consistent with other reports

**Table 7**

Textural ground characteristics and mean water content: BG = barren ground plot; M = mosses plot; JRI = James Ross; ED = Edmonson Point; S = Signy Island.

| Site  | BG-JRI | BG-ED | BG-S | M-JRI | M-ED | M-S  |
|-------|--------|-------|------|-------|------|------|
| sand  | 70     | 95.8  | 92.5 | 61.6  | 80.5 | 97.9 |
| silt  | 21.2   | 4.2   | 6    | 23.5  | 17.6 | 2    |
| clay  | 8.1    | 0     | 1.5  | 13.8  | 1.9  | 0.1  |
| water | 20     | 16    | 11.3 | 50    | 27.6 | 27.1 |

from Arctic, sub-Arctic and Antarctic locations (Cannone et al., 2006; Guglielmin et al., 2008; Guglielmin and Cannone, 2012).

Differently from what reported by Fisher et al. (2016) and Park et al. (2018) we observed that at our sites the ALT decrease was not proportional to the moss thickness. The decoupling between the moss thickness and ALT reduction it is not only due to the moss thermal properties but also to the thermal properties of the soils below the mosses. Considering the grain size characteristics and the water content for the different soils reported in Table 7, it is possible to see that the grain size is approximately the same for the bare ground and the moss covered soils both at Signy Island and James Ross Island, although the water content is higher under the moss site especially at James Ross Island (50% vs 20%). At Edmonson Point the soil under the moss is richer in silt and in water than the coarser regolith of the bare ground.

Therefore, the water retention capacity and the amount of water occurring in the field apparently may play a more important role than canopy thickness and/or architecture in determining the amount of the buffering effect exerted by each moss species.

#### 5.4. Active layer thickness of bare grounds

Normally the ALT is related to the summer GST (e.g. Guglielmin, 2006), although the thermal properties of the ground (e.g. water/ice content; organic matter content, quartz content) can significantly affect the maximum thawing (e.g. Williams and Smith, 1989). However, our data show a clear decoupling between summer GST and ALT when comparing the different study sites. The minimum ALT of 36–40 cm was observed at Edmonson Point, where maximum summer GST was reached. In contrast, about 4 times deeper ALT was found on Signy Island where the GST was 2.4 to 4.1 °C lower. Considering Table 7, the grain size of the sediments at Edmonson Point and Signy are very similar and the water content too is not so different (< 5% of difference). James Ross Island is more different because the clay content is not irrelevant (8.1%), and both the silt and the water are higher than in the other sites. The slight differences of sediment characteristics between Edmonson Point and Signy can't explain the observed huge difference in ALT. However, it is likely that the much lower winter and annual ground temperatures at Edmonson Point require a greater amount of energy during the summer to achieve deeper ground thawing.

The variability in ALT at local scale can be strongly affected by the lithology (e.g. Hrbáček et al., 2017b). This is consistent with observations from separate locations close to two of the study areas, which showed that ALT could reach more than 100 cm on James Ross Island (Hrbáček et al., 2017a), and more than 75 cm in the Victoria Land region (e.g. Bockheim et al., 2007; Adlam et al., 2010; Guglielmin et al., 2014b). Similar observations have not been reported on Signy Island, where the only relevant study documenting large variability in ALT between two bare-ground sites inferred that this was related to different snow cover characteristics (Guglielmin et al., 2012).

Generally, the ALT values observed under bare ground conditions reached average values typical of large part of James Ross Island (e.g.; Hrbáček et al., 2017a, 2017b) and of Victoria Land region (e.g. Bockheim et al., 2007; Adlam et al., 2010; Guglielmin et al., 2014b). ALT at the bare ground site studied here on Signy Island was one of the highest values recorded across Antarctica when considering only bare

ground sites (e.g. Vieira et al., 2010; Bockheim et al., 2013; Hrbáček et al., 2019). The only significantly greater ALTs recorded in Antarctica have been in solid bedrock (e.g. Vieira et al., 2010; Guglielmin et al., 2011; Bockheim et al., 2013).

## 6. Conclusion

Among the three contrasting study locations between 74 and 60°S our data emphasize the role of incoming radiation, being the most important driver of summer GST of barren ground surfaces at the southernmost site, and explaining the apparent paradox that the highest summer GST occurred where the lowest summer air temperature was recorded. The cloudiness increase at the other two sites was mainly related to the global circulation (westerly winds) at Signy Island and, to a lesser extent, at James Ross Island, which strongly decreased the incoming radiation in summer. During the winter the main driver of the barren ground GST was air temperature, although at Edmonson Point and JRI some net cooling due to the thin snow cover was detected.

Our data confirm the importance of the buffering effect of the moss cover in Antarctic terrestrial ecosystems. Furthermore, the intensity of the effect of moss cover on GST and ALT mainly depends on the species-specific moss water retention capacity (and density) and therefore by their structure, but not its thickness. Indeed, a thin but dense and dry moss can insulate the ground more efficiently than a thick but less dense and wetter moss.

The data obtained emphasise that there is a decoupling between ALT and summer GST, with the highest GST recorded at the site with the thinnest ALT (Edmonson Point). At this site, despite a limited moss thickness the highest buffering effect was recorded probably related to the lowest water retention of this moss. This apparent paradox could be a result of the buffering effect of the moss, but also by the much higher energy required to increase the temperature where the lowest winter ground temperatures are reached (Edmonson Point).

## Declaration of Competing Interest

The authors declare that they have no known competing financial interests or personal relationships that could have appeared to influence the work reported in this paper.

## Acknowledgements

The work of FH and MK was supported by the Ministry of Education, Youth and Sports of the Czech Republic projects LM2015078 and Z.02.1.01/0.0/0.0/16\_013/0001708 and by Masaryk University project MUNI/A/1576/2018. FH acknowledge SCAR for the fellowship funding support. The research at Signy Island and Edmonson Point was funded by the Projects “PNRA 16\_0194” led by MG and “PNRA16\_00224” by NC. Work on Signy Island logistically supported by the British Antarctic Survey. PC is supported by NERC core funding to the BAS ‘Biodiversity, Evolution and Adaptation’ Team.

## Funding

For MG, NC and FM: the projects PNRA 16\_0194 and PNRA 16\_00224 of the Italian Ministry of Research; for PC the project “Biodiversity, Evolution and Adaptation of British Antarctic Survey, United Kingdom; for FH and MK the projects LM2015078 and Z.02.01/0.0/0.0/16\_013/0001708 of Ministry of Youth and Sports of the Czech Republic and the project MUNI/A/1576/2018 of Masaryk University, Brno.

## Appendix A. Supplementary material

Supplementary data to this article can be found online at <https://doi.org/10.1016/j.catena.2020.104562>.

## References

- Adlam, L.S., Balks, M.R., Seybold, C.A., Campbell, D.I., 2010. Temporal and spatial variation in active layer depth in the McMurdo Sound Region, Antarctica. *Antarct. Sci.* 22, 45–52.
- Almeida, I.C.C., Schaefer, C.E.G.R., Fernandes, R.B.A., Pereira, T.T.C., Nieuwendam, A., Pereira, A.B., 2014. Active layer thermal regime at different vegetation covers at Lions Rump, King George Island, Maritime Antarctica. *Geomorphology* 225, 36–46.
- Blok, D., Heijmans, M.M.P.D., Schaepman-Strub, G., van Ruijven, J., Parmentier, F.J.W., Maximov, T.C., Berendse, F., 2011. The Cooling capacity of mosses: controls on water and energy fluxes in a Siberian tundra site. *Ecosystems* 14, 1055–1065.
- Bockheim, J., Campbell, I.B., McLeod, M., 2007. Permafrost distribution and active-layer depths in the McMurdo dry valleys. *Antarctica Permafrost Periglac.* 18, 217–227.
- Bockheim, J., Vieira, G., Ramos, M., López-Martínez, J., Serrano, E., Guglielmin, M., Wilhelm, K., Nieuwendam, A., 2013. Climate warming and permafrost dynamics in the Antarctic Peninsula region. *Glob. Planet. Chang.* 100, 215–223.
- Bromwich, D.H., Nicolas, J.P., Monaghan, A.J., 2011. An assessment of precipitation changes over Antarctica and the Southern Ocean since 1989 in contemporary global reanalyses. *J. Climate* 24, 4189–4209.
- Burn, C.R., Smith, C.A.S., 1988. Observations of the “thermal offset” in near-surface mean annual ground temperatures at several sites near Mayo, Yukon Territory, Canada. *Arctic* 41, 99–104.
- Cannone, N., 2006. A network for monitoring terrestrial ecosystems along a latitudinal gradient in continental Antarctica. *Antarct. Sci.* 18, 549–560.
- Cannone, N., Ellis Evans, J.C., Strachan, R., Guglielmin, M., 2006. Interactions between climate, vegetation and active layer in Maritime Antarctica. *Antarct. Sci.* 18, 323–333.
- Cannone, N., Dalle Fratte, M., Convey, P., Worland, M.R., Guglielmin, M., 2017. Ecology of moss banks on Signy Island (maritime Antarctic). *Bot. J. Linn. Soc.* 184, 518–533.
- Cannone, N., Seppelt, R.D., 2008. A preliminary floristic classification of Northern and Southern Victoria Land vegetation (continental Antarctica). *Antarct. Sci.* 20, 553–562.
- Cannone, N., Guglielmin, M., 2009. Influence of vegetation on the ground thermal regime in continental Antarctica. *Geoderma* 15, 215–223.
- Convey, P., 2017. Antarctic Biodiversity. Reference Module in Life Sciences. Elsevier. Doi: 10.1016/B978-0-12-809633-8.02182-8.
- De Pablo, M.A., Ramos, M., Molina, A., 2017. Snow cover evolution, on 2009–2014, at the Limnopolar Lake CALM-S site on Byers Peninsula, Livingston Island, Antarctica. *Catena* 149 (2), 538–547.
- Elumeeva, T.G., Soudzilovskaia, N.A., During, H.J., Cornelissen, J.H.C., 2011. The importance of colony structure versus shoot morphology for the water balance of 22 subarctic bryophyte species. *J. Veg. Sci.* 22, 152–164.
- Ferreira, A., Vieira, G., Ramos, M., Nieuwendam, A., 2017. Ground temperature and permafrost distribution in Hurd Peninsula (Livingston Island, Maritime Antarctic): an assessment using freezing indexes and TTOP modelling. *Catena* 149 (2), 560–571.
- Fisher, J.P., Estop-Aragoñes, C., Thierry, A., Charman, D.J., Wolf, S.A., Hartley, I.P., Murton, J.B., Williams, M., Phoenix, G.K., 2016. The influence of vegetation and soil characteristics on active-layer thickness of permafrost soils in boreal forest. *Global Change Biol.* 22, 3127–3140.
- Gadek, B., Leszkiewicz, J., 2010. Influence of snow cover on ground surface temperature in the zone of sporadic permafrost, Tatras Mountains, Poland and Slovakia. *Cold Regions Sci. Technol.* 60, 205–211.
- Gornall, J.L., Jonsdottir, I.S., Woodin, S.J., Van der Wal, R., 2007. Arctic mosses govern below-ground environment and ecosystem processes. *Oecologia* 153, 931–941.
- Gubler, S., Fiddes, J., Keller, M., Gruber, S., 2011. Scale-dependent measurement and analysis of ground surface temperature variability in alpine terrain. *The Cryosphere* 5 (431–443), 2011. <https://doi.org/10.5194/tc-5-431-2011>.
- Guglielmin, M., 2006. Ground surface temperature (GST), active layer, and permafrost monitoring in continental Antarctica. *Permafrost Periglac.* 17, 133–143.
- Guglielmin, M., Dramis, F., 1997. Permafrost as a climatic indicator in northern Victoria Land, Antarctica. *Ann. Glaciol* 29, 131–135.
- Guglielmin, M., Ellis Evans, J.C., Cannone, N., 2008. Ground thermal regime under different vegetation conditions in permafrost areas and sensitivity to climate change. A case study at Signy Island (maritime Antarctica). *Geoderma* 144, 73–85.
- Guglielmin, M., Balks, M., Adlam, L.S., Baio, F., 2011. Permafrost thermal regime from two 30m deep boreholes in Southern Victoria Land, Antarctica. *Permafrost Periglac.* 22, 129–139.
- Guglielmin, M., Cannone, N., 2012. A permafrost warming in a cooling Antarctica? *Climatic Change* 111, 177.
- Guglielmin, M., Worland, M.R., Cannone, N., 2012. Spatial and temporal variability of ground surface temperature and active layer thickness at the margin of maritime Antarctica, Signy Island. *Geomorphology* 155–156, 20–33.
- Guglielmin, M., Dalle Fratte, M., Cannone, N., 2014a. Permafrost warming and vegetation changes in continental Antarctica. *Environ. Res. Lett.* 9. <https://doi.org/10.1088/1748-9326/9/4/045001>.
- Guglielmin, M., Worland, M.R., Baio, F., Convey, P., 2014b. Permafrost and snow monitoring at Rothera Point (Adelaide Island, Maritime Antarctica): Implications for rock weathering in cryotic conditions. *Geomorphology* 225, 47–56.
- Hrbáček, F., Láška, K., Engel, Z., 2016. Effect of snow cover on the active-layer thermal regime – a case study from James Ross Island, Antarctic Peninsula. *Permafrost Periglac.* 27, 307–315.
- Hrbáček, F., Kňazková, M., Nývlt, D., Láška, K., Mueller, C.W., Ondruch, J., 2017a. Active layer monitoring at CALM-S site near J.G.Mendel Station, James Ross Island, Eastern Antarctic Peninsula. *Sci. Tot. Environ.* 601–602, 987–997.
- Hrbáček, F., Nývlt, D., Láška, K., 2017b. Active layer thermal dynamics at two lithologically different sites on James Ross Island, Eastern Antarctic Peninsula. *Catena* 149,

- 592–602.
- Hrbáček, F., Vieira, G., Oliva, M., Balks, M., Guglielmin, M., de Pablo, M.A., Molina, A., Ramos, M., Goyanes, G., Meiklejohn, I., Abramov, A., Demidov, N., Fedorov-Davydov, D., Lupachev, A., Rivkina, E., Láska, K., Kňazková, M., Nývlt, D., Raffi, R., Strelin, J., Sone, T., Fukui, K., Dolgikh, A., Zazovskaya, E., Mergelov, N., Osokin, N., Miamin, V., 2019. Active layer monitoring in Antarctica (CALM-S): results from 2006–2015 and new perspectives. *Polar Geogr.* <https://doi.org/10.1080/1088937X.2017.1420105>.
- King, J.C., Turner, J., 1997. *Antarctic Meteorology and Climatology*. Cambridge Atmospheric and Space Science Series. University Press, Cambridge, pp. 409.
- Lacelle, D., Lapalme, C., Davila, A.F., Pollard, W., Marinova, M., Heldmann, J., McKay, C.P., 2016. Solar radiation and air and ground temperature relations in the cold and hyper-arid Quartermain mountains, McMurdo dry valleys of Antarctica. *Permafrost Periglac.* 27, 163–176.
- Matthews, D.H., Maling, D.H., 1967. The geology of the South Orkney Islands: I Signy Island, Falkland Islands. *Dependencies Survey Sci. Rep.* 25, 32 pp.
- Michel, R.F.M., Schaefer, C.E.G.R., Poelking, E.L., Simas, F.N.B., Fernandes Filho, E.L., Bockheim, J.G., 2012. Active layer temperature in two Cryosols from King George Island, Maritime Antarctica. *Geomorphology* 155–156, 12–19.
- Mlčoch, B., Nývlt, D., Mixa, P. (Eds.), 2018. James Ross Island. Geological map of the northern part. 1:25 000. Unpublished manuscript, Czech Geological Survey, Praha.
- Nelson, F.E., Shiklomanov, N.I., Mueller, G.R., Hinkel, K.M., Walker, D.A., Bockheim, J.G., 1997. Estimating active layer thickness over a large region: Kuparuk River Basin, Alaska, USA. *Arctic Alpine Res.* 29 (4), 367–378.
- Obryk, M.K., Fountain, A.G., Doran, P.T., Lyons, W.B., Eastman, R., et al., 2018. Drivers of solar radiation variability in the McMurdo Dry Valleys, Antarctica. *Sci. Rep.* 8, 5002. <https://doi.org/10.1038/s41598-018-23390-7>.
- Ochyra, R., Smith, R.L.L., Bernarek-Ochyra, A., 2008. *The Illustrated Moss Flora of Antarctica*. Cambridge University Press, Cambridge.
- O'Donnell, J.A., Romanovsky, V.E., Harden, J.W., McGuire, A.D., 2009. The effect of moisture content on the thermal conductivity of moss and organic soil horizons from black spruce ecosystems in interior Alaska. *Soil Sci.* 174, 646–651.
- Oliva, M., Hrbáček, F., Ruiz-Fernández, J., de Pablo, M.A., Vieira, G., Ramos, M., Antoniades, D., 2017. Active layer dynamics in three topographically distinct lake catchments in Byers Peninsula (Livingston Island, Antarctica). *Catena* 149 (2), 548–559.
- Park, H., Launiainen, S., Konstantinov, P.Y., Iijima, Y., Fedorov, A.N., 2018. Modeling the effect of moss cover on soil temperature and carbon fluxes at a tundra site in Northeastern Siberia. *J. Geophys. Res.-Bioge.* 123, 3028–3044.
- Porada, P., Ekici, A., Beer, C., 2016. Effects of bryophyte and lichen cover on permafrost soil temperature at large scale. *Cryosphere* 10 (5), 2291–2315.
- Porada, P., Poschl, U., Kleidon, A., Beer, C., Weber, B., 2017. Estimating global nitrous oxide emissions by lichens and bryophytes with a process-based productivity model. *Biogeosciences* 14, 1593–1602.
- Romanovsky, V., Burgess, M., Smith, S., Yoshikawa, K., Brown, J., 2002. Permafrost temperature records: Indicators of climate change. *Eos Trans. Amer. Geophys. Union* 50, 589–594.
- Schmid, M.O., Gubler, S., Fiddes, J., Gruber, S., 2012. Inferring snowpack ripening and melt-out from distributed measurements of near-surface ground temperatures. *The Cryosphere* 6, 1127–1139. <https://doi.org/10.5194/tc-6-1127-2012>.
- Soudzilovskaia, N.A., van Bodegom, P.M., Cornelissen, J.H.C., 2013. Dominant bryophyte control over high-latitude soil temperature fluctuations predicted by heat transfer traits, field moisture regime and laws of thermal insulation. *Funct. Ecol.* 2, 1442–1454.
- Terauds, A., Chown, S.L., Morgan, F.J., Peat, H.J., Watts, D.J., Keys, H., Convey, P., Bergstrom, D.M., 2012. Conservation biogeography of the Antarctic. *Div. Distrib.* 18, 726–741.
- Terauds, A., Lee, J.R., 2016. Antarctic biogeography revisited: updating the Antarctic Conservation Biogeographic Regions. *Div. Distrib.* 22, 836–840.
- Thomas, J.L., Waugh, D.W., Gnanadesikan, A., 2015. Southern Hemisphere extratropical circulation: recent trends and natural variability. *Geophys. Res. Lett.* 42, 5508–5515.
- Turetsky, M.R., Bond-Lamberty, B., Euskirchen, E., Talbot, J., Frolking, S., McGuire, A.D., Tuittila, E.S., 2012. The resilience and functional role of moss in boreal and arctic ecosystems. *New Phytol.* 196, 49–67.
- Turner, J., Bindschadler, R.A., Convey, P., di Prisco, G., Fahrback, E., Gutt, J., Hodgson, D.A., Mayewski, P.A., Summerhayes, C.P. (Eds.), 2009. *Antarctic climate change and the environment*. Scientific Committee on Antarctic Research, Cambridge.
- Smith, M.W., Risborough, D., 2002. Climate and the limits of permafrost: a zonal analysis. *Permafrost Periglac.* 13, 1–15.
- Van Loon, H., 1967. The half-yearly oscillations in middle and high southern latitudes and the coreless winter. *J. Atmos. Sci.* 24, 472–486.
- Van Lipzig, N.P.M., King, J.C., Lachlan-Cope, T.A., van der Broeke, M.R., 2004. Precipitation, sublimation and snow drift in the Antarctic Peninsula region from a regional atmospheric model. *J. Geophys. Res.* 109, D24106.
- Vieira, G., Bockheim, J., Guglielmin, M., Balks, M., Abramov, A.A., Boelhouwers, J., Cannone, N., Ganzert, L., Gilichinsky, D., Goryachkin, S., López-Martínez, J., Meiklejohn, I., Raffi, R., Ramos, M., Schaefer, C., Serrano, E., Simas, F., Sletten, R., Wagner, D., 2010. Thermal state of permafrost and active-layer monitoring in the Antarctic: advances during the International Polar Year 2007–2008. *Permafrost Periglac.* 21, 182–197.
- Williams, P.J., Smith, M.W., 1989. *The Frozen Earth. Fundamentals of Geocryology*. Cambridge University Press, Cambridge, pp. 306.
- Wilhelm, K.R., Bockheim, J.G., 2017. Climatic controls on active layer dynamics: Amsler Island, Antarctica. *Antarctic Sci.* 29 (2), 173–182.
- Zhang, T., 2005. Influence of the seasonal snow cover on the ground thermal regime: an overview. *Rev. Geophys.* 43. <https://doi.org/10.1029/2004RG000157>.



# The evolution of a near-surface ground thermal regime and modeled active-layer thickness on James Ross Island, Eastern Antarctic Peninsula, in 2006–2016

Filip Hrbáček<sup>1</sup> | Tomáš Uxa<sup>2,3</sup>

<sup>1</sup>Department of Geography, Faculty of Science, Masaryk University, Brno, Czech Republic

<sup>2</sup>Department of Geothermics, Institute of Geophysics, Czech Academy of Sciences, Prague, Czech Republic

<sup>3</sup>Department of Physical Geography and Geoecology, Faculty of Science, Charles University, Prague, Czech Republic

## Correspondence

Filip Hrbáček, Department of Geography, Faculty of Science, Masaryk University, Brno, Czech Republic.  
Email: hrbacekfilip@gmail.com

## Funding information

Ministry of Education, Youth and Sports of the Czech Republic, Grant/Award Numbers: LM2015078, LM2015079, Z.02.1.01/0.0/0.0/16\_013/0001708

## Abstract

Thermal regime and thickness of the active layer respond rapidly to climate variations, and thus they are important measures of cryosphere changes in polar environments. We monitored air temperature and ground temperature at a depth of 5 cm and modeled active-layer thickness using the Stefan and Kudryavtsev models at the Abernethy Flats site, James Ross Island, Eastern Antarctic Peninsula, in the period March 2006 to February 2016. The decadal average of air and ground temperature was  $-7.3$  and  $-6.1^{\circ}\text{C}$ , respectively, and the average modeled active-layer thickness reached 60 cm. Mean annual air temperature increased by  $0.10^{\circ}\text{C y}^{-1}$  over the study period, while mean annual ground temperature showed the opposite tendency of  $-0.05^{\circ}\text{C y}^{-1}$ . The cooling took place mainly in summer and caused thawing season shortening and active-layer thinning of  $1.6\text{ cm y}^{-1}$ . However, these trends need to be taken carefully because all were non-significant at  $p < 0.05$ . The Stefan and Kudryavtsev models reproduced the active-layer thickness with mean absolute errors of 2.6 cm (5.0%) and 3.4 cm (5.9%), respectively, which is better than in most previous studies, making them promising tools for active-layer modeling over Antarctica.

## KEYWORDS

climate change, ground physical properties, ground temperature, modeling, permafrost, validation

## 1 | INTRODUCTION

The active layer is the top layer of the ground underlain by permafrost, which thaws in summer and freezes again in autumn. It reacts sensitively to the variability of climate parameters such as air temperature, global radiation or snow cover, and therefore it represents one of the key parameters of the cryosphere, which indicate climate change in polar regions (e.g. <sup>1-3</sup>). Unlike the Arctic, where permafrost areas occupy more than 25 million  $\text{km}^2$ , these environments are very rare in Antarctica as they cover only about 32 000  $\text{km}^2$ , representing around 0.2% of the continent.<sup>4,5</sup> The active layer has been most intensively investigated in Victoria Land, where research started as early as

the 1960s,<sup>6</sup> and recently in the Antarctic Peninsula (AP) region.<sup>5,7</sup> The AP is the warmest area in Antarctica and it has been considered to be among the most rapidly warming regions on Earth in the second half of the 20th century.<sup>8</sup> However, recent studies have shown that summer air temperature has been decreasing since around 2000,<sup>9</sup> which has impacted some cryospheric components including the thermal regime and thickness of the active layer.<sup>10</sup>

Nonetheless, temporal analyses of the active layer state in the AP region remain limited (e.g. <sup>5,11,12</sup>) as the majority of monitoring sites were established after the International Polar Year (IPY) 2007–2009.<sup>13</sup> Moreover, most observations are made through manual probing at the Circumpolar Active Layer Monitoring – South sites or in shallow boreholes (< 2 m) that frequently do not reach below the permafrost table<sup>5,7,13</sup> and, as such, they might be unrepresentative of the

Filip Hrbáček and Tomáš Uxa contributed equally to this paper.

full active-layer thickness (ALT). In the latter cases, the ALT has been mostly established as the depth of the 0°C isotherm by extrapolating the temperature gradient determined by continuous data-logger tracking of maximum annual ground temperatures (e.g. <sup>11,14,15</sup>) or by one-at-a-time probing using portable thermometers.<sup>2,16</sup> In particular, the former approach has been widely used across the AP region, with only slight modifications in the number and depth of temperature sensors and curve-fitting methods.<sup>17–21</sup> However, it may deviate substantially at places where the distance between the deepest temperature sensor and the permafrost table is large because the temperature gradient decreases non-linearly with depth, and thus it can be very small, (e.g. <sup>18,20,21</sup>) requiring highly accurate measurements.

Valuable insights into the dynamics of the thermal regime and thickness of the active layer can provide diverse thermal modeling techniques (e.g. <sup>22,23</sup>). Beside complex numerical models that account for many of the processes involved in surface and subsurface energy exchange and are capable of capturing the transient evolution of the active layer and permafrost conditions, (e.g. <sup>24–26</sup>) there also exist so-called equilibrium models which can define simple climate–permafrost relationships on an annual basis and evaluate such parameters as permafrost presence or absence, mean annual ground temperature or ALT.<sup>22</sup> Of these models, the Stefan<sup>27</sup> and Kudryavtsev<sup>28</sup> equations have been most widely used to calculate the ALT.<sup>22</sup> Simplicity and low requirements for input parameters have made these analytical solutions popular, particularly in modeling ALT over larger spatial scales or in situations where insufficient data were available to drive more sophisticated numerical models.<sup>22,29</sup> Despite their simplicity

and several simplifying assumptions, which may be restricting in specific settings (e.g. <sup>30,31</sup>), these models have been extensively validated to provide thawing or freezing depth estimates with a reasonable degree of accuracy (e.g. <sup>1,30,32–37</sup>). Nonetheless, they have been used inexplicably rarely in Antarctica (e.g. <sup>38,39</sup>) compared to their long-term and widespread use in polar and alpine areas of the northern hemisphere.

In this study, we describe a 10-year period (March 2006 to February 2016) of air and ground surface temperature monitoring at the Abernethy Flats site, James Ross Island (JRI), Eastern AP, and we apply two equilibrium thermal models, the Stefan and Kudryavtsev equations, to assess the interannual variability of ALT. Our aims in bridging the gaps in active layer and permafrost research in Antarctica are twofold. First, we analyse the behavior of air and ground surface temperature and ALT over one decade (including the pre-IPY 2007–2009 period), which is unique within the region. Second, we use simple modeling tools to predict the ALT, which have been used only sporadically in this area before now. We further compare our results with observations from other parts of Antarctica and general climate patterns.

## 2 | REGIONAL SETTING

JRI is ~2,600 km<sup>2</sup> in area and is located on the northeastern coast of the AP (Figure 1). Glaciers cover about 75% of the island, but only a few occur in its northern part, the Ulu Peninsula, where the study area

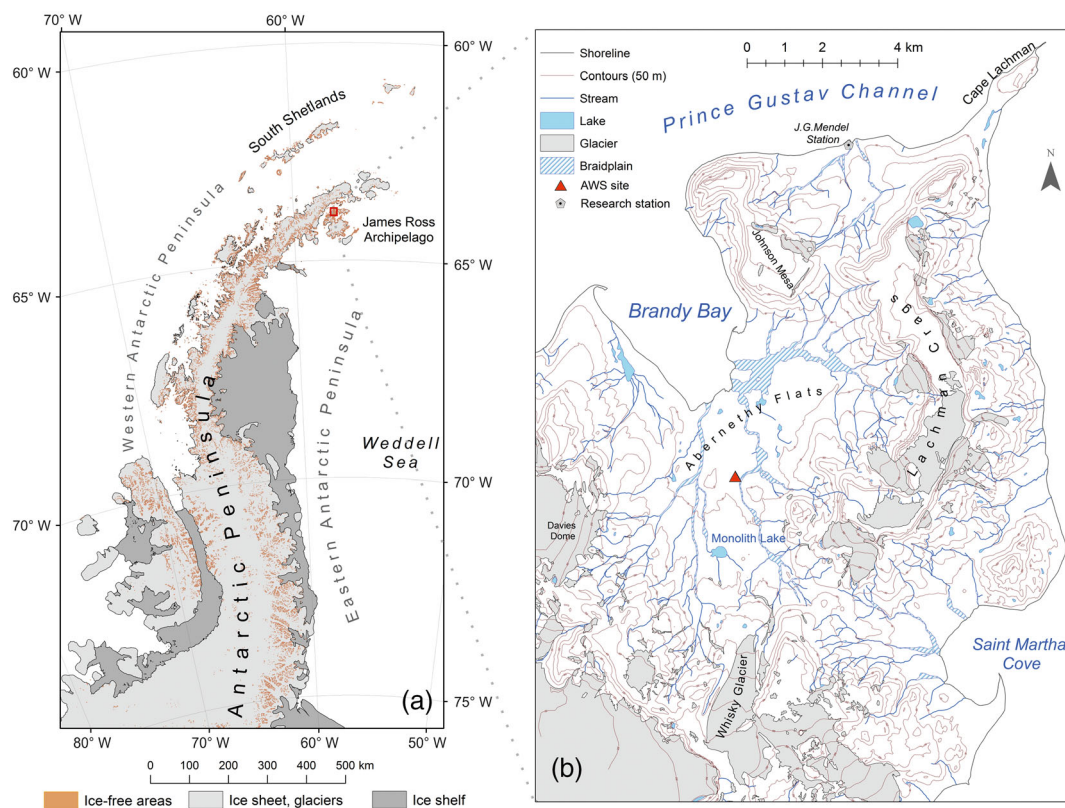


**FIGURE 1** Regional setting (a) and location of the study site (b) [Colour figure can be viewed at [wileyonlinelibrary.com](http://wileyonlinelibrary.com)]

is located.<sup>40</sup> Deglaciation of the Ulu Peninsula started  $12.9 \pm 1.2$  ka<sup>41</sup> and resulted in exposure of more than 300 km<sup>2</sup> of land that represents one of the largest glacier-free areas within the AP region.<sup>42</sup> The geology of the Ulu Peninsula consists mostly of Neogene volcanic rocks, which built volcanic mesas, and Cretaceous sedimentary rocks in the lowlands, partially covered by Quaternary sediments.<sup>43</sup>

The climate of the Ulu Peninsula has a semi-arid polar-continental character,<sup>44</sup> with a mean annual air temperature (MAAT) around  $-7.0^\circ\text{C}$  at sea level near the Johann Gregor Mendel Station<sup>5</sup> and estimated annual precipitation as low as 300–500 mm of water equivalent<sup>45</sup> because of a rain-shadow effect caused by the mountain ranges of the Northern AP.<sup>44</sup> Precipitation occurs largely as snow, but high wind speeds cause intense snow drifting and very irregular, topography-controlled snow deposition.<sup>46,47</sup>

The glacier-free surfaces are underlain by continuous permafrost,<sup>7</sup> the thickness of which reaches from around 3.4 m on coastal marine terraces to more than 67 m in lower-lying inland areas.<sup>48,49</sup> ALT depends strongly on local lithology, and usually ranges between approximately 50 and 145 cm.<sup>5,42,49,50</sup> Vegetation cover is sparse and is mostly concentrated in moist and nutrient-rich areas.<sup>46</sup>

### 3 | METHODS

#### 3.1 | Measurement setting and data processing

The study site is located in the Abernethy Flats area ( $63^\circ52'53''\text{S}$ ,  $57^\circ56'5''\text{W}$ ; 41 m a.s.l.), which is a flat lowland of the Ulu Peninsula with a slope of up to  $5^\circ$  (Figures 1 and 2). It is built of fine-grained calcareous sandstones and siltstones of the Alpha Member, Santa Marta Formation,<sup>43,51</sup> partially covered by Holocene glacial sediments,<sup>40,43</sup> and it is completely vegetation-free (Figure 2).

Air temperature and ground temperature were monitored from March 2006 to February 2016. Air temperature was measured using an EMS33 sensor (EMS Brno) equipped with a Pt100/A resistance temperature detector (accuracy of  $\pm 0.15^\circ\text{C}$  at  $0^\circ\text{C}$ ) placed in a solar radiation shield 2 m above the ground surface. Ground temperature was measured with A-class Pt100/8 resistance temperature detectors (EMS Brno; accuracy of  $\pm 0.15^\circ\text{C}$  at  $0^\circ\text{C}$ ) placed directly into the ground at depths of 5, 10, 20, 30, 40 and 50 cm, and from February 2012 also at 75 cm. All the detectors were connected to an EdgeBox V12 data logger (EMS Brno) set to measure and record the temperature every 30 min.

Daily, monthly, seasonal and annual means of air temperature and ground temperature at a depth of 5 cm were calculated from the half-hour temperature data. A period from March 1 to February 28 or 29 of the following year was set to calculate the annual means in order to cover a 12-month period from the active-layer freezeback to the maximum thaw depth of the next year. Missing air and ground temperature data due to data logger malfunction in the period from September 17, 2011 to February 6, 2012 were complemented in a monthly or seasonal resolution using multiple regression based on data from two equally instrumented stations located at a distance of

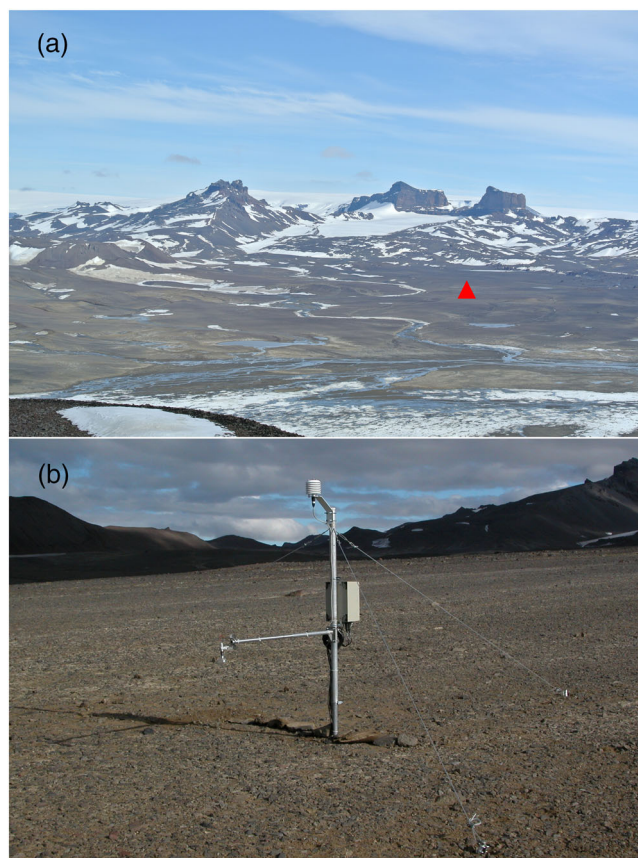


**FIGURE 2** The Abernethy flats area (a) and a detailed photo of the study site (b). The red triangle indicates the position of the automatic weather station [Colour figure can be viewed at [wileyonlinelibrary.com](http://wileyonlinelibrary.com)]

5 and 7 km that have similar topography and bare surface, which ensured high accuracy of the regression models ( $R^2 > 0.9$  in all cases). The temporal trends of selected characteristics were assessed using the non-parametric Mann–Kendall trend test<sup>52,53</sup> and Sen's slope estimator.<sup>54</sup> Relations between ALT (section 3.2) and selected air and ground temperature attributes were examined using the Pearson correlation coefficient. All statistics were tested at  $p < 0.05$ .

Thawing and freezing seasons were defined based on the continuous persistence of positive and negative mean daily temperatures, respectively, at a depth of 5 cm. For air temperature, the seasons were set to be equal to those at a depth of 5 cm. Subsequently, thawing and freezing degree-days for air ( $TDD_a$  and  $FDD_a$ ) and ground at a depth of 5 cm ( $TDD_5$  and  $FDD_5$ ) were calculated as sums of all positive and negative mean daily temperatures ( $^\circ\text{C}$  days) during the thawing and freezing seasons, respectively. The degree-days were further used to calculate the dimensionless thawing ( $n_t$ ) and freezing ( $n_f$ )  $n$ -factors, which summarize the energy balance between air and ground surface at the end of the thawing and freezing seasons, respectively:<sup>55</sup>

$$n_t = \frac{TDD_5}{TDD_a} = \frac{\sum_{i=1}^{L_t} T_5(i) [T_5 > 0^\circ\text{C}]}{\sum_{i=1}^{L_a} T_a(i) [T_a > 0^\circ\text{C}]} \quad (1)$$

$$n_f = \frac{FDD_5}{FDD_a} = \frac{\sum_{i=1}^{L_f} T_5(i) [T_5 < 0^\circ\text{C}]}{\sum_{i=1}^{L_f} T_a(i) [T_a < 0^\circ\text{C}]} \quad (2)$$

where  $T_a$  and  $T_5$  are the mean daily air temperature and ground temperature at a depth of 5 cm, respectively, during the thawing or freezing season, and  $L_t$  and  $L_f$  refer to the number of days in the thawing and freezing seasons, respectively.

Data from deeper parts of the profile were used only to determine the temperature-based *ALT* (hereafter referred to as observed *ALT*), which was used to validate the outputs of *ALT* modeling (section 3.2). It was defined as the maximum depth of the  $0^\circ\text{C}$  isotherm during the particular thawing season calculated by linear interpolation between the maximum temperature of the deepest sensor with at least one measurement  $>0^\circ\text{C}$  and the maximum temperature of the shallowest sensor with all measurements  $\leq 0^\circ\text{C}$ . The observed *ALT* was available from a very cold season 2009/10 and from the period 2012/13 to 2015/16 when the measurement profile already reached a depth of 75 cm.

### 3.2 | Active-layer thickness modeling

The *ALT* over the period March 2006 to February 2016 was modeled via the Stefan<sup>27</sup> and Kudryavtsev<sup>28</sup> models. Both models were forced with ground temperature data from a depth of 5 cm and two sets of time-invariant ground physical properties based on ground samples from depths of 10 and 30 cm that were considered homogeneous across the entire ground profile for each model run. The outputs of the Stefan model are therefore hereafter called scenarios  $S_{10}$  and  $S_{30}$ , while the products of the Kudryavtsev model are termed scenarios  $K_{10}$  and  $K_{30}$ .

#### 3.2.1 | Stefan model

The Stefan model<sup>27</sup> was applied on  $TDD_5$  to predict the *ALT* (m) as follows:

$$ALT = z_5 + \lambda \sqrt{\frac{2k_t TDD_5 SF}{Q_L}} \quad (3)$$

where  $z_5$  (m) is the depth of the ground temperature measurement,  $k_t$  is the thawed thermal conductivity ( $\text{W m}^{-1} \text{K}^{-1}$ ),  $SF$  is the scaling factor of 86,400 seconds per day, and  $Q_L$  is the volumetric latent heat of fusion of water-ice ( $\text{J m}^{-3}$ ) expressed as:

$$Q_L = L\rho\omega \quad (4)$$

where  $L$  is the specific latent heat of fusion of water-ice ( $334,000 \text{ J kg}^{-1}$ ),  $\rho$  is the dry bulk density ( $\text{kg m}^{-3}$ ), and  $\omega$  is the gravimetric water content (dimensionless). Because the Stefan model tends to overestimate the *ALT* due to errors arising from disregarding sensible heat or due to low ground temperatures at the onset of thawing,<sup>30,56</sup> we adopted a polynomial correction factor for ground thawing with sub-zero initial temperature ( $\lambda$ ) in Equation (3) in order to improve its performance:<sup>56</sup>

$$\lambda = \left[ 1 + 0.147S_{te} \left( \kappa \frac{T_{init}}{MGTS_5} \right)^2 + 0.535\sqrt{S_{te}} \kappa \frac{T_{init}}{MGTS_5} \right] \times (1 - 0.16S_{te} + 0.038S_{te}^2) \quad (5)$$

with

$$S_{te} = \frac{C_t MGTS_5}{Q_L} \quad (6)$$

$$\kappa = \sqrt{\frac{k_f C_f}{k_t C_t}} \quad (7)$$

where  $S_{te}$  is the dimensionless Stefan number, which is proportional to the ratio of sensible heat to latent heat absorbed during thawing,<sup>57,58</sup>  $\kappa$  is a dimensionless parameter accounting for different thermal properties of the thawed and frozen zones within the ground profile,<sup>56</sup>  $T_{init}$  is the initial temperature corresponding to the mean ground temperature across the seasonally thawing layer at the onset of thawing ( $^\circ\text{C}$ ),  $MGTS_5$  is the mean ground temperature of the thawing season at depth  $z_5$  ( $^\circ\text{C}$ ),  $k_f$  is the frozen thermal conductivity ( $\text{W m}^{-1} \text{K}^{-1}$ ), and  $C_f$  and  $C_t$  are the frozen and thawed volumetric heat capacity, respectively ( $\text{J m}^{-3} \text{K}^{-1}$ ).

We calculated the sub-zero initial temperature by logarithmic fitting of the mean daily ground temperature profile one day before the start of thawing and then integrating this function across the depth range defined by  $z_5$  and initial *ALT* estimate ( $ALT_{init}$ ) based on the uncorrected Stefan model:

$$T_{init} = \frac{1}{ALT_{init} - z_5} \int_{z_5}^{ALT_{init}} a \ln z + b dz \quad (8)$$

where  $a$  and  $b$  are empirical constants. The initial temperature was determined for seasons 2012/13 to 2015/16, and the resulting average value of  $-3^\circ\text{C}$  was subsequently used in the final *ALT* estimates in each thawing season.

#### 3.2.2 | Kudryavtsev model

The Kudryavtsev model<sup>28</sup> was applied to ground temperature data at a depth of 5 cm to predict the *ALT* analogously to the Stefan model:

$$ALT = z_5 + \frac{2(A_5 - |T_{TOP}|) \sqrt{\frac{k_t C_t P_5}{\pi}} + \frac{(2A_{TOP} C_t Z_c + Q_L (ALT - z_5)) Q_L \sqrt{\frac{k_t P_5}{\pi C_t}}}{2A_{TOP} C_t Z_c + Q_L (ALT - z_5) + \sqrt{\frac{k_t P_5}{\pi C_t}} (2A_{TOP} C_t + Q_L)}}{2A_{TOP} C_t + Q_L} \quad (9)$$

with

$$A_{TOP} = \frac{A_5 - |T_{TOP}|}{A_5 + \frac{Q_L}{2C_t}} - \frac{Q_L}{2C_t} \quad (10)$$

$$Z_c = \frac{2(A_5 - |T_{TOP}|) \sqrt{\frac{k_t C_t P_5}{\pi}}}{2A_{TOP} C_t + Q_L} \quad (11)$$

Equation (9) can, however, be solved only numerically, and thus we used the modified Kudryavtsev model,<sup>30</sup> which is more convenient as it allows an analytical solution:

$$ALT = z_5 + ALT^* \sqrt{\frac{k_t P_5}{\pi C_t}} \quad (12)$$

with

$$ALT^* = B + \sqrt{B^2 + D} \quad (13)$$

$$B = \delta + \frac{\delta}{2\gamma} - \frac{\gamma}{2\delta} - \frac{\gamma}{2} \quad (14)$$

$$D = \delta + \delta\gamma + \gamma - \delta^2 - \frac{\delta^2}{\gamma} \quad (15)$$

$$\gamma = \alpha - \beta \quad (16)$$

$$\delta = \ln \frac{\alpha + 1}{\beta + 1} \quad (17)$$

$$\alpha = \frac{2C_t A_5}{Q_L} \quad (18)$$

$$\beta = \frac{2C_t |T_{TOP}|}{Q_L} \quad (19)$$

where  $P_5$  is the period at depth  $z_5$  calculated as the sum of the lengths of the thawing season for which the ALT is modeled and the preceding freezing season (s),  $A_5$  is the physical amplitude (i.e. half range) of the annual ground temperature oscillations at depth  $z_5$  (°C) and  $T_{TOP}$  is the mean annual ground temperature at the top of the permafrost (°C).

Previous studies have expressed the annual amplitude of ground temperature oscillations as half the annual range in the mean daily or mean monthly air or ground temperature (e.g. <sup>33,37,59-62</sup>) or as the difference between the maximum mean monthly ground surface temperature and the mean annual ground surface temperature.<sup>30</sup> However, daily or monthly temperatures might overestimate or underestimate, respectively, the annual ground temperature amplitude. Moreover, they might be unrepresentative of variously long thawing and freezing seasons whose summary length does not match the period of one year exactly. Accordingly, we calculated  $A_5$  as the difference between the annual maximum of the 31-day moving average of ground temperature at depth  $z_5$  and the mean annual ground

temperature at depth  $z_5$  ( $MAGT_5$ ). We believe that this design is more representative of the ALT dynamics because it prefers the thawing season when calculating the amplitude and, as such, it emphasizes its utmost importance for active-layer formation. By contrast, it suppresses the freezing season, and thus it eliminates the potential attenuation of ground temperature amplitude caused by snow cover insulation.

The  $T_{TOP}$  for permafrost conditions ( $T_{TOP} \leq 0^\circ\text{C}$ ) was calculated using a semi-empirical equation after Garagulya:<sup>63</sup>

$$T_{TOP} = \frac{MAGT_5 (k_f + k_t) + A_5 \frac{k_t - k_f}{\pi} \left( \frac{MAGT_5}{A_5} \arcsin \frac{MAGT_5}{A_5} + \sqrt{1 - \frac{MAGT_5^2}{A_5^2}} \right)}{k_f} \quad (20)$$

If a sinusoidal temperature wave is assumed, Equation (20) produces identical results to the thermal offset equation,<sup>64</sup> which has been extensively employed in the  $T_{TOP}$  model.<sup>65,66</sup> However, for consistency of the calculations, we preferably use the former approach because it incorporates  $A_5$  as an input parameter, like both forms of the Kudryavtsev model (Equations 9 and 12).

### 3.3 | Ground physical properties

Ground physical parameters (Table 1) are based on analyses of intact ground samples collected in duplicate from depths of 10 and 30 cm into 400-cm<sup>3</sup> plastic cylinders in February 2017 near the temperature measurement site. The ground samples were weighed twice before and after oven-drying for 24 h at 105°C. Afterwards, the dry bulk density was calculated as the ratio of the mass of dry ground to the total volume of the sample, the gravimetric water content was determined as the ratio of the mass of water to the mass of dry ground, and the volumetric water content ( $\phi$ ) was computed as the product of the above parameters (dimensionless). Ground texture characteristics were acquired by wet sieving of particles >63  $\mu\text{m}$  and X-ray sedimentation of the finest fractions  $\leq 63 \mu\text{m}$  (Sedigraph III Plus, Micrometrics).

In addition, seven replicate measurements on intact thawed samples were made with an ISOMET 104 device (Applied Precision Ltd) to determine the average thawed thermal conductivity and thawed volumetric heat capacity. The frozen thermal conductivity and frozen volumetric heat capacity were subsequently estimated based on the thermal properties of the thawed samples and their volumetric water contents, neglecting volume changes due to phase transitions. For the frozen thermal conductivity, we assumed a geometric mean

**TABLE 1** Selected ground physical properties at the Abernethy flats site

| Depth | $\omega$ (%) | $\phi$ (%) | $\rho$ (kg m <sup>-3</sup> ) | $k_t$ (W m <sup>-1</sup> K <sup>-1</sup> ) | $k_f$ (W m <sup>-1</sup> K <sup>-1</sup> ) | $C_t$ (J m <sup>-3</sup> K <sup>-1</sup> ) | $C_f$ (J m <sup>-3</sup> K <sup>-1</sup> ) | Sand (%) | Silt (%) | Clay (%) |
|-------|--------------|------------|------------------------------|--|--|--|--|----------|----------|----------|
| 10 cm | 18.0         | 23.4       | 1,302                        | 0.45                                       | 0.62                                       | 1.38                                       | 0.83                                       | 50       | 22       | 28       |
| 30 cm | 18.2         | 26.5       | 1,457                        | 0.61                                       | 0.87                                       | 1.68                                       | 1.06                                       | 53       | 20       | 27       |

$\omega$  (gravimetric water content);  $\phi$  (volumetric water content);  $\rho$  (dry bulk density);  $k_t$  (thawed thermal conductivity);  $k_f$  (frozen thermal conductivity);  $C_t$  (thawed volumetric heat capacity);  $C_f$  (frozen volumetric heat capacity).

equation based on the thermal conductivity of the ground constituents and their volume fractions:<sup>67</sup>

$$k_f = k_t \left( \frac{k_i}{k_w} \right)^\phi \quad (21)$$

where  $k_i$  is the thermal conductivity of ice ( $2.22 \text{ W m}^{-1} \text{ K}^{-1}$ ) and  $k_w$  is the thermal conductivity of water ( $0.57 \text{ W m}^{-1} \text{ K}^{-1}$ ). Calculation of the frozen volumetric heat capacity builds on a weighted average of volumetric heat capacity of the ground constituents and their volume fractions:<sup>66</sup>

$$C_f = C_t - \phi(C_w - C_i) \quad (22)$$

where  $C_w$  is the volumetric heat capacity of water ( $4.21 \text{ MJ m}^{-3} \text{ K}^{-1}$ ) and  $C_i$  is the volumetric heat capacity of ice ( $2.05 \text{ MJ m}^{-3} \text{ K}^{-1}$ ).

## 4 | RESULTS

### 4.1 | Air and ground temperature regimes

MAAT at Abernethy Flats was  $-7.3^\circ\text{C}$  in the period March 2006 to February 2016 and ranged from  $-5.1^\circ\text{C}$  (2006/07) to  $-8.9^\circ\text{C}$  (2009/10) (Figure 3). The warmest season was summer (DJF) with a mean seasonal air temperature (MSAT) average of  $0.4^\circ\text{C}$ , which varied between  $2.0^\circ\text{C}$  (2007/08) and  $-1.0^\circ\text{C}$  (2009/10). The coldest season was winter (JJA)

with MSAT average of  $-14.8^\circ\text{C}$ . Winter MSAT varied between  $-9.9^\circ\text{C}$  in 2010/11 and  $-18.3^\circ\text{C}$  in 2009/10 (Table 2). The highest mean monthly air temperature was mostly recorded in January and averaged  $1.2^\circ\text{C}$  with a range between  $2.7^\circ\text{C}$  (2007 and 2009) and  $-0.6^\circ\text{C}$  (2010). The coldest month was usually July with an average of  $-15.5^\circ\text{C}$  and substantially higher temperature variability compared to the warmest month of between  $-9.8^\circ\text{C}$  (2006) and  $-21.9^\circ\text{C}$  (2007). The highest mean daily temperatures slightly exceeded  $5^\circ\text{C}$  and occasionally even  $10^\circ\text{C}$  during the summer months, while the minimum mean daily temperatures usually dropped below  $-25^\circ\text{C}$  and rarely decreased even below  $-30^\circ\text{C}$  (Figure 3). The MAAT tended to increase on average by  $+0.10^\circ\text{C y}^{-1}$  over the entire period of March 2006 to February 2016. The major warming of  $+0.31^\circ\text{C y}^{-1}$  was observed for the autumn months (MAM), while cooling of  $-0.16^\circ\text{C y}^{-1}$  was found for the winter months (JJA). However, in all cases the trends were non-significant at  $p < 0.05$ .

MAGT<sub>5</sub> was  $-6.1^\circ\text{C}$  in the period March 2006 to February 2016 and ranged from  $-3.3^\circ\text{C}$  (2008/09) to  $-8.2^\circ\text{C}$  (2007/08 and 2009/10) (Figure 3). Mean seasonal ground temperature at 5 cm (MSGT<sub>5</sub>) in the summer months averaged  $3.3^\circ\text{C}$  and varied between  $5.1^\circ\text{C}$  (2007/08 and 2008/09) and  $0.4^\circ\text{C}$  (2009/10). The coldest season was winter when MSGT<sub>5</sub> decreased on average to  $-14.7^\circ\text{C}$ , with a range between  $-9.6^\circ\text{C}$  in 2008/09 and  $-18.9^\circ\text{C}$  in 2007/08 (Table 2). The highest mean monthly ground temperature at a depth of 5 cm was mostly recorded in January and averaged  $4.8^\circ\text{C}$ , with variations between  $7.1^\circ\text{C}$  (2009) and  $2.7^\circ\text{C}$  (2010). The coldest months were July and

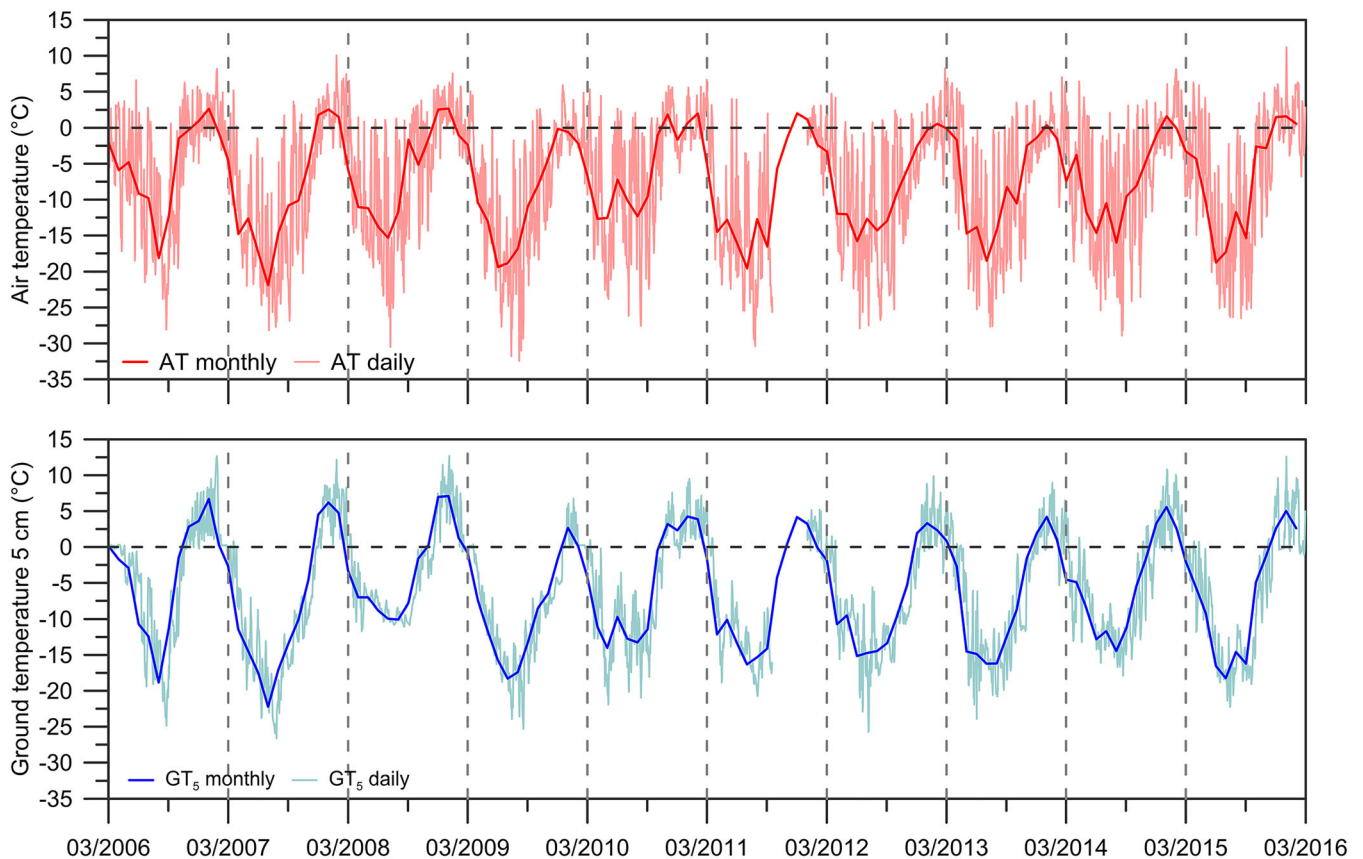


**FIGURE 3** Daily and monthly air temperature (AT) and ground temperature at a depth of 5 cm (GT<sub>5</sub>) [Colour figure can be viewed at [wileyonlinelibrary.com](http://wileyonlinelibrary.com)]

**TABLE 2** Annual and seasonal means of air temperature (AT) and ground temperature at a depth of 5 cm ( $GT_5$ ) and the temperature trends for the period March 2006 to February 2016

| Period  | Annual |        | MAM   |        | JJA   |        | SON   |        | DJF   |        |
|---------|--------|--------|-------|--------|-------|--------|-------|--------|-------|--------|
|         | AT     | $GT_5$ | AT    | $GT_5$ | AT    | $GT_5$ | AT    | $GT_5$ | AT    | $GT_5$ |
| 2006/07 | -5.1   | -3.8   | -4.2  | -1.5   | -12.4 | -14.0  | -4.6  | -3.3   | 0.9   | 3.5    |
| 2007/08 | -8.8   | -8.2   | -10.7 | -9.5   | -18.0 | -18.9  | -8.6  | -9.4   | 2.0   | 5.1    |
| 2008/09 | -6.1   | -3.3   | -9.4  | -5.8   | -13.6 | -9.6   | -2.8  | -3.1   | 1.4   | 5.1    |
| 2009/10 | -8.9   | -8.2   | -8.6  | -6.6   | -18.3 | -17.1  | -7.8  | -9.4   | -1.0  | 0.4    |
| 2010/11 | -5.8   | -5.3   | -10.6 | -9.7   | -9.9  | -11.9  | -2.9  | -2.9   | 0.3   | 3.5    |
| 2011/12 | -8.6   | -6.6   | -10.8 | -8.0   | -16.1 | -15.0  | -7.7  | -5.6   | 0.5   | 3.0    |
| 2012/13 | -8.3   | -7.3   | -9.1  | -7.4   | -14.3 | -14.8  | -9.3  | -9.4   | -0.8  | 2.5    |
| 2013/14 | -7.2   | -6.6   | -5.5  | -5.4   | -15.5 | -15.8  | -7.1  | -7.6   | -0.8  | 2.4    |
| 2014/15 | -7.1   | -5.3   | -7.6  | -6.0   | -13.7 | -13.0  | -7.3  | -6.0   | 0.2   | 3.8    |
| 2015/16 | -6.9   | -6.5   | -6.0  | -5.6   | -15.9 | -16.5  | -6.9  | -7.5   | 1.2   | 3.4    |
| 2006/16 | -7.3   | -6.1   | -8.3  | -6.5   | -14.8 | -14.7  | -6.5  | -6.4   | 0.4   | 3.3    |
| Trend   | 0.10   | -0.05  | 0.31  | 0.13   | -0.16 | -0.20  | -0.08 | -0.13  | -0.09 | -0.16  |

August, both having identical average of  $-15.2^\circ\text{C}$ . The mean ground temperature of these two months varied considerably, between  $-10.0^\circ\text{C}$  (2008) and  $-22.2^\circ\text{C}$  (2007) (Figure 3). The highest mean daily ground temperatures at a depth of 5 cm usually reached around  $10^\circ\text{C}$  and occasionally even exceeded  $15^\circ\text{C}$  during summer months, while the minimum daily means usually dropped below  $-20^\circ\text{C}$  and rarely even below  $-25^\circ\text{C}$  (Figure 3). A negative trend of  $-0.05^\circ\text{C y}^{-1}$  was detected on an annual basis. Seasonally, ground temperature increased by  $0.13^\circ\text{C y}^{-1}$  in autumn months (MAM), while a negative trend of  $-0.20^\circ\text{C y}^{-1}$  was found for the winter months (JJA). However, all the trends were non-significant at  $p < 0.05$ .

Thawing seasons started between October 18 (2011/12) and December 20 (2010/11), while they ended between February 13 (2013/14) and March 19 (2011/12). These days also delimit the freezing seasons. The thawing seasons lasted for 153 days (2010/11) to 64 days (2009/10) with an average length of 105 days (Table 3). The

thawing seasons shortened by an average of 1.5 days per year. Mean air temperature during the thawing season averaged  $0.7^\circ\text{C}$ , with the warmest thawing season in 2008/09 ( $2.0^\circ\text{C}$ ) and the coldest in 2013/14 ( $-0.8^\circ\text{C}$ ). The average  $TDD_a$  was  $169^\circ\text{C days}$  and varied between  $242^\circ\text{C days}$  (2015/16) and  $37^\circ\text{C days}$  (2009/10). Relatively high  $FDD_a$  values were observed during thawing seasons as well, averaging  $-92^\circ\text{C days}$ , with a maximum of  $-41^\circ\text{C days}$  (2008/09) and minimum of  $-162^\circ\text{C days}$  (2013/14). Mean ground temperature during the thawing season at a depth of 5 cm was on average  $3.4^\circ\text{C}$  and varied between  $5.3^\circ\text{C}$  (2008/2009) and  $1.7^\circ\text{C}$  (2009/10). Similarly to seasonal ground temperature,  $TDD_5$  reached a maximum of  $520^\circ\text{C days}$  in 2008/09 and minimum of  $107^\circ\text{C days}$  in 2009/10. The average  $TDD_5$  was  $368^\circ\text{C days}$ . Summer  $FDD_5$  was very low, with an average of  $-8^\circ\text{C days}$ . The  $FDD_5$  was zero in 2009/10, whereas it reached  $-32^\circ\text{C days}$  in 2013/14. The average  $n_t$  was 2.35, with a maximum of 3.21 in 2013/14 and minimum of 1.59 in 2015/16 (Table 3).

**TABLE 3** Characteristics of mean seasonal air temperature ( $MATS_a$ ) and ground temperature at a depth of 5 cm ( $MGTS_5$ ), thawing ( $TDD$ ) and freezing ( $FDD$ ) degree-days, thawing  $n$ -factor ( $n_t$ ) and duration of thawing seasons in the period 2006/07–2015/16

| Period  | $MATS_a$ ( $^\circ\text{C}$ ) | $MGTS_5$ ( $^\circ\text{C}$ ) | $TDD_a$ ( $^\circ\text{C days}$ ) | $TDD_5$ ( $^\circ\text{C days}$ ) | $FDD_a$ ( $^\circ\text{C days}$ ) | $FDD_5$ ( $^\circ\text{C days}$ ) | $n_t$ (-) | Duration (days) |
|---------|-------------------------------|-------------------------------|-----------------------------------|-----------------------------------|-----------------------------------|-----------------------------------|-----------|-----------------|
| 2006/07 | 0.8                           | 3.3                           | 190                               | 432                               | -84                               | -1                                | 2.27      | 129             |
| 2007/08 | 1.6                           | 4.4                           | 236                               | 475                               | -70                               | -1                                | 2.01      | 107             |
| 2008/09 | 2.0                           | 5.3                           | 233                               | 520                               | -41                               | -1                                | 2.23      | 97              |
| 2009/10 | -0.6                          | 1.7                           | 37                                | 107                               | -77                               | 0                                 | 2.89      | 64              |
| 2010/11 | 0.6                           | 3.0                           | 225                               | 461                               | -131                              | -6                                | 2.05      | 153             |
| 2011/12 | -                             | 3.0*                          | -                                 | 347*                              | -                                 | -                                 | -         | -               |
| 2012/13 | 0.4                           | 2.9                           | 145                               | 311                               | -106                              | -13                               | 2.14      | 100             |
| 2013/14 | -0.8                          | 2.3                           | 84                                | 270                               | -162                              | -32                               | 3.21      | 103             |
| 2014/15 | 0.6                           | 4.2                           | 132                               | 370                               | -81                               | -2                                | 2.80      | 88              |
| 2015/16 | 1.6                           | 3.5                           | 242                               | 386                               | -74                               | -13                               | 1.59      | 108             |
| 2006/16 | 0.7                           | 3.4                           | 169                               | 370                               | -92                               | -8                                | 2.35      | 105             |

\*Value calculated by regression; it is not used to compute the period average.

Freezing seasons were substantially longer than thawing seasons, with an average length of 262 days and range between 302 days (2012/13) and 214 days (2006/07) (Table 4). Their duration was prolonged by an average of 3.8 days per year during the study period. Mean air temperature during freezing seasons dropped on average to  $-10.2^{\circ}\text{C}$ . The warmest freezing season was in 2006/07 ( $-8.8^{\circ}\text{C}$ ), while the coldest was in 2007/08 ( $-12.5^{\circ}\text{C}$ ). Likewise,  $FDD_a$  also reached its maximum of  $-1,973^{\circ}\text{C days}$  in 2006/07 and minimum of  $-3,448^{\circ}\text{C days}$  in 2007/08. The average  $FDD_a$  was  $-2,757^{\circ}\text{C days}$ . The positive air temperature events during winter (Figure 3) resulted in the occurrence of  $TDD_a$  in the freezing season, the average of which was  $60^{\circ}\text{C days}$  and it ranged from  $87^{\circ}\text{C days}$  in 2015/16 to  $29^{\circ}\text{C days}$  in 2007/08. Mean ground temperature during freezing seasons at a depth of 5 cm was  $-9.8^{\circ}\text{C}$  and varied between  $-7.0^{\circ}\text{C}$  in 2008/09 and  $-12.7^{\circ}\text{C}$  in 2007/08. The average  $FDD_5$  was  $-2,586^{\circ}\text{C days}$  and reached a maximum of  $-1,745^{\circ}\text{C days}$  in 2008/09 and minimum of  $-3,477^{\circ}\text{C days}$  in 2007/08. Unlike  $TDD_a$ ,  $TDD_5$  was very limited during the freezing seasons. The average was as low as  $3^{\circ}\text{C days}$ , and the maximum reached  $12^{\circ}\text{C days}$  in 2014/15, while only  $1^{\circ}\text{C day}$  was detected in the freezing seasons 2008/09 and 2013/14. The average  $n_f$  was 0.93, with a maximum of 1.03 in 2010/11 and minimum of 0.71 in 2008/09 (Table 4).

## 4.2 | Active-layer thickness

The average ALT modeled for the  $S_{10}$  scenario was 58 cm and ranged from 33 cm (2009/10) to 70 cm (2008/09). Model outputs for scenario  $S_{30}$  exhibited 2–5 cm thicker ALT (Figure 4) with an average of 62 cm and range between 35 cm (2009/10) and 75 cm (2008/09). Both scenarios showed non-significant ALT thinning at a rate of  $1.1 \text{ cm y}^{-1}$ .

ALT modeled for scenario  $K_{10}$  achieved an average of 57 cm and ranged from 35 cm (2009/10) to 79 cm (2008/09). The Kudryavtsev model also tended to provide 2–6 cm thicker active layer for the  $K_{30}$  scenario compared to  $K_{10}$  (Figure 4). The average ALT modeled for the  $K_{30}$  scenario was 62 cm and it varied between 37 cm (2009/10)

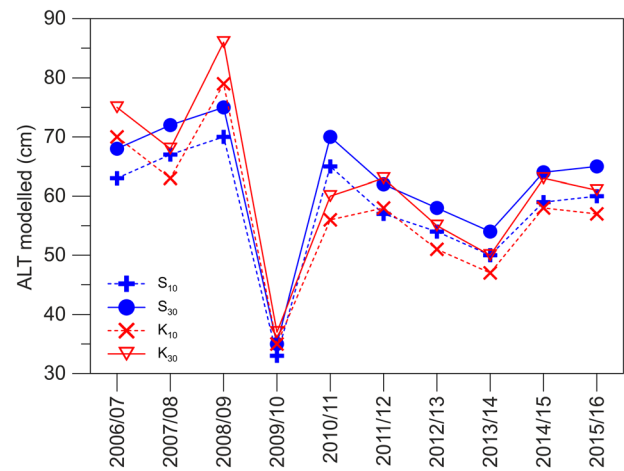


**FIGURE 4** Interannual variability of the active-layer thickness (ALT) modeled by the Stefan ( $S_{10}$ ,  $S_{30}$ ) and Kudryavtsev ( $K_{10}$ ,  $K_{30}$ ) models [Colour figure can be viewed at [wileyonlinelibrary.com](http://wileyonlinelibrary.com)]

and 86 cm (2008/09). Likewise, scenarios  $K_{10}$  and  $K_{30}$  modeled non-significant ALT thinning at rates of  $1.5$  and  $2.0 \text{ cm y}^{-1}$ , respectively.

The average ALT of all four scenarios reached 60 cm, ranging from 35 cm (2009/10) to 78 cm (2008/09). The average annual range of all four model scenarios was 9 cm. The annual range also positively correlated with the ALT, as the smallest model range of 4 cm was achieved when the mean modeled ALT reached its minimum, while the largest model range of 15 cm corresponded to its maximum (Figure 4). The thinning rate of the mean ALT was  $1.6 \text{ cm y}^{-1}$ , but it was also non-significant at  $p < 0.05$ .

The mean ALT modeled by the Stefan and Kudryavtsev models was controlled in particular by the summer ground temperature ( $r = 0.95$  and  $0.89$ , respectively), but it correlated highly significantly with the summer air temperature as well ( $r = 0.81$  and  $0.80$ , respectively; Figure 5). The influence of annual as well as winter air and ground temperatures was usually moderate ( $r = 0.43$  to  $0.61$ ), with the only significant relationship ( $r = 0.75$ ) found between the mean ALT modeled by the Kudryavtsev model and  $MAGT_5$  (Figure 5).

**TABLE 4** Characteristics of mean seasonal air temperature ( $MAFS_a$ ) and ground temperature at a depth of 5 cm ( $MGFS_5$ ), freezing ( $FDD$ ) and thawing ( $TDD$ ) degree-days, freezing  $n$ -factor ( $n_f$ ) and duration of freezing seasons in the period 2006/07–2015/16

| Period  | $MAFS_a$ ( $^{\circ}\text{C}$ ) | $MGFS_5$ ( $^{\circ}\text{C}$ ) | $FDD_a$ ( $^{\circ}\text{C days}$ ) | $FDD_5$ ( $^{\circ}\text{C days}$ ) | $TDD_a$ ( $^{\circ}\text{C days}$ ) | $TDD_5$ ( $^{\circ}\text{C days}$ ) | $n_f$ (-) | Duration (days) |
|---------|---------------------------------|---------------------------------|-------------------------------------|-------------------------------------|-------------------------------------|-------------------------------------|-----------|-----------------|
| 2006/07 | -8.8                            | -8.6                            | -1,973                              | -1,836                              | 81                                  | 3                                   | 0.93      | 214             |
| 2007/08 | -12.5                           | -12.7                           | -3,448                              | -3,477                              | 29                                  | 2                                   | 1.01      | 273             |
| 2008/09 | -9.6                            | -7.0                            | -2,449                              | -1,745                              | 44                                  | 1                                   | 0.71      | 251             |
| 2009/10 | -10.7                           | -10.4                           | -3,291                              | -3,116                              | 75                                  | 2                                   | 0.95      | 300             |
| 2010/11 | -9.5                            | -10.0                           | -2,307                              | -2,384                              | 45                                  | 2                                   | 1.03      | 238             |
| 2011/12 | -                               | -12.7*                          | -                                   | -3,126*                             | -                                   | -                                   | -         | -               |
| 2012/13 | -10.3                           | -9.7                            | -3,146                              | -2,925                              | 49                                  | 3                                   | 0.93      | 302             |
| 2013/14 | -10.7                           | -10.9                           | -2,712                              | -2,706                              | 72                                  | 1                                   | 0.99      | 247             |
| 2014/15 | -10.0                           | -8.9                            | -2,691                              | -2,332                              | 54                                  | 12                                  | 0.87      | 263             |
| 2015/16 | -10.0                           | -10.2                           | -2,799                              | -2,757                              | 87                                  | 5                                   | 0.98      | 271             |
| 2006/16 | -10.2                           | -9.8                            | -2,757                              | -2,586                              | 60                                  | 3                                   | 0.93      | 262             |

\*Value calculated by regression; it is not used to compute the period average.

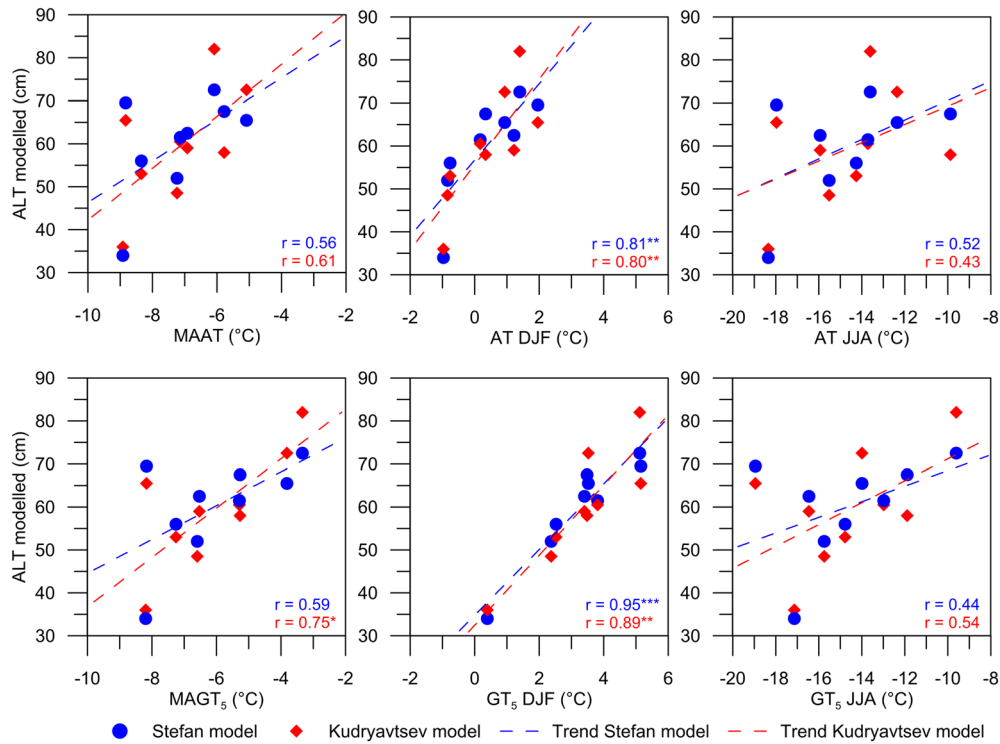


**FIGURE 5** Correlations between mean active-layer thickness (ALT) modeled by the Stefan and Kudryavtsev models and mean annual air temperature (MAAT), mean annual ground temperature at a depth of 5 cm (MAGT<sub>5</sub>), and mean seasonal air temperature (AT) and ground temperature at a depth of 5 cm (GT<sub>5</sub>) in summer (DJF) and winter (JJA). Statistical significance is expressed as \*\*\**p* < 0.001, \*\**p* < 0.01, \**p* < 0.05 [Colour figure can be viewed at wileyonlinelibrary.com]

The differences between the modeled and observed ALT reached on average -4.2 cm (-7.9%) and -5.8 cm (-10.3%) for scenarios S<sub>10</sub> and K<sub>10</sub>, respectively (Figure 6), with deviations from -1 to -8 cm (-1.1 to

-15.4%) and -2 to -11 cm (-3.3 to -16.2%), respectively. Because both scenarios underestimated the ALT in all cases, the corresponding mean absolute errors were 4.2 cm (7.9%) and 5.8 cm (10.3%), respectively.

More accurate ALT was modeled for scenarios S<sub>30</sub> and K<sub>30</sub>, which deviated on average by -0.2 cm (-0.8%) and -2.2 cm (-3.9%), with variations from -4 to 4 cm (-10.3 to 6.7%) and from -7 to 3 cm (-10.3 to 5.0%), respectively (Figure 6). Because the scenarios both underestimated and overestimated the ALT, the corresponding mean absolute errors were 2.6 cm (5.0%) and 3.4 cm (5.9%) for S<sub>30</sub> and K<sub>30</sub>, respectively.

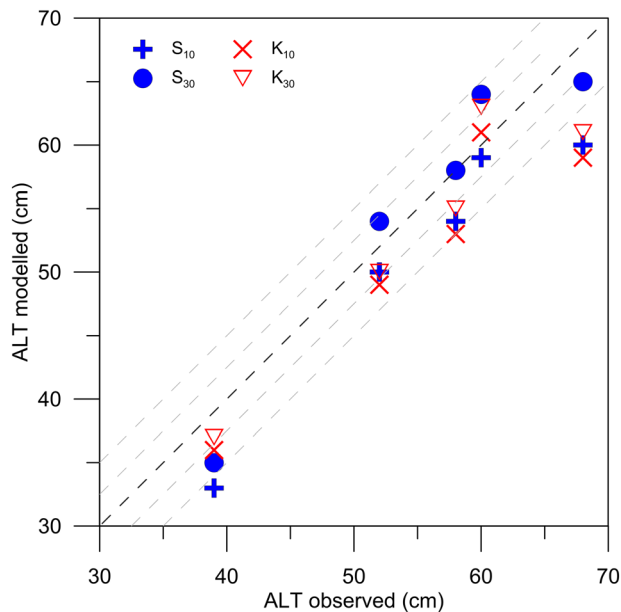


**FIGURE 6** Validation of modeled active-layer thickness (ALT) by the Stefan (S<sub>10</sub>, S<sub>30</sub>) and Kudryavtsev (K<sub>10</sub>, K<sub>30</sub>) models with observed ALT. A dark dashed line indicates a 1:1 relationship between the observed and modeled ALT, and grey dashed lines indicate the error bands of 2.5 and 5.0 cm [Colour figure can be viewed at wileyonlinelibrary.com]

## 5 | DISCUSSION

### 5.1 | Climate and active-layer thickness

The climate on the Eastern AP, where JRI is located, has a prevailing continental character but also some patterns of an oceanic climate (e. g. <sup>44,68</sup>). In contrast to the Western AP where an oceanic climate is dominant, the MAAT at the same latitudes of the Eastern AP is about 4 to 6°C lower<sup>69</sup> and the annual amplitude of air temperature is almost two times larger.<sup>70</sup> Yet, the area of JRI is among the warmest parts of Antarctica as MAAT in the coastal areas of Eastern Antarctica is typically between -10 and -15°C and decreases to about -15 to -20°C in the southernmost coastal areas in the region of the McMurdo Dry Valleys.<sup>71</sup>

Active-layer formation is mainly controlled by summer temperatures (Figure 5), as has also been reported from numerous sites in polar and subpolar as well as mountain regions (e.g. <sup>72-75</sup>). The mean

DJF air temperature on JRI reached 0.4°C in the period March 2006 to February 2016, which was 0.2–0.8°C lower than at sites along the Western AP in the same period.<sup>10</sup> The mean DJF ground temperature on JRI differed from those on some sites on the South Shetlands, usually by –1 to +1°C.<sup>11,76</sup> Higher ground temperature differences in contrast to that of air temperature might be attributed to the specific conditions of each study site, such as snow cover presence, vegetation coverage, moisture content, topography or lithological properties.<sup>77</sup>

Despite lower summer air temperature and more variable summer ground temperature differences, the near-surface thawing degree-days were usually higher on the Abernethy Flats than on the South Shetlands (e.g. <sup>11,20,70</sup>). This can be explained by the almost two times higher mean daily global radiation during the summer months on JRI (~240 W m<sup>-2</sup>)<sup>78</sup> than on the South Shetlands (~130 W m<sup>-2</sup>)<sup>79</sup> associated with a prevailing oceanic climate causing higher cloudiness on the Shetlands. The eminent role of global radiation on ground temperature can be mainly exemplified on Victoria Land where its mean summer value can exceed 240 W m<sup>-2</sup> and cause over 700°C days, despite mean summer air temperature being around –2°C.<sup>80</sup>

A significant air temperature decrease started around 2000 along most of the Western AP. The cooling triggered by natural variability of cyclonic activity and increasing sea-ice concentrations near coastlines caused MAAT trends of –0.16 to 0.05°C y<sup>-1</sup> in the period 2006–2015.<sup>9,10</sup> In contrast, the MAAT on JRI was increasing at a non-significant rate of 0.10°C y<sup>-1</sup>, which corresponds to observations from other sites of the north-eastern AP where positive, but non-significant, trends between 0.02 and 0.08°C y<sup>-1</sup> have been reported.<sup>10</sup> Unlike MAAT, there was a non-significant negative trend of –0.05°C y<sup>-1</sup> for MAGT<sub>5</sub>. Interestingly, the MSAT and MSGT<sub>5</sub> trends were positive only in autumn (MAM), at 0.30 and 0.13°C y<sup>-1</sup>, respectively, while they were negative in the other three seasons. Yet, the north-eastern AP region exhibited a MAAT more than 1°C lower in the period 2006–2015 compared to 1996–2005, and autumn (MAM) air temperature was even about 1.5°C lower.<sup>10</sup>

Among JRI sites of similar altitude, the average modeled ALT on Abernethy Flats of 60 cm was comparable to that at the site near the Johann Gregor Mendel station, where about 20% higher TDD<sub>5</sub> was observed, but ALT was reduced by lower thermal conductivity of around 0.30 W m<sup>-1</sup> K<sup>-1</sup> (see <sup>42,50</sup>), while about 20–30 cm higher ALT was reported at two other sites, mostly because of their higher thermal conductivity >0.7 W m<sup>-1</sup> K<sup>-1</sup> and slightly higher TDD<sub>5</sub>.<sup>42,50</sup>

Despite similar summer ground surface temperatures, the ALT on Abernethy Flats was lower than in the Western AP, where it usually exceeds 80 cm (e.g. <sup>5,7,13</sup>) and sub-Antarctica with ALT > 100 cm.<sup>19</sup> In these areas, permafrost is much warmer as the temperature at the top of the permafrost table is about 4–5°C higher than on JRI.<sup>70</sup> Therefore, thaw propagation during summer can be more rapid because less heat is needed for active-layer thawing. Moreover, thawing can be accelerated by higher input of liquid precipitation, which frequently occurs in the Western AP in the summer months. Slightly higher ALT values (~65 to 100 cm) were also observed in the coastal parts of Enderby Land and Princess Elizabeth Land in eastern Antarctica. MAAT in these regions is about 3°C lower than on JRI,

but summer air temperature is only about 1.0°C lower.<sup>81,82</sup> The difference might therefore be caused by contrasting ground physical properties as well as the slightly higher temperature amplitude of these areas. Lower ALT (< 50 cm) values were typical for cold areas with MAAT < –15°C such as northern Victoria Land,<sup>2,5,16,75</sup> McMurdo Dry Valleys,<sup>5,83</sup> and the mountainous areas in Dronning Maud Land<sup>5,84</sup> or the Ellsworth Mountains.<sup>85</sup> Mean monthly air temperatures during the summer only rarely exceeded –2°C in these areas, which probably enhanced the role of solar radiation in active-layer formation.<sup>75,80</sup>

Although the MAAT trend on JRI was positive, MAGT<sub>5</sub> decreased slightly, and the mean modeled ALT thinned by 1.6 cm y<sup>-1</sup> during the study period. The thinning can be mainly related to the decreasing DJF temperatures (Figure 5) and shortening of the thawing seasons, which occurred across the whole AP region<sup>10</sup> and caused similar active-layer thinning of 1.5 cm y<sup>-1</sup> on Deception Island during the period 2006–2014<sup>12</sup> as well as a thaw depth reduction of 1.6 cm y<sup>-1</sup> on the South Shetlands in the period 2009–2016.<sup>86</sup> The long-term ALT observations from other regions of Antarctica are sparse, but show that ALT remained stable in the McMurdo Dry Valley region,<sup>5,83</sup> while even slight thickening of 0.3 cm y<sup>-1</sup> was reported from northern Victoria Land in the period 1997–2012.<sup>16</sup> Generally, the summer season is the most important part of the year for active-layer development, while the effect of annual temperature is of lesser significance. Besides temperature, incoming solar radiation might become an important factor governing active-layer thawing in regions where no trend of summer air temperature was detected.<sup>16,75</sup>

## 5.2 | Model suitability

The Stefan and Kudryavtsev models have been widely used in different parts of the northern hemisphere for local ALT prediction based on *in situ* ground surface or subsurface measurements (e.g. <sup>30,32,60,61</sup>) as well as for regional or global ALT modeling (e.g. <sup>1,33,34,59,62,87–89</sup>), but until now they have been applied only twice in Antarctica.<sup>38,39</sup> The ALT values modeled in these two cases are, however, thought to be overestimated by up to hundreds of percent.<sup>90</sup> The present study is therefore the first one which provides validated ALT estimates based on the Stefan and Kudryavtsev models in Antarctica because their outputs based on ground physical parameters at a depth of 30 cm differ from the observed ALT on average by 2.6 and 3.4 cm or 5.0 and 5.9%, respectively (Table 5). Such accuracy is substantially better than in most previous studies, which showed average mean absolute errors of 3.6–58.8 cm and 2.8–65.7 cm for the Stefan and Kudryavtsev models, respectively, while their average mean absolute percentage errors were 6.0–26.1% and 5.8–24.7%, respectively (Table 5). Only two of these investigations reached an average mean absolute percentage error less than 10% for both the Stefan<sup>60,86</sup> and the Kudryavtsev models.<sup>30,88</sup> Romanovsky and Osterkamp<sup>30</sup> even achieved slightly better relative accuracy than this study, 5.8%, but on the other hand, they reached it by adapting the initially measured ground thermal properties through numerical modeling. The majority of studies have, however, reported average mean percentage errors

**TABLE 5** Overview of the accuracy of the Stefan and Kudryavtsev models for selected studies from across the Earth

| Model  | Solution       | ALT observed (cm)      | ALT modeled (cm)       | Mean error (cm)  | Mean absolute error (cm)                          | Mean percentage error (%)                        | Mean absolute percentage error (%)                | Source   |                                 |
|--------|----------------|------------------------|------------------------|--|---|--|---|--|---------------------------------|
| Stefan | Classic        | 50.2 (35.5 to 62.0)    | 62.3 (44.5 to 79.3)    | 12.2 (9.0 to 17.3)                                     | 12.3 (9.3 to 17.3)                                | 25.7 (20.4 to 28.6)                              | 26.1 (20.4 to 29.6)                               | Romanovsky and Osterkamp (1997)                    |                                 |
|        |                | 46.8 (40.2 to 60.3)    | 49.9 (37.9 to 66.7)    | 3.1 (-8.7 to 12.8)                                     | 6.7 (3.6 to 12.8)                                 | 7.3 (-16.1 to 31.8)                              | 14.9 (8.5 to 31.8)                                | Klene et al. (2001)                                |                                 |
|        |                | 328.8 (100.0 to 480.0) | 295.0 (130.0 to 410.0) | -33.8 (-100.0 to 70.0)                                 | 58.8 (20.0 to 100.0)                              | -1.5 (-25.0 to 50.0)                             | 21.5 (6.3 to 50.0)                                | Heggem et al. (2006)                               |                                 |
|        |                | 284.3 (150.0 to 480.0) | 281.4 (160.0 to 460.0) | -2.9 (-90.0 to 60.0)                                   | 37.1 (0.0 to 90.0)                                | 2.9 (-25.0 to 33.3)                              | 13.8 (0 to 33.3)                                  | Zorigt et al. (2016)                               |                                 |
|        | Semi-empirical | 39.7 (37.3 to 44.8)    | 40.9 (37.3 to 42.8)    | 1.2 (-2.0 to 4.8)                                      | 3.6 (2.0 to 4.8)                                  | 4.3 (-4.9 to 13.6)                               | 9.8 (5.1 to 13.6)                                 | Nelson et al. (1997)                               |                                 |
|        |                | 43.3 (29.0 to 56.0)    | 44.1 (35.0 to 59.0)    | 0.8 (-10.0 to 14.0)                                    | 4.4 (0.0 to 14.0)                                 | 2.1 (-18.5 to 46.7)                              | 10.4 (0.0 to 46.7)                                | Shiklomanov and Nelson (2002)                      |                                 |
|        | Corrected      | 217.4 (170.0 to 261.2) | 218.2 (176.8 to 277.5) | 0.8 (-10.5 to 16.3)                                    | 13.6 (6.8 to 22.3)                                | 0.4 (-5.0 to 6.4)                                | 6.0 (4.0 to 8.7)                                  | Yin et al. (2016)                                  |                                 |
|        |                | 55.4                   | 51.2/55.2 <sup>a</sup> | -4.2/ -0.2 <sup>a</sup>                                | 4.2/2.6 <sup>a</sup>                              | -7.9/ -0.8 <sup>a</sup>                          | 7.9/5.0 <sup>a</sup>                              | This study   |                                 |
|        | Kudryavtsev    |                        | 172.5 (29.3 to 298.9)  | 173.3 (39.2 to 272.5)                                  | 0.7 (-44.1 to 52.5)                               | -  | 6.6 (-15.8 to 43.1)                               | -  | Anisimov et al. (1997)          |
|        |                |                        | 50.2 (35.5 to 62.0)    | 51.9 (33.5 to 68.0) / 51.6 (36.3 to 63.0) <sup>a</sup> | 1.7 (-2.0 to 6.0) / 1.4 (0.8 to 2.5) <sup>a</sup> | 5.4 (3.5 to 7.7) / 2.8 (2.2 to 3.7) <sup>a</sup> | 2.0 (-4.8 to 9.4) / 2.8 (1.3 to 5.1) <sup>a</sup> | 11.5 (6.8 to 15.4) / 5.8 (5.1 to 6.4) <sup>a</sup> | Romanovsky and Osterkamp (1997) |
|        |                | 49.6 (43.0 to 55.0)    | 49.4 (41.0 to 58.0)    | -0.2 (-8.0 to 6.0)                                     | 4.6 (2.0 to 8.0)                                  | -0.4 (-16.3 to 14.0)                             | 9.6 (3.6 to 16.3)                                 | Shiklomanov and Nelson (1999)                      |                                 |
|        |                | 51.6 (33.0 to 65.0)    | 49.0 (26.0 to 67.0)    | -2.6 (-16.0 to 15.0)                                   | -   | -4.8 (-27.1 to 34.1)                             | -   | Sazonova and Romanovsky (2003)                     |                                 |
|        |                | 237.1 (159.9 to 379.7) | 228 (181.7 to 269.4)   | -9.0 (-110.3 to 80.3)                                  | 38.4 (5.7 to 110.3)                               | -0.3 (-29.0 to 47.1)                             | 16.0 (2.7 to 47.1)                                | Pang et al. (2012)                                 |                                 |
|        |                | 43.8 (37.0 to 56.0)    | 44.3 (31.0 to 59.0)    | 0.5 (-10.0 to 3.0)                                     | -   | 1.0 (-24.4 to 8.1)                               | -   | Streletskiy et al. (2012)                          |                                 |
|        |                | 217.4 (170.0 to 261.2) | 236.5 (216.7 to 254.0) | 19.1 (-7.3 to 46.7)                                    | 22.7 (7.3 to 46.7)                                | 10.5 (-2.7 to 27.5)                              | 11.9 (2.7 to 27.5)                                | Yin et al. (2016)                                  |                                 |
|        |                | 284.3 (150.0 to 480.0) | 275.7 (160.0 to 390.0) | -8.6 (-170.0 to 90.0)                                  | 65.7 (10.0 to 170.0)                              | 4.6 (-51.5 to 40.9)                              | 24.7 (2.8 to 51.5)                                | Zorigt et al. (2016)                               |                                 |
|        |                | 55.4                   | 49.6/53.2 <sup>a</sup> | -5.8/ -2.2 <sup>a</sup>                                | 5.8/3.4 <sup>a</sup>                              | -10.3/ -3.9 <sup>a</sup>                         | 10.3/5.9 <sup>a</sup>                             | This study   |                                 |

<sup>a</sup>Based on two sets of ground thermal properties.

mostly well below  $\pm 10\%$  (Table 5). This probably relates to the fact that equilibrium models assume stationary conditions,<sup>22</sup> and thus they well represent multi-year or multi-site averages that moderate the energy imbalances introduced by short-term and/or long-term climate variations, while they tend to fail to capture interannual transient departures from the equilibrium state.<sup>91</sup> Yet, this and other studies<sup>30,60</sup> have shown that equilibrium models can perform reasonably well even on an annual basis regardless of their limitations.

Theoretical studies have shown that the Stefan model tends to overestimate *ALT* by up to tens of percent.<sup>30,56,92</sup> This drawback is nicely illustrated by the *ALT* modeled through the basic form of the solution, which deviated on average by 13.8–26.1% from the observed *ALT* and exhibited the highest mean absolute percentage errors of up to 50% as well (Table 5). Somewhat better accuracy, with average mean absolute percentage errors of 9.8–10.4%, but at the same time with maximum deviations of up to 46.7%, was achieved if the ground physical parameters were substituted by the single empirically estimated edaphic parameter (Table 5). The latter approach simply overcomes the main model shortcomings and even coarse temperature data alone are needed to force the model successfully,<sup>87,89</sup> but despite the range of the edaphic parameter is relatively low,<sup>93</sup> it has limited transferability because it is valid only where observed *ALT* is available for model calibration.<sup>94</sup> The most accurate *ALT* estimates utilizing the Stefan model have been achieved by this study and by Yin et al<sup>60</sup> which both employed correction factors accommodating sensible heat and ground temperature prior to thawing,<sup>56</sup> resulting in average mean absolute percentage errors as low as 5.0–6.0%. Likewise, the annual ground surface temperature amplitude calculated from the difference between the maximum of the 31-day moving average ground temperature at a depth of 5 cm and *MAGT*<sub>5</sub> and usage of the actual length of the freezing and thawing seasons instead of the standard annual period of 365 days probably better represent the ground surface temperature behavior, which is reflected in the lower bias of the Kudryavtsev model than in most previous studies (Table 5). However, note that these comparisons need to be taken with caution because the validation data as well as the length of the validation periods in Table 5 differ, which prevents precise assessment of the modeling accuracy.

Both models also benefited greatly from adding the depth of the driving ground temperature measurements to their outputs,<sup>95</sup> which reduced the mean absolute percentage error of the Stefan and Kudryavtsev models by 5.1 and 7.3%, respectively. However, it has not yet been used in other investigations utilizing the ground temperature to run the models for ground thawing.<sup>30,32,34,60</sup> Undoubtedly, driving temperature data measured directly in the ground might also significantly contribute to the high accuracy of the models compared to the case of air temperature forcing; the earlier studies are, however, inconclusive in this regard for both the Stefan and the Kudryavtsev models. Nonetheless, the model adjustments proved to be highly useful, but at the same time, they require more input data. Furthermore, it is unclear to what extent the high accuracy of the models is due to their modifications alone and what is the role of ground surface and subsurface characteristics.

Because ground physical parameters enter the models as constants, the accuracy of the models depends on how the parameters are representative of the entire profile, which inherently relates to their temporal variability. Besides meteorological conditions, the main drivers of their changes are such factors as vegetation, snow cover or ground texture, which significantly alter air–ground fluxes and hence the moisture content or thermal properties of the ground.<sup>22</sup> However, the study site is vegetation-free and winter snow cover, which comprises most of the total precipitation, is believed to be low and rather episodic<sup>96</sup> as the freezing *n*-factor mostly ranged between 0.93 and 1.03 (Table 4).<sup>42,50</sup> Likewise, ground texture and moisture are homogeneous at least in the upper half of the active layer (Table 1).<sup>42</sup> In contrast, bulk density tends to increase with depth, being about 12% higher at 30 cm than at 10 cm, which also led to about 22–40% higher values of ground thermal conductivity and volumetric heat capacity at this depth (Table 1), probably due to enhanced particle contact caused by a reduction in porosity.<sup>67,97</sup> The *ALT* modeled based on ground physical properties at a depth of 30 cm was more accurate, on average by about 2.9 and 4.4% for the Stefan and Kudryavtsev models, respectively, than those based on the characteristics at 10 cm. Ground physical parameters at a depth of 30 cm are therefore more representative of the entire profile, probably because they are closer to half the depth between the ground surface and the base of the active layer and, as such, they are close to their optimal values. Naturally, this applies for uniform profiles such as in this study, but would be invalid for multilayer systems, especially those consisting of materials in high contrast to soil such as a surface layer of peat or shallow bedrock.

The higher accuracy of the Stefan and Kudryavtsev models on JRI than in most other regions might therefore be attributed both to the application of recent model enhancements<sup>56</sup> and other modifications improving their performance as well as to comparably lower temporal variability of ground surface and subsurface parameters and to their relatively homogeneous distribution across the profile. High model accuracy can also be assumed especially in other cold and dry regions of Antarctica where ground physical properties, particularly water content, remain stable over the years. They might therefore help to better understand the spatial variability of *ALT* as well as its sensitivity to climate changes there. Further testing of the models is, however, highly desirable in more temperate and humid regions of maritime Antarctica.

## 6 | CONCLUSIONS

Study of the active-layer thermal regime and thickness on Abernethy Flats, James Ross Island, Eastern Antarctic Peninsula, in the period March 2006 to February 2016 led to the following main conclusions:

1. Decadal *MAAT* and *MAGT*<sub>5</sub> values were  $-7.3$  and  $-6.1^{\circ}\text{C}$ , respectively, and the average modeled *ALT* reached 60 cm.
2. The *MAAT* increased on average by  $0.10^{\circ}\text{C y}^{-1}$ , but a negative trend of  $-0.05^{\circ}\text{C y}^{-1}$  was detected for *MAGT*<sub>5</sub>. The modeled *ALT* thinned on average by  $1.6\text{ cm y}^{-1}$ , which mainly related to a decrease in summer temperatures and to shortening of the thawing seasons. However, all the trends were statistically non-significant at  $p < 0.05$ .

3. The modeled ALT strongly and significantly correlated with summer air and ground temperature. It also showed moderate, but mostly non-significant, positive correlations with annual as well as winter air and ground temperatures.
4. The modeled ALT based on ground physical parameters at a depth of 30 cm showed a mean absolute error of 2.6 cm (5.0%) and 3.4 cm (5.9%) for the Stefan and Kudryavtsev models, respectively. This is therefore the first validated outcome of these analytical models in Antarctica. Their accuracy was, moreover, better than in most previous studies from the northern hemisphere, which is probably linked to the model modifications, rather low temporal variations of ground surface and subsurface characteristics, and homogeneous distribution of ground physical parameters within the active layer.

Our 10-year series is one of the longest datasets of simultaneous air temperature, ground temperature and ALT observations ever published in the Antarctic Peninsula region as well as throughout the Antarctica and it documents the short- to medium-term climate variations in the area. However, any trends should be taken carefully because the time series remains too short to capture a reliable climate signal.

The Stefan and Kudryavtsev models have been demonstrated to be simple tools that require a small amount of input data, while maintaining high accuracy of ALT estimates. They have considerable potential for reliable reconstructions of ALT at a local scale as well as its spatial modeling over Antarctica.

## ACKNOWLEDGEMENTS

This research was supported by the Ministry of Education, Youth and Sports of the Czech Republic projects LM2015078, LM2015079 and Z.02.1.01/0.0/0.0/16\_013/0001708. The authors thank Kamil Láška for maintenance of the meteorological station and providing meteorological data, Carsten W. Mueller for ground texture analysis, and Barret L. Kurylyk for discussing the calculation of the Stefan correction factors.

## ORCID

Filip Hrbáček  <https://orcid.org/0000-0001-5032-9216>

Tomáš Uxa  <https://orcid.org/0000-0001-9911-6529>

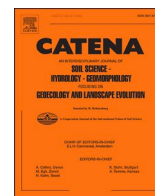
## REFERENCES

1. Anisimov OA, Shiklomanov N, Nelson FE. Global warming and active-layer thickness: results from transient general circulation models. *Global Planet Change*. 1997;15(3-4):61-77.
2. Guglielmin M. Ground surface temperature (GST), active layer, and permafrost monitoring in continental Antarctica. *Permafrost Periglacial Process*. 2006;17:133-143.
3. Romanovsky VE, Smith SL, Christiansen HH. Permafrost thermal state in the polar northern hemisphere during the international polar year 2007-2009: a synthesis. *Permafrost Periglacial Process*. 2010;21(2):106-116.
4. Burton-Johnson A, Black M, Fretwell PT, Kaluza-Gilbert J. An automated methodology for differentiating rock from snow, clouds and sea in Antarctica from Landsat 8 imagery: a new rock outcrop map and area estimation for the entire Antarctic continent. *Cryosphere*. 2010;10:1665-1677.
5. Hrbáček F, Vieira G, Oliva M, et al. Active layer monitoring in Antarctica: an overview of results from 2006 to 2015. *Polar Geogr*. 2019;n/a. <https://doi.org/10.1080/1088937X.2017.14201056>
6. Campbell IB, Claridge GGC. Permafrost properties, patterns and processes in the Transantarctic Mountains region. *Permafrost Periglacial Process*. 2006;17(3):215-2327.
7. Bockheim J, Vieira G, Ramos M, et al. Climate warming and permafrost dynamics in the Antarctic peninsula region. *Global Planet Change*. 2013;100:215-223.
8. Turner J, Colwell SR, Marshall GJ, et al. Antarctic climate change during last 50 years. *Int J Climatol*. 2005;25(3):279-294.
9. Turner J, Lu H, White I, et al. Absence of 21st century warming on Antarctic peninsula consistent with natural variability. *Nature*. 2016;535(7612):411-415.
10. Oliva M, Navarro F, Hrbáček F, et al. Recent regional climate cooling on the Antarctic peninsula and associated impacts on the cryosphere. *Sci Total Environ*. 2017;580:210-223.
11. Almeida ICC, Schaefer CEGR, Michel RFM, et al. Long term active layer monitoring at a warm-based glacier front from maritime Antarctica. *Catena*. 2016;149(2):572-581.
12. Ramos M, Vieira G, de Pablo MA, Molina A, Abramov A, Goyanes G. Recent shallowing of the thaw depth at Crater Lake, Deception Island, Antarctica (2006-2014). *Catena*. 2017;149(2):519-528.
13. Vieira G, Bockheim J, Guglielmin M, et al. Thermal state of permafrost and active-layer monitoring in the Antarctic: advances during the international polar year 2007-2008. *Permafrost Periglacial Process*. 2010;21(2):182-197.
14. Cannone N, Ellis Evans JC, Strachan R, Guglielmin M. Interactions between climate, vegetation and the active layer in soils at two maritime Antarctic sites. *Antarct Sci*. 2006;18(3):323-333.
15. Michel RFM, Schaefer CEGR, Poelking EL, Simas, Filho, Bockheim JG. Active layer temperature in two Cryosols from King George Island, Maritime Antarctica. *Geomorphology*. 2012;155-156:12-19.
16. Guglielmin M, Dalle Fratte M, Cannone N. Permafrost warming and vegetation changes in continental Antarctica. *Environ Res Lett*. 2014;9. <https://doi.org/10.1088/1748-9326/9/4/045001>
17. Guglielmin M, Evans CJE, Cannone N. Active layer thermal regime under different vegetation conditions in permafrost areas. A case study at Signy Island (maritime Antarctica). *Geoderma*. 2008;144(1-2):73-85.
18. Ramos M, Vieira G. Evaluation of the ground surface enthalpy balance from bedrock temperatures (Livingston Island, maritime Antarctic). *The Cryosphere*. 2009;3(1):133-145.
19. Guglielmin M, Worland MR, Cannone N. Spatial and temporal variability of ground surface temperature and active layer thickness at the margin of maritime Antarctica, Signy Island. *Geomorphology*. 2012;155:20-33.
20. De Pablo MA, Ramos M, Molina A. Thermal characterization of the active layer at the Limnopolar Lake CALM-S site on byers peninsula (Livingston Island), Antarctica. *Solid Earth*. 2014;5(2):721-739.
21. Oliva M, Hrbáček F, Ruiz-Fernandéz J, et al. Active layer dynamics in three topographically distinct lake catchments in byers peninsula (Livingston Island, Antarctica). *Catena*. 2017;149(2):548-559.
22. Riseborough D, Shiklomanov N, Etzelmüller B, Gruber S, Marchenko S. Recent advances in permafrost modelling. *Permafrost Periglacial Process*. 2008;19:137-156.
23. Bonnaventure PP, Lamoreaux SF. The active layer: a conceptual review of monitoring, modelling techniques and changes in a warming climate. *Prog Phys Geog*. 2013;37(3):352-376.
24. Weismüller J, Wollschläger U, Boike J, Pan X, Yu Q, Roth K. Modeling the thermal dynamics of the active layer at two contrasting permafrost

- sites on Svalbard and on the Tibetan plateau. *The Cryosphere*. 2011;5(3):741-757.
25. Jafarov EE, Marchenko SS, Romanovsky VE. Numerical modeling of permafrost dynamics in Alaska using a high spatial resolution dataset. *The Cryosphere*. 2012;6(3):613-624.
  26. Westermann S, Langer M, Boike J, et al. Simulating the thermal regime and thaw processes of ice-rich permafrost ground with the land-surface model CryoGrid 3. *Geosci Model Dev*. 2016;9(2):523-546. <https://doi.org/10.5194/gmd-9-523-2016>
  27. Stefan J. Über die Theorie der Eisbildung, insbesondere über die Eisbildung im Polarmee. *Ann Phys*. 1891;278(2):269-286. <https://doi.org/10.1002/andp.18912780206>
  28. Kudryavtsev VA, Garagulya LS, Kondrat'yeva KA, Melamed VG. *Fundamentals of frost forecasting in geological engineering investigations. Draft Translation 606*. U.S. Army Cold Regions Research and Engineering Laboratory; Hanover, NH; 1977.
  29. Shiklomanov NI, Nelson F. Active Layer Processes. In: Elias SA, ed. *Encyclopedia of Quaternary Science*. Vol.3 Oxford, UK: Elsevier; 2007:138-2147.
  30. Romanovsky VE, Osterkamp TE. Thawing of the active layer on the coastal plain of the Alaskan Arctic. *Permafrost Periglacial Processes*. 1997;8(1):1-22.
  31. Kurylyk BL. Discussion of 'a simple thaw-freeze algorithm for a multi-layered soil using the Stefan equation' by Xie and Gough (2013). *Permafrost Periglacial Processes*. 2015;26(2):200-206.
  32. Klene A, Nelson FE, Shiklomanov NI, Hinkel KM. The N-factor in natural landscapes: variability of air and soil-surface temperatures, Kuparuk River basin, Alaska, USA. *Arct Antarct Alp Res*. 2001;33(2):140-148.
  33. Sazonova TS, Romanovsky VE. A model for regional-scale estimation of temporal and spatial variability of active layer thickness and mean annual ground temperatures. *Permafrost Periglacial Processes*. 2003;14(2):125-139.
  34. Heggem ESF, Eitzelmüller B, Anarmaa S, Sharkhuu N, Goulden CE, Nandinsetseg B. Spatial distribution of ground surface temperatures and active layer depths in the Hövsgöl area, northern Mongolia. *Permafrost Periglacial Processes*. 2006;17(4):357-369.
  35. Shiklomanov NI, Anisimov OA, Zhang T, Marchenko S, Nelson FE, Oelke C. Comparison of model-produced active layer fields: results for northern Alaska. *J Geophys Res: Earth Surface*. 2007;112. <https://doi.org/10.1029/2006JF000571>
  36. Smith SL, Wolfe SA, Riseborough DW, Nixon FM. Active-layer characteristics and summer climate indices, Mackenzie Valley, Northwest Territories, Canada. *Permafrost Periglacial Processes*. 2009;20(2):201-220.
  37. Peng X, Zhang T, Frauenfeld OW, et al. Response of seasonal soil freeze depth to climate change across China. *The Cryosphere*. 2017;11(3):1059-1073.
  38. Wilhelm KR, Bockheim JG, Kung S. Active layer thickness prediction on the Western Antarctic peninsula. *Permafrost Periglacial Processes*. 2015;26(2):188-199.
  39. Wilhelm KR, Bockheim JG. Influence of soil properties on active layer thermal propagation along the western Antarctic peninsula. *Earth Surf Process Landf*. 2016;41(11):1550-1563.
  40. Davies BJ, Glasser NF, Carrivick JL, Hambrey MJ, Smellie JL, Nývlt D. Landscape evolution and ice-sheet behaviour in a semi-arid polar environment: James Ross Island, NE Antarctic Peninsula. In: Hambrey MJ, Barker PF, Barrett PJ, et al., eds. *Antarctic Palaeoenvironments and Earth-Surface Processes*. Vol.381 London, UK: Geological Society, Special Publications; 2013:353-395.
  41. Nývlt D, Braucher R, Engel Z, Mičoch B. ASTER team. Timing of the northern Prince Gustav ice stream retreat and the deglaciation of northern James Ross island, Antarctic peninsula during the last glacial-interglacial transition. *Quatern Res*. 2014;82(2):441-449.
  42. Hrbáček F, Kňázková M, Nývlt D, Láska K, Mueller CW, Ondruch J. Active layer monitoring at CALM-S site near J.G.Mendel Station, James Ross Island, Eastern Antarctic Peninsula. *Sci Total Environ*. 2017;601-602:987-997.
  43. Mičoch B, Nývlt D, Mixa P, et al. *Geological map of James Ross Island - Northern part 1: 25,000*. Praha, Czech Republic: Czech Geological Survey; 2019.
  44. Martin PJ, Peel DA. The spatial distribution of 10 m temperatures in the Antarctic peninsula. *J Glaciol*. 1978;20(83):311-317.
  45. Van Lipzig NPM, King JC, Lachlan-Cope TA, van der Broeke MR. Precipitation, sublimation and snow drift in the Antarctic peninsula region from a regional atmospheric model. *J Geophys Res*. 2004;109(D24):D24106.
  46. Nývlt D, Nývltová FM, Barták M, et al. Death age, seasonality, taphonomy and colonization of seal carcasses from ulu peninsula, James Ross island, Antarctic Peninsula. *Antarct Sci*. 2016;28(1):3-16.
  47. Kňázková M, Hrbáček F, Nývlt D, Kavan J. Effect of hyaloclastite breccia boulders on meso-scale periglacial-aeolian landsystem in semi-arid Antarctic environment, James Ross Island, Antarctic Peninsula. *Cuadernos de Investigacion Geografica*. 2019; online first. <https://doi.org/10.18172/cig.3800>
  48. Fukuda M, Shimokawa K, Takahashi N, Sone T. Permafrost in Seymour Island and James Ross island, Antarctic peninsula region. *Geogr Rev Jpn Ser a*. 1992;65(2):124-131.
  49. Borzotta E, Trombotto D. Correlation between frozen ground thickness measured in Antarctica and permafrost thickness estimated on the basis of the heat flow obtained from magnetotelluric soundings. *Cold Reg Sci Technol*. 2004;40(1-2):81-96.
  50. Hrbáček F, Nývlt D, Láska K, Kňázková M, Kampová B, Engel Z, Oliva M, Müller CW. Permafrost and active layer research on James Ross Island: An overview. *Czech Polar Reports*. 2019;9(1):20-36.
  51. Olivero E, Scasso RA, Rinaldi CA. Revision of the Marambio Group, James Ross Island, Antarctica. Instituto Antártico Argentino, Contribución. 1986;331:28.
  52. Mann HB. Non-parametric tests against trend. *Econometrica*. 1945;13:163-171.
  53. Kendal MG. *Rank Correlation Methods*. 4th ed. London, UK: Charles Griffin; 1975 XX pp.
  54. Sen PK. Estimates of the regression coefficient based on Kendall's tau. *J Am Stat Assoc*. 1968;63(324):1379-1389.
  55. Lunardini VJ. Theory of N-factors and correlation of data. In: *Proceedings of the Third International Conference on Permafrost*. Vol.1 National Council of Canada: Ottawa; 1978:40-46.
  56. Kurylyk BL, Hayashi M. Improved Stefan equation correction factors to accommodate sensible heat storage during soil freezing or thawing. *Permafrost Periglacial Processes*. 2016;27(2):189-203.
  57. Lunardini VJ. *Heat transfer in cold climate*. New York: Van Nostrand Reinhold; 1981.
  58. Kurylyk BL, McKenzie JM, MacQuarrie KTB, Voss CI. Analytical solutions for benchmarking cold regions subsurface water flow and energy transport models: one-dimensional soil thaw with conduction and advection. *Adv Water Resour*. 2014;70:172-184.
  59. Streletskiy DA, Shiklomanov NI, Nelson FE. Spatial variability of permafrost active-layer thickness under contemporary and projected climate in northern Alaska. *Polar Geogr*. 2012;35(2):95-116.

60. Yin G, Niu F, Lin Z, Luo J, Liu M. Performance comparison of permafrost models in Wudaoliang Basin, Qinghai-Tibet plateau, China. *J Mt Sci*. 2016;13(7):1162-1173.
61. Zorrig M, Kwadijk J, Van Beek E, Kenner S. Estimating thawing depths and mean annual ground temperatures in the Khuvsgul region of Mongolia. *Environ Earth Sci*. 2016;75(10):897.
62. Pang Q, Zhao L, Li S, Ding Y. Active layer thickness variations on the Qinghai-Tibet plateau under the scenarios of climate change. *Environ Earth Sci*. 2012;66(3):849-857.
63. Garagulya LS. *Application of Mathematical Methods and Computers in Investigations of Geocryological Processes*. Moscow, Russia: Moscow University Press; 1990.
64. Romanovsky VE, Osterkamp TE. Interannual variations of the thermal regime of the active layer and near-surface permafrost in northern Alaska. *Permafrost Periglacial Process*. 1995;6(4):313-335.
65. Smith MW, Riseborough DW. Permafrost monitoring and detection of climate change. *Permafrost Periglacial Process*. 1996;7(4):301-309.
66. Smith S, Riseborough D. Climate and the limits of permafrost: a zonal analysis. *Permafrost Periglacial Process*. 2002;13(1):1-15.
67. Farouki OT. *Thermal Properties of Soils*. U.S. Army Cold Regions Research and Engineering Laboratory Monograph. 1981: 81-1.
68. King JC, Comiso JC. The spatial coherence of interannual temperature variations in the Antarctic peninsula. *Geophys Res Lett*. 2003;30(2):1040.
69. Cook AJ, Vaughan DG. Overview of areal changes of the ice shelves on the Antarctic peninsula over the past 50 years. *The Cryosphere*. 2010;4(1):77-98.
70. Hrbáček F, Oliva M, Láška K, et al. Active layer thermal regime in two climatically contrasted sites of the Antarctic peninsula region. *Cuadernos de Investigacion Geografica*. 2016;42(2):457-474.
71. Comiso JC. Variability and trends in Antarctic surface temperatures from in situ and satellite infrared measurements. *J Climate*. 1999;13:1674-1696.
72. Kennedy AD. Water as a limiting factor in the Antarctic terrestrial environment: a biogeographical synthesis. *Arct Antarct Alp Res*. 1993;25(4):308-315.
73. Smith S, Romanovsky V, Lewkowicz A, et al. Thermal state of permafrost in North America: a contribution to the international polar year. *Permafrost Periglacial Process*. 2010;21(2):117-135.
74. Wu Q, Zhang T. Recent permafrost warming on the Qinghai-Tibetan Plateau. *J Geophys Res: Atmos*. 2008;113:D13. <https://doi.org/10.1029/2007JD009539>
75. Guglielmin M, Cannone N. A permafrost warming in a cooling Antarctica? *Clim Change*. 2012;111(2):177-195. <https://doi.org/10.1007/s10584-011-0137-2>
76. Arazny A, Kejna M, Sobota I. Ground temperature at the Henryk Arctowski station (King George Island, Antarctic) – case study from the period January 2012 to February 2013. *Bull Geogr Phys Geogr Ser*. 2013;6(1):59-80.
77. French H. *The periglacial environment* (p. 458). 3rd ed. England: John Wiley & Sons Ltd.; 2007.
78. Láška K, Budík L, Budíková M, Prošek P. Method of estimating solar UV radiation in high-latitude location based on satellite ozone retrieval with an improved algorithm. *Int J Remote Sens*. 2011;32(11):3165-3177.
79. Banon M, Justel A, Velazquez D, Queasada A. Regional weather survey on byers peninsula, Livingston Island, South Shetland Islands, Antarctica. *Antarct Sci*. 2013;25(2):146-156.
80. Cannone N, Guglielmin M. Influence of vegetation on the ground thermal regime in continental Antarctica. *Geoderma*. 2009;151(3-4):215-223.
81. Mergelov NS. Soils of wet valleys in the Larsemann Hills and Vestfold Hills oases (Princess Elizabeth land, East Antarctica). *Eurasian Soil Sci*. 2014;47(9):845-862.
82. Bockheim JG. *The soils of Antarctica*. Cham, Switzerland: Springer International; 2015:332.
83. Adlam LS, Balks MR, Seybold CA, Campbell DI. Temporal and spatial variation in active layer depth in the McMurdo Sound region, Antarctica. *Antarct Sci*. 2010;22(1):45-52.
84. Kotzé C, Meiklejohn I. Temporal variability of ground thermal regimes on the northern buttress of the Vesleskarvet nunatak, western Dronning Maud land, Antarctica. *Antarct Sci*. 2016;29(1):73-81.
85. Schaefer CEGR, Michel RFM, Delpupo C, Senra CO, Bremer UF, Bockheim JG. Active layer thermal monitoring of a Dry Valley of the Ellsworth Mountains, Continental Antarctica. *Antarctica Catena*. 2017;149(2):603-615.
86. De Pablo MA, Ramos M, Molina A, Prieto M. Thaw depth spatial and temporal variability at the Limnopolar Lake CALM-S site, byers peninsula, Livingston Island, Antarctica. *Sci Total Environ*. 2018;615:814-827.
87. Nelson FE, Shiklomanov NI, Mueller GR, Hinkel KM, Walker DA, Bockheim JG. Estimating active-layer thickness over a large region: Kuparuk river basin, Alaska, USA. *Arct Antarct Alp Res*. 1997;29(4):367-378.
88. Shiklomanov NI, Nelson FE. Analytic representation of the active layer thickness field, Kuparuk River basin, Alaska. *Ecol Modell*. 1999;123(2-3):105-125.
89. Shiklomanov NI, Nelson FE. Active-layer mapping at regional scales: a 13-year spatial time series for the Kuparuk region, north-Central Alaska. *Permafrost Periglacial Process*. 2002;13(3):219-230.
90. Uxa T. Discussion on, 'active layer thickness prediction on the Western Antarctic peninsula' by Wilhelm et al. 2015. *Permafrost Periglacial Process*. 2016;28:493-498.
91. Riseborough DW. The effect of transient conditions on an equilibrium permafrost-climate model. *Permafrost Periglacial Process*. 2007;18(1):21-32.
92. Aldrich HP, Paynter HM. *Analytical Studies of Freezing and Thawing of Soils*. U.S. Army Arctic Construction and Frost Effects Laboratory: Boston, MA; 1953.
93. McRoberts EC. Field observations of thawing in soils. *Can Geotech J*. 1975;12(1):126-130. <https://doi.org/10.1139/t75-011>
94. Zhang Y, Carey SK, Quinton WL. Evaluation of the algorithms and parameterizations for ground thawing and freezing simulation in permafrost regions. *J Geophys Res*. 2008;113(D17):D17116. <https://doi.org/10.1029/2007JD009343>
95. Hayashi M, Goeller N, Quinton WL, Wright N. A simple heat-conduction method for simulating the frost-table depth in hydrological models. *Hydrol Process*. 2007;21(19):2610-2622. <https://doi.org/10.1002/hyp.6792>
96. Hrbáček F, Láška K, Engel Z. Effect of snow cover on the active-layer thermal regime – a case study from James Ross island, Antarctic Peninsula. *Permafrost Periglacial Process*. 2016;27(3):307-315.
97. Abu-Hamdeh NH, Reeder R. Soil thermal conductivity: effects of density, moisture, salt concentration, and organic matter. *Soil Sci Soc Am J*. 2000;64(4):1285-1290.

**How to cite this article:** Hrbáček F, Uxa T. The evolution of a near-surface ground thermal regime and modeled active-layer thickness on James Ross island, eastern Antarctic peninsula, in 2006–2016. *Permafrost and Periglacial Process*. 2020;31:141-155. <https://doi.org/10.1002/ppp.2018>



# Effect of summer snow cover on the active layer thermal regime and thickness on CALM-S JGM site, James Ross Island, eastern Antarctic Peninsula

Filip Hrbáček<sup>a,\*</sup>, Zbyněk Engel<sup>b,1</sup>, Michaela Kňázková<sup>a</sup>, Jana Smolíková<sup>a,b</sup>

<sup>a</sup> Department of Geography, Faculty of Science, Masaryk University, Brno, Czech Republic

<sup>b</sup> Department of Physical Geography and Geoecology, Faculty of Science, Charles University, Prague, Czech Republic

## ARTICLE INFO

### Keywords:

Antarctica  
Soils  
Periglacial environment  
Ground penetrating radar  
Ground temperature

## ABSTRACT

This study aims to assess the role of ephemeral snow cover on ground thermal regime and active layer thickness in two ground temperature measurement profiles on the Circumpolar Active Layer Monitoring Network – South (CALM-S) JGM site on James Ross Island, eastern Antarctic Peninsula during the high austral summer 2018. The snowstorm of 13–14 January created a snowpack of recorded depth of up to 38 cm. The snowpack remained on the study site for 12 days in total and covered 46% of its area six days after the snowfall. It directly affected ground thermal regime as indicates temperature record at snow-covered profile AWS-JGM which subsurface section was nearly 5 °C colder compared to the snow-free AWS-CALM profile. The thermal insulation effect of snow cover is also reflected in the mean monthly (January) and summer (DJF) ground temperatures on AWS-JGM that decreased by ca 1.1 and 0.7 °C, respectively. Summer thawing degree days at a depth of 5 cm decreased by ca 10% and active layer was ca 5–10 cm thinner when compared to previous snow-free summer seasons. Surveying by ground penetrating radar revealed a general active layer thinning of up to 20% in those parts of the CALM-S which were covered by snow of >20 cm depth for at least six days.

## 1. Introduction

Seasonal occurrence of snow cover, its thickness and spatial distribution significantly affect ground thermal regime as well as active layer refreezing in regions underlain by permafrost. It is estimated that a snow accumulation about 40 cm deep has the maximum insulating effect (e.g., Zhang, 2005). Generally, thinner snow accumulation tends to have a cooling effect on the ground while a thicker and long-lasting snow cover can increase the ground temperature. The insulating effect of snow cover in permafrost conditions is the most prominent in winter due to maximum snow thickness, high surface albedo and the porosity of snow, and a large temperature difference between the atmosphere and the ground surface (Harris et al., 2009; Callaghan et al., 2011). Under these conditions, the solar energy absorbed by the snow surface is reduced, thermal conduction within the snowpack is low, and the transfer of heat between the air and the soil surface is limited. The net influence of snow over the cold period amounts to an increase of mean ground temperatures and maximum thaw depths, but these effects vary greatly in space

and time (Zhang, 2005). At the end of winter the insulating effect of snow decreases, and meltwater becomes the primary influence.

During the summer period, the effect of snow on ground temperature and thaw depth is considered to be relatively small under permafrost conditions (Goodrich, 1982). The ground remains frozen underneath long-lasting snow patches but warms rapidly in snow-free areas (Harris and Corte, 1992). The infiltration of meltwater increases the thermal conductivity of the ground, enhancing heat transfer from the ground surface to the permafrost table (Campbell et al., 1998). When ephemeral snow cover builds up during the summer, snow protects the ground from warm air and the active layer may eventually refreeze from the permafrost table upwards. However, this cooling effect is limited and its impact on the ground is controlled primarily by the duration of the snow cover, snow properties and a temperature difference between the air and the ground surface. The insulating capacity of snow increases in late summer when the thaw plane tends to rise rapidly (Goodrich, 1982). The impact of summer snow cover on ground temperatures and active layer thickness was studied rarely in the high mountains (Hoelzle et al., 2003;

\* Corresponding author.

E-mail address: [hrbacekfilip@gmail.com](mailto:hrbacekfilip@gmail.com) (F. Hrbáček).

<sup>1</sup> Both authors contributed equally to this paper.

<https://doi.org/10.1016/j.catena.2021.105608>

Received 13 May 2021; Received in revised form 29 June 2021; Accepted 14 July 2021

Available online 25 July 2021

0341-8162/© 2021 Elsevier B.V. All rights reserved.

Luetschg et al., 2008; Magnin et al., 2017; Mena et al., 2021), arctic environment (Christiansen, 2004; Hinkel and Hurd, 2006; Park et al., 2015) and Maritime Antarctic (Guglielmin and Cannone, 2012; Guglielmin et al., 2014b; de Pablo et al., 2017; Ramos et al., 2017, 2020). Most of these studies deal with the cooling effect of a delayed snow cover melt due to its albedo and the latent heat flux. Changes in the ground thermal regime induced by summer snowfall events were reported only from the Alps (Hanson and Hoelzle, 2004; Draebing et al., 2017; Magnin et al., 2017), Tianshan Mountains (Zhao et al., 2018) and arid Andes in Chile (Mena et al., 2021).

The snow cover effect on ground thermal regime or active layer thawing has been widely studied in the Arctic regions during the past decades (e.g., Zhang, 2005; Callaghan et al., 2011; Johansson et al., 2013; Park et al., 2015). However, the knowledge on snow-ground interactions in Antarctica is limited mostly to sites within the Antarctic Peninsula region (AP) with only a few studies from different parts of the continent. Generally, snowpack controls the ground thermal regime and active layer thickness in Antarctica in different ways depending on its seasonal duration and prevailing depth. Only a negligible effect of winter snowpack on ground thermal regime was observed in dry and cold conditions of the north-eastern AP where snow cover in winter is irregular and usually thinner than 30 cm (Hrbáček et al., 2016). A ground temperature increase was observed in cases when snow persists for the majority of the winter with a thickness between 30 and 70 cm. Such conditions are characteristic for the study sites on the South Shetlands in the north-western AP (Oliva et al., 2017a; de Pablo et al., 2017; Ramos et al., 2017) and they were also observed in topographically similar sites on James Ross Island (Kňažková et al., 2020). Importantly, ground warming during the thaw season can lead to permafrost degradation especially in areas on the border conditions between continuous and discontinuous permafrost of the north-western AP (Hrbáček et al., 2020).

At the same time, however, persistent snowpack can lead to active layer thinning and its effect can eventually promote permafrost aggradation. The main reason is a shortening of the thawing season (Ramos et al., 2017). Consequently, the heat deficit reduces active layer thawing propagation. Such conditions were observed on the South Shetlands after 2010 (de Pablo et al., 2017; Ramos et al., 2017) and they were related to a recent climate cooling (Turner et al., 2016; Oliva et al., 2017b) and an associated increase in snow precipitation within the AP region (Carrasco and Cordero, 2020). Similar effect of long-lasting snow

cover was reported from the Victoria Land where the presence of snow prevented the active layer from thawing in the summer completely (Guglielmin et al., 2014a). General cooling of the active layer and permafrost was further observed in areas where snowpack exceeded 1 m, as reported by Guglielmin et al. (2014b) from Adelaide Island. According to Ramos et al. (2020), permanent accumulation of >4.5 m can even lead to a complete insulation of the ground from atmosphere, causing permafrost aggradation and forming a specific subnival thermal regime of the ground.

This study brings a new perspective on the effect of snow on ground thermal regime and active layer thickness. We assess the role of a relatively thick ephemeral snowpack that occurred in the high summer 2018 on the area of Circumpolar Active Layer Monitoring site (CALM-S) JGM on James Ross Island. The objectives of this study are to (i) describe the spatial variability of snow cover thickness in the study area in January 2018, (ii) assess the differences in ground thermal regime and active layer thickness between the snow-covered and snow-free sites, and (iii) determine the effect of ephemeral snowpack on active layer thaw depth.

## 2. Study area

James Ross Island is located in the north-eastern sector of the AP (Fig. 1). The northern part of James Ross Island, Ulu Peninsula, constitutes the largest ice-free area in the entire AP. The mean annual air temperature (MAAT) in the lowland parts of JRI (<50 m asl) was  $-7.0\text{ }^{\circ}\text{C}$  in the period 2006–2015 with a positive trend of annual temperatures but a cooling trend in the summer (DJF) months (Hrbáček and Uxa, 2020). The annual precipitation is estimated to about 300–700 mm  $\text{w.e.y}^{-1}$  (van Wessem et al., 2016; Palermé et al., 2017). Snow cover is distributed irregularly as indicated by perennial snowfields on lee-slopes and snow patches around topographic obstacles. Snow thickness in the flat lowland areas is usually less than 20 cm, but can rarely exceed 40 cm (Hrbáček et al., 2016; Kňažková et al., 2020). The ice-free area is underlain by continuous permafrost with a modelled temperature between  $-4\text{ }^{\circ}\text{C}$  and  $-8\text{ }^{\circ}\text{C}$  (Obu et al., 2020). The active layer thickness strongly depends on lithology and varies between 50 and 120 cm (Hrbáček et al., 2019).

The study site is located on the CALM-S JGM which is the part of a continental database under code A27 (CALM-S database, 2021). The area of 80 m by 70 m was established in February 2014 following recommendations for CALM-S sites proposed by Guglielmin (2006). The

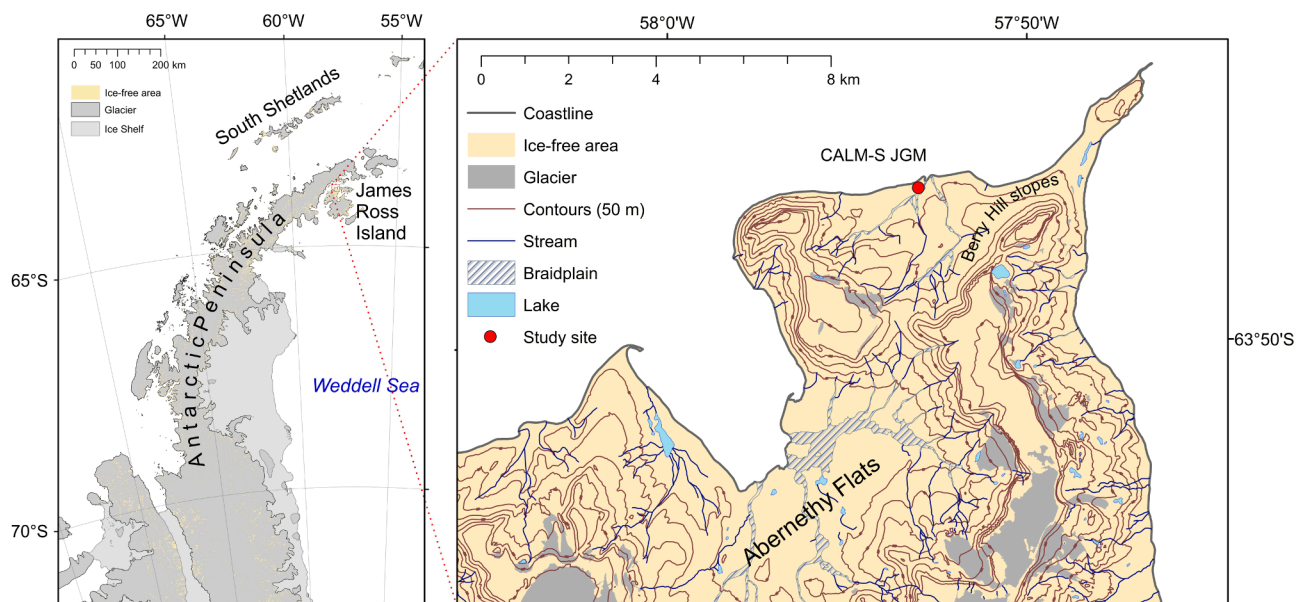


Fig. 1. Regional setting (left) and the location of CALM-S JGM site (right).

area comprises diverse geological units, with a Holocene marine terrace covering ca 80% of the northern part of the site and Cretaceous Whisky Bay Fm. forming the remaining 20% of the site (Fig. 2). The geological conditions lead to a variability of general ground physical characteristics and consequently drive the variability of active layer thaw depth which is about 20 cm thicker in the southern part underlain by the Cretaceous sediments (Hrbáček et al., 2017).

### 3. Material and methods

#### 3.1. Temperature monitoring and data processing

There are two automatic weather stations (AWS) installed within the CALM-S JGM grid. The fully equipped site AWS-JGM is located in the part formed by the marine terrace. It provides data on air temperature at 2 m above ground measured by Pt100/8 sensor (accuracy  $\pm 0.15$  °C) placed in a radiation shield, and ground temperature measured by Pt100/8 thermometers (accuracy  $\pm 0.15$  °C) placed directly in the ground. The second automatic weather station (AWS-CALM) is installed in the Cretaceous sediments about 60 m to the west from AWS-JGM and provides data on ground temperature only. The measurement is conducted by the same thermistors and placed at the same depths as on AWS-JGM. Missing data in the AWS-CALM record in the period 18 December 2016 to 20 January 2017 were replaced using a multiple regression according to air and ground temperature data from AWS-JGM. With regards to the size of the CALM-S JGM area, the air temperatures from AWS-JGM site are considered to be representative also for AWS-CALM (Hrbáček et al., 2017).

Climate data were analysed for the austral summer periods 2016/17 and 2017/18. Particularly, the following parameters were calculated:

- Daily and seasonal mean air and ground temperatures at depths of 5, 50 and 75 cm;
- Thawing degree days of air and ( $TDD_A$ ) ground at a depth of 5 cm ( $TDD_5$ ) calculated as a sum of positive daily temperatures;
- Isothermal days at a depth of 5 cm set as an event with the maximum and minimum daily temperatures within the interval 0.5 °C to  $-0.5$  °C (Guglielmin, 2006).

Further, we evaluated 30 min variability of air, and ground temperatures at depths of 5, 50 and 75 cm and 2 h variability of snow depth in the period from 10 January to 25 January 2018. The daily variability of active layer thickness (ALT) was defined as a maximum daily depth of 0 °C isotherm for the entire period of thawing season and the maximum seasonal ALT is calculated accordingly.

#### 3.2. ALT measurements

Mechanical probing and ground penetrating radar (GPR) soundings were used to determine seasonal changes of active layer thickness. Thaw depths were measured on 31 January and 12 February during the summer period 2016/17 and on 20 January, 12 and 24 February in the 2017/18 summer period. The gridded sampling design with evenly distributed nodes at 10 m spacing was used for the probing, which was carried out at each of the grid nodes with a 1 cm diameter steel rod of 120 cm length. GPR data were collected along nine parallel profiles with north–south orientation, four profiles (Fig. 2) were selected for a detailed analysis. GPR sounding was carried out using a shielded 500 MHz antenna and RAMAC CU-II control unit (MALÅ GeoScience, 2005). A wheel encoder was used to trig the measurements and control the distance along the profiles. The time window was set to 54.6 ns and scan spacing to 0.049 m. GPR data were processed using the REFLEXW software version 8.5 (Sandmeier, 2017). The depth axis of raw GPR profiles was converted from the time axis using the wave velocity determined from thaw depths probed at grid nodes and from the position of relevant reflector in GPR scans. The velocity obtained for each sampling date ranged between 0.071 and 0.094 m ns<sup>-1</sup> increasing towards the late summer season with decreasing soil moisture (Fig. 3a). This velocity range and the electromagnetic pulse width yield a maximum vertical (depth) resolution length of 4–5 cm, assuming a resolution of one quarter of the GPR signal wavelength (Knapp, 1990). The position of the permafrost table is actually determined less precisely due to changes in water content within active layer associated with various sediment types, grain size, porosity and compaction (e.g. Jol and Bristow, 2003). To cover uncertainties in the location of a target, the vertical resolution is usually approximated by half of the signal wavelength (Luo et al., 2019), which corresponds to the range of 7–9 cm in case of the 500 MHz antennae and the above-mentioned velocity

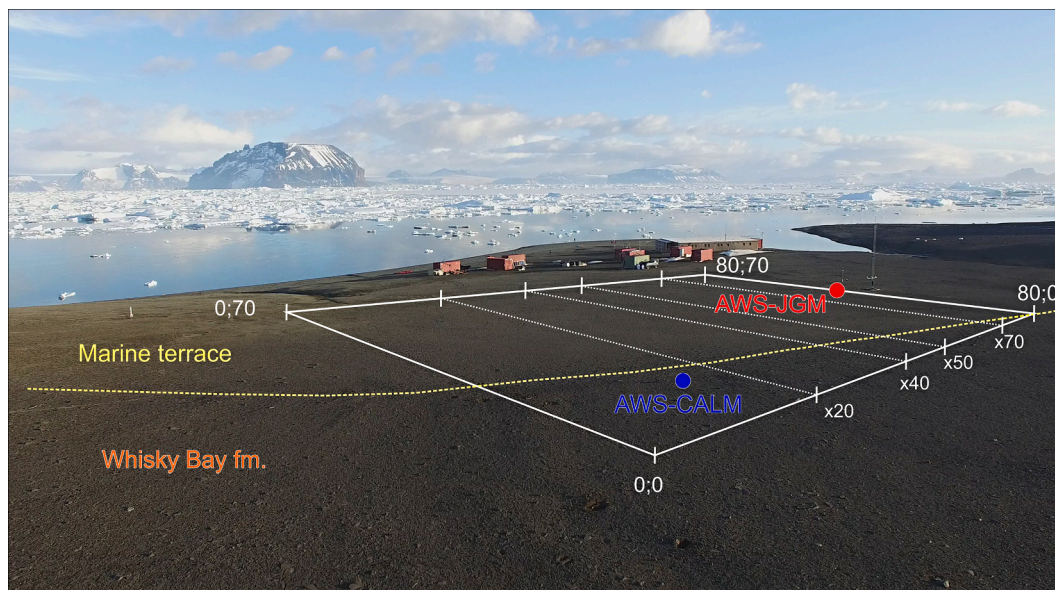
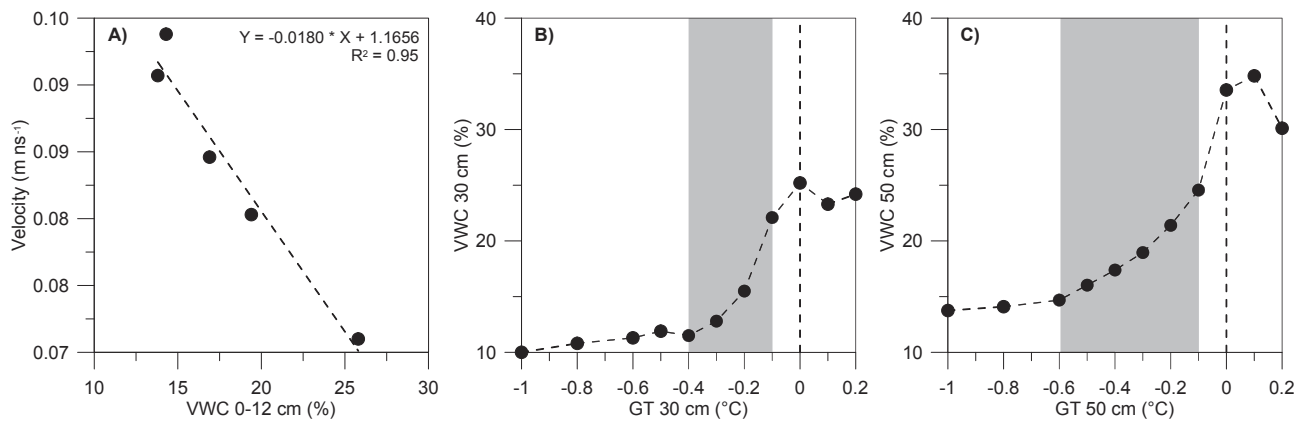


Fig. 2. Study site from the south-west. The white polygon with local coordinates (x;y) in the corners delimits the area of CALM-S JGM, white dotted lines indicate selected ground penetrating radar profiles shown in Fig. 7, and the yellow dotted line represents the boundary between the geological formations of Holocene marine terrace and Cretaceous Whisky Bay Fm. Colour points represent positions of ground temperature monitoring profiles. (For interpretation of the references to colour in this figure legend, the reader is referred to the web version of this article.)



**Fig. 3.** Linear correlation is observed between mean surficial volumetric water content (VWC) on CALM-S JGM and GPR wave velocities in active layer (A). Relationship between mean volumetric water content and associated mean ground temperature (GT) at 30 cm (B) and 50 cm (C) depth indicates the temperature interval of soil water phase change (shaded rectangle).

range. The volumetric soil moisture was set as a mean value of 72 measurements recorded at each grid point of CALM-S JGM within 12 cm thick subsurface layer of the ground using the HydroSense II measuring device paired with the CS658 soil–water sensor (Campbell Scientific, Inc.). Volumetric water content measured by CS650 sensor (Campbell Scientific, Inc.) in the depths of 30 and 50 cm was used together with ground temperature records on AWS-CALM to construct the soil freezing curves. The active layer phase change occurred between  $-0.1$  °C and  $-0.6$  °C (Fig. 3b, c) reflecting the variability in salt content in the ground, which may decrease the freezing point temperature nearly by 2 °C (Harris et al., 2018).

### 3.3. Snow cover observations

A long-term year-round monitoring of snow depths is provided at 2-hour interval using the Judd (accuracy  $\pm 1$  cm) ultrasonic sensor installed at the AWS-JGM since 2011 (Hrbáček et al., 2016). The sensor is located within 5-meter distance from ground temperature measurement profile. Raw readings from the sensor were corrected against actual air temperatures following the specification of the manufacturer (Judd Communication). Snow depth data are available for the summer season 2017/18 due to sensor failure prior to the summer 2016/17.

The extent of snow cover in the 2017/2018 summer was identified using an unmanned aerial vehicle (UAV) imagery. DJI Phantom 3 Professional was used for the survey at a flight height of 30 m allowing the ground sample distance of approximately 1.0 cm. Pictures from the UAV were processed and orthorectified in Metashape (Agisoft) and used for the delimitation of snow patches in ArcMap 10.4 (ESRI). The spatial distribution of snow depth was assessed based on the GPR scanning and mechanical probing. The scanning with a shielded 800 MHz antenna was carried out along nine parallel GPR profiles designed for ALT measurements and probing was done at a rectangular array of the CALM-S grid nodes with a steel rod covering both the ice-covered and bare parts of the test site. The signal acquisition time of GPR scanning was set to 38.1 ns and scan spacing to 0.019 m. The probed snow depths were used to adjust the position of snow/ground interface in obtained GPR scans allowing for a precise conversion of time axis to depth, and interpolation of snow depth using the Radial Basis Function in Surfer 15 (Golden Software).

## 4. Results

### 4.1. Air temperatures during the period 2016–2018

Data from the AWS-JGM site provide a general understanding of climate conditions at the study site over the period 2016–2018. MAAT

ranged from  $-6.7$  °C to  $-3.9$  °C with a mean temperature of  $-5.5$  °C for the 3-year period. The value of  $-3.9$  °C obtained for the year 2016 represents the highest annual air temperature recorded at the study site since the beginning of measurements in 2004. The warmest year was followed by significantly colder year 2017 with the MAAT of  $-6.7$  °C, which is, however, only 0.1 °C colder compared to the mean air temperature for the period 2004–2018. The year 2018 with the MAAT of  $-5.8$  °C belongs to warmer years in the AWS-JGM temperature record.

Mean summer air temperatures over the investigated period coincide within the measurement uncertainty of temperature sensors, varying between 0.1 °C in 2016/17 and 0.0 °C in 2017/18. Similarly, mean monthly air temperatures for the warmest month (January) ranged from 0.2 °C (2016/17) to  $-0.1$  °C (2017/18). Mean daily air temperatures mostly varied between 5.0 °C and  $-2.0$  °C (Fig. 4) and the warmest period occurred at the turn of January and February in both summer seasons. Summer TDD<sub>A</sub> reached 83 °Cdays in 2016/17 and 67 °Cdays in 2017/18 (Table 1).

The most prominent cooling over the summer period 2017/18 was connected with the snowstorm event that occurred on 13 to 14 January 2018. The air temperature decreased from above-zero values to  $-5.4$  °C immediately after the snowstorm but remained rather positive with a mean of 1.0 °C from 16 to 25 January. Fig. 4b shows air temperature variation during this event and its effect on ground temperatures at snow covered/snow free sites. While air temperature controlled ground temperature fluctuations at bare ground, it did not affect subsurface temperatures below the snow cover.

### 4.2. Ground thermal regime in the summer seasons 2016/17 and 2017/18

Mean seasonal ground temperatures on AWS-JGM ranged from 4.3 °C (2016/17) and 3.4 °C (2017/18) at a depth of 5 cm to  $-1.2$  °C (2016/17) and  $-1.4$  °C (2017/18) at a depth of 75 cm. Mean daily temperatures at a depth of 5 cm were mostly positive with the maximum values exceeding 10.0 °C in 2016/17 and 8.0 °C in 2017/18 (Fig. 4a). Isothermal days at a depth of 5 cm occurred only twice in 2016/17, whereas 9 such days were observed in 2017/18 (Table 1). The summer TDD<sub>5</sub> were 398 °C days (2016/17) and 311 °C days (2017/18). The detailed view on the ground thermal regime in January 2018 (Fig. 4a) indicates that the temperature at the depth of 5 cm remained between  $-0.2$  °C and  $-0.3$  °C under the snow cover >10 cm deep. Over the same period, the ground temperature at the depth of 50 cm decreased from positive (0.1 to 0.4 °C) to negative values of  $-0.3$  °C. The snowpack melted earlier at the site of ground temperature measurement than below the ultrasonic snow depth sensor (Fig. 5). Therefore, the ground temperature regime shows positive values with typical daily regime

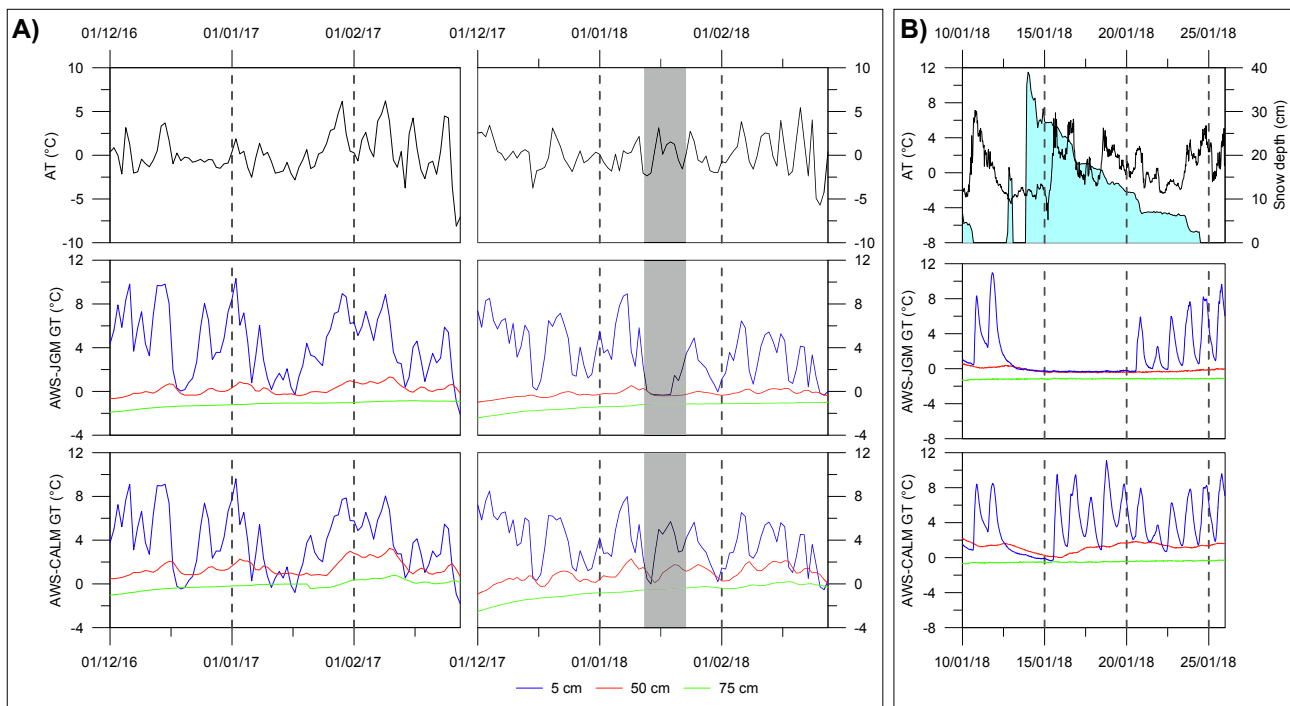


**Fig. 4.** Variability of air temperature (AT) and ground temperatures (GT) at depths of 5, 50 and 75 cm on AWS-JGM and AWS-CALM. Temperatures are presented as daily means of summer seasons 2016/17 and 2017/18 (A) and 30-min records in the period 10 January to 25 January 2018 (B). Grey rectangle in plot A) indicates the period with compact snow cover detected on AWS-JGM.

**Table 1**

Selected thermal characteristics of air temperature (AT) and ground temperature at a depth of 5 cm (GT<sub>5</sub>) on AWS-JGM and AWS-CALM in the summer periods 2016/17 and 2017/18.

| Season  | Period  | AT   | TDD <sub>A</sub> | AWS-JGM         |                  |      | AWS-CALM        |                  |      |
|---------|---------|------|------------------|-----------------|------------------|------|-----------------|------------------|------|
|         |         |      |                  | GT <sub>5</sub> | TDD <sub>5</sub> | ITD* | GT <sub>5</sub> | TDD <sub>5</sub> | ITD* |
| 2016/17 | DJF     | 0.1  | 83               | 4.3             | 398              | 2    | 3.9             | 354              | 0    |
|         | January | 0.2  | 26               | 4.0             | 117              | 0    | 3.5             | 101              | 0    |
| 2017/18 | DJF     | 0.0  | 67               | 3.4             | 311              | 9    | 3.8             | 340              | 1    |
|         | January | -0.1 | 17               | 2.8             | 82               | 9    | 3.7             | 112              | 1    |

\* ITD = isothermal days.

since 21 January, three days before the snow completely melted.

Different pattern of mean seasonal ground temperatures was observed on AWS-CALM. While the temperature at a depth of 5 cm differed only slightly between 3.9 °C (2016/17) and 3.8 °C (2017/18), the differences in the depths of 50 and 75 cm were greater. Observed means were 1.5 °C (2016/17) and 0.9 °C (2017/18) at a depth of 50 cm and -0.1 °C (2016/17) and -0.7 °C (2017/18) at 75 cm. Mean daily temperatures at a depth of 5 cm only rarely dropped below 0 °C (Fig. 4). Their seasonal maximums exceeded 8.5 °C (2016/17) and 6.5 °C (2017/18). Only one isothermal day appeared in the season 2017/18. The summer TDD<sub>5</sub> were 354 °Cdays (2016/17) and 340 °Cdays (2017/18). The ground temperature at the depth of 5 cm dropped to -0.4 °C after the cooling and snowstorm event in January 2018. However, the temperature ranged from 1.2 °C and 11.1 °C for the rest of the period with snow presence on AWS-JGM. The temperature at the depth of 50 cm decreased from 2.2 °C (10 January) to 0.0 °C (16 January), but it increased rapidly up to 2.0 °C (21 January) as the snow cover melted.

#### 4.3. Snow cover at CALM-S JGM site in January 2018

Snowstorm occurred between 13 January 22:00 UTC and 14 January 4:00 UTC. A relatively short period of 6 hr was sufficient to create snow cover that reached a maximum depth of 38 cm at AWS-JGM site. The

most rapid thinning of the snowpack was observed on the 16 January when the snow depth decreased by 8 cm as a result of relatively high air temperatures that reached 6.0 °C in maximum (Fig. 4b). Snow persisted until 24 January when the last shallow snowpack (3 cm) melted (Fig. 4b).

The distribution and thickness of snow were surveyed six days after the snowstorm, when snow cover extent was reduced to 46% of the CALM-S JGM area. The ground plan of the snow patch was complex and snow depth variable (Fig. 5) due to the redistribution by strong wind during the snowstorm and irregular melting after the storm. Snow drift produced irregular pattern of elongated zastrugi features and interleaving troughs with the SW-NE orientation. Owing to the drift, snow depth ranged from 20 to 30 cm on the ridges to less than 5 cm in troughs. While the maximum snow depths determined at probed profiles was 25 cm, the modelled mean snow depth was 10 cm. Within the snow patch, wind-blown ground appeared at seven places that increased rapidly in extent due to the enhanced snowmelt on the margins of bare ground.

#### 4.4. Evolution of ALT during summer seasons 2016/17 and 2017/18

The active layer thawing in 2016/17 begun in early October, while it started around mid-November in 2017/18. The most rapid thawing propagation in the early thawing season at the turn of November and

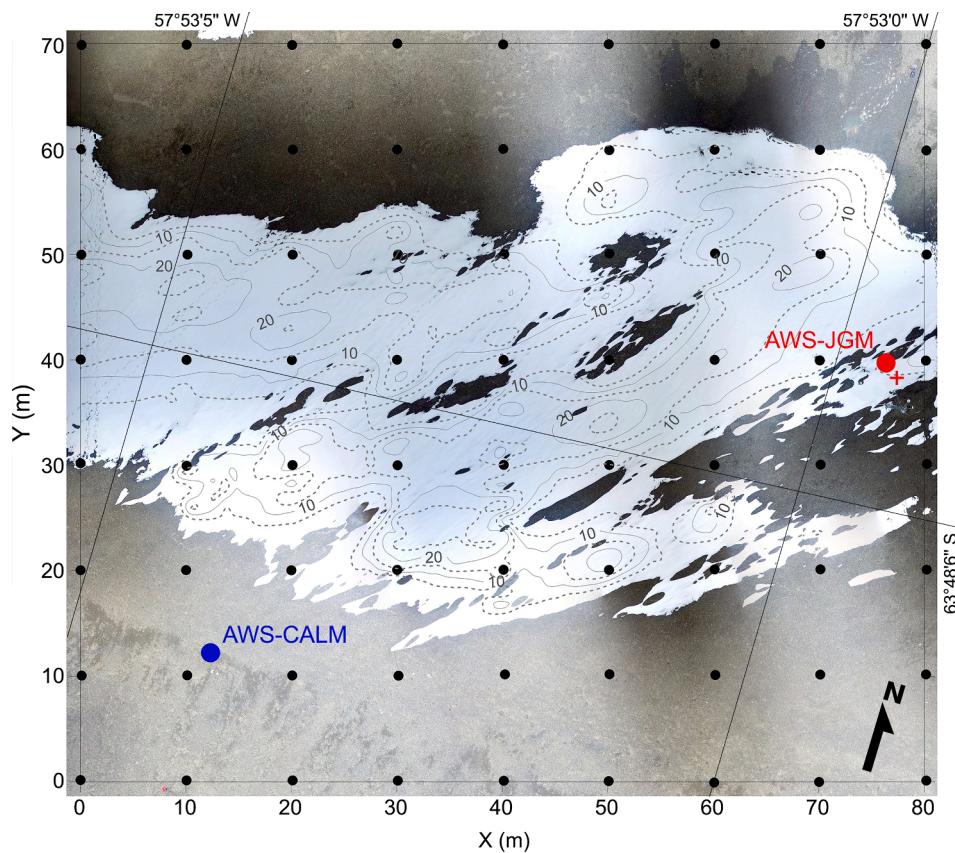


**Fig. 5.** Distribution of snow with 5 cm isohyets of snow depth on CALM-S JGM on 20th January 2018. Black points mark 10 m grid nodes, colour points represent the position of ground temperature measurement profiles AWS-JGM (red) and AWS-CALM (blue), red cross represents the position of snow depth sensor on AWS-JGM. The image was derived from a UAV flight. (For interpretation of the references to colour in this figure legend, the reader is referred to the web version of this article.)

December was connected with a rapid increase in total TDD<sub>5</sub> during this period (Fig. 6). Thaw depths were around 50 cm (AWS-JGM) and 65 cm (AWS-CALM) in mid-December when the thawing propagation started to slow down (Fig. 6). The most pronounced interruption of thawing

progress was observed on AWS-JGM in January 2018 when the active layer refroze completely after a snowstorm. The maximum thicknesses on AWS-JGM reached 66 cm (10 February 2017) and 59 cm (8 January 2018). Observed maximums on AWS-CALM were 90 cm (11 February

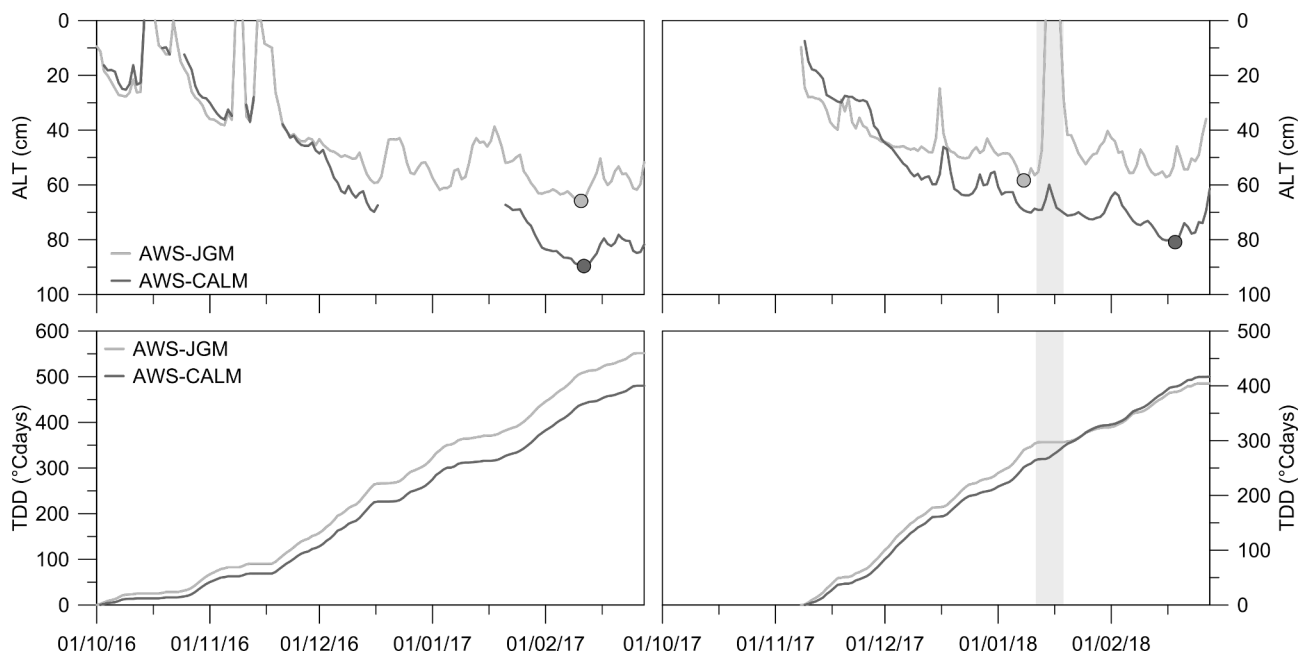


**Fig. 6.** Seasonal evolution of active layer thickness (ALT) and thawing degree days (TDD<sub>5</sub>) on AWS-JGM and AWS-CALM in the seasons 2016/17 and 2017/18. Dots indicate maximum active layer thickness on both AWS sites. Grey rectangle indicates the period with compact snow cover detected on AWS-JGM.

2017) and 81 cm (18 February 2018). Total TDD<sub>5</sub> in thawing seasons reached 552 °C days (2016/17) and 404 °C days (2017/18) on AWS-JGM. The TDD<sub>5</sub> on AWS-CALM were 512 °C days (2016/17) and 416 °C days (2017/18).

The difference in ALT between the two subsequent summer seasons is clearly visible in Fig. 7 that also reveals relatively even thaw plane during the summer 2016/17 and its irregular course in January 2018. The largest interannual difference in thaw depths coincides with those sections of the scanned profiles that were covered with thick continuous snowpack during the January 2018 measurement in profiles X20 and X40 (Fig. 7). Within these sections, the thaw plane is located 20 to 30 cm higher compared to the snow-free parts of the profiles. The thaw plane along the predominantly snow-free profile 70 in January 2018 is more or less parallel to the permafrost table observed in 2017 (Fig. 7). This is also the case of February measurements in all measured profiles. The observed discrepancy between zero thaw depth values (Fig. 6) and detected active layer thickness (Fig. 7) is explained by the fact, that the actual active layer freezing temperature is lower than 0 °C (Fig. 3b, c). Therefore, we were able to detect unfrozen active layer even under negative ground temperature conditions (Fig. 4b).

Spatial distribution of thaw depth for the CALM-S JGM site during the late summer 2016/17 and 2017/18 is illustrated in Fig. 8. Thaw depths were more spatially uniform in February 2017 although two geologically distinct parts of the study area are clearly visible. The bimodal distribution with prevailing lower ALT (less than 80 cm) and

thaw depths as high as 115 cm along the southern margin of the study area have already been observed over the years 2014–16. This large contrast in thaw depth has been tentatively attributed to different grain size distribution and moisture content in two sedimentary units within the study area (Hrbáček et al., 2017). The strongly bimodal pattern can be seen in the 2018 grid that shows even more pronounced difference in thaw depths between the two parts. The region of decreased ALT coincides with maximum snow depths in January 2018 that is also consistent with the difference between mean thaw depths over the period 2014–17 and 2018 grid (Fig. 8D).

## 5. Interpretation and discussion

### 5.1. Climate conditions in the study area in the context of previous years

Air temperatures in the study area during the summer periods 2016/17 and 2017/18 were below long-term (2006–2015) summer average of 0.4 °C reported for the AWS-JGM and nearby Abernethy Flats sites (Hrbáček and Uxa, 2020). Although the lowest mean air temperature on CALM-S site was recorded in the summer 2014/15 (Hrbáček et al., 2017), the lowest TDDA was observed in 2017/18 (Table 2) indicating a decrease in a total number of days with prevailing positive temperatures. The mean summer ground temperatures at a depth of 5 cm were the lowest in the season 2017/18. By contrast to the previous summer seasons when both summer and January ground temperature was 0.1 to

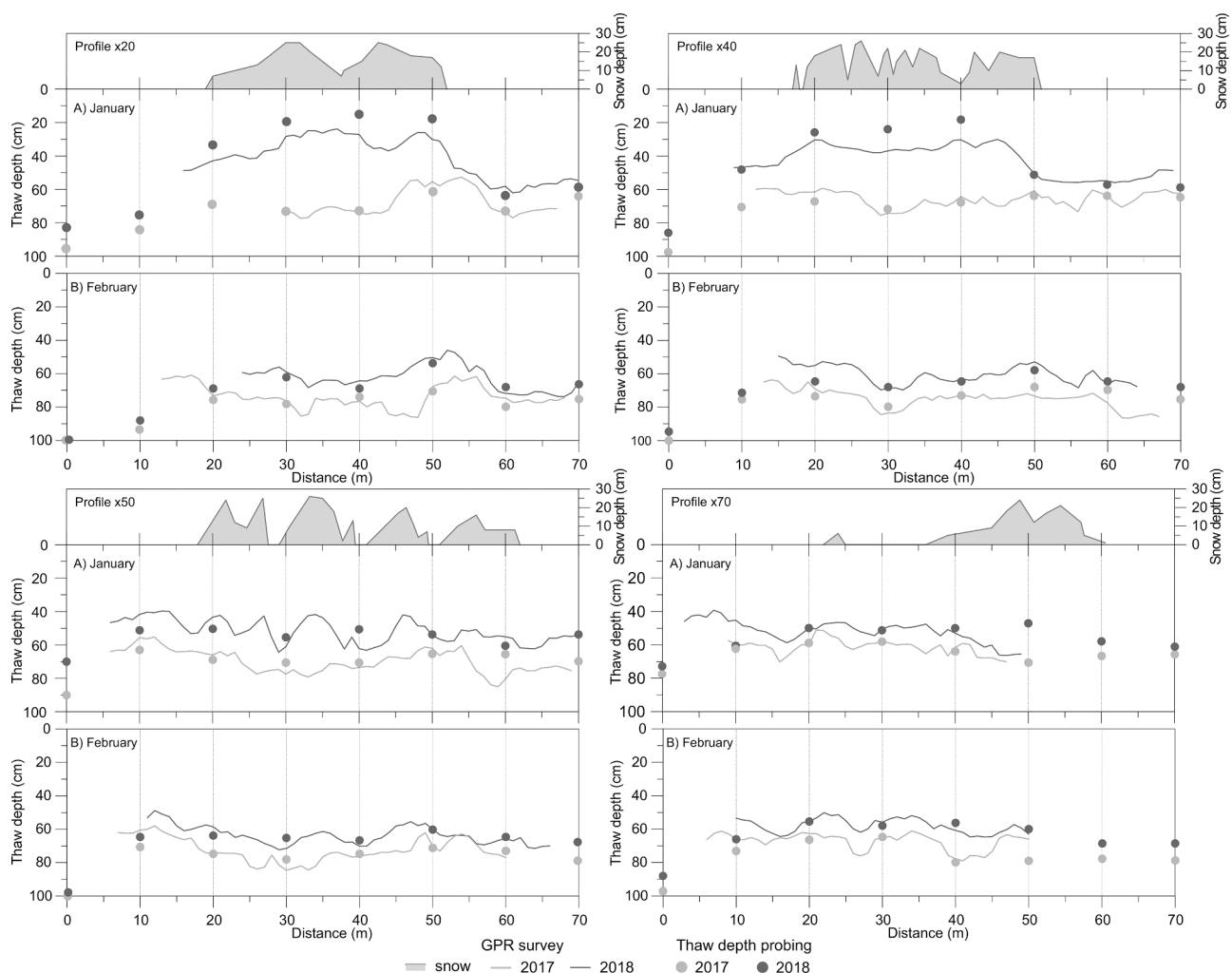
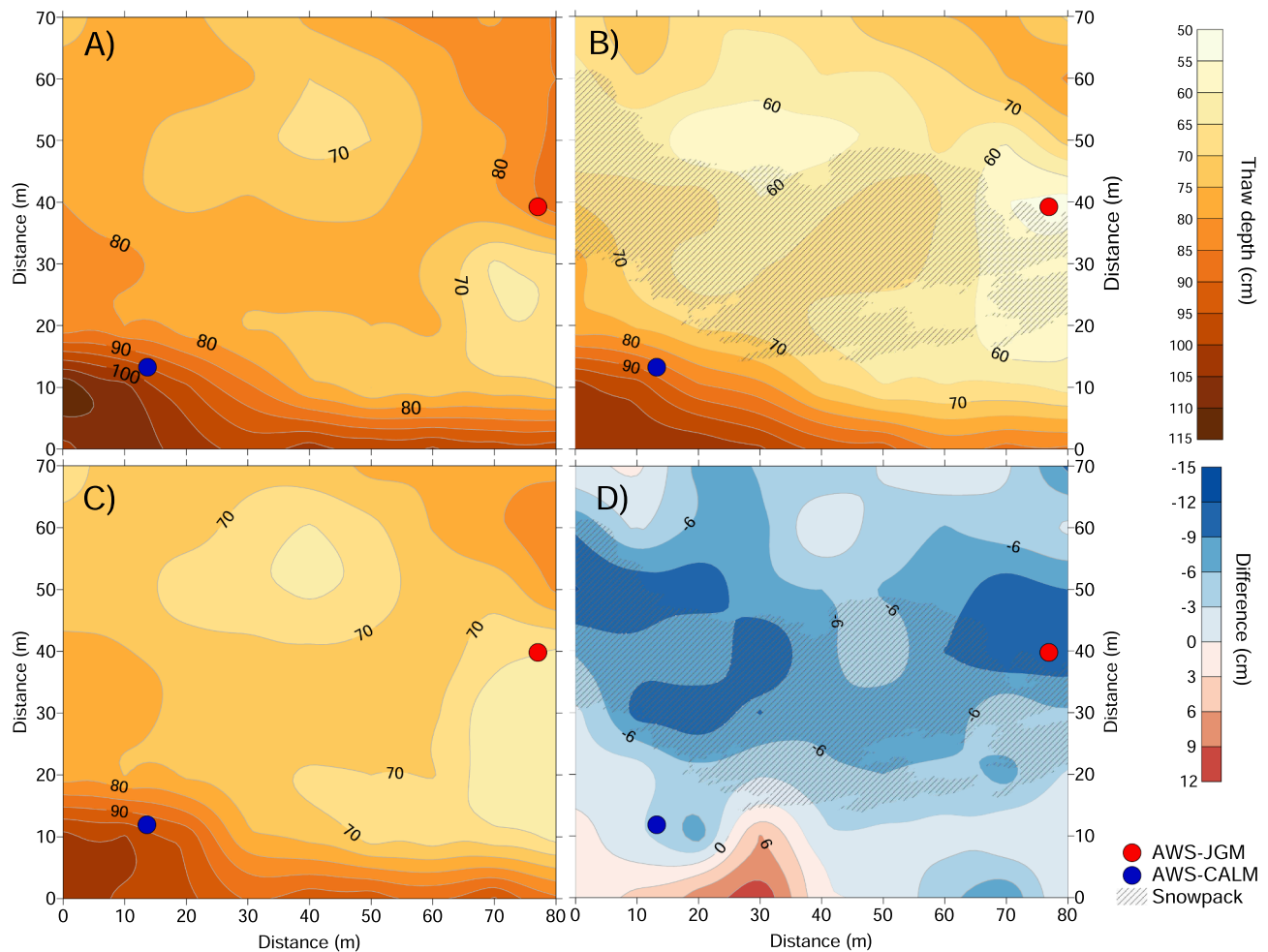


Fig. 7. Snow cover depth (grey polygons) in January 2018 and thaw depths in January and February 2017 and 2018 determined from GPR and probing measurements at CALM-S JGM site.



**Fig. 8.** Spatial variability of thaw depth on CALM-S JGM in A) February 2017, B) February 2018, C) mean thaw depth in the period 2014–2017 and D) difference between February 2018 and the 2014–2017 mean.

**Table 2**

Variability of mean summer (DJF) of air temperature (AT) and ground temperature (GT) at the depth of 5 cm, thawing degree days of ground (TDD<sub>5</sub>) and active layer thickness (ALT) on AWS-JGM and AWS-CALM in the period 2014/15 to 2017/18.

| Season       | AT<br>DJF<br>(°C) | GT<br>DJF<br>AWS-<br>CALM<br>JGM<br>(°C) | GT DJF<br>AWS-<br>CALM<br>JGM<br>(°C) | TDD <sub>5</sub><br>AWS-<br>JGM<br>(°Cdays) | TDD <sub>5</sub><br>AWS-<br>CALM<br>JGM<br>(°Cdays) | ALT<br>AWS-<br>JGM<br>(cm) | ALT<br>AWS-<br>CALM<br>(cm) |
|--------------|-------------------|--|---------------------------------------|---|---|----------------------------|-----------------------------|
| 2014/<br>15* | -0.5              | 4.7                                      | 4.4                                   | 456   | 418   | 63                         | 86                          |
| 2015/<br>16* | 0.4               | 4.7                                      | 4.6                                   | 506   | 478   | 65                         | 87                          |
| 2016/<br>17  | 0.1               | 4.3                                      | 3.9                                   | 552   | 502   | 67                         | 90                          |
| 2017/<br>18  | 0                 | 3.4                                      | 3.8                                   | 404   | 416   | 59                         | 82                          |

\* Data according to Hrbáček et al. (2017).

0.5 °C higher on AWS-JGM than AWS-CALM, we observed opposite pattern during the summer 2017/18. The ground temperature was 0.4 °C (DJF) to 0.9 °C (January) higher on AWS-CALM than AWS-JGM (Fig. 9). We associated this unusual pattern with the presence of snow cover during January 2018 which caused the differences of the mean daily ground temperatures up to 6.0 °C and the 30-min temperatures even up to 11.4 °C (Fig. 4a, b).

Regardless of relatively cold summer ground surface temperatures, the thickest active layer and the highest TDD<sub>5</sub> on both AWS-JGM and AWS-CALM were observed in 2016/17 (Table 2). This was primarily caused by unusually warm spring months (September to November) in the north-eastern part of the AP (Turner et al., 2020). Such conditions favoured early melting of the active layer in the beginning of October which started weeks earlier than usually (Hrbáček et al., 2017; Hrbáček and Uxa, 2020). Sandy soil texture together with lower moisture also supports warmer surficial conditions on AWS-JGM as documented by TDD<sub>5</sub> higher by 28–50 °Cdays than on AWS-CALM. However, TDD<sub>5</sub> were 12 °C days lower in 2017/18 on AWS-JGM than on AWS-CALM (Fig. 9).

### 5.2. Snow cover effect on ground thermal regime

Variations in summer air temperature and the length of the thaw season control ALT but snow cover may reduce it significantly (e.g., Guglielmin, 2004; Zhang, 2005; Guglielmin et al., 2012). While a cooling effect of thick long-lasting snow patches has been reported from different regions including AP (Guglielmin et al., 2014b; Ramos et al., 2017, 2020), the influence of thin snow cover that rapidly builds and melts during the warm period remains poorly known. The ground thaw depths recorded in January 2018 at the CALM-S JGM site demonstrate a decrease in active layer thickness underneath ephemeral snow cover with limited depth that protected the ground surface only for six days prior to ALT measurements. The initial maximum snow depth of 38 cm falls within the range of 30–70 cm that is considered sufficient to isolate the ground from temperature variations (e.g., de Pablo et al., 2017;

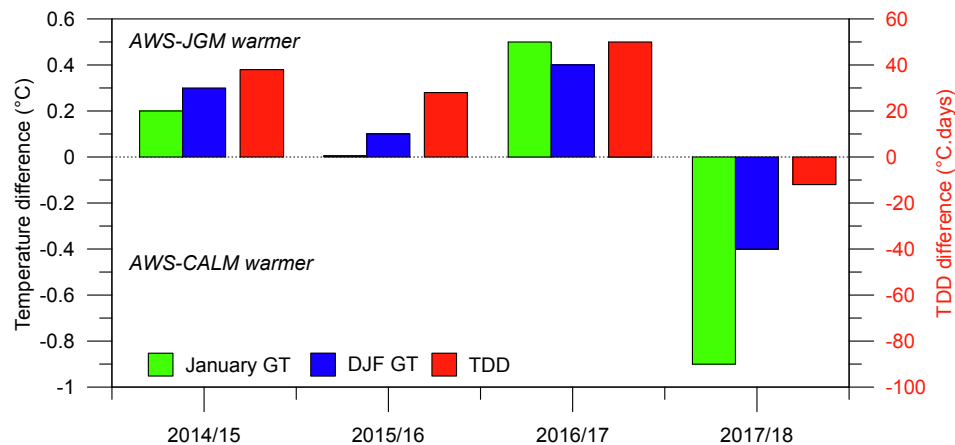


Fig. 9. Difference in ground temperature (GT) and thawing degree days (TDD) between AWS-JGM and AWS-CALM in the period 2014/15 to 2017/18. Data from period 2014/15 and 2015/16 adopted from Hrbáček et al. (2017).

Kňažková et al., 2020). However, the maximum snow depth of 25 cm observed on the CALM-S JGM at the time of ALT measurements indicates much lower snow depth over most of the study area. Considering that ALT thinning was observed far beyond the margin of the snowpack, a mean snow depth of 10 cm has sufficient influence on the ground thermal regime. This value is significantly lower than the effective snow depth of 20 cm considered with respect to the insulation effect of snow in AP region (de Pablo et al., 2016; Oliva et al., 2017a). This suggests that main impact of ephemeral summer snow cover on ground temperature results from the strong reflection of solar radiation due to high albedo of the snow surface rather than from the insulating effect of a thin snowpack.

The largest impact of ephemeral snow cover on thaw depths in the study area can be seen underneath thick continuous snowpack in profiles X20 and X40 (Fig. 7), where active layer thinning reaches 20 to 30 cm. By contrast, a slight overall decrease (lower than 10 cm) in ALT was observed along profile X50 across irregularly thick snowpack with frequent holes and at predominantly snow-free profile X70 (Fig. 7). The difference in thaw depths between snow-covered and bare surface decreases rapidly after the snowmelt. The snow cover disappeared from the study area on 24 January and measurements from 12 February reveal the unimodal distribution of ALT. The rapid restoration of a more or less uniform thaw plane results from the combination of relatively high air temperatures and an enhanced conduction of heat from the ground surface due to meltwater percolation (*sensu* de Pablo et al., 2014; Farzaman et al., 2020). The influence of ephemeral snow cover on thaw depths is apparent in the timing of the maximum ALT on snow-covered and bare sites. Whereas the maximum ALT on snow-affected AWS-JGM site was observed before the snowstorm event on 9 January, the ALT maximum on a snow-free site occurred on 18 February. The later culmination of the thaw depth at the snow-free site coincides well with the timing of the maximum ALT in previous summer seasons which is typically around mid-February (Hrbáček et al., 2017).

The ground temperatures recorded at the CALM-S JGM indicate that ephemeral snow cover may also affect thermal regime of the active layer. As Fig. 4 shows, the presence of snow cover with an initial depth of 38 cm eliminates diurnal temperature fluctuations down to a depth of 50 cm and results in a substantial decrease in the mean daily ground temperatures. The mean monthly ground surface temperature in January is reduced by nearly one degree below the snow cover (with the depth decreasing from 38 to 12 cm over six days) compared to the bare surface (Tables 1 and 2). Although the net cooling effect of ephemeral snow over the summer season is limited, the number of isothermal days increases and TDD<sub>5</sub> are reduced by ca 10% compared to snow-free summer seasons (Tables 1 and 2). This is in line with the reported insulating effect of snow patches that persist over the warm season in

permafrost conditions (de Pablo et al., 2017). Guglielmin et al. (2014b) and Oliva et al. (2017a) reported a cooling of the ground surface and a reduced magnitude of ground temperature fluctuations on Adelaide Island, western AP; and Livingston Island, north-western AP, respectively. De Pablo et al. (2017) observed an increase in the minimum ground surface temperatures below quasi-permanent snow patches on Livingston Island, north-western AP. The observed changes in recorded ground temperatures confirm that the presence of snow cover may be more important for the active layer refreezing and thaw plane position than summer temperatures (Zhang, 2005; de Pablo et al., 2017; Ramos et al., 2017). This also implies that the seasonal active-layer measurement should not be done immediately after summer snowfall events.

### 5.3. Assessment of the results in a wider regional context

The previous studies on JRI considered the winter snowpack as too thin and temporally unstable to create a sufficient insulation layer on the ground (Hrbáček et al., 2016). This is mostly because of dynamic weather conditions during winter and prevailing strong southern winds which remove the snow from flat surfaces resulting in its irregular distribution within the terrain (Kavan et al., 2020). In specific conditions of long-lasting snow accumulations, a snowpack >30 cm deep causes isothermal regime of ground temperature during the winter months (Kňažková et al., 2020).

Most of the studies dealing with relationships between snow and the ground thermal regime in Antarctica are located in the South Shetlands in the north-western AP. The oceanic climate makes this part of AP one of the wettest regions in Antarctica with precipitation rates of >1000 mm yr<sup>-1</sup> (Carrasco and Cordero, 2020). This results in high annual net snow accumulation and snow cover depth, with mean values of about 0.5 m (de Pablo et al., 2017). Such snowpack can cause a significant warming of the ground compared to windswept areas (Oliva et al., 2017a). As the northern AP is located in border conditions between continuous and discontinuous permafrost (Bockheim et al., 2013; Obu et al., 2020), regular and thick snowpack in the winter months can lead to permafrost degradation (Hrbáček et al., 2020). On the other hand, mean annual air temperature has decreased at a statistically significant rate since the beginning of the 20th century, with a most rapid cooling during the summer season (Turner et al., 2016, Oliva et al., 2017b). This was reflected in an increase in the number of snowfall events on the north-western side of the AP since the mid-2010s during the summer period (Carrasco and Cordero, 2020). Despite the fact that the trends in the annual total of precipitation from extreme precipitation events over 1979–2016 are small (Turner et al., 2019), positive trends in the precipitation total and summer snowfall events may result in a more frequent accumulation of ephemeral snow cover with a temporary

cooling effect.

This study brings new insight into the functioning of the snow cover in relation to active layer thickness. So far, the active layer thinning was attributed mostly to long-lasting snow accumulation which prevented active layer thawing during the early warm season. Therefore, its thinning was directly related to the shortening of the thawing season (Ramos et al., 2017; de Pablo et al., 2017). Consequently, the long-term active layer thinning rate was more likely connected with an increased duration of the snow cover in the northwestern AP, rather than with the climate variability during summer months (Ramos et al., 2017, 2020). In other Antarctic regions, like Victoria Land, snowpack can persist for an entire summer and completely prevent active layer thawing (Guglielmin et al., 2014a). However, the ephemeral snowpack's role in summer has not been described yet from neither Antarctic nor Arctic regions. The influence of summer snowfalls and related snowpack on the thermal regime and thickness of the active layer has been reported from alpine areas (Magnin et al., 2017; Zhao et al., 2018; Mena et al., 2021), but snow and ground conditions in the mountains differ strongly from those in high latitudes (Hoelzle and Gruber, 2008). Usually, the period of high summer is characterized by a low snowfall intensity and predominantly bare ground surface in ice-free areas across Antarctica. Therefore, snowfall events leading to an accumulation of >30 cm deep snow cover are scarce in this region and the snow control on ground thermal regime is primarily related to its high albedo.

## 6. Conclusions

This study brings a new perspective on the effect of snow cover on active layer thermal regime and thickness in the Antarctic Peninsula region. The recent research deals mostly with the role of winter or permanent snow cover, whereas the role of ephemeral snow occurring during the high summer was not documented at all in Antarctica. This study shows that even short-term presence of a relatively thick snow cover during the high summer can significantly affect active layer thermal regime and thawing propagation. Considering the observations from 2017/18 within the context of the snow-free seasons with similar air temperature conditions, the ephemeral snow cover considerably affected the ground thermal regime and active layer thickness. The magnitude of the snow insulation effect was controlled by the snow depth and duration of snowpack. The observed snowpack with an initial snow depth of 38 cm lasted for 12 days during the high summer season. Below the ephemeral snow cover, the diurnal temperature fluctuations were limited down to a depth of 50 cm, thaw depths decreased by nearly 20%, the maximum active layer thickness was observed almost six weeks prior to the maximum on a snow-free site, and the mean monthly ground temperature was reduced by nearly one degree compared to the snow-free surface. The number of isothermal days increased and TDD<sub>5</sub> were reduced by ca 10% in the presence of snow cover.

## Declaration of Competing Interest

The authors declare that they have no known competing financial interests or personal relationships that could have appeared to influence the work reported in this paper.

## Acknowledgement

The research was supported by the Ministry of Education, Youth and Sports of the Czech Republic projects LM2015078 and CZ.02.1.01/0.0/0.0/16\_013/0001708; by the Masaryk University project MUNI/A/1517/2020; and by the Czech Science Foundation project GC20-20240S. The authors acknowledge the crew of JGM station, particularly Jakub Ondruch for providing UAV imagery and Kamil Laska for the support on the meteorological measurements setting and maintenance.

## References

- Bockheim, J., Vieira, G., Ramos, M., López-Martínez, J., Serrano, E., Guglielmin, M., Wilhelm, K., Nieuwendam, A., 2013. Climate warming and permafrost dynamics in the Antarctic Peninsula region. *Glob. Planet. Change* 100, 215–223. <https://doi.org/10.1016/j.gloplacha.2012.10.018>.
- Callaghan, T.V., Johansson, M., Brown, R.D., Groisman, P.Y., Labba, N., Radionov, V., Bradley, R.S., Blangy, S., Bulygina, O.N., Christensen, T.R., Colman, J.E., Essery, R.L.H., Forbes, B.C., Forchhammer, M.C., Golubev, V.N., Honrath, R.E., Juday, G.P., Meshcherskaya, A.V., Phoenix, G.K., Pomeroy, J., Rautio, A., Robinson, D.A., Schmidt, N.M., Serreze, M.C., Shevchenko, V.P., Shiklomanov, A.I., Shmakin, A.B., Skold, P., Sturm, M., Woo, M.K., Wood, E.F., 2011. Multiple effects of changes in arctic snow cover. *Ambio* 40, 32–45. <https://doi.org/10.1007/s13280-011-0213-x>.
- Campbell, I.B., Claridge, G.G.C., Campbell, D.I., Balks, M.R., 1998. The Soil Environment of the McMurdo Dry Valleys, Antarctica. In: Prisco, J.C., (Ed.), *Ecosystem Dynamics in a Polar Desert: the McMurdo Dry Valleys, Antarctica*. Am. Geophys. Union, Washington. <https://doi.org/10.1029/AR072p0297>.
- Carrasco, J.F., Cordero, R.R., 2020. Analyzing precipitation changes in the northern tip of the Antarctic Peninsula during the 1970–2019 period. *Atmosphere* 11 (12), 1270. <https://doi.org/10.3390/atmos11121270>.
- Christiansen, H.H., 2004. Meteorological control on interannual spatial and temporal variations in snow cover and ground thawing in two northeast Greenlandic Circumpolar-Active-Layer-Monitoring (CALM) sites. *Permafrost Periglac.* 15, 155–169. <https://doi.org/10.1002/ppp.489>.
- de Pablo, M.A., Ramos, M., Molina, A., 2014. Thermal characterization of the active layer at the Linnopolar Lake CALM-S site on Byers Peninsula (Livingston Island), Antarctica. *Solid Earth* 5, 721–739. <https://doi.org/10.5194/se-5-721-2014>.
- de Pablo, M.A., Ramos, M., Molina, A., Vieira, G., Hidalgo, M.A., Prieto, M., Jiménez, J.J., Fernández, S., Recondo, C., Calleja, J.F., Peón, J.J., Mora, C., 2016. Frozen ground and snow cover monitoring in the South Shetland Islands, Antarctica: instrumentation, effects on ground thermal behaviour and future research. *Cuad. Investig. Geográfica* 42, 475–495.
- de Pablo, M.A., Ramos, M., Molina, A., 2017. Snow cover evolution, on 2009–2014, at the Linnopolar lake CALM-S site on Byers peninsula, Livingston island, Antarctica. *Catena* 149, 538–547. <https://doi.org/10.1016/j.catena.2016.06.002>.
- Draebing, D., Haberkorn, A., Krautblatter, M., Kenner, R., Phillips, M., 2017. Thermal and mechanical responses resulting from spatial and temporal snow cover variability in permafrost rock slopes, Steintaelli. *Swiss Alps. Permafrost Periglac.* 28 (1), 140–157. <https://doi.org/10.1002/ppp.v28.110.1002/ppp.1921>.
- Farzaman, M., Vieira, G., Monteiro Santos, F.A., Yaghoobi Tabar, B., Hauck, C., Catarina Paz, M., Bernardo, I., Ramos, M., Angel De Pablo, M., 2020. Detailed detection of active layer freeze-thaw dynamics using quasi-continuous electrical resistivity tomography (Deception Island, Antarctica). *Cryosphere* 14, 1105–1120. <https://doi.org/10.5194/tc-14-1105-2020>.
- Goodrich, L.E., 1982. The influence of snow cover on the ground thermal regime. *Can. Geotech. J.* 19 (4), 421–432. <https://doi.org/10.1139/82-0407>.
- Guglielmin, M., 2004. Observations on permafrost ground thermal regimes from Antarctica and the Italian Alps, and their relevance to global climate change. *Glob. Planet. Change* 40 (1–2), 159–167. [https://doi.org/10.1016/S0921-8181\(03\)00106-1](https://doi.org/10.1016/S0921-8181(03)00106-1).
- Guglielmin, M., 2006. Ground surface temperature (GST), active layer and permafrost monitoring in continental Antarctica. *Permafrost Periglac.* 17 (2), 133–143. [https://doi.org/10.1002/\(ISSN\)1099-153010.1002/ppp.v17.210.1002/ppp.553](https://doi.org/10.1002/(ISSN)1099-153010.1002/ppp.v17.210.1002/ppp.553).
- Guglielmin, M., Cannone, N., 2012. A permafrost warming in a cooling Antarctica? *Clim. Change* 111 (2), 177–195. <https://doi.org/10.1007/s10584-011-0137-2>.
- Guglielmin, M., Worland, M.R., Cannone, N., 2012. Spatial and temporal variability of ground surface temperature and active layer thickness at the margin of maritime Antarctica, Signy Island. *Geomorphology* 155, 20–33. <https://doi.org/10.1016/j.geomorph.2011.12.016>.
- Guglielmin, M., Dalle Fratte, M., Cannone, N., 2014a. Permafrost warming and vegetation changes in continental Antarctica. *Environ. Res. Lett.* 9 (4), 045001. <https://doi.org/10.1088/1748-9326/9/4/045001>.
- Guglielmin, M., Worland, M.R., Baio, F., Convey, P., 2014b. Permafrost and snow monitoring at Rothera Point (Adelaide Island, Maritime Antarctica): implications for rock weathering in cryotic conditions. *Geomorphology* 225, 47–56. <https://doi.org/10.1016/j.geomorph.2014.03.051>.
- Hanson, S., Hoelzle, M., 2004. The thermal regime of the active layer at the Murtèl rock glacier based on data from 2002. *Permafrost Periglac.* 15 (3), 273–282. [https://doi.org/10.1002/\(ISSN\)1099-153010.1002/ppp.v15.310.1002/ppp.499](https://doi.org/10.1002/(ISSN)1099-153010.1002/ppp.v15.310.1002/ppp.499).
- Harris, C., Arenson, L.U., Christiansen, H.H., Etzelmüller, B., Frauenfelder, R., Gruber, S., Haerberli, W., Hauck, C., Hölzle, M., Humlum, O., Isaksen, K., Käab, A., Kern-Lütschg, M.A., Lehning, M., Matsuoka, N., Murton, J.B., Nötzli, J., Phillips, M., Ross, N., Seppälä, M., Springman, S.M., Vonder Mühll, D., 2009. Permafrost and climate in Europe: monitoring and modelling thermal, geomorphological and geotechnical responses. *Earth-Science Rev.* 92 (3), 117–171. <https://doi.org/10.1016/j.earscirev.2008.12.002>.
- Harris, S.A., Corte, A.E., 1992. Interactions and relations between mountain permafrost, glaciers, snow and water. *Permafrost Periglac.* 3 (2), 103–110. [https://doi.org/10.1002/\(ISSN\)1099-153010.1002/ppp.v3.210.1002/ppp.3430030207](https://doi.org/10.1002/(ISSN)1099-153010.1002/ppp.v3.210.1002/ppp.3430030207).
- Harris, S.A., Brouckov, A., Guodong, C., 2018. *Geocryology: Characteristics and Use of Frozen Ground and Permafrost Landforms*. CRC Press, London, p. 765.
- Hinkel, K.M., Hurd, J.K., 2006. Permafrost destabilization and thermokarst following snow fence installation, Barrow, Alaska, USA. *Arct. Antarct. Alp. Res.* 38 (4), 530–539. [https://doi.org/10.1657/1523-0430\(2006\)38\[530:PDATFS\]2.0.CO;2](https://doi.org/10.1657/1523-0430(2006)38[530:PDATFS]2.0.CO;2).
- Hoelzle, M., Gruber, S., 2008. Borehole and ground surface temperatures and their relationship to meteorological conditions in the Swiss Alps. In: Kane, D.L., Hinkel, K.

- M. (Eds.), 9th International Conference on Permafrost, 29 June – 03 July 2008, Fairbanks, Alaska. Institute of Northern Engineering, Fairbanks, pp. 723–728. <https://doi.org/10.5167/uzh-2825>.
- Hoelzle, M., Haeberli, W., Stocker-Mittaz, C., 2003. Miniature ground temperature data logger measurements 2000–2002 in the Murtèl-Corvatsch area. In: Phillips, M., Springman, S., Arenson, L. (Eds.), Proceedings of the 8th International Conference on Permafrost. Swets & Zeitlinger, Lisse, pp. 419–424.
- Hrbáček, F., Láška, K., Engel, Z., 2016. Effect of snow cover on the active-layer thermal regime – a case study from James Ross Island, Antarctic Peninsula. *Permafrost Periglac.* 27 (3), 307–315. <https://doi.org/10.1002/ppp.v27.310.1002/ppp.1871>.
- Hrbáček, F., Kňazková, M., Nývlt, D., Láška, K., Mueller, C.W., Ondruch, J., 2017. Active layer monitoring at CALM-S site near J.G. Mendel station, James Ross Island, eastern Antarctic Peninsula. *Sci. Total Environ.* 601–602, 987–997. <https://doi.org/10.1016/j.scitotenv.2017.05.266>.
- Hrbáček, F., Nývlt, D., Láška, K., Kňazková, M., Kampová, B., Engel, Z., Oliva, M., Mueller, C.W., 2019. Permafrost and active layer research on James Ross Island: An overview. *Czech Polar Reports* 9 (1), 20–36. <https://doi.org/10.5817/CPR2019-1-3>.
- Hrbáček, F., Oliva, M., Fernández, J.-R., Kňazková, M., de Pablo, M.A., 2020. Modelling ground thermal regime in bordering (dis)continuous permafrost environments. *Environ. Res.* 181, 108901. <https://doi.org/10.1016/j.envres.2019.108901>.
- Hrbáček, F., Uxa, T., 2020. The evolution of a near-surface ground thermal regime and modelled active-layer thickness on James Ross Island, Eastern Antarctic Peninsula, in 2006–2016. *Permafrost Periglac.* 31, 141–155. <https://doi.org/10.1002/ppp.2018>.
- Johansson, M., Callaghan, T.V., Bosiò, J., Åkerman, H.J., Jackowicz-Korczynski, M., Christensen, T.R., 2013. Rapid responses of permafrost and vegetation to experimentally increased snow cover in sub-arctic Sweden. *Environ. Res. Lett.* 8 (3), 035025. <https://doi.org/10.1088/1748-9326/8/3/035025>.
- Jol, H.M., Bristow, C.S., 2003. GPR in sediments: advice on data collection, basic processing and interpretation, a good practice guide. In: Bristow, C.S., Jol, H.M. (Eds.), *Ground Penetrating Radar in Sediments*. Geol. Soc. Spec. Publ., London, pp. 9–27. <https://doi.org/10.1144/GSL.SP.2001.211.01.02>.
- Judd Communications, 2011. Judd Communications Depth Sensor. Available at: <http://static1.1.sqspcdn.com/static/f/1146254/15414722/1322862508567/ds2m anual.pdf>. (accessed 31 January 2020).
- Kavan, J., Nývlt, D., Láška, K., Engel, Z., Kňazková, M., 2020. High-latitude dust deposition in snow on the glaciers of James Ross Island, Antarctica. *Earth Surf. Proc. Land.* 45 (7), 1569–1578. <https://doi.org/10.1002/esp.v45.710.1002/esp.4831>.
- Knapp, R.W., 1990. Vertical resolution of thick beds, thin beds and thin-bed cyclothem. *Geophysics* 55 (9), 1183–1190. <https://doi.org/10.1190/1.1442934>.
- Kňazková, M., Hrbáček, F., Kavan, J., Nývlt, D., 2020. Effect of hyaloclastite breccia boulders on meso-scale periglacial-aeolian landsystem in semi-arid antarctic environment, James Ross Island, Antarctic Peninsula. *Geogr. Res. Lett.* 46, 7–31.
- Luetschg, M., Lehning, M., Haeberli, W., 2008. A sensitivity study of factors influencing warm/thin permafrost in the Swiss Alps. *J. Glaciol.* 54 (187), 696–704. <https://doi.org/10.3189/002214308786570881>.
- Luo, T.X.H., Lai, W.W.L., Chang, R.K.W., Goodman, D., 2019. GPR imaging criteria. *J. Appl. Geophys.* 165, 37–48. <https://doi.org/10.1016/j.jappgeo.2019.04.008>.
- Magnin, F., Westermann, S., Pogliotti, P., Ravanel, L., Deline, P., Malet, E., 2017. Snow control on active layer thickness in steep alpine rock walls (Aiguille du Midi, 3842 m a.s.l., Mont Blanc massif). *Catena* 149 (2), 648–662. <https://doi.org/10.1016/j.catena.2016.06.006>.
- MALÁ GeoScience, 2005. Ramac GPR. Hardware manual. Malá: MALÁ GeoScience.
- Mena, G., Yoshikawa, K., Schorghofer, N., Pastén, C., Ochoa, F.A., Yoshii, Y., Doi, M., Miyata, T., Takahashi, H., Casassa, G., Sone, T., 2021. Freeze–thaw cycles and snow impact at arid permafrost region in Chajnantor Volcano, Atacama, northern Chile. *Arct. Antarct. Alp. Res.* 53 (1), 60–66. <https://doi.org/10.1080/15230430.2021.1878739>.
- Obu, J., Westermann, S., Vieira, G., Abramov, A., Balks, M.R., Bartsch, A., Hrbáček, F., Kääh, A., Ramos, M., 2020. Pan-Antarctic map of near-surface permafrost temperatures at 1 km<sup>2</sup> scale. *Cryosphere* 14, 497–519. <https://doi.org/10.5194/tc-14-497-2020>.
- Oliva, M., Hrbáček, F., Ruiz-Fernández, J., de Pablo, M.Á., Vieira, G., Ramos, M., Antoniadis, D., 2017a. Active layer dynamics in three topographically distinct lake catchments in Byers Peninsula (Livingston Island, Antarctica). *Catena* 149, 548–559. <https://doi.org/10.1016/j.catena.2016.07.011>.
- Oliva, M., Navarro, F., Hrbáček, F., Hernández, A., Nývlt, D., Perreira, P., Ruiz-Fernández, J., Trigo, R., 2017b. Recent regional climate cooling on the Antarctic Peninsula and associated impacts on the cryosphere. *Sci. Total Environ.* 580, 210–223. <https://doi.org/10.1016/j.scitotenv.2016.12.030>.
- Palermo, C., Genthon, C., Claud, C., Kay, J.E., Wood, N.B., L'Ecuyer, T., 2017. Evaluation of current and projected Antarctic precipitation in CMIP5 models. *Clim. Dyn.* 48 (1–2), 225–239. <https://doi.org/10.1007/s00382-016-3071-1>.
- Park, Hotaek, Fedorov, Alexander N., Zheleznyak, Mikhail N., Konstantinov, Pavel Y., Walsh, John E., 2015. Effect of snow cover on pan-Arctic permafrost thermal regimes. *Clim. Dyn.* 44 (9–10), 2873–2895. <https://doi.org/10.1007/s00382-014-2356-5>.
- Ramos, M., Vieira, G., de Pablo, M.A., Molina, A., Abramov, A., Goyanes, G., 2017. Recent shallowing of the thaw depth at Crater Lake, Deception Island, Antarctica (2006–2014). *Catena* 149 (2), 519–528. <https://doi.org/10.1016/j.catena.2016.07.019>.
- Ramos, M., Vieira, G., de Pablo, M.A., Molina, A., Jimenez, J.J., 2020. Transition from a Subaerial to a Subnival Permafrost Temperature Regime Following Increased Snow Cover (Livingston Island, Maritime Antarctic). *Atmosphere* 11, 1332. <https://doi.org/10.3390/atmos11121332>.
- Sandmeier, K.J., 2017. Reflexw Processing Program for Seismic, Acoustic and Electromagnetic Reflection, Refraction and Transmission Data, Version 8.5. Sandmeier Scientific Software, Karlsruhe.
- Turner, J., Lu, H., White, I., King, J.C., Phillips, T., Hosking, J.S., Bracegirdle, T.J., Marshall, G.J., Mulvaney, R., Deb, P., 2016. Absence of 21st century warming on Antarctic Peninsula consistent with natural variability. *Nature* 535 (7612), 411–415. <https://doi.org/10.1038/nature18645>.
- Turner, J., Phillips, T., Thamban, M., Rahaman, W., Marshall, G.J., Wille, J.D., Favier, V., Winton, V. H.L., Thomas, E., Wang, Z., Broeke, M., Hosking, J.S., Lachlan-Cope, T., 2019. The dominant role of extreme precipitation events in Antarctic snowfall variability. *Geophys. Res. Lett.* 46 (6), 3502–3511. <https://doi.org/10.1029/2018GL081517>.
- Turner, J., Marshall, G.J., Clem, K., Colwell, S., Phillips, T., Lu, H., 2020. Antarctic temperature variability and change from station data. *Int. J. Climatol.* 40 (6), 2986–3007. <https://doi.org/10.1002/joc.v40.610.1002/joc.6378>.
- van Wessem, J.M., Ligtenberg, S.R.M., Reijmer, C.H., van de Berg, W.J., van den Broeke, M.R., Barrand, N.E., Thomas, E.R., Turner, J., Wuite, J., Scambos, T.A., van Meijgaard, E., 2016. The modelled surface mass balance of the Antarctic Peninsula at 5.5 km horizontal resolution. *Cryosphere* 10, 271–285. <https://doi.org/10.5194/tc-10-271-2016>.
- Zhang, T., 2005. Influence of the seasonal snow cover on the ground thermal regime: An overview. *Rev. Geophys.* 43, RG4002. <https://doi.org/10.1029/2004RG000157>.
- Zhao, J.Y., Chen, J., Wu, Q.B., Hou, X., 2018. Snow cover influences the thermal regime of active layer in Urumqi River Source, Tianshan Mountains. *China. J. Mt. Sci.* 15 (12), 2622–2636. <https://doi.org/10.1007/s11629-018-4856-y>.

## Variability of soil moisture on three sites in the Northern Antarctic Peninsula in 2022/23

Filip Hrbáček<sup>1\*</sup>, Michaela Kňazková<sup>1</sup>, Mohammad Farzamian<sup>2,3</sup>, Joana Baptista<sup>3</sup>

<sup>1</sup>*Polar-Geo-Lab, Department of Geography, Masaryk University, Kotlářská 2, 611 37 Brno, Czech Republic*

<sup>2</sup>*Instituto Nacional de Investigação Agrária e Veterinária (INIAV), 2780-157 Oeiras, Portugal*

<sup>3</sup>*Centro de Estudos Geográficos, IGOT - Universidade de Lisboa, Portugal*

### Abstract

Soil moisture represents one of the crucial parameters of the terrestrial environments in Antarctica. It affects the biological abundance and also the thermal state of the soils. In this study, we present one year of volumetric water content and soil temperature measurements on James Ross Island, Nelson Island and King George Island. The volumetric water content at all sites increased with depth. The mean summer values were between 0.24 and 0.37 cm<sup>3</sup>/cm<sup>3</sup> (James Ross Island), 0.30 and 0.40 cm<sup>3</sup>/cm<sup>3</sup> (Nelson Island) and 0.11 and 0.36 cm<sup>3</sup>/cm<sup>3</sup> (King George Island). We found that the freezing point of the soils was close to 0°C on Nelson Island and King George Island. We attributed the lower temperature of soil freezing around -0.5°C on James Ross Island to the site location close to the sea. Even though the sites are located in the distinctive climate zones and comprise of contrasting soil types, the only differences of moisture regime were observed the surficial layer of the studied sites.

**Key words:** soil moisture, soil thermal regime, permafrost, freeze-thaw processes

**DOI:** 10.5817/CPR2023-1-2

### Introduction

Antarctic terrestrial environments occupy only about 0.5% of the whole continent (Brooks et al. 2019). One of the most important parameters which can affect ecological and geomorphological processes in these areas is the availability of liquid water in the summer months.

Soil moisture is an important parameter driving the dynamics of the periglacial environment. Many of the geomorphological landforms and features are the result of frost weathering or freeze-thaw processes. Moreover, soil moisture acts as an important driver affecting soil thermal regime,

---

Received June 17, 2023, accepted August 22, 2023.

\*Corresponding author: F. Hrbáček <hrbacekfilip@gmail.com>

*Acknowledgements:* This work was supported by Czech Scientific Foundation project (GM22-28659M) and Czech Antarctic Research Programme funded by MEYS of Czech Republic and Thawimpact project (2022.06628.PTDC) funded by Fundação para a Ciência e a Tecnologia of Portugal. We acknowledge Ondřej Zvěřina and Christopher Stringer for the annual maintenance of the site on Nelson Island.

heat transfer and active layer seasonal thawing (*e.g.* Farouki 1981, Clayton *et al.* 2021). Even though an increase of soil moisture usually leads to an increase in soil thermal conductivity (*e.g.* Farouki 1981, Abu-Hamdeh and Reeder 2000, Wessolek *et al.* 2023), it increases the amount of latent heat necessary for the phase change at the same time. As a consequence, the active layer tends to be thinner under moist conditions (*e.g.* Clayton *et al.* 2021).

Besides being an important land-forming parameter, soil moisture is obviously one of the most important ecological factors and one of the major drivers of the Antarctic vegetation abundance (Kennedy 1993, Ugolini and Bockheim 2008, Royles *et al.* 2013, Guglielmin *et al.* 2014). Yet, the particular limits of soil water content and seasonal dynamics favouring vegetation presence are unknown. The shortage of available liquid water can lead to a rapid worsening of vegetation condition as was observed over a 13-year period in East Antarctica (Robinson *et al.* 2018).

The knowledge on soil moisture in Antarctica is mostly limited to the area of McMurdo Dry Valleys where general soil research is carried out in the last few decades (*e.g.* Hrbáček *et al.* 2023). The vast majority of soils in the McMurdo region are very dry with water content lower than 5% (Seybold *et al.* 2010). The zones with a clearly distinguishable moisture regime are

called water tracks and form specific ecosystems of the McMurdo region promoting also the abundance of biota or microbial diversity (Levy *et al.* 2011, Wlostowski *et al.* 2018, George *et al.* 2021). In the Antarctic Peninsula region, soil moisture was monitored on some sites in the South Shetlands area. Higher moisture content was observed on sites below vegetation as compared to bare ground on King George Island (Almeida *et al.* 2014). On Robert Island, moisture content was identified as an important factor affecting the variability of soil CO<sub>2</sub> flux (Thomazini *et al.* 2020).

A thorough examination of soil moisture variability therefore represents one of the challenges and an important step for the advance in Antarctic soil research in general (Horrocks *et al.* 2020, Hrbáček *et al.* 2023). The aim of our study is to evaluate the general patterns and variability of volumetric soil water content (VWC) measured on three sites with diverse climate conditions and lithological properties in the northern Antarctic Peninsula region (James Ross Island, Nelson Island and King George Island) in the period 2022-2023. Particularly we focus on:

- 1) Assessment of seasonal variability of soil moisture on each site;
- 2) Evaluation of vertical changes of soil moisture;
- 3) Determination of freeze-thaw behaviour of soils.

## Study sites

The study sites are located on James Ross Island in the north-eastern part of Antarctic Peninsula region and on Nelson Island and King George Island in the South Shetlands (Fig. 1). There is a climate contrast between the study sites. The South Shetlands have oceanic climate with a mean annual air temperature around -2.0°C (*e.g.* Turner *et al.* 2020) and annual precipitation around 500-1000 mm, during

summer even in the liquid form (*e.g.* Kejna *et al.* 2013). In contrast, the climate conditions on James Ross Island are semi-arid polar continental with mean annual temperature around -6.0°C (Kaplan Pastířiková *et al.* 2023) and the precipitation estimated between 300 and 700 mm, mostly in the snowy form (van Wessem *et al.* 2016).

### James Ross Island

Located off the north-eastern coast of the Antarctic Peninsula, James Ross Island has a total area of approximately 2400 km<sup>2</sup>, a quarter of which is currently ice-free. The largest continuous ice-free area on the island and also within the whole northern Antarctic Peninsula region is called the Ulu Peninsula and extends over 300 km<sup>2</sup> in the northern part of James Ross Island. The deglaciation of this part of James Ross Island dates to around 12 900 ka ago (Nývlt et al. 2014). The area is underlain by continuous permafrost, thickness of which

has been estimated to 67 meters (Borzotta and Trombotta 2004).

The study site is located approximately 100 meters from the Czech Antarctic research station Johann Gregor Mendel in the northern coast of the Ulu Peninsula. It is situated on a Holocene marine terrace, overlying the Cretaceous sedimentary rocks of Whisky Bay Formation ([1]), characteristic by predominantly flat or gently sloping terrain. The soil is comprised of a loose, fine-grained sediment of prevailing sandy texture (Stachoň et al. 2014).

### Nelson Island

The total area of Nelson Island is 165 km<sup>2</sup>, of which 95% is covered by ice sheet and only around 8 km<sup>2</sup> is ice-free, scattered into multiple small ice-free areas along the coast. One of the ice-free areas, the Stansbury Peninsula, is located in the northern part of Nelson Island and covers approximately 2.89 km<sup>2</sup> (Meier et al. 2023). Nelson Island lies in the zone of sporadic permafrost (Bockheim et al. 2013), with mean annual ground temperatures around 0°C (Obu et al. 2020).

The study site is located in the central

part of the Stansbury Peninsula, on a plateau with multiple lakes. The closest lake is ca. 50 m far from the study site. Geologically, the area is formed by volcanic rocks, mainly basalts, andesites and tuffs (Smellie et al. 1984). The relief of the interior part of Stansbury Peninsula forms a transition between paraglacial and periglacial domain, with moraines, lakes and patterned ground as dominant landforms. Soils in the study area are classified as clay loam to sandy loam with low organic matter content (Meier et al. 2023).

### King George Island

Barton Peninsula is the second largest ice-free area of King George Island with an area of 10 km<sup>2</sup> and was exposed after the retreat of Collins Glacier that started at 15 ka ago (Oliva et al. 2019). The exposed surface is composed of stratified volcanic rocks (andesites) and a plutonic intrusion (Birkenmajer 1989, Hwang et al. 2011).

The study site is located approximately 20 meters away from the King Sejong Station borehole, which was installed at 127 m a.s.l. in bedrock and reaches a depth of 13 meters. It is also situated in close proximity to the Automated Electrical Re-

sistivity Tomography (A-ERT) setup aimed to the detection of active layer freeze–thaw dynamics using quasi-continuous electrical resistivity tomography (Farzamian et al. 2020). The ground itself is composed of a diamicton, featuring angular boulders and gravels embedded in a sandy-silty matrix. Periglacial processes occur with the formation of stone circles, solifluction lobes, and striped ground. Based on the A-ERT data (Farzamian et al. 2020), the estimated thickness of the active layer in the soils is approximately 1–1.5 meters.

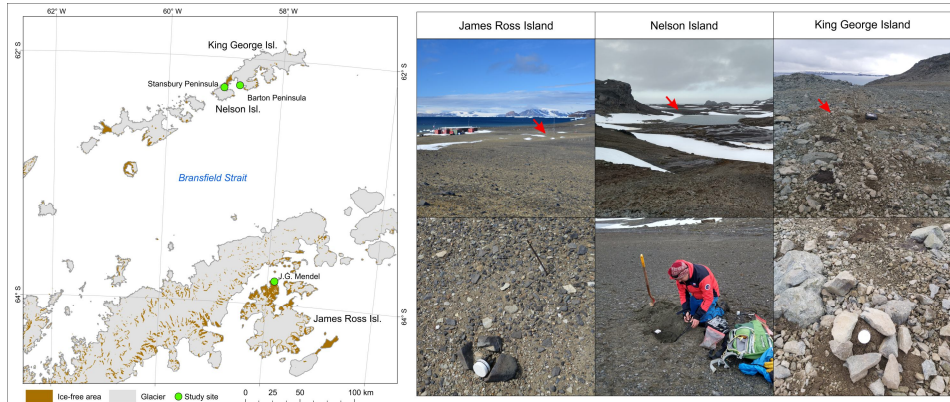


**Fig. 1.** Regional setting and study sites.

## Methods

We used VWC data from three profiles located on James Ross Island, Nelson Island and King George Island (Fig. 1, Table 1). At all sites, VWC was measured by three time-domain reflectometry sensors CS655 (Campbell Sci.) with an accuracy of  $\pm 3\%$  placed at different depths connected to Microlog SDI-MP datalogger (EMS Brno). The measurement and storing interval was 60 minutes. With the respect to the local conditions, the sensors were installed both in horizontal and vertical position (Table 1). Besides VWC, the CS655 sensors also provide data of soil temperature with an accuracy between  $\pm 0.1^\circ\text{C}$  (range  $0^\circ\text{C}$  to  $+40^\circ\text{C}$ ) and  $\pm 0.5^\circ\text{C}$  (full temperature range).

The daily VWC data are represented by a single measurement obtained at 16:00 UTC, which corresponds to the midday in local time of the study sites. The VWC variability was studied only for the unfrozen conditions defined by the mean daily ground temperature  $> 0^\circ\text{C}$ . In case of frozen ground (ground temperature  $< 0^\circ\text{C}$ ), we consider VWC as approximate value of unfrozen water content (*e.g.* Zhou *et al.* 2014)

Finally, we used hourly data of VWC and ground temperature to construct the soil freezing curve for both phases of soil freezing and soil thawing at the bottom-most sensors.

| Study site                | Installation depth [cm]   | Measurement period | Elevation |
|---------------------------|---|--------------------|-----------|
| <b>James Ross Island</b>  | $5^{\text{h}}$ , $30^{\text{h}}$ , $50^{\text{h}}$ cm                       | 1/1/2022–28/2/2023 | 10 m      |
| <b>Nelson Island</b>      | $5^{\text{h}}$ , $20\text{--}30^{\text{v}}$ , $50\text{--}60^{\text{v}}$ cm | 1/1/2022–2/2/2023  | 30 m      |
| <b>King George Island</b> | $10^{\text{h}}$ , $20\text{--}30^{\text{v}}$ , $60^{\text{h}}$ cm           | 23/2/2022–7/2/2023 | 127 m     |

**Table 1.** Description of the study sites. *Note:* <sup>h</sup> – horizontal placement of the sensor, <sup>v</sup> – vertical placement of the sensor.

## Results

### *Variability of soil moisture and temperature*

#### **James Ross Island**

Mean VWC on James Ross Island within the study period for the unfrozen soil was  $0.24 \text{ cm}^3/\text{cm}^3$  in 5 cm depth, ranging from the minimum of 0.13 to the maximum of  $0.30 \text{ cm}^3/\text{cm}^3$ . Both the mean and the minimum and maximum values increase with depth, so that in 50 cm depth, mean VWC reached  $0.33 \text{ cm}^3/\text{cm}^3$  and the minimum and maximum were 0.28 and  $0.37 \text{ cm}^3/\text{cm}^3$ , respectively. The amplitude between the minimum and maximum decreased with depth, from  $0.17 \text{ cm}^3/\text{cm}^3$  in 5 cm depth to  $0.09 \text{ cm}^3/\text{cm}^3$  in 50 cm depth (Table 2).

Ground temperature in 2022 reached an average of  $-3.22^\circ\text{C}$  at 5 cm below surface and decreased with depth to  $-3.79^\circ\text{C}$  at 50 cm depth. Maximum and minimum temperatures of  $10.5^\circ\text{C}$  and  $-21.1^\circ\text{C}$ , respectively, were observed close to ground surface at 5 cm depth, with temperature amplitude spanning over  $31^\circ\text{C}$ . The absolute value of recorded temperature extremes decreased with depth as well as the amplitude between maximum and minimum (Table 3). The thawing period of 2021/2022 ended on March 13<sup>th</sup>, while the thawing period of 2022/2023 began on November 6<sup>th</sup>.

#### **Nelson Island**

Closely below ground surface at 5 cm depth, mean VWC on Nelson Island reached  $0.30 \text{ cm}^3/\text{cm}^3$  and increased with depth, to  $0.34 \text{ cm}^3/\text{cm}^3$  in 20–30 cm and  $0.40 \text{ cm}^3/\text{cm}^3$  in 50 cm depth. The maximum observed in 5 and 20–30 cm depths were similar to each other, while in 50 cm depth the maximum was higher and reached  $0.51 \text{ cm}^3/\text{cm}^3$ . The amplitude of fluctuations in VWC decreased with depth, with over  $0.32 \text{ cm}^3/\text{cm}^3$  in 5 cm to approximately  $0.20 \text{ cm}^3/\text{cm}^3$  in 50 cm depth (Table 2).

Mean annual ground temperatures in 2022 were above  $0^\circ\text{C}$  throughout the whole profile, ranging from  $0.3^\circ\text{C}$  at 5 cm depth to  $0.1^\circ\text{C}$  in 50 cm depth. The absolute value of maximum and minimum observed temperature decreased with depth, same as the amplitude of temperature fluctuations, from over  $15^\circ\text{C}$  on top to approximately  $6^\circ\text{C}$  in the bottom part of the profile (Table 3). The thawing period of 2021/2022 ended on April 25<sup>th</sup>, 2022 and the thawing period of 2022/2023 began on November 18<sup>th</sup>, 2022.

#### **King George Island**

Mean VWC in 10 cm depth on King George Island site was  $0.11 \text{ cm}^3/\text{cm}^3$  and exhibited pronounced differences between the upper and lower layers of soil, with mean VWC more than three times higher at 60 cm depth ( $0.36 \text{ cm}^3/\text{cm}^3$ ). The amplitude of the fluctuations was highest in 20–30 cm depth, with maximum and minimum values of 0.39 and  $0.08 \text{ cm}^3/\text{cm}^3$ ,

respectively. In contrast, the difference between maximum and minimum VWC in 60 cm depth reached only  $0.03 \text{ cm}^3/\text{cm}^3$  (Table 2).

Mean ground temperature during the period from February 23<sup>rd</sup>, 2022 until February 7<sup>th</sup>, 2023 reached  $-0.7^\circ\text{C}$  in 10 cm depth and slightly decreased with depth down to  $-1.0^\circ\text{C}$  in the bottommost part of

the profile. The temperature amplitude decreased with depth, ranging from over 10°C on the top to approximately 6°C in 60 cm depth (Table 3). Similar to the

Nelson Island site, the thawing period of 2021/2022 ended on April 26<sup>th</sup>, 2022 and the thawing period of 2022/2023 began on November 18<sup>th</sup>, 2022.

|                           | Sensor depth | VWC <sub>mean</sub><br>[cm <sup>3</sup> /cm <sup>3</sup> ] | VWC <sub>max</sub><br>[cm <sup>3</sup> /cm <sup>3</sup> ] | VWC <sub>min</sub><br>[cm <sup>3</sup> /cm <sup>3</sup> ] |
|---------------------------|--------------|--|---|---|
| <b>James Ross Island</b>  | 5 cm         | 0.24 ± 0.03  | 0.30  | 0.13  |
|                           | 30 cm        | 0.27 ± 0.06  | 0.37  | 0.20  |
|                           | 50 cm        | 0.33 ± 0.03  | 0.37  | 0.28  |
| <b>Nelson Island</b>      | 5 cm         | 0.30 ± 0.07  | 0.47  | 0.15  |
|                           | 20–30 cm     | 0.34 ± 0.04  | 0.46  | 0.28  |
|                           | 50 cm        | 0.40 ± 0.04  | 0.51  | 0.30  |
| <b>King George Island</b> | 10 cm        | 0.11 ± 0.05  | 0.19  | 0.04  |
|                           | 20–30 cm     | 0.18 ± 0.06  | 0.39  | 0.08  |
|                           | 60 cm        | 0.36 ± 0.01  | 0.38  | 0.35  |

**Table 2.** Volumetric water content variability at various depths for the three study sites.

|                           | Sensor depth | GT <sub>mean</sub><br>[°C] | GT <sub>max</sub><br>[°C] | GT <sub>min</sub><br>[°C] | TP <sub>end</sub> | TP <sub>start</sub> |
|---------------------------|--------------|----------------------------|---------------------------|---------------------------|-------------------|---------------------|
| <b>James Ross Island</b>  | 5 cm         | -3.2                       | 10.5                      | -21.0                     | 13/03/2022        | 06/11/2022          |
|                           | 30 cm        | -3.7                       | 4.8                       | -15.1                     |                   |                     |
|                           | 50 cm        | -3.8                       | 1.9                       | -11.8                     |                   |                     |
| <b>Nelson Island</b>      | 5 cm         | 0.3                        | 6.5                       | -8.6                      | 25/04/2022        | 18/11/2022          |
|                           | 20–30 cm     | 0.2                        | 5.0                       | -5.4                      |                   |                     |
|                           | 50 cm        | 0.1                        | 3.4                       | -2.2                      |                   |                     |
| <b>King George Island</b> | 10 cm        | -0.7                       | 3.5                       | -6.6                      | 26/04/2022        | 18/11/2022          |
|                           | 20–30 cm     | -0.9                       | 2.6                       | -5.4                      |                   |                     |
|                           | 60 cm        | -1.0                       | 1.1                       | -4.6                      |                   |                     |

**Table 3.** Ground temperature variability at various depths with the dates of the end of thawing period 2021/2022 and the beginning of thawing period 2022/2023 for the three study sites.

### *Soil freeze-thawing characteristics*

#### **James Ross Island**

The period of soil freezing occurred between March 16<sup>th</sup> and April 7<sup>th</sup>, 2022 on James Ross Island. The temperature of the soil during zero-curtain period was -0.5°C. The more pronounced decrease of soil mois-

ture to the values below 0.3 cm<sup>3</sup>/cm<sup>3</sup> was visible around March 28<sup>th</sup>, 2022 (Fig. 3) which was in ca 2/3 of zero-curtain phase duration.

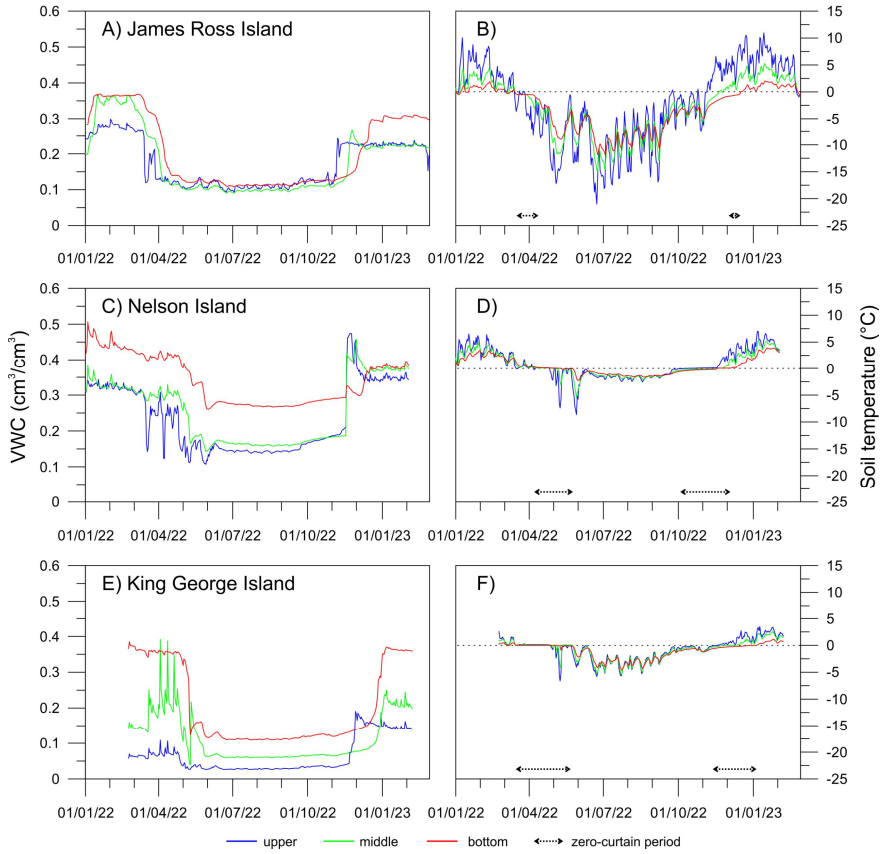


**Fig. 2.** Variability of studied parameters on the three sites – (A) VWC and (B) ground temperature on James Ross Island; (C) VWC and (D) ground temperature on Nelson Island; (E) VWC and (F) ground temperature on King George Island.

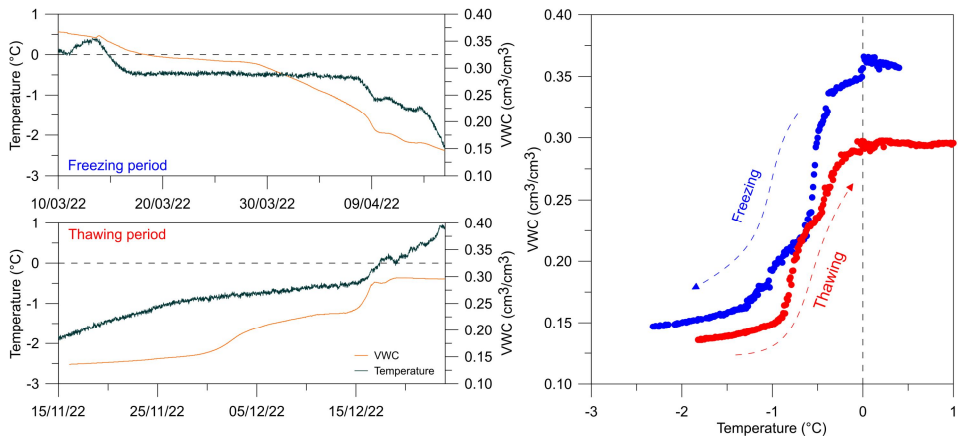


**Fig. 3.** The variability of VWC and soil temperature on James Ross Island during the freezing and thawing phase.

As indicated by the soil freezing curve, the inflection point representing the beginning of the soil freezing process is for the values of  $0.3 \text{ cm}^3/\text{cm}^3$  and  $-0.45^\circ\text{C}$  for moisture and temperature, respectively. The residual (unfrozen) water content is around  $0.15 \text{ cm}^3/\text{cm}^3$  for the temperature

$-2.0^\circ\text{C}$ . The soil thawing process was relatively fast. The thawing zero-curtain period occurred within a short period between December 10<sup>th</sup> and 15<sup>th</sup>, 2022 (see Fig. 3) when temperature was kept around  $-0.6^\circ\text{C}$  and VWC around  $-0.23 \text{ cm}^3/\text{cm}^3$ .

### Nelson Island

Soil freeze-thaw curves on the Nelson Island site were distorted by the fact that the sensor at the bottommost level was and still is placed in the vertical position. Therefore, during freezing and thawing, the soil temperature sensor is above or below the freeze-thaw front. Therefore, we observed the initial patterns of soil phase change represented by a decrease of soil moisture from  $0.45$  to  $0.37 \text{ cm}^3/\text{cm}^3$  under measured temperature of  $0.1^\circ\text{C}$  (Fig. 4). The pronounced decrease of moisture from  $0.37$  to  $0.32 \text{ cm}^3/\text{cm}^3$  occurred between

May 9<sup>th</sup> and 14<sup>th</sup>, 2022 when temperature dropped from  $0.1$  to  $-0.1^\circ\text{C}$ . Notably, the values of unfrozen water content remain around  $0.25$  to  $0.27 \text{ cm}^3/\text{cm}^3$  over the whole winter season (Fig. 2). During the thawing phase, VWC exhibited the highest increase during a short period between November 17<sup>th</sup> and 18<sup>th</sup>, 2022. We assume, that the sudden increase in temperature from  $-0.1$  to  $0.1^\circ\text{C}$  might be conditioned by the sensor parameters. Yet, the change is within the accuracy of the sensor.

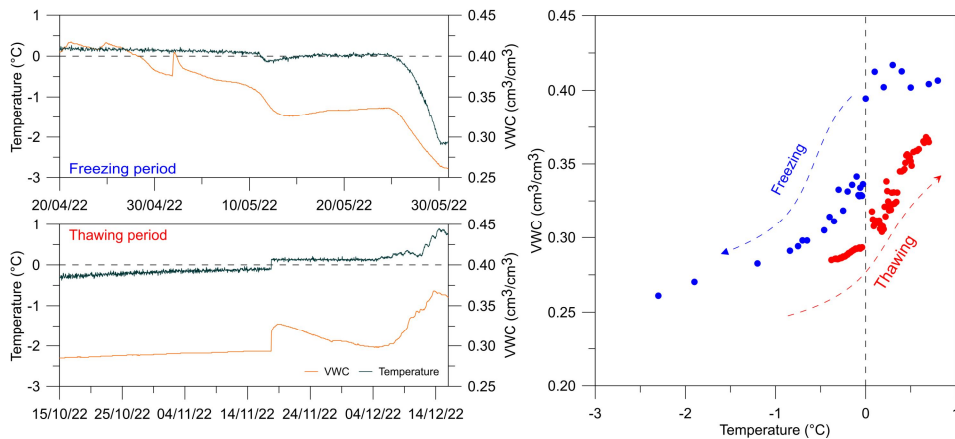


**Fig. 4.** The variability of VWC and soil temperature on Nelson Island during the freezing and thawing phase.

### King George Island

The zero-curtain period ended on May 9<sup>th</sup>, 2022 when a clear and rapid decrease of soil temperature and moisture started

(Fig. 5). Soil freezing process starts at the temperature closely below  $0^\circ\text{C}$ . The stable frozen soil is around temperature  $-0.5^\circ\text{C}$

with a residual water content of  $0.14 \text{ cm}^3/\text{cm}^3$ . The soil thawing process begun on December 15<sup>th</sup>, 2022 when soil moisture started to increase considerably and ended

on December 27<sup>th</sup>, 2022 when the moisture values have stabilized. The temperature during the thawing process was between  $-0.2$  and  $-0.05^\circ\text{C}$  (Fig. 5).

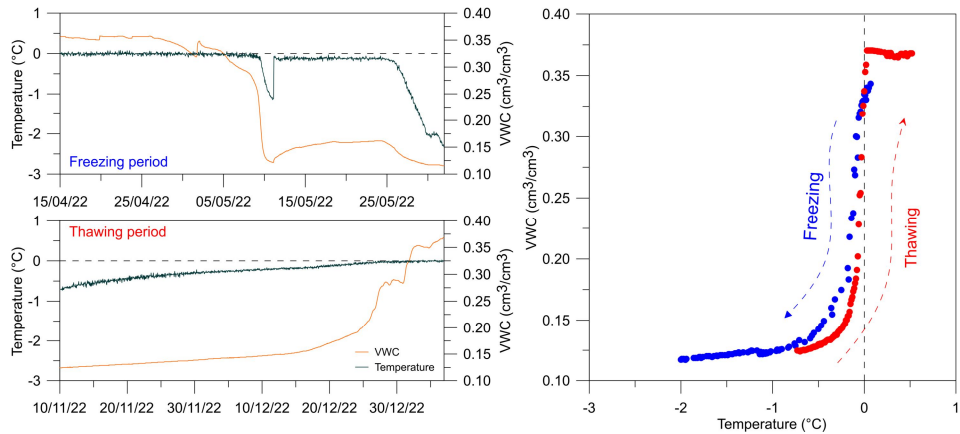


**Fig. 5.** The variability of VWC and soil temperature on King George Island during the freezing and thawing phase.

## Discussion

The study sites are located in the parts of Antarctic Peninsula with distinctive air temperature average (e.g. Oliva et al. 2017, Turner et al. 2020), precipitation rates (e.g. van Wessem et al. 2017, Palerme et al. 2017) and the overall soil thermal conditions (e.g. Hrbáček et al. 2023). Yet, the VWC variability on the study sites exhibited a relatively similar pattern. The highest VWC was observed on Nelson Island, on the side of the Antarctic Peninsula with higher annual precipitation rates and the soils with relatively fine matrix favouring the soil retention. The lowest VWCs were observed on Barton Peninsula, which we mostly associated with the gravelly matrix of the study site (Fig. 1; Farzadian, personal communication).

Notably, the site on James Ross Island, which is often classified as semi-arid polar-continental climate zone (Martin and Peel 1978), had also relatively high VWCs reaching up to  $0.37 \text{ cm}^3/\text{cm}^3$ . However,

when compared to the hyper-arid climate conditions typical for McMurdo Dry Valleys where soil moisture is very often lower than  $0.05 \text{ cm}^3/\text{cm}^3$  (Seybold et al. 2010, Levy et al. 2011), VWC data from AWS-JGM site indicate relatively humid soils. Indeed, the analysis of gravimetric water content on other sites on James Ross Island showed that the moisture content can be 7 to 12% than on AWS-JGM (Hrbáček et al. 2019).

All of the study sites followed a similar pattern of increasing moisture with increasing depth. Such a pattern is typical for the moisture profiles in permafrost affected areas where the frozen soil creates an impermeable layer and the moisture is accumulated at the base of the active layer (e.g. Shur et al. 2005, Andresen et al. 2020). We attribute the differences between the maximum seasonal water content values mostly to the differences in soil texture. The sites on Nelson Island and

James Ross Island are comprised of soils with relatively high content of fine material (Stachoň *et al.* 2014, Meier *et al.* 2023) which creates favourable conditions to keep a relatively high amount of soil water even in the surficial part of the profile. The gravelly matrix in the topmost part of soil on King George Island has a low capability to keep the water (*e.g.* Scheinost *et al.* 1997) which is transported downwards through the soil profile and accumulated above the permafrost table (*e.g.* Andresen *et al.* 2020).

The beginning of the thawing season showed different patterns of VWC when all three sites are compared. A VWC regime with a pronounced short-term maximum peak was observed on Nelson Island and was very likely caused by the infiltration of snowmelt water which very often lead to full water saturation (*e.g.* Mohammed *et al.* 2019). We assume that some meltwater infiltration occurred also on King George Island, as the VWC values at top and middle sensors were twice higher than at the end of the thawing season 2022 (Fig. 2). The overall occurrence of snow on Nelson and King George Islands is also suggested by the isothermal ground thermal regime prior to the zero-curtain period, which is one of the indicators of snow presence (*e.g.* Zhang 2005, Oliva *et al.* 2017). In contrast, the initial thawing on James Ross Island does not show any signs of possible snowmelt infiltration. The VWC values in the beginning of thawing season 2022/23 are even lower than they were at the end of the thawing

season 2021/22. The moisture loss during winter was ca.  $0.02$  to  $0.05$   $\text{cm}^3/\text{cm}^3$

The soil freezing curves reveal that the freezing temperature is very close to  $0^\circ\text{C}$  on the sites on Nelson and King George Island, whereas the freezing temperature on James Ross Island was around  $-0.5^\circ\text{C}$ . We suppose that the major reason is the close proximity to the sea and the fact, that the site is located on the marine terrace presumably exhibiting some level of salinity. A laboratory experiment found that salt content lower than 0.5% is sufficient to decrease the freezing point to  $-1.0^\circ\text{C}$  in sandy soils (Bing and Ma 2011). The soil freeze-thawing hysteresis exhibited typical loop with higher VWC values in freezing phase than thawing at all sites (Devoie *et al.* 2022).

We also detected noticeable values of unfrozen water content especially on Nelson Island, where the VWC during winter did not dropped below  $0.25$   $\text{cm}^3/\text{cm}^3$  at the depth of 50 cm. Even though the TDR are considered to slightly overestimate the amount unfrozen water content (*e.g.* Watanabe and Wake 2009), the absolute value of overestimation of non-calibrated sensors was found lower than  $0.05$   $\text{cm}^3/\text{cm}^3$  in many studies (*e.g.* Watanabe and Wake 2009, Zhang *et al.* 2011, Zhou *et al.* 2014). High amount of unfrozen water content in the frozen ground can increase the heat transport and generally promote the permafrost thawing (*e.g.* Romanovsky and Osterkamp 2000, Oldenborger and LeBlanc 2018).

## Conclusion

This study brings the first results from a newly established network for soil moisture monitoring in the northern Antarctic Peninsula region. Even though the distinctive conditions between oceanic climate on South Shetlands and semi-arid climate on James Ross Island create a prerequisite for

distinctive soil moisture regime, the observation shows rather small differences between study sites. In absolute values, the moistest site was Nelson Island where soil moisture exceeded  $0.50$   $\text{cm}^3/\text{cm}^3$ , which can be related to the overall moist climate and fines soil matrix favouring water re-

tention. The moisture values on King George Island and James Ross Island were comparable in the bottommost zone. We assume that the lowest moisture in the top layer on King George Island was attributed to coarse and highly permeable soils.

Importantly, we observed a noticeable amount of unfrozen water content at all of the sites. High amount of unfrozen water

can significantly promote heat transfer to the ground and favour the active layer thickening. Therefore, mainly in the border conditions of permafrost presence on the South Shetlands, the variability of soil moisture can be one of the crucial parameters affecting the distribution of active layer thickness and permafrost.

## References

- ABU-HAMDEH, N. H., REEDER, R. C. (2000): Soil thermal conductivity: Effects of density, moisture, salt concentration, and organic matter. *Soil Science Society of America Journal*, 64: 1285-1290. doi: 10.2136/sssaj2000.6441285x
- ALMEIDA, I., SCHAEFER, C. E. G. R., FERNANDES, R. B. A., PEREIRA, T. T. C., NIEUWENDAM, A. and PEREIRA, A. B. (2014): Active layer thermal regime at different vegetation covers at Lions Rump, King George Island, Maritime Antarctica. *Geomorphology*, 225: 36-46.
- ANDRESEN, C. G., LAWRENCE, D. M., WILSON, C. J., MCGUIRE, A. D., KOVEN, C., SCHAEFER, K., JAFAROV, E., PENG, S., CHEN, X., GOUTTEVIN, I., BURKE, E., CHADBURN, S., JI, D., CHEN, G., HAYES, D. and ZHANG, W. (2020): Soil moisture and hydrology projections of the permafrost region – a model intercomparison. *The Cryosphere*, 14: 445-459, doi: 10.5194/tc-14-445-2020
- BING, H., MA, W. (2011): Laboratory investigation of the freezing point of saline soil. *Cold Regions Science and Technology*, 67(1–2): 79-88. doi: 10.1016/j.coldregions.2011.02.008
- BIRKENMAJER, K. (1989): A guide to Tertiary geochronology of King George Island, West Antarctica. *Polish Polar Research*, 10(4): 555-579.
- BOCKHEIM, J., VIEIRA, G., RAMOS, M., LÓPEZ-MARTÍNEZ, J., SERRANO, E., GUGLIELMIN, M., WILHELM, K. and NIEUWENDAM, A. (2013): Climate warming and permafrost dynamics in the Antarctic Peninsula region. *Global and Planetary Change*, 100: 215-223. doi: 10.1016/j.gloplacha.2012.10.018
- BORZOTTA, E., TROMBOTTO, D. (2004): Correlation between frozen ground thickness measured in Antarctica and permafrost thickness estimated on the basis of the heat flow obtained from magnetotelluric soundings. *Cold Regions Science and Technology*, 40: 81-96. doi: 10.1016/j.coldregions.2004.06.002
- BROOKS, S. T., JABOUR, J., VAN DEN HOFF, J. and BERGSTROM, D. M. (2019): Our footprint on Antarctica competes with nature for rare ice-free land. *Nature Sustainability*, 2: 185-190. doi: 10.1038/s41893-019-0237-y
- CLAYTON, L.K., SCHAEFER, K., BATTAGLIA, M.J., BOURGEOU-CHAVEZ, L., CHEN, J., CHEN, R.H., CHEN, A., BAKIAN-DOGAHEH, K., GRELIK, S., JAFAROV, E., LIU, L., MICHAELIDES, R.J., MOGHADDAM, M., PARSEKIAN, A.D., ROCHA, A.V., SCHAEFER, S.R., SULLIVAN, T., TABATABAENEJAD, A., WANG, K., WILSON, K.J., ZEBKER, H.A., ZHANG, T. and ZHAO, Y. (2021): Active layer thickness as a function of soil water content. *Environmental Research Letters*, 16: 055028. doi: 10.1088/1748-9326/abfa4c
- DEVOIE, É. G., GRUBER, S. and MCKENZIE, J. M. (2022): A repository of measured soil freezing characteristic curves: 1921 to 2021. *Earth System Science Data*, 14: 3365-3377. doi: 10.5194/essd-14-3365-2022
- FAROUKI, O. T. (1981): Thermal properties of soil. U.S. Army Corps of Engineers, Cold Regions Research and Engineering Laboratory, Hanover, 136 p.
- FARZAMIAN, M., VIEIRA, G., MONTEIRO SANTOS, F. A., YAGHOOBI TABAR, B., HAUCK, C., PAZ, M. C., BERNARDO, I., RAMOS, M. and DE PABLO, M. A. (2020): Detailed detection of active layer freeze-thaw dynamics using quasi-continuous electrical resistivity tomography (Deception Island, Antarctica). *The Cryosphere*, 14: 1105-1120. doi: 10.5194/tc-14-1105-2020

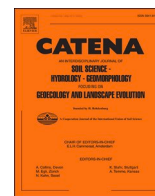
- GEORGE, S. F., FIERER, N., LEVY, J. S. and ADAMS B. (2021): Antarctic water tracks: Microbial community responses to variation in soil moisture, pH, and salinity. *Frontiers in Microbiology*, 12: 616730. doi: 10.3389/fmicb.2021.616730
- GUGLIELMIN, M., DALLE FRATTE, M. and CANNONE, N. (2014): Permafrost warming and vegetation changes in continental Antarctica. *Environmental Research Letters*, 9(4): 045001. doi: 10.1088/1748-9326/9/4/045001
- HORROCKS, C. A., NEWSHAM, K. K., COX, F., GARNETT, M. H., ROBINSON, C. H. and DUNGAIT, J. A. J. (2020): Predicting climate change impacts on maritime Antarctic soils: A space-for-time substitution study. *Soil Biology and Biochemistry*, 141: 107682. doi: 10.1016/j.soilbio.2019.107682
- HRBÁČEK, F., NÝVLT, D., LÁSKA, K., KŇAŽKOVÁ, M., KAMPOVÁ, B., ENGEL, Z., OLIVA, M. and MUELLER, C. W. (2019): Permafrost and active layer research on James Ross Island: An overview. *Czech Polar Reports*, 9(1): 20-36. doi: 10.5817/CPR2019-1-3
- HRBÁČEK, F., OLIVA, M., HANSEN, C., BALKS, M., O'NEILL, T.A., DE PABLO, M.A., PONTI, S., RAMOS, M., VIEIRA, G., ABRAMOV, A., KAPLAN PASTÍRIKOVÁ, L., GUGLIELMIN, M., GOYANES, G., FRANCELLINO, M.R., SCHAEFER, C. and LACELLE, D. (2023): Active layer and permafrost thermal regimes in the ice-free areas of Antarctica. *Earth Science Reviews*, 242: 104458. doi: 10.1016/j.earscirev.2023.104458
- HWANG, J., ZHENG, X., RIPLEY, E. M., LEE, J. I. and SHIN, D. (2011): Isotope geochemistry of volcanic rocks from the Barton Peninsula, King George Island, Antarctica. *Journal of Earth Science*, 22(1): 40-51. doi: 10.1007/s12583-011-0156-y
- KAPLAN PASTÍRIKOVÁ, L., HRBÁČEK, F., UXA, T. and LÁSKA, K. (2023): Permafrost table temperature and active layer thickness variability on James Ross Island, Antarctic Peninsula, in 2004–2021. *Science of the Total Environment*, 869: 161690. doi: 10.1016/j.scitotenv.2023.161690
- KEJNA, M., ARAZNY, A. and SOBOTA, I. (2013): Climatic change on King George Island in the years 1948–2011. *Polish Polar Research*, 34(2): 213-225.
- KENNEDY, A. D. (1993): Water as a limiting factor in the antarctic terrestrial environment: A biogeographical synthesis. *Arctic and Alpine Research*, 25(4): 308-315.
- LEVY, J. S., FOUNTAIN, A. G., GOOSEFF, M. N., WELCH, K. A. and BERRY LYONS, W. (2011): Water tracks and permafrost in Taylor Valley, Antarctica: Extensive and shallow groundwater connectivity in a cold desert ecosystem. *GSA Bulletin*, 123(11–12): 2295-2311. doi: 10.1130/B30436.1
- MARTIN, P. J., PEEL, D. A. (1978): The spatial distribution of 10 m temperatures in the Antarctic Peninsula. *Journal of Glaciology*, 20(83): 311-317. doi: 10.3189/S0022143000013861
- MEIER, M., FRANCELLINO, M. R., GASPARINI, A. S., THOMAZINI, A., PEREIRA, A. B., VON KRUGER, F. L., FERNANDES-FILHO, E. I. and SCHAEFER, C. E. G. R. (2023): Soils and geoenvironments at Stansbury Peninsula, Nelson Island, maritime Antarctica. *Catena*, 223: 106884. doi: 10.1016/j.catena.2022.106884
- MOHAMMED, A., PAVLOVSKII, I., CEY, E. and HAYASHI, M. (2019): Effects of preferential flow on snowmelt partitioning and groundwater recharge in frozen soils. *Hydrology and Earth System Sciences*, 23(12): 5017-5031. doi: 10.5194/hess-23-5017-2019
- NÝVLT, D., BRAUCHER, R., ENGEL, Z., MLČOCH, B., ASTER Team (2014): Timing of the Northern Prince Gustav Ice Stream retreat and the deglaciation of northern James Ross Island, Antarctic Peninsula during the last glacial–interglacial transition. *Quaternary Research*, 82: 441-449.
- OBU, J., WESTERMANN, S., VIEIRA, G., ABRAMOV, A., BALKS, M., BARTSCH, A., HRBÁČEK, F., KÄÄB, A. and RAMOS, M. (2020): Pan-Antarctic map of near-surface permafrost temperatures at 1 km<sup>2</sup> scale. *The Cryosphere*, 14: 497-519.
- OLDENBORGER, G. A., LEBLANC, A. M. (2018): Monitoring changes in unfrozen water content with electrical resistivity surveys in cold continuous permafrost. *Geophysical Journal International*, 215(2): 965-977. doi: 10.1093/gji/ggy321
- OLIVA, M., NAVARRO, F., HRBÁČEK, F., HERNÁNDEZ, A., NÝVLT, D., PERREIRA, P., RUIZ-FERNÁNDEZ, J. and TRIGO, R. (2017): Recent regional climate cooling on the Antarctic Peninsula and associated impacts on the cryosphere. *Science of the Total Environment*, 580: 210-223. doi: 10.1016/j.scitotenv.2016.12.030

- OLIVA, M., ANTONIADES, D., SERRANO, E., GIRALT, S., LIU, E. J., GRANADOS, I., PLA-RABES, S., TORO, M., HONG, S. G. and VIEIRA, G. (2019): The deglaciation of Barton Peninsula (King George Island, South Shetland Islands, Antarctica) based on geomorphological evidence and lacustrine records. *Polar Record*, 55(3): 177-188. doi: 10.1017/S0032247419000469
- PALERME, C., GENTHON, C., CLAUD, C., KAY, J. E., WOOD, N. B. and L'ECUYER, T. (2017): Evaluation of current and projected Antarctic precipitation in CMIP5 models. *Climate Dynamics*, 48: 225-239. doi: 10.1007/s00382-016-3071-1
- ROBINSON, S. A., KING, D. H., BRAMLEY-ALVES, J., WATERMAN, M. J., ASHCROFT, M. B., WASLEY, J., TURNBULL, J. D., MILLER, R. E., RYAN-COLTON, E., BENNY, T., MULLANY, K., CLARKE, L. J., BARRY, L. A. and HUA, Q. (2018): Rapid change in East Antarctic terrestrial vegetation in response to regional drying. *Nature Climate Change*, 8(10): 879-884. doi: 10.1038/s41558-018-0280-0
- ROMANOVSKY, V. E., OSTERKAMP, T. E. (2000): Effects of unfrozen water on heat and mass transport processes in the active layer and permafrost. *Permafrost and Periglacial Processes*, 11: 219-239. doi: 10.1002/1099-1530(200007/09)11:3<219::AID-PPP352>3.0.CO;2-7
- ROYLES, J., AMESBURY, M. J., CONVEY, P., GRIFFITHS, H., HODGSON, D. A., LENG, M. J. and CHARMAN, D. J. (2013): Plants and soil microbes respond to recent warming on the Antarctic Peninsula. *Current Biology*, 23(17): 1702-1706. doi: 10.1016/j.cub.2013.07.011
- SCHINOST, A. C., SINOWSKI, W. and AUERSWALD, K. (1997): Regionalization of soil water retention curves in a highly variable soilscape, I. Developing a new pedotransfer function. *Geoderma*, 78(3-4): 129-143. doi: 10.1016/S0016-7061(97)00046-3
- SEYBOLD, C. A., BALKS, M. R. and HARMS, D. S. (2010): Characterization of active layer water contents in the McMurdo Sound region, Antarctica. *Antarctic Science*, 22(6): 633-645. doi: 10.1017/S0954102010000696
- SHUR, Y., HINKEL, K. M. and NELSON, F. E. (2005): The transient layer: Implications for geocryology and climate-change science. *Permafrost and Periglacial Processes*, 16: 5-17. doi: 10.1002/ppp.51
- SMELLIE, J. L., PANKHURST, R. J., THOMSON, M. R. A. and DAVIES, R. E. S. (1984): The geology of the South Shetland Islands: IV. Stratigraphy, Geochemistry and Evolution. *British Antarctic Survey Scientific Reports*, 87: 1-85.
- STACHOŇ, Z., RUSSNÁK, J., NÝVLT, D. and HRBÁČEK, F. (2014): Stabilisation of geodetic points in the surroundings of Johann Gregor Mendel Station, James Ross Island, Antarctica. *Czech Polar Reports*, 4(1): 80-89. doi: 10.5817/CPR2014-1-9
- THOMAZINI, A., FRANCELINO, M. R., PEREIRA, A. B., SCHÜNEMANN, A. L., MENDONÇA, E. S., MICHEL, R. F. M. and SCHAEFER, C. E. G. R. (2020): The current response of soil thermal regime and carbon exchange of a paraglacial coastal land system in maritime Antarctica. *Land Degradation and Development*, 31: 655-666. doi: 10.1002/ldr.3479
- TURNER, J., MARSHALL, G. J., CLEM, K., COLWELL, S., PHILLIPS, T. and LU, H. (2020): Antarctic temperature variability and change from station data. *International Journal of Climatology*, 40(6): 2986-3007. doi: 10.1002/joc.6378
- UGOLINI, F. C., BOCKHEIM, J. G. (2008): Antarctic soils and soil formation in a changing environment: A review. *Geoderma*, 144(1-2): 1-8. doi: 10.1016/j.geoderma.2007.10.005
- VAN WESSEM, J. M., LIGTENBERG, S. R. M., REIJMER, C. H., VAN DE BERG, W. J., VAN DEN BROEKE, M. R., BARRAND, N. E., THOMAS, E. R., TURNER, J., WUITE, J., SCAMBOS, T. A. and VAN MEIJAARD, E. (2016): The modelled surface mass balance of the Antarctic Peninsula at 5.5 km horizontal resolution. *The Cryosphere*, 10: 271-285. doi: 10.5194/tc-10-271-2016
- WATANABE, K., WAKE, T. (2009): Measurement of unfrozen water content and relative permittivity of frozen unsaturated soil using NMR and TDR. *Cold Region Science and Technology*, 59(1): 34-41. doi: 10.1016/j.coldregions.2009.05.011
- WESSOLEK, G., BOHNE, K. and TRINKS, S. (2023): Validation of soil thermal conductivity models. *International Journal of Thermophysics*, 44: 20. doi: 10.1007/s10765-022-03119-5
- WLOSTOWSKI, A. N., GOOSEFF, M. N. and ADAMS, B. J. (2018): Soil moisture controls the thermal habitat of active layer soils in the McMurdo Dry Valleys, Antarctica. *Journal of Geophysical Research: Biogeosciences*, 123: 46-59. doi: 10.1002/2017JG004018

- ZHANG, T. (2005): Influence of the seasonal snow cover on the ground thermal regime: An overview. *Reviews of Geophysics*, 43(4): RG4002. doi: 10.1029/2004RG000157
- ZHANG, Y., TREBERG, M. and CAREY, S. K. (2011): Evaluation of the heat pulse probe method for determining frozen soil moisture content. *Water Resources Research*, 47: W05544. doi: 10.1029/2010WR010085
- ZHOU, X., ZHOU, J., KINZELBACH, W. and STAUFFER, F. (2014): Simultaneous measurement of unfrozen water content and ice content in frozen soil using gamma ray attenuation and TDR. *Water Resources Research*, 50(12): 9630-9655. doi: 10.1002/2014WR015640

### **Web sources / Other sources**

- [1] MLČOCH, B., NÝVLT, D. and MIXA, P. (eds.)(2020): Geological map of James Ross Island – Northern part 1: 25,000. Czech Geological Survey, Praha.



# Interannual variability of soil thermal conductivity and moisture on the Abernethy Flats (James Ross Island) during thawing seasons 2015–2023

Michaela Kňázková<sup>a,\*</sup>, Filip Hrbáček<sup>a</sup>

<sup>a</sup> Polar-Geo-Lab, Department of Geography, Masaryk University, Kotlářská 2, 611 37 Brno, Czech Republic

## ARTICLE INFO

### Keywords:

Soil thermal properties  
Soil thermal regime  
Active layer thickness  
Antarctic Peninsula  
Climate change

## ABSTRACT

The knowledge of soil thermal properties is important for determining how a soil will behave under changing climate conditions, especially in the sensitive environment of permafrost affected soils. This paper represents the first complex study of the interplay between the different parameters affecting soil thermal conductivity of soils in Antarctica. Antarctic Peninsula is currently the most rapidly warming region of the whole Antarctica, with predictions of this warming to continue in the upcoming decades. This study focuses on James Ross Island, where the Abernethy Flats automatic weather station is located in a lowland area with semi-arid climate. Air and ground temperature, soil heat flux and soil moisture during the thawing season were monitored on this site from 2015 to 2023. Moreover, two approaches to determining soil thermal conductivity were compared – laboratory measurements and calculation from field data. During this period, mean annual temperatures have increased dramatically for both air (from  $-6.9\text{ }^{\circ}\text{C}$  in 2015/2016 to  $-3.8\text{ }^{\circ}\text{C}$  in 2022/2023) and ground (from  $-6.5\text{ }^{\circ}\text{C}$  to  $-3.2\text{ }^{\circ}\text{C}$ ), same as active layer thickness (from 68 cm to 95 cm). Average soil thermal conductivity for the thawing period reached values between 0.49 and 0.74  $\text{W/m.K}^{-1}$  based on field data. Statistically significant relationships were found between the seasonal means of volumetric water content and several other parameters – soil thermal conductivity ( $r = 0.91$ ), thawing degree days ( $r = -0.87$ ) and active layer thickness ( $r = -0.88$ ). Although wetter soils generally have a higher conductivity, the increase in temperature exhibits a much stronger control over the active layer thickening, also contributing to the overall drying of the upper part of the soil profile.

## 1. Introduction

Soil thermal conductivity represents one of the key physical parameters of the ground affecting the active layer thawing in the polar regions (Farouki, 1981). Soils with different thermal conductivity typically exhibit distinct thawing patterns since the layer of soil can either work as an insulator or accelerate the thawing. Soils in the permafrost regions are sensitive to disturbances which can have far-reaching consequences (e.g., de Bruin et al., 2021; Cannone et al., 2021). The ongoing changes in these environments will likely result in the shifts of some of the factors affecting soil thermal properties, which in turn will contribute to changes in thawing patterns and, in extreme cases, might even lead to permafrost degradation. It is therefore of key importance to better integrate soil thermal conductivity with existing models of permafrost development (Li et al., 2023).

There are several factors which determine the thermal conductivity of a particular soil. Some of these are inherent to the soil, such as its

mineralogical composition, dry bulk density, texture and organic matter content (e.g., Farouki, 1981; Abu-Hamdeh & Reeder, 2000), others can to an extent vary over time, such as salinity and water content. Also, soils in frozen state tend to exhibit higher values of soil thermal conductivity than soils in unfrozen state due to the higher thermal conductivity of ice when compared to water ( $0.54\text{ W/m.K}^{-1}$  for water at  $4\text{ }^{\circ}\text{C}$  and  $2.22\text{--}2.35\text{ W/m.K}^{-1}$  for ice; Yershov, 1998). However, of these factors, as the one generally considered the most important in moderating in-situ variability of soil thermal conductivity, water content has received the most attention. Numerous studies have concluded that a rise in water content of the soil typically leads to an increase in soil thermal conductivity (e.g., Abu-Hamdeh & Reeder, 2000; O'Donnell et al., 2009; Rasmussen et al., 2018 Schjønning, 2021; Wessolek et al., 2023), which can facilitate heat transfer into the deeper levels of the ground. On the other hand, higher amount of soil water in permafrost affected soils increases the necessity of incoming heat for the phase change between water and ice. Consequently, active layer tends to be

\* Corresponding author.

E-mail address: [michaelaknazkova@gmail.com](mailto:michaelaknazkova@gmail.com) (M. Kňázková).

<https://doi.org/10.1016/j.catena.2023.107640>

Received 15 May 2023; Received in revised form 4 October 2023; Accepted 26 October 2023

Available online 2 November 2023

0341-8162/© 2023 Elsevier B.V. All rights reserved.

thinner in the moist soils regardless of their higher thermal conductivity as opposed to dry soils (Clayton et al., 2021) and less freeze–thaw cycles were observed in wetter soils (Wlostowski et al., 2017). Thus, the presence of unfrozen water content in fine-grained soils might actually slow down or even prevent permafrost degradation (Nicolosky & Romanovsky, 2018).

Currently, there are many approaches on how to estimate or measure soil thermal conductivity. In general, the three major groups are i) direct measurements in the field or a laboratory; ii) calculations based on the Fourier law of heat transfer based on measurements of soil temperature and heat flux and iii) calculations using theoretical or empirical models based on soil physical properties. Each of these general approaches present their own challenges and limitations and encompass many different methods and equations developed during the past several decades. As a conclusion, there is not a general agreement on which method generates the most accurate results across a wide variety of soil types. For example, Wessolek et al. (2023) compared 10 models concluding that the pedo-transfer functions models based on De Vries (1963) and Brakelmann (1984) approaches had the best performance. In contrast, He et al. (2020) preferred the models based on Kersten empirical function (Kersten, 1949).

In permafrost regions, soil thermal conductivity is a parameter used in many models for active layer thickness (ALT) or permafrost temperature calculation (Riseborough et al., 2008). Therefore, the knowledge of its natural variability can provide important information allowing for a substantial increase in the model accuracy. Li et al. (2023) suggest that the rate of permafrost degradation on the Qiangtang plateau in China is twice of that previously calculated, once improved parametrisation for soil thermal conductivity is considered. Similarly, an uncertainty in the parametrisation of soil thermal conductivity of Antarctic soils is one of the reasons why the continental predictions of temperature on the top of permafrost had a lower accuracy in Antarctica (Obu et al., 2020) when compared with the Arctic (Obu et al., 2019).

As mentioned, the knowledge of soil thermal conductivity remains sparse in Antarctica (Hrbáček et al., 2023). It has been reported that values  $<0.3 \text{ W/m.K}^{-1}$  occur in the very dry and dry sandy soils (Levy & Schmidt, 2016; Hrbáček et al., 2017; Liu et al., 2018), while the thermal conductivity reaches over  $2.5 \text{ W/m.K}^{-1}$  in solid bedrock (Guglielmin et al., 2011; Correia et al., 2012). These values were mostly generated by direct measurements under laboratory conditions (Guglielmin et al., 2011; Correia et al., 2012; Levy & Schmidt, 2016; Hrbáček et al., 2017; Hrbáček & Uxa, 2020). Calculated values of thermal conductivity of Antarctic soils were published by Liu et al. (2018), who employed the Johansen semiempirical equation which is based on the determination of soil physical properties including dry density and porosity (Johansen, 1977).

There is therefore at present a significant research gap in understanding the spatial and temporal variability of thermal conductivity of Antarctic soils. While ice-free areas currently only occupy less than 0.5% of the total area of the Antarctic continent (Brooks et al., 2019), their extent is likely to increase substantially in the near future (Lee et al., 2017) and the understanding of the dynamics of these environments is therefore of high importance. In these ice-free areas, the spatial variability of ALT is strongly associated with the variability of soil thermal conductivity. In our previous study from James Ross Island, we concluded that the ALT can differ by more than 40 cm within a Circumpolar Active Layer Monitoring (CALM) grid with dimensions of  $80 \times 70 \text{ m}$  (Hrbáček et al., 2017), which is linked to the variability of soil thermal conductivity stemming from different soil physical properties and variation in soil moisture within the grid.

The main objective of this study is to provide an assessment of the interannual variability of soil thermal conductivity and moisture on the Abernethy Flats automatic weather station on James Ross Island over a total of eight Antarctic summer seasons (2015–2023). Particularly we focus on: i) analysis of air and ground temperature and ALT, ii) employing a numerical model based on Fourier law of heat conduction

to determine soil thermal conductivity from the soil temperature and heat flux measurements, iii) investigating how soil thermal conductivity is affected by changes in soil volumetric water content and in turn how it translates into the changes in ALT, and iv) evaluating mutual relationships between the main studied parameters – soil thermal conductivity, volumetric water content, ALT and selected thermal indices.

## 2. Study site

The area of interest for this study lies on the Ulu Peninsula, the northernmost extension of James Ross Island, which is located off the north-eastern coast of the Antarctic Peninsula (Fig. 1). James Ross Island has a total area of around  $2500 \text{ km}^2$ , of which approximately 25% is not covered by glaciers. Ulu Peninsula therefore with its more than  $300 \text{ km}^2$  of ice-free terrain represents one of the largest ice-free areas in the whole Antarctic Peninsula region. The topography of Ulu Peninsula is dominated by a contrast between the volcanic mesas located at elevations around 500 m above sea level and lowlands predominantly formed by Cretaceous and Quaternary sediments. The Abernethy Flats automatic weather station (AWS) is located in the largest area of low, flat terrain on the Ulu Peninsula, the Abernethy Flats, at 41 m a.s.l. ( $63^\circ 52' 53''\text{S}$ ,  $57^\circ 56' 5''\text{W}$ ). Abernethy Flats is a vast lowland consisting of Cretaceous sediments, predominantly sandstones and siltstones of the Santa Marta Formation, locally overlain by younger sediments of marine, lacustrine and slope origin (Mlcoch et al., 2020). The area is underlain by continuous permafrost with an estimated thickness of over 67 m in the low-lying inland areas (Borzotta & Trombotto, 2004).

Climate of James Ross Island is characterised as semi-arid polar continental, with average air and ground (5 cm depth) temperatures on the Abernethy Flats site for the period 2006–2016 being  $-7.3$  and  $-6.1$  °C, respectively, and mean modelled ALT of 60 cm (Hrbáček & Uxa, 2020). Mean annual precipitation estimates range from 300 to 700 mm (van Wessem et al., 2016) and the precipitation is predominantly in the form of snow. However, the distribution of snow within the landscape is extremely uneven due to frequent winds blowing from the southwestern direction (Kavan et al., 2020) and is strongly controlled by topography. In the flat areas such as around the Abernethy Flats AWS, the accumulation rarely exceeds 50 cm. However, large snow accumulations can develop in the terrain depressions or around obstacles (Křažková et al., 2020). Patterns of snow accumulation also exert a strong control over the ground thermal regime and soil water content distribution, with meltwater being the primary source of moisture for the soils and also for the sparse, predominantly moss and lichen vegetation on James Ross Island.

## 3. Methods

### 3.1. Instrumental measurements

#### 3.1.1. Air and ground temperature

Instrumental measuring of air and ground temperature has been established at the Abernethy Flats AWS in 2006. Data from the period 2006–2016 have been presented by Hrbáček & Uxa (2020), where they were used for the modelling of ALT. In this study, we include data for the austral summer seasons spanning the period between 20 November 2015 and 28 February 2023; eight seasons in total.

The instruments utilised in this study for temperature measurements are Pt100/8 resistance thermometers with an accuracy of  $\pm 0.15$  °C (manufacturer EMS Brno). The air temperature probe EMS33 was mounted inside a radiation shield 2 m above terrain. Ground temperature is measured by probes placed directly in the ground within a 75 cm deep profile at the depths of 5, 10, 20, 30, 40, 50 and 75 cm. Air and ground temperature is measured in a 30-minute interval and data is stored using an EdgeBox V12 datalogger (EMS Brno). During the study period, approximately one-month break occurred resulting from a datalogger malfunction which lasted from 20 February until 19 March

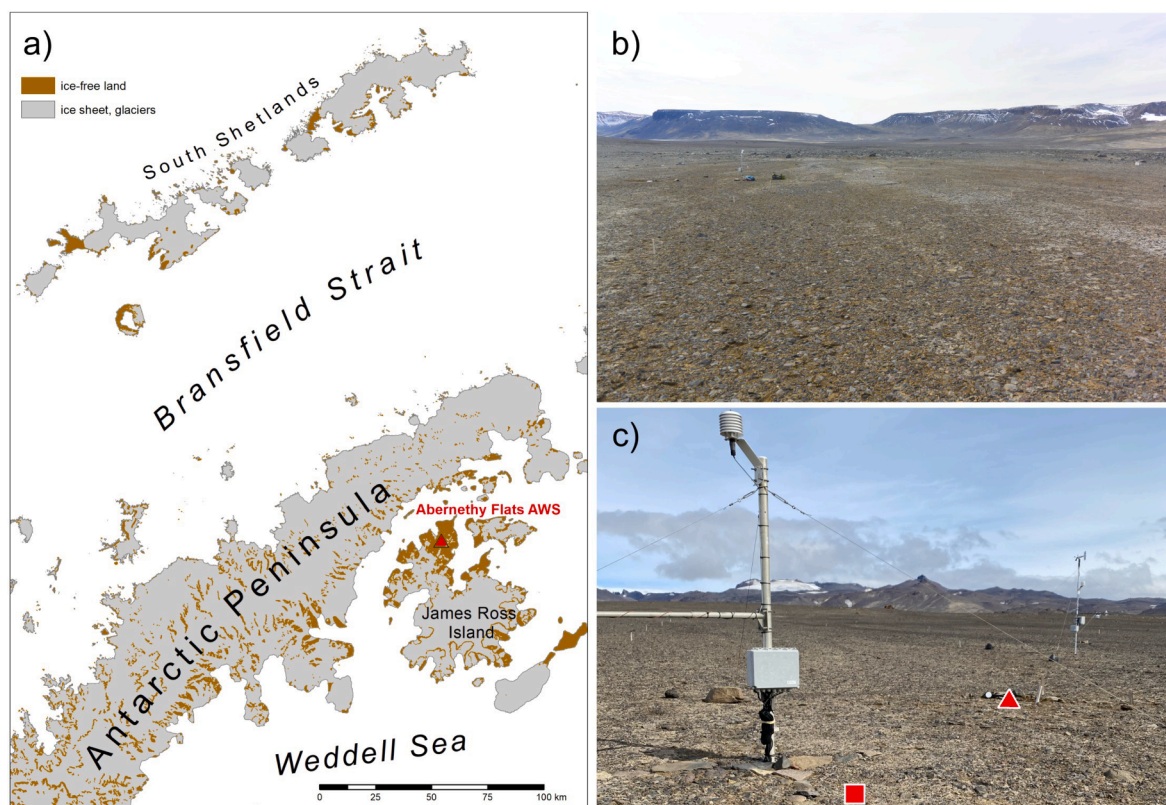


**Fig. 1.** Location of the study site within the northern Antarctic Peninsula region (a); characteristic view of the Abernethy Flats lowland (b) and Abernethy Flats AWS with square indicating the location of ground temperature profile and triangle indicating soil moisture measurement (c).

2018. Also, the data for the season of 2022/2023 ends on 28 February 2023, which means some part of the thawing season might not be included.

### 3.1.2. Soil heat flux

In the beginning of February 2015, heat flux monitoring has also been established on this site. Soil heat flux is measured in 30-minute interval using Hukseflux HFP01 heat plate with an accuracy of  $-15\%$  to  $+5\%$  (manufacturer Hukseflux Thermal Sensors) installed horizontally within the soil at the depths of 5 and 20 cm. This setting allows for the determination of soil thermal conductivity in the upper layer of soil (5–20 cm), following the methodology proposed by Mondal et al. (2015).

### 3.1.3. Soil moisture

Soil volumetric water content monitoring has been set up in February 2017 using CS655 probe with an accuracy of  $\pm 3\%$  (manufacturer Campbell Sci.) operating on the principle of dielectric permittivity measurement. These probes measure in 30-minute interval and are installed at the depth of 5 and 30 cm in the close proximity of the ground temperature measuring profile. Since dielectric properties of soil are influenced by temperature, a subsequent correction of soil moisture data was carried out using a general approach described by Jeewantini Kapilaratne & Lu (2017), which helps to remove the apparent daily variability of volumetric water content due to soil temperature fluctuations.

## 3.2. Data analysis

### 3.2.1. Thermal indices

Climate variability for the given study period is analysed using mean annual air and ground temperatures. Mean annual temperatures are calculated from the 30-minute data for the interval of March–February

so as to include the whole of one summer season. The summer (or thawing) season is defined as the period with daily average ground temperatures in 5 cm depth reaching above  $0\text{ }^{\circ}\text{C}$ . Thermal indices were calculated, such as thawing degree-days (TDD) which represent the sum of all positive temperatures within the summer season. These are calculated for air as well as ground at 5, 20, 30 and 50 cm depth. Thawing n-factor is determined as the ratio between the sum of positive near-surface ground temperatures at 5 cm depth ( $\text{TDD}_5$ ) and the sum of positive air temperatures ( $\text{TDD}_{\text{air}}$ ).

### 3.2.2. Thaw depths

Thaw depth for each day within the thawing season was calculated from maximum daily ground temperature observed at each individual sensor within the measuring profile. By way of assuming a linear decrease of temperature between the deepest sensor showing a daily maximum above  $0\text{ }^{\circ}\text{C}$  and the shallowest sensor with maximum below  $0\text{ }^{\circ}\text{C}$ , the position of  $0\text{ }^{\circ}\text{C}$  isotherm was identified as an intersection of the temperature decrease trend with the depth axis. For situations when the thaw depth exceeded 75 cm, which is the depth of the deepest sensor, the position of the  $0\text{ }^{\circ}\text{C}$  isotherm was extrapolated using the daily maximums measured by the two bottommost sensors. ALT was subsequently determined as the maximum observed depth of the  $0\text{ }^{\circ}\text{C}$  isotherm during the particular season.

### 3.2.3. Thermal properties

According to Farouki (1981), soil thermal conductivity is defined as the amount of heat passing through a unit of soil under a temperature gradient. Multiple studies (e.g., Zhang et al., 2002; Li et al., 2017; Li et al., 2019) have employed the method of calculating soil thermal conductivity from soil heat flux and temperature measurements, using equations derived from Fourier law of heat conduction such as Eq. (1), where  $G_z$  is the average heat flux through a layer of soil and  $\frac{\Delta T}{\Delta z}$  represents the temperature gradient between the depths delimiting the layer for

which the thermal conductivity is calculated. However, these solutions also produce a relatively large number of unrealistic values which need to be subsequently filtered out, especially when the soil temperature gradient or heat flow are close to zero.

$$G_z = -\lambda \frac{\Delta T}{\Delta z} \quad (1)$$

Instead, we calculated soil thermal conductivity using the numerical solution described by Romio et al. (2019), where the use of Least Squares Method trend-fitting has been proposed to avoid possible numerical divergences resulting from the direct solution of Eq. (1). We use ground temperatures and the average of measured values of soil heat flux at 5 and 20 cm, assuming that the layer of soil between these depths comprises of homogenous material and neglecting transfer of heat in horizontal direction. The relationship between half-hourly measurements of soil heat flux  $G_z$  and temperature gradient  $\frac{\Delta T}{\Delta z}$  over a 24-hour period (Fig. 2a, c) can be displayed using a scatter plot (Fig. 2b, d) and fitted with a linear trend expressed by a function  $y = ax + b$ , from which soil thermal conductivity  $\lambda$  can be subsequently extracted as the proportionality constant ( $a$ ; also expressing the slope of the function) using Eq. (1). The suitability of the linear trend fit for a particular set of 24-hour values of soil heat flux and ground temperature gradient is expressed by the coefficient of determination ( $R^2$ ). Only those values of soil thermal conductivity which exhibit  $R^2$  values of more than 0.9 were considered reliable and used for the calculation of daily, weekly and seasonal averages. This limiting value of  $R^2 \geq 0.9$  was chosen arbitrarily as the optimal way to filter out non-representative values of soil thermal conductivity, which are generated by the changing of meteorological conditions, or a presence of snow.

### 3.3. Sample collection and analysis

To determine soil physical properties and also to validate the values of soil thermal conductivity calculated from the experimental data, a series of measurements has been conducted under laboratory conditions. Sampling took place in the close proximity of the Abernethy Flats AWS in February 2023. Smaller soil samples were collected in an undisturbed state from 5, 20, 30 and 50 cm depth into a metal cylinder of 100 cm<sup>3</sup> and were dried subsequently in the oven for 72 h to determine dry bulk density and texture (proportion of the main texture components – clay, silt and sand). Two cylinders were collected from each depth and the values were then calculated as an average.

Larger samples of approximately 1 kg were also collected, dried and subsequently poured into a plastic container of sufficient volume so that the testing probe of ISOMET 2114 soil thermal properties analyser (manufacturer Applied Precision) could be fully immersed in the sample. The measurement operates on the principle of the thermal response of the analysed material to heat flow input via a heated needle probe. Using this method, samples from depths of 10–20, 25–35 and 40–50 cm were tested. These samples were compacted to the approximate dry bulk density of 1.4, 1.45 and 1.5 g/cm<sup>3</sup>, representative of the values obtained from the metal cylinders for the particular depth. Water was gradually added to the samples in increments of 20 ml and thermal properties measured to obtain values of soil thermal conductivity at a given soil moisture level.

## 4. Results

### 4.1. Air and ground temperature variability

Interannual variability of air and ground temperature at the

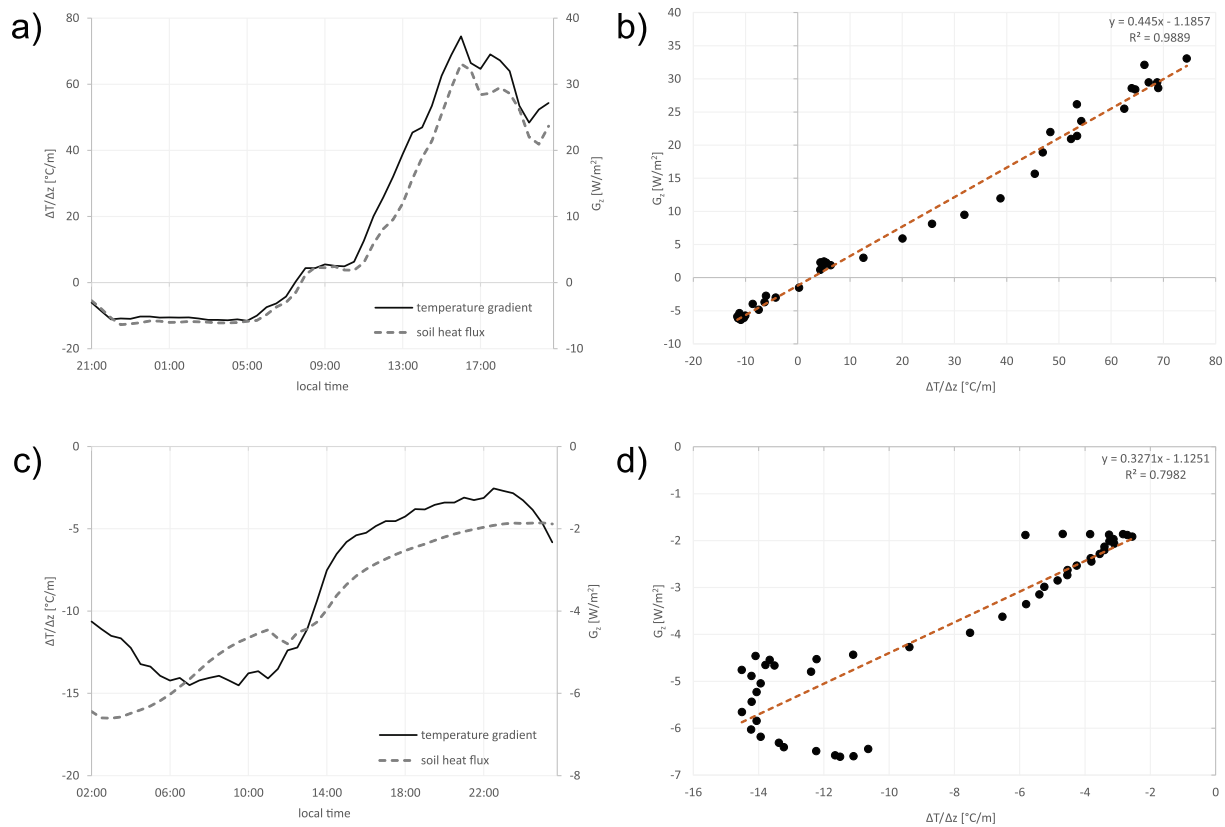


**Fig. 2.** Determination of soil thermal conductivity from the values of soil heat flux and ground temperature gradient; a) evolution of these parameters under near ideal conditions over 24 h, b) scatter plot of the 24-hour values where the linear trend represents a good fit ( $R^2 \geq 0.9$ ), c) evolution of soil heat flux and ground temperature gradient under less than ideal conditions and d) scatter plot of the values where the linear trend does not represent a good fit ( $R^2 \leq 0.9$ ).

Abernethy Flats AWS is considerable and the mean annual air and ground temperatures exhibit rather pronounced differences between the individual years. Table 1 sums up the mean annual temperatures (with the year spanning March to February) over the period 2015–2023. Overall, air temperatures show a slightly higher variability ( $-3.8$  to  $-6.9$  °C) than ground temperatures ( $-3.2$  to  $-6.5$  °C). Also, as a predominant rule, mean ground temperatures drop with increasing depth, same as the amplitude of the temperature fluctuations. However, occasionally the mean temperature in 30 cm depth may be the same or lower than the temperature in 50 cm depth.

The year 2015/2016 was the coldest from the perspective of mean air temperature ( $-6.9$  °C) and also the year when lowest mean ground temperatures overall ( $-6.5$  °C) were recorded. Mean air and ground temperatures stayed at a relatively steady level during the years 2015–2019 (with the exception of a very warm year 2016/2017), however, since then they started increasing quite rapidly, with the mean air temperatures rising by 2.6 °C and ground temperatures by up to 2.8 °C within the course of three years, overcoming the level of the year 2016/2017. By far the warmest year within the studied period was 2022/2023, when mean air temperatures reached  $-3.8$  °C and very high annual averages were also observed for ground temperatures (ranging from  $-3.2$  °C in 5 cm and  $-4.1$  °C in 50 cm). Compared to the period average, the year 2022/2023 was up to 1.9 °C warmer (Table 1).

The thawing n-factor as well shows great variability over the studied period. It ranges from 1.59 to 2.93 and can change dramatically from one year to the next. However, there has been a steady increase in the n-factor from 2015 up until the 2020, from which point it started decreasing until 2022.

#### 4.1.1. Thawing degree days, thawing season duration and ALT

From the perspective of seasonal thawing degree-days, the summer seasons of 2020/2021, 2021/2022 and 2022/2023 represent the warmest summer seasons within the studied period (Fig. 3), with TDD<sub>air</sub> reaching over 300 °C.days and TDD<sub>5</sub> close to or over 600 °C.days. Values of thawing degree-days have risen dramatically over the course of the seasons 2019–2023, especially in the greater depths of 30 and 50 cm, where there is a stark contrast between the summer season 2018/2019 and the subsequent season 2019/2020, with TDD<sub>50</sub> of 5 and 72 °C.days, respectively (Fig. 3), with even greater increases since, reaching a maximum of 209 °C.days in 2022/2023.

The start and end dates of the thawing season on the Abernethy Flats are quite changeable, as well as its total duration. Typically, the ground starts to thaw in the beginning to mid-November (Fig. 4). In some years, however, the start of the thawing season can shift as early as the start of October (2016/2017) or as late as mid to end of November (2018/2019). The ground again freezes over at the end of the thawing season in late February to early March. It is not uncommon that the beginning and end of the thawing season are difficult to ascertain as there are several short thawing episodes before the main season begins or after it ends. Sometimes even the main season is fragmented by freezing episodes as was the case in the season 2015/2016, when the ground froze over completely for two weeks around mid-December.

**Table 1**

Mean annual (March–February) air and ground temperatures (°C) at the Abernethy Flats AWS.

| year      | AT   | GT <sub>5</sub> | GT <sub>20</sub> | GT <sub>30</sub> | GT <sub>50</sub> | n-factor |
|-----------|------|-----------------|------------------|------------------|------------------|----------|
| 2015/2016 | -6.9 | -6.5            | -6.8             | -6.9             | -6.8             | 1.59     |
| 2016/2017 | -4.3 | -4.1            | -4.5             | -4.8             | -4.9             | 2.12     |
| 2017/2018 | -6.5 | -5.9            | -6.0             | -6.2             | -6.1             | 2.66     |
| 2018/2019 | -5.7 | -5.8            | -6.1             | -6.3             | -6.2             | 2.93     |
| 2019/2020 | -6.4 | -6.0            | -6.4             | -6.6             | -6.6             | 2.54     |
| 2020/2021 | -6.3 | -5.4            | -5.8             | -6.1             | -6.1             | 2.10     |
| 2021/2022 | -4.8 | -4.2            | -4.6             | -4.9             | -4.9             | 1.91     |
| 2022/2023 | -3.8 | -3.2            | -3.7             | -4.0             | -4.1             | 2.12     |
| 2015–2023 | -5.6 | -5.1            | -5.5             | -5.7             | -5.7             | 2.24     |

The maximum of thaw depth for the majority of the study period falls within the interval between 5 and 15 February, with the exception of season 2022/2023, where the maximum was reached already on 25 January. Despite the increase in TDD<sub>5</sub>, the ALT increased only slightly between the seasons 2015/2016 and 2016/2017, from 68 to 69 cm. The following two years, ALT dropped to its minimum of 62 cm, however, in 2019/2020 it reached 77 cm and since then started increasing every year, up to a maximum of 95 cm in 2022/2023 (Fig. 3).

#### 4.2. Soil physical properties

The dry bulk density of soil at the Abernethy Flats increases with depth and ranges from 1.34 g/cm<sup>3</sup> in 5 cm to 1.55 g/cm<sup>3</sup> in 50 cm (Table 2). Sand is the dominant fraction, with texture analysis results showing more than 50% sand content in all depths. While the proportion of silt stays relatively even throughout the soil profile, with only mild variation between 20.2 and 22.7%, there is some variability in the ratio between sand and clay content, with the highest percentage of clay (28.3%) near the ground surface level and in 30 cm depth (Table 2).

Seasonal variability of volumetric water content during the seasons 2017–2023 is depicted for each individual season in Fig. 5. Freezing episodes (when the ground temperature in 5 cm drops below 0 °C) are characterised by a rapid decrease in volumetric water content, typically below the level of 0.1 cm<sup>3</sup>/cm<sup>3</sup> (10%). Moisture levels in 5 cm depth show an overall higher variability than in the greater depth of 30 cm. There is usually a distinct peak in the beginning of the thawing season, where values of volumetric water content in 5 cm depth reach close to 0.5 cm<sup>3</sup>/cm<sup>3</sup> (50%). This peak lasts for up to two weeks, after which the surface moisture levels typically drop to around 20%, with the exception of the summer season 2018/2019 and also the subsequent season 2019/2020, when surface moisture level stayed relatively high throughout nearly the entire season, at over 25%. Volumetric water content at 30 cm depth typically has a much lower variability with minimum values (below 20%) at the beginning of the season, a subsequent rapid increase and then remains at a relatively steady level (over 30%) for the rest of the season, with the exception of the season 2017/2018, when higher variability was observed, with the increase divided into multiple stages and peaks reaching over 40% (Fig. 5).

##### 4.2.1. Soil thermal conductivity

In the upper layer of soil (5–20 cm), average thermal conductivity  $\lambda$  of the unfrozen soil calculated from the AWS data ranged from 0.49 to 0.74 W/m.K<sup>-1</sup> within the period 2015–2023. Seasonal average of soil thermal conductivity can be observed as the proportionality constant of the linear trend in Fig. 6 (shown in bold), while Fig. 5 presents the variability of soil thermal conductivity weekly moving average in relation to soil moisture for the seasons 2017–2023. The lowest values of soil thermal conductivity were recorded in the summer season 2015/2016 (0.49 W/m.K<sup>-1</sup>), from which point it has been on a steady increase up until the season 2018/2019, when it reached a maximum value of 0.74 W/m.K<sup>-1</sup>. During the following seasons, it fluctuates between 0.70 W/m.K<sup>-1</sup> in 2019/2020, 0.61 W/m.K<sup>-1</sup> in 2020/2021, 0.68 W/m.K<sup>-1</sup> in the summer season 2021/2022 and drops again to 0.60 W/m.K<sup>-1</sup> in 2022/2023 (Fig. 7).

The soil thermal conductivity typically varies within each individual season starting with a distinct peak at the beginning of each season (Fig. 5). During this peak, the values can reach over 0.9 W/m.K<sup>-1</sup>, with the exception of 2022/2023, when this peak was present, but somewhat less pronounced. Overall, the season 2022/2023 exhibits the lowest variability of soil thermal conductivity of all studied seasons. The values stay steady at a level below 0.6 W/m.K<sup>-1</sup> for most of the season and even drop towards the end of the season. In all the previous seasons, several peaks during the season are present, and the variability is much higher.

Laboratory measurements of soil thermal conductivity at different dry bulk density (Fig. 7) show an increase in conductivity with increasing volumetric water content. For extremely dry soil with close to

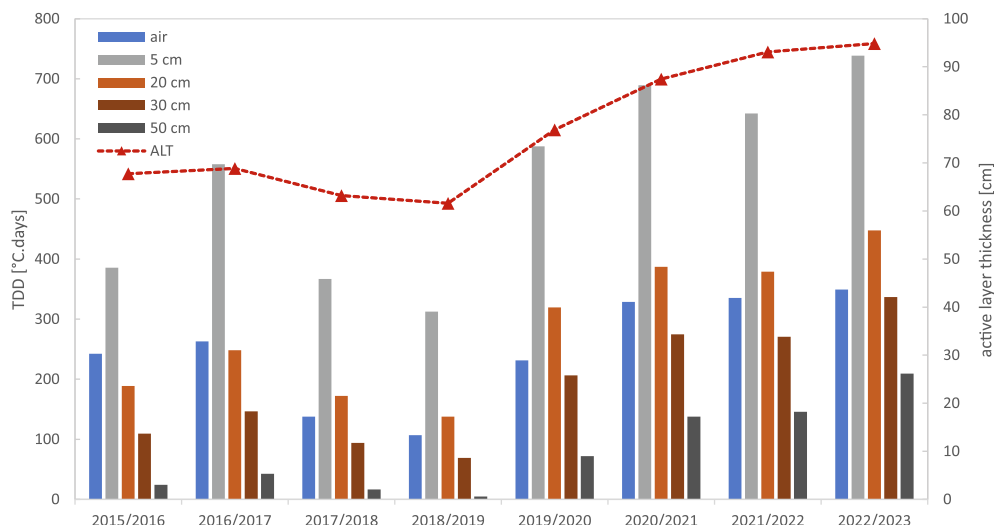


Fig. 3. ALT with ground thawing degree-days (TDD) for the thawing seasons 2015–2023 on the Abernethy Flats AWS.

0% moisture content, soil thermal conductivity exhibits values between 0.24 and 0.29 W/m.K<sup>-1</sup>. Conductivity starts to increase very rapidly especially after the volumetric water content passes 10%. Between 10 and 15% of soil moisture, thermal conductivity more than doubles, from around 0.3 W/m.K<sup>-1</sup> to between 0.6 and 0.8 W/m.K<sup>-1</sup>, rising more rapidly in a soil with higher bulk density. However, after the volumetric water content reaches over 20%, the increasing trend of soil thermal conductivity slows down. For soil with dry bulk density of 1.4 g/cm<sup>3</sup>, it reaches peak values of 0.9 W/m.K<sup>-1</sup> between 25 and 30% soil moisture, afterwards oscillates around this value. For denser soil with a density of 1.45 g/cm<sup>3</sup> the soil thermal conductivity peaks at around 1 W/m.K<sup>-1</sup>. In the densest soil with a density of 1.5 g/cm<sup>3</sup>, conductivity reaches maximum values of 1.1 W/m.K<sup>-1</sup> already between 20 and 25% of moisture, with no further significant increase afterwards.

## 5. Discussion

### 5.1. Ground surface temperature and ALT evolution

The increasing trend of ALT is especially pronounced on the Abernethy Flats AWS during the past several seasons, starting in the year 2019. This is coupled with a dramatic rise in seasonal air and ground TDD (Fig. 3). From the perspective of mean annual air and ground temperatures (-3.8 and -3.2 °C, respectively), 2022/2023 was also the warmest year since the establishment of measurement on this AWS in 2006. According to Hrbáček & Uxa (2020), average modelled ALT on the Abernethy Flats reached 60 cm in the period 2006–2016 and it ranged between 35 and 78 cm in the individual seasons. For the study period 2015–2023, which is the scope of the current paper, the average ALT calculated from the ground temperature data has been 77 cm and the range was between 62 (2018/2019) and 95 cm (2022/2023). There has been therefore an increase of 17 cm from the perspective of the period average and also a new overall seasonal maximum ALT was reached.

Increase in air and ground temperatures and a thickening of active layer has been reported from other sites around the Antarctic Peninsula ((Hrbáček et al., 2023)), which is considered one of the most rapidly warming parts of Antarctica (Turner et al., 2020). This trend is likely to continue in the following decades, with predictions of up to 0.5–1.4 °C increase in annual air temperatures before the year 2044 in the eastern part of Antarctic Peninsula (Bozkurt et al., 2021).

### 5.2. Variability of soil thermal conductivity based on other physical properties

Hrbáček & Uxa (2020) reported soil thermal conductivity values on the Abernethy Flats in 10 cm depth at dry bulk density of 1.30 g/cm<sup>3</sup> and volumetric water content of 23.4% to be 0.45 W/m.K<sup>-1</sup>; in 30 cm depth with dry bulk density of 1.47 g/cm<sup>3</sup> and volumetric water content of 26.5% to be 0.61 W/m.K<sup>-1</sup>. While these values are lower than the values presented in this study to be typical of soil at that dry bulk density and moisture level, they still fall within the range of natural variability of soil thermal conductivity at the Abernethy Flats.

#### 5.2.1. Volumetric water content

Both the laboratory measurements and experimental data confirm that there is a link between soil moisture and soil thermal conductivity, as already reported from permafrost affected soils over different regions by many authors (e.g., Farouki, 1981; O'Donnell et al., 2009; Rasmussen et al., 2018). The linear regression between calculated soil thermal conductivity and instrumentally measured volumetric water content revealed  $R^2 > 0.49$  to 0.78 for the individual seasons (Fig. 8), all statistically significant ( $p > 0.01$ ), which means that at least about a half of the variability of soil thermal conductivity can be attributed to changes in soil moisture. The nature of the regression changes between the individual seasons, in some seasons revealing a much stronger relationship between the two variables than in others. This might be related to irregularities in measuring soil moisture caused by factors such as the several metres of distance between the moisture sensor and the ground temperature measurement profile. As proven by investigations in CALM grids (e.g., Smith et al., 2009; Mergelov, 2014), the variation of soil moisture can be rather significant even within a relatively small area, which is primarily connected with microtopography and the resulting uneven distribution of snow and subsequently meltwater or local variation in physical properties such as soil texture and dry bulk density.

However, determining the exact nature of the relationship between volumetric water content and soil thermal conductivity from the experimental data itself is rather difficult, because the natural variability of soil moisture on the Abernethy Flats site does not include the whole range from totally dry soil to its full saturation. The naturally observed variability of soil thermal conductivity, at least in the uppermost layer of soil, is not considerable. On the other hand, laboratory measurements of soil thermal properties suggest that soil thermal conductivity has the potential to change significantly within quite a narrow window of variation in volumetric water content (Fig. 7).

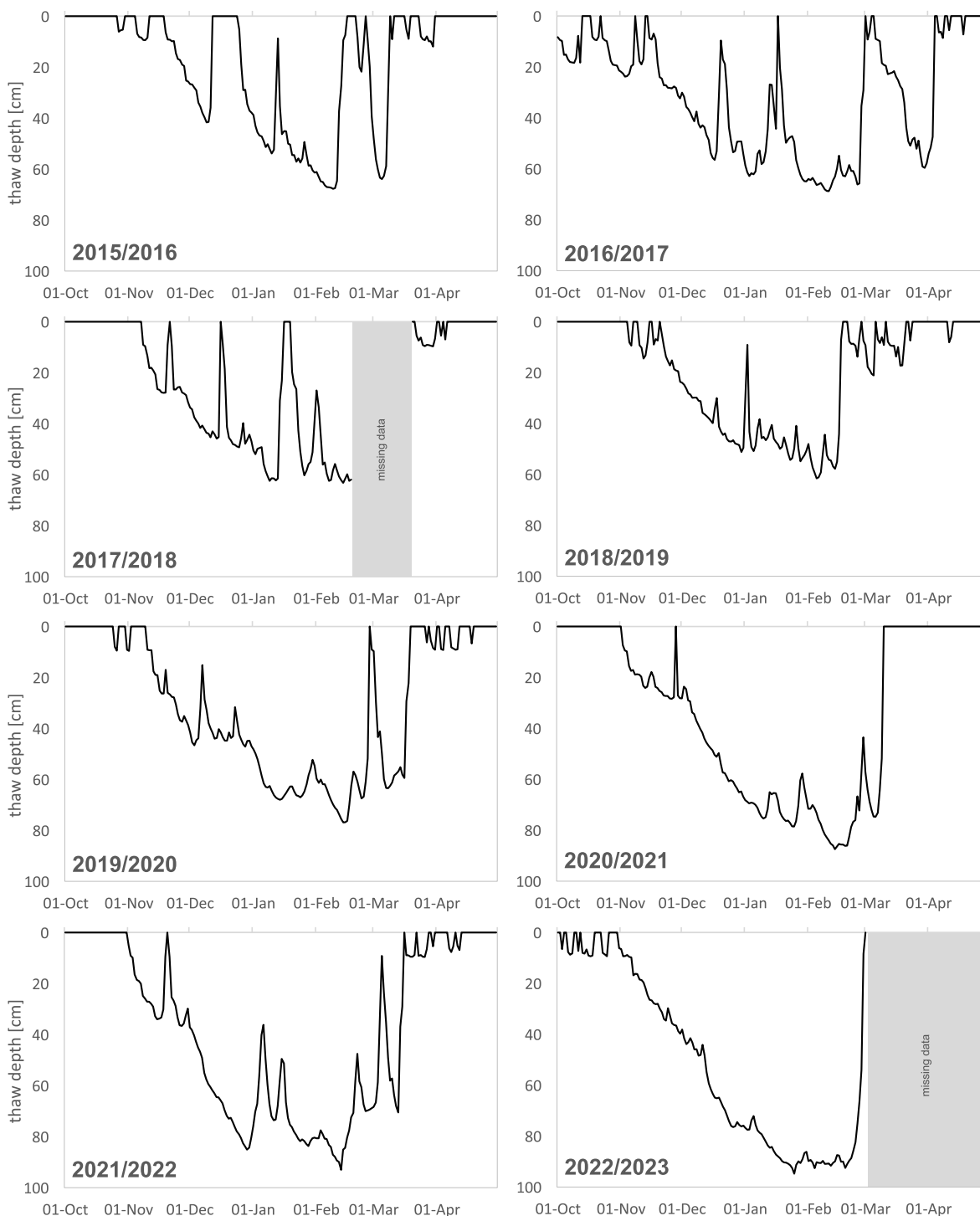


Fig. 4. Daily evolution of thaw depth over the course of the individual thawing seasons 2015–2023 on the Abernethy Flats AWS.

**Table 2**  
Physical properties of soil at the Abernethy Flats AWS site at different depths.

| depth | dry bulk density [g/cm <sup>3</sup> ] | sand [%] | silt [%] | clay [%] |
|-------|---------------------------------------|----------|----------|----------|
| 5 cm  | 1.34                                  | 50.1     | 21.6     | 28.3     |
| 20 cm | 1.41                                  | 56.4     | 20.2     | 23.4     |
| 30 cm | 1.41                                  | 53.1     | 20.3     | 26.5     |
| 50 cm | 1.55                                  | 55.2     | 22.7     | 22.1     |

5.2.2. Dry bulk density

At the same time, soil thermal conductivity is significantly affected by dry bulk density (e.g., Hinzman et al., 1991; Abu-Hamdeh & Reeder, 2000; Loranty et al., 2018). In our laboratory experiment, soil with higher dry bulk density by 0.1 g/cm<sup>3</sup> exhibited higher thermal conductivity by 0.2 W/m.K<sup>-1</sup> and also the difference was more pronounced for higher volumetric water content.

Sampling showed that there is also a gradient from less dense soil at the ground surface to more dense soil in the lower part of the profile, therefore it is assumed that the soil thermal conductivity increases with depth. With the thickening of the active layer and the penetration of

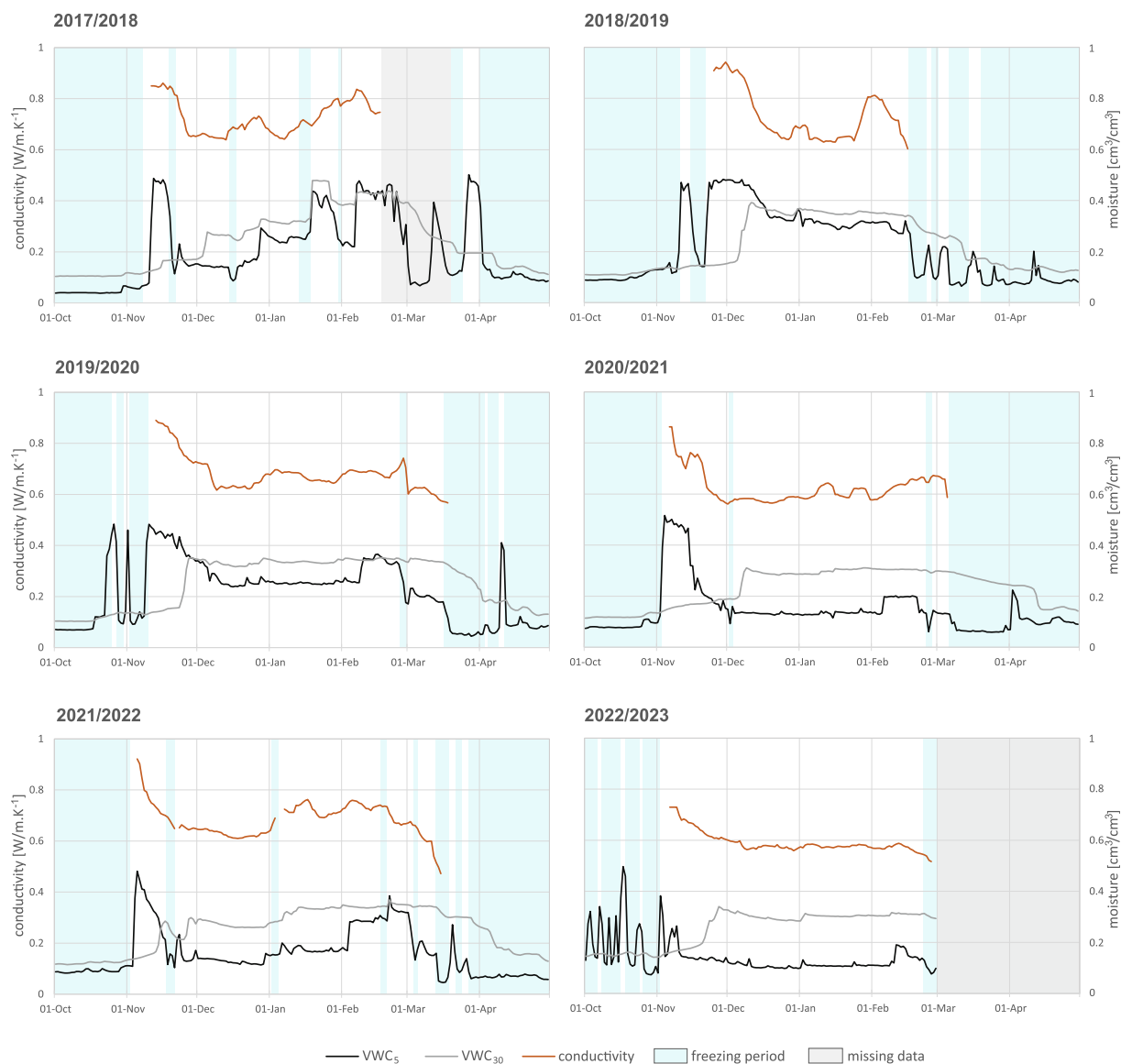


**Fig. 5.** Daily average of volumetric water content for 5 and 30 cm depth and weekly moving average of soil thermal conductivity (5–20 cm) in the summer seasons 2017–2023.

liquid moisture into still greater depths of the soil (e.g., [Andresen et al., 2020](#)), there is a potential for an increase of soil thermal conductivity in these depths and therefore of more heat reaching deeper parts of the soil profile, driving the thawing of the active layer ([Clayton et al., 2021](#)). A positive feedback loop is thus generated.

### 5.2.3. Correlation of seasonal means of selected parameters

While there is, depending on the season, still up to a half of the variability in soil thermal conductivity unaccounted for by changes in volumetric water content, the correlation between the seasonal means of these two parameters is very strong ( $r = 0.91$ ) and statistically significant for  $p < 0.01$  ([Fig. 9](#)). There is also a high correlation between both volumetric water content and thermal conductivity with thawing  $n$ -factor, which effectively describes the exchange of heat between the air and ground ([Klene et al., 2001](#)). In the years when ground surficial layer was moister and the soil was more conductive, higher values of  $n$ -factor were observed.

However, no significant relationship had been detected between soil thermal conductivity and ALT ( $r = -0.20$ ). Presumably the leading parameter affecting seasonal variability of ALT is  $TDD_5$  ( $r = 0.92$ ). Such a correlation value confirms the previous findings of a strong effect of

summer temperature on ALT on the Abernethy Flats ([Hrbáček and Uxa, 2020](#)). It is necessary to note that the relationship between ALT and TDD is highly predictable as TDD is the only temporal variable input to the widely used Stefan model for ALT modelling (e.g., [Riseborough et al., 2008](#)). Further, ALT ( $r = -0.88$ ) and  $TDD_5$  ( $r = -0.92$ ) both correlate negatively with volumetric water content. It means that even though it has been established that an increase in volumetric water content generates an increase in soil thermal conductivity ([Figs. 7–9](#)), this itself does not lead to a thickening of the active layer. On the contrary, active layer tends to be shallower in wet soils, due to a greater amount of latent heat needed for the phase change. Our results are therefore in agreement with the findings from other regions like Alaska ([Clayton et al. 2021](#)) and Tibetan Plateau (e.g., [Dörfer et al., 2013](#), [Jin et al., 2020](#)) who also concluded that the latent heat mechanism had a greater control than soil thermal conductivity on ALT in soils.

Notably, an increase of summer temperatures expressed by  $TDD_5$  will lead to soil drying and thickening of the active layer and it will also have consequences for the hydric regime of the active layer and the underlying permafrost. The occurrence of thicker active layer during the summer period allows for the migration of liquid moisture into greater depth and may result in the drying up of the surface layer of soil (e.g.,

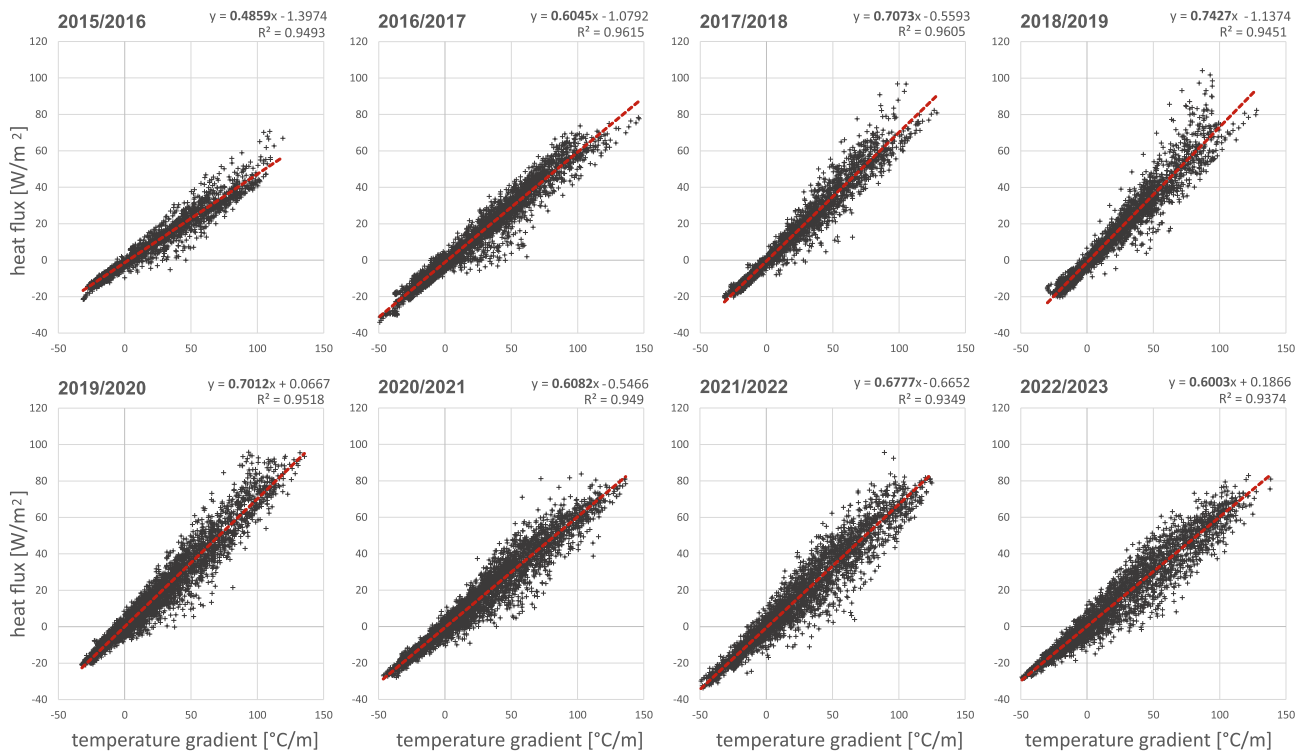


Fig. 6. Seasonal variability of soil thermal conductivity (marked in bold in the regression equation) determined from measured heat flux and temperature gradient values within the period 2015–2023.

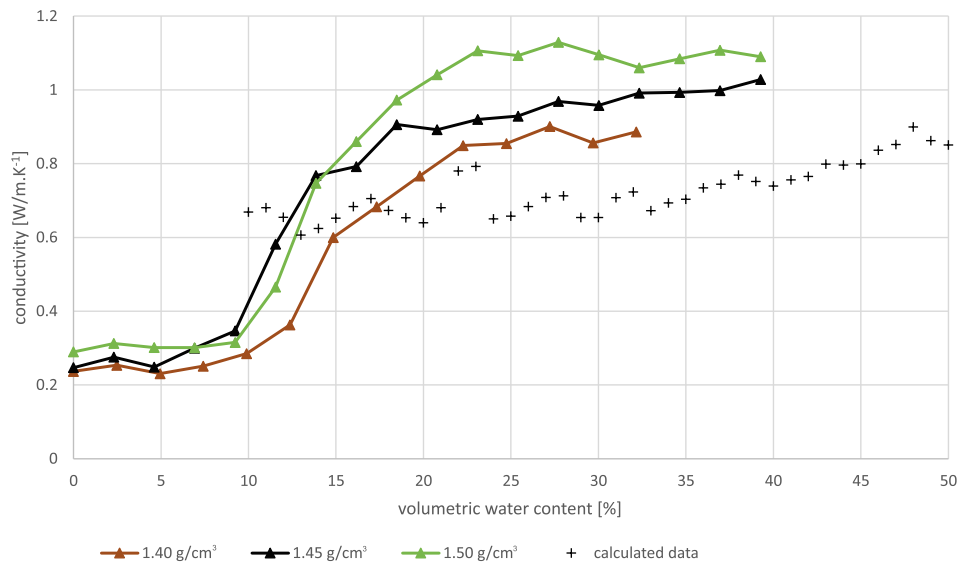


Fig. 7. Variability of soil thermal conductivity from the laboratory measurements at different volumetric water content and dry bulk density compared to the calculated data from field measurements.

Lawrence et al., 2015; Andresen et al., 2020). Surficial drying can lead to further acceleration of active layer thickening (Clayton et al., 2021), but it might also negatively affect the already very scarce vegetation which greatly relies on the presence of moisture, mostly derived from melt-water (Colesie et al., 2022), as there is very little liquid precipitation on James Ross Island and the eastern part of the Antarctic Peninsula in general.

## 6. Summary and conclusions

This paper describes the natural variability of soil thermal

conductivity on the Abernethy Flats, James Ross Island, during the period 2015–2023, contributing to a better understanding of how thermal properties and moisture affect the thermal regime of soils in the Antarctic ice-free areas. Instrumental measurements of air and ground temperature, as well as ground heat flux and water content are analysed to fulfil this purpose. We also conducted a laboratory measurement of thermal properties on soil samples from different depths to determine their response to a rising volumetric water content. Our findings show that the soil thermal conductivity increases rapidly up to a certain level of moisture, however the increase slows down and the further increments of moisture do not generate significantly higher conductivity

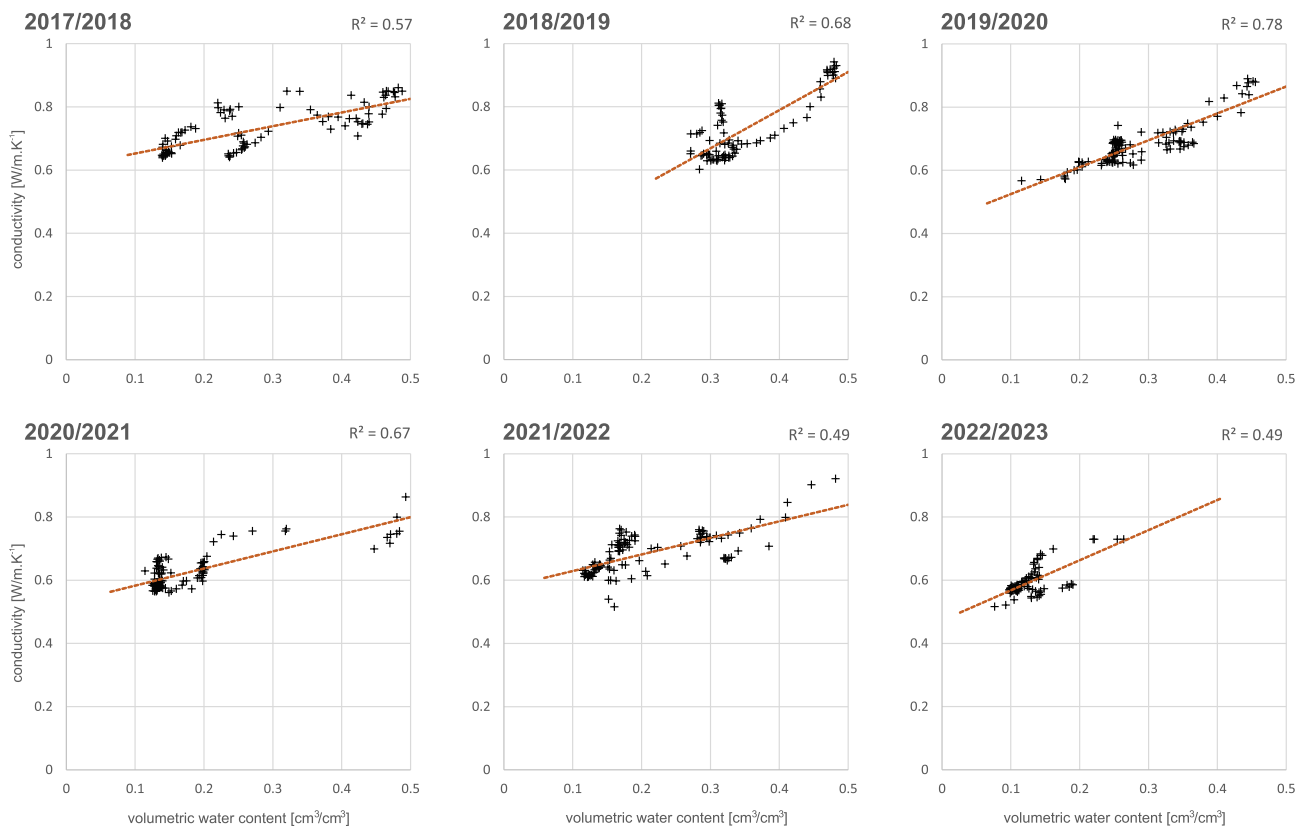


Fig. 8. Relationship between volumetric water content and soil thermal conductivity for individual seasons 2017–2023.

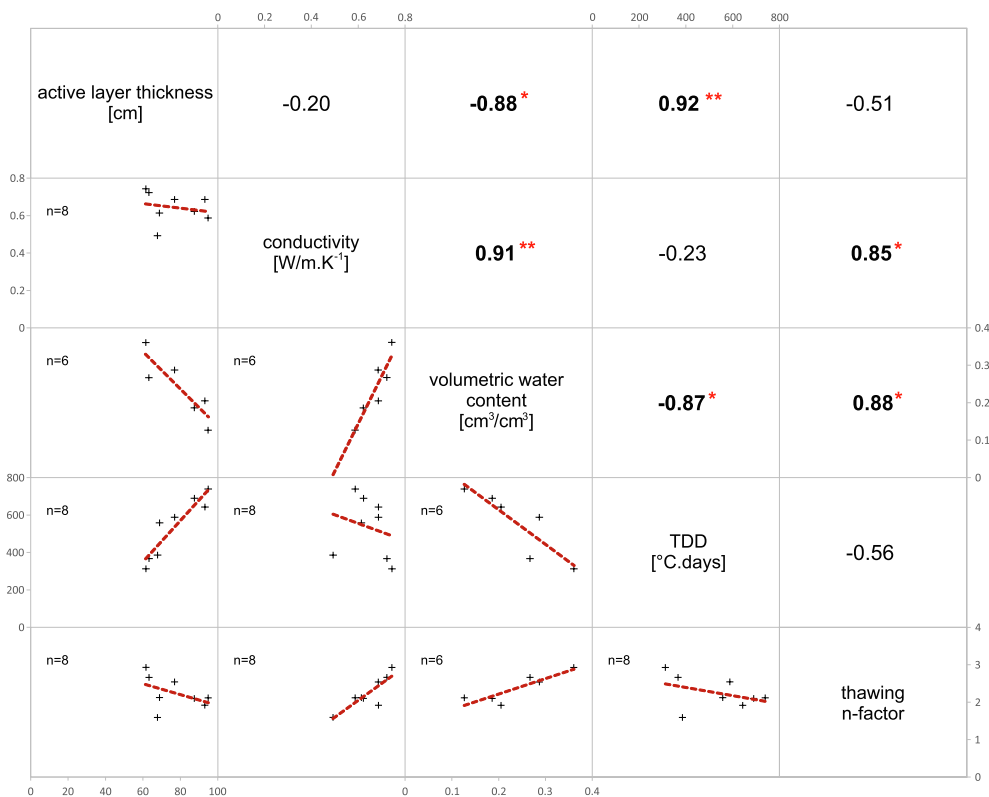


Fig. 9. Correlation matrix of the main soil parameters mentioned in this study (statistical significance expressed as \* for  $p < 0.05$ ; \*\* for  $p < 0.01$ ).

values. The relatively low observed natural variability of soil thermal conductivity is therefore in agreement with how the samples performed under laboratory conditions.

While soil thermal properties, such as its thermal conductivity, are mainly affected by water content, an increase in thermal conductivity does not directly lead to a deepening of the active layer. In fact, evidence was found to the contrary, when the active layer was actually shallower in the years with higher overall soil moisture levels. While wet soil is more efficient at conducting heat from the atmosphere into the ground, this is offset by the greater amount of heat needed to thaw the ice present within the soil. The main control of active layer depth is therefore the sum of positive temperatures within the season, which has indirect control over the soil water content as well, through evaporation and migration of available liquid moisture into the deeper parts of the soil profile.

The warming trend observed in this part of the Antarctic Peninsula in the recent seasons has led to a dramatic increase of thaw depths on the Abernethy Flats. The rapidly changing conditions will most likely affect the hydric and thermal regime of the underlying permafrost in the future and have consequences also for the local biota, which, being mostly dependent on meltwater for its only source of moisture, is very sensitive to these ongoing changes.

### Declaration of Competing Interest

The authors declare the following financial interests/personal relationships which may be considered as potential competing interests: Filip Hrbáček reports financial support was provided by Czech Science Foundation.

### Data availability

Data will be made available on request.

### Acknowledgements

This research was supported by Ministry of Education, Youth and Sports of the Czech Republic project (VAN 2022) and Czech Science Foundation project (GM22-28659M). The authors would like to acknowledge the staff of Czech Antarctic Johann Gregor Mendel station for help with installation and maintenance of the instrumental measurements. Furthermore, we thank Miguel Ángel de Pablo and two anonymous reviewers for providing suggestions on improving this manuscript.

### References

- Abu-Hamdeh, N.H., Reeder, R.C., 2000. Soil Thermal Conductivity: Effects of Density, Moisture, Salt Concentration, and Organic Matter. *Soil Sci. Soc. Am. J.* 64, 1285–1290. <https://doi.org/10.2136/sssaj2000.6441285x>.
- Andresen, C.G., Lawrence, D.M., Wilson, C.J., McGuire, A.D., Koven, C., Schaefer, K., Jafarov, E., Peng, S., Chen, C., Gouttevin, I., Burke, E., Chadburn, S., Ji, D., Chen, G., Hayes, D., Zhang, W., 2020. Soil moisture and hydrology projections of the permafrost region – a model intercomparison. *Cryosphere* 14, 445–459. <https://doi.org/10.5194/tc-14-445-2020>.
- Borzotta, E., Trombotto, D., 2004. Correlation between frozen ground thickness measured in Antarctica and permafrost thickness estimated on the basis of the heat flow obtained from magnetotelluric soundings. *Cold Reg. Sci. Technol.* 40, 81–96. <https://doi.org/10.1016/j.coldregions.2004.06.002>.
- Bozkurt, D., Bromwich, D.H., Carrasco, J., Rondanelli, R., 2021. Temperature and precipitation projections for the Antarctic Peninsula over the next two decades: contrasting global and regional climate model simulations. *Clim. Dyn.* 56, 3853–3874. <https://doi.org/10.1007/s00382-021-05667-2>.
- Brakelmann, H., 1984. *Physical principles and calculation methods of moisture and heat transfer in cable trenches*. VDE-Verlag, Berlin, p. 93.
- Brooks, S.T., Jabour, J., van den Hoff, J., Bergstrom, D.M., 2019. Our footprint on Antarctica competes with nature for rare ice-free land. *Nat. Sustainability* 2, 185–190. <https://doi.org/10.1038/s41893-019-0237-y>.
- Cannone, N., Guglielmin, M., Malfasi, F., Hubberten, H.W., Wagner, D., 2021. Rapid soil and vegetation changes at regional scale in continental Antarctica. *Geoderma* 394, 115017. <https://doi.org/10.1016/j.geoderma.2021.115017>.
- Clayton, L.K., Schaefer, K., Battaglia, M.J., Bourgeau-Chavez, L., Chen, J., Chen, R.H., Chen, A., Bakian-Dogaheh, K., Grelik, S., Jafarov, E., Liu, L., Michaelides, R.J., Moghaddam, M., Parsekian, A.D., Rocha, A.V., Schaefer, S.R., Sullivan, T., Tabatabaenejad, A., Wang, K., Wilson, K.J., Zebker, H.A., Zhang, Y., Zhao, Y., 2021. Active layer thickness as a function of soil water content. *Environ. Res. Lett.* 16, 055028. <https://doi.org/10.1088/1748-9326/abfa4c>.
- Colesie, C., Walshaw, C.V., Garcia Sancho, L., Davey, M.P., Gray, A., 2022. Antarctica's vegetation in a changing climate. *WIREs Clim. Change* 14, e810.
- Correia, A., Vieira, G., Ramos, M., 2012. Thermal conductivity and thermal diffusivity of cores from a 26 meter deep borehole drilled in Livingston Island, Maritime Antarctic. *Geomorphology* 155–156, 7–11. <https://doi.org/10.1016/j.geomorph.2011.12.012>.
- de Bruin, J.G.H., Bense, V.F., van der Ploeg, M.J., 2021. Inferring Permafrost Active Layer Thermal Properties from Numerical Model Optimization. *Geophys. Res. Lett.* 48, e2021GL093306. [doi.org/10.1029/2021GL093306](https://doi.org/10.1029/2021GL093306).
- De Vries, D.A., 1963. *Thermal properties of soils*. In: Van Wijk, W.R. (Ed.), *Physics of Plant Environment*. Wiley, New York, pp. 210–235.
- Dörfer, C., Kühn, P., Baumann, F., He, J., Scholten, T., 2013. *Soil Organic Carbon Pools and Stocks in Permafrost-Affected Soils on the Tibetan Plateau*. *PLoS One* 8, e57024.
- Farouki, O.T., 1981. *Thermal Properties of Soil*. U.S. Army Corps of Engineers, Cold Regions Research and Engineering Laboratory, Hanover, 136 pp.
- Guglielmin, M., Balks, M.R., Adlam, L.S., Baio, F., 2011. Permafrost thermal regime from two 30-m deep boreholes in Southern Victoria Land, Antarctica. *Permafrost. Periglac. Process.* 22, 129–139. <https://doi.org/10.1002/ppp.715>.
- He, H., He, D., Jin, J., Smits, K.M., Dyck, M., Wu, Q., Si, B., Lv, J., 2020. Room for improvement: A review and evaluation of 24 soil thermal conductivity parameterization schemes commonly used in land-surface, hydrological, and soil-vegetation-atmosphere transfer models. *Earth-Sci. Rev.* 211, 103419. [doi.org/10.1016/j.earscirev.2020.103419](https://doi.org/10.1016/j.earscirev.2020.103419).
- Hinzman, L.D., Kane, D.L., Gieck, R.E., Everett, K.R., 1991. Hydrologic and thermal properties of the active layer in the Alaskan Arctic. *Cold Reg. Sci. Technol.* 19, 95–110. [https://doi.org/10.1016/0165-232X\(91\)90001-W](https://doi.org/10.1016/0165-232X(91)90001-W).
- Hrbáček, F., Kňazková, M., Nývlt, D., Láška, K., Mueller, C.W., Ondruch, J., 2017. Active layer monitoring at CALM-S site near J.G.Mendel Station, James Ross Island, Eastern Antarctic Peninsula. *Sci. Total Environ.* 601–602, 987–997. [dx.doi.org/10.1016/j.scitotenv.2017.05.266](https://doi.org/10.1016/j.scitotenv.2017.05.266).
- Hrbáček, F., Uxa, T., 2020. The evolution of a near-surface ground thermal regime and modeled active-layer thickness on James Ross Island, Eastern Antarctic Peninsula, in 2006–2016. *Permafrost. Periglac. Process.* 31, 141–155. <https://doi.org/10.1002/ppp.2018>.
- Hrbáček, F., Oliva, M., Hansen, C., Balks, M., O'Neill, T.A., de Pablo, M.A., Ponti, S., Ramos, M., Vieira, G., Abramov, A., Kaplan Pastříková, L., Guglielmin, M., Goyanes, G., Francellino, M.R., Schaefer, C., Lancelle, D., 2023. Active layer and permafrost thermal regimes in the ice-free areas of Antarctica. *Earth Sci. Rev.* 242, 104458. <https://doi.org/10.1016/j.earscirev.2023.104458>.
- Jeevantinie Kapilaratne, R.G.C., Lu, M., 2017. Automated general temperature correction method for dielectric soil moisture sensors. *J. Hydrol.* 551, 203–216. [doi.org/10.1016/j.jhydrol.2017.05.050](https://doi.org/10.1016/j.jhydrol.2017.05.050).
- Jin, X., Jin, H., Wu, X., Luo, D., Yu, S., Li, X., He, R., Wang, Q., Knops, J.M.H., 2020. Permafrost Degradation Leads to Biomass and Species Richness Decreases on the Northeastern Qinghai-Tibet Plateau. *Plants* 9, 1453. <https://doi.org/10.3390/plants9111453>.
- Johansen, O., 1977. *Thermal Conductivity of Soils*. U.S. Army Corps of Engineers, Cold Regions Research and Engineering Laboratory, Hanover, 291 pp.
- Kavan, J., Nývlt, D., Láška, K., Engel, Z., Kňazková, M., 2020. High latitude dust deposition in snow on the glaciers of James Ross Island, Antarctica. *Earth Surf. Proc. Land.* 45, 1569–1578.
- Kersten, M.S., 1949. *Thermal Properties of Soils*. Bulletin No. 28, University of Minnesota.
- Klene, A.E., Nelson, F.E., Shiklomanov, N.I., Hinkel, K.M., 2001. The N-Factor in Natural Landscapes: Variability of Air and Soil-Surface Temperatures, Kuparuk River Basin, Alaska, U.S.A. *Arct. Antarct. Alp. Res.* 33, 140–148.
- Kňazková, M., Hrbáček, F., Kavan, J., Nývlt, D., 2020. Effect of hyaloclastite breccia boulders on meso-scale periglacial-aeolian landsystem in semi-arid Antarctic environment, James Ross Island, Antarctic Peninsula. *Cuadernos de Investigación Geográfica* 46, 7–31.
- Lawrence, D.M., Koven, C.D., Swenson, S.C., Riley, W.J., Slater, A.G., 2015. Permafrost thaw and resulting soil moisture changes regulate projected high-latitude CO<sub>2</sub> and CH<sub>4</sub> emissions. *Environ. Res. Lett.* 10, 094011. <https://doi.org/10.1088/1748-9326/10/9/094011>.
- Lee, J.R., Raymond, B., Bracegirdle, T.J., Chadès, I., Fuller, R.A., Shaw, J.D., Terauds, A., 2017. Climate change drives expansion of Antarctic ice-free habitat. *Nature* 547, 49–54. <https://doi.org/10.1038/nature22996>.
- Levy, J.S., Schmidt, L.M., 2016. Thermal properties of Antarctic soils: wetting controls subsurface thermal state. *Antarct. Sci.* 28, 361–370. <https://doi.org/10.1017/S0954102016000201>.
- Li, W., Weng, B., Yan, D., Lai, Y., Li, M., Wang, H., 2023. Underestimated permafrost degradation: Improving the TTOP model based on soil thermal conductivity. *Science of the Total Environment*, 854, 158564. [dx.doi.org/10.1016/j.scitotenv.2022.158564](https://doi.org/10.1016/j.scitotenv.2022.158564).
- Li, Z., Yang, J., Zheng, Z., Yu, Y., Zhang, T., Hou, X., Wei, Z., 2017. Comparative study of the soil thermal regime in arid and semi-humid areas. *Environ. Earth Sci.* 76, 28. <https://doi.org/10.1007/s12665-016-6354-2>.
- Li, R., Zhao, L., Wu, T., Wang, Q., Ding, Y., Yao, J., Wu, X., Hu, G., Xiao, Y., Du, Y., Zhu, X., Qin, Y., Yang, S., Bai, R., Du, E., Liu, G., Zou, D., Qiao, Y., Shi, J., 2019. Soil thermal conductivity and its influencing factors at the Tanggula permafrost region on the Qinghai-Tibet Plateau. *Agric. For. Meteorol.* 264, 235–246. <https://doi.org/10.1016/j.agrformet.2018.10.011>.

- Liu, L., Sletten, R.S., Hallet, B., Waddington, E.D., 2018. Thermal Regime and Properties of Soils and Ice-Rich Permafrost in Beacon Valley, Antarctica. *J. Geophys. Res. Earth* 123, 1797–1810. <https://doi.org/10.1029/2017JF004535>.
- Lorant, M.M., Abbott, B.W., Blok, D., Douglas, T.A., Epstein, H.E., Forbes, B.C., Jones, B. M., Kholodov, A.L., Kropp, H., Malhotra, A., Mamet, S.D., Myers-Smith, I.H., Natali, S.M., O'Donnell, J.A., Phoenix, G.K., Rocha, A.V., Sonnentag, O., Tape, K.D., Walker, D.A., 2018. Reviews and syntheses: Changing ecosystem influences on soil thermal regimes in northern high-latitude permafrost regions. *Biogeosciences* 15, 5287–5313. <https://doi.org/10.5194/bg-15-5287-2018>, 2018.
- Mergelov, N.S., 2014. Soils of wet valleys in the Larsemann Hills and Vestfold Hills oases (Princess Elizabeth Land, East Antarctica). *Eurasian Soil Sci.* 47, 845–862. <https://doi.org/10.1134/S1064229314090099>.
- Mlčoch, B., Nývlt, D., Mixa, P. (Eds.), 2020. *Geological Map of James Ross Island – Northern Part 1: 25,000*. Czech Geological Survey, Praha.
- Mondal, S., Padmakumar, G.P., Sharma, V., Singh, D.N., Baghini, M.S., 2015. A methodology to determine thermal conductivity of soils from flux measurement. *Geomech. Geoen.: Int. J.* 11, 73–85. [dx.doi.org/10.1080/17486025.2015.1020346](https://doi.org/10.1080/17486025.2015.1020346).
- Nicolisky, D.J., Romanovsky, V.E., 2018. Modeling Long-Term Permafrost Degradation. *J. Geophys. Res. Earth* 123, 1756–1771. <https://doi.org/10.1029/2018JF004655>.
- Obu, J., Westermann, S., Bartsch, A., Berdnikov, N., Christiansen, H.H., Dashtseren, A., Delaloye, R., Elberling, B., Eitzmüller, B., Kholodov, A., Khomutov, A., Kääh, A., Leibman, M.O., Lewkowicz, A.G., Panda, S.K., Romanovsky, V., Way, R.G., Westergaard-Nielsen, A., Wu, T., Yamkhin, Y., Zou, D., 2019. Northern Hemisphere permafrost map based on TTOP modelling for 2000–2016 at 1 km<sup>2</sup> scale. *Earth Sci. Rev.* 193, 299–316. <https://doi.org/10.1016/j.earscirev.2019.04.023>.
- Obu, J., Westermann, S., Vieira, G., Abramov, A., Balks, M., Bartsch, A., Hrbáček, F., Kääh, A., Ramos, M., 2020. Pan-Antarctic map of near-surface permafrost temperatures at 1 km<sup>2</sup> scale. *Cryosphere* 14, 497–519.
- O'Donnell, J.A., Romanovsky, V.E., Harden, J.W., McGuire, A.D., 2009. The Effect of Moisture Content on the Thermal Conductivity of Moss and Organic Soil Horizons From Black Spruce Ecosystems in Interior Alaska. *Soil Sci.* 174, 646–651. <https://doi.org/10.1097/SS.0b013e3181c4a7f8>.
- Rasmussen, L.H., Zhang, W., Hollesen, J., Cable, S., Christiansen, H.H., Jansson, P., Elberling, B., 2018. Modelling present and future permafrost thermal regimes in Northeast Greenland. *Cold Reg. Sci. Technol.* 146, 199–213. <https://doi.org/10.1016/j.coldregions.2017.10.011>.
- Riseborough, D., Shiklomanov, N., Eitzmüller, B., Gruber, S., Marchenko, S., 2008. Recent Advances in Permafrost Modelling. *Permafrost Periglac. Process.* 19, 137–156. <https://doi.org/10.1002/ppp.615>.
- Romio, L.C., Roberti, D.R., Buligon, L., Zimmer, T., Degrazia, G.A., 2019. A Numerical Model to Estimate the Soil Thermal Conductivity Using Field Experimental Data. *Appl. Sci.* 9, 4799. <https://doi.org/10.3390/app9224799>.
- Schjønning, P., 2021. Thermal conductivity of undisturbed soil – Measurements and predictions. *Geoderma* 402, 115188. <https://doi.org/10.1016/j.geoderma.2021.115188>.
- Smith, S.L., Wolfe, S.A., Riseborough, D.W., Nixon, F.M., 2009. Active-layer characteristics and summer climatic indices, Mackenzie Valley, Northwest Territories, Canada. *Permafrost Periglac. Process.* 20, 201–220. <https://doi.org/10.1002/ppp.651>.
- Turner, J., Marshall, G.J., Clem, K., Colwell, S., Phillips, T., Lu, H., 2020. Antarctic temperature variability and change from station data. *Int. J. Climatol.* 40 (6), 2986–3007. <https://doi.org/10.1002/joc.6378>.
- van Wessem, J.M., Ligtgenberg, S.R.M., Reijmer, C.H., van de Berg, W.J., van den Broeke, M.R., Barrand, N.E., Thomas, E.R., Turner, J., Wuite, J., Scambos, T.A., van Meijgaard, E., 2016. The modelled surface mass balance of the Antarctic Peninsula at 5.5 km horizontal resolution. *Cryosphere* 10, 271–285. <https://doi.org/10.5194/tc-10-271-2016>.
- Wessolek, G., Bohne, K., Trinks, S., 2023. Validation of Soil Thermal Conductivity Models. *Int. J. Thermophys.* 44, 20. <https://doi.org/10.1007/s10765-022-03119-5>.
- Wlostowski, A.N., Gooseff, M.N., Adams, B.J., 2017. Soil Moisture Controls the Thermal Habitat of Active Layer Soils in the McMurdo Dry Valleys, Antarctica. *J. Geophys. Res.* Bioge. 123, 46–59. <https://doi.org/10.1002/2017JG004018>.
- Yershov, E.D., 1998. *General Geocryology*. Cambridge University Press, Cambridge. doi: 10.1017/CBO9780511564505.
- Zhang, Q., Cao, X., Wei, G., Huang, R., 2002. Observation and study of land surface parameters over Gobi in typical arid region. *Adv. Atmos. Sci.* 19, 121–135. <https://doi.org/10.1007/s00376-002-0039-3>.



## Permafrost table temperature and active layer thickness variability on James Ross Island, Antarctic Peninsula, in 2004–2021

Lucia Kaplan Pastřířková<sup>a,\*</sup>, Filip Hrbáčřek<sup>a</sup>, Tomáš Uxa<sup>b</sup>, Kamil Lářka<sup>a</sup>

<sup>a</sup> Department of Geography, Masaryk University, Brno, Czech Republic

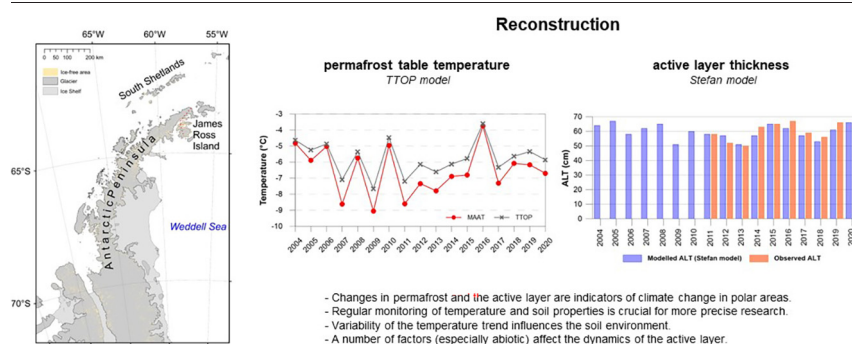
<sup>b</sup> Institute of Geophysics, Czech Academy of Sciences, Prague, Czech Republic



### HIGHLIGHTS

- Permafrost and active layer changes are important indicators of climate variability.
- Regular study of the properties and changes of permafrost and the active layer is crucial for revealing long-term trends.
- TTOP and Stefan model has advantages in obtaining data of the frozen ground.

### GRAPHICAL ABSTRACT



### ARTICLE INFO

Editor: Manuel Esteban Lucas-Borja

#### Keywords:

Permafrost  
Active layer  
TTOP model  
Stefan model  
Antarctic Peninsula  
Climate change

### ABSTRACT

Climate change and its impacts on sensitive polar ecosystems are relatively little studied in Antarctic regions. Permafrost and active layer changes over time in periglacial regions of the world are important indicators of climate variability. These changes (e. g. permafrost degradation, increasing of the active layer thickness) can have a significant impact on Antarctic terrestrial ecosystems. The study site (AWS-JGM) is located on the Ulu Peninsula in the north of James Ross Island. Ground temperatures at depths of 5, 50, and 75 cm have been measured at the site since 2011, while air temperature began to be measured in 2004. The main objective is to evaluate the year-to-year variability of the reconstructed temperature of the top of the permafrost table and the active layer thickness (ALT) since 2004 based on air temperature data using TTOP and Stefan models, respectively. The models were verified against direct observations from a reference period 2011/12–2020/21 showing a strong correlation of 0.95 (RMSE = 0.52) and 0.84 (RMSE = 3.54) for TTOP and Stefan models, respectively. The reconstructed average temperature of the permafrost table for the period 2004/05–2020/21 was  $-5.8\text{ }^{\circ}\text{C}$  with a trend of  $-0.1\text{ }^{\circ}\text{C}/\text{decade}$ , while the average air temperature reached  $-6.6\text{ }^{\circ}\text{C}$  with a trend of  $0.6\text{ }^{\circ}\text{C}/\text{decade}$ . Air temperatures did not have an increasing trend throughout the period, but in the first part of the period (2004/05–2010/11) showed a decreasing tendency ( $-1.3\text{ }^{\circ}\text{C}/\text{decade}$ ). In the period 2011/12–2020/21, it was a warming of  $1.9\text{ }^{\circ}\text{C}/\text{decade}$ . The average modelled ALT for the period 2004/05–2020/21 reached a value of 60cm with a trend of  $-1.6\text{ cm}/\text{decade}$ . Both models were found to provide reliable results, and thus they significantly expand the information about the permafrost and ALT, which is necessary for a better understanding of their spatiotemporal variability and the impact of climate change on the cryosphere.

\* Corresponding author at: Department of Geography, Masaryk University, Kotlářská 267/2, 601 77 Brno, Czech Republic.  
E-mail address: [l.pastirikova17@gmail.com](mailto:l.pastirikova17@gmail.com) (L. Kaplan Pastřířková).

## 1. Introduction

Antarctica, as the least human-disturbed continent, is one of the key areas for understanding the overall global climate (Stammerjohn et al., 2021). Properties of perennially frozen ground (permafrost) and seasonal thaw layer (active layer) are important indicators of climate change in the polar areas because they are sensitive to even slight changes in air and ground temperatures (Smith and Riseborough, 1996; Vaughan et al., 2003). Thawing of permafrost is reflected in various landscape processes and hazards such as coastal instability, ground subsidence, changes in hydrological regime, ecosystems, or surface vegetation (French, 2017; Cannone et al., 2021). The response of permafrost and active layer to current climate change depends on the interactions of many parameters and factors, including topography, structure and properties of the ground, the presence and type of vegetation or the occurrence of snow (e. g. Smith and Riseborough, 1996; French, 2017; Biskaborn et al., 2019). Temperature changes in these ecosystems might be significantly influenced by the presence of vegetation dominated by mosses and lichens (Guglielmin et al., 2014). In recent decades, there have been rapid changes in the range and abundance of several populations of vegetation in relation to climate change (Chown and Convey, 2007). Surface coverage by vegetation provides an insulating effect and consequently the vegetation affects the energy exchange of the ground. This has a feedback effect on the active layer thickness and the temperature of the permafrost (Guglielmin et al., 2014).

Continuous permafrost currently occurs mostly in the Arctic and the Tibetan Plateau, underlying  $\sim 10,700,000\text{km}^2$  (Obu et al., 2019). In contrast, ice-free areas in Antarctica hosting such ecosystems are estimated to occupy as low as about  $55,000\text{--}71,000\text{km}^2$  of the entire continent (Lee et al., 2017; Brooks et al., 2019). A significant extent of permafrost occurs in the Antarctic Peninsula region where ice-free areas occupy about  $6500\text{km}^2$  (Brooks et al., 2019). The Antarctic Peninsula region has been exposed to accelerated atmospheric warming in the last decades of the 20th century when the air temperatures locally increased by  $>3\text{ }^\circ\text{C}$  (e. g. Doran et al., 2002; Vaughan et al., 2003; Turner et al., 2020). The warming of the Antarctic Peninsula region has been confirmed on the basis of numerous studies especially in its western part, which shows mean annual air temperatures ranging from  $-2$  to  $-4\text{ }^\circ\text{C}$  (Turner et al., 2020). However, atmospheric cooling was observed since the late 1990s (Turner et al., 2016; Oliva et al., 2017), which also affected the cryosphere, including active layer and permafrost temperatures (Oliva et al., 2017; Hrbáček and Uxa, 2020).

The recent studies from other parts of Antarctica also report fast changes of vegetation state (Robinson et al., 2018) and soil biogeochemical properties (Cannone et al., 2021) in response to changes in soil thermal and moisture regimes. Unlike atmospheric measurements, long-term data on active layer and permafrost in Antarctica are unavailable, especially before the International Polar Year 2007–2008. The research has been less systematic and spatially worse distributed than in the northern hemisphere due to the remoteness of the continent (Vieira et al., 2010). Hence, long-term changes in the temperature and thickness of the active layer and permafrost in Antarctica mostly cannot be accurately assessed (Biskaborn et al., 2015), and the studies remain scarce (Guglielmin and Cannone, 2012; Ramos et al., 2017; Biskaborn et al., 2019; Hrbáček and Uxa, 2020; Hrbáček et al., 2021). Understanding of long-term variability of the active layer and permafrost thermal regime can be key for the complex comprehension of the geomorphic and soil dynamic in the Antarctic terrestrial environments (Convey and Peck, 2019). The knowledge of active layer and permafrost thermal regime will be also crucial for the predictions of the evolution of newly exposed ice-free areas which are expected to double in extent in the Antarctic Peninsula region until the end of 21st century (Lee et al., 2017).

One of the possibilities how to bridge this gap in data availability may be active layer and permafrost modelling using specific proven models, which has been common in the northern hemisphere over last decades (e.g.; Smith and Riseborough, 1996, 2002; Gislén et al., 2013; Westermann et al., 2013; Kurylyk, 2015; Obu et al., 2019). On the contrary,

only a few early modelling studies have so far emerged in Antarctica for permafrost temperature (Ferreira et al., 2017; Hrbáček et al., 2020; Obu et al., 2020) as well as ALT (Guglielmin and Cannone, 2012; Wilhelm and Bockheim, 2016; Uxa, 2017; Hrbáček and Uxa, 2020). The models are generally controlled by ground temperature and ground thermal properties, but it is also possible to use parameterized air temperatures (Smith and Riseborough, 1996). An important part of the current study of permafrost changes is the integration of models that mostly contain input parameters related to thawing and freezing processes. Modelled permafrost temperature based on other measured parameters in the field can reveal local climate change. The models generally differ in their complexity. Numerical models (e. g. CoupModel, CryoGrid 2, CryoGrid 3, GIPL2-MPI) are more sophisticated and can accommodate energy transfer between the atmosphere, snow cover and permafrost, but they need many inputs (Jafarov et al., 2012; Westermann et al., 2013; Rasmussen et al., 2018). On the other hand, analytical models, such as the TTOP or Stefan model, tend to be simpler and require fewer inputs while maintaining good accuracy (Riseborough et al., 2008).

The main aim of this study is to reconstruct and analyse the variability of permafrost table temperature and ALT at the Johann Gregor Mendel station (AWS-JGM) on James Ross Island, Antarctic Peninsula, using analytical models. The specific objectives are as follows:

- 1) Evaluation of the variability of air temperature, ground temperature at depths of 5, 50 and 75 cm and changes in the active layer thickness observed in the period 2011/12–2020/21.
- 2) Reconstruction of the permafrost table temperature using the TTOP model and ALT using the Stefan model in the period 2004/05–2020/21 based on the air temperature data.
- 3) Assessment of long-term variability of air temperature, permafrost table temperature and ALT in the period 2004/05–2020/21.

## 2. Study area

James Ross Island is located in the north-eastern part of the Antarctic Peninsula region (Fig. 1). It lies in the transition zone between the oceanic and continental climate. Compared to the western part of the Antarctic Peninsula, it is an area with colder and drier conditions, caused by the orographic barrier of the Trinity Peninsula, which prevents air masses from the west (Martin and Peel, 1978; King et al., 2013).

About 75 % of the area of James Ross Island is covered by glaciers, which are located mainly in its central and southern part (Davies et al., 2013). The study site AWS-JGM ( $63^\circ 48' \text{S}$ ,  $57^\circ 52' \text{W}$ , 10 m a.s.l.) is located in the northern part of Ulu Peninsula, where deglaciated surfaces of  $312\text{ km}^2$  form the largest ice-free area in the Antarctic Peninsula region (Kavan et al., 2017; Hrbáček et al., 2017). It is situated on a Holocene marine terrace (Fig. 2) formed by beach deposits composed of gravelly sand (Hrbáček et al., 2017) with a surface gently inclined ( $<3^\circ$ ) towards north.

The mean annual air temperature (MAAT) was around  $-7.0\text{ }^\circ\text{C}$  in the period 2005–2015 at sea level on the AWS-JGM site (Ambrožová and Láška, 2016; Hrbáček et al., 2016b). A positive trend of MAAT and a negative trend of mean summer air temperature was reported in the study area in the period 2006–2015 (Hrbáček et al., 2021). July and August are the coldest months as mean daily air temperatures can drop below  $-30\text{ }^\circ\text{C}$ . January is usually the warmest month as the highest mean daily air temperatures can exceed  $8\text{--}9\text{ }^\circ\text{C}$  (Láška et al., 2011). Local climate is characterized by  $4\text{--}5\text{ }^\circ\text{C}$  lower MAAT compared to the north-western part of the Antarctic Peninsula (Hrbáček et al., 2016b).

Precipitation occurs mostly in the form of snow, especially from March to November, and it is estimated at  $300\text{--}700\text{ mm}$  of water equivalent per year (van Wessem et al., 2016). The influence of snow cover on ground temperature is rather limited as its depth during winter is reduced by wind redistribution (Kavan et al., 2020), and it usually does not exceed 30 cm (Hrbáček et al., 2016a). The Ulu Peninsula is underlain by continuous permafrost (Bockheim et al., 2013; Obu et al., 2020), with estimated thickness in coastal areas of ca.  $6\text{--}67\text{ m}$  (Borzotta and Trombotto, 2004). The ALT

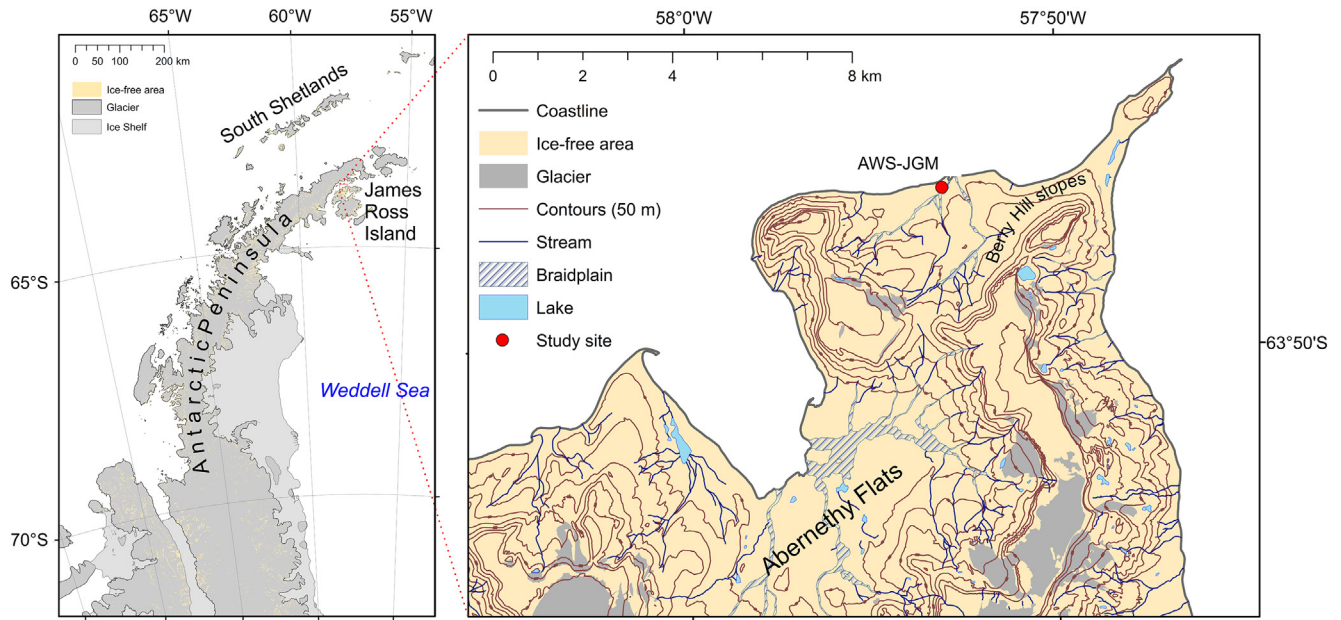


Fig. 1. Regional setting and location of the study site the AWS-JGM (James Ross Island) [Czech Geological Survey, 2009; SCAR Antarctic Digital Database].

strongly depends on lithological properties and usually ranges from ca. 0.5 to 1.2 m (Hrbáček et al., 2017).

### 3. Data and methods

#### 3.1. Data measuring and processing

##### 3.1.1. Temperature data

Air temperature was measured using Minikin TH datalogger (EMS Brno) with an accuracy of  $\pm 0.15$  °C at 0 °C, which was installed at 2 m above the ground surface in a solar radiation shield from March 2004 to February 2021. Ground temperatures were measured with A-class Pt100/8 resistance temperature detectors (EMS Brno) placed directly into the ground at depths of 5, 50 and 75 cm during the period from March 2011 to February 2021. Both air and ground temperatures were measured and stored every 30 min.

Daily, monthly, seasonal and annual means of air and ground temperatures at individual depths were subsequently calculated from the 30-min temperature records. The mean annual air and ground temperatures were calculated for the period from March 1 to February 28/29 because it usually contains an almost complete sequence of the freezing and thawing seasons. This approach respects the natural annual cycle of ground temperature and is consistent with previous studies from the area (e. g. Hrbáček et al., 2017; Hrbáček and Uxa, 2020). The ALT was calculated as a maximum depth of 0

°C isotherm interpolated from the maximum annual temperatures at depths of 50 and 75 cm. Subsequently, we used the values of the observed ALT and annual temperature means from the depths of 50 and 75 cm for the interpolation of the mean annual ground temperature at the top of the permafrost (ITOP). ITOP values, similar to TTOP (mean annual temperature at the top of permafrost), were calculated for individually defined annual periods, which corresponded to the composite sums of the lengths of the freezing and thawing seasons.

Daily mean air and ground temperatures measured at a depth of 5 cm were used to define the duration of the thawing ( $D_t$ ) and freezing ( $D_f$ ) seasons with prevailing positive and negative temperatures, respectively, as has been used in other studies from the Antarctic Peninsula region (e. g. Ferreira et al., 2017; de Pablo et al., 2017; Hrbáček et al., 2017).  $D_t$  and  $D_f$  were defined by the air temperature for the period 2004/05–2020/21 and also by the ground temperature measured at a depth of 5 cm for the period 2011/12–2020/21 when ground temperature has been measured at the AWS-JGM. For each season, thawing and freezing degree-days were defined for air ( $TDD_A$  and  $FDD_A$ ) and ground at a depth of 5 cm ( $TDD_{GT5}$  and  $FDD_{GT5}$ ). Thawing degree-days ( $TDD$ ) are calculated as the total seasonal sum of mean daily temperatures  $> 0$  °C:

$$TDD = \sum_{i=1}^{D_t} T_{(i)} [T > 0 \text{ °C}] \quad (1)$$

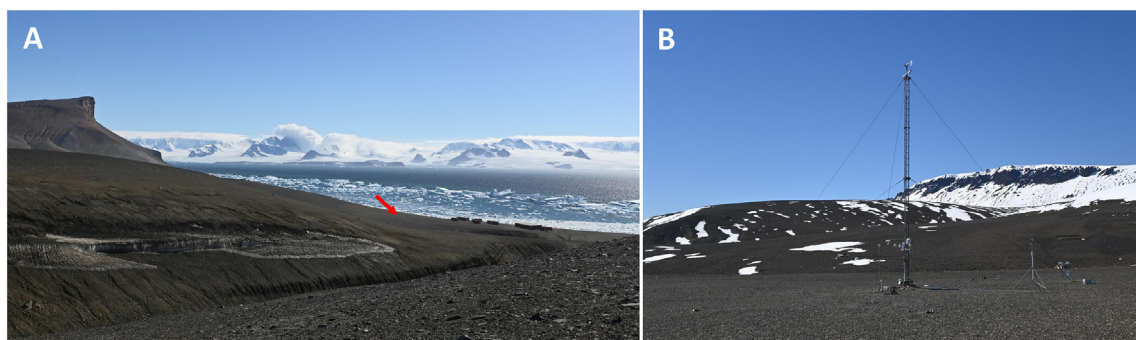


Fig. 2. (A) Position of the study site near the AWS-JGM on the Holocene marine terrace in the northern part of the Ulu Peninsula and (B) a detailed photo of the automatic weather station there.

Freezing degree-days ( $FDD$ ) are calculated as the total seasonal sum of mean daily temperatures  $<0$  °C:

$$FDD = \sum_{i=1}^{Df} T_{(i)} [T < 0 \text{ °C}] \quad (2)$$

Both permafrost table temperature and ALT reconstructions are based on  $TDD_A$  and  $FDD_A$  available for the period 2004/05–2020/21. We avoided the commonly used n-factors to transfer between the air and near-surface degree-days (e. g. Lunardini, 1978; Riseborough, 2002; Hrbáček and Uxa, 2020) due to their temporal variability, and instead we used the degree-day relationships based on the 2011/12–2020/21 time series. A statistically significant ( $p < 0.01$ ) linear functions best fitted the  $TDD_A/TDD_{GT5}$  and  $FDD_A/FDD_{GT5}$  relationship, respectively (Fig. 3). The regression relationships were used to model the near-surface thawing and freezing degree-days ( $TDD_M$  and  $FDD_M$ ) for the period 2004/05–2020/21.

### 3.1.2. Ground physical properties

We determined the physical properties of thawed ground samples such as volumetric water content ( $\phi$ ), thermal conductivity ( $k_t$ ) and volumetric heat capacity ( $C_t$ ) for a depth of 20–30 cm, which was found to provide representative data for the active layer on James Ross Island (Hrbáček and Uxa, 2020). Volumetric water content was measured by CS650 sensor (Campbell Scientific, Inc.) and thermal properties using an ISOMET 2114 instrument (Applied Precision). The mean values of these characteristics were calculated from multiple measurements on intact samples in the laboratory in 2014 (Hrbáček et al., 2017) and updated by field measurements carried out during four summer seasons in 2017/18–2020/21 (Table 1).

Subsequently, we calculated the value of thermal conductivity of frozen ground ( $k_f$ ) based on the measured value of the thermal conductivity of thawed ground and the volumetric water content, neglecting the volumetric changes associated with phase transitions:

$$k_f = k_t \left( \frac{k_i}{k_w} \right)^\phi \quad (3)$$

where  $k_i$  is the thermal conductivity of ice ( $2.22 \text{ W.m}^{-1}.\text{K}^{-1}$ ) and  $k_w$  is the thermal conductivity of water ( $0.57 \text{ W.m}^{-1}.\text{K}^{-1}$ ). Calculation of the frozen volumetric heat capacity was as follows:

$$C_f = C_t - \phi (C_w - C_i) \quad (4)$$

where  $C_w$  is the volumetric heat capacity of water ( $4.21 \text{ MJ.m}^{-3}.\text{K}^{-1}$ ) and  $C_i$  is the volumetric heat capacity of ice ( $2.05 \text{ MJ.m}^{-3}.\text{K}^{-1}$ ).

**Table 1**

Ground physical properties for the study site AWS-JGM.

| Depth    | $\phi$ (%) | $k_t$<br>( $\text{W.m}^{-1}.\text{K}^{-1}$ ) | $k_f$<br>( $\text{W.m}^{-1}.\text{K}^{-1}$ ) | $C_t$<br>( $\text{MJ.m}^{-3}.\text{K}^{-1}$ ) | $C_f$<br>( $\text{MJ.m}^{-3}.\text{K}^{-1}$ ) |
|----------|------------|--|--|---|---|
| 20–30 cm | 26.5       | 0.39   | 0.56   | 1.21  | 0.64  |

$\phi$  - volumetric water content;  $k_t$  - thawed thermal conductivity;  $k_f$  - frozen thermal conductivity;  $C_t$  - thawed volumetric heat capacity;  $C_f$  - frozen volumetric heat capacity.

### 3.2. Permafrost table temperature and active layer thickness modelling

#### 3.2.1. TTOP model

One of the most adopted models for permafrost temperature calculation and reconstruction is the TTOP model (Temperature at the Top of Permafrost model) (Smith and Riseborough, 1996, 2002). In general, this model provides information on the relationship between climate and permafrost. The model joins permafrost temperature conditions with ground surface temperatures through subsurface thermal properties and surface thawing and freezing degree-days (Riseborough, 2002; Riseborough, 2003). The TTOP model for permafrost conditions estimates the mean annual ground temperature at the permafrost table (the base of the active layer) and is independent of its thickness as an input parameter (Smith and Riseborough, 1996; Wright et al., 2003).

The following formula was used to calculate the  $TTOP$  (°C) under permafrost conditions:

$$TTOP = \frac{k_t TDD_M + k_f FDD_M}{k_f P} \quad (5)$$

where  $P$  is the length of the annual period defined based on the sum of the length of the freezing ( $Df$ ) and thawing ( $Di$ ) seasons.

#### 3.2.2. Stefan model

The active layer thickness was estimated using the Stefan (1891) model, which is a simple analytical solution that has been widely used in permafrost areas (e. g. Klene et al., 2001; Shiklomanov and Nelson, 2002; Hrbáček and Uxa, 2020). Since the model itself does not account for sensible heat and assumes that the active layer is at zero temperature before

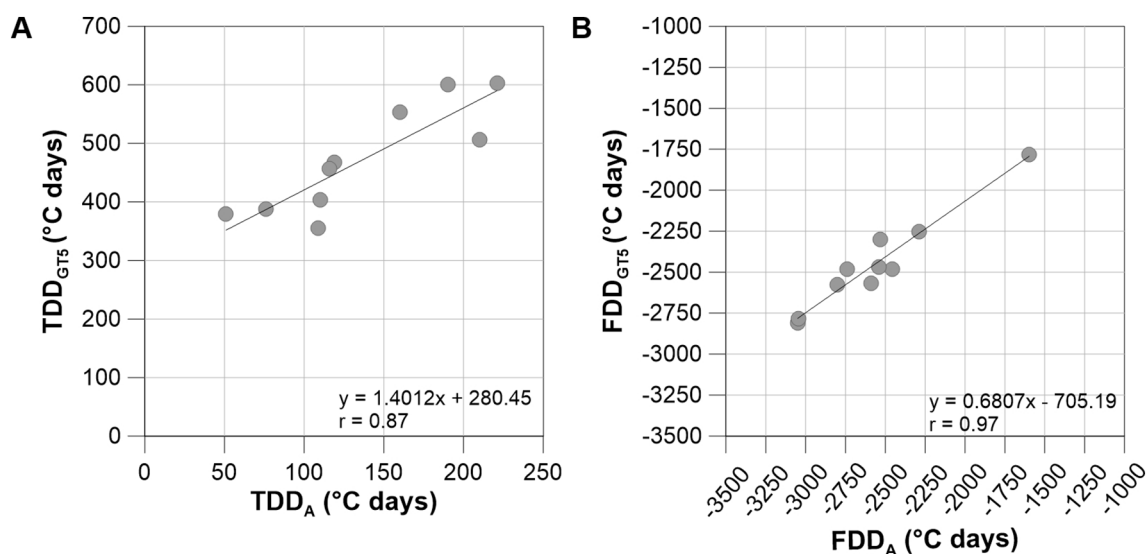


**Fig. 3.** (A) Linear relationships between  $TDD_A$  and  $TDD_{GT5}$  and (B) between  $FDD_A$  and  $FDD_{GT5}$  at AWS-JGM in the period 2004/05 to 2020/21.

thaw, which causes an exaggerated ALT, it was refined by the correction factor proposed by Kurylyk and Hayashi (2016) as follows:

$$ALT = z_5 + \lambda \sqrt{\frac{2k_t TDD_M SF}{L \phi \rho}}, \tag{6}$$

where  $z_5$  (m) is the depth of the ground temperature measurement used to force the model,  $SF$  (86,400 s) is the time-scaling factor,  $L$  (334,000 J.kg<sup>-1</sup>) is the specific latent heat of fusion of water-ice and  $\rho$  (1000 kg.m<sup>-3</sup>) is the density of water.  $\lambda$  is the dimensionless polynomial correction factor, which accounts for the sensible heat required to raise the active-layer temperature as well as for the subzero active-layer temperature before thaw (Kurylyk and Hayashi, 2016):

$$\lambda = \left[ 1 + 0.147 S_{te} \left( \beta \frac{T_{init}}{MGTS_5} \right)^2 + 0.535 \sqrt{S_{te}} \beta \frac{T_{init}}{MGTS_5} \right] \times (1 - 0.16 S_{te} + 0.038 S_{te}^2), \tag{7}$$

with

$$S_{te} = \frac{C_t MGTS_5}{L \phi \rho}, \tag{8}$$

$$\kappa = \sqrt{\frac{k_f C_f}{k_i C_i}}, \tag{9}$$

where  $S_{te}$  is the dimensionless Stefan number, which is the ratio of the sensible to latent heat,  $\beta$  is the dimensionless parameter that accommodates the difference between the thawed and frozen ground thermal properties,  $T_{init}$  (°C) is the initial temperature of the active layer just before thaw, and  $MGTS_5$  (°C) is the mean ground temperature in the thawing season at a depth  $z_5$ .

The initial temperature of the active layer was computed using the logarithmic fit of the mean daily ground temperature profile one day before thaw for the depth range between  $z_5$  and the initial ALT ( $ALT_{init}$ ) estimate from the uncorrected Stefan model (Hrbáček and Uxa, 2020) as follows:

$$T_{init} = \frac{1}{ALT_{init} - z_5} \int_{z_5}^{ALT_{init}} a \ln z + b dz, \tag{10}$$

where  $a$  and  $b$  are the regression coefficients. The initial temperature of the active layer was determined for seasons 2011/12–2020/21 and its mean value of  $-3.8$  °C was then used for ALT correction in all seasons. Note that all ALT values were converted from meters to centimeters, which are used hereafter.

### 3.3. Model validation and data analysis

The modelled TTOP and ALT values were verified against the interpolated values of ground temperature at the permafrost table (ITOP) and ALT from the period 2011/12–2020/21. Their agreements and relationships with other air and ground temperature characteristics were assessed using the mean error, mean absolute error, root-mean-square error (RMSE), and correlation coefficient ( $r$ ). The temporal trends of air and ground temperatures, TTOP and ALT were evaluated by the non-parametric Mann-Kendell test and Sen's slope estimator (Sen, 1968) using the MakeSens application (Salmi et al., 2002). The statistics were tested at  $p < 0.001$ ,  $p < 0.01$  or  $p < 0.05$ .

## 4. Results

### 4.1. Variability of air and ground temperature in the period 2011/12–2020/21

MAAT at AWS-JGM was  $-6.7$  °C in the period from March 2011 to February 2021. The maximum MAAT ( $-3.9$  °C) was recorded in 2016/

17 whereas the minimum MAAT ( $-8.2$  °C) in 2011/12 (Table 2). The highest mean monthly air temperature ( $2.7$  °C) was recorded in February 2020/21, although January was usually the warmest month (from  $-0.6$  °C to  $1.4$  °C). The coldest month was typically July (from  $-9.0$  °C to  $-18.8$  °C), despite the lowest mean monthly air temperature ( $-20.1$  °C) was recorded in August 2020/21. The highest annual mean daily air temperature usually exceeded  $9$  °C with a maximum of  $11.2$  °C recorded on the 2nd of January 2016. The lowest daily mean air temperatures usually dropped below  $-25$  °C in July or August, with a minimum of  $-30.2$  °C on 26th of July 2011 (Fig. 4). MAAT followed a strong warming trend of  $1.9$  °C/decade, statistically significant at  $p < 0.01$  (Table 2).

Mean annual ground temperature at a depth of 5 cm ( $MAGT_5$ ) was  $-5.4$  °C in the period 2011/12–2020/21. It ranged from  $-3.4$  °C (2016/17) to  $-6.8$  °C (2012/13).  $MAGT_{50}$  showed the same mean as  $MAGT_5$  ( $-5.4$  °C), but the temperature variability was slightly lower ( $-4.0$  °C in 2016/17 to  $-6.2$  °C in 2011/12).  $MAGT_{75}$  was  $0.2$  °C lower ( $-5.6$  °C) during the period 2011/12–2020/21 and it ranged from  $-4.4$  °C in 2016/17 to  $-6.3$  °C in 2011/12 (Table 2). Daily and monthly means indicate a decrease in variability from ground temperature measured at a depth of 5 cm to ground temperature at a depth of 75 cm. The annual course of mean monthly ground temperatures shows that the ground temperatures fluctuate more in the winter months whereas they are relatively stable during the summer (Fig. 4).

The maximum monthly ground temperatures reached  $6.8$  °C in December 2020/21 (5 cm) to  $-0.9$  °C in February 2016/17 (75 cm) whereas the minimum monthly ground temperatures dropped to  $-19.1$  °C in July 2019/20 (5 cm) to  $-12.8$  °C in August 2011/12 (75 cm). The maximum mean daily ground temperature reached  $13.0$  °C at a depth of 5 cm (on the 2nd of January 2016), but it did not exceed  $0$  °C at a depth of 75 cm ( $-0.8$  °C on the 15th of February 2017). Whereas  $MAGT_5$  followed the statistically significant ( $p < 0.05$ ) warming trend of  $1.3$  °C/decade, the warming trends of  $MAGT_{50}$  ( $1.0$  °C/decade) and  $MAGT_{75}$  ( $0.8$  °C/decade) were statistically insignificant at  $p < 0.05$ .

The mean observed ALT in the period 2011/12–2020/21 reached 60 cm. It varied between 50 cm (2013/14) and 67 cm (2016/17). ALT followed a strong positive trend of 12 cm/decade, but statistically insignificant at  $p < 0.05$ .

Throughout the period 2011/12–2020/21, the thawing seasons were more than twice as short as the freezing seasons (according to ground temperature). Their length varied between 91 (2014/15) and 186 days (2016/17) with an average of 117 days, whereas the length of freezing seasons was between 206 (2016/17) and 303 days (2012/13) with an average of 248 days. The total duration of annual period then ranged from 329 (2017/18) to 403 days (2012/13). The mean duration of the annual cycle was equal to 365 days, which coincides with the duration of the clearly defined annual cycle from March to February.

**Table 2**

MAAT,  $MAGT_5$ ,  $MAGT_{50}$ ,  $MAGT_{75}$ , ALT and their trends for the period from March 2011 to February 2021.

| Period       | MAAT (°C) | $MAGT_5$ (°C) | $MAGT_{50}$ (°C)    | $MAGT_{75}$ (°C)    | ALT (cm)           |
|--------------|-----------|---------------|---------------------|---------------------|--------------------|
| 2011/12      | -8.2      | -6.4          | -6.2                | -6.3                | 58                 |
| 2012/13      | -8.1      | -6.8          | -6.1                | -6.1                | 52                 |
| 2013/14      | -7.4      | -5.7          | -5.5                | -5.7                | 50                 |
| 2014/15      | -6.7      | -5.0          | -5.2                | -5.4                | 63                 |
| 2015/16      | -7.0      | -5.6          | -5.8                | -5.9                | 65                 |
| 2016/17      | -3.9      | -3.4          | -4.0                | -4.4                | 67                 |
| 2017/18      | -6.6      | -5.6          | -5.2                | -5.2                | 59                 |
| 2018/19      | -6.0      | -5.1          | -5.2                | -5.3                | 56                 |
| 2019/20      | -6.5      | -5.5          | -5.6                | -5.8                | 66                 |
| 2020/21      | -6.4      | -5.0          | -5.3                | -5.5                | 66                 |
| Average      | -6.7      | -5.4          | -5.4                | -5.6                | 60                 |
| Trend/decade | 1.9**     | 1.3*          | 1.0 <sup>n.s.</sup> | 0.8 <sup>n.s.</sup> | 12 <sup>n.s.</sup> |

n.s. not significant.

\*\* Trend at  $p < 0.01$  level of significance.

\* Trend at  $p < 0.05$  level of significance.

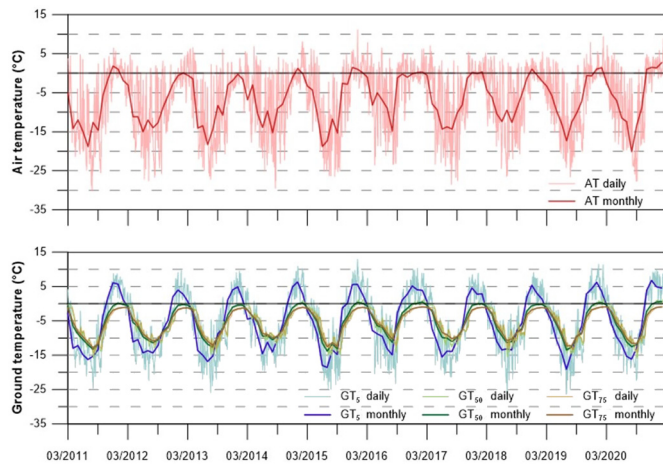


Fig. 4. Daily and monthly air temperature (AT) and ground temperature at a depth of 5 cm (GT<sub>5</sub>), 50 cm (GT<sub>50</sub>) and 75 cm (GT<sub>75</sub>) in the period from March 2011 to February 2021.

4.2. Permafrost table temperature and active layer thickness reconstruction in the period 2004/05–2020/21

ITOP had an average of  $-5.5\text{ }^{\circ}\text{C}$  in the period 2011/12–2020/21. The highest ITOP ( $-4.0\text{ }^{\circ}\text{C}$ ) was recorded in 2016/17 and the lowest ITOP ( $-6.6\text{ }^{\circ}\text{C}$ ) in 2011/12, which was the only value lower than  $-6\text{ }^{\circ}\text{C}$ . Most of the ITOP values are in a very narrow range of  $-5.3\text{ }^{\circ}\text{C}$  to  $-5.8\text{ }^{\circ}\text{C}$  (Table 3). ITOP followed a positive trend of  $0.4\text{ }^{\circ}\text{C}/\text{decade}$  (non-significant at  $p < 0.05$ ).

The average TTOP value was  $-5.8\text{ }^{\circ}\text{C}$ , with a maximum of  $-3.6\text{ }^{\circ}\text{C}$  (2016/17) and a minimum of  $-7.7\text{ }^{\circ}\text{C}$  (2009/10) (Table 3, Fig. 5B). Comparing the modelled TTOP with the ITOP, the absolute differences varied from  $0.03\text{ }^{\circ}\text{C}$  to  $0.82\text{ }^{\circ}\text{C}$ . The results of the TTOP model were all underestimated by  $-0.1\text{ }^{\circ}\text{C}$  to  $-0.8\text{ }^{\circ}\text{C}$  except for the year 2016/17, in which the model overestimated the permafrost table temperature by  $0.5\text{ }^{\circ}\text{C}$ . Statistically significant correlation ( $p < 0.001$ ) of 0.95 between the modelled TTOP and ITOP was found during the period 2011/12–2020/21 (Fig. 5A). The mean absolute error was  $0.36\text{ }^{\circ}\text{C}$  and the RMSE was  $0.52\text{ }^{\circ}\text{C}$ .

Table 3

Seasonal thawing and freezing degree-days (TDD<sub>A</sub>, FDD<sub>A</sub>, TDD<sub>GT5</sub>, FDD<sub>GT5</sub>, TDD<sub>M</sub>, FDD<sub>M</sub>), duration of thawing and freezing seasons, observed ALT and modelled ALT<sub>M</sub>, ITOP and TTOP in the period 2004/05–2020/21.

| Period  | TDD <sub>A</sub><br>( $^{\circ}\text{C days}$ ) | TDD <sub>GT5</sub><br>( $^{\circ}\text{C days}$ ) | TDD <sub>M</sub><br>( $^{\circ}\text{C days}$ ) | FDD <sub>A</sub><br>( $^{\circ}\text{C days}$ ) | FDD <sub>GT5</sub><br>( $^{\circ}\text{C days}$ ) | FDD <sub>M</sub><br>( $^{\circ}\text{C days}$ ) | Dt <sub>A</sub> (days) | Df <sub>A</sub> (days) | Dt <sub>GT5</sub> (days) | Df <sub>GT5</sub> (days) | ALT<br>(cm) | ALT <sub>M</sub><br>(cm) | ITOP<br>( $^{\circ}\text{C}$ ) | TTOP<br>( $^{\circ}\text{C}$ ) |
|---------|---|---|---|---|---|---|------------------------|------------------------|--------------------------|--------------------------|-------------|--------------------------|--------------------------------|--------------------------------|
| 2004/05 | 195   | –   | 554   | –2027   | –   | –2085   | 115                    | 252                    | –                        | –                        | –           | 64                       | –                              | –4,63                          |
| 2005/06 | 234   | –   | 608   | –2355   | –   | –2308   | 114                    | 245                    | –                        | –                        | –           | 67                       | –                              | –5,25                          |
| 2006/07 | 122   | –   | 451   | –1943   | –   | –2028   | 110                    | 242                    | –                        | –                        | –           | 58                       | –                              | –4,87                          |
| 2007/08 | 168   | –   | 516   | –3420   | –   | –3033   | 86                     | 291                    | –                        | –                        | –           | 62                       | –                              | –7,09                          |
| 2008/09 | 199   | –   | 559   | –2290   | –   | –2264   | 84                     | 266                    | –                        | –                        | –           | 65                       | –                              | –5,35                          |
| 2009/10 | 40  | –   | 336   | –3169   | –   | –2862   | 36                     | 307                    | –                        | –                        | –           | 51                       | –                              | –7,66                          |
| 2010/11 | 155   | –   | 498   | –2182   | –   | –2190   | 131                    | 281                    | –                        | –                        | –           | 60                       | –                              | –4,47                          |
| 2011/12 | 119   | 468   | 447   | –3050   | –2812   | –2781   | 100                    | 243                    | 101                      | 243                      | 58          | 58                       | –6.6                           | –7,20                          |
| 2012/13 | 109   | 355   | 433   | –3044   | –2782   | –2777   | 82                     | 321                    | 100                      | 303                      | 52          | 57                       | –5.5                           | –6,14                          |
| 2013/14 | 51  | 379   | 352   | –2741   | –2480   | –2571   | 83                     | 269                    | 111                      | 239                      | 50          | 51                       | –5.8                           | –6,61                          |
| 2014/15 | 116   | 456   | 443   | –2531   | –2302   | –2428   | 82                     | 264                    | 91                       | 261                      | 63          | 57                       | –5.4                           | –6,12                          |
| 2015/16 | 210   | 506   | 575   | –2803   | –2579   | –2613   | 107                    | 276                    | 106                      | 272                      | 65          | 65                       | –5.7                           | –5,78                          |
| 2016/17 | 190   | 600   | 547   | –1597   | –1783   | –1792   | 166                    | 226                    | 186                      | 206                      | 67          | 62                       | –4.0                           | –3,60                          |
| 2017/18 | 110   | 404   | 435   | –2458   | –2483   | –2378   | 110                    | 218                    | 109                      | 220                      | 59          | 57                       | –5.7                           | –6,33                          |
| 2018/19 | 76  | 388   | 387   | –2289   | –2251   | –2263   | 83                     | 271                    | 116                      | 240                      | 56          | 53                       | –5.3                           | –5,63                          |
| 2019/20 | 160   | 554   | 505   | –2589   | –2566   | –2468   | 127                    | 269                    | 128                      | 265                      | 66          | 61                       | –5.4                           | –5,34                          |
| 2020/21 | 221   | 603   | 590   | –2539   | –2467   | –2433   | 115                    | 230                    | 117                      | 229                      | 66          | 66                       | –5.7                           | –5,86                          |
| 2004/21 | 146   | –   | 484   | –2531   | –   | –2428   | 102                    | 263                    | –                        | –                        | –           | 60                       | –                              | –5,80                          |
| 2011/21 | 132   | 471   | 471   | –2564   | –2451   | –2451   | 106                    | 259                    | 117                      | 248                      | 60          | 59                       | –5.5                           | –5,90                          |

The variability of measured MAAT and modelled TTOP values has a similar pattern (Fig. 5B), although MAAT varied more ( $-7.2\text{ }^{\circ}\text{C}$  to  $-3.5\text{ }^{\circ}\text{C}$ ) than TTOP ( $-6.6\text{ }^{\circ}\text{C}$  to  $-4.0\text{ }^{\circ}\text{C}$ ). MAAT and TTOP show a high year-on-year variability especially until 2011/12. In the second part of the period (2012/13–2020/21), their variability decreased, except for 2016/17.

Mean modelled ALT during the period 2004/05–2020/21 was 60 cm. ALT varied relatively slightly between 51 cm in 2009/10 and 67 cm in 2005/06 (Fig. 6B). The ALT trend during 2004/05–2020/21 was found as a slightly negative, showing active-layer thinning of  $1.6\text{ cm}/\text{decade}$  (non-significant at  $p < 0.05$ ). The validation against the observed ALT confirmed that the corrected Stefan model provided reliable results. The differences varied between  $-6$  and  $5\text{ cm}$ , which corresponded to  $-10.5$  and  $8.8\%$ , respectively. Generally, the model tended to slightly underestimate ALT in 5 of 10 cases whereas it overestimated it in 2 cases. The mean error and mean absolute error were  $-1.5\text{ cm}$  and  $2.7\text{ cm}$ , respectively. The RMSE was  $3.54\text{ cm}$ .

As documented in Fig. 7, the TTOP correlated with MAAT strongly and significantly ( $r = 0.99; p < 0.001$ ) whereas the ALT correlated with the MAAT significantly but on a moderate level ( $r = 0.44; p < 0.01$ ). The analysis of the relationship between modelled ALT and TTOP showed a moderate, statistically significant correlation ( $r = 0.48, p < 0.01$ ). TTOP was controlled strongly by the FDD<sub>M</sub> values ( $r = 0.90, p < 0.001$ ). TTOP and TDD<sub>M</sub> exhibited a moderate relationship only ( $r = 0.54, p < 0.05$ ). Since the Stefan model is a function of TDD, we did not consider ALT values for this analysis.

5. Discussion

5.1. Variability of air and ground temperatures and active layer thickness

In general, there is a long-term rising trend of permafrost temperatures in many locations around the world (e. g. Biskaborn et al., 2019; Stammerjohn et al., 2021). Yet, the variability in local level also depends on several factors such as MAAT, ground thermal properties, lithologic conditions, occurrence of vegetation, snow cover, or surface type and characteristics (Chaves et al., 2017; Smith and Riseborough, 2002; Bockheim et al., 2013; French, 2017). In the shorter term, regions with warm permafrost ( $2\text{--}3\text{ }^{\circ}\text{C}$  below zero) are more endangered in terms of permafrost thawing.

The global permafrost temperatures at the depth of zero annual amplitude rose by  $0.29 \pm 0.12\text{ }^{\circ}\text{C}/\text{decade}$  (Biskaborn et al., 2019). The most

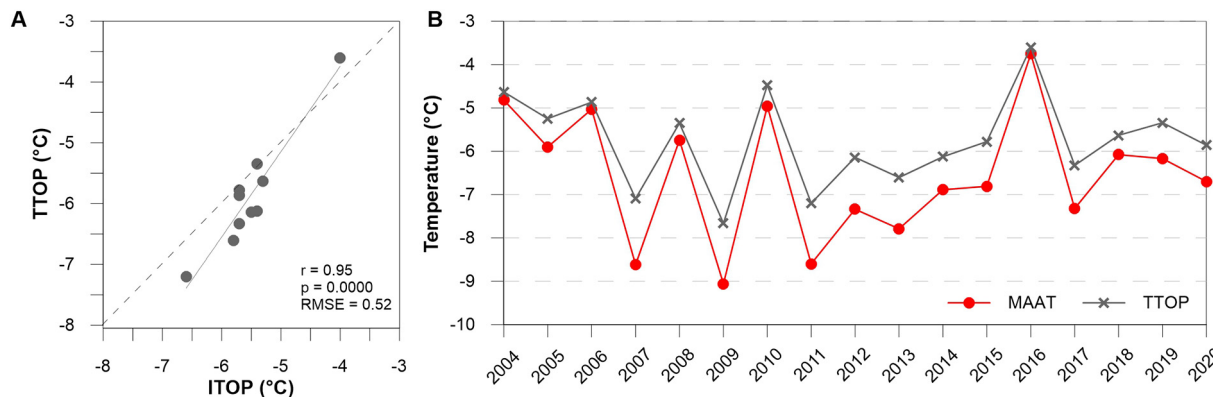


Fig. 5. (A) The 1:1 plot of the modelled TTOP and observed ITOP and (B) the variability of mean annual air temperature (MAAT) (averages for individually defined years) and TTOP during period 2004/05–2020/21.

pronounced warming rates of permafrost are currently in the Arctic regions (e. g. Stammerjohn et al., 2021; Li et al., 2022). According to Biskaborn et al. (2019), the permafrost temperatures in the Arctic continuous permafrost zone increased by  $0.39 \pm 0.15$  °C/decade during the period 2007–2016. The permafrost in Antarctica showed a warming trend of  $0.37 \pm 0.10$  °C/decade. However, their findings from Antarctica are not statistically significant and might be related to the lack of data and the scarce coverage of study sites. It is also important to note that only three sites from western Antarctic Peninsula were involved into their study. The sites in South Shetlands exhibited a warming trend of 0.25 to 0.73 °C/decade whereas the trend was negative at the site in western Antarctic Peninsula (Faraday/Vernadsky station) of  $-0.15$  °C/decade.

Notably, the results on active layer thermal regime or thickness presented from Antarctic Peninsula in the period before 2015 reported near-surface temperature cooling (e.g. Hrbáček et al., 2021) or active layer thinning (e.g. Ramos et al., 2017; de Pablo et al., 2017; Hrbáček and Uxa, 2020) as results of atmospheric cooling in the region (Turner et al., 2016; Oliva et al., 2017).

Our results from AWS-JGM represent the longest dataset of continuous ground temperature and ALT presented in the Antarctica Peninsula region to date. The 17-year period 2004/05–2020/21 is characterized by a positive trend of 0.6 °C/decade for MAAT,  $-0.1$  °C/decade for TTOP and  $-1.6$  cm/decade for ALT, all statistically non-significant at  $p < 0.05$  (see Fig. 8). The mismatch between MAAT and TTOP trend is very likely the result of non-linear evolution of the temperatures over the study period and the sensitivity of used statistics for trend analysis (Fig. 8). A similar mismatch between trends is also mentioned in a study by Hrbáček and Uxa (2020).

For MAAT, TTOP and ALT (see Fig. 8), the breaking point with the most negative temperature and thickness anomalies is the year 2011/12, and since 2013/14 at the latest, there has been a stable growth of these parameters. Before, there was a decline in their values. The temperature anomalies values of the centred moving averages at the beginning and end of the study period was similar. Likewise, the results from other regions in Antarctica reported rather stable conditions without any notable trend (Carshalton et al., 2022) or warming and thickening trends (Cannone et al., 2021). Seasonality of cooling thus presents challenges for models dealing with climate change and ecosystems (Doran et al., 2002).

However, when dividing the time series into two parts, the temperature trends are quite different. In the period 2004/05–2010/11, MAAT and TTOP at AWS-JGM tended to decrease at a rate of  $-1.3$  °C/decade and  $-1.8$  °C/decade, respectively (non-significant at  $p < 0.05$ ), while in the period 2011/12–2020/21 they showed an increasing tendency of 1.9 °C/decade and 1.5 °C/decade, respectively (significant at  $p < 0.01$ ). Similar pattern also exhibited ALT which followed a trend  $-2.3$  cm/year in the short period 2004/05 to 2010/11 whereas the trend was 0.3 cm/year in the period 2011/12 to 2020/21.

Data from other surrounding stations in the Antarctic Peninsula region were used to compare air temperature trends (Fig. 8). These stations provide continuous datasets and were included also to recent studies reporting the air temperature variability in the region (Turner et al., 2016; Oliva et al., 2017; Turner et al., 2020). The similar course of 5-years centred moving average and the warming trends between 0.15 and 0.6 °C/decade were observed on the station located in northern part of Antarctic Peninsula (Esperanza, Marambio and Bellinghausen) whereas the air temperature course on Faraday/Vernadsky located in Western Antarctic Peninsula was

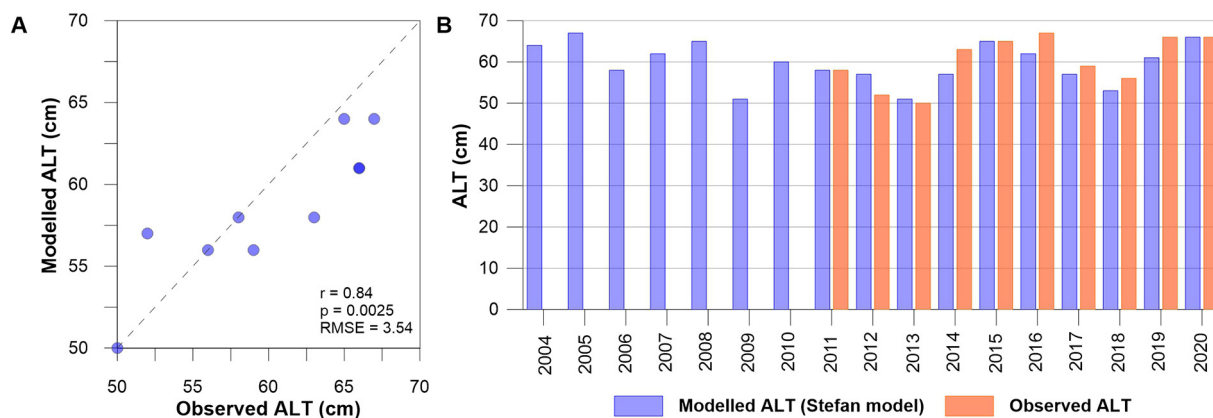
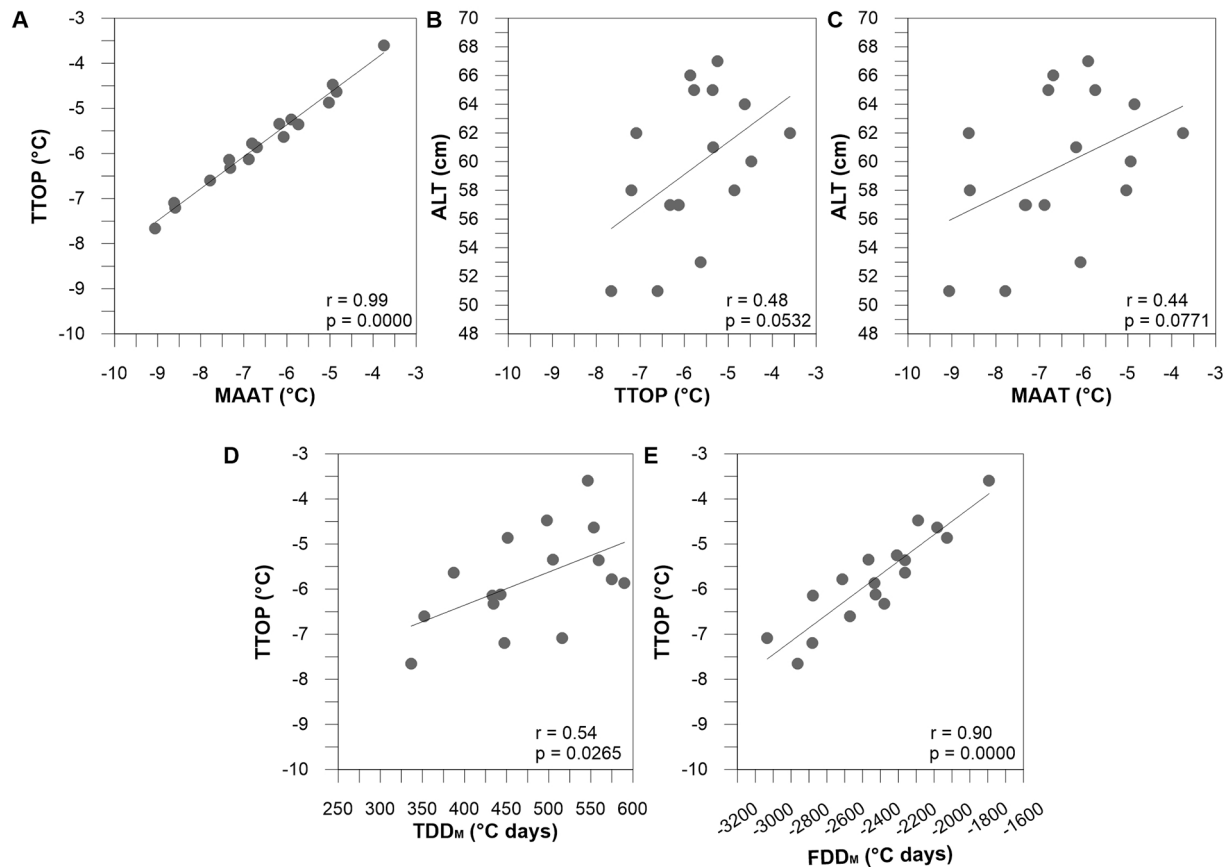


Fig. 6. (A) The 1:1 plot of the modelled and observed ALT and (B) the variability of the modelled ALT in the period 2004/05–2020/21 and the observed ALT in the period 2011/12–2020/21.



**Fig. 7.** Relationships of (A) mean annual air temperature (MAAT) and permafrost table temperature (TTOP) to the (B and C) modelled active layer thickness (ALT) and modelled (D) thawing (TDD<sub>M</sub>) and (E) freezing (FDD<sub>M</sub>) degree-days.

considerably different. The common result of all stations is the turning point in the year 2013/14. Such temperature conditions suggest that the results from AWS-JGM can be representative for the wider area of the northern part of Antarctic Peninsula region.

Air temperature trends at all selected stations are within a range of  $-0.02$  to  $0.6$  °C/decade, indicating a warming in the first half of the 21st century. The temperature trend of the upper part of the permafrost points to relatively more stable conditions in the soil environment in the Antarctic Peninsula region. The apparent mismatch in the temperature trends suggests that in terms of statistical significance it is necessary to consider any short-term values with a big caution because even small change (extension/shortening) of the reference period can turn the trend direction from positive to negative or cause (in)significance (Turner et al., 2005). Such statistically-based changes and generally large mismatch of results reporting atmospheric cooling (e.g. Turner et al., 2016; Oliva et al., 2017; Ramos et al., 2017; de Pablo et al., 2017; Hrbáček and Uxa, 2020) or warming (Biskaborn et al., 2019; this study) and associated impacts on active layer and permafrost thermal regime document large short-term variability of the climate conditions and high sensitivity of trends on the specific selection of study period. This fact generally confirms the suggestion by Gonzalez and Fortuny (2018) that at least 30-year long dataset is necessary to reliably interpret the trend magnitude. The problem is that only short time series of air temperatures and even shorter ground or permafrost temperatures are available from Antarctica so far.

## 5.2. Suitability of the TTOP and Stefan model

### 5.2.1. TTOP model

In the case of our results, the TTOP model outputs were validated over a 10-year reference period 2011/12–2020/21 using ITOP derived from ground temperatures at a depth of 50 and 75 cm and ALT. A statistically

significant correlation ( $p < 0.001$ ) of 0.95 was identified between the modelled and observed data (see Fig. 5). Despite the validation and verified model outputs, there are several limitations, which are reflected in the results of reconstruction and caused mainly underestimation of the modelled values (except for 2016/17) with an average difference of the measured values  $0.36$  °C. Table 3 includes outputs of the modelled and reconstructed permafrost table temperatures, which mostly ranged from  $-5$  °C to  $-7$  °C (with an average of  $-5.8$  °C in the period 2004/05–2020/21).

Part of the analysis of Obu et al. (2020), which was based on ERA-Interim and parameterized data, was the James Ross Island region, which was characterized by ground temperatures in the range of  $-3$  °C to  $-7$  °C, depending on the altitude. Specifically for the AWS-JGM, the modelled average MAGT was  $-4.98$  °C, while the difference compared to the measured values of MAGT was  $0.62$  °C. The model showed the mean error of  $-0.17$  °C and RMSE of  $1.94$  °C (for the entire territory of Antarctica). RMSE turned out better in our results and was lower, specifically  $0.52$  °C. In the case of the Arctic regions and the use of the TTOP model, the modelled temperatures were compared with the measured temperatures from the boreholes, with the mean error of  $-0.08$  °C and the RMSE being  $1.99$  °C, slightly higher than in Antarctica (Obu et al., 2019). In the case of using the CryoGRID 1.0 model (CryoGRID 1.0 is based on the TTOP-modelling approach, Smith and Riseborough, 1996) the results show a good agreement with the mean annual ground temperatures with RMSE of  $0.7$  °C (in Norway) (Gisnås et al., 2013). The TTOP model or its further adaptations (e. g. mentioned CryoGRID 1) has been used in various regions to calculate the permafrost table temperature, especially in the northern hemisphere (e. g. Smith and Riseborough, 2002; Gisnås et al., 2013; Obu et al., 2019). However, it has been applied and validated only a few times in Antarctica (Ferreira et al., 2017; Hrbáček et al., 2020; Obu et al., 2020). The disadvantage of the TTOP model is the assumption of a homogeneous profile. The model also assumes a state of thermal

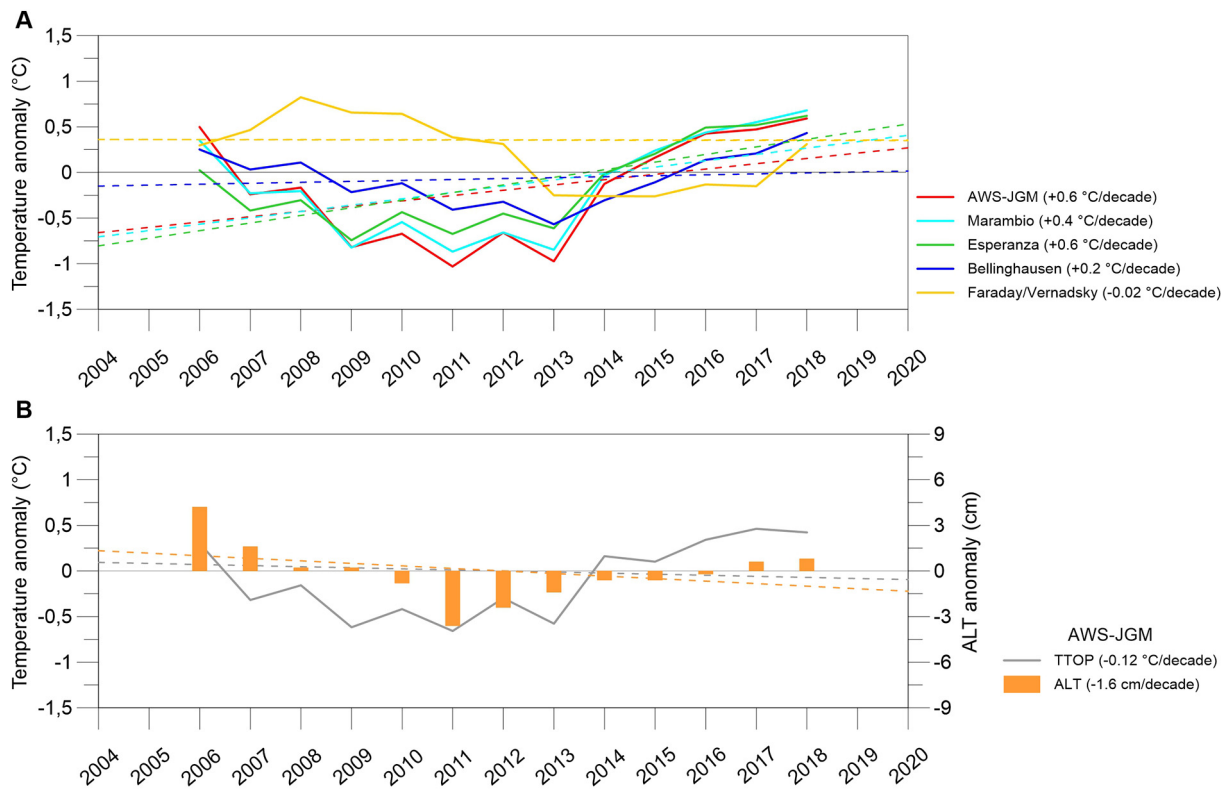


**Fig. 8.** Centered moving averages with 5-year window for anomalies of (A) MAAT at Bellinghausen, Faraday/Vernadsky, Esperanza, AWS-JGM, Marambio stations and (B) modelled permafrost table temperature (TTOP) and ALT at the AWS-JGM station supplemented by their trend values during the period 2004/05–2020/21. [Data (AT) from stations (except AWS-JGM) were obtained from the Reference Antarctic Data for Environmental Research (READER) database.].

equilibrium between the atmosphere and the ground. Equilibrium within the year is also assumed, as the modelled values represent the mean annual temperatures of the permafrost table (Riseborough, 2003; Wright et al., 2003). On the other hand, it is a great advantage that for the calculation itself it is enough to know the ratio of thawed and frozen thermal conductivity (Riseborough et al., 2008; Ferreira et al., 2017; Hrbáček and Uxa, 2020). Due to the lower input data requirements, the TTOP model is also suitable for spatial permafrost mapping on a regional scale, which can reveal the potential impacts of climate change on permafrost (Wright et al., 2003).

### 5.2.2. Stefan model

The overall suitability and accuracy of the Stefan model was discussed in detail in our previous work (Hrbáček and Uxa, 2020 and references therein). Results from AWS-JGM generally confirm a very high reliability of the Stefan model for bare-ground conditions on James Ross Island. The model validation showed that the mean absolute error was 2.7 cm (4.7 %), which is slightly better than that observed on Abernethy Flats site (Hrbáček and Uxa, 2020). Notably, the validation of the modelled ALT at AWS-JGM was done against more robust dataset, which substantially increased the reliability of the used approach. Our results also confirm that the polynomial correction proposed by Kurylyk and Hayashi (2016) significantly improved the accuracy of the model, as without this correction it would have a mean absolute error of 4.5 cm (7.0 %). The general tendency of slight ALT overestimation on James Ross Island might be caused by the fact that maximum thaw depths are usually observed in the mid-February, whereas the usual end of thawing seasons occurs at the turn of February and March (e. g. Hrbáček et al., 2017). The TDD covering the entire thawing season is therefore slightly higher than what it would be for the period between the beginning of thawing season and the time of maximum thaw depth. Certain inaccuracy of Stefan model on AWS-JGM can be related to the fact that, we modelled  $TDD_{GT5}$  from air temperature data. The difference between  $TDD_{GT5}$  and  $TDD_M$  in the reference period 2011/12–2020/21 was 78 and  $-53$  °C days (see Table 3). Consequently, the highest errors

of modelled ALT occurred in the years 2012/13, 2014/15 and 2019/20 when the differences between  $TDD_{GT5}$  and  $TDD_M$  were highest. Other possible source of the inaccuracy is the use of constant thermal and moisture parameters, because these can vary from year to year. However, the small mean absolute error suggests that this affects the model outputs only to a limited extent. Additionally, constant ground physical parameters have been used previously to successfully model the temporal variability of ALT (e.g. Romanovsky et al., 1997; Sazanova and Romanovsky, 2003; Hrbáček and Uxa, 2020).

### 5.3. Effect of changes in ground thermal regime and ALT

Our observations confirmed only medium correlation of 0.44 ( $p < 0.001$ ) between MAAT and ALT which was reported from other site on James Ross Island (Hrbáček and Uxa, 2020). Very strong positive correlation of 0.99 between MAAT and TTOP (see Fig. 7) is a result of bare-ground conditions (without vegetation) and limited snow cover. The result of the correlation is also influenced by the calculation of TTOP from the modelled seasonal indices. The daily and monthly means indicate a decrease in interannual variability from air temperature to ground temperature measured at a depth of 75 cm (see Fig. 4). The difference between the TTOP and the mean annual surface temperature is referred to as the thermal offset (Goodrich, 1982; Smith and Riseborough, 2002; French, 2017). The average thermal offset for the period 2011/12–2020/21 ranged from  $-0.1$  °C (2011/12, 2015/16, 2018/19) to  $-0.7$  °C (2014/15; 2017/18; 2020/21). The thermal offset is conditioned by different thermal conductivity of thawed and frozen ground (Burn and Smith, 1988). However, the difference may be even larger due to the fact that the ground temperature was not measured at the surface but at a depth of 5 cm. Permafrost could thus occur in a given location and influence the soil environment even if the mean annual temperatures on the near-surface reach positive temperatures.

Even though we observed slightly negative trend of permafrost table temperature and ALT over study period, it is predicted that the atmospheric warming by 0.5 to 1.5 °C will occur in the Antarctic Peninsula region in the near-future period 2020–2044 (Bozkurt et al., 2021). The second part of our study period also points to positive temperature trends. Considering very strong correlation between MAAT and TTOP observed on AWS-JGM (see Fig. 7), we can expect gradual increase in the permafrost table temperature also on James Ross Island. It is also highly probable that active-layer thickening will occur as the predictions expect summer air temperature increase by 0.3 and 0.8 °C in the leeward side of Antarctic Peninsula (Bozkurt et al., 2021). Such an air temperature change corresponds to TDD<sub>A</sub> increase by ca. 30–80 °C.days during summer months. In total, TDD<sub>A</sub> might increase from current long-term mean of 146 °C.days to values around 170–230 °C.days, which then corresponds to TDD<sub>GTS</sub> > 600 °C.days. Under such conditions, the ALT will very likely reach >70 cm, which is ca. 15 % more than its current average (see Table 2).

Notably, expected changes in soil thermal regime and ALT may significantly affect the environment on James Ross Island area. Considering the analogue scenarios from another parts of Antarctica, we can conclude that even a short warming period can alter the soil biogeochemical properties relatively rapidly (Cannone et al., 2021). For example, acceleration of soil carbon cycling can foster the conditions allowing the vegetation growth and soil organic matter forming on James Ross Island (Prater et al., 2021). On the other hand, the active-layer thickening will most likely cause the draining of surficial water into the deeper part of the soil profile, which, together with more intensive soil vapour caused by surface warming, will very likely lead to drying of the surficial part of the ground (e. g. Xue et al., 2009; Andresen et al., 2020), which might have a negative effect on the health and the abundance of the local vegetation (Robinson et al., 2018). The drying of the surfaces could subsequently increase the amount of the finest soil fraction, which is relocated by the dust storms typical for the area of James Ross Island (Kavan et al., 2018).

## 6. Conclusions

Study of the permafrost table temperature and active layer thickness on AWS-JGM, James Ross Island, Eastern Antarctic Peninsula region, in the period from March 2004 to February 2021, has these main conclusions:

- 1) The TTOP and Stefan models are suitable tools for modelling the permafrost table temperature and the active layer thickness, respectively, in the James Ross Island region.
- 2) The measured MAAT reached  $-6.6$  °C and ranged from  $-3.9$  °C (2016/17) to  $-9.1$  °C (2009/10), the permafrost table temperature using the TTOP model averaged  $-5.8$  °C, ranging from  $-3.6$  °C (2016/17) to  $-7.7$  °C (2009/10).
- 3) The modelled ALT using the Stefan model reached an average of 60 cm, with a minimum thickness of 51 cm (2009/10) and a maximum thickness of 67 cm (2005/06).
- 4) A statistically significant correlation ( $p < 0.001$ ) of 0.95 was observed between TTOP and ITOP in the reference period 2011/12–2020/21. The mean absolute error was 0.36 °C and the RMSE was 0.52 °C.
- 5) A statistically significant correlation ( $p < 0.01$ ) of 0.84 was detected between modelled and observed values of ALT in the reference period 2011/12–2020/21. The RMSE was 3.54 cm.
- 6) The positive trend of the measured AT was 0.6 °C/decade whereas the trend of the modelled permafrost table temperature (TTOP) showed a slight cooling of  $-0.1$  °C/decade and active layer thickness thinned by  $-1.6$  cm/decade. However, all trends were not statistically significant.
- 7) MAAT in the period up to 2010/11 showed a decreasing tendency of  $-1.3$  °C/decade (non-significant at  $p < 0.05$ ) and the period from 2011/12 has a warming character of 1.9 °C/decade (significant at  $p < 0.01$ ). The tendency of the TTOP indicates a cooling of  $-1.8$  °C/decade by 2010 (non-significant at  $p < 0.05$ ) and warming of 1.5 °C/

decade by 2020 (significant at  $p < 0.01$ ). For ALT, there was a thinning of  $-6.7$  cm/decade until 2010/11 and a thickening of 3.3 cm/decade until 2020/21 (both non-significant at  $p < 0.05$ ).

Further changes in climatic conditions are expected to affect the local environment in the next decades. Systematic monitoring and advance in thermal modelling of the ice-free area is essential for assessing the impacts of climate change on the Antarctic terrestrial environment. The dynamics of permafrost and active layer are affected by a number of environmental, mainly abiotic, factors like moisture, texture or geochemical composition that are not always systematically monitored in remote regions, such as Antarctica. Therefore, numerical modelling of permafrost and active layer is challenging and always requires verification using in-situ observations to get more accurate results.

## CRedit authorship contribution statement

**Lucia Kaplan Pastřířková:** Conceptualization, Data curation, Writing – original draft, Visualization. **Filip Hrbáček:** Conceptualization, Data curation, Writing – review & editing, Resources, Investigation, Supervision, Funding acquisition. **Tomáš Uxa:** Data curation, Writing – review & editing, Formal analysis. **Kamil Láška:** Writing – review & editing, Resources, Investigation.

## Data availability

Data will be made available on request.

## Declaration of competing interest

The authors declare that they have no known competing financial interests or personal relationships that could have appeared to influence the work reported in this paper.

## Acknowledgement

This research was supported by the Ministry of Education, Youth and Sports of the Czech Republic project (VAN 2022), Czech Science Foundation project (GM22-28659M) and Specific research - support for student projects (MUNI/A/1393/2021).

## References

- Ambrožová, K., Láška, K., 2016. Změny teploty vzduchu na ostrově Jamese Rosse v kontextu Antarktického poloostrova (The Air Temperature Change on James Ross Island within the context of the Antarctic Peninsula). In: Nováček, A. (Ed.), Sborník příspěvků Výroční konference České geografické společnosti 2016. Jihočeská univerzita v Českých Budějovicích, České Budějovice, pp. 20–25.
- Andresen, C.G., Lawrence, D.M., Wilson, C.J., McGuire, A.D., Koven, C., Schaefer, K., Jafarov, E., Peng, S., Chen, X., Gouttevin, I., Burke, E., Chadburn, S., Ji, D., Chen, G., Hayes, D., Zhang, W., 2020. Soil moisture and hydrology projections of the permafrost region – a model intercomparison. *Cryosphere* 14 (2), 445–459. <https://doi.org/10.5194/tc-14-445-2020>.
- Biskaborn, B.K., Lanckman, J.-P., Lantuit, H., Elger, K., Streletskiy, D.A., Cable, W.L., Romanovsky, V.E., 2015. The new database of the Global Terrestrial Network for Permafrost (GTN-P). *Earth Syst. Sci. Data* 7 (2), 245–259. <https://doi.org/10.5194/essd-7-245-2015>.
- Biskaborn, B.K., Smith, S.L., Noetzli, J., Matthes, H., Vieira, G., Streletskiy, D.A., Schoeneich, P., Romanovsky, V.E., Lewkowicz, A.G., Abramov, A., Allard, M., Boike, J., Cable, W.L., Christiansen, H.H., Delaloye, R., Diekmann, B., Drozdov, D., Etzelmüller, B., Grosse, G., Guglielmin, M., Ingeman-Nielsen, T., Isaksen, K., Ishikawa, M., Johansson, M., Johansson, H., Joo, A., Kaverin, D., Kholodov, A., Konstantinov, P., Kröger, T., Lambiel, Ch., Lanckman, J.-P., Luo, D., Malkova, G., Meiklejohn, I., Moskalenko, N., Oliva, M., Phillips, M., Ramos, M., Sannel, A.B.K., Sergeev, D., Seybold, C., Skryabin, P., Vasiliev, A., Wu, Q., Yoshikawa, K., Zheleznyak, M., Lantuit, H., 2019. Permafrost is warming at a global scale. *Nat. Commun.* 10 (1), 264. <https://doi.org/10.1038/s41467-018-08240-4>.
- Bockheim, J., Vieira, G., Ramos, M., López-Martínez, J., Serrano, E., Guglielmin, M., Wilhelm, K., Nieuwendam, A., 2013. Climate warming and permafrost dynamics in the Antarctic Peninsula region. *Glob. Planet. Chang.* 100, 215–223. <https://doi.org/10.1016/j.gloplacha.2012.10.018>.
- Borzotta, E., Trombotto, D., 2004. Correlation between frozen ground thickness measured in Antarctica and permafrost thickness estimated on the basis of the heat flow obtained from

- magnetotelluric soundings. *Cold Reg. Sci. Technol.* 40 (1–2), 81–96. <https://doi.org/10.1016/j.coldregions.2004.06.002>.
- Bozkurt, D., Bromwich, D.H., Carrasco, J., Rondanelli, R., 2021. Temperature and precipitation projections for the Antarctic peninsula over the next two decades: contrasting global and regional climate model simulations. *Clim. Dyn.* 56 (11–12), 3853–3874. <https://doi.org/10.1007/s00382-021-05667-2>.
- Brooks, S.T., Jabour, J., van den Hoff, J., Bergstrom, D.M., 2019. Our footprint on Antarctica competes with nature for rare ice-free land. *Nat. Sustain.* 2 (3), 185–190. <https://doi.org/10.1038/s41893-019-0237-y>.
- Burn, C.R., Smith, C.A.S., 1988. Observations of the “thermal offset” in near-surface mean annual ground temperatures at several sites near Mayo, Yukon Territory, Canada. *Arctic* 41 (2). <https://doi.org/10.14430/arctic1700>.
- Cannone, N., Guglielmin, M., Malfasi, F., Hubberten, H.W., Wagner, D., 2021. Rapid soil and vegetation changes at regional scale in continental Antarctica. *Geoderma* 394, 115017. <https://doi.org/10.1016/j.geoderma.2021.115017>.
- Carshalton, A.G., Balks, M.R., O'Neill, T.A., Bryan, K.R., Seybold, C.A., 2022. Climatic influences on active layer depth between 2000 and 2018 in the McMurdo Dry Valleys, Ross Sea Region, Antarctica. *Geoderma Reg.* 29, e00497. <https://doi.org/10.1016/j.geodrs.2022.e00497>.
- Chaves, D., Lyra, G., Francelino, M., Silva, L., Thomazini, A., Schaefer, C., 2017. Active layer and permafrost thermal regime in a patterned ground soil in Maritime Antarctica, and relationship with climate variability models. *Sci. Total Environ.* 584–585, 572–585. <https://doi.org/10.1016/j.scitotenv.2017.01.077>.
- Chown, S.L., Convey, P., 2007. Spatial and temporal variability across life's hierarchies in the terrestrial Antarctic. *Philos. Trans. R. Soc., B Biol. Sci.* 362 (1488), 2307–2331. <https://doi.org/10.1098/rstb.2006.1949>.
- Convey, P., Peck, L., 2019. Antarctic environmental change and biological responses. *Sci. Adv.* 5 (11). <https://doi.org/10.1126/sciadv.aaz0888>.
- Czech Geological Survey, 2009. JRI—northern part. Topographic Map 1: 25 000, 1st edition Czech Geological Survey, Prague.
- Davies, B.J., Glasser, N.F., Carrivick, J.L., Hambrey, M.J., Smellie, J.L., Nývlt, D., 2013. Landscape evolution and ice-sheet behaviour in a semi-arid polar environment: James Ross Island, NE Antarctic Peninsula. *Geol. Soc. Lond., Spec. Publ.* 381 (1), 353–395. <https://doi.org/10.1144/SP381.1>.
- Doran, P.T., Priscu, J.C., Lyons, W.B., Walsh, J.E., Fountain, A.G., McKnight, D.M., Moorhead, D.L., Virginia, R.A., Wall, D.H., Clow, G.D., Fritsen, C.H., McKay, C.P., Parsons, A.N., 2002. Antarctic climate cooling and terrestrial ecosystem response. *Nature* 415 (6871), 517–520. <https://doi.org/10.1038/nature710>.
- Ferreira, A., Vieira, G., Ramos, M., Nieuwendam, A., 2017. Ground temperature and permafrost distribution in Hurd Peninsula (Livingston Island, Maritime Antarctic): an assessment using freezing indexes and TTOP modelling. *Catena* 149, 560–571. <https://doi.org/10.1016/j.catena.2016.08.027>.
- French, H.M., 2017. *The Periglacial Environment*. 4th edition. Wiley-Blackwell, Oxford.
- Gisnås, K., Eitzelmüller, B., Farbrøt, H., Schuler, T.V., Westermann, S., 2013. CryoGRID 1.0: permafrost distribution in Norway estimated by a spatial numerical model. *Permafrost. Periglac. Process.* 24 (1), 2–19. <https://doi.org/10.1002/ppp.1765>.
- Gonzalez, S., Fortuny, D., 2018. How robust are the temperature trends on the Antarctic Peninsula? *Antarct. Sci.* 30 (5), 322–328. <https://doi.org/10.1017/S0954102018000251>.
- Goodrich, L.E., 1982. The influence of snow cover on the ground thermal regime. *Can. Geotech. J.* 19 (4), 421–432. <https://doi.org/10.1139/t82-047>.
- Guglielmin, M., Cannone, N., 2012. A permafrost warming in a cooling Antarctica? *Clim. Chang.* 111 (2), 177–195. <https://doi.org/10.1007/s10584-011-0137-2>.
- Guglielmin, M., Dalle Fratte, M., Cannone, N., 2014. Permafrost warming and vegetation changes in continental Antarctica. *Environ. Res. Lett.* 9 (4), 045001. <https://doi.org/10.1088/1748-9326/9/4/045001>.
- Hrbáček, F., Uxa, T., 2020. The evolution of a near-surface ground thermal regime and modeled active-layer thickness on James Ross Island, eastern Antarctic Peninsula, in 2006–2016. *Permafrost. Periglac. Process.* 31 (1), 141–155. <https://doi.org/10.1002/ppp.2018>.
- Hrbáček, F., Láška, K., Engel, Z., 2016a. Effect of snow cover on the active-layer thermal regime - a case study from James Ross Island, Antarctic Peninsula. *Permafrost. Periglac. Process.* 27 (3), 307–315. <https://doi.org/10.1002/ppp.1871>.
- Hrbáček, F., Oliva, M., Láška, K., Ruiz-Fernández, J., de Pablo, M.A., Vieira, G., Ramos, M., Nývlt, D., 2016b. Active layer thermal regime in two climatically contrasted sites of the Antarctic Peninsula region. *Cuad. Investig. Geogr.* 42 (2), 457–474. <https://doi.org/10.18172/cig.2915>.
- Hrbáček, F., Kňázková, M., Nývlt, D., Láška, K., Mueller, C.W., Ondruch, J., 2017. Active layer monitoring at CALM-S site near J.G.Mendel Station, James Ross Island, eastern Antarctic peninsula. *Sci. Total Environ.* 601–602, 987–997. <https://doi.org/10.1016/j.scitotenv.2017.05.266>.
- Hrbáček, F., Oliva, M., Fernández, J.-R., Kňázková, M., de Pablo, M.A., 2020. Modelling ground thermal regime in bordering (d)continuous permafrost environments. *Environ. Res.* 181, 108901. <https://doi.org/10.1016/j.envres.2019.108901>.
- Hrbáček, F., Vieira, G., Oliva, M., Balks, M., Guglielmin, M., de Pablo, M.A., Molina, A., Ramos, M., Goyanes, G., Meiklejohn, I., Abramov, A., Demidov, N., Fedorov-Davydov, D., Lupachev, A., Rivkina, E., Láška, K., Kňázková, M., Nývlt, D., Raffi, R., Strelin, J., Sone, T., Fukui, K., Dolgikh, A., Zazovskaya, E., Mergelov, N., Osokin, N., Miamin, V., 2021. Active layer monitoring in Antarctica: an overview of results from 2006 to 2015. *Polar Geogr.* 44 (3), 217–231. <https://doi.org/10.1080/1088937X.2017.1420105>.
- Jafarov, E.E., Marchenko, S.S., Romanovsky, V.E., 2012. Numerical modeling of permafrost dynamics in Alaska using a high spatial resolution dataset. *Cryosphere* 6 (3), 613–624. <https://doi.org/10.5194/tc-6-613-2012>.
- Kavan, J., Ondruch, J., Nývlt, D., Hrbáček, F., Carrivick, J.L., Láška, K., 2017. Seasonal hydrological and suspended sediment transport dynamics in proglacial streams, James Ross Island, Antarctica. *Geogr. Ann. Ser. B* 99 (1), 38–55. <https://doi.org/10.1080/04353676.2016.1257914>.
- Kavan, J., Dagsson-Waldhauserova, P., Renard, J.B., Láška, K., Ambrožová, K., 2018. Aerosol concentrations in relationship to local atmospheric conditions on James Ross Island, Antarctica. *Front. Earth Sci.* 6. <https://doi.org/10.3389/feart.2018.00207>.
- Kavan, J., Nývlt, D., Láška, K., Engel, Z., Kňázková, M., 2020. High-latitude dust deposition in snow on the glaciers of James Ross Island, Antarctica. *Earth Surf. Process. Landf.* 45 (7), 1569–1578. <https://doi.org/10.1002/esp.4831>.
- King, J.C., Turner, J., Marshall, G.J., Connolly, W.M., Lachlan-Cope, T.A., 2013. Antarctic Peninsula Climate Variability and Its Causes as Revealed by Analysis of Instrumental Records, pp. 17–30. <https://doi.org/10.1029/AR079p0017>.
- Klene, A.E., Nelson, F.E., Shiklomanov, N.I., Hinkel, K.M., 2001. The N-factor in natural landscapes: variability of air and soil-surface temperatures, Kuparuk River Basin, Alaska, U.S.A. *Arct. Antarct. Alp. Res.* 33 (2), 140. <https://doi.org/10.2307/1552214>.
- Kurylyk, B.L., 2015. Discussion of ‘A simple thaw-freeze algorithm for a multi-layered soil using the Stefan equation’ by Xie and Gough (2013). *Permafrost. Periglac. Process.* 26 (2), 200–206. <https://doi.org/10.1002/ppp.1834>.
- Kurylyk, B.L., Hayashi, M., 2016. Improved Stefan equation correction factors to accommodate sensible heat storage during soil freezing or thawing. *Permafrost. Periglac. Process.* 27 (2), 189–203. <https://doi.org/10.1002/ppp.1865>.
- Láška, K., Barták, M., Hájek, J., Prošek, P., Bohuslavová, O., 2011. Climatic and ecological characteristics of deglaciated area of James Ross Island, Antarctica, with a special respect to vegetation cover. *Czech Polar Rep.* 1 (1), 49–62. <https://doi.org/10.5817/CPR2011-1-5>.
- Lee, J.R., Raymond, B., Bracegirdle, T.J., Chadès, I., Fuller, R.A., Shaw, J.D., Terauds, A., 2017. Climate change drives expansion of Antarctic ice-free habitat. *Nature* 547 (7661), 49–54. <https://doi.org/10.1038/nature22996>.
- Li, G., Zhang, M., Pei, W., Melnikov, A., Khristoforov, I., Li, R., Yu, F., 2022. Changes in permafrost extent and active layer thickness in the Northern Hemisphere from 1969 to 2018. *Sci. Total Environ.* 804, 150182. <https://doi.org/10.1016/j.scitotenv.2021.150182>.
- Lunardini, V.J., 1978. Theory of n-factors and correlation of data. *Proceedings of the Third International Conference on Permafrost*. National Research Council of Canada, Ottawa, pp. 40–46.
- Martin, P.J., Peel, D.A., 1978. The spatial distribution of 10 m temperatures in the Antarctic Peninsula. *J. Glaciol.* 20 (83), 311–317. <https://doi.org/10.3189/S0022143000013861>.
- Obu, J., Westermann, S., Bartsch, A., Berdnikov, N., Christiansen, H.H., Dashtseren, A., Delaloye, R., Elberling, B., Eitzelmüller, B., Kholodov, A., Khomutov, A., Kääh, A., Leibman, M.O., Lewkowicz, A.G., Panda, S.K., Romanovsky, V., Way, R.G., Westergaard-Nielsen, A., Wu, T., Yamkhin, J., Zou, D., 2019. Northern Hemisphere permafrost map based on TTOP modelling for 2000–2016 at 1 km2 scale. *Earth Sci. Res.* 193, 299–316. <https://doi.org/10.1016/j.earscirev.2019.04.023>.
- Obu, J., Westermann, S., Vieira, G., Abramov, A., Balks, M.R., Bartsch, A., Hrbáček, F., Kääh, A., Ramos, M., 2020. Pan-Antarctic map of near-surface permafrost temperatures at 1 km2 scale. *Cryosphere* 14 (2), 497–519. <https://doi.org/10.5194/tc-14-497-2020>.
- Oliva, M., Navarro, F., Hrbáček, F., Hernández, A., Nývlt, D., Pereira, P., Ruiz-Fernández, J., Trigo, R., 2017. Recent regional climate cooling on the Antarctic Peninsula and associated impacts on the cryosphere. *Sci. Total Environ.* 580, 210–223. <https://doi.org/10.1016/j.scitotenv.2016.12.030>.
- de Pablo, M.A., Ramos, M., Molina, A., 2017. Snow cover evolution, on 2009–2014, at the limnopol lake CALM-S site on Byers Peninsula, Livingston Island, Antarctica. *Catena* 149, 538–547. <https://doi.org/10.1016/j.catena.2016.06.002>.
- Prater, I., Hrbáček, F., Braun, C., Vidal, A., Meier, L.A., Nývlt, D., Mueller, C.W., 2021. How vegetation patches drive soil development and organic matter formation on polar islands. *Geoderma Reg.* 27, e00429. <https://doi.org/10.1016/j.geodrs.2021.e00429>.
- Ramos, M., Vieira, G., de Pablo, M.A., Molina, A., Abramov, A., Goyanes, G., 2017. Recent shallowing of the thaw depth at Crater Lake, Deception Island, Antarctica (2006–2014). *Catena* 149, 519–528. <https://doi.org/10.1016/j.catena.2016.07.019>.
- Rasmussen, L.H., Zhang, W., Hollesen, J., Cable, S., Christiansen, H.H., Jansson, P.-E., Elberling, B., 2018. Modelling present and future permafrost thermal regimes in North-east Greenland. *Cold Reg. Sci. Technol.* 146, 199–213. <https://doi.org/10.1016/j.coldregions.2017.10.011>.
- Riseborough, D.W., 2002. The mean annual temperature at the top of permafrost, the TTOP model, and the effect of unfrozen water. *Permafrost. Periglac. Process.* 13 (2), 137–143. <https://doi.org/10.1002/ppp.418>.
- Riseborough, D.W., 2003. Thawing and freezing indices in the active layer. *Proceedings of the 8th International Conference on Permafrost*. AA Balkema Rotterdam, pp. 953–958.
- Riseborough, D., Shiklomanov, N., Eitzelmüller, B., Gruber, S., Marchenko, S., 2008. Recent advances in permafrost modelling. *Permafrost. Periglac. Process.* 19 (2), 137–156. <https://doi.org/10.1002/ppp.615>.
- Robinson, S.A., King, D.H., Bramley-Alves, J., Waterman, M.J., Ashcroft, M.B., Wasley, J., Turnbull, J.D., Miller, R.E., Ryan-Colton, E., Benny, T., Mullany, K., Clarke, L.J., Barry, L.A., Hua, Q., 2018. Rapid change in East Antarctic terrestrial vegetation in response to regional drying. *Nat. Clim. Chang.* 8 (10), 879–884. <https://doi.org/10.1038/s41558-018-0280-0>.
- Romanovsky, V.E., Osterkamp, T.E., Duxbury, N.S., 1997. An evaluation of three numerical models used in simulations of the active layer and permafrost temperature regimes. *Cold Reg. Sci. Technol.* 26 (3), 195–203. [https://doi.org/10.1016/S0165-232X\(97\)00016-5](https://doi.org/10.1016/S0165-232X(97)00016-5).
- Salmi, T., Määttä, A., Anttila, P., Ruoho-Airola, T., Amnell, T., 2002. *Detecting Trends of Annual Values of Atmospheric Pollutants by the Mann-Kendall Test and Sen's Slope Estimates*. Finnish Meteorological Institute, Helsinki.
- Sazanova, T.S., Romanovsky, V.E., 2003. A model for regional-scale estimation of temporal and spatial variability of active layer thickness and mean annual ground temperatures. *Permafrost. Periglac. Process.* 14 (2), 125–139. <https://doi.org/10.1002/ppp.449>.
- Sen, P.K., 1968. Estimates of the regression coefficient based on Kendall's tau. *J. Am. Stat. Assoc.* 63 (324), 1379–1389. <https://doi.org/10.1080/01621459.1968.10480934>.

- Shiklomanov, N.I., Nelson, F.E., 2002. Active-layer mapping at regional scales: a 13-year spatial time series for the Kuparuk region, north-central Alaska. *Permafrost. Periglac. Process.* 13 (3), 219–230. <https://doi.org/10.1002/ppp.425>.
- Smith, M.W., Riseborough, D.W., 1996. Permafrost monitoring and detection of climate change. *Permafrost. Periglac. Process.* 7 (4), 301–309. [https://doi.org/10.1002/\(SICI\)1099-1530\(199610\)7:4<301::AID-PPP231>3.0.CO;2-R](https://doi.org/10.1002/(SICI)1099-1530(199610)7:4<301::AID-PPP231>3.0.CO;2-R).
- Smith, M.W., Riseborough, D.W., 2002. Climate and the limits of permafrost: a zonal analysis. *Permafrost. Periglac. Process.* 13 (1), 1–15. <https://doi.org/10.1002/ppp.410>.
- Stammerjohn, S., Scambos, T.A., Adusumilli, S., Barreira, S., Bernhard, G.H., Bozkurt, D., Bushinsky, S.M., Clem, K.R., Colwell, S., Coy, L., de Laat, J., du Plessis, M.D., Fogt, R.L., Foppert, A., Fricker, H.A., Gardner, A.S., Gille, S.T., Gorte, T., Johnson, B., Keenan, E., Kennett, D., Keller, L.M., Kramarova, N.A., Lakkala, K., Lazzara, M.A., Lenaerts, J.T.M., Lieser, J.L., Li, Z., Liu, H., Long, C.S., MacFerrin, M., MacLennan, M.L., Massom, R.A., Mikolajczyk, D., Montgomery, L., Mote, T.L., Nash, E.R., Newman, P.A., Petropavlovskii, I., Pitts, M., Reid, P., Rintoul, S.R., Santee, M.L., Shadwick, E.H., Silvano, A., Stierle, S., Strahan, S., Sutton, A.J., Swart, S., Tamsitt, V., Tilbrook, B., Wang, L., Williams, N.L., Yuan, X., 2021. Antarctica and the Southern Ocean. *Bull. Am. Meteorol. Soc.* 102 (8), 317–356. <https://doi.org/10.1175/BAMS-D-21-0081.1>.
- Stefan, J., 1891. Ueber die theorie der eisbildung, insbesondere über die eisbildung im polarmeere. *Ann. Phys.* 278 (2), 269–286. <https://doi.org/10.1002/andp.18912780206>.
- Turner, J., Colwell, S.R., Marshall, G.J., Lachlan-Cope, T.A., Carleton, A.M., Jones, P.D., Lagun, V., Reid, P.A., Iagovkina, S., 2005. Antarctic climate change during the last 50 years. *Int. J. Climatol.* 25 (3), 279–294. <https://doi.org/10.1002/joc.1130>.
- Turner, J., Lu, H., White, I., King, J.C., Phillips, T., Hosking, J.S., Bracegirdle, T.J., Marshall, G.J., Mulvaney, R., Deb, P., 2016. Absence of 21st century warming on Antarctic Peninsula consistent with natural variability. *Nature* 535 (7612), 411–415. <https://doi.org/10.1038/nature18645>.
- Turner, J., Marshall, G.J., Clem, K., Colwell, S., Phillips, T., Lu, H., 2020. Antarctic temperature variability and change from station data. *Int. J. Climatol.* 40 (6), 2986–3007. <https://doi.org/10.1002/joc.6378>.
- Uxa, T., 2017. Permafrost. *Periglac. Process.* 28 (2), 493–498. <https://doi.org/10.1002/ppp.1888>.
- Vaughan, D.G., Marshall, G.J., Connolley, W.M., Parkinson, C., Mulvaney, R., Hodgson, D.A., King, J.C., Pudsey, C.J., Turner, J., 2003. Recent rapid regional climate warming on the Antarctic Peninsula. *Clim. Chang.* 60 (3), 243–274. <https://doi.org/10.1023/A:1026021217991>.
- Vieira, G., Bockheim, J., Guglielmin, M., Balks, M., Abramov, A.A., Boelhouwers, J., Cannone, N., Ganzert, L., Gilichinsky, D.A., Goryachkin, S., López-Martínez, J., Meiklejohn, I., Raffi, R., Ramos, M., Schaefer, C., Serrano, E., Simas, F., Sletten, R., Wagner, D., 2010. Thermal state of permafrost and active-layer monitoring in the antarctic: advances during the international polar year 2007–2009. *Permafrost. Periglac. Process.* 21 (2), 182–197. <https://doi.org/10.1002/ppp.685>.
- van Wessem, J.M., Ligtenberg, S.R.M., Reijmer, C.H., van de Berg, W.J., van den Broeke, M.R., Barrand, N.E., Thomas, E.R., Turner, J., Wuite, J., Scambos, T.A., van Meijgaard, E., 2016. The modelled surface mass balance of the Antarctic Peninsula at 5.5 km horizontal resolution. *Cryosphere* 10 (1), 271–285. <https://doi.org/10.5194/tc-10-271-2016>.
- Westermann, S., Schuler, T.V., Gislås, K., Eitzelmüller, B., 2013. Transient thermal modeling of permafrost conditions in Southern Norway. *Cryosphere* 7 (2), 719–739. <https://doi.org/10.5194/tc-7-719-2013>.
- Wilhelm, K., Bockheim, J., 2016. Influence of soil properties on active layer thermal propagation along the western Antarctic Peninsula. *Earth Surf. Process. Landf.* 41 (11), 1550–1563. <https://doi.org/10.1002/esp.3926>.
- Wright, J.F., Duchense, C., Coté, M.M., 2003. Regional-scale permafrost mapping using the TTOP ground temperature model. In: Phillips, M., Springman, S.M., Arenson, L.U. (Eds.), *Permafrost: Proceedings of the 8th International Conference on Permafrost*. Balkema Publishers, Zurich, pp. 1241–1246.
- Xue, X., Guo, J., Han, B., Sun, Q., Liu, L., 2009. The effect of climate warming and permafrost thaw on desertification in the Qinghai-Tibetan Plateau. *Geomorphology* 108 (3–4), 182–190. <https://doi.org/10.1016/j.geomorph.2009.01.004>.

## RESEARCH ARTICLE OPEN ACCESS

# Active Layer Warming and Thickening on CALM-S JGM, James Ross Island, in the Period 2013/14–2022/23

Filip Hrbáček  | Michaela Kňázková | Kamil Láska | Lucia Kaplan Pastířiková

Department of Geography, Masaryk University, Brno, Czech Republic

**Correspondence:** Filip Hrbáček ([hrbacekfilip@gmail.com](mailto:hrbacekfilip@gmail.com))

**Received:** 20 February 2025 | **Revised:** 24 February 2025 | **Accepted:** 12 March 2025

**Funding:** This research was supported by the Czech Science Foundation project (GM22-28659M) and internal grant of Masaryk University (MUNI/A/1323/2022).

## ABSTRACT

The Circumpolar Active Layer Monitoring-South (CALM-S) site was established near the Johann Gregor Mendel (JGM) research station on James Ross Island in February 2014. The CALM-S JGM grid, measuring 80 × 70 m, encompasses two distinct lithological units: a Holocene marine terrace (covering approximately 75% of the grid) and Cretaceous sediments of the Whisky Bay Formation (covering the remaining 25%). Within each lithology, a monitoring profile was established to track the active layer thermal regime and thickness. Additionally, active layer thaw depth probing has been conducted annually around mid-February. Since 2017, the dataset has been further supplemented by surficial soil water content measurements. During the study period (2013/14–2022/23), air temperature increased at a rate of 0.2°C per year. Consequently, the active layer thickness, defined by the 0°C isotherm, increased by an average of 1.5 cm per year, while mechanically probed thaw depths showed an annual increase of 1.9 cm. This study confirms that local lithology strongly influences active layer thermal regime. On average, the active layer thickness was 24 cm greater on AWS-CALM (Cretaceous sediments) than on AWS-JGM (marine terrace). The thaw depth was 28 cm greater in the Cretaceous sediment part of CALM-S compared with the marine terrace part. A strong correlation ( $r=0.82$  to  $r=0.91$ ) was found between active layer thickness and thaw depth with thawing degree days of air and near-surface ground temperature in both lithologies.

## 1 | Introduction

Active layer thickness (ALT) and temperature are two important climatic variables of permafrost environments [1, 2]. The Circumpolar Active Layer Monitoring (CALM) programme is one of the first international projects to standardise the monitoring of the active layer thermal regime and thaw depth. The predominant monitoring approach is to use mechanical probing to detect the active layer thaw depth within the grid nodes (e.g. [1, 3]). Furthermore, the CALM sites are equipped with active layer and permafrost temperature monitoring systems, which provide data for the ALT derived as the depth of the 0°C

isotherm and the overall climatic conditions of the CALM sites. Recently, CALM monitoring results have been summarised for North America [4], Siberia [5, 6], and Antarctica [7]. Moreover, a number of studies conducted over the past two decades have focused on a detailed assessment of thaw depth variability at CALM sites situated in various regions of the Arctic (e.g. [8–13]) and Antarctica (e.g. [7, 14–21]).

The estimated extent of global permafrost is between 14 and 16 million km<sup>2</sup> [22]. Of this total, only 45,000 to 70,000 km<sup>2</sup> is located in the ice-free areas of Antarctica [23]. These ice-free areas are fragmented into a mosaic of very small rock outcrops

This is an open access article under the terms of the [Creative Commons Attribution](https://creativecommons.org/licenses/by/4.0/) License, which permits use, distribution and reproduction in any medium, provided the original work is properly cited.

© 2025 The Author(s). *Permafrost and Periglacial Processes* published by John Wiley & Sons Ltd.

covering up to a few hectares and larger Antarctic oases covering tens or hundreds of square kilometres. In contrast to the permafrost and active layer monitoring sites listed in the Global Terrestrial Network for Permafrost database (GTN-P), which have more than 80 profiles [23], the CALM-S (Circumpolar Active Layer Monitoring - South) database contains only nine sites [24]. Most of the CALM-S sites (six out of nine) are located in the Antarctic Peninsula region. This limited number of CALM-S sites in Antarctica is primarily caused by the local conditions that are unfavourable for thaw depth probing measurements (e.g. [1, 15]). Other limitations include logistic constraints or climate conditions like long-lasting snow cover presence, preventing the measurements (e.g. [20]). Nevertheless, the few CALM-S sites in Antarctica have provided valuable data to understand active layer thaw depth variability under different conditions. In particular, the factors studied in Antarctica were local lithology [18], snow cover [16, 20, 25], and vegetation [16]. The effect of these factors can result in a local thaw depth variability of up to 50 cm over the 100 × 100 m area.

The objective of this study is to evaluate the first decade (2014–2023) of active layer thermal regime, ALT and thaw depth monitoring on the CALM-S near Johann Gregor Mendel station (CALM-S JGM), including the first years (2017–2023) of surficial volumetric water content (VWC) monitoring. The initial results from CALM-S JGM have already been published, focusing on a general description and the role of lithology on thaw depth variability [18], an assessment of the effect of summer snow cover on active layer thaw depth and an example of a reference plot for a geophysical survey [26]. This study will particularly focus on the following:

- a. evaluation of decadal trends in active layer thermal regime, thickness and thaw depth,
- b. assessment of temperature influence on ALT and thaw depth,

- c. analysis of the spatial and temporal variability of VWC and its influence on thaw depth.

## 2 | Methods

### 2.1 | Study Area

James Ross Island is located in the northeastern part of the Antarctic Peninsula. It is the largest island in the region (approximately 2400 km<sup>2</sup>), with ice-free areas covering more than 500 km<sup>2</sup> of its surface. Such an extension forms the largest mosaics of ice-free areas in the Antarctic Peninsula region (e.g. [23]). The area of interest is the northern part of James Ross Island, called Ulu Peninsula. The mean annual air temperature near sea level was −6.7°C in the period 2004–2021 [27]. Precipitation is estimated to be between 300 and 700 mm w.e./year [28], mainly snowy. The snow is strongly redistributed by wind [29], leading to relatively low accumulations in flat areas (e.g. [30]). The permafrost is continuous [31], with ALT generally ranging from about 40 up to 120 cm (e.g. [23]).

### 2.2 | CALM-S JGM

The CALM-S JGM grid of 80 × 70 m has a reduced size in respect to the CALM standard due to Johann Gregor Mendel station facilities located to the north and the area formed by soils that are difficult to probe to the south (Figure 1). The site is elevated between 8 and 12 m a.s.l., and it is gently inclined (1–5°) towards the north. The lithology of the CALM-S JGM consists of about 75% of gravelly to sandy sediments of a Holocene marine terrace and the remaining 25% of silt-loam sediments of the Whisky Bay Fm. of Cretaceous origin [18]. The CALM-S JGM area was delineated using a total station connected to the local geodetic network [32].

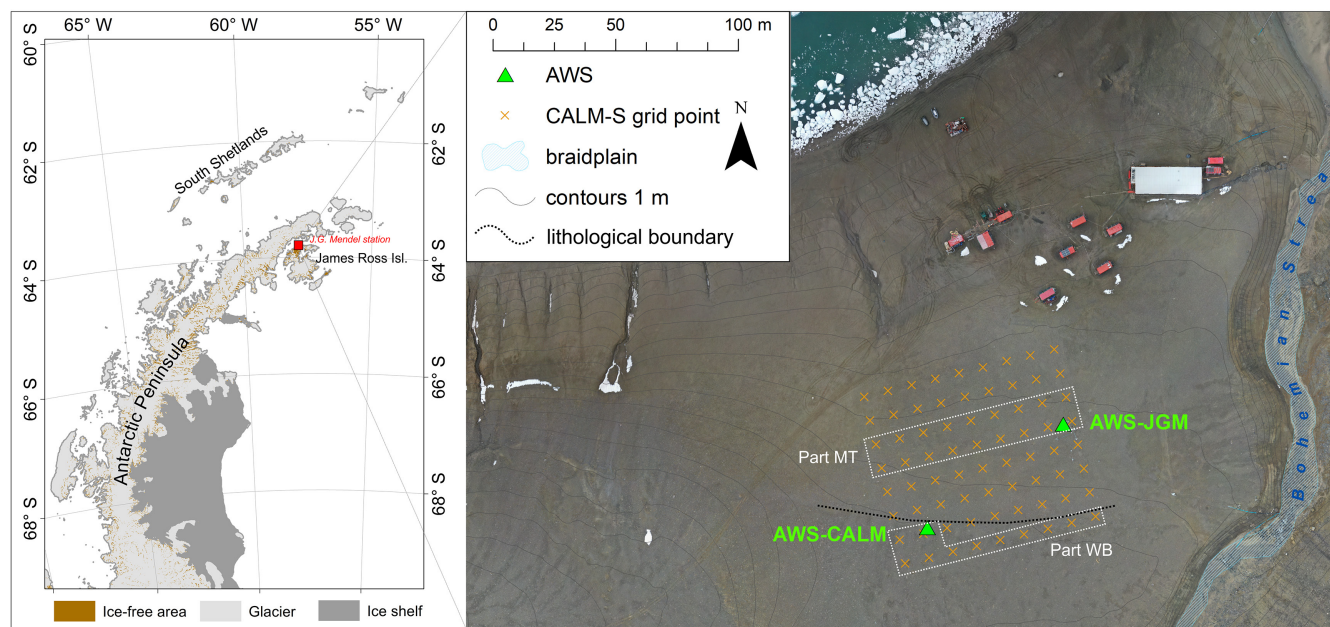


**FIGURE 1** | Regional setting (left) and a detailed image of the CALM-S JGM site and its vicinity (right). White dotted polygons represent the area used as a reference for Holocene marine terrace sediments and Whisky Bay Formation. [Colour figure can be viewed at [wileyonlinelibrary.com](https://onlinelibrary.wiley.com/doi/10.1002/ppp.2274)] <https://onlinelibrary.wiley.com/doi/10.1002/ppp.2274>

## 2.3 | Automatic Monitoring Stations

The CALM-S JGM is equipped with an automatic weather station (AWS) and two profiles for ground temperature monitoring. The profile AWS-JGM is located on a Holocene marine terrace, whereas the profile AWS-CALM is located within the Cretaceous sediments of Whisky Bay Formation (Figure 1). The AWS-JGM provides air temperature data measured at 2 m above the ground surface using a Minikin TH sensor (EMS Brno) with an accuracy of  $\pm 0.15^\circ\text{C}$  placed in a protective radiation shield. AWS-JGM and AWS-CALM provide ground temperature data measured in a 200-cm deep profile using Pt100/8 thermometers (accuracy  $\pm 0.15^\circ\text{C}$ ; EMS Brno) placed directly to the ground. Data are recorded at 30-min intervals using dataloggers EdgeBox V12 (EMS Brno).

### 2.3.1 | Data Processing

The data from the air temperature and ground temperature sensors at 5-, 50-, 75-, 100-, and 200-cm depths were used from the AWS-JGM and AWS-CALM. The raw 30-min data from the temperature measurements were used to calculate daily means and subsequently utilised to compute monthly and annual averages. In accordance with previous studies (e.g. [18, 27]), the annual means were calculated for the period from March to February to contain a complete sequence of a freezing and thawing season. The temporal trends of selected parameters were established using the MAKESENS 1.0 application [33].

The datasets were continuous, with the exception of AWS-CALM ground temperatures, which were missing due to data logger malfunction in the period between 11 October 2016 to 21 January 2017. The mean daily temperatures were recalculated using linear regression models ( $R^2 > 0.99$  in all cases) based on relationships between ground temperatures of particular depths measured on AWS-CALM and AWS-JGM from 1 September 2016 to 28 February 2017.

The mean daily ground temperatures at a depth of 5 cm were further used for the determination of thawing seasons and freezing seasons defined as a period with the prevailing positive and negative temperatures, respectively, and for the calculation of degree days indices (e.g. [34–36]):

1. Thawing degree day (TDD) indices summarise the positive daily mean temperatures during the thawing season. For each season, TDD of air (TDD<sub>a</sub>) and ground temperatures at depths of 5 cm (TDD<sub>5</sub>) and 50 cm (TDD<sub>50</sub>) were defined for the periods (a) from the beginning of the thawing season until the day with maximum ALT (e.g. [1]), further referred to as TDD<sub>e</sub>, and (b) residual TDD for the whole thawing season, further referred to as TDD<sub>t</sub>.
2. Freezing degree day (FDD) indices summarise the negative daily mean temperatures during the freezing season. FDDs were calculated for air temperature (FDD<sub>A</sub>) and ground temperature at a depth of 5 cm (FDD<sub>5</sub>).

## 2.4 | ALT

ALT refers to the maximum annual depth of  $0^\circ\text{C}$  isotherm. It was calculated for the day when the maximum positive temperature was detected on the bottommost sensor in the active layer using a linear interpolation with the closest sensor recording temperature  $< 0^\circ\text{C}$ . The pairs of these depths were 50 and 75 cm and 75 and 100 cm on AWS-JGM and AWS-CALM, respectively.

### 2.5 | Active Layer Thaw Depth and Volumetric Water Content

Thaw depth measurements were conducted using frost probes with a diameter of 1 cm and lengths of 120 or 140 cm. Measurements were taken 1 to 3 times during the thawing season to obtain data as close as possible to the seasonal ALT maximum. The annual thaw depth was calculated as the mean value of the 72 points. Data visualization was performed in Surfer 23 (Golden Software) using the kriging method. The data from 2021 were missing due to technical difficulties with the probing and were substituted using a multiple regression model ( $R^2 = 0.88$ ;  $p < 0.01$ ) based on the relationship between thaw depth and ALT during the period 2014 to 2023:

$$TD = ALT_{AWS-JGM} \times -0.004 + ALT_{AWS-CALM} \times 1.02 - 10.863$$

where  $TD$  represents the mean thaw depth value on the CALM-S JGM site, and  $ALT_{AWS-JGM}$  and  $ALT_{AWS-CALM}$  represent annual ALTs observed on both study profiles.

Since 2017, the VWC has been measured using a Hydrosense II device equipped with a TDR probe CS659 (Campbel Sci.) with an electrode length of 12 cm (accuracy  $\pm 3\%$ ). The measurement was carried out within a 1-m radius from each grid node of CALM-S JGM. The representative value was obtained as a mean from at least two measurements with a less than 5% difference. VWC measurements were conducted on the same day as the active layer thaw depth probed. Finally, to obtain values of thaw depth and VWC representing both lithological formations, we defined two areas, counting 10 nodes and 18 nodes for Whisky Bay Fm. (Part WB) and Holocene marine terrace (Part MT), respectively (Figure 1).

## 3 | Results

### 3.1 | Air and Ground Thermal Regime

#### 3.1.1 | Air Temperature AWS-JGM

The mean annual air temperature (MAAT) was  $-5.8^\circ\text{C}$ , and it ranged from  $-3.6^\circ\text{C}$  (2022/23) to  $-7.4^\circ\text{C}$  (2013/14) (Table 1). During the study period, the MAAT exhibited an increasing trend of  $0.2^\circ\text{C}/\text{year}$  (significant at  $p < 0.05$ ). The mean monthly air temperature was positive only during the summer months from December to February. The warmest month recorded was January 2023 ( $3.0^\circ\text{C}$ ). Mean daily temperatures exceeded  $5^\circ\text{C}$  in each summer season. The maximum mean daily temperature ( $11.2^\circ\text{C}$ ) was recorded on 2 January 2016 (Figure 2). The mean value of TDD<sub>Ae</sub> was  $139^\circ\text{C}\text{-days}$  ( $25^\circ\text{C}\text{-days}$  in 2013/14 to  $256^\circ\text{C}\text{-days}$  in 2022/23), while the mean value of TDD<sub>At</sub> was

**TABLE 1** | Mean annual air (AT) and ground temperatures (GT) on the AWS-JGM and AWS-CALM in the seasons 2013–2023.

|              | AWS-JGM |      |      |       |       | AWS-CALM |      |       |       |
|--------------|---------|------|------|-------|-------|----------|------|-------|-------|
|              | AT      | GT5  | GT50 | GT100 | GT200 | GT5      | GT50 | GT100 | GT200 |
| 2013/2014    | -7.4    | -5.4 | -5.5 | -6.0  | -6.0  | —        | —    | —     | —     |
| 2014/2015    | -6.7    | -5.0 | -5.1 | -5.7  | -5.6  | -4.9     | -5.0 | -5.2  | -5.2  |
| 2015/2016    | -7.0    | -5.6 | -5.8 | -6.3  | -6.0  | -5.6     | -5.8 | -5.7  | -5.7  |
| 2016/2017    | -3.9    | -3.3 | -4.0 | -4.8  | -5.1  | -3.5     | -4.2 | -4.6  | -4.7  |
| 2017/2018    | -6.6    | -5.6 | -5.1 | -5.4  | -5.2  | -5.3     | -5.3 | -5.1  | -5.1  |
| 2018/2019    | -6.0    | -5.1 | -5.1 | -5.6  | -5.4  | -4.6     | -4.7 | -4.7  | -4.8  |
| 2019/2020    | -6.5    | -5.4 | -5.6 | -6.1  | -5.8  | -4.6     | -4.9 | -5.1  | -5.1  |
| 2020/2021    | -6.4    | -5.0 | -5.3 | -5.8  | -5.6  | -5.0     | -5.3 | -5.4  | -5.4  |
| 2021/2022    | -4.7    | -4.3 | -4.7 | -5.3  | -5.4  | -4.1     | -4.4 | -4.6  | -4.7  |
| 2022/2023    | -3.6    | -3.0 | -3.7 | -4.5  | -4.7  | -2.7     | -3.2 | -3.6  | -3.8  |
| 2013–2023    | -5.9    | -4.8 | -5.0 | -5.5  | -5.5  | -4.5     | -4.8 | -4.9  | -5.0  |
| Annual trend | 0.20*   | 0.12 | 0.10 | 0.09  | 0.08  | 0.16     | 0.18 | 0.13  | 0.10  |

\*Statistically significant at  $p < 0.05$ .

185°C·days (61°C·days in 2013/14) to 274°C·days in 2021/22) (Figure 3). The mean monthly air temperature in winter occasionally dropped below  $-15^{\circ}\text{C}$ . The minimum observed monthly temperature was  $-20.1^{\circ}\text{C}$  in August 2020, and the daily minimum of  $-29.5^{\circ}\text{C}$  was recorded on 18 August 2014 (Figure 2). The mean FDD<sub>a</sub> was  $-2397^{\circ}\text{C}\cdot\text{days}$ , ranging from  $-2767^{\circ}\text{C}\cdot\text{days}$  (2013) to  $-1648^{\circ}\text{C}\cdot\text{days}$  (2022) (Figure 3).

### 3.1.2 | Ground Temperature AWS-JGM

The mean annual ground temperature (MAGT) on AWS-JGM ranged from  $-4.8^{\circ}\text{C}$  (5 cm) to  $-5.5^{\circ}\text{C}$  (200 cm) during the period from 1 March 2013 to 28 February 2023. The highest MAGT was observed in 2022/23, with ground temperatures between  $-3.0^{\circ}\text{C}$  (5 cm) and  $-4.7^{\circ}\text{C}$  (200 cm), whereas the coldest year was 2015/16, with temperatures between  $-5.6^{\circ}\text{C}$  (5 cm) and  $-6.0^{\circ}\text{C}$  (200 cm). The mean monthly ground temperature at the depth of 5 cm was usually  $> 0^{\circ}\text{C}$  for 4 months from November to February and occasionally exceeded  $5^{\circ}\text{C}$  in December and January. The warmest month recorded was December 2021 ( $7.4^{\circ}\text{C}$ ) (Figure 2). The mean TDD<sub>5e</sub> was  $448^{\circ}\text{C}\cdot\text{days}$  (287 to  $594^{\circ}\text{C}\cdot\text{days}$ ) days, while the mean TDD<sub>5t</sub> reached  $513^{\circ}\text{C}\cdot\text{days}$  (379 to  $623^{\circ}\text{C}\cdot\text{days}$ ) (Figure 3). The mean monthly temperature at a depth of 50 cm exceeded  $0^{\circ}\text{C}$  only in January and February. The recorded maximum was  $1.3^{\circ}\text{C}$  in January 2023 (Figure 2). The mean TDD<sub>50e</sub> reached  $22^{\circ}\text{C}\cdot\text{days}$  ( $0^{\circ}\text{C}\cdot\text{days}$  in 2013/14 to  $74^{\circ}\text{C}\cdot\text{days}$  in 2022/23). The mean TDD<sub>50t</sub> was only slightly higher ( $24^{\circ}\text{C}\cdot\text{days}$ ), with a range from  $0^{\circ}\text{C}\cdot\text{days}$  (2013/14) to  $76^{\circ}\text{C}\cdot\text{days}$  (2022/23) (Figure 3).

The mean monthly ground temperature at a depth of 5 cm occasionally dropped below  $-15^{\circ}\text{C}$  in winter. The coldest month was July 2019 ( $-19.1^{\circ}\text{C}$ ), when the lowest mean daily temperature of  $-26.5^{\circ}\text{C}$  was recorded (1 July 2019). Mean FDD<sub>5</sub> reached  $-2292^{\circ}\text{C}\cdot\text{days}$  ( $-2566^{\circ}\text{C}\cdot\text{days}$  to  $-1731^{\circ}\text{C}\cdot\text{days}$ ). Mean monthly temperatures at a depth of 50 cm usually dropped below  $-10^{\circ}\text{C}$ .

The coldest month was July 2015 ( $-13.8^{\circ}\text{C}$ ), while the lowest mean daily temperature was recorded on 22 August 2021 ( $-16.1^{\circ}\text{C}$ ).

### 3.1.3 | Ground Temperature AWS-CALM

The MAGT on AWS-CALM varied between  $-4.5^{\circ}\text{C}$  (5 cm) and  $-5.0^{\circ}\text{C}$  (200 cm). The highest MAGT was recorded in the 2022/23 season ( $-2.7^{\circ}\text{C}$  at 5 cm and  $-3.8^{\circ}\text{C}$  at 200 cm). The coldest year was 2015/16, with MAGT between  $-5.6^{\circ}\text{C}$  (5 cm) and  $-5.8^{\circ}\text{C}$  (50 cm) (Table 1). In a similar manner to AWS-JGM, the mean monthly ground temperatures at a depth of 5 cm on AWS-CALM were above  $0^{\circ}\text{C}$  in the period from November to February. The temperatures even exceeded  $5^{\circ}\text{C}$  in December and January. The warmest month was December 2021 ( $7.3^{\circ}\text{C}$  at 5 cm) 2021 (Figure 2). The mean TDD<sub>5e</sub> was  $452^{\circ}\text{C}\cdot\text{days}$  ( $345^{\circ}\text{C}\cdot\text{days}$  to  $570^{\circ}\text{C}\cdot\text{days}$ ) while the mean TDD<sub>5t</sub> was  $497^{\circ}\text{C}\cdot\text{days}$  ( $381^{\circ}\text{C}\cdot\text{days}$  to  $621^{\circ}\text{C}\cdot\text{days}$ ) (Figure 3). In contrast to AWS-JGM, mean monthly temperatures at a depth of 50 cm exceeded  $0^{\circ}\text{C}$  in January and February. Furthermore, since 2017, positive monthly mean temperatures have also been observed in December. In particular, the mean monthly ground temperature at a depth of 50 cm exceeded  $0^{\circ}\text{C}$  in March 2016, 2020 and 2022. The maximum mean monthly temperature at a depth of 50 cm ( $3.3^{\circ}\text{C}$ ) was recorded in January 2023 (Figure 2). The mean TDD<sub>50e</sub> reached  $107^{\circ}\text{C}\cdot\text{days}$  ( $63^{\circ}\text{C}\cdot\text{days}$  in 2018/19 to  $183^{\circ}\text{C}\cdot\text{days}$  in 2022/23). The mean TDD<sub>50t</sub> was higher ( $134^{\circ}\text{C}\cdot\text{days}$ ) with a range from  $71^{\circ}\text{C}\cdot\text{days}$  (2018/19) to  $210^{\circ}\text{C}\cdot\text{days}$  (2022/23) (Figure 3).

The mean monthly ground temperature at a depth of 5 cm usually dropped below  $-15^{\circ}\text{C}$  during winter. The coldest month was July 2019 ( $-19.1^{\circ}\text{C}$ ). The lowest daily temperature was recorded on 20 August 2021 ( $-24.5^{\circ}\text{C}$ ). The mean monthly temperatures at a depth of 50 cm regularly dropped below  $-10^{\circ}\text{C}$ . The

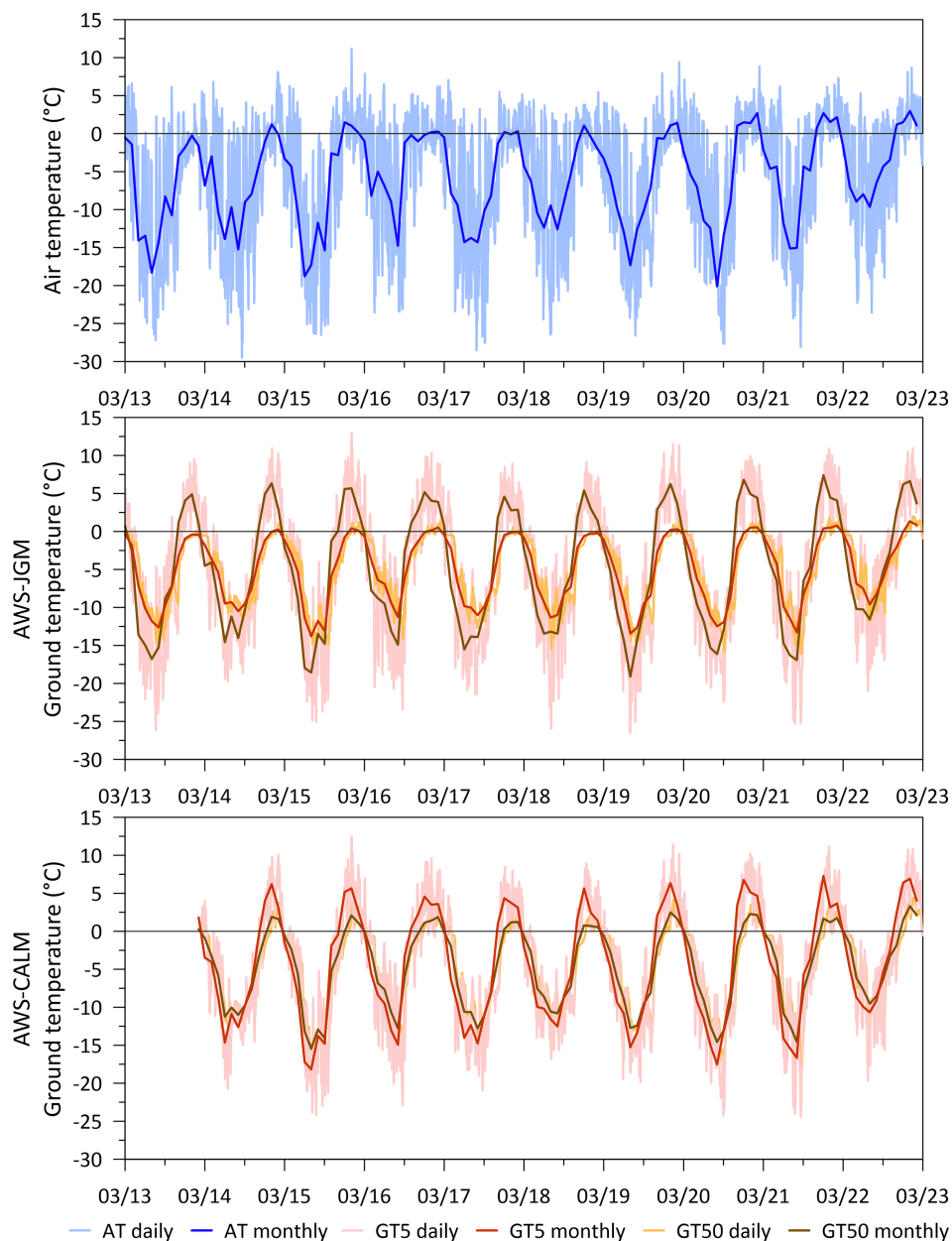


**FIGURE 2** | Variability of mean daily and mean monthly air temperature (AT) and ground temperatures at depths of 5 cm (GT5) and 50 cm (GT50) temperatures measured in the period between March 1, 2013, and February 28, 2023, on AWS-JGM and AWS-CALM. [Colour figure can be viewed at [wileyonlinelibrary.com](https://onlinelibrary.wiley.com)]

coldest month was July 2015 ( $-15.6^{\circ}\text{C}$ ); the lowest mean daily temperature was  $-18.7^{\circ}\text{C}$  (4 September 2020). The mean  $\text{FDD}_5$  reached  $-2121^{\circ}\text{C}\cdot\text{days}$ , with a range from  $-2510^{\circ}\text{C}\cdot\text{days}$  (2015) to  $-1605^{\circ}\text{C}\cdot\text{days}$  (2022) (Figure 3).

## 3.2 | ALT and Thaw Depth

### 3.2.1 | ALT Variability

The mean ALTs on study sites were 64 cm (AWS-JGM) and 88 cm (AWS-CALM). The maximum ALT of 73 cm (AWS-JGM) and 98 cm (AWS-CALM) was detected in 2022/23, while the lowest ALT was 51 cm (AWS-JGM) and 77 cm (AWS-CALM) in 2013/14. Statistically significant thickening trends reached

1.5 cm/year on AWS-JGM and 1.1 cm/year on AWS-CALM (Table 2). The date of maximum ALT occurrence was between 9 January and 21 February on AWS-JGM and between 25 January and 21 February on AWS-CALM (Table 2). The average thaw propagation period was 94 days (62 to 135 days) on AWS-JGM and 101 days (76 to 133 days) on AWS-CALM (Table 2).

The strongest correlation was found between ALT and  $\text{TDD}_{\text{Ae}}$  ( $r=0.91$ ) and  $\text{TDD}_{5\text{e}}$  ( $r=0.90$ ) on AWS-JGM. The relationships between ALT and annual temperatures were less pronounced, expressed by  $r=0.68$  (ALT vs MAAT) and  $r=0.62$  (ALT vs MAGT). ALT also strongly correlated with  $\text{TDD}_{\text{Ae}}$  ( $r=0.82$ ) and  $\text{TDD}_{5\text{e}}$  ( $r=0.91$ ) on AWS-CALM. Nevertheless, only moderate correlations were observed between ALT and MAAT ( $r=0.51$ ) and MAGT ( $r=0.57$ ) (Figure 4).

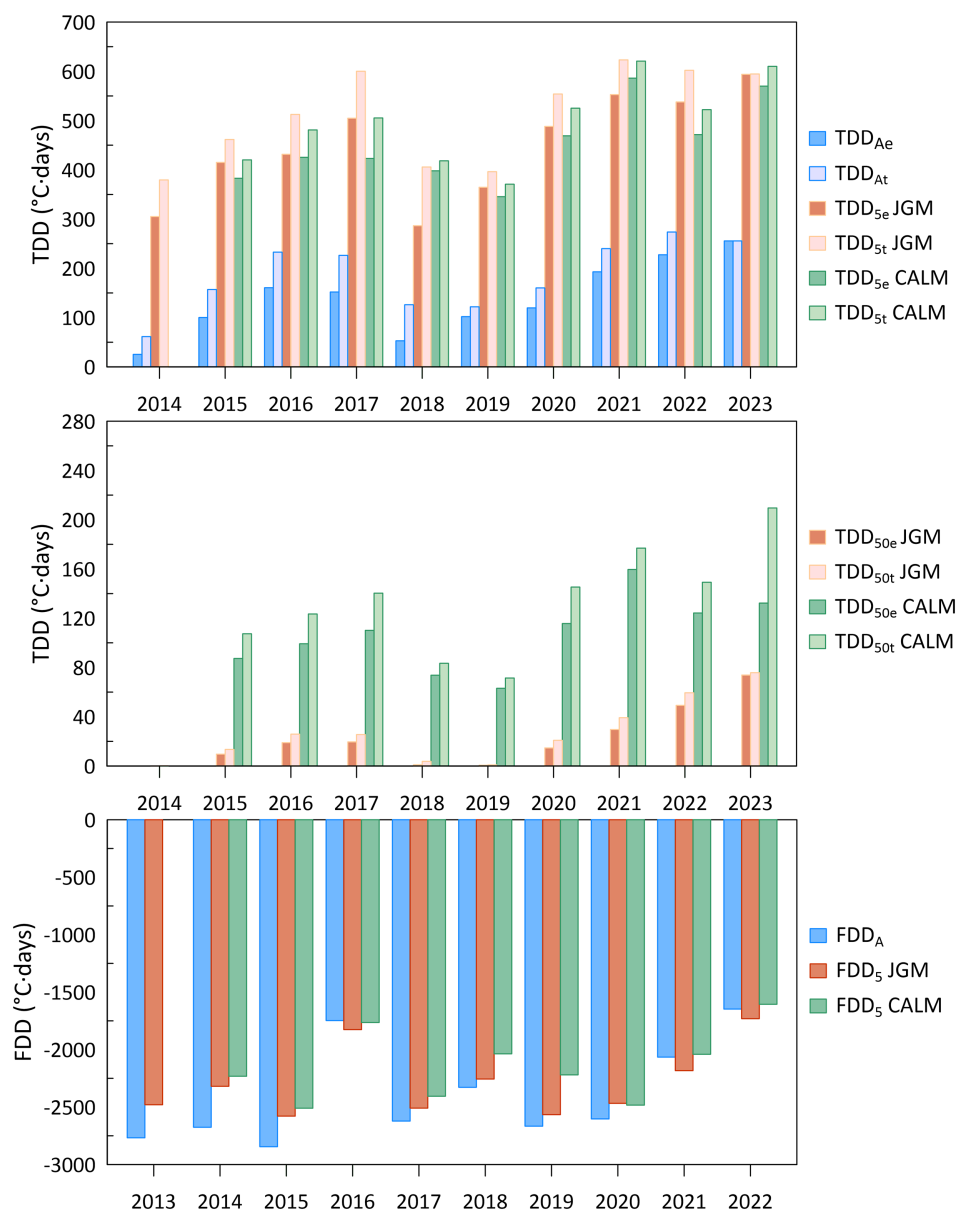


**FIGURE 3** | Annual variations of thawing (TDD) and freezing (FDD) degree days of air (A) and ground at a depth of 5 and 50cm on AWS-JGM and AWS-CALM. The subscripts  $e$  and  $t$  refers to TDD prior ALT maximum and total TDD during thawing season, respectively. [Colour figure can be viewed at [wileyonlinelibrary.com](https://onlinelibrary.wiley.com)]

### 3.2.2 | Thaw Depth Distribution and Variability

The mean active layer thaw depth on CALM-S JGM was 78 cm, with an annual range from 66 cm (2014) to 93 cm (2023) (Table 2). The year-to-year increase in thaw depths displayed a statistically significant thickening trend of 1.9 cm/year during the period 2014 to 2023 (Table 2). The maximum thaw depths increased from 100 cm (2014) to 130 cm (2023), while the minimum thaw depths increased from 51 cm (2014) to 72 cm (2023) (Figure 5). A clear pattern emerges in the thaw depth variation between the northern, larger grid area located on a Holocene marine terrace, with the thaw depths typically less than 80 cm, and the southern part, which is underlain by the Cretaceous sediments of the Whisky Bay Fm. Here, thaw depths regularly exceed 100 cm (Figure 5). A comparison of the reference zones revealed that the thaw depth on the Whisky Bay Fm. was, on average, 28 cm thicker than that of Holocene marine sediments,

with a stronger thickening trend of 2.2 cm/year compared with 1.3 cm/year (Table 2). The thaw depth exhibited a very strong correlation with  $TDD_{Ae}$  ( $r=0.83$ ) and  $TDD_{5e}$  both on AWS-JGM ( $r=0.84$ ) and AWS-CALM ( $r=0.87$ ). Strong correlations were found with MAAT and MAGT on AWS-JGM (both  $r=0.67$ ) and MAGT on AWS-CALM ( $r=0.66$ ) (Figure 4).

### 3.3 | Surficial Volumetric Water Content

The mean surficial VWC on CALM-S JGM ranged from 13.4% (2023) to 21.0% (2018). Similar to ALT, the strongest gradient of VWC was observed in the southern part of CALM-S, where the wettest patches with soil moisture exceeding 25% were located. The annual maximums reached 31% (2023) to 38% (2022). In some years (2018, 2020 and 2022), the patches with  $VWC > 25\%$  were also present in the northeast corner of the grid (Figure 6).

**TABLE 2** | General overview of active layer thickness (ALT) and surficial volumetric water content (VWC) on AWS-JGM and AWS-CALM and thaw depth on CALM-S JGM.

| Season          | AWS JGM  |                      |                      |                  |                      |               | AWS-CALM         |                      |                      |              |                  |                 | CALM-S JGM       |      |                  |            |                  |         |                  |      |         |
|-----------------|----------|----------------------|----------------------|------------------|----------------------|---------------|------------------|----------------------|----------------------|--------------|------------------|-----------------|------------------|------|------------------|------------|------------------|---------|------------------|------|---------|
|                 | ALT (cm) |                      | Thawing season start |                  | Season (days)        |               | ALT (cm)         |                      | Thawing season start |              | Season (days)    |                 | Thaw depth       |      | VWC (%)          |            | Thaw depth       |         | VWC (%)          |      |         |
|                 | ALT date | Thawing season start | Season (days)        | ALT (cm)         | Thawing season start | Season (days) | ALT date         | Thawing season start | Season (days)        | Probing date | Thaw depth       | VWC (%)         | Thaw depth       | MT   | VWC (%)          | Thaw depth | MT               | VWC (%) | Thaw depth       | WB   | VWC (%) |
| 2013/2014       | 51       | 24 February 2014     | 69                   | —                | 17 November 2013     | —             | —                | —                    | —                    | —            | 5 February 2014  | 66              | 65               | —    | 80               | —          | —                | —       | —                | —    | —       |
| 2014/2015       | 63       | 7 February 2015      | 76                   | 86               | 24 November 2014     | 8             | 8 February 2015  | 25 November 2014     | 76                   | 6            | 6 February 2015  | 78              | 73               | —    | 102              | —          | —                | —       | —                | —    | —       |
| 2015/2016       | 65       | 5 February 2016      | 76                   | 88               | 22 November 2015     | 8             | 8 February 2016  | 22 November 2015     | 79                   | 29           | 29 January 2016  | 77              | 70               | —    | 98               | —          | —                | —       | —                | —    | —       |
| 2016/2017       | 66       | 10 February 2017     | 135                  | 90               | 29 September 2016    | 11            | 11 February 2017 | 2 November 2016      | 133                  | 9            | 9 February 2017  | 80              | 75               | 15.6 | 100              | 13.9       | 100              | 13.9    | 100              | 21.4 | 21.4    |
| 2017/2018       | 59       | 9 January 2018       | 62                   | 81               | November 2017        | 18            | 18 February 2018 | 10 November 2017     | 101                  | 12           | 12 February 2018 | 75              | 66               | 21   | 106              | 19.6       | 106              | 19.6    | 106              | 27.3 | 27.3    |
| 2018/2019       | 56       | 5 February 2019      | 105                  | 77               | 24 October 2018      | 7             | 7 February 2019  | 27 November 2018     | 104                  | 12           | 12 February 2019 | 67              | 61               | 16.6 | 91               | 15.3       | 91               | 15.3    | 91               | 22.4 | 22.4    |
| 2019/2020       | 66       | 11 February 2020     | 95                   | 92               | 9 November 2019      | 13            | 13 February 2020 | 10 November 2019     | 96                   | 21           | 21 February 2020 | 80              | 75               | 16.9 | 102              | 14.9       | 102              | 14.9    | 102              | 25.1 | 25.1    |
| 2020/2021       | 66       | 12 February 2021     | 105                  | 92               | 31 October 2020      | 13            | 13 February 2021 | 31 October 2020      | 106                  | —            | —                | 83 <sup>#</sup> | 73 <sup>#</sup>  | 16.7 | 107 <sup>#</sup> | 15.5       | 107 <sup>#</sup> | 15.5    | 107 <sup>#</sup> | 20.4 | 20.4    |
| 2021/2022       | 71       | 12 February 2022     | 105                  | 92               | 31 October 2021      | 13            | 13 February 2022 | 1 November 2021      | 105                  | 9            | 9 February 2022  | 81              | 77               | 19.3 | 99               | 17.5       | 99               | 17.5    | 99               | 22.5 | 22.5    |
| 2022/2023       | 73       | 21 February 2023     | 108                  | 98               | 6 November 2022      | 13            | 13 February 2023 | 6 November 2022      | 100                  | 11           | 11 February 2023 | 93              | 85               | 13.4 | 124              | 12         | 124              | 12      | 124              | 21   | 21      |
| Mean            | 64       | 5 February           | 94                   | 88               | 5 November           | 12            | 12 February      | 5 November           | 100                  | —            | —                | 82              | 75               | 16.1 | 103              | 15.3       | 103              | 15.3    | 103              | 22.3 | 22.3    |
| Trend (cm/year) | 1.5*     | —                    | —                    | 1.1 <sup>+</sup> | —                    | —             | —                | —                    | —                    | —            | —                | 1.9*            | 1.3 <sup>+</sup> | —    | 2.2 <sup>+</sup> | —          | —                | —       | —                | —    | —       |

<sup>#</sup>Data reconstructed using a regression model from AWS-JGM and AWS-CALM.

\*Significant at  $p < 0.05$ .

<sup>+</sup>Significant at  $p < 0.1$ .

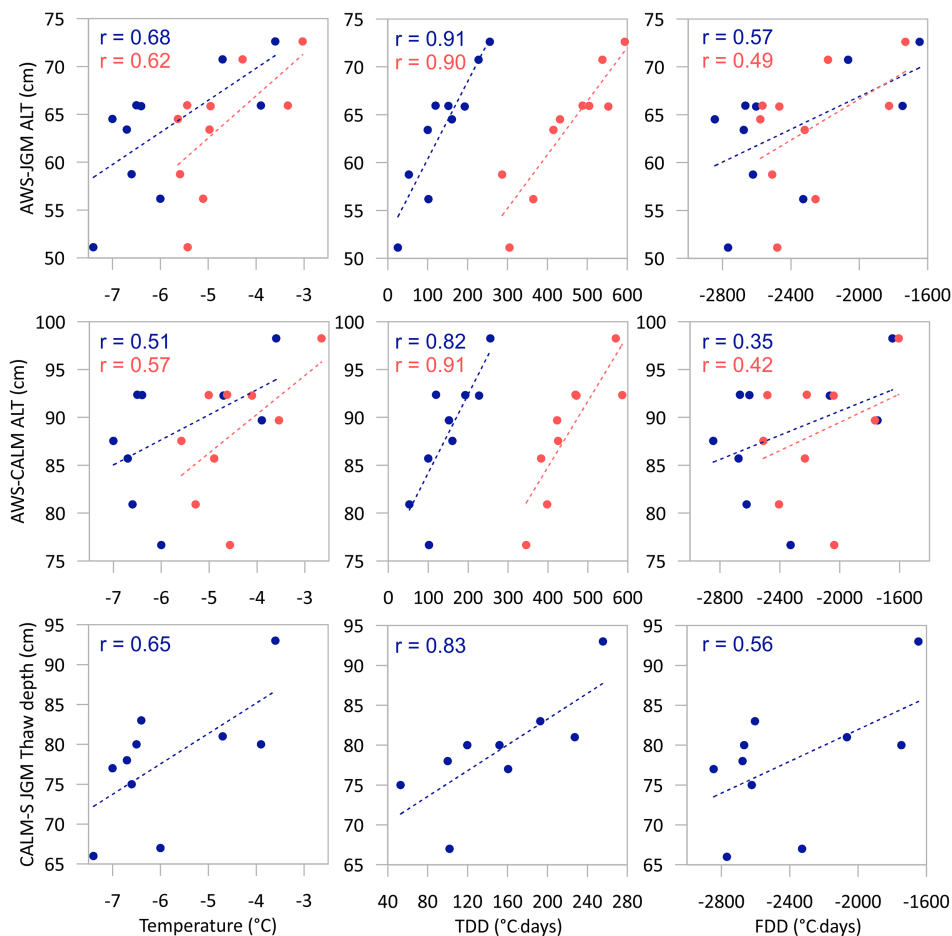


**FIGURE 4** | Correlation plots between active layer thickness (ALT)/thaw depth and parameters of air temperature (blue) and ground temperature at a depth of 5 cm (red) on AWS-JGM (top row), AWS-CALM (middle row) and CALM-S JGM (bottom row). The  $r$  value expresses the Pearson correlation coefficient. [Colour figure can be viewed at [wileyonlinelibrary.com](https://onlinelibrary.wiley.com)]

The drier parts with VWC lower than 15% were presented mostly in a diagonal direction from northwest to southeast (Figure 6). The vast majority of the CALM-S JGM had VWC < 15% in 2023, including several larger patches with VWC < 10% detected in the north and southeast part (Figure 6). Overall, the VWC was about 7% higher in the reference part WB than in the part MT (Table 2; Figure 6). We found a moderate negative correlation ( $r = -0.52$  and  $-0.57$ ; statistically not significant) between mean thaw depth and mean VWC for the whole CALM-S JGM and for the part MT, respectively. A very weak negative correlation ( $r = -0.18$ ; statistically not significant) was found in the MB part (Figure 6).

## 4 | Discussion

### 4.1 | Sustainability of CALM-S JGM

After 10 seasons, the monitoring experience, quality and representativeness of the dataset generated by the CALM-S JGM can be evaluated. Managing a CALM-S site in Antarctica is challenging, and several obstacles can be faced related to the climatic conditions and the general remoteness of the continent. This threatens the homogeneity of the dataset [15]. Some of the same problems were encountered with the CALM-S

JGM, but overall, the grid provided a unique and consistent dataset.

Although the CALM-S JGM is located in a relatively flat area, it is possible to clearly distinguish between the two main lithological units, which is reflected in the variability of soil physical properties such as texture, density, moisture and thermal properties. In particular, soil thermal properties are considered the primary factor causing the variability of thaw depth on the CALM-S JGM [18]. As the site consists entirely of bare ground, there is no effect of vegetation [16] or organic matter or peat content (e.g. [6, 11]).

The variability of thaw depth on other CALM sites is also often related to uneven distribution of snow cover (e.g. [12, 16, 20]). However, our previous studies from the area of CALM-S JGM found that the typical snow cover was thinner than 30 cm and irregular. Therefore, the snow effect on the active layer thermal regime was generally negligible [30]. A notable influence of snow on the thaw depth was only observed in 2018 when short-term snow presence during the summer led to a distinctive reduction of the thaw depth [26].

Physical properties, namely soil texture, also affect the practical aspects of thaw depth probing. The sandy soil matrix of the

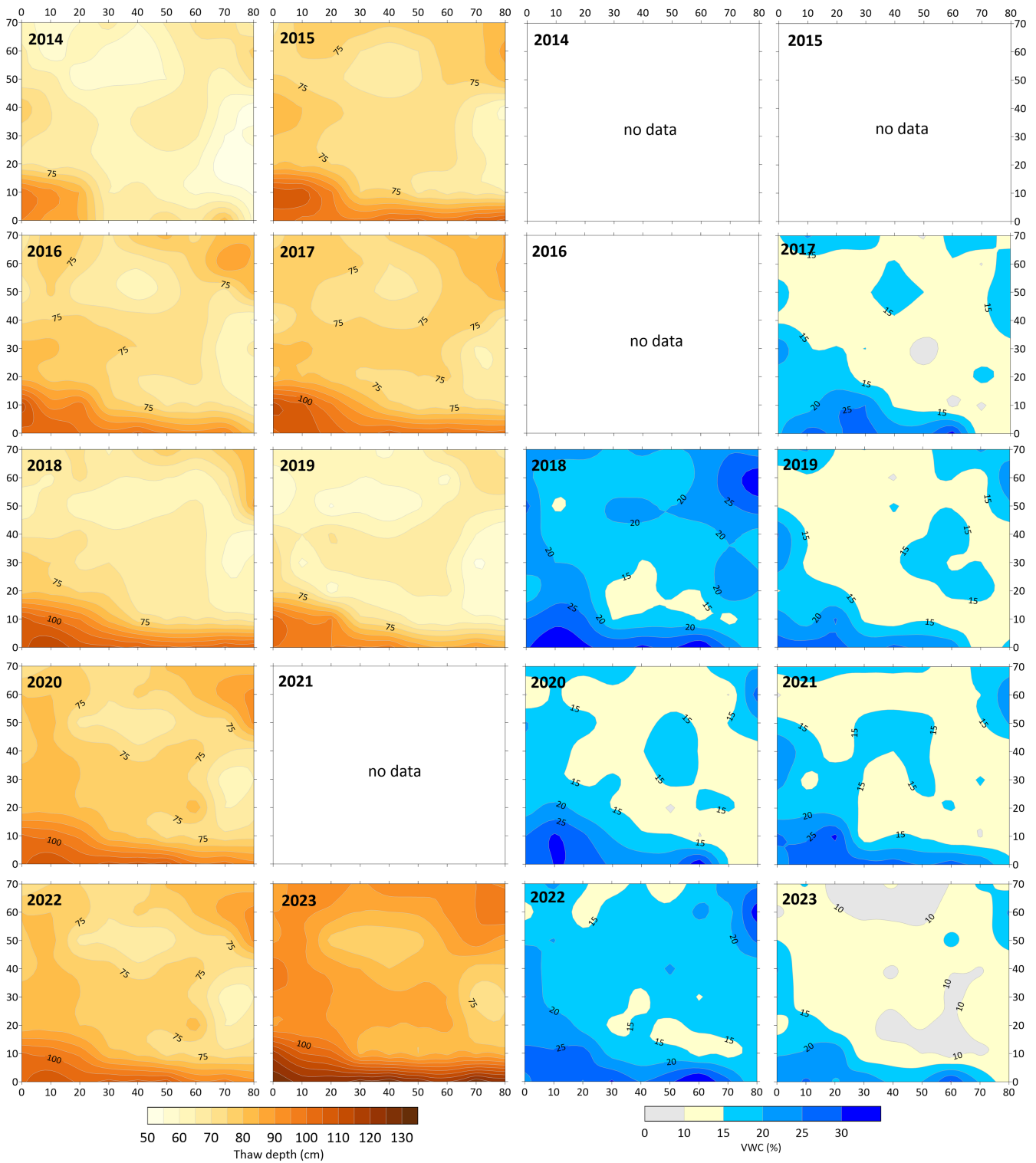


**FIGURE 5** | The variability of active layer thaw depth and surficial volumetric water content (VWC) in the period 2014 to 2023 (data missing in 2021). [Colour figure can be viewed at [wileyonlinelibrary.com](https://onlinelibrary.wiley.com)]

marine terrace that forms the northern part of the CALM-S JGM provides favourable conditions for the probing, making it fast and reliable. However, this lithological unit represents only a small part of the total area of the Ulu Peninsula [37]. Due to the low values of soil thermal conductivity of this lithological unit, the ALT observed on the AWS-JGM is a

few decimetres thinner than in other lowland areas of the JRI (e.g. [18, 38, 39]). On the other hand, the smaller part of the CALM-S JGM plot underlain by Cretaceous sediments can be considered representative for a much larger part of the Ulu Peninsula, as this particular lithological unit covers larger areas there [37]. Notably, the soil thermal properties

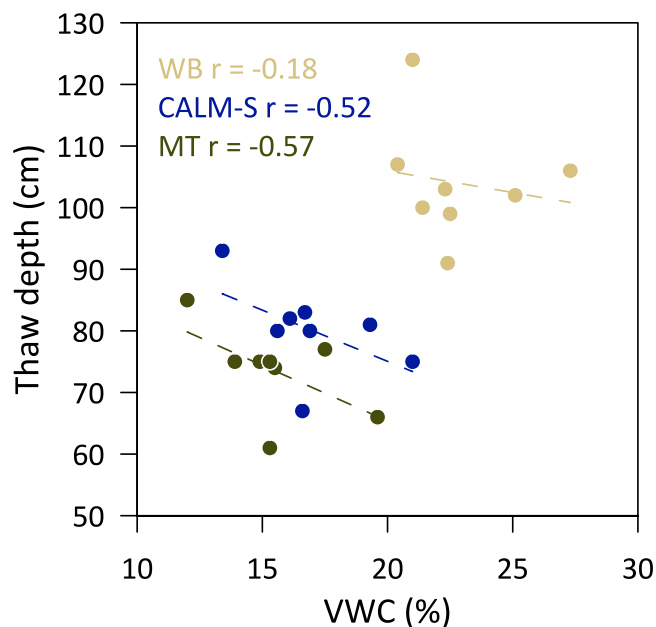


**FIGURE 6** | Relationship between surficial volumetric water content (VWC) and thaw depth in CALM-S JGM and reference parts of marine terrace (MT) and Whisky Bay Fm. sediments (WB). The  $r$  value expresses the Pearson correlation coefficient. [Colour figure can be viewed at [wileyonlinelibrary.com](https://onlinelibrary.wiley.com)]

determined for AWS-CALM are similar to other sites in the northern part of the Ulu Peninsula, which is also reflected in similar ALTs between 80 and 100 cm ([23]; unpublished data). However, this part of CALM-S is difficult to survey by mechanical probing due to the high adhesion of the silty to clayey soils and the presence of larger boulders hidden in the ground. For this reason, it was decided that the probing would be conducted in only 10 nodes of this lithological unit to ensure the sustainability of the monitoring.

Finally, logistical constraints preventing the measurement as close as possible to the time of maximum ALT represent a noticeable issue of CALM-S monitoring in Antarctica [15], which is the main objective on the Arctic CALM sites (e.g. [1]). In Antarctica, a difference of a few weeks between the probing and the maximum ALT occurrence is an issue, especially on the sites at the South Shetlands, where field probing is typically conducted in early February, while maximum ALT is observed in March or even April (e.g. [36]). Consequently, the reported thaw depth can be several decimetres thinner than the ALT [23]. In the case of CALM-S JGM, the maximum ALT was most often recorded between 5th and 13th February. Therefore, our approach of 2–3 measurements during the period from late January to late February ensures that the thaw depth measurement will be within a few days of the ALT maximum.

#### 4.2 | Effect of Thermal Regime and Moisture on Active Layer Thaw

Our results showed a very strong correlation between ALT/thaw depth and TDD of both air ( $r = 0.82$  to  $0.90$ ) and ground ( $r = 0.90$  to  $0.91$ ), confirming our observations, which generally

neglect the role of the snow cover and the absence of other important factors such as vegetation or organic matter content, which typically reduce the correlation to  $r < 0.7$  (e.g. [11, 12]). In contrast to summer temperature, the relationship between ALT/thaw depth and mean annual temperature or winter temperature was only moderate and statistically insignificant. However, a general pattern can be observed suggesting a thicker active layer in warmer years, including the winter season.

Unlike our recent study from the Abernethy Flats area on James Ross Island [39], the relationship between soil moisture and thaw depth on CALM-S were not statistically significant, which, is caused by the short dataset of only 7 years. Nevertheless, the negative correlation suggests the tendency of increasing thaw depth with decreasing surficial VWC. This pattern points towards a relatively even distribution of soil water in the profile, amplifying the effect of latent heat over the soil thermal conductivity (e.g. [40]).

#### 4.3 | Response of Active Layer to Climate Variability

In the Antarctic Peninsula region, the beginning of the 21st century until about 2012 to 2014 was connected with atmospheric cooling [41] and the associated impacts on the cryosphere, such as permafrost cooling, active layer thinning and glacier advance [42]. In particular, the active layer thinning of more than 1 cm/year was observed on James Ross Island [35] and the South Shetlands [21] during the period 2006 to 2015. However, our study period 2013/14 to 2023 was under the influence of a substantial increase in air temperature with a trend of  $2.0^\circ\text{C}/\text{decade}$  (significant at  $p < 0.05$ ). As a result, observed ground temperatures increased by  $0.8^\circ\text{C}/\text{decade}$  (200 cm) to  $1.8^\circ\text{C}/\text{decade}$  (5 cm), but both trends are not statistically significant. Renewed warming was observed across all of the Antarctic Peninsula (e.g. [43]) and resulted in 2022 being the warmest year ever observed in the northeastern Antarctic Peninsula [44].

Thickening of the thaw depth by 1.9 cm/year (CALM-S JGM) and ALT by 1.5 cm and 1.1 cm on AWS-JGM and AWS-CALM, respectively, resulted from the strong relationship between thaw depth and summer temperatures. These trends were higher than reported in the period 2012 to 2021 [27], emphasising the effect of the warm period after 2015. When analysing the complete dataset of ALT available for AWS-JGM (2012 to 2023), the ALT thickening reached 1.1 cm/year.

These results are consistent with the global behaviour of the active layer, which shows thickening trend rates between 0.27 and 4.0 cm/year in the period 1995 to 2020 [4–6, 12, 23]. The only area with a relatively stable or even decreasing active layer was found in the Dry Valleys in Antarctica, where the trends ranged from  $-0.5$  to  $0.04$  cm/year [23].

#### 5 | Conclusions

CALM-S JGM is the first continuously operated CALM site in the northeastern part of the Antarctic Peninsula region.

Although the site has atypical dimensions of 80×70 m, it provides valuable results on the thermal regime and thickness of the active layer. Results from 2013/14 to 2022/23 confirmed our initial hypothesis that distinctive lithology can significantly affect ALT and thaw depth at CALM-S JGM. The active layer was, on average, 24 cm thicker on AWS-CALM than on AWS-JGM, although TDD was higher on AWS-JGM. The thaw depth was, on average, 28 cm thicker in the part formed by Cretaceous sediments compared with marine sediments. ALT and thaw depth showed significant thickening trends between 1.1 and 2.2 cm/year, which can be associated with the 2.0°C increase in air temperature during the study period. Finally, surface soil moisture distribution was clearly affected by distinctive lithology. On average, soil moisture was 7.3% higher in the silty soils of the Whisky Bay Fm. than in the sandy soils of the Holocene marine terrace. The negative correlation between annual mean soil moisture and active layer thaw depth further suggests that soil drying will favour active layer deepening on the CALM-S JGM. However, this assumption so far lacks statistical significance due to the temporal limitation of moisture monitoring.

### Acknowledgments

The authors would like to thank Czech Antarctic Research Programme and the crew of the Johann Gregor Mendel for field support, namely, Zdeněk Stachoň, Jakub Ondruch, Matěj Roman, Jana Smolíková, and Zbyněk Engel who participated in the CALM-S measurement fieldwork. Open access publishing facilitated by Masarykova univerzita, as part of the Wiley - CzechELib agreement.

### Data Availability Statement

Data are available upon request.

### References

1. J. Brown, K. M. Hinkel, and F. E. Nelson, “The Circumpolar Active Layer Monitoring (CALM) Program: Research Designs and Initial Results,” *Polar Geography* 24, no. 3 (2000): 165–258, <https://doi.org/10.1080/10889370009377698>.
2. F. E. Nelson, N. E. Shiklomanov, and K. E. Nyland, “Cool, CALM, Collected: The Circumpolar Active Layer Monitoring Program and Network,” *Polar Geography* 44, no. 3 (2021): 155–166, <https://doi.org/10.1080/1088937X.2021.1988001>.
3. P. P. Bonnaventure and S. F. Lamoureux, “The Active Layer: A Conceptual Review of Monitoring, Modelling Techniques and Changes in a Warming Climate,” *Progress in Physical Geography: Earth and Environment* 37, no. 3 (2013): 352–376, <https://doi.org/10.1177/0309133313478314>.
4. K. E. Nyland, N. I. Shiklomanov, D. A. Streletskiy, F. E. Nelson, A. E. Klene, and A. L. Kholodov, “Long-Term Circumpolar Active Layer Monitoring (CALM) Program Observations in Northern Alaskan Tundra,” *Polar Geography* 44, no. 3 (2021): 167–185, <https://doi.org/10.1080/1088937X.2021.1988000>.
5. A. Abramov, S. Davydov, A. Ivashchenko, et al., “Two Decades of Active Layer Thickness Monitoring in Northeastern Asia,” *Polar Geography* 44, no. 3 (2021): 186–202, <https://doi.org/10.1080/1088937X.2019.1648581>.
6. D. Kaverin, G. Malkova, D. Zamolodchikov, et al., “Long-Term Active Layer Monitoring at CALM Sites in the Russian European North,” *Polar Geography* 44, no. 3 (2021): 203–216, <https://doi.org/10.1080/1088937X.2021.1981476>.
7. F. Hrbáček, G. Vieira, M. Oliva, et al., “Active Layer Monitoring in Antarctica: An Overview of Results From 2006 to 2015,” *Polar Geography* 44, no. 3 (2021): 1–16, <https://doi.org/10.1080/1088937X.2017.1420105>.
8. H. H. Christiansen, “Meteorological Control on Interannual Spatial and Temporal Variations in Snow Cover and Ground Thawing in two Northeast Greenlandic Circumpolar-Active-Layer-Monitoring (CALM) Sites,” *Permafrost and Periglacial Processes* 15, no. 2 (2004): 155–169, <https://doi.org/10.1002/ppp.489>.
9. K. M. Hinkel and F. E. Nelson, “Spatial and Temporal Patterns of Active Layer Thickness at Circumpolar Active Layer Monitoring (CALM) Sites in Northern Alaska, 1995–2000,” *Journal of Geophysical Research: Atmospheres* 108 (2003): 8168, <https://doi.org/10.1029/2001JD000927>.
10. G. Mazhitova, G. Malkova, O. Chestnyk, and D. Zamolodchikov, “Active-Layer Spatial and Temporal Variability at European Russian Circumpolar-Active-Layer-Monitoring (CALM) Sites,” *Permafrost and Periglacial Processes* 15, no. 2 (2004): 123–139, <https://doi.org/10.1002/ppp.484>.
11. S. L. Smith, S. A. Wolfe, D. W. Riseborough, and F. M. Nixon, “Active-Layer Characteristics and Summer Climatic Indices, Mackenzie Valley, Northwest Territories, Canada,” *Permafrost and Periglacial Processes* 20 (2009): 201–220, <https://doi.org/10.1002/ppp.651>.
12. S. M. Strand, H. H. Christiansen, M. Johansson, J. Akerman, and O. Humlum, “Active Layer Thickening and Controls on Interannual Variability in the Nordic Arctic Compared to the Circum-Arctic,” *Permafrost and Periglacial Processes* 32, no. 1 (2021): 47–58, <https://doi.org/10.1002/ppp.2088>.
13. M. Sudakova, M. Sadurtdinov, A. Skvortsov, et al., “Using Ground Penetrating Radar for Permafrost Monitoring From 2015–2017 at CALM Sites in the Pechora River Delta,” *Remote Sensing* 13 (2021): 3271, <https://doi.org/10.3390/rs13163271>.
14. M. Guglielmin, “Observations on Permafrost Ground Thermal Regimes From Antarctica and the Italian Alps, and Their Relevance to Global Climate Change,” *Global and Planetary Change* 40, no. 1–2 (2004): 159–167, [https://doi.org/10.1016/S0921-8181\(03\)00106-1](https://doi.org/10.1016/S0921-8181(03)00106-1).
15. M. Guglielmin, “Ground Surface Temperature (GST), Active Layer and Permafrost Monitoring in Continental Antarctica,” *Permafrost Periglac* 17 (2006): 133–143, <https://doi.org/10.1002/ppp.553>.
16. M. Guglielmin, M. Dalle Fratte, and N. Cannone, “Permafrost Warming and Vegetation Changes in Continental Antarctica,” *Environmental Research Letters* 9, no. 4 (2014): 045001, <https://doi.org/10.1088/1748-9326/9/4/045001>.
17. M. Guglielmin, M. R. Worland, and N. Cannone, “Spatial and Temporal Variability of Ground Surface Temperature and Active Layer Thickness at the Margin of Maritime Antarctica, Signy Island,” *Geomorphology* 155 (2012): 20–33, <https://doi.org/10.1016/j.geomorph.2011.12.016>.
18. F. Hrbáček, M. Kňazková, D. Nývlt, K. Láška, C. W. Mueller, and J. Ondruch, “Active Layer Monitoring at CALM-S Site Near J.G.Mendel Station, James Ross Island, Eastern Antarctic Peninsula,” *Science of the Total Environment* 601–602 (2017): 987–997, <https://doi.org/10.1016/j.scitotenv.2017.05.266>.
19. M. A. de Pablo, J. J. Blanco, A. Molina, M. Ramos, A. Quesada, and G. Vieira, “Interannual Active Layer Variability at the Limnopol Lake CALM Site on Byers Peninsula, Livingston Island, Antarctica,” *Antarctic Science* 25 (2013): 167–180, <https://doi.org/10.1017/S0954102012000818>.
20. M. A. de Pablo, M. Ramos, A. Molina, and M. Prieto, “Thaw Depth Spatial and Temporal Variability at the Limnopol Lake CALM-S Site, Byers Peninsula, Livingston Island, Antarctica,” *Science of the Total Environment* 615 (2018): 814–827, <https://doi.org/10.1016/j.scitotenv.2017.09.284>.

21. M. Ramos, G. Vieira, M. A. de Pablo, A. Molina, A. Abramov, and G. Goyanes, "Recent Shallowing of the Thaw Depth at Crater Lake, Deception Island, Antarctica (2006–2014)," *Catena* 149, no. 2 (2017): 519–528, <https://doi.org/10.1016/j.catena.2016.07.019>.
22. J. Obu, "How Much of the Earth's Surface Is Underlain by Permafrost?," *Journal of Geophysical Research: Earth Surface* 126 (2021): e2021JF006123, <https://doi.org/10.1029/2021JF006123>.
23. F. Hrbáček, M. Oliva, C. Hansen, et al., "Active Layer and Permafrost Thermal Regimes in the Ice-Free Areas of Antarctica," *Earth Science Reviews* 242 (2023): 104458, <https://doi.org/10.1016/j.earscirev.2023.104458>.
24. CALM Site, (2024), Available online: <https://www2.gwu.edu/~calm/>.
25. M. A. de Pablo, M. Ramos, and A. Molina, "Snow Cover Evolution, on 2009–2014, at the Limnopolar Lake CALM-S Site on Byers Peninsula, Livingston Island, Antarctica," *Catena* 149 (2017): 538–547, <https://doi.org/10.1016/j.catena.2016.06.002>.
26. F. Hrbáček, Z. Engel, M. Kňázková, and J. Smolíková, "Effect of Summer Snow Cover on the Active Layer Thermal Regime and Thickness on CALM-S JGM Site, James Ross Island, Eastern Antarctic Peninsula," *Catena* 207 (2021): 105608, <https://doi.org/10.1016/j.catena.2021.105608>.
27. L. Kaplan Pastířiková, F. Hrbáček, T. Uxa, and K. Láška, "Permafrost Table Temperature and Active Layer Thickness Variability on James Ross Island, Antarctic Peninsula, in 2004–2021," *Science of the Total Environment* 869 (2023): 161690, <https://doi.org/10.1016/j.scitotenv.2023.161690>.
28. J. M. van Wessem, S. R. M. Ligtenberg, C. H. Reijmer, et al., "The Modelled Surface Mass Balance of the Antarctic Peninsula at 5.5 km Horizontal Resolution," *Cryosphere* 10 (2016): 271–285, <https://doi.org/10.5194/tc-10-271-2016>.
29. J. Kavan, D. Nývlt, K. Láška, Z. Engel, and M. Kňázková, "High Latitude Dust Deposition in Snow on the Glaciers of James Ross Island, Antarctica," *Earth Surface Processes and Landforms* 45 (2020): 1569–1578, <https://doi.org/10.1002/esp.4831>.
30. F. Hrbáček, K. Láška, and Z. Engel, "Effect of Snow Cover on the Active-Layer Thermal Regime — A Case Study From James Ross Island, Antarctic Peninsula," *Permafrost and Periglacial Processes* 27 (2016): 307–315, <https://doi.org/10.1002/ppp.1871>.
31. J. Obu, S. Westermann, G. Vieira, et al., "Pan-Antarctic Map of Near-Surface Permafrost Temperatures at 1 km<sup>2</sup> Scale," *Cryosphere* 14, no. 2 (2020): 497–519.
32. Z. Stachoň, J. Russnák, D. Nývlt, and F. Hrbáček, "Stabilisation of Geodetic Points in the Surroundings of Johann Gregor Mendel Station, James Ross Island, Antarctica," *Czech Polar Reports* 4 (2014): 81–90, <https://doi.org/10.5817/CPR2014-1-9>.
33. T. Salmi, A. Määttä, P. Anttila, T. Ruoho-Airola, and T. Amnell, *Detecting Trends of Annual Values of Atmospheric Pollutants by the Mann-Kendall Test and Sen's Slope Estimates* (Finnish Meteorological Institute, 2002).
34. D. W. Riseborough, "Thawing and freezing indices in the active layer," in *Permafrost, Proceedings of the Eighth International Conference on Permafrost 21–25 July 2003, Zurich, Switzerland*, eds. M. Phillips, S. M. Springman, L. U. Arenson (A.A. Balkema, Lisse, 2003), 953–958.
35. F. Hrbáček and T. Uxa, "The Evolution of a Near-Surface Ground Thermal Regime and Modeled Active-Layer Thickness on James Ross Island, Eastern Antarctic Peninsula, in 2006–2016," *Permafrost and Periglacial Processes* 31 (2020): 141–155, <https://doi.org/10.1002/ppp.2018>.
36. M. A. de Pablo, M. Ramos, and A. Molina, "Thermal Characterisation of the Active Layer at the Limnopolar Lake CALM-S Site on Byers Peninsula (Livingston Island), Antarctica," *Solid Earth* 5, no. 2 (2014): 721–739, <https://doi.org/10.5194/se-5-721-2014>.
37. B. Mlčoch, D. Nývlt, and P. Mixa, eds., *Geological Map of James Ross Island – Northern Part 1: 25,000* (Czech Geological Survey, 2020).
38. F. Hrbáček, D. Nývlt, K. Láška, et al., "Permafrost and Active Layer Research on James Ross Island: An Overview," *Czech Polar Reports* 9, no. 1 (2019): 20–36, <https://doi.org/10.5817/cpr2019-1-3>.
39. M. Kňázková and F. Hrbáček, "Interannual Variability of Soil Thermal Conductivity and Moisture on the Abernethy Flats (James Ross Island) During Thawing Seasons 2015–2023," *Catena* 234 (2024): 107640, <https://doi.org/10.1016/j.catena.2023.107640>.
40. L. K. Clayton, K. Schaefer, M. J. Battaglia, et al., "Active Layer Thickness as a Function of Soil Water Content," *Environmental Research Letters* 16 (2021): 055028, <https://doi.org/10.1088/1748-9326/abfa4c>.
41. J. Turner, H. Lu, I. White, et al., "Absence of 21st Century Warming on Antarctic Peninsula Consistent With Natural Variability," *Nature* 535 (2016): 411–415, <https://doi.org/10.1038/nature18645>.
42. M. Oliva, F. Navarro, F. Hrbáček, et al., "Recent Regional Climate Cooling on the Antarctic Peninsula and Associated Impacts on the Cryosphere," *Science of the Total Environment* 580 (2017): 210–223, <https://doi.org/10.1016/j.scitotenv.2016.12.030>.
43. J. F. Carrasco, D. Bozkurt, and R. R. Cordero, "A Review of the Observed Air Temperature in the Antarctic Peninsula. Did the Warming Trend Come Back After the Early 21st hiatus?," *Polar Science* 28 (2021): 100653, <https://doi.org/10.1016/j.polar.2021.100653>.
44. R. J. H. Dunn, C. Sandford, M. Kendon, C. P. Morice, J. J. Kennedy, and N. A. Rayner, "Global and Regional Climate in 2022," *Weather* 78, no. 12 (2023): 328–336, <https://doi.org/10.1002/wea.4500>.



# Modelling ground thermal regime in bordering (dis)continuous permafrost environments

Filip Hrbáček<sup>a,\*</sup>, Marc Oliva<sup>b</sup>, Jesus-Ruiz Fernández<sup>c</sup>, Michaela Kňázková<sup>a</sup>, Miguel Angel de Pablo<sup>d</sup>

<sup>a</sup> Department of Geography, Faculty of Science, Masaryk University, Brno, Czech Republic

<sup>b</sup> Department of Geography, Universitat de Barcelona, C/ Montalegre 6-8, 3r, 08001, Barcelona, Spain

<sup>c</sup> Department of Geography, University of Oviedo, Spain

<sup>d</sup> Department of Geology, Geography and Environment, University of Alcalá, 28805, Madrid, Spain

## ARTICLE INFO

### Keywords:

Ground thermal regime  
Permafrost distribution  
Snow cover  
Deglaciation  
Maritime Antarctica

## ABSTRACT

Permafrost controls geomorphological dynamics in maritime Antarctic ecosystems. Here, we analyze and model ground thermal regime in bordering conditions between continuous and discontinuous permafrost to better understand its relationship with the timing of glacial retreat. In February 2017, a transect including 10 sites for monitoring ground temperatures was installed in the eastern fringe of Byers Peninsula (Livingston Island, northern Antarctic Peninsula), together with one station recording air temperatures and snow thickness. The sites were selected following the Mid-Late Holocene deglaciation of the area at a distance ranging from 0.30 to 3.15 km from the current Rotch Dome glacier front. The transect provided data on the effects of topography, snow cover and the timing of ice-free exposure, on the ground thermal regime. From February 2017 to February 2019, the mean annual air temperature was  $-2.0^{\circ}\text{C}$ , which was  $> 0.5^{\circ}\text{C}$  higher than 1986–2015 average in the Western Antarctic Peninsula region. Mean annual ground temperature at 10 cm depth varied between  $0.3$  and  $-1.1^{\circ}\text{C}$ , similar to the modelled Temperatures on the Top of the Permafrost (TTOP) that ranged from  $0.06 \pm 0.08^{\circ}\text{C}$  to  $-1.33 \pm 0.07^{\circ}\text{C}$ . The positive average temperatures at the warmest site were related to the long-lasting presence of snow which favoured warmer ground temperatures and may trigger permafrost degradation. The role of other factors (topography, and timing of the deglaciation) explained intersite differences, but the overall effect was not as strong as snow cover.

## 1. Introduction

The Antarctic Peninsula (AP) region has experienced shifting climate conditions over the last decades (Oliva et al., 2017a; Turner et al., 2005, 2016) that have driven large environmental changes on terrestrial ecosystems, including glacier oscillations (Engel et al., 2018; Kunz et al., 2012; Navarro et al., 2013), geomorphic activity (Oliva and Ruiz-Fernández, 2015), variations of permafrost and active layer dynamics (Bockheim et al., 2013; Vieira et al., 2010; Hrbáček et al., 2019a), and alterations of ecological processes (Convey et al., 2009; Ruiz-Fernández et al., 2019).

Permafrost, despite being a key component of the Cryosphere, is one of the less studied elements in Antarctic terrestrial ecosystems. Apart from frozen water, permafrost stores a large number of natural elements (e.g.;  $\text{CO}_2$ ,  $\text{CH}_4$ , Hg, etc) as well as products of anthropogenic pollution that have the potential to trigger dramatic climatic and environmental

changes in terrestrial and marine ecosystems (Potapowicz et al., 2019; Oliva and Fritz, 2018). Therefore, an accurate characterization of its distribution, thermal state and associated biogeochemical processes is crucial to anticipate future changes in a warming climate scenario. Recent studies have reported a global increase of permafrost temperatures between 2007 and 2016 of  $0.29 \pm 0.12^{\circ}\text{C}$ , up to  $0.37 \pm 0.10^{\circ}\text{C}$  in Antarctica (Biskaborn et al., 2019). However, the limited number of boreholes for permafrost monitoring distributed across this vast continent increases the uncertainties of the observed trends. In the AP region, the number of studies focusing on permafrost and active layer thickness has increased significantly over the last decade following the scientific efforts made during the International Polar Year 2007–2008 (Vieira et al., 2010). The majority of the research has focused on the islands surrounding the northern tip of the AP where mean annual air temperatures (MAAT) are slightly negative at sea level, namely the South Shetland Islands (SSI) (De Pablo et al., 2013; Goyanes et al.,

\* Corresponding author.

E-mail address: [hrbacekfilip@gmail.com](mailto:hrbacekfilip@gmail.com) (F. Hrbáček).

2014; Oliva et al., 2017b; Ramos et al., 2007), James Ross Island (Hrbáček et al., 2019b), Signy Island (Cannone et al., 2006; Guglielmin et al., 2008), with data from AP also discussed in some review papers encompassing the entire continent (Bockheim et al., 2013; Vieira et al., 2010).

The monitoring of permafrost and active layer temperatures has been accompanied by several approaches to improve our understanding of the spatial distribution of permafrost, such as geophysical surveying in different landforms to identify the spatial extent of permafrost domain (Correia et al., 2017; Hauck et al., 2007), geomorphological approaches focused on the study of frozen ground measurements and related processes (Oliva and Ruiz-Fernández, 2015, 2017;), as well as modelling subsurface temperatures based on surface properties and microclimatic conditions to better represent ground-atmosphere interactions (Ferreira et al., 2017; Hrbáček and Uxa, 2019). Whereas the understanding of the role of some factors such as snow (de Pablo et al., 2017; Hrbáček et al., 2019b) and lithology (Hrbáček et al., 2017) on permafrost and active layer development is increasing, there are several questions that have not been addressed yet, such as the relationship between the deglaciation and permafrost degradation/aggradation, or the role of cold/warm-based glaciers on permafrost following deglaciation (Oliva et al., 2019). The timing of the deglaciation affects the compactness of the soil, its exposure to intense physical and chemical weathering, as well as the possible presence of mosses and lichen communities (Ruiz-Fernández et al., 2019); in turn, these factors over time trigger changes of the surface albedo, soil texture and porosity that may also impact the active layer thermal regime.

With the purpose of better understanding the interaction between glacial retreat and active layer dynamics, we present here a new research study consisting of modelling ground temperatures to detect the spatial limits of permafrost in the boundary between continuous and discontinuous permafrost conditions (e.g. Nelson et al., 2002; Smith and Riseborough, 2002), as is the case of the coastal fringes of the SSI. Based on the data collected from ten active layer monitoring sites distributed along a transect stretching from the present-day moraine of Rotch Dome glacier to the lowest slopes of the central plateau of the Byers Peninsula (Livingston Island, SSI), we modelled the possible occurrence of permafrost using different thermal parameters (TTOP model, freezing-thawing degree days, etc). Here, in the largest ice-free environment on the SSI, there is a reasonably good chronological control of the timing of the deglaciation based on the existence of radiocarbon dates and tephrochronology from several lakes revealing that the eastern fringe became ice-free during the Mid-Late Holocene (Oliva et al., 2016a; 2016b). The difference in the time of deglaciation ranging from several hundreds of years between sites up to ca. 5–6 ka between the edges of the transect makes this a very appropriate environment to study if the time scale of glacier retreat conditions active layer thermal regime or if it rapidly adapts to the new environmental setting.

## 2. Material and methods

### 2.1. Study area

The Byers Peninsula lies on the western tip of Livingston Island at 62° 34' 35" S – 62° 40' 35" S latitude and 60° 54' 14" W – 61° 13' 07" W longitude (Fig. 1). With a land area of roughly 60 km<sup>2</sup>, this peninsula is the largest ice-free area on SSI. This archipelago has a polar maritime climate with relatively abundant rainfall, occurring mainly in summer (500–800 mm/year), both in the form of rain and snow (Bañón et al., 2013). Throughout the 2002–2010 period, the MAAT in the Byers Peninsula at 70 m.a.s.l was –2.8 °C, with a moderate thermal range (Bañón et al., 2013).

This peninsula is composed of volcanic, volcanoclastic and sedimentary rocks (mainly sandstones, mudstones and conglomerates) dating from Jurassic and Cretaceous periods. There are also sills, dikes

and other intrusive rocks of Cretaceous age (Hathway and Lomas, 1998; Parica et al., 2007). The relief is organised around several staggered platforms at different elevations (the highest one develops between 70 and 100 m.a.s.l), from which some isolated volcanic plugs stand out, such as Penca Hill (217 m.a.s.l), Chester Cone (188 m.a.s.l) and Cerro Negro (143 m.a.s.l). The lowest areas are formed by both deposits of Holocene raised beaches and present-day beaches (López-Martínez et al., 1996, 2012).

As in the rest of the SSI, Livingston Island is mostly covered by glaciers, with only around 10% of ice-free terrain (Serrano, 2003). Whereas the highest areas on the island are covered by alpine glaciers, the lower terrain is occupied by coalescing glacial domes with the fronts reaching the sea. One of them corresponds to Rotch Dome glacier, the retreat of which has exposed the ice-free terrain of the Byers Peninsula. Following the deglaciation, several lakes appeared, whose sediments are indicative of past glacial oscillations, volcanic activity and climate variability (Toro et al., 2013; Liu et al., 2016; Oliva et al., 2016a,b; Antoniadis et al., 2018).

Present-day geomorphological dynamics in the Byers Peninsula is subject to the presence of permafrost and the annual evolution of the active layer. Periglacial processes are very active, even at lower altitudes, with abundant landforms derived from cryoturbation dynamics such as stone sorted-circles and stone stripes (López-Martínez et al., 2012; Ruiz-Fernández and Oliva, 2016). On the other hand, the abundant surface runoff resulting from snow melting during a few months of the year has an important geomorphological impact as it enhances fluvial erosion, thus triggering changes in the peninsula drainage network (Mink et al., 2014).

### 2.2. Measurement setting and data processing

In order to evaluate the potential influence of the timing of deglaciation on ground thermal conditions, in February 2017 we established a 2.8-km long transect from the present-day front of Rotch Dome glacier to the edges of the central plateau including 9 shallow boreholes for the monitoring of active layer temperatures in different topographical conditions (Fig. 1 in Supplementary Material). The monitoring sites were set at an increasing distance from the glacier within a narrow elevation belt (Table 1 in Supplementary Material), including the AWS-Domo station where air temperatures and snow cover thickness were also monitored.

Air temperature at the AWS-Domo was measured every 2 h using Tinytag sensor (accuracy ± 0.25 °C) placed 1.5 m above the ground within the radiation protective shield. The evolution of snow cover thickness was determined following the method proposed by Lewkowicz (2008) using iButtons DS 1922L (accuracy ± 0.5 °C) mounted on a vertical array and recording data every 6 h. The same type of iButton sensors was used for ground temperature monitoring at intervals of 6 h. Whereas at the AWS-Domo iButtons were installed in a borehole at the depths of 2, 5, 10, 20, 40, and 80 cm, at the other sites of the transect two iButtons were set directly into the ground at 10 and 40 cm depth. The obtained data were used to calculate mean, maximum and minimum daily values. The temporal analysis of the data was subdivided considering different periods:

- The study period from 10 February 2017 to 9 February 2019.
- Seasons 2017/18 consisted of freezing seasons 2017 and thawing seasons 2017/18

According to the recently published studies from the Maritime Antarctica region (e. g. de Pablo et al., 2017; Hrbáček et al., 2017), the freezing season was defined as a period with prevailing ground temperatures < 0 °C at the depth of 10 cm whereas the thawing season was defined as a period with prevailing ground temperatures > 0 °C at the depth of 10 cm. Further, we calculated the mean seasonal temperatures, seasonal duration as well as the parameters commonly used to

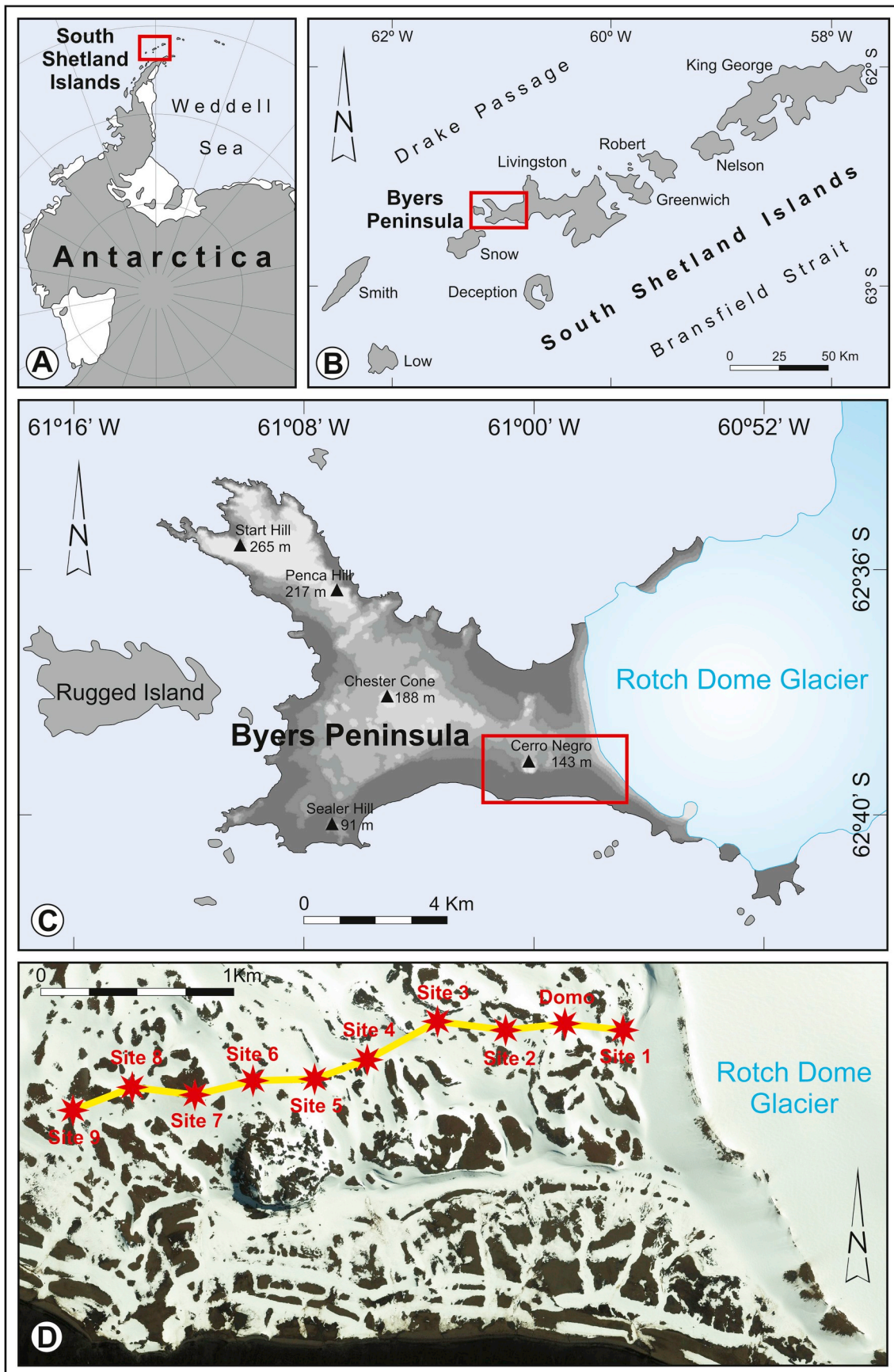


Fig. 1. Regional setting and the localization of the study area.

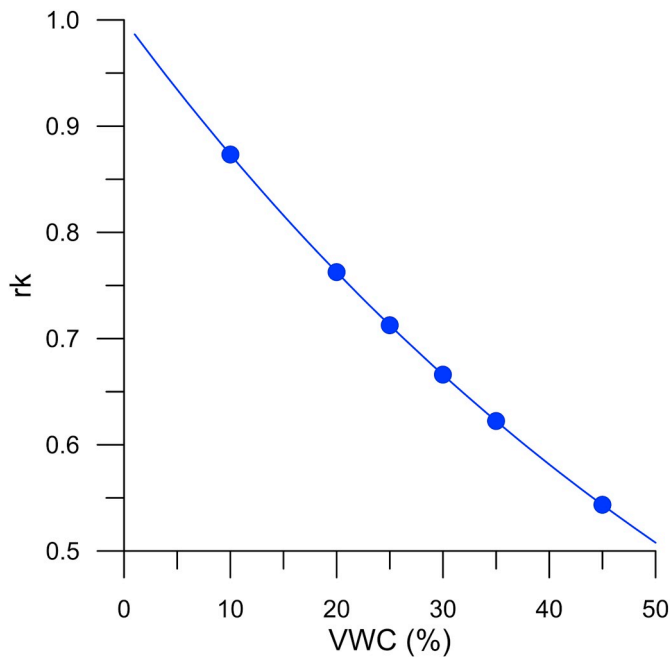


Fig. 2. The relationship between  $rk$  and volumetric water content (VWC) calculated using equation (2). The blue dots represent the  $rk$  used for TTOP model calculation. (For interpretation of the references to colour in this figure legend, the reader is referred to the Web version of this article.)

characterize the ground thermal regime considering the mean daily temperature (e.g., Guglielmin et al., 2008):

- a) Thawing degree days (TDD) – the seasonal sum of the mean daily temperatures  $> 0\text{ }^{\circ}\text{C}$
- b) Freezing degree days (FDD) – the seasonal sum of the mean daily temperatures  $< 0\text{ }^{\circ}\text{C}$ .

The TDD and FDD were calculated for both air (AT) and ground (GT) temperatures at different depths (5, 10, 40 and 80 cm). These indexes were also used for the calculation of:

- c) Freezing n-factor – the ratio between  $FDD_{GT}$  of the topmost part of the ground and  $FDD_{AT}$ .
- d) Thawing n-factor – the ratio between  $TDD_{GT}$  of the topmost part of the ground and  $TDD_{AT}$ .

Table 1

Selected thermal characteristics of the transect for in the monitoring period (10 February 2017 to 12 February 2019).

| Site     | MPGT <sup>a</sup> at 10 cm (°C) | MPGT <sup>a</sup> at 40 cm (°C) | TDD <sub>10cm</sub> (°C:days) <sup>b</sup> | TDD <sub>40cm</sub> (°C:days) <sup>c</sup> | FDD <sub>10cm</sub> (°C:days) <sup>d</sup> | FDD <sub>40cm</sub> (°C:days) <sup>e</sup> | TTOP (°C) <sup>f</sup> | Frost number |
|----------|---------------------------------|---------------------------------|--|--|--|--|------------------------|--------------|
| T1       | -0.5                            | -0.5                            | 569  | 434  | -926                                       | -773                                       | -0.73 ± 0.09           | 0.56         |
| T2       | -1.1                            | -1.1                            | 432  | 291  | -1270                                      | -1107                                      | -1.33 ± 0.09           | 0.63         |
| T3       | -1.0                            | -1.1                            | 377  | 205  | -1139                                      | -1027                                      | -1.20 ± 0.08           | 0.63         |
| T4       | -0.8                            | -0.9                            | 659  | 537  | -1277                                      | -1230                                      | -1.12 ± 0.14           | 0.58         |
| T5       | -0.9                            | -                               | 655  | -  | -1277                                      | -  | -1.13 ± 0.14           | 0.60         |
| T6       | -1.1                            | -1.0                            | 377  | 262  | -1161                                      | -1017                                      | -1.23 ± 0.08           | 0.64         |
| T7       | -0.6                            | -1.0                            | 575  | 333  | -1019                                      | -1054                                      | -0.85 ± 0.12           | 0.57         |
| T8       | -0.8                            | -0.6                            | 516  | 372  | -1070                                      | -831                                       | -0.97 ± 0.11           | 0.59         |
| T9       | 0.3                             | 0.3                             | 485  | 457  | -290                                       | -238                                       | 0.06 ± 0.10            | 0.44         |
| AWS-Domo | -1.0                            | -0.9                            | 404  | 227  | -1156                                      | -883                                       | -1.20 ± 0.09           | 0.64         |

<sup>a</sup> Mean period ground temperature.

<sup>b</sup> Thawing degree days at 10 cm.

<sup>c</sup> Thawing degree days at 40 cm.

<sup>d</sup> Freezing degree days at 10 cm.

<sup>e</sup> Freezing degree days at 40 cm.

<sup>f</sup> Modelled temperature on the top of the permafrost.

Due to the low inter-site variability of degree-days of air temperatures on the Byers Peninsula already described by Oliva et al. (2017), we used the data from AWS-Domo for the rest of the sites to calculate the n-factors. The active layer thickness was set on the AWS-Domo in the thawing season 2017/18 as a depth of  $0\text{ }^{\circ}\text{C}$  isotherm as it was defined by extrapolation of the best fitting exponential curve of the maximum seasonal ground temperatures at all depths of the profile (e.g. Guglielmin, 2006).

### 2.3. Permafrost temperature and threshold condition modelling

The occurrence of permafrost at the study sites was tested using the Temperature on the TOP of the Permafrost (TTOP) model (1), a commonly used approach for detecting the existence of permafrost in boundary environments between continuous and discontinuous permafrost (Smith and Riseborough, 1996; Riseborough et al., 2008), calculated as follows:

$$TTOP = \frac{rk \times TDD_G + FDD_G}{p} \tag{1}$$

where,  $rk$  is the ratio between the thermal conductivity of thawed and frozen ground,  $TDD_g$  represents the thawing degree days at the depth of 10 cm and  $FDD_g$  represents freezing degree days at the depth of 10 cm;  $p$  is the duration of the period in days.

Following Riseborough and Smith (1998), the  $rk$  can be expressed as the function of the soil water content:

$$rk = \frac{k_w^n}{k_i^{(n-w_u)}} k_w^{w_u} \tag{2}$$

where,  $k_i$  is the thermal conductivity of ice ( $2.21\text{ W m}^{-1}\text{K}^{-1}$ ),  $k_w$  is the thermal conductivity of water ( $0.56\text{ W m}^{-1}\text{K}^{-1}$ ) and  $w_u$  is the unfrozen volumetric water content.

Due to the absence of data on moisture conditions or the soil thermal properties, we calculated the TTOP using six  $rk$  between 0.87 and 0.54 which corresponds to soil volumetric water content of 10–45% (Fig. 2) and accordingly calculated mean TTOP value and a standard deviance. We used moisture usually measured at the Byers Peninsula (Nielsen et al., 2010).

Another parameter derived from degree days indices is the Frost number (FN) index (3), which can be calculated following the formula proposed by Nelson and Outcalt (1987):

$$FN = \frac{\sqrt{FDD}}{\sqrt{FDD} + \sqrt{TDD}} \tag{3}$$

The FN is a simple tool for predicting the probability of permafrost occurrence.  $FN < 0.5$  indicates the progressive ground thawing,

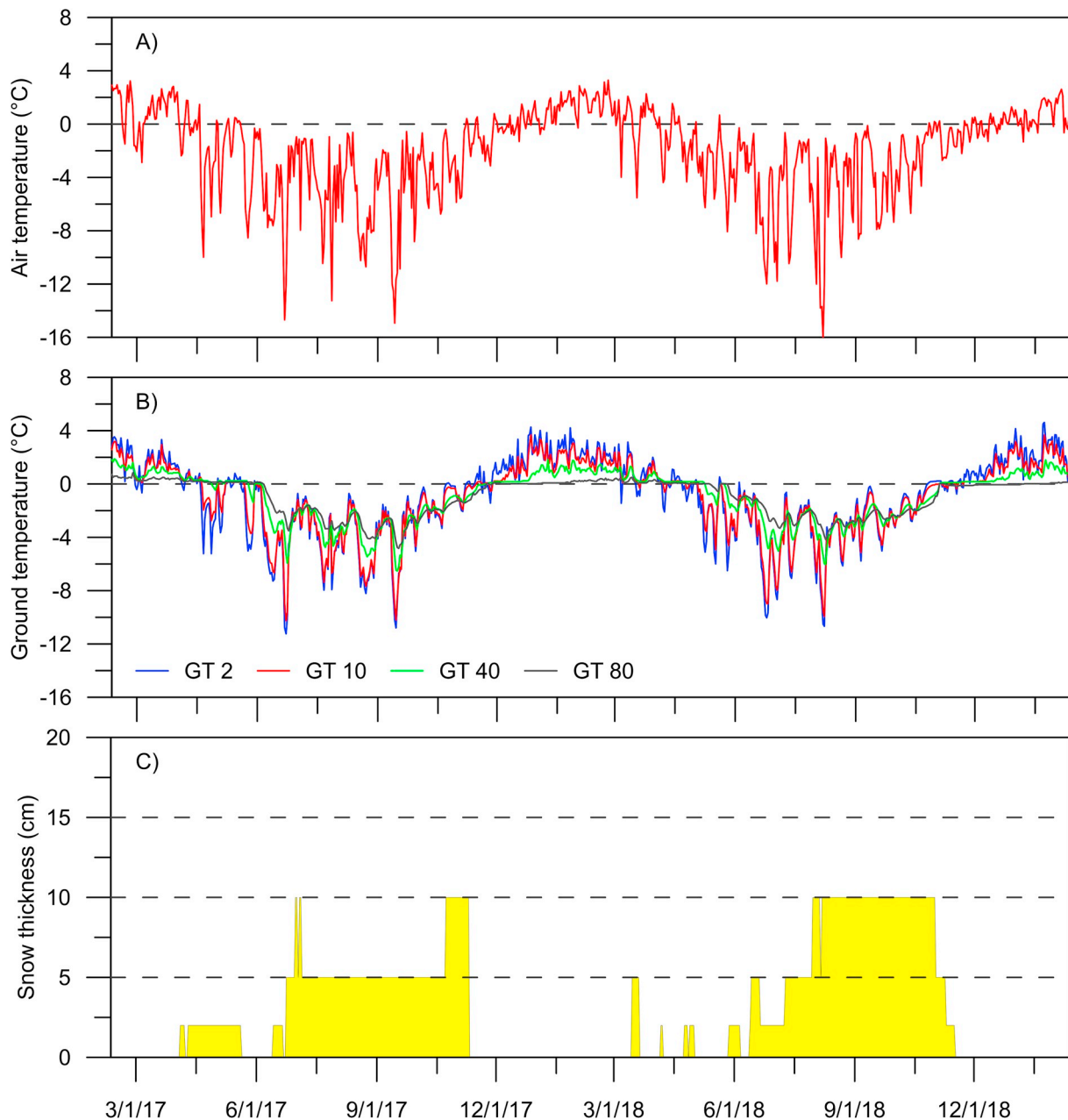


**Fig. 3.** Variability of the mean daily air temperature (A), ground temperature at the depths of 2, 10, 40 and 80 cm (B) and snow cover thickness (C) in the period 2/2017 to 2/2019 on AWS-Domo site.

deepening of active layer thickness and permafrost degradation, while  $FN > 0.5$  indicates a prevailing freezing regime that favours permafrost stability.

### 3. Results

#### 3.1. Air, snow and ground thermal regime at AWS-Domo

The MAAT between 10 February 2017 and 9 February 2019 was  $-2.1^{\circ}\text{C}$ . Interannual variability in this polar maritime environment was very low, ranging between  $-2.2^{\circ}\text{C}$  (2017/18) and  $-2.0^{\circ}\text{C}$  (2018/19). The maximum air temperature reached  $7.9^{\circ}\text{C}$  (15 December 2017), whereas the minimum dropped to  $-17.1^{\circ}\text{C}$  (7 August 2018). The warmest month was February 2018 ( $1.8^{\circ}\text{C}$ ), and the coldest month was August 2018 ( $-5.9^{\circ}\text{C}$ ). The mean daily air temperatures averaged positive values from October to May, with negative values from June to

September (Fig. 3). Snow cover was continuous from 30 June 2017 to 10 November 2017 and from 13 June 2018 to 16 November 2018. In both cases, the maximum thickness did not exceed 10 cm (Fig. 3).

The mean annual ground temperature (MAGT) at AWS-Domo showed a very low variability throughout the borehole during the study period (Fig. 4). The lowest MAGT of  $-1.2^{\circ}\text{C}$  was observed at 5 cm depth, and the highest values of  $-0.9^{\circ}\text{C}$  were recorded at 40 cm depth. The MAGT was almost equal in both years with the maximum difference of  $0.1^{\circ}\text{C}$  at 5, 10 and 20 cm.

The complete period including the freezing season of 2017 and the thawing season of 2017/18 lasted for 351 days. The freezing season lasted for 201 days from 20 April 2017 to 14 November 2017 (Table 2). The mean air temperature of the freezing season was  $-4.0^{\circ}\text{C}$  and the  $FDD_{AT}$  reached  $-902^{\circ}\text{C}\cdot\text{days}$ . There were very few days recording only positive air temperatures, with a total  $TDD_{AT}$  of  $3^{\circ}\text{C}\cdot\text{days}$ . The mean ground temperature of the freezing season at 5 cm depth was  $-2.9^{\circ}\text{C}$ ,

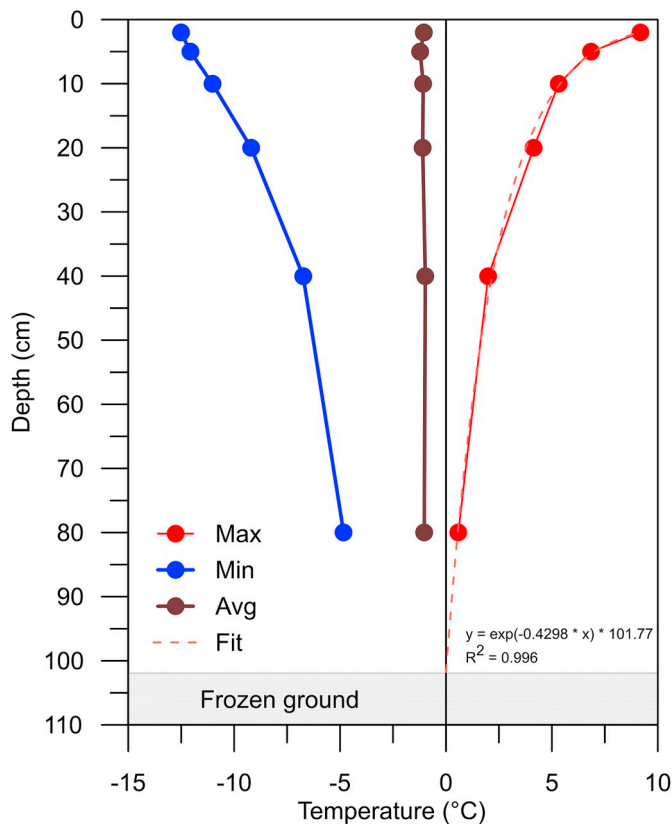


Fig. 4. Vertical temperature profile on AWS-Domo in the season 2017/18.

Table 2

The thermal characteristics of the freezing season 2017/18.

| Site                  | Beginning | End      | Duration | FDD <sub>10cm</sub> (°Cdays) <sup>a</sup> | MSGT (°C) <sup>b</sup> | n-factor |
|-----------------------|-----------|----------|----------|---|------------------------|----------|
| T1                    | 21.04.17  | 24.12.17 | 248      | -541                                      | -2.2                   | 0.60     |
| T2                    | 20.04.17  | 05.12.17 | 230      | -664                                      | -2.9                   | 0.74     |
| T3                    | 20.04.17  | 10.12.17 | 235      | -539                                      | -2.3                   | 0.60     |
| T4                    | 19.04.17  | 10.11.17 | 206      | -681                                      | -3.3                   | 0.75     |
| T5                    | 21.04.17  | 04.12.17 | 228      | -682                                      | -3                     | 0.76     |
| T6                    | 21.04.17  | 28.11.17 | 222      | -611                                      | -2.7                   | 0.68     |
| T7                    | 20.04.17  | 11.11.17 | 206      | -639                                      | -3.1                   | 0.71     |
| T8                    | 22.04.17  | 14.11.17 | 207      | -548                                      | -2.6                   | 0.61     |
| T9                    | 26.04.17  | 24.12.17 | 243      | -241                                      | -1.1                   | 0.27     |
| AWS-Domo              | 19.04.17  | 14.11.17 | 210      | -602                                      | -2.9                   | 0.66     |
| AWS-Domo <sup>b</sup> | 06.06.17  | 28.11.17 | 176      | -399                                      | -2.3                   | -        |

<sup>3</sup> Data from 80 cm depth.

<sup>a</sup> Freezing degree days at 10 cm depth.

<sup>b</sup> Mean seasonal ground temperature.

FDD<sub>10cm</sub> reached -602 °C·days and TDD<sub>10cm</sub> yielded only 3 °C·days. The freezing n-factor was 0.66. There was a considerable time lag of re-freezing between the surficial parts of the ground (10 cm) and the lowest section of the borehole (80 cm). The active layer at 80 cm depth froze on 6 June 2017, while re-thawing occurred on 28 November. The mean ground temperature during the freezing season at 80 cm depth was -2.3 °C, and FDD<sub>80cm</sub> was considerably higher compared to 5 cm depth, with -399 °C·days (Table 2).

The thawing season lasted for 129 days from 28 November 2017 to 5 April 2018. The mean air temperature of the thawing season was 0.7 °C (Table 4). Prevailing positive air temperatures resulted in a TDD<sub>AT</sub> of 122 °C·days. A numerous days (33) with negative temperatures resulted in a FDD<sub>AT</sub> of -28 °C·days. The mean seasonal ground temperature at 5 cm depth was 1.5 °C, and TDD<sub>5cm</sub> reached 203 °C·days. Only several days with negative temperatures (12) occurred during the

Table 3

The thermal characteristics of the thawing seasons 2017/18.

| Site                  | Beginning | End      | Duration | TDD <sub>10cm</sub> (°C·days) <sup>a</sup> | MSGT (°C) <sup>b</sup> | Thawing n-factor |
|-----------------------|-----------|----------|----------|--|------------------------|------------------|
| T1                    | 25.12.17  | 06.04.18 | 103      | 245  | 2.4                    | 2.01             |
| T2                    | 06.12.17  | 07.04.18 | 123      | 207  | 1.7                    | 1.70             |
| T3                    | 11.12.17  | 24.04.18 | 135      | 183  | 1.3                    | 1.50             |
| T4                    | 11.11.17  | 23.04.18 | 164      | 321  | 1.9                    | 2.63             |
| T5                    | 05.12.17  | 07.04.18 | 124      | 301  | 2.5                    | 2.47             |
| T6                    | 23.11.17  | 08.04.18 | 137      | 195  | 1.4                    | 1.60             |
| T7                    | 12.11.17  | 03.05.18 | 173      | 292  | 1.7                    | 2.39             |
| T8                    | 15.11.17  | 04.05.18 | 171      | 261  | 1.5                    | 2.14             |
| T9                    | 25.12.17  | 08.05.18 | 135      | 241  | 2.2                    | 2.01             |
| AWS-Domo              | 15.11.17  | 03.05.18 | 170      | 192  | 1.1                    | 1.57             |
| AWS-Domo <sup>b</sup> | 29.11.17  | 12.05.18 | 166      | 21   | 0.1                    | -                |

<sup>3</sup> Data from 80 cm depth.

<sup>a</sup> Thawing degree days at 10 cm depth.

<sup>b</sup> Mean seasonal ground temperature.

thawing seasons, which resulted in a FDD<sub>5cm</sub> of -4 °C·days. The active layer thawing at 80 cm depth started on 29 November and the ground remained unfrozen for 166 days until 12 May. Ground temperatures remained almost in the isothermal state for the whole period with mean daily ground temperatures close to 0 °C, which determined a mean seasonal ground temperature at 80 cm depth of only 0.1 °C. TDD<sub>80cm</sub> reached only 21 °C·days and no FDD was detected. The active layer thickness in 2017/18 was extrapolated to reach 101 cm, with the maximum depth observed on 14 March 2018.

The predicted TTOP was -1.24 ± 0.06 °C at AWS-Domo for the season 2017/18 (Fig. 5; Table 5) and -1.20 ± 0.09 °C for the whole study period (Table 1). The TTOP slightly underestimated the observed ground temperatures at 80 cm depth, which reached -1.1 °C (2017/18) and -1.0 °C (2017/19), respectively.

### 3.2. Ground thermal regime at transect sites

The MAGT at the individual sites of the transect ranged from -1.1 °C (T2) to 0.3 °C (T9), both at 10 cm and 40 cm depth (Fig. 6, Table 1). The offsets between 10 cm and 40 cm were within ± 0.1 °C in 7 profiles, and the only site that showed a stronger negative offset of -0.4 °C was T7. The total TDD<sub>10cm</sub> varied between 377 °C·days (T3) and 659 °C·days (T4), whereas TDD<sub>40cm</sub> was generally about 30% lower reaching 205 °C·days (T3) to 537 °C·days (T4). The total FDD<sub>10cm</sub> recorded the highest values at T9 with -290 °C·days (Table 1).

The beginning of the freezing season 2017 fluctuated between the sites from 19 April (T4) to 26 April (T9) (Fig. 6, Table 1). The duration of the freezing season oscillated between 206 (T4, T7) and 248 days (T1). The mean seasonal temperature ranged from -1.1 °C (T9) and -3.3 °C (T4). Consequently, the highest FDD<sub>10cm</sub> of -241 °C·days were observed at T9, while the lowest FDD<sub>10cm</sub> of -681 °C·days at T4. The freezing n-factor ranged from 0.6 at T1 and T3 up to 0.75 at T4. The only exception was T9 site with a freezing n-factor of 0.27 (Table 2).

The thawing season 2017/18 lasted between 106 (T9) and 173 (T7) days (Table 3tbl3). The onset occurred between 11 November (T4) and 25 December (T9) and the end started between 6 April (T1) and 4 May (T8). The mean ground temperature of thawing season ranged from 1.3 °C (T3) to 2.2 °C (T9), whereas TDD<sub>10cm</sub> oscillated between 183 °C·days (T3) and 321 °C·days (T4). Thawing n-factor varied between 1.50 (T3) and 2.63 (T5).

The whole season 2017/18 lasted from 351 (T1) to 379 (T7) days (Table 5). The mean seasonal ground temperature dropped below -1.0 °C at sites T2-T6, and it reached 0.0 °C at T9. The TTOP prediction suggested the occurrence of permafrost at all sites. The coldest permafrost temperatures were found in T2 (-1.47 ± 0.07 °C) whereas the highest temperature was predicted at T9 (-0.19 ± 0.07 °C; Fig. 5, Table 5). The TTOP model predicted slightly higher temperatures for

**Table 4**  
The thermal characteristics of the season 2017/18.

| Site     | Beginning  | End      | Duration | MSGT (°C) <sup>a</sup> | TTOP (°C) <sup>b</sup> | Frost number |
|----------|------------|----------|----------|------------------------|------------------------|--------------|
| T1       | 21.04.17   | 06.04.18 | 351      | -0.8                   | -1.06 ± 0.08           | 0.60         |
| T2       | 20.04.17   | 07.04.18 | 353      | -1.3                   | -1.47 ± 0.07           | 0.64         |
| T3       | 20.04.17   | 24.04.18 | 370      | -1.0                   | -1.11 ± 0.06           | 0.63         |
| T4       | 19.04.17   | 23.04.18 | 370      | -1.0                   | -1.24 ± 0.10           | 0.59         |
| T5       | 21.04.17   | 07.04.18 | 352      | -1.1                   | -1.34 ± 0.10           | 0.60         |
| T6       | 21.04.17   | 08.04.18 | 353      | -1.2                   | -1.32 ± 0.06           | 0.64         |
| T7       | 20.04.17   | 03.05.18 | 379      | -0.9                   | -1.15 ± 0.09           | 0.60         |
| T8       | 22.04.17   | 04.05.18 | 378      | -0.8                   | -0.97 ± 0.08           | 0.59         |
| T9       | 26.04.17   | 08.05.18 | 378      | 0.0                    | -0.19 ± 0.07           | 0.50         |
| AWS-Domo | 20.04.2017 | 03.05.18 | 379      | -1.1                   | -1.24 ± 0.06           | 0.64         |

<sup>a</sup> Mean seasonal ground temperature.

<sup>b</sup> Modelled temperature on the top of the permafrost.

**Table 5**  
Comparison of the mean annual air temperature in the selected sites in the Western Antarctic Peninsula region.

| Station        | 1986–2015 <sup>a</sup> | 2006–2015 <sup>a</sup> | II/2017 – I/2019 <sup>b</sup> |
|----------------|------------------------|------------------------|-------------------------------|
| Bellingshausen | -2.3                   | -2.3                   | -1.6                          |
| Rothera        | -4.1                   | -3.8                   | -3.2                          |
| Faraday        | -2.8                   | -2.5                   | -2.3                          |

<sup>a</sup> Oliva et al. (2017b)

<sup>b</sup> Database READER (2019).

the whole period 2017/19. The modelled values varied between  $-1.33 \pm 0.07$  °C (T2) and  $0.06 \pm 0.08$  °C (T9). The positive temperature at T9 is associated with a FN of 0.44, which varied between 0.56 and 0.64 at the rest of the sites of the transect (Table 1).

#### 4. Discussion

Distinguishing the extent of permafrost conditions is a challenging scientific exercise in transitional environments between continuous and discontinuous permafrost (e.g. Oesterkamp and Romanovsky, 1999; Nelson et al., 2002; Smith and Riseborough, 2002). This transition in the Northern Hemisphere can encompass large regions as the boundary between continuous and discontinuous permafrost zone is usually defined as areas delimited by MAAT isotherms between  $-8.0$  °C and  $-2.0$  °C (e.g. Smith and Riseborough, 2002; Romanovsky et al., 2010). However, in the scarce ice-free environments of Antarctica this transition mainly occurs in narrow elevation belts, and thus, the boundary between the continuous and discontinuous permafrost is difficult to detect and other approaches need to be implemented.

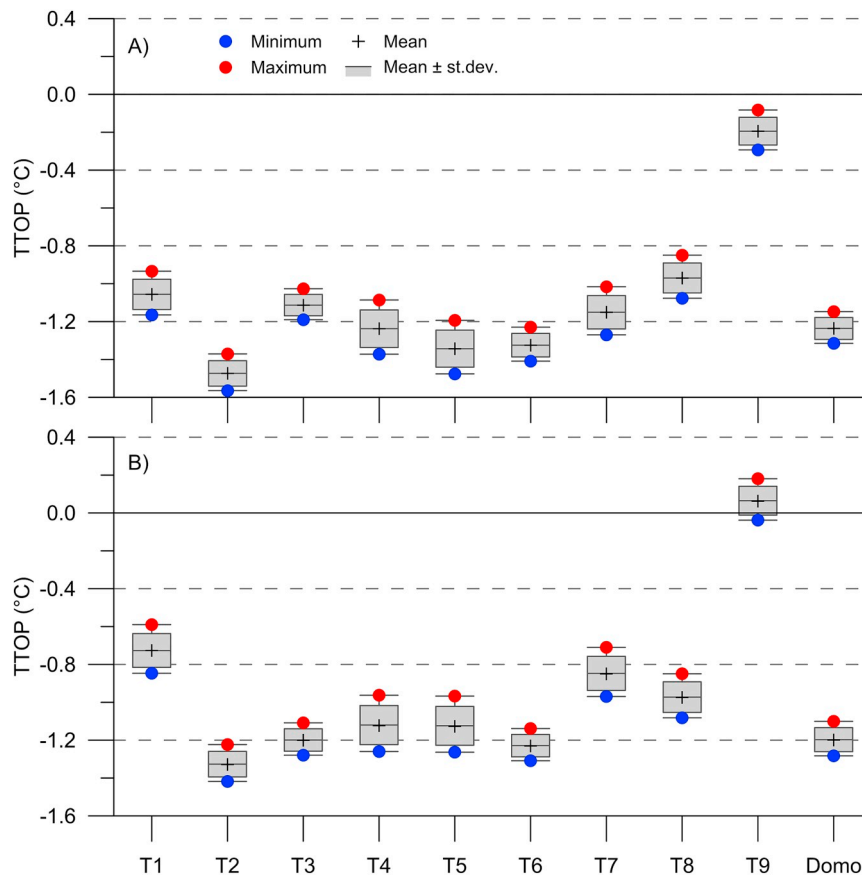


**Fig. 5.** Variability of predicted TTOP on the transect sites and AWS-Domo a) in the seasons 2017/18 b) in the period 2/2017 to 2/2019. The grey box indicates the range of standard deviation around mean value.

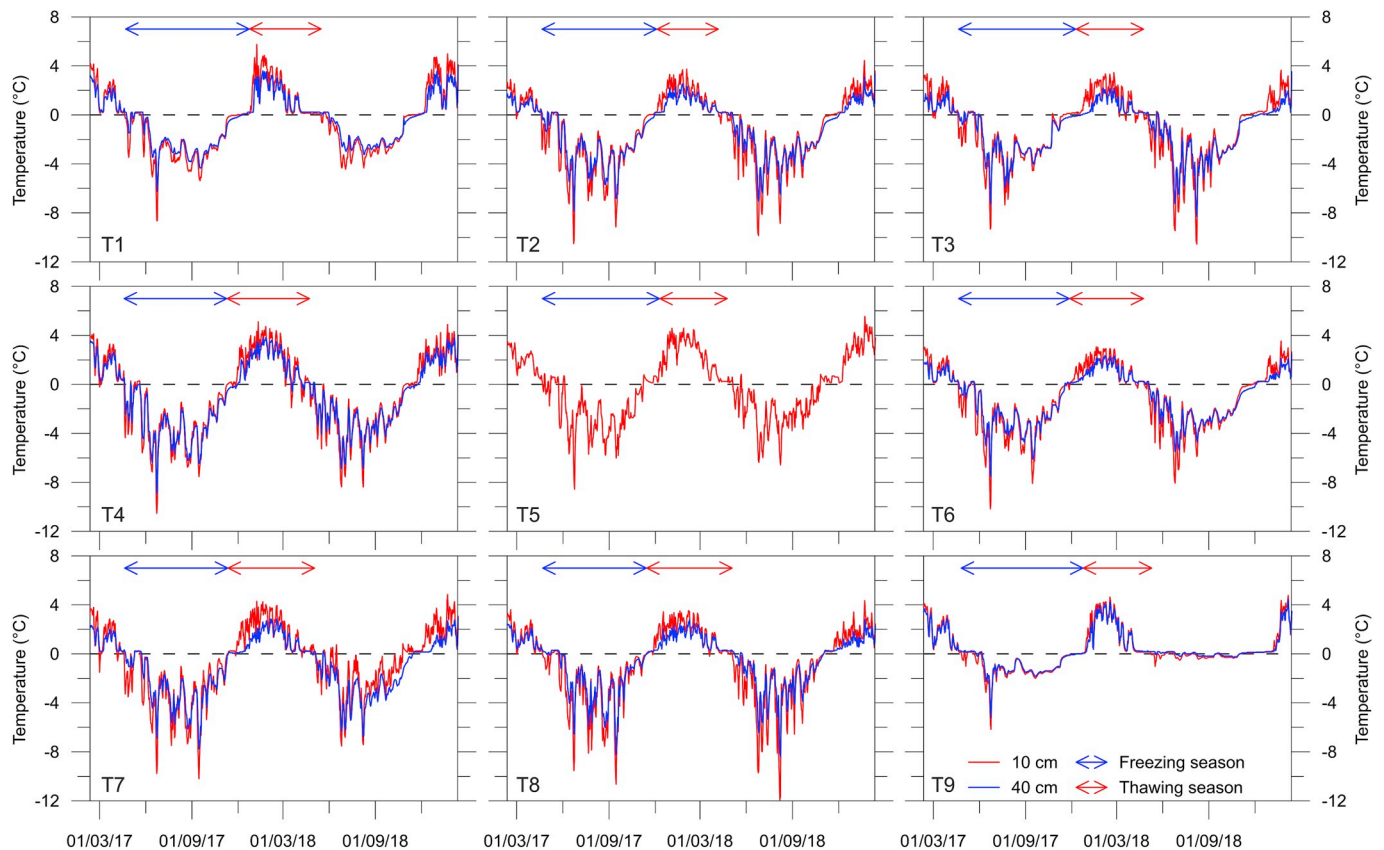


Fig. 6. Variability of mean daily ground temperature at the depths of 10 and 40 cm on the transect sites T1-T9.

#### 4.1. Permafrost thermal state and spatial distribution

With that purpose, a transect for monitoring ground thermal regime was established on the Byers Peninsula following the spatial pattern of deglaciation from the recent moraine of Rotch Dome glacier to the slopes descending to the coast. The transect crosses the AWS-Domo site (Fig. 1), which reported MAAT around  $-2.0^{\circ}\text{C}$  during the study period. Such MAAT was  $0.8^{\circ}\text{C}$  higher than 2002–2010 average for Livingston Island (Bañón et al., 2013) and also the MAAT on stations providing long-term climate data in the Western Antarctic Peninsula that showed MAAT of  $0.5^{\circ}\text{C}$ – $0.8^{\circ}\text{C}$  higher in the period 2017–2019 than the long-term average (Table 5).

The MAAT of  $-2.0^{\circ}\text{C}$  is a boundary temperature indicating a very intense cryogenic regime pointing to the boundary conditions of continuous vs discontinuous permafrost occurrence (e.g.; Washburn, 1979). Therefore, the low altitude gradient of the transect (33–82 m.a.s.l), together with the wide time span of the age of deglaciation (5–6 ka), makes it an ideal transect to examine how the deglaciation may affect the ground thermal dynamics.

The direct ground measurements and the modelled ground temperatures agree on the permafrost occurrence at 9 out of the 10 sites of the transect, with the predicted temperatures ranging between  $-0.7$  and  $-1.3^{\circ}\text{C}$  (Fig. 5). Despite the lack of data on moisture conditions and ground thermal properties, predictions of the TTOP model fit the observed values. The comparison to the measured value of the MAGT at the depth of 80 cm at the AWS-Domo site showed a very good match with a small underestimation of the TTOP model of  $0.1$ – $0.2^{\circ}\text{C}$ . Such a low span of the TTOP predictions was achieved thanks to the low absolute values of both TDD and FDD. For example, Smith and Riseborough (1996) proposed the relationship between rk and TTOP in MAAT regimes similar to Livingston Island around  $-1.5^{\circ}\text{C}$ . Due to considerably higher TDD ( $1500^{\circ}\text{C}\cdot\text{days}$ ) and FDD ( $-2000^{\circ}\text{C}\cdot\text{days}$ ), their predicted TTOP ranged from  $-4.3^{\circ}\text{C}$  for rk 0.3 to  $-2.0^{\circ}\text{C}$  for rk

0.9.

Additional information about the permafrost distribution is provided by the FN. In the Northern Hemisphere, a FN of 0.5 was defined as a border value between the sporadic and discontinuous permafrost zone and a FN of 0.57 as a boundary between the discontinuous and continuous permafrost (e.g. Nelson and Outcalt, 1987; Crichton et al., 2014). Therefore, the T9 site that reported a FN value of 0.44 would be placed within the sporadic permafrost area and T1 and T7 ranging from 0.56 to 0.64 fit within the relatively stable continuous permafrost belt.

In fact, T9 is located at 33 m.a.s.l and continuous permafrost conditions have been described in the SSI as starting at ca. 30–40 m (Vieira et al., 2010; Bockheim et al., 2013). In the case of the Byers Peninsula, the occurrence of stable permafrost conditions has already been confirmed by direct profile ground temperature measurements in areas above 50 m.a.s.l (e.g. de Pablo et al., 2017; Oliva et al., 2017a). Our data confirm the spatial pattern of continuous permafrost conditions in areas  $> 50$  m.a.s.l, showing that a MAAT of ca.  $-2.0^{\circ}\text{C}$  is sufficient to maintain permafrost with an active layer thickness around 100 cm (Fig. 3). On the other hand, isolated permafrost patches suggesting discontinuous permafrost were detected by geophysical surveying almost at sea level, developed on Late Holocene marine terraces (Correia et al., 2017). In the neighbouring ice-free areas of Livingston Island, such as on the Hurd Peninsula, permafrost was absent also at the low-elevated bedrock sites (Ferreira et al., 2017). In other areas across the AP, permafrost was not detected at bedrock sites even in areas above 50 m.a.s.l, as in the Palmer Archipelago (Bockheim et al., 2013).

#### 4.2. Controlling factors of permafrost distribution in the maritime Antarctica

Apart from MAAT, the ground thermal conditions are controlled by several other factors. In the Maritime Antarctica, the most important factors seem to be topography, snow cover, lithology or water content

(Ferreira et al., 2017; Hrbáček et al., 2019b; Oliva et al., 2017a; de Pablo et al., 2017), though others such as the geomorphological setting and the age of deglaciation may also play an important role influencing the ground thermal regime.

In the case of the SSI, most ice caps are polythermal and include both cold and warm-based surfaces (). On the Byers Peninsula, the Rotch Dome glacier near T1 constitutes a cold-based glacier as revealed by seismic and ground-penetrating radar (Navarro, *personal communication*). The decreasing thickness of the dome-shaped glacier in its margins facilitates the penetration of the cold flow down to the surface freezing the basement of the glacier. Immediately after the glacier retreat, the proglacial environment of cold-based glaciers includes the presence of permafrost as it already pre-existed in this area before the deglaciation. By contrast, in the forelands of warm-based glaciers, permafrost may have aggraded (or simply not formed) following the deglaciation or even due to the gradual thinning of the ice in this dome-shaped glacier (Oliva and Ruiz-Fernández, 2015). Consequently, the absence or existence of permafrost after the deglaciation must be determined by the basal temperature of the retreating glacier (Harris and Murton, 2005).

Our transect follows the deglaciation pattern occurred on the Byers Peninsula since the Mid-Late Holocene. Whereas the closest station (T1) is located on the moraine that is known to have developed over the last few centuries, the AWS-Domo site must have become ice-free before 1.8 ka cal BP and the westernmost sites were deglaciated between 5 and 6 ka cal BP (Oliva et al., 2016a,b). The ground thermal regime detected between the sites T2-T9 and AWS-Domo suggests that the age of ice-free exposure plays no role in the active layer temperatures centuries after the glacial retreat. The more important factors like snow cover or local topography cause the inter-site variability and differences in ground temperature.

In this context of relatively stable glacial fronts as revealed by the chronology of glacial retreat (Oliva et al., 2017a), the future variations of snow cover in a changing climate may have a prominent role in altering the permafrost and active layer stability. Microtopographic conditions determine the substantial differences in the accumulation and duration of snow cover along the transect, which can explain inter-site differences in the active layer dynamics. Although the T1 site is located on an ice-cored moraine built by the Rotch Dome glacier (John and Sudgen, 1971), it is not the coldest site in terms of average temperatures. The presence of the frozen mass beneath the moraine keeps the ground temperature more stable and closer to 0 °C at the end of freezing seasons, which favours a more persistent snow cover and relatively higher mean temperatures (Fig. 6).

A clear example of the snow-affected warming of the permafrost was observed at T9. Here, a very low value of the freezing n-factor (0.27) suggests the snow thickness exceeded 80 cm. Such thicknesses related to similar n-factor (< 0.30) occurred in previous seasons recording similar freezing n-factors in several sites of the Byers Peninsula (de Pablo et al., 2017; Oliva et al., 2017a). Such snow thickness favoured higher ground temperatures between 1.1 and 2.2 °C at T9 than at the other sites of the transect during the freezing season 2017. The snow cover insulating effect at the other sites including AWS-Domo was rather negligible, even though a thin snow cover of 5–10 cm persisted for almost the whole winter (Fig. 2). Except for T2, the sites with freezing n-factor > 0.7 (T4, T5) are located on the north-faced > 10° steep slope. Due to such topographical conditions, these sites should receive a higher amount of incoming solar radiation in the summer season, which explains the > 20% higher amount of TDD. At the same time, the lowest TDDs were observed in the south-exposed sites (T3, T6).

In summary, despite the above-average MAAT during the study period (Table 5), the ground thermal regime data confirmed the presence of continuous permafrost conditions on the Byers Peninsula in areas above, at least, 50 m.a.s.l. Data suggests that permafrost stability in a future warmer Antarctica can be threatened by the combination of

higher temperatures and the increase of the total precipitation by the end of 21st century (Palermo et al., 2017). A long-lasting thick snow cover persisting during the winter can favour the warming of the ground, which can accelerate the permafrost thawing. Concurrently, the higher annual rates of liquid precipitation can also lead to progressive ground warming as predicted in the Arctic (Bintanja, 2018).

## 5. Conclusions

The occurrence of permafrost has major implications for edaphic, geomorphological and hydrological processes prevailing in polar terrestrial ecosystems. Under the present-day warming climate, higher temperatures are impacting the ground thermal regime, thus affecting ecosystem dynamics. Some of the major changes may occur in the transitional areas between continuous and discontinuous permafrost conditions, such as coastal fringes of the northern AP region where MAATs are ca. –2 °C at sea level. Here, the distribution of permafrost is still poorly known and the factors controlling its spatial occurrence are still under debate.

In the ice-free area of the Byers Peninsula, we conducted an experiment to infer the potential role of the timing of deglaciation on ground thermal regime. We established 10 shallow boreholes within a 2.8-km long transect from the Rotch Dome ice-cored moraine to the lowest slopes of the central plateau to monitor the active layer thermal regime. This almost flat transect follows the deglaciation pattern following the retreat of Rotch Dome glacier towards the east of this peninsula, from the Mid-Holocene glacial retreat at the western sites to the stations situated near the present-day glacier front that became exposed only a few centuries ago.

Climate conditions report a MAAT of around –2.0 °C, which is sufficient to maintain continuous permafrost along the transect with ground temperatures of the topmost part of the permafrost ranging between –0.7 °C and –1.3 °C on 9 of 10 monitoring sites. Soil moisture variability and consequently changes of the rk factor do not have a great impact on the variability of TTOP predictions. In fact, there are not great variations of the temperature of the active layer along the transect, with the highest values located at the site deglaciated more recently several centuries ago. Here, the existence of an ice-cored moraine determines a longer snow cover duration that isolates the ground and favours higher temperatures near the surface.

This geomorphic control seems to be a matter of time, as at the rest of the sites where buried glacial ice already melted away, there is a more similar ground thermal regime. The most important factor affecting permafrost temperatures is the duration and thickness of snow cover, which is highly controlled by the topography (including aspect and slope). Long-lasting snow cover during the winter exceeding 80 cm can form such a strong insulating layer that can lead to ground temperatures close to 0 °C. Differences are slightly higher in the summer, being warmer in the north-exposed sites and colder in the south-exposed slopes. However, the role of the topography is not strong enough to affect the presence or absence of permafrost.

## Acknowledgements

The work of FH and MK was supported by the Ministry of Education Youth and Sports of Czech Republic large infrastructure projects LM2015078 and CZ.02.1.01/0.0/0.0/16\_013/0001708 and by the Masaryk University project MUNI/A/1576/2018. MO is supported by the Ramón y Cajal Program (RYC-2015-17597) and the Research Group ANTALP (Antarctic, Arctic, Alpine Environments; 2017-SGR-1102) funded by the Government of Catalonia through the AGAUR agency. The work complements the research topics examined in the NUNANTAR project (02/SAICT/2017–32002) of the Fundação para a Ciência e a Tecnologia and CRONOBYSERS Project of the Portuguese Polar Program (PROPOLAR), Fundação para a Ciência e a Tecnologia. The work of JRF was supported by Cronoantar project CTM 2016-77878-P. Work of

MAAdP was partially supported by CTM 2014-52021R (PERMASNOW) research project from Spanish Research Agency, Government of Spain. Finally, we are grateful to two anonymous referees and the managing editor Dr. Paulo Pereira for their beneficial comments, which significantly improved the final version of manuscript.

## Appendix A. Supplementary data

Supplementary data to this article can be found online at <https://doi.org/10.1016/j.envres.2019.108901>.

## References

- Antoniades, D., Giral, S., Geyer, Álvarez-Valero, A.M., Pla-Rabes, S., Granados, I., Liu, E.J., Toro, M., Smellie, J., Oliva, M., 2018. The timing and widespread effects of the largest Holocene volcanic eruption in Antarctica. *Nat. Sci. Rep.* 8, 17279.
- Bañón, M., Justel, A., Velázquez, D., Quesada, A., 2013. Regional weather survey on Byers peninsula, Livingston island, South Shetland islands, Antarctica. *Antarct. Sci.* 25, 146–156.
- Bintanja, R., 2018. The impact of Arctic warming on increased rainfall. *Sci. Rep.* 8, 16001.
- Biskaborn, B.K., Smith, S.L., Noetzi, J., Matthes, H., Vieira, G., Streletskiy, D.A., Schoeneich, P., Romanovsky, V.E., Lewkowicz, A.G., Abramov, A., Allard, M., Boike, J., Cable, W.L., Christiansen, H.H., Delaloye, R., Diekmann, B., Drozdov, D., Eitzelmüller, B., Grosse, G., Guglielmin, M., Ingeman-Nielsen, T., Isaksen, K., Ishikawa, M., Johansson, M., Johannsson, H., Joo, A., Kaverin, D., Kholodov, A., Konstantinov, P., Kröger, T., Lambiel, C., Lanckman, J.P., Luo, D., Malkova, G., Meiklejohn, I., Moskalenko, N., Oliva, M., Phillips, M., Ramos, M., Sannel, A.B.K., Sergeev, D., Seybold, C., Skryabin, P., Vasiliev, A., Wu, Q., Yoshikawa, K., Zheleznyak, M., Lantuit, H., 2019. Permafrost is warming at a global scale. *Nat. Commun.* 10, 1–11. <https://doi.org/10.1038/s41467-018-08240-4>.
- Bockheim, J., Vieira, G., Ramos, M., López-Martínez, J., Serrano, E., Guglielmin, M., Wilhelm, K., Nieuwendam, A., 2013. Climate warming and permafrost dynamics in the Antarctic Peninsula region. *Glob. Planet. Chang.* 100, 215–223. <https://doi.org/10.1016/j.gloplacha.2012.10.018>.
- Cannone, N., Ellis Evans, J.C., Strachan, R., Guglielmin, M., 2006. Interactions between climate, vegetation and the active layer in soils at two Maritime Antarctic sites. *Antarct. Sci.* 18, 323–333. <https://doi.org/10.1017/S095410200600037X>.
- Convey, P., Bindschadler, R., di Prisco, G., Fahrbach, E., Gutt, J., Hodgson, D.A., Mayewski, P.A., Summerhayes, C.P., Turner, J., 2009. Antarctic climate change and the environment. *Antarct. Sci.* 21, 541. <https://doi.org/10.1017/S0954102009990642>.
- Correia, A., Oliva, M., Ruiz-Fernández, J., 2017. Evaluation of frozen ground conditions along a coastal topographic gradient at Byers Peninsula (Livingston Island, Antarctica) by geophysical and geoecological methods. *Catena* 149, 529–537. <https://doi.org/10.1016/j.catena.2016.08.006>.
- Crichton, K.A., Roche, D.M., Krinner, G., Chappellaz, J., 2014. A simplified permafrost-carbon model for long-term climate studies with the CLIMBER-2 coupled earth system model. *Geosci. Model Dev. (GMD)* 7, 3111–3134.
- De Pablo, M.A., Blanco, J.J., Molina, A., Ramos, M., Quesada, A., Vieira, G., 2013. Interannual active layer variability at the limnopolar lake CALM site on Byers peninsula, Livingston island, Antarctica. *Antarct. Sci.* 25, 167–180. <https://doi.org/10.1017/S0954102012000818>.
- de Pablo, M.A., Ramos, M., Molina, A., 2017. Snow cover evolution, on 2009–2014, at the limnopolar lake CALM-S site on Byers peninsula, Livingston island, Antarctica. *Catena* 149, 538–547. <https://doi.org/10.1016/j.catena.2016.06.002>.
- Engel, Z., Láška, K., Nývlt, D., Stachoň, Z., 2018. Surface mass balance of small glaciers on James Ross island, north-eastern antarctic peninsula, during 2009–2015. *J. Glaciol.* 64, 349–361. <https://doi.org/10.1017/jog.2018.17>.
- Ferreira, A., Vieira, G., Ramos, M., Nieuwendam, A., 2017. Ground temperature and permafrost distribution in Hurd Peninsula (Livingston Island, Maritime Antarctic): an assessment using freezing indexes and TTOP modelling. *Catena* 149, 560–571. <https://doi.org/10.1016/j.catena.2016.08.027>.
- Goyanes, G., Vieira, G., Caselli, A., Mora, C., Ramos, M., de Pablo, M.A., Neves, M., Santos, F., Bernardo, I., Gilichinsky, D., Abramov, A., Batista, V., Melo, R., Trindade Nieuwendam, A., Ferreira, A., Oliva, M., 2014. Regimen termico y variabilidad espacial de la capa activa en isla Decepcion, Antártida. *Rev. Asoc. Geol. Argent.* 71, 112–124.
- Guglielmin, M., 2006. Ground surface temperature (GST), active layer, and permafrost monitoring in continental Antarctica. *Permafrost. Periglac. Process.* 17, 133–143.
- Guglielmin, M., Ellis Evans, C.J., Cannone, N., 2008. Active layer thermal regime under different vegetation conditions in permafrost areas. A case study at Signy Island (Maritime Antarctica). *Geoderma* 144, 73–85. <https://doi.org/10.1016/j.geoderma.2007.10.010>.
- Harris, C., Murton, J.B., 2005. Interactions between glaciers and permafrost: an introduction. In: Harris, C., Murton, J.B. (Eds.), *Cryospheric Systems: Glaciers and Permafrost*. The Geological Society, London, pp. 1–9. Special Publications of the Geological Society of London 242.
- Hathway, B., Lomas, S.A., 1998. The upper jurassic-lower cretaceous Byers Group, South Shetland islands, Antarctica: revised stratigraphy and regional correlations. *Cretac. Res.* 19, 43–67.
- Hauk, C., Vieira, G., Gruber, S., Blanco, J., Ramos, M., 2007. Geophysical identification of permafrost in Livingston island, maritime Antarctica. *J. Geophys. Res. Earth Surf.* 112, 1–15. <https://doi.org/10.1029/2006JF000544>.
- Hrbáček, F., Uxa, T., 2019. The Evolution of a Near-Surface Ground Thermal Regime and Modelled Active-Layer Thickness on James Ross Island, Eastern Antarctic Peninsula, in 2006–2016. *Permafrost and Periglacial Processes*.
- Hrbáček, F., Kňázková, M., Nývlt, D., Láška, K., Mueller, C.W., Ondruch, J., 2017. Active layer monitoring at CALM-S site near J.G.mendel station, James Ross island, eastern antarctic peninsula. *Sci. Tot. Environ.* 601–602, 987–997. <https://doi.org/10.1016/j.scitotenv.2017.05.266>.
- Hrbáček, F., Vieira, G., Oliva, M., Balks, M., Guglielmin, M., de Pablo, M.A., Molina, A., Ramos, M., Goyanes, G., Meiklejohn, I., Abramov, A., Demidov, N., Fedorov-Davydov, D., Lupachev, A., Rivkina, E., Láška, K., Kňázková, M., Nývlt, D., Raffi, R., Strelin, J., Sone, T., Fukui, K., Dolgikh, A., Zazovskaya, E., Mergelov, N., Osokin, N., Miamin, V., 2019a. Active Layer Monitoring in Antarctica: an Overview of Results from 2006 to 2015. *Polar Geography* <https://doi.org/10.1080/1088937X.2017.1420105>. (in press).
- Hrbáček, F., Nývlt, D., Láška, K., Kňázková, M., Kampová, B., Engel, Z., Oliva, M., Mueller, C.W., 2019b. Permafrost and active layer research on James Ross Island: an overview. *Czech Polar Reports* 9 (1), 20–36.
- John, B.S., Sugden, D.E., 1971. Raised marine features and phases of glaciation in the South Shetland Islands. *Br. Antarct. Surv. Bull.* 24, 45–111.
- Kunz, M., King, M.A., Mills, J.P., Miller, P.E., Fox, A.J., Vaughan, D.G., Marsh, S.H., 2012. Multi-decadal glacier surface lowering in the Antarctic Peninsula. *Geophys. Res. Lett.* 39, 1–5. <https://doi.org/10.1029/2012GL052823>.
- Lewkowicz, A., 2008. Evaluation of miniature temperature-loggers to monitor snowpack evolution at mountain permafrost sites, Northwestern Canada. *Permafrost and Periglacial Processes* 19 (3), 323–331.
- Liu, E.J., Oliva, M., Antoniades, D., Giral, S., Granados, I., Pla-Rabes, S., Toro, M., Geyer, A., 2016. Expanding the tephrostratigraphical framework for the South Shetland Islands, Antarctica, by combining compositional and textural tephra characterisation. *Sediment. Geol.* 340, 49–61.
- López-Martínez, J., Martínez de Pisón, E., Serrano, E., Arche, A., 1996. Geomorphological Map of Byers Peninsula, Livingston Island. BAS Geomap Series. Sheet 5-A, 1:25,000. British Antarctic Survey, Cambridge, UK.
- López-Martínez, J., Serrano, E., Schmid, T., Mink, S., Linés, C., 2012. Periglacial processes and landforms in the south Shetland islands (northern antarctic peninsula region). *Geomorphology* 155, 62–79.
- Mink, S., López-Martínez, J., Maestro, A., Garrote, J., Ortega, J.A., Serrano, E., Durán, J.J., Schmid, T., 2014. Insights into deglaciation of the largest ice-free area in the South Shetland Islands (Antarctica) from quantitative analysis of the drainage system. *Geomorphology* 225, 4–24.
- Navarro, F.J., Jonsell, U.Y., Corcuera, M.I., Martín-Español, A., 2013. Decelerated mass loss of Hurd and Johnsons glaciers, Livingston island, antarctic peninsula. *J. Glaciol.* 59 (213), 115–128. <https://doi.org/10.3189/2013JoG12J144>.
- Nelson, F.E., Outcalt, S.I., 1987. A computational method for prediction and regionalization of permafrost. *Arct. Alp. Res.* 19 (3), 279–288.
- Nelson, F.E., Anisimov, O.A., Shiklomanov, N., 2002. Climate change and hazard zonation in the circum-arctic permafrost regions. *Nat. Hazards* 26 (3), 203–225.
- Nielsen, U.N., Wall, D.H., Li, G., Toro, M., Adams, B.J., Ross, V.A., 2010. Nematode communities of Byers peninsula, Livingston island, maritime Antarctica. *Antarct. Sci.* 23 (4), 348–357.
- Oesterkamp, T.E., Romanovsky, V.E., 1999. Evidence for warming and thawing discontinuous permafrost in Alaska. *Permafrost. Periglac. Process.* 10, 17–37.
- Oliva, M., Ruiz-Fernández, J., 2015. Coupling patterns between para-glacial and permafrost degradation responses in Antarctica. *Earth Surf. Process. Landf.* 40, 1227–1238. <https://doi.org/10.1002/esp.3716>.
- Oliva, M., Ruiz-Fernández, J., 2017. Geomorphological processes and frozen ground conditions in elephant point (Livingston island, South Shetland islands, Antarctica). *Geomorphology* 293, 368–379. <https://doi.org/10.1016/j.geomorph.2016.01.020>.
- Oliva, M., Antoniades, D., Giral, S., Granados, I., Pla-Rabes, S., Toro, M., Liu, E.J., Sanjurjo, J., Vieira, G., 2016a. The Holocene deglaciation of the Byers Peninsula (Livingston Island, Antarctica) based on the dating of lake sedimentary records. *Geomorphology* 261, 89–102. <https://doi.org/10.1016/j.geomorph.2016.02.029>.
- Oliva, M., Antoniades, D., Giral, S., Granados, I., Pla-Rabes, S., Toro, M., Sanjurjo, J., 2016b. La deglaciación de las áreas libres de hielo de las islas Shetland del Sur (Antártida): ejemplos de Byers (Livingston) y Barton (King George). *Cuaternario Geomorfol.* 30, 105–118. <https://doi.org/10.17735/cyg.v30i1-2.48665>.
- Oliva, M., Frit, M., 2018. Permafrost degradation on a warmer earth: Challenges and perspectives. *Current Opinion in Environ. Sci. Health* 5, 14–18.
- Oliva, M., Hrbáček, F., Ruiz-Fernández, J., de Pablo, M.A., Vieira, G., Ramos, M., Antoniades, D., 2017a. Active layer dynamics in three topographically distinct lake catchments in Byers Peninsula (Livingston Island, Antarctica). *Catena* 149, 548–559. <https://doi.org/10.1016/j.catena.2016.07.011>.
- Oliva, M., Navarro, F., Hrbáček, F., Hernández, A., Nývlt, D., Pereira, P., Ruiz-Fernández, J., Trigo, R., 2017b. Recent regional climate cooling on the Antarctic Peninsula and associated impacts on the cryosphere. *Sci. Total Environ.* 580, 210–223. <https://doi.org/10.1016/j.scitotenv.2016.12.030>.
- Oliva, M., Mercier, D., Ruiz-Fernández, J., McColl, S., 2019. Paraglacial processes in recently deglaciated environments. *Land Degrad. Dev.* <https://doi.org/10.1002/ldr.3283>.
- Palmer, C., Genthon, C., Claud, C., Kay, J.E., Wood, N.B., L'Ecuyer, T., 2017. Evaluation of current and projected Antarctic precipitation in CMIP5 models. *Clim. Dyn.* 48 (1–2), 225–239.
- Parica, C.A., Salani, F.M., Vera, E., Remesal, M., Césari, S.N., 2007. Geología de la formación Cerro Negro (Cretácico) en la isla Livingston: aportes a su geocronología y contenido paleontológico. *Rev. Asoc. Geol. Argent.* 62, 553–567.
- Potapowicz, J., Szuminska, D., Szopinska, M., Polkowska, Z., 2019. The influence of

- global climate change on the environmental fate of anthropogenic pollution released from the permafrost: Part I. Case study of Antarctica. *Sci. Total Environ.* 651 (1), 1534–1548.
- Ramos, M., Vieira, G., Gruber, S., Blanco, J.J., Hauck, C., Hidalgo, M.A., Tomé, D., Neves, M., Trindade, A., 2007. Permafrost and Active Layer Monitoring in the Maritime Antarctic: Preliminary Results from CALM Sites on Livingston and Deception Islands. *U.S. Geol. Surv. Natl. Acad. USGS OF-2007-1047, Short Research Papers*, 070 1–5. <https://doi.org/10.3133/of2007-1047.srp070>.
- READER, 2019. REference Antarctic Data for Environmental Research Project. Scientific Committee on Antarctic Research Available online (1. 9. 2019) at. <https://legacy.bas.ac.uk/met/READER/surface/stationpt.html>.
- Riseborough, D., Shiklomanov, N., Etzelmüller, B., Gruber, S., Marchenko, S., 2008. Recent advances in permafrost modelling. *Permafrost Periglac. Process* 19, 137–156.
- Riseborough, D., Smith, S., 1998. Exploring the limits of permafrost. In: *Seventh International Conference on Permafrost (Proceedings), Yellowknife (Canada). Collection Nordicana* 55. pp. 935–941.
- Romanovsky, V., Smith, S.L., Christiansen, H., 2010. Permafrost thermal state in the polar northern Hemisphere during the international polar year 2007–2009: a synthesis. *Permafrost Periglac. Process.* 21 (2), 106–116.
- Ruiz-Fernández, J., Oliva, M., 2016. Relative paleoenvironmental adjustments following deglaciation of the Byers peninsula (Livingston island, Antarctica). *Arctic Antarctic Alpine Res.* 48 (2), 345–359.
- Ruiz-Fernández, J., Oliva, M., Nývlt, D., Cannone, N., García-Hernández, C., Guglielmin, M., Hrbáček, F., Roman, M., Fernández, S., López-Martínez, J., Antoniades, D., 2019. Patterns of spatio-temporal paraglacial response in the Antarctic Peninsula region and associated ecological implications. *Earth Sci. Rev.* 192, 379–402. <https://doi.org/10.1016/j.earscirev.2019.03.014>.
- Serrano, E., 2003. Boletín de la AGE In: *Paisaje y pisos geocológicos en las áreas libres de hielo de la Antártida Marítima (Islas Shetland del Sur)*, vol. 35. pp. 5–32.
- Smith, M.W., Riseborough, D., 1996. Permafrost monitoring and detection of climate change. *Permafrost Periglac. Process.* 7, 301–309.
- Smith, M.W., Riseborough, D., 2002. Climate and limits of permafrost: a zonal analysis. *Permafrost Periglac. Process.* 13 (1), 1–15.
- Toro, M., Granados, I., Pla, S., Giral, S., Antoniades, D., Galán, L., Martínez-Cortizas, A., Lim, H.S., Appleby, P.G., 2013. «Chronostratigraphy of the sedimentary record of limnopolake, Byers peninsula, Livingston island, Antarctica». *Antarct. Sci.* 25, 198–212.
- Turner, J., Colwell, S.R., Marshall, G.J., Lachlan-Cope, T.A., Carleton, A.M., Jones, P.D., Lagun, V., Reid, P.A., Iagovkina, S., 2005. Antarctic climate change during the last 50 years. *Int. J. Climatol.* 25, 279–294. <https://doi.org/10.1002/joc.1130>.
- Turner, J., Lu, H., White, I., King, J.C., Phillips, T., Hosking, J.S., Bracegirdle, T.J., Marshall, G.J., Mulvaney, R., Deb, P., 2016. Absence of 21st century warming on Antarctic Peninsula consistent with natural variability. *Nature* 535, 411–415. <https://doi.org/10.1038/nature18645>.
- Vieira, G., Bockheim, J., Guglielmin, M., Balks, M., Abramov, A.A., Boelhouwers, J., Cannone, N., Ganzert, L., Gilichinsky, D.A., Goryachkin, S., López-Martínez, J., Meiklejohn, I., Raffi, R., Ramos, M., Schaefer, C., Serrano, E., Simas, F., Sletten, R., Wagner, D., 2010. Thermal state of permafrost and active-layer monitoring in the antarctic: advances during the international polar year 2007–2009. *Permafrost Periglac. Process.* 21, 182–197. <https://doi.org/10.1002/ppp.685>.
- Washburn, A.L., 1979. *Geocryology. A Survey of Periglacial Processes and Environments*. Edward Arnold, London.



# Pan-Antarctic map of near-surface permafrost temperatures at 1 km<sup>2</sup> scale

Jaroslav Obu<sup>1</sup>, Sebastian Westermann<sup>1</sup>, Gonçalo Vieira<sup>2</sup>, Andrey Abramov<sup>3</sup>, Megan Ruby Balks<sup>4</sup>, Annett Bartsch<sup>5,a</sup>, Filip Hrbáček<sup>6</sup>, Andreas Kääh<sup>1</sup>, and Miguel Ramos<sup>7</sup>

<sup>1</sup>Department of Geosciences, University of Oslo, Oslo, Sem Sælands vei 1, 0371 Oslo, Norway

<sup>2</sup>Centre for Geographical Studies, Institute of Geography and Spatial Planning, University of Lisbon, R. Branca Edmée Marques, 1600-276 Lisbon, Portugal

<sup>3</sup>Institute of Physicochemical and Biological Problems in Soil Science, Russian Academy of Sciences, Pushchino, Russia

<sup>4</sup>Department of Earth and Ocean Sciences, University of Waikato, Private Bag 3105, Hamilton, New Zealand

<sup>5</sup>Zentralanstalt für Meteorologie und Geodynamik, Hohe Warte 39, Vienna, Austria

<sup>6</sup>Department of Geography, Masaryk University, Kotlářská 2, 61137 Brno, Czech Republic

<sup>7</sup>Department of Physics and Mathematics, University of Alcalá, Campus universitario, 28805 Alcalá de Henares, Madrid, Spain

<sup>a</sup>now at: b.geos GmbH, Vienna, Industriestraße 1 2100, Korneuburg, Austria

**Correspondence:** Jaroslav Obu (jaroslav.obu@geo.uio.no)

Received: 18 June 2019 – Discussion started: 25 June 2019

Revised: 2 December 2019 – Accepted: 12 December 2019 – Published: 7 February 2020

**Abstract.** Permafrost is present within almost all of the Antarctic's ice-free areas, but little is known about spatial variations in permafrost temperatures except for a few areas with established ground temperature measurements. We modelled a temperature at the top of the permafrost (T<sub>TOP</sub>) for all the ice-free areas of the Antarctic mainland and Antarctic islands at 1 km<sup>2</sup> resolution during 2000–2017. The model was driven by remotely sensed land surface temperatures and downscaled ERA-Interim climate reanalysis data, and subgrid permafrost variability was simulated by variable snow cover. The results were validated against in situ-measured ground temperatures from 40 permafrost boreholes, and the resulting root-mean-square error was 1.9 °C. The lowest near-surface permafrost temperature of −36 °C was modelled at Mount Markham in the Queen Elizabeth Range in the Transantarctic Mountains. This is the lowest permafrost temperature on Earth, according to global-scale modelling results. The temperatures were most commonly modelled between −23 and −18 °C for mountainous areas rising above the Antarctic Ice Sheet and between −14 and −8 °C for coastal areas. The model performance was good where snow conditions were modelled realistically, but er-

rors of up to 4 °C occurred at sites with strong wind-driven redistribution of snow.

## 1 Introduction

Permafrost in the Antarctic is present beneath all ice-free terrain, except for the lowest elevations of the maritime Antarctic and sub-Antarctic islands (Vieira et al., 2010). Ice- and snow-free land occupies 0.22 % (30 900 km<sup>2</sup>) of Antarctica (Burton-Johnson et al., 2016; Hrbáček et al., 2018). Major ice-free areas include Queen Maud Land, Enderby Land, the Vestfold Hills, Wilkes Land, the Transantarctic Mountains, the Ellsworth Mountains, Marie Byrd Land and the Antarctic Peninsula (Greene et al., 1967; Fig. 1). Despite the relatively small area, in comparison to glaciated areas, permafrost is one of the major factors controlling terrestrial ecosystem dynamics in the Antarctic (Bockheim et al., 2008).

Compared with the Northern Hemisphere, where the first permafrost investigations date back to the 19th century (Shiklomanov, 2005; Humlum et al., 2003), the ground temperatures in the Antarctic have been systematically stud-

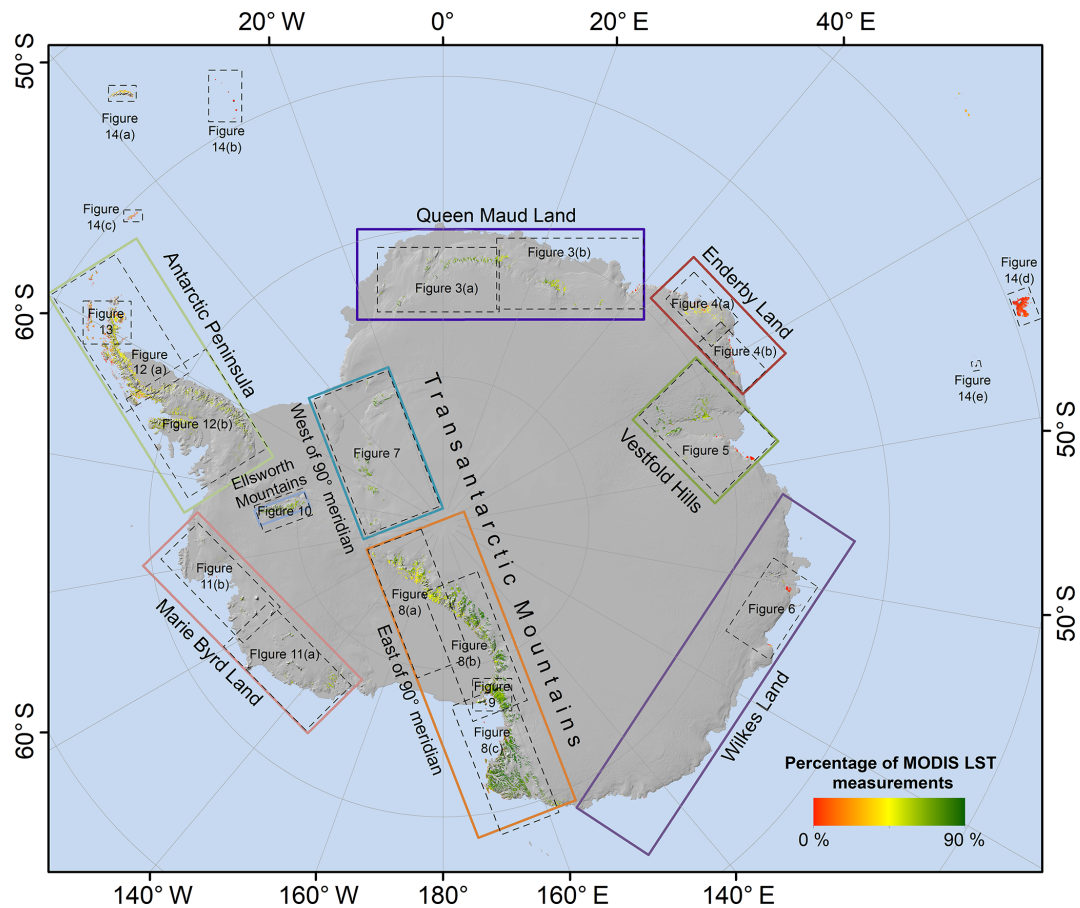


**Figure 1.** Overview map of the ice-free Antarctic regions and extents of the maps presented in the paper. The ice-free areas are shown according to percentage of MODIS LST measurements in the combined MODIS ERA surface temperature product. Background topography, on this and all following maps, is from the Quantarctica 3 database (Roth et al., 2017).

ied only during the last 2 decades. Permafrost was studied in relation to patterned ground since the 1960s and during the Dry Valley Drilling Project in the 1970s, but temperatures have been measured only occasionally (Decker and Bucher, 1977; Guglielmin, 2012). The first Antarctic permafrost borehole network was implemented in 1999 in Victoria Land (Transantarctic Mountains) and was extended during the International Polar Year 2007–2009 to cover all eight major ice-free regions (Vieira et al., 2010).

Permafrost distribution was estimated and mapped on the Antarctic Peninsula by Bockheim et al. (2013) based on mean annual temperature, periglacial features, shallow excavations, borehole measurements, geophysical surveys and existing permafrost models. Bockheim et al. (2007) characterised permafrost in the McMurdo Dry Valleys based on ground ice properties and active-layer thickness from more than 800 shallow excavations.

Antarctic permafrost modelling efforts were limited to small areas in the Antarctic Peninsula region and sub-Antarctic islands. Ferreira et al. (2017) modelled freezing indices and the temperature at the top of the permafrost

(TTOP) for eight monitored sites on the Hurd Peninsula and Livingston Island for the 2007 and 2009 seasons to study the controlling factors of ground temperatures. Rocha et al. (2010) ran the H-TESSEL scheme forced by ERA-Interim reanalysis to simulate ground temperatures at Reina Sofía Peak on Livingston Island. Ground temperature measurements and permafrost modelling efforts have been limited to point sites, and little is known about spatial variability in ground temperatures at the regional and continent-wide scales.

In this study we employed the TTOP modelling scheme based on the Moderate Resolution Imaging Spectroradiometer (MODIS) land surface temperature (LST) and ERA-Interim reanalysis to model the spatial distribution of temperatures at the top of permafrost on all ice-free areas of Antarctica and the Antarctic islands. We adapted the existing modelling scheme from the Northern Hemisphere (Westermann et al., 2015; Obu et al., 2019a) according to the available input data and their characteristics for the Antarctic.

## 2 Methods

### 2.1 The CryoGrid 1 model

The CryoGrid 1 model (Gisnås et al., 2013) calculates the mean annual ground temperature (MAGT) and is based on the TTOP equilibrium approach (Smith and Riseborough, 1996):

$$\text{MAGT} = \begin{cases} \frac{1}{\tau} (n_f \text{FDDs} + r_k n_t \text{TDDs}) & \text{for } (n_f \text{FDDs} + r_k n_t \text{TDDs}) \leq 0, \\ \frac{1}{\tau} \left( \frac{1}{r_k} n_f \text{FDDs} + n_t \text{TDDs} \right) & \text{for } (n_f \text{FDDs} + r_k n_t \text{TDDs}) > 0, \end{cases} \quad (1)$$

where FDDs represents freezing degree days, and TDDs represents thawing degree days in the surface meteorological forcing accumulated over the model period  $\tau$  (in days). The influence of seasonal snow cover, vegetation and ground thermal properties was taken into account by the semi-empirical adjustment factors  $r_k$  (ratio of thermal conductivity of the active layer in thawed and frozen state),  $n_f$  (scaling factor between average winter surface and ground surface temperature) and  $n_t$  (scaling factor between average summer surface and ground surface temperature). We use land surface temperature (LST) to compute FDDs and TDDs (see following section) instead of the air temperature that was used initially by Smith and Riseborough (2002) and hence omit the thawing  $n_t$  factors.

### 2.2 Freezing and thawing degree days

Spatially distributed datasets of TDDs and FDDs were compiled from remotely sensed land surface temperature products and climate reanalysis data following the procedure of Obu et al. (2019a). We used LST data (level 3 product in processing version 6) from MODIS aboard the Terra and Aqua satellites, which contain up to two daytime and two nighttime measurements per day at a spatial resolution of 1 km starting in the year 2000 (Wan, 2014). For this reason, the study extends from 2000 to the end of 2017. Data gaps in the MODIS LST time series due to cloud cover can result in a systematic cold bias in seasonal averages (Westerman et al., 2012; Soliman et al., 2012; Østby et al., 2014), so a gap filling with near-surface air temperatures from the ERA-Interim and ERA-5 reanalysis was applied (Westermann et al., 2015).

The ERA-Interim reanalysis provides gap-free meteorological data from 1979 onwards at a spatial resolution of  $0.75^\circ \times 0.75^\circ$  (Dee et al., 2011). The ERA-5 reanalysis is an ERA-Interim upgrade and provides the data at improved  $0.28125^\circ \times 0.28125^\circ$  (31 km) spatial resolution but was, at the time of the study, available only from 2008 onwards (Hersbach and Dee, 2016). ERA-Interim data were, for this reason, used before 2008, and ERA-5 data were used afterwards. The reanalysis data were downscaled to the 1 km resolution of individual MODIS pixels using atmospheric lapse rates and the Global Multi-resolution Terrain Elevation

Data 2010 (GMTED2010; Danielson and Gesch, 2011). The downscaling methodology was described in detail by Fiddes and Gruber (2014), Westermann et al. (2015), and Obu et al. (2019a). The gap-filled MODIS LST time series were averaged to 8 d periods from which FDDs and TDDs were finally accumulated for the 2000–2017 study period.

### 2.3 Average annual snowfall and $n_f$ factors

Spatially distributed datasets of  $n_f$  factors were generated from average annual snowfall forced by ERA-Interim and ERA-5 reanalysed data. Snow cover in the majority of the Antarctic is dominated by sublimation and processes related to blowing snow (Gallée, 1998; Bintanja and Reijmer, 2001), which were not taken into account by the snowfall and degree-day model that Obu et al. (2019a) used to estimate the  $n_f$  factor for the Northern Hemisphere. Thus, only mean annual snowfall was calculated using the downscaled ERA-Interim precipitation data from before 2008 and the ERA-5 precipitation after 2008. Precipitation was downscaled based on the difference between reanalysis elevation data and GMTED2010 data using a precipitation gradient, found in drier areas (Hevesi et al., 1992), of 2 % per 100 m up to 1000 m and 1 % per 100 m for elevations above 1000 m. Snowfall was defined as precipitation at air temperatures below  $0^\circ\text{C}$ , using the downscaled ERA-Interim air temperatures as employed for the gap filling of MODIS LST (see above). For a detailed downscaling procedure description, see Obu et al. (2019a).

$N_f$  factors were defined based on average annual snowfall; however the reported  $n_f$  factors in Antarctica were calculated with respect to snow depth. Oliva et al. (2017) identified  $n_f$  factor values of around 0.3 for snow accumulations of 80 cm on Livingston Island, although the  $n_f$  factors can increase to 0.55 in the same accumulations due to their temporal variability (de Pablo et al., 2017).  $N_f$  factors close to, or even greater than, 1 were measured in areas with little or no snow cover on Vesleskarvet nunatak (Kotzé and Meiklejohn, 2017), in the McMurdo Dry Valleys (Lacelle et al., 2016) and on James Ross Island (Hrbáček et al., 2016). This range was used to constrain the  $n_f$  factor ranges in relation to average annual snowfall (Table 1). Since the snow model was not able to simulate snow-free sites, nor snowdrifts, due to strong wind distribution, we used a maximum  $n_f$  factor of 0.95 and a minimum of 0.3. However, smaller snow-depth variations on a local scale were taken into account, with an ensemble of different values of mean annual snowfall for each 1 km<sup>2</sup> pixel (e.g. Gisnås et al., 2014).

### 2.4 $r_k$ factors

The  $r_k$  factor is defined as the ratio of thawed and frozen thermal conductivities of the active-layer material (Romanovsky and Osterkamp, 1995) and is related to water and organic matter contents (e.g. Gisnås et al., 2013). Soil moisture prop-

**Table 1.** Ranges of  $n_f$  factors that were assigned to mean annual snowfall values.

| Mean annual snowfall (mm) | $n_f$ min | $n_f$ max |
|---------------------------|-----------|-----------|
| < 3                       | 0.85      | 0.95      |
| 3–10                      | 0.77      | 0.85      |
| 10–30                     | 0.75      | 0.77      |
| 30–50                     | 0.73      | 0.75      |
| 50–75                     | 0.67      | 0.73      |
| 75–100                    | 0.64      | 0.67      |
| 100–125                   | 0.55      | 0.64      |
| 125–150                   | 0.5       | 0.55      |
| 150–200                   | 0.45      | 0.5       |
| 200–300                   | 0.4       | 0.45      |
| > 300                     | 0.3       | 0.4       |

erties were mapped on a regional scale (Bockheim et al., 2007), but no pan-Antarctic datasets related to soil water or organic contents were available. The ESA CCI Land Cover that Obu et al. (2019a) used for the Northern Hemisphere study contains only a “permanent snow and ice” class on the Antarctic mainland; therefore, a rock outcrop dataset (Burton-Johnson et al., 2016) was used to constrain non-glaciated areas. An  $r_k$  factor of 0.85 was used for the whole of the Antarctic, representing an average value between very dry sites on continental Antarctica and moderately moist sites on the Antarctic Peninsula.

## 2.5 Ensemble-based modelling of subpixel heterogeneity

Ground temperatures can vary considerably at short distances due to heterogeneous snow cover, vegetation, topography and soil properties (Beer, 2016; Gislén et al., 2014, 2016; Zhang et al., 2014). We ran an ensemble of 200 model realisations with different combinations of  $n_f$  and  $r_k$  factors to simulate the variability.  $R_k$  factor values were drawn randomly from a uniform distribution to vary by  $\pm 0.1$  between 0.75 and 0.95 to represent both very dry sites and locations with higher soil moisture. The distribution of snowfall within the 1 km pixel was simulated using a log-normal distribution function where mean annual snowfall determined the mean of the distribution. The coefficient of variation in the distribution for the open areas (0.9) according to Liston (2004) was assigned to all modelled areas. An  $n_f$  factor was assigned to the estimated average annual snowfall according to Table 1. The pixels not overlapping with rock outcrops were masked out. A fraction of the model runs, with MAGT < 0 °C, was used to derive the permafrost type (zone) on Antarctic islands (see Obu et al., 2019a, for detailed description).

## 2.6 Model validation

We compared our results to available in situ measurements in 40 permafrost boreholes and shallow boreholes at soil-climate stations. The ensemble mean of modelled MAGTs was compared to the borehole measurements to take the simulated spatial variability, provided by the ensemble spread, into account. The accuracy of the model was estimated, with root-mean-square error (RMSE) and mean absolute error, between the modelled and measured MAGT.

The validation data were provided by the authors for the McMurdo Dry Valleys, ice-free areas near Russian stations (Bunger Hills, Schirmacher Hills, Larsemann Hills, Thala Hills, King George Island and Hobs Coast) and the northern Antarctic Peninsula. Ground temperatures from these locations represent mean MAGT at the top of the permafrost and usually overlap well with the modelling period 2000–2017 (Appendix A). Validation data for Queen Maud Land (Troll Station, Flårjuven Bluff and Vesleskarvet) and the Baker Rocks site were obtained from Hrbáček et al. (2018), and MAGTs from Terra Nova Bay (Oasi New and Boulder Clay) were obtained from Vieira et al. (2010). MAGTs from Hope Bay, Mount Dolence, the Marble Point borehole and Limnopolar Lake were obtained from Schaefer et al. (2017a, b), Guglielmin et al. (2011) and de Pablo et al. (2014), respectively. The borehole data from Signy Island and Rothera Point were extracted from Guglielmin et al. (2012, 2014). The data reported in publications were not necessarily calculated for the top of the permafrost and do not completely overlap with the modelling period and are, thus, less reliable than the author-supplied validation data. For instance, the data from Vieira et al. (2010) represent MAGT for the periods before 2010, usually lasting only few years (Table A1).

## 3 Results

### 3.1 Comparison to borehole measurements

Ground temperatures can vary significantly inside a 1 km<sup>2</sup> model pixel, which is, to a certain extent, represented by the TTOP model ensemble runs. Average MAGT derived from the ensemble runs was compared to the measured site ground temperatures, which might limit representativeness for sites with locally specific ground and snow properties. The comparison yielded a RMSE of 1.94 °C and a mean absolute error for all boreholes of −0.17 °C (Fig. 2). The small mean absolute error is partly achieved with fine adjustment of the  $n_f$  factor class limits. For 50 % of the boreholes, the agreement between borehole temperatures and modelled MAGT was better than 1 °C, while it is better than 2 °C for 75 % and better than 3 °C for 85 % of the boreholes. Assuming a Gaussian distribution of standard deviation  $\sigma_{\text{MAGT}}$ , 68 % of borehole comparisons should fall within 1  $\sigma_{\text{MAGT}}$ , while 95 % falls within 3  $\sigma_{\text{MAGT}}$ , and 99 % should be within 3

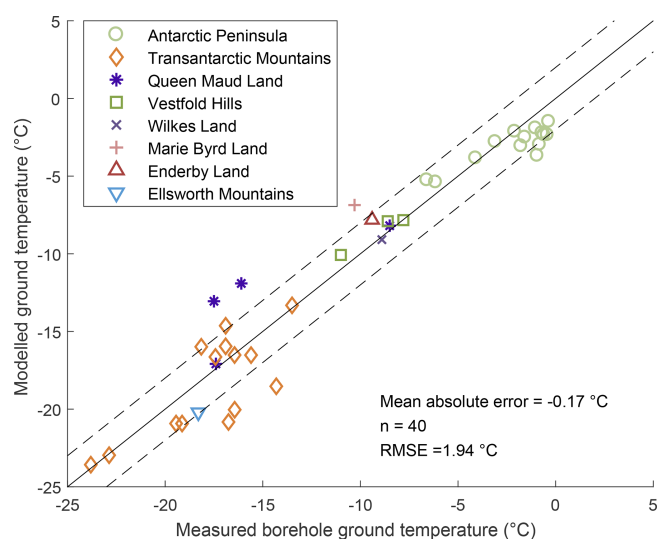


**Figure 2.** Measured vs. modelled permafrost temperatures for all boreholes. The dashed lines represent  $\pm 2$  °C intervals around the 1 : 1 solid line.

$\sigma$  MAGT. For the comparison with Antarctic boreholes, 18 (45 %) boreholes were contained within 1, 29 (73 %) within 2 and 31 (78 %) within 3 standard deviations from the mean, which is comparable to the results for the Northern Hemisphere (Obu et al., 2019a).

### 3.2 Queen Maud Land

There are 2430 km<sup>2</sup> of ice-free areas in Queen Maud Land according to the rock outcrop map (Burton-Johnson et al., 2016; Hrbáček et al., 2018). The average MAGT is  $-18.2$  °C, and it ranges from  $-26.2$  °C in the highest parts of the Fimbulheimen Range to  $-6.3$  °C on the Prince Olav Coast, where MAGTs down to  $-10$  °C were modelled at elevations exceeding 200 m (Fig. 3). MAGTs above  $-10$  °C can be found also at the Schirmacher Oasis (Hills) and reach above  $-8$  °C. MAGTs in the Sør Rondane Mountains and in the Fimbulheimen Range range from  $-12$  °C at elevations of around 800 m a.s.l. to  $-24$  °C at elevations exceeding 3000 m a.s.l. The Kirwan Escarpment (elevations usually exceeding 2000 m) is characterised by MAGTs between  $-23$  and  $-20$  °C, and in the Heimefront Range (with slightly lower elevations) the MAGTs were between  $-22$  and  $-18$  °C. MAGTs were modelled as being from  $-21$  to  $-17$  °C on the Borg Massif and between  $-16$  and  $-12$  °C on the Ahlmann Ridge.

### 3.3 Enderby Land

Permafrost occupies 1140 km<sup>2</sup> of ice-free area in Enderby Land, which is predominantly mountaintops and a few coastal sites. The modelled average MAGT was  $-11.7$  °C, ranging from  $-22.4$  °C, on summits exceeding 2000 m el-

evation, to  $-6.3$  °C in the north-western part of the coast (Fig. 4). The MAGT was modelled as being around  $-8$  °C along the majority of the coast and around  $-10$  °C in the coastal areas of the Nye, Scott and Tula mountains, dropping below  $-15$  °C at elevations exceeding 1000 m a.s.l. In the Framnes Mountains, MAGT was modelled at between  $-17$  and  $-12$  °C.

### 3.4 Vestfold Hills

The ice-free area of the Vestfold Hills region is 2750 km<sup>2</sup>. The modelling showed an average MAGT of  $-17.4$  °C in this region. The MAGT ranged from  $-6.6$  °C on the islands of the Ingrid Christensen Coast to  $-28.3$  °C in the highest parts of the Prince Charles Mountains (Fig. 5). The MAGT in Amery Oasis, which is a part of the Prince Charles Mountains, was modelled as  $-13$  °C, in the lowest-lying areas, down to  $-18$  °C at elevations approaching 1000 m a.s.l. At similar elevations on the Mawson Escarpment, significantly lower MAGTs, from  $-19$  °C at 200 m a.s.l down to  $-24$  °C at 1500 m a.s.l, were recognised. In the coastal lowland areas of the Larsemann and Vestfold Hills the MAGT ranged between  $-10$  to  $-7$  °C.

### 3.5 Wilkes Land

The majority of the 400 km<sup>2</sup> of ice-free area in Wilkes Land lies in the area surrounding the Bunger Hills, where MAGTs of around  $-9$  °C were modelled close to the Shackleton Ice Shelf. The lowest MAGT of  $-15.9$  °C was modelled on the adjacent mountains at 1300 m elevation (Fig. 6). Modelled MAGTs were  $-8$  to  $-6$  °C at the Budd Coast,  $-8$  °C at the Adélie Coast and  $-10$  to  $-11$  °C at the George V Coast. Due to the prevalence of low-lying regions the mean MAGT of the region was only  $-8.9$  °C.

### 3.6 Transantarctic Mountains

The Transantarctic Mountains are the largest ice-free region, comprising 19 750 km<sup>2</sup> and extending from Cape Adare to Coats Land. The part west of the 90° meridian (Fig. 7) consists of mountain ranges mostly lower than 2000 m (except for the Thiel Mountains) that do not extend to sea level. The highest MAGT, of  $-17.0$  °C, was modelled at the foot of the Shackleton Range and at the Pensacola Mountains. The MAGTs decreased down to  $-29$  °C in the high mountains. The lowest MAGT of  $-29.8$  °C was modelled in the Thiel Mountains.

The region east of 90° E (Fig. 8) consists of numerous mountain ranges extending from the Ross Ice Shelf and Ross Sea up to more than 4000 m elevation and from 69 to 85° S latitude. The results show the widest range of MAGTs among all the regions, with the lowest temperature of  $-33.5$  °C at Mount Markham in the Queen Elizabeth Range and the warmest at  $-8.5$  °C on the Oates Coast. The modelled MAGTs close to the Ross Ice Shelf decreased

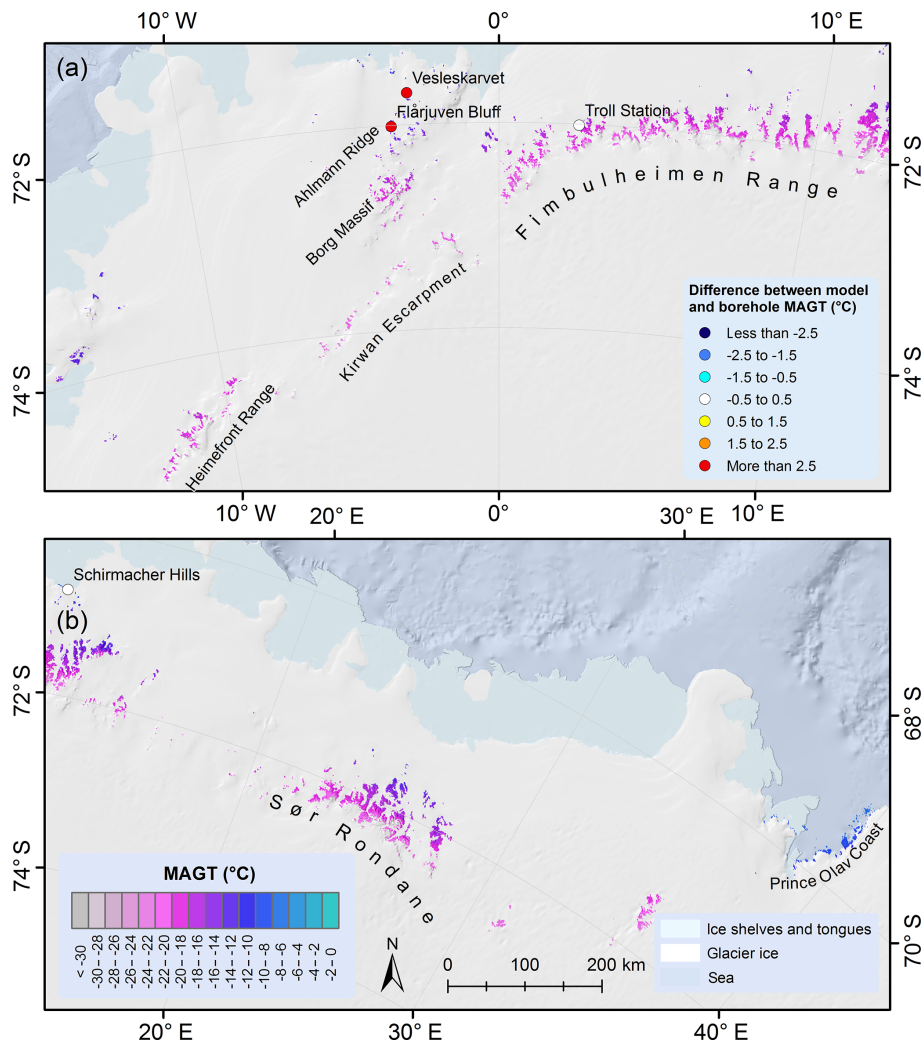


**Figure 3.** Permafrost temperature maps of Queen Maud Land and differences between borehole and modelled MAGT. Legends, scale and north arrow are valid for both panels. See Fig. 1 for location of panels (a) and (b).

northwards, from  $-15^{\circ}\text{C}$  at the Amundsen Coast to  $-18^{\circ}\text{C}$  to the north of the Dufek Coast. Similar MAGTs, between  $-19$  and  $-17^{\circ}\text{C}$ , were modelled further north along the ice shelf at the Shackleton and Hillary coasts. Similar decreases in MAGT at higher elevations in the northward direction were observed, but local MAGT variations in relation to altitude were considerable. However, MAGTs below  $-30^{\circ}\text{C}$  were modelled at the highest parts of the mountain ranges along the Ross Ice Shelf. Higher MAGTs were modelled along the Ross Sea and range between  $-15$  and  $-12^{\circ}\text{C}$  along the Scott and Borchgrevink coasts. The modelled MAGTs were around  $-10^{\circ}\text{C}$  at Cape Adare and between  $-13$  and  $-10^{\circ}\text{C}$  on the Pennell Coast. MAGT was modelled down to  $-26^{\circ}\text{C}$  in the Prince Albert Mountains at elevations above 2000 m a.s.l. They approach  $-30^{\circ}\text{C}$  at the highest elevations, which exceed 3000 m a.s.l., in the Deep Freeze Range. Despite the elevations reaching 4000 m a.s.l.

in the Admiralty Mountains, the MAGT was only down to  $-23^{\circ}\text{C}$ .

### McMurdo Dry Valleys

The McMurdo Dry Valleys are a part of the Transantarctic Mountains, include a large ice-free area (4500 km<sup>2</sup>) and are one of the most extensively studied permafrost regions in Antarctica (Levy, 2013; Bockheim et al., 2007). The lowest MAGT among the dry valleys is modelled in the Victoria Valley, falling below  $-24^{\circ}\text{C}$  at the lowest part (Fig. 9). A winter ground temperature inversion is pronounced with MAGTs in the surrounding valleys, modelled at around  $-21^{\circ}\text{C}$ . The MAGT also increases up the valleys to  $-21^{\circ}\text{C}$  in the McKelvey, Balham and Barwick Valleys. No MAGT inversion was modelled in the Wright Valley, where MAGTs ranged between  $-21$  and  $-19^{\circ}\text{C}$  and in the Taylor Valley, which is the warmest, with an MAGT of  $-17^{\circ}\text{C}$  in the lower-lying

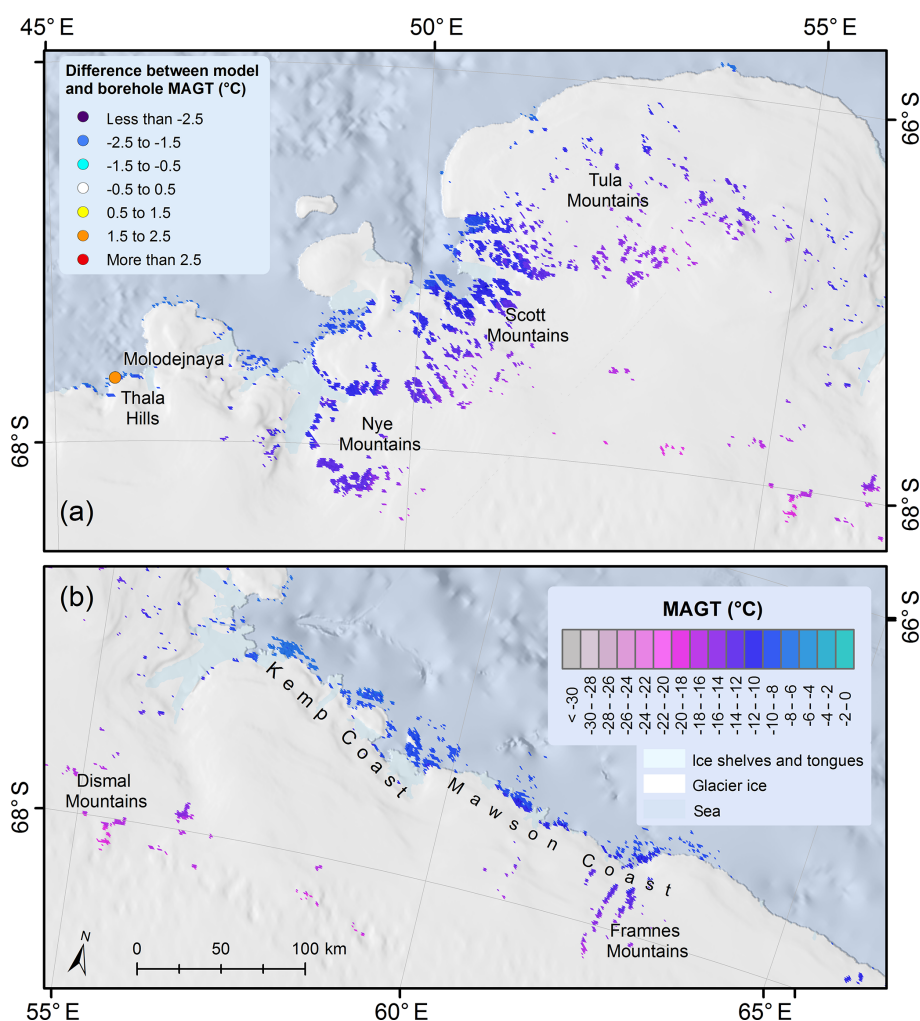


**Figure 4.** Permafrost temperature maps of Enderby Land and differences between borehole and modelled MAGT. Legends, scale and north arrow are valid for both panels. See Fig. 1 for location of panels (a) and (b).

parts and  $-20^{\circ}\text{C}$  in the upper part of the valley. At the Olympus and Asgard ranges and the Kukri Hills, which surround the valleys, MAGTs between  $-23$  and  $-20^{\circ}\text{C}$  were modelled. In the surrounding mountains, close to the ice sheet, modelled MAGTs were around  $-25^{\circ}\text{C}$  and reached  $-27^{\circ}\text{C}$  at the highest and the most east-lying mountains. MAGTs along the coast of McMurdo Sound ranged from  $-13$  to  $-17^{\circ}\text{C}$ . On Ross Island, the MAGT was modelled as  $-16^{\circ}\text{C}$  at the Scott and McMurdo bases, which are near sea level, and down to  $-24^{\circ}\text{C}$  at higher altitudes on Mount Erebus.

### 3.7 Ellsworth Mountains

The ice-free area of the Ellsworth Mountains occupies  $380\text{ km}^2$  of high-elevation terrain, with a modelled mean MAGT of  $-21.5^{\circ}\text{C}$ . The highest temperature was modelled at the foot of the mountains ( $-17.4^{\circ}\text{C}$ ) at  $500\text{ m a.s.l.}$ , with  $-21^{\circ}\text{C}$  at  $1000\text{ m a.s.l.}$ ,  $-22^{\circ}\text{C}$  at  $2000\text{ m}$  and  $-26.1^{\circ}\text{C}$  at the highest elevations of Vinson Massif (Fig. 10).

### 3.8 Marie Byrd Land

The ice-free areas in Marie Byrd Land occupy only  $210\text{ km}^2$  and consist mostly of rock outcrops at lower elevations close to the coast and volcanos protruding through the ice sheet. In the Ford Ranges, MAGT was modelled as from  $-10^{\circ}\text{C}$  close to sea level to  $-16^{\circ}\text{C}$  at elevations exceeding  $1000\text{ m a.s.l.}$  (Fig. 11). MAGTs between  $-11$  and  $-8^{\circ}\text{C}$  were modelled at the Hobbs, Walgreen, Eights and Ruppert coasts, reaching  $-6^{\circ}\text{C}$  on the islands surrounded by open sea. The volcano mountain ranges reaching  $3000\text{ m a.s.l.}$  (Flood and Kohler Range) had MAGTs typically ranging between  $-16$  to  $-14^{\circ}\text{C}$  at their peaks. Modelled MAGTs were between  $-25$  and  $-21^{\circ}\text{C}$  on the Executive Committee Range, where rock outcrops occur above  $2000\text{ m a.s.l.}$  and the highest peaks extend to over  $4000\text{ m a.s.l.}$

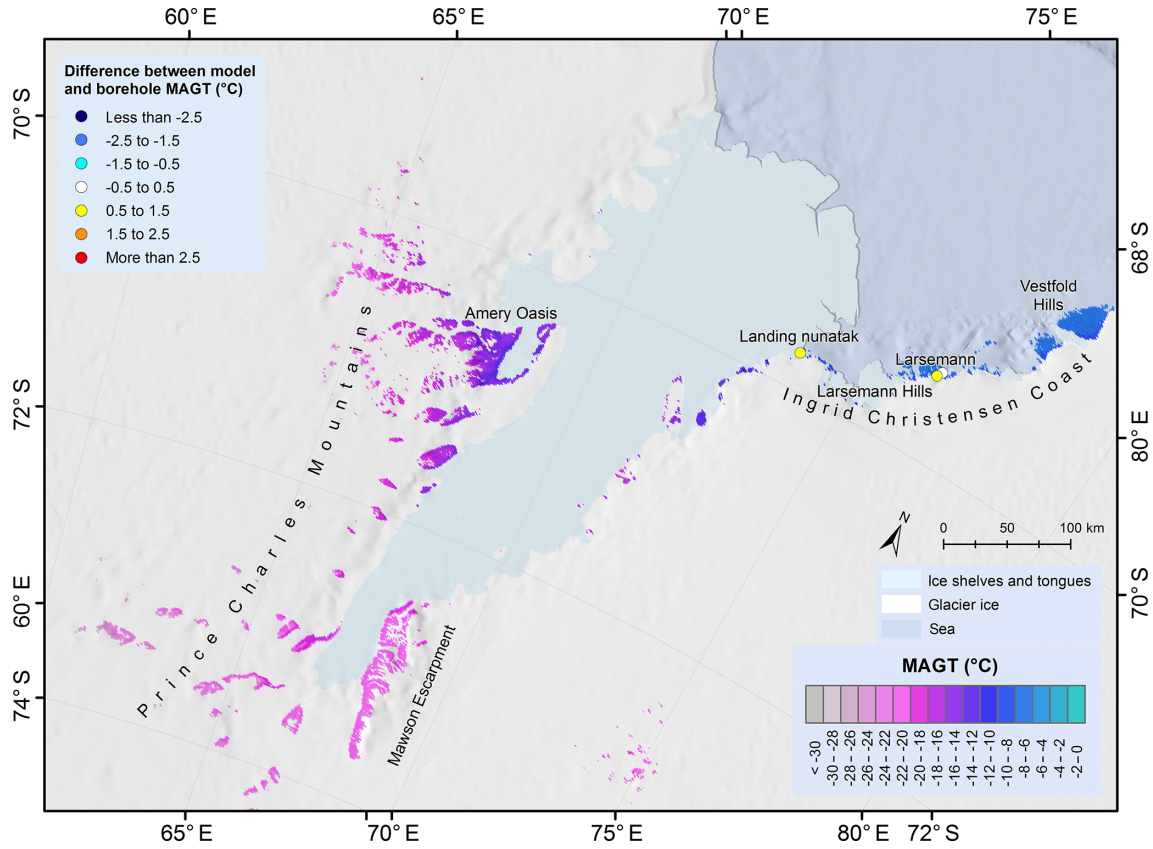


Figure 5. Permafrost temperature map of the Vestfold Hills and differences between borehole and modelled MAGT.

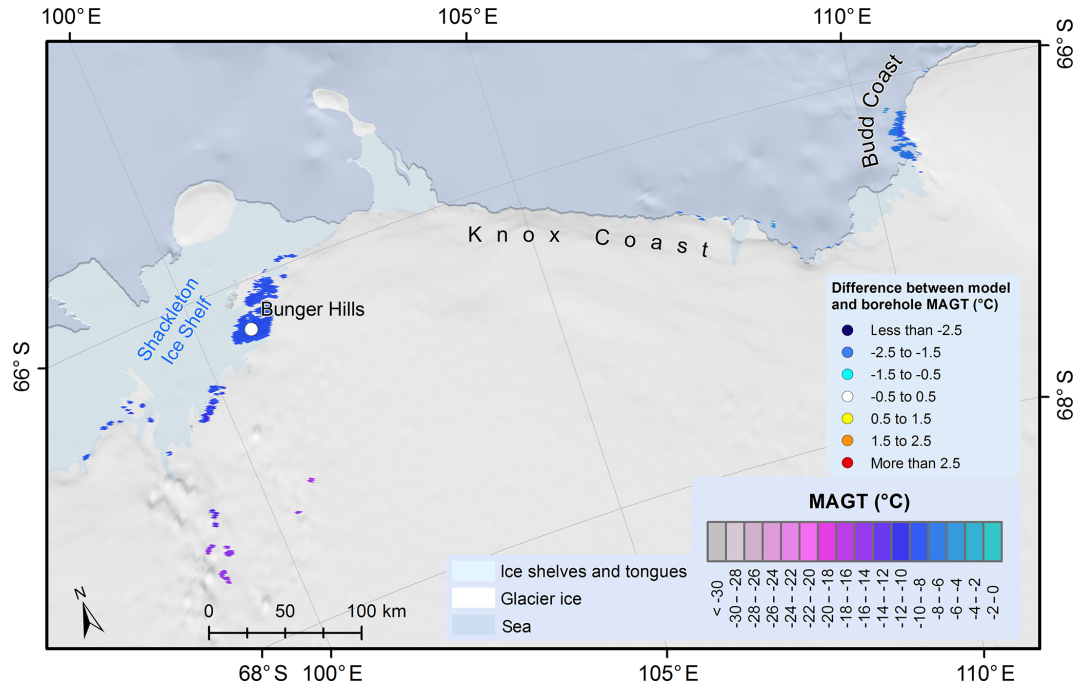
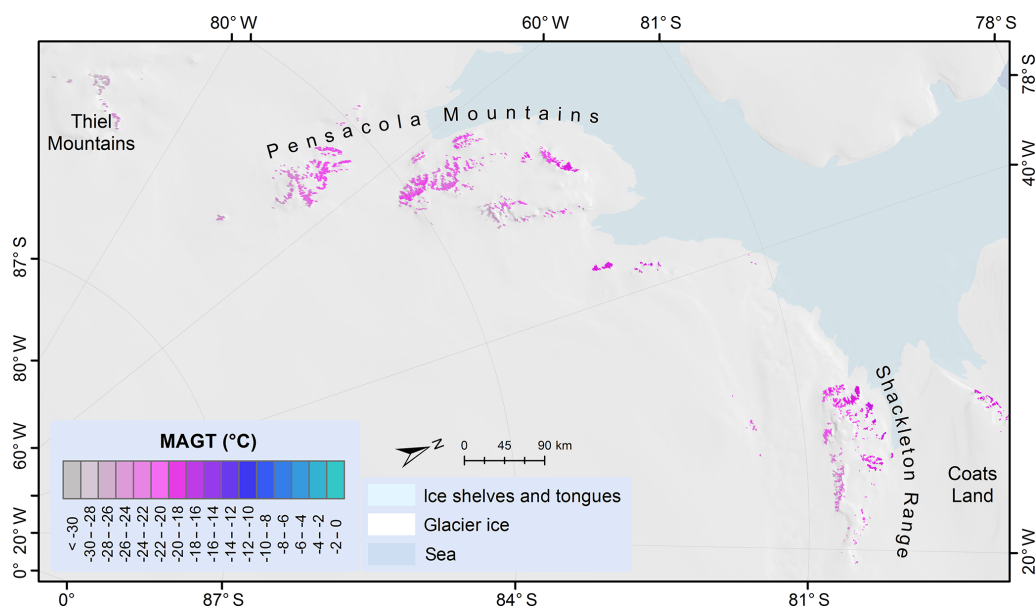


Figure 6. Permafrost temperature maps of Wilkes Land and differences between borehole and modelled MAGT. See Fig. 1 for location.



**Figure 7.** Permafrost temperature map of the Transantarctic Mountains west of the 90° meridian. See Fig. 1 for location.

### 3.9 Antarctic Peninsula

The ice-free areas of the Antarctic Peninsula cover 3800 km<sup>2</sup>, including the South Shetland Islands, where the modelled MAGT was slightly below 0 °C, and the mountains of the south-eastern Antarctic Peninsula, with modelled MAGTs of around −19 °C. The modelled near-surface permafrost temperatures in the Antarctic Peninsula were the warmest among all Antarctic regions, with an average modelled MAGT of −7.3 °C (Fig. 12).

#### 3.9.1 Palmer Land

The mountains of Palmer Land show considerable differences between the eastern and western parts of the peninsula. Modelled MAGTs at the mountains of the Orville Coast were around −17 °C, increasing to about −12 to −15 °C at the Black Coast and eventually rising above −10 °C at the Wilkins Coast. On the western side at the Fallières Coast, MAGTs of up to −4 °C were modelled. Temperatures decreased to −6 to −8 °C at the Rymill Coast, around −10 °C at 1000 m a.s.l. and approaching −12 °C at 1500 m a.s.l. Similar MAGT ranges were modelled on Alexander Island, where MAGTs close to the coast were around −5 °C, decreasing to between −9 and −7 °C at 1000 m a.s.l. and falling below −10 °C at elevations above 2000 m a.s.l.

#### 3.9.2 Graham Land

A considerable increase in modelled MAGT from the east to the west of Graham Land was observed, where the southern part of the eastern coast is protected by the Larsen Ice Shelf. Ground temperatures gradually increased in the north-

ward direction on both sides of the peninsula. MAGTs at the Bowman and Foyn coasts ranged between −8 and −6 °C and slowly increased from −6 °C at the Oscar II Coast to around −4 °C at the northernmost part of the mainland, although still falling below −8 °C at higher elevations. On the western side, MAGT gradually decreased from around −2 °C on the northern Davis Coast to −5 °C at the south of the Danco Coast and Anvers Island, where MAGT also fell below −6 °C at higher elevations. Similar MAGT ranges were observed at the Graham and Loubet coasts and at Adelaide Island but were lower than −7 °C at higher elevations. Small Island along the western coast of the Antarctic Peninsula had a modelled MAGT between −3 and −1 °C.

#### 3.9.3 South Shetland Islands and James Ross Island

Another frequently studied area in the Antarctic is the northern Antarctic Peninsula, especially the South Shetland Islands. At sites close to sea level, the modelled MAGT was usually above −1 °C on the South Shetland Islands (Fig. 13). MAGT decreased below −2 °C on sites that are not adjacent to the coast but still low-lying, such as Byers and Hurd Peninsulas on Livingston Island and Fildes Peninsula on King George Island. The MAGT was below −4 °C on the highest unglaciated peaks of Livingston and Smith Islands and reached −3 °C on Deception Island.

Modelled MAGTs were noticeably colder on James Ross Island than on the South Shetland Islands, and, at sites adjacent to the sea, ranged from −3 °C in the north down to −5 °C in the south. Lower-lying ice-free areas, including Seymour Island, had MAGTs typically between −6 and −5 °C. The MAGTs on the highest rock outcrops were modelled as being down to −7 °C.

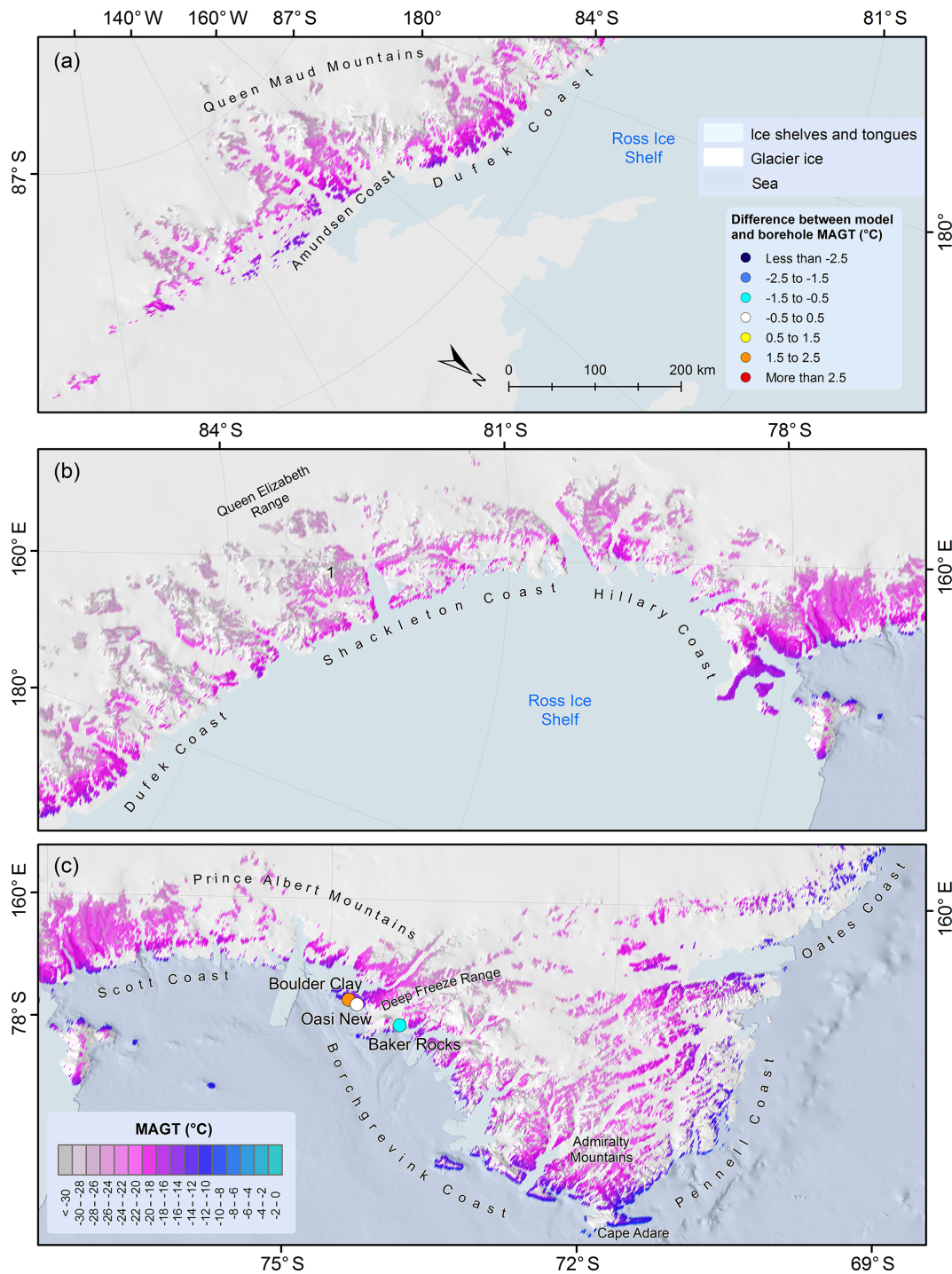


**Figure 8.** Permafrost temperature maps of the Transantarctic Mountains east of the 90° meridian and differences between borehole and modelled MAGT. Legends, scale and north arrow are valid for all panels. See Fig. 1 for location of panels (a), (b) and (c).

### 3.10 Other Antarctic and sub-Antarctic islands

The modelling results were derived for the Antarctic islands and sub-Antarctic islands, where the size and ice-free area of the island is sufficient that MODIS LST data were avail-

able. The MAGT on Signy Island ranged from  $-1.5\text{ }^{\circ}\text{C}$  at the coast to  $-4\text{ }^{\circ}\text{C}$  in the interior. Permafrost was modelled on all South Sandwich Islands, with similar MAGT ranges to those on Signy Island (Fig. 14). Less permafrost is modelled on South Georgia Island, where MAGTs at the coast increase

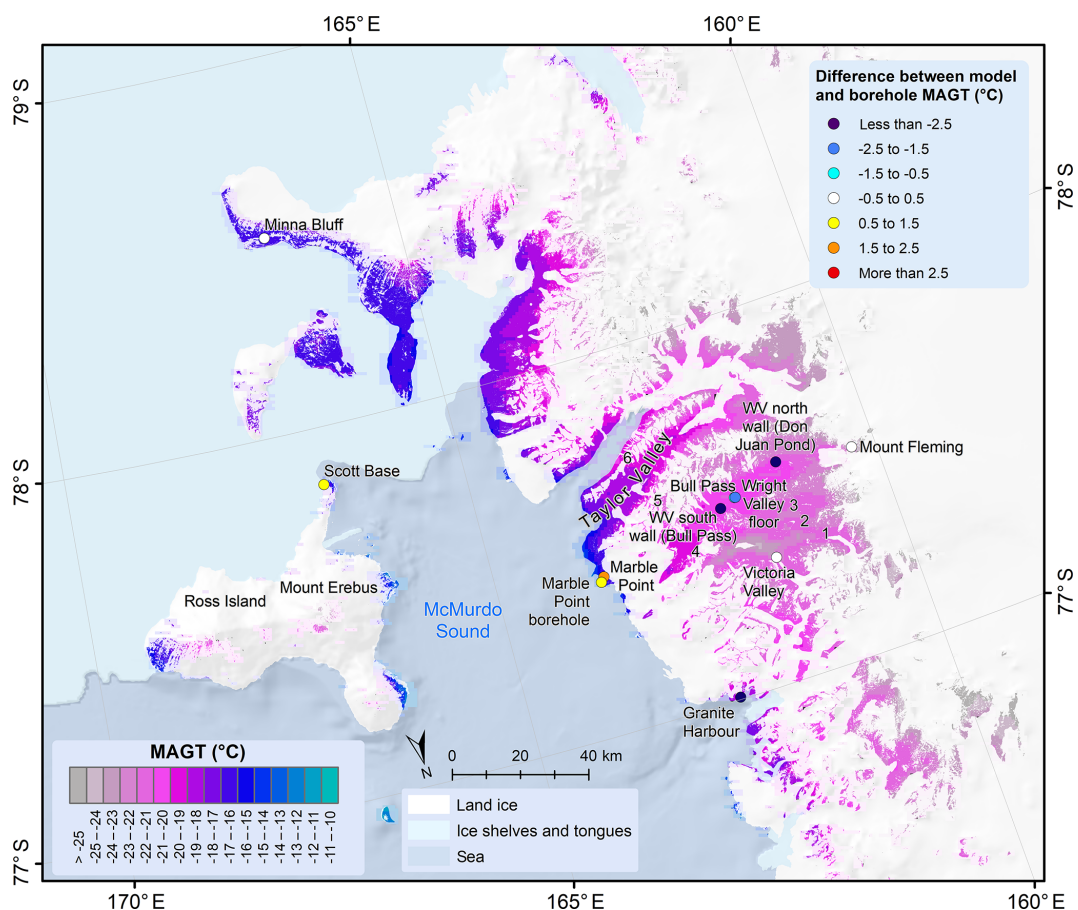


**Figure 9.** Permafrost temperature map of the McMurdo Dry Valleys and differences between borehole and modelled MAGT. See Fig. 1 for location. Note: the MAGT colour ramp is different from other figures. 1: McKelvey Valley. 2: Balham Valley. 3: Barwick Valley. 4: Olympus Range. 5: Asgard Range. 6: Kukri Hills.

to +1 °C and sporadic permafrost starts to occur at elevations above 100 m. The MAGTs decreased below −2 °C at the highest-lying rock outcrops. No permafrost was modelled on the Crozet Islands. MAGTs below 0 °C were modelled at the highest elevations of Kerguelen Island and in isolated permafrost patches occurring above 500 m a.s.l. Permafrost is present also on the southernmost ice-free area of Heard Island.

### 3.11 Regional MAGT distribution

The MAGT distribution of Antarctic is bimodal, with the most pronounced peak at −21 °C and the second peak at −7 °C (Fig. 15). The peaks correspond to the two largest ice-free areas of the Transantarctic Mountains and the Antarctic Peninsula; however the temperatures around the −20 °C peak also occur in other regions, such as Queen Maud Land, the Vestfold Hills and the Ellsworth Mountains. The most commonly modelled temperatures were between −23 and −18 °C and usually occurred in the mountains rising above the Antarctic Ice Sheet and glaciers. MAGTs between −10

and −6 °C occurred in the coastal areas of Wilkes Land, Marie Byrd Land, Queen Maud Land, Enderby Land and the Vestfold Hills. However the peak of temperature distribution at coastal sites shifted towards −7 °C because of MAGTs on the Antarctic Peninsula. The peak of coastal areas would be at −9 °C if the Antarctic Peninsula were excluded.

### 3.12 Altitudinal MAGT gradients

Average MAGT lapse rate for the whole Antarctic was 0.40 °C (100 m)<sup>−1</sup>, ranging from 0.15 °C (100 m)<sup>−1</sup> in the Ellsworth Mountains to 0.59 °C (100 m)<sup>−1</sup> in Enderby Land. The lapse rates increased from 0.21 °C (100 m)<sup>−1</sup> in Wilkes Land to 0.38 °C (100 m)<sup>−1</sup> in the Transantarctic Mountains, 0.44 °C (100 m)<sup>−1</sup> in the Vestfold Hills, 0.47 °C (100 m)<sup>−1</sup> in Marie Byrd Land and in the Antarctic Peninsula, and 0.49 °C (100 m)<sup>−1</sup> in Queen Maud Land.

The lapse rates indicate significant regional differences in the modelled MAGT patterns in relation to elevation (Fig. 16). The warmest among all regions was the Antarctic Peninsula, which had MAGTs similar to Marie Byrd Land

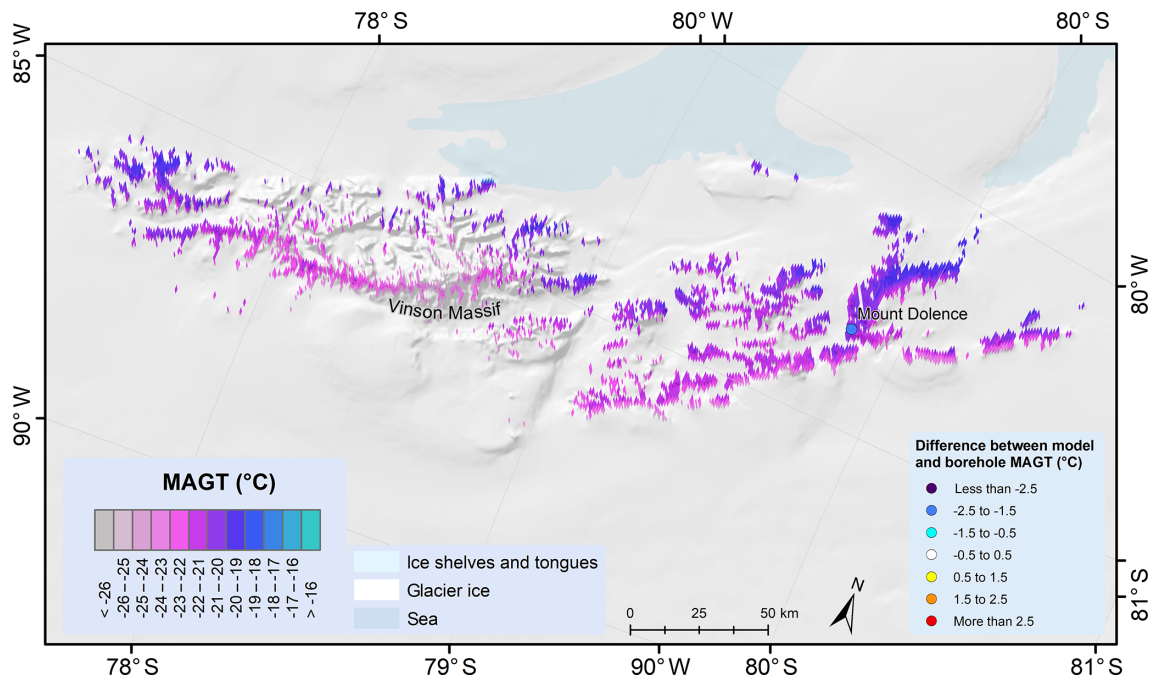


**Figure 10.** Permafrost temperature map of the Ellsworth Mountains and differences between borehole and modelled MAGT. See Fig. 1 for location.

of  $-12^{\circ}\text{C}$  only at around 1300 m a.s.l. Marie Byrd Land, Queen Maud Land, Enderby Land and Wilkes Land had MAGTs of  $-9^{\circ}\text{C}$  at the coast but show varying characteristics of temperature decrease with elevation. Marie Byrd Land was the warmest, with a decrease in MAGT up to 1500 m a.s.l. and a faster decrease to  $-25^{\circ}\text{C}$  at 3000 m a.s.l. The slower decrease in temperature with altitude to the 1500 m elevation was also modelled in Enderby Land, but the MAGT was colder. The MAGT decreased rapidly to  $-13^{\circ}\text{C}$  at 700 m a.s.l. in Queen Maud Land, where it slightly increased with elevation and then dropped steadily to  $-22^{\circ}\text{C}$  at 2800 m a.s.l. The MAGT increase with elevation could be explained by presence of rock outcrops with similar elevation in different latitudes or in different settings regarding continentality.

The modelled MAGT in the Vestfold Hills dropped rapidly, from  $-10^{\circ}\text{C}$  at the coast to  $-17^{\circ}\text{C}$  at 200 m a.s.l., and then gradually decreased to  $-24^{\circ}\text{C}$  at 2000 m a.s.l. There are no rock outcrops close to sea level in the Ellsworth Mountains, and the MAGT at 100 m a.s.l. was  $-20^{\circ}\text{C}$ . In the Ellsworth Mountains there was a slow decrease in the modelled MAGT, to  $-25^{\circ}\text{C}$  at 3000 m a.s.l. The coldest MAGTs (below  $-30^{\circ}\text{C}$ ) were modelled in the Transantarctic Mountains. In the part west of the  $90^{\circ}$  meridian, the MAGT dropped from  $-20^{\circ}\text{C}$  at 500 m a.s.l. to  $-27^{\circ}\text{C}$  at 2000 m a.s.l., but the absolute temperatures were lower east of the  $90^{\circ}$  meridian, where elevations exceed 4000 m a.s.l.

According to the gradients for subregions of the northern Antarctic Peninsula, the warmest were the South Shetland

Islands, followed by Palmer Archipelago (Fig. 17). The altitudinal MAGT profiles showed clear differences between the western and eastern parts of the northern Antarctic Peninsula mainland, although James Ross Island had a similar altitudinal profile to the western Antarctic Peninsula mainland. A significant decrease in MAGT from sea level to 100 m elevation was observed on the South Shetland Islands, Palmer Archipelago and on the western Antarctic Peninsula mainland.

## 4 Discussion

### 4.1 Comparison to borehole measurements

#### 4.1.1 Queen Maud Land

The modelled MAGT was, according to validation data, overestimated in Queen Maud Land (Fig. 3). Overestimation in Schirmacher Hills and Troll Station was below  $1^{\circ}\text{C}$  but was higher than  $4^{\circ}\text{C}$  in Flårjuven Bluff and Vesleskarvet. Both stations are located on nunataks, which are exposed to wind that blows the snow away. The estimated 120 mm of annual snowfall resulted in  $n_f$  factors that were too low for snow-free conditions. However, the minimum MAGT of the ensemble spread approaches the measured MAGT at both stations (Appendix A).

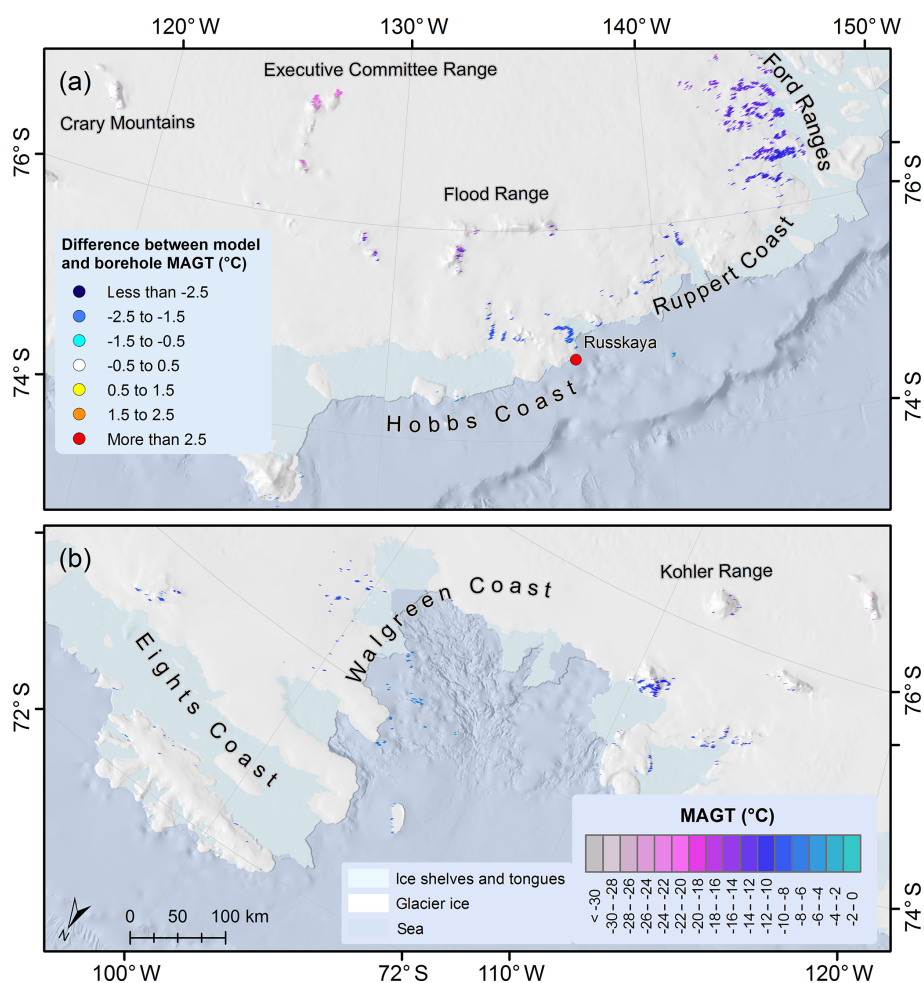


**Figure 11.** Permafrost temperature maps of Marie Byrd Land and differences between borehole and modelled MAGT. Legends, scale and north arrow are valid for both panels. See Fig. 1 for location of panels (a) and (b).

#### 4.1.2 Enderby Land, Vestfold Hills and Wilkes Land

The borehole data in Enderby Land were from the Molodejnaya station (Thala Hills), where modelled MAGT was overestimated by 1.6 °C (Fig. 4). The overestimation can be explained by rather thin snow cover due to strong winds and snow redistribution at the borehole site, which is confirmed by small differences between measured winter air and ground surface temperatures. The MAGT was accurately modelled in the coastal parts of the Vestfold Hills region, where validation data were available (Fig. 5). The difference between modelled and measured MAGT was small at the Larsemann Hills borehole, but slight MAGT overestimation (between 0.6 and 0.9 °C) was observed in comparison to the Larsemann and Landing Nunatak borehole measurements. Similarly, the MAGT was accurately modelled at the Bunger Hills station in the Wilkes Land region, with only small differences in comparison to measured ground temperature (Fig. 6).

#### 4.1.3 Transantarctic Mountains

The majority of the available validation data in the Transantarctic Mountains region were in the vicinity of the McMurdo Dry Valleys (Fig. 9). The sites on the floors of the McMurdo Dry Valleys (Victoria Valley, Wright Valley floor and Bull Pass) were modelled well, with slight overestimation in Victoria Valley and underestimation of around 1 °C in the Wright Valley. Two observation sites on small terraces on the walls of the Wright Valley (WV south wall and WV north wall) were modelled 3–4 °C too cold. The difference can be explained by the micro-location of both sites, which are sheltered from katabatic winds, are above the winter inversion layer and receive abundant summer solar radiation. The MAGT was overestimated by up to 1 °C at Mount Fleming, Scott Base and the Marble Point borehole, which lie outside the valleys. The MAGT at the Marble Point site, characterised by glacial till, was overestimated by 2.2 °C; however, the Marble Point borehole, which was drilled in granite bedrock approximately 1 km away, showed smaller overesti-

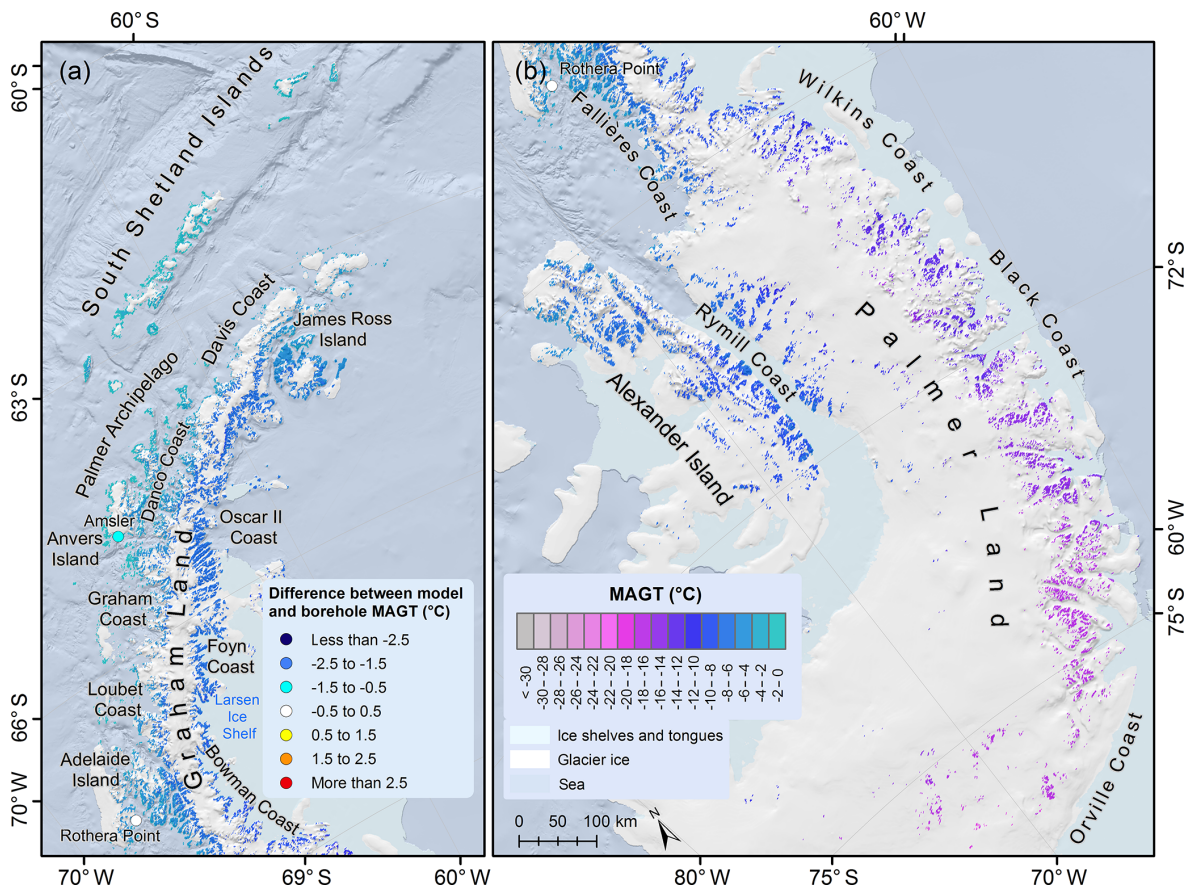


**Figure 12.** Permafrost temperature maps of the Antarctic Peninsula and differences between borehole and modelled MAGT. Legends, scale and north arrow are valid for both panels. See Fig. 1 for location of panels (a) and (b).

mation. The MAGT was underestimated by more than 4 °C at the Granite Harbour site, which has a warm microclimate, as it is situated on a north-facing moraine that receives a lot of meltwater from upslope.

Outside the McMurdo Dry Valleys, MAGT measurements from the Zucchelli Station and Baker Rocks were available (Fig. 9). The MAGT was overestimated by 2.3 °C at the Boulder clay borehole, which was drilled in a glacial till, exposed to katabatic winds and characterised by numerous snow drifts (Guglielmin, 2006), causing high local variability in permafrost conditions. On the other hand, the MAGT was overestimated by only 0.2 °C at the Oasi New borehole, which is located in a granitic outcrop. MAGT at the Baker Rocks site, which is situated in littoral deposits (Raffi and Stenni, 2011), was underestimated by 0.9 °C.

#### 4.1.4 Marie Byrd Land

The only available borehole data in Marie Byrd Land (Fig. 11) were from the Russian research station Russkaya. According to the measured MAGT between 2008–2013 the modelled MAGT was overestimated by 3.4 °C. The area is characterised by frequent storms and strong winds, which

blow off most of the snow on one hand and decrease the number and quality of the MODIS measurements on the other hand. The snow-free conditions at the Hobbs Coast borehole site were likely not simulated by the snow model, which resulted in the MAGT overestimation. An alternative explanation could be the measurement period, which was only 5 years in comparison to 17 modelled years. No validation data were available for the higher elevations of the volcanic ranges. The modelled MAGTs there might be underestimated because the TTOP model does not account for the ground heat flux. This can especially be the case in the locations with recent volcanic activity.

#### 4.1.5 Antarctic Peninsula

Comparison of the modelled MAGT with measured MAGT in boreholes showed an underestimation on the western Antarctic Peninsula and slight overestimation on the eastern Antarctic Peninsula (Fig. 13). The MAGTs are underestimated by between 1 and 2.1 °C on the South Shetland Islands (King George, Livingston and Deception Island). The underestimations may be explained by heat advection from meltwater and rain that is not simulated by the model but is

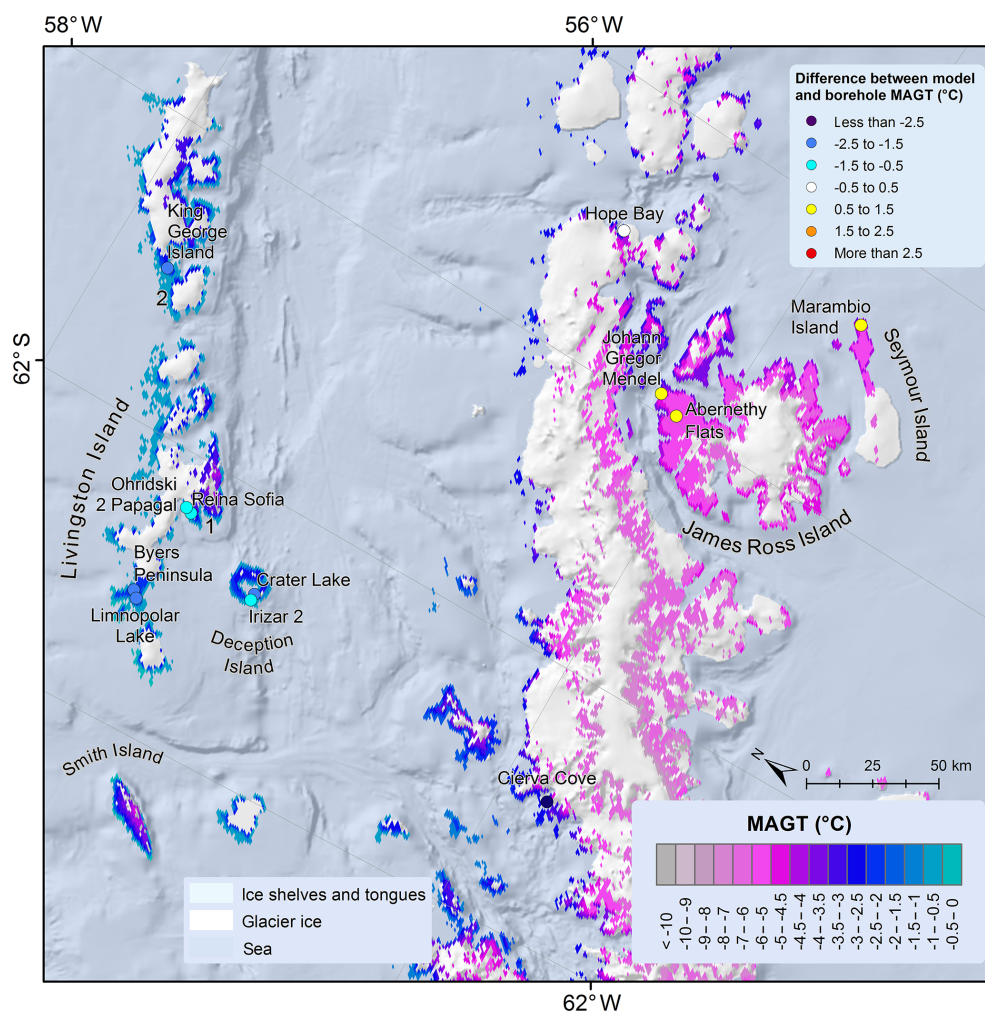


**Figure 13.** Permafrost temperature map of the northern Antarctic Peninsula and differences between borehole and modelled MAGT. See Fig. 1 for location. Note: the MAGT colour ramp is different from other figures. 1: Hurd Peninsula. 2: Fildes Peninsula.

especially common in this part of the Antarctic. Another possible explanation for deviations of the modelled MAGT on the north-eastern Antarctic Peninsula are the frequent cloudy conditions. Although clouds are generally masked out by the MODIS LST and replaced by ERA reanalysis temperatures, measurements in some areas are still contaminated with cloud temperatures, which results in MAGT underestimation (Østby et al., 2014).

Recent shallowing of thaw depth and ground cooling were observed on Deception Island by Ramos et al. (2017). However, similar cooling was recorded also on the eastern Antarctic Peninsula, but MAGT was overestimated by 1.4 °C at Marambio Island and by 0.8 °C at Abernethy Flats and by 0.6 °C at the Johann Gregor Mendel borehole sites. MAGT was overestimated by only 0.2 °C at the Hope Bay mainland site, which suggests that there was a continuous gradient of MAGT overestimation from the eastern Antarctic Peninsula to MAGT underestimation on the western Antarctic Peninsula.

## 4.2 Permafrost controls

The modelled permafrost temperatures reflect the climatic characteristics of the Antarctic, with major controls of latitude, elevation and continentality (Vieira et al., 2010). The effects of the ocean and continentality are well reflected in altitudinal MAGT profiles in Figs. 16 and 17. Regions with areas close to the open sea generally show faster MAGT decrease with elevation, which was observed especially in the Vestfold Hills, the Transantarctic Mountains east of the 90° meridian and in Marie Byrd Land, where the MAGT dropped significantly with the first elevation increase of 100 or 200 m. The same phenomenon was observed on the North Antarctic Peninsula, on the South Shetland Islands, in the Palmer Archipelago and on the western Antarctic Peninsula mainland, where there is less sea ice than on James Ross Island, and the western Antarctic Peninsula mainland, where a MAGT decrease was not observed. The continental mountainous regions of the Ellsworth Mountains, and the

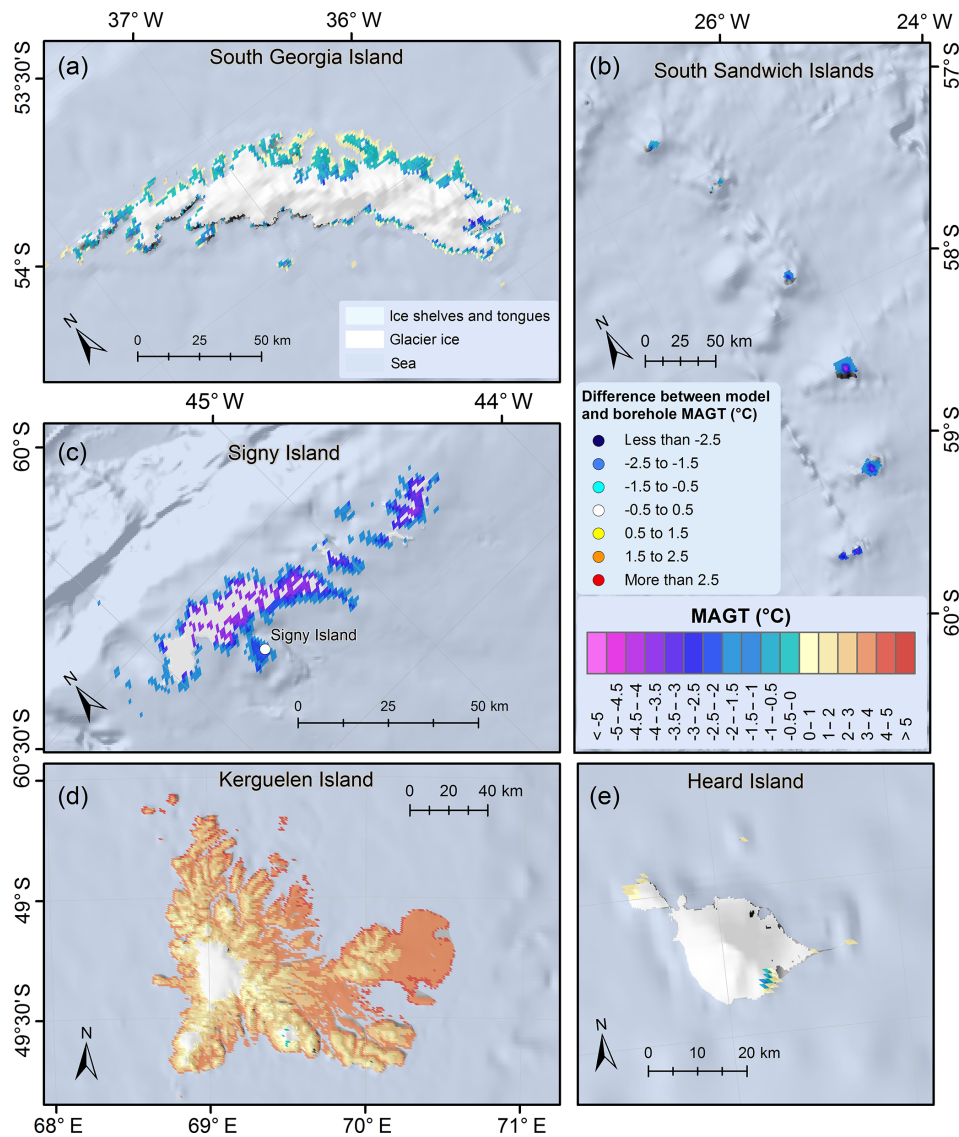


**Figure 14.** Permafrost temperature maps of Antarctic islands and difference between borehole and modelled MAGT. Legends are valid for all panels. See Fig. 1 for location of panels (a), (b), (c), (d) and (e). Note: the MAGT colour ramp is different from other figures.

Transantarctic Mountains west of the 90° meridian, have no open sea in the vicinity and had a significantly slower MAGT drop with the altitude.

The modelled MAGT lapse rate of  $0.40\text{ }^{\circ}\text{C}\text{ (100 m)}^{-1}$  for the whole Antarctic is lower than the average air temperature lapse rate of  $0.65\text{ }^{\circ}\text{C}\text{ (100 m)}^{-1}$  in the International Standard Atmosphere (ISO 2533:1975) but is, however, the same as the mean air temperature lapse rate measured for ice-free sites on James Ross Island from 2013–2016 (Ambrozova et al., 2019). Small increases in MAGTs with elevation were observed in many regions. This might be attributed to the nature of the analysis rather than a presence of temperature inversions. The rock outcrops on the scale of the regions are often present at different elevations far from each other, which results in occurrence of higher MAGTs at higher elevations.

Additionally, some elevation bins have only a few rock outcrop pixels, which makes the averaged MAGT less representative for the whole region.

The lowest MAGT ensemble mean of  $-33.5\text{ }^{\circ}\text{C}$  was modelled in the Transantarctic Mountains at the Queen Elizabeth Range, where the highest peak reaches 4350 m. The MAGT there could fall below  $-36\text{ }^{\circ}\text{C}$  according to the coldest ensemble member. This is the lowest MAGT modelled on Earth according to the modelling in the other parts of the globe (Obu et al., 2019a, b). On the highest Antarctic peak, Mount Vinson in the Ellsworth Mountains, reaching 4892 m, a MAGT of only  $-26.1\text{ }^{\circ}\text{C}$  was modelled. The Queen Elizabeth Range lies approximately  $5^{\circ}$  further south than Mount Vinson, illustrating the effect of latitude on permafrost temperatures.

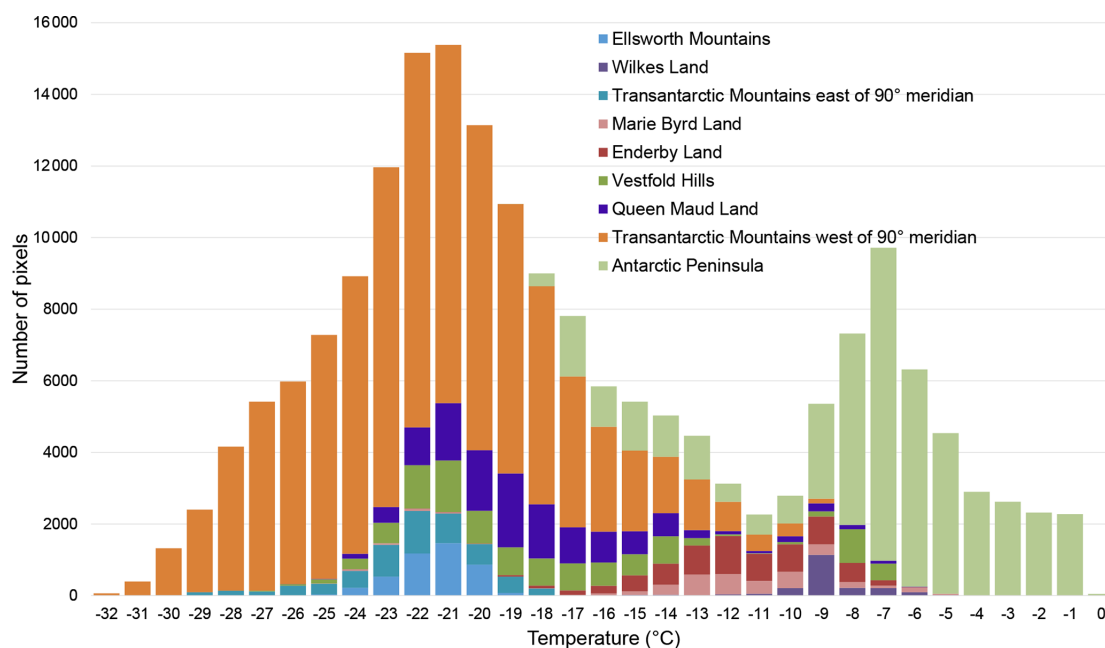


**Figure 15.** Histogram of temperature distribution across the Antarctic for 1 °C bins. Note: the ice-free areas were often smaller than the analysed pixel size.

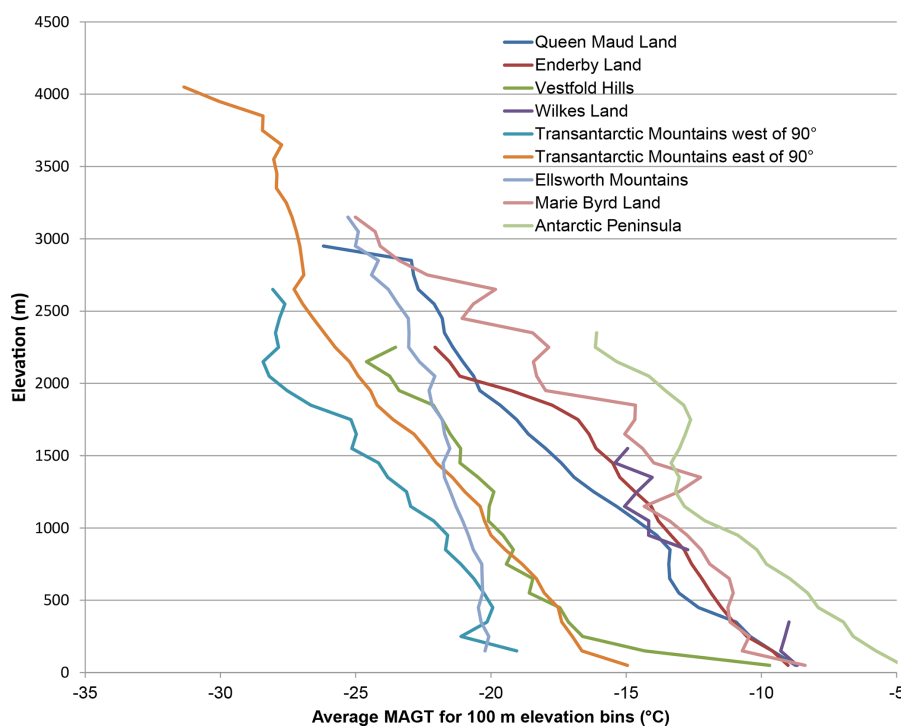


**Figure 16.** Altitudinal MAGT gradients for Antarctic soil regions calculated for 100 m elevation bins.

The winter air temperature inversions that occur in the McMurdo Dry Valleys result in air temperatures that are about 10 °C lower in the valleys than in the surroundings, but inversions are occasionally disrupted by winter storms. The winter inversions reflect MAGTs being approximately 3 °C colder

on the floor than the in surrounding areas in Victoria Valley, where the inversions are particularly intense in comparison to other valleys. No MAGT inversions were modelled in the Wright Valley, at only 50 m a.s.l (though winter temperature

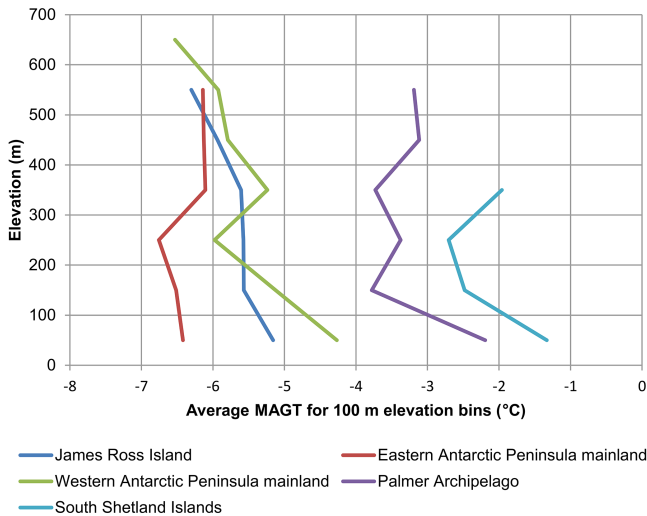


**Figure 17.** Altitudinal MAGT gradients for the northern Antarctic Peninsula calculated for 100 m elevation bins.

inversions do occur there), or in the Taylor Valley, which is opened to the coast and can drain cold air.

### 4.3 Model performance and limitations

As the LST data are primarily derived from satellite data, their availability and accuracy depend on cloud cover. On one hand the frequent cloud cover might be a reason for general underestimation of modelled MAGT at Antarctic Peninsula. However, the clear-sky conditions in the McMurdo Dry Valleys might explain the relatively successful modelling results in this area.

The absence of vegetation in the Antarctic results in high snow redistribution by wind and highly spatially variable snow cover, which influences ground temperatures in many parts of the Antarctic (Guglielmin et al., 2014; Ramos et al., 2017; Ferreira et al., 2017). Neither snow redistribution nor sublimation are simulated by our snowfall model, and the average snow depths could not be estimated, so  $n_f$  factors could not be derived for the Antarctic in the same manner as was done for the Northern Hemisphere by Obu et al. (2019a). Although an ensemble of 200 model runs with varying annual snowfall is used, the mean of the ensemble runs does not always represent the borehole site microclimate and ground properties. In the case of wind-exposed nunataks where the snow presence is overestimated on larger areas, such as Flårjuven Bluff and Vesleskarvet, the MAGTs were overestimated by up to 4 °C, but the modelled ensemble minimum still approached the measured MAGT.

Several permafrost and active-layer studies in the Antarctic have noted occurrence of  $n_f$  factors above 1 (Lacelle et al., 2016; Kotzé and Meiklejohn, 2017), which indicates that average air temperatures are higher than ground surface temperatures. The likely explanation could be a presence of

snow during the warmer part of the year, which is insulating ground from heat, unlike from cold in the winter. However Kotzé and Meiklejohn (2017) mention also a presence of blocky deposits at the Vesleskarvet site, which could result in ground cooling due to cold air advection. The concept of  $n_f$  factors was introduced for the Northern Hemisphere to account for the effect of snow cover during freezing conditions (Smith and Riseborough, 1996), which challenges the derivation of  $n_f$  factors for TTOP modelling on the Antarctic sites with highly temporarily variable snow cover.

Ground properties such as water or organic matter contents could not be taken into account by  $r_k$  factors due to the absence of datasets on a pan-Antarctic scale. However, the  $r_k$  factors are multiplied only with TDDs in the TTOP model. The TDDs are low in comparison to FDDs in the Antarctic, which results in limited influence of the  $r_k$  factors on the results. There were no TDDs present in the Antarctic interior according to the input data. TDDs in coastal areas usually contributed less than 1 % to the whole sum of FDDs and TDDs, and this contribution increased up to 15 % at the lowland sites on the South Shetland Islands. However, ground stratigraphies are crucial for transient permafrost models in the Antarctic.

Elevation is one of the major permafrost controlling factors in the Antarctic (Vieira et al., 2010). In steep terrain, the model input datasets are less likely to be representative for the micro-locations within the modelled pixel or the borehole site, as, for example, shown on the borehole sites on the walls of the Wright Valley. A number of the Antarctic boreholes are situated in mountainous environments, which might explain some of the discrepancies between measured and modelled MAGT. Elevation uncertainties in digital elevation model are inherited by the model and reflected in the estimated average annual snowfall and downscaled ERA re-analysis temperatures. The elevations of some peaks might also not be well represented at the spatial resolution of 1 km; therefore the modelled MAGT might appear warmer than the MAGT found on the top a peak.

## 5 Conclusions

Near-surface permafrost temperatures in the Antarctic were most commonly modelled as being between −23 and −18 °C for mountainous areas rising above the Antarctic Ice Sheet. The Earth's lowest permafrost temperature of −36 °C was modelled at Mount Markham in the Queen Elizabeth Range in the Transantarctic Mountains. Coastal regions were usually characterised with ground temperatures between −14 and −8 °C, approaching 0 °C in the coastal areas of the Antarctic Peninsula and rising above 0 °C in the Antarctic islands. The regional variations in permafrost temperatures can be explained by (1) continentality, which influences permafrost temperatures, especially at elevations of up to 200 m, (2) elevation and (3) latitude, which explains differences in

permafrost temperatures at similar elevations. Snow cover and snow redistribution have strong influence on local permafrost temperature variations in the Antarctic.

Comparison of modelled temperatures to 40 permafrost boreholes and soil-climate stations yielded root-mean-square error of 1.9 °C, but the accuracy varied significantly between borehole sites. The difference was smaller than 1 °C for more than 50 % of the sites but can exceed 4 °C. The greatest differences between the modelled and measured permafrost temperatures occurred where snow conditions were not successfully represented in the model. These sites are generally exposed to a strong wind-driven redistribution of snow, as, for example, at nunataks in Queen Maud Land, on the Hobs Coast and in Marie Byrd Land. Considerable differences between modelled and measured MAGTs also occurred at sites with microclimate and ground properties that are not representative for the respective modelled 1 km<sup>2</sup> pixel. Permafrost temperatures on the walls of Wright Valley and in Granite Harbour were underestimated by up to 4 °C, which can be explained by warm microclimates of the borehole sites compared to surroundings. The model performed well in areas with frequent cloud-free conditions, such as the McMurdo Dry Valleys, where even winter air temperature inversions are reflected in the modelled permafrost temperatures. Frequent cloudy conditions on the north-western Antarctic Peninsula can to some extent explain the systematic underestimation of modelled permafrost temperatures in this area.

This study is the first continent-wide modelling of permafrost temperatures for the Antarctic. It reports near-surface permafrost temperatures for remote regions without observations, which is highly valuable for research fields, such as climate change, terrestrial ecology, microbiology or astrobiology. Our study suggests that extended networks of currently sparse borehole temperature measurements and spatially distributed information on snow cover and ground properties are crucial for improving future permafrost modelling results in the Antarctic.

## Appendix A

Table A1. List of borehole properties, measurements and modelled results. NA: not available.

| Borehole name         | Latitude  | Longitude  | Sensor depth (cm) | Elevation (m) | Measured MAGT | MAGT calculation period    | Modelled mean MAGT | Difference between modelled and measured MAGT | Modelled max MAGT | Modelled min MAGT | Modelled SD | Source                      | Soil region              |
|-----------------------|-----------|------------|-------------------|---------------|---------------|----------------------------|--------------------|---|-------------------|-------------------|-------------|-----------------------------|--------------------------|
| Johann Gregor Mendel  | -63.80000 | -57.86670  | 75                | 10            | -5.60         | 2011–2017                  | -4.98              | 0.62  | -2.83             | -6.43             | 0.89        | Hrbáček et al. (2017a)      | Antarctic Peninsula      |
| Abernethy Flats       | -63.88140 | -57.94830  | 75                | NA            | -6.15         | 2006–2016                  | -5.38              | 0.77  | -2.89             | -6.89             | 1.08        | Hrbáček et al. (2017b)      | Antarctic Peninsula      |
| Bunger Hills          | -66.27530 | 100.76000  | 500               | 7             | -8.90         | 2008–2014                  | -9.09              | -0.19   | -4.41             | -11.50            | 1.41        | Andrey Abramov              | Wilkes Land              |
| Schirmacher Hills     | -70.77177 | 11.73673   | 100               | 80            | -8.50         | 2009–2016                  | -8.19              | 0.31  | -3.91             | -9.95             | 1.08        | Andrey Abramov              | Queen Maud Land          |
| Larsemann Hills       | -69.38669 | 76.37538   | 500               | 96            | -7.80         | 2013–2015                  | -7.83              | -0.03   | -3.53             | -9.82             | 1.23        | Andrey Abramov              | Vestfold Hills           |
| Larsemann             | -69.40421 | 76.34465   | 300               | 96            | -8.60         | 2008, 2010–2015            | -7.90              | 0.70  | -3.64             | -9.76             | 1.17        | Andrey Abramov              | Vestfold Hills           |
| Landing nunatak       | -69.74781 | 73.70503   | 100               | 96            | -11.00        | 2011–2012                  | -10.08             | 0.93  | -6.10             | -12.39            | 1.33        | Andrey Abramov              | Vestfold Hills           |
| King George Island    | -62.19667 | -58.96556  | 500               | 20            | -0.70         | 2008–2009, 2014            | -2.21              | -1.51   | -0.93             | -2.75             | 0.47        | Andrey Abramov              | Antarctic Peninsula      |
| Russkaya              | -74.76333 | -136.79639 | 50                | 76            | -10.30        | 2008–2013                  | -6.86              | 3.44  | -4.06             | -10.14            | 1.66        | Andrey Abramov              | Marie Byrd Land          |
| Molodnejnaya          | -67.66556 | 45.84194   | 50                | 45            | -9.40         | 2008, 2011–2013, 2015–2016 | -7.81              | 1.59  | -4.06             | -10.19            | 1.66        | Andrey Abramov              | Enderby Land             |
| Reina Sofia           | -62.67028 | -60.38222  | NA                | 275           | -1.78         | NA                         | -3.05              | -1.27   | -1.54             | -3.97             | 0.67        | Miguel Ramos                | Antarctic Peninsula      |
| Cierva Cove           | -64.16195 | -60.95093  | 1500              | 182           | -0.95         | NA                         | -3.67              | -2.72   | -1.95             | -5.51             | 0.86        | Gonçalo Vieira              | Antarctic Peninsula      |
| Amsler                | -64.77619 | -64.06057  | 900               | 67            | -0.36         | 2016–2017                  | -1.48              | -1.12   | -0.65             | -2.42             | 0.49        | Gonçalo Vieira              | Antarctic Peninsula      |
| Crater Lake           | -62.98333 | -60.66667  | NA                | 85            | -0.83         | NA                         | -2.93              | -2.13   | -1.51             | -4.01             | 0.65        | Gonçalo Vieira              | Antarctic Peninsula      |
| Byers Peninsula       | -62.62981 | -61.06013  | NA                | 92            | -0.43         | NA                         | -2.36              | -1.90   | -1.10             | -2.95             | 0.50        | Oliva et al. (2017)         | Antarctic Peninsula      |
| Linnpolar Lake        | -62.64959 | -61.10405  | 130               | 90            | -0.60         | 2009–2012                  | -2.34              | -1.74   | -1.04             | -2.90             | 0.47        | de Pablo et al. (2014)      | Antarctic Peninsula      |
| Rothera Point         | -67.57070 | -68.11879  | NA                | 31            | -3.10         | 2009–2011                  | -2.78              | 0.32  | -1.36             | -3.95             | 0.74        | Guglielmin et al. (2014)    | Antarctic Peninsula      |
| Marambio Island       | -64.23333 | -56.61667  | NA                | 200           | -6.60         | NA                         | -5.24              | 1.36  | -3.01             | -6.58             | 0.83        | Jorge Strelin               | Antarctic Peninsula      |
| Signy Island          | -60.71655 | -45.59978  | NA                | 90            | -2.10         | 2006–2009                  | -2.11              | -0.01   | -0.97             | -2.86             | 0.45        | Guglielmin et al. (2012)    | Antarctic islands        |
| Ohridski 2 Papagal    | -62.64811 | -60.36375  | 400               | 147           | -1.04         | 2008–2018                  | -1.90              | -0.87   | -0.93             | -2.80             | 0.43        | Gonçalo Vieira              | Antarctic Peninsula      |
| Irizar 2              | -62.98263 | -60.71562  | 80                | 130           | -1.58         | 2009–2017                  | -2.49              | -0.91   | -1.21             | -3.33             | 0.60        | Gonçalo Vieira              | Antarctic Peninsula      |
| Troll Station         | -72.01139 | 2.53306    | 3                 | 1275          | -17.40        | 2007–2015                  | -17.09             | 0.31  | -9.41             | -19.56            | 1.19        | Hrbáček et al. (2018)       | Queen Maud Land          |
| Flårjuven Bluff       | -72.01167 | -3.38833   | 3                 | 1220          | -17.50        | 2008–2015                  | -13.06             | 4.45  | -6.46             | -16.84            | 2.68        | Hrbáček et al. (2018)       | Queen Maud Land          |
| Vestleskarvet         | -71.68998 | -2.84758   | 3                 | 805           | -16.10        | 2009–2014                  | -11.91             | 4.19  | -6.01             | -15.09            | 2.57        | Hrbáček et al. (2018)       | Queen Maud Land          |
| Boulder Clay          | -74.74583 | 164.02139  | NA                | 205           | -16.90        | 1996–2009                  | -14.63             | 2.27  | -8.83             | -16.78            | 1.22        | Vieira et al. (2010)        | Transantarctic Mountains |
| Oasis New             | -74.70000 | 164.10000  | NA                | 80            | -13.50        | 2005–2009                  | -13.32             | 0.18  | -8.24             | -15.08            | 0.84        | Vieira et al. (2010)        | Transantarctic Mountains |
| Bull Pass             | -77.51847 | 161.86269  | 60                | 141           | -19.44        | 2000–2017                  | -20.93             | -1.49   | -17.24            | -22.65            | 0.95        | USDA (Seybold et al., 2010) | Transantarctic Mountains |
| WV south wall         | -77.50219 | 162.06475  | 50                | 832           | -16.44        | 2013–2017                  | -20.04             | -3.60   | -17.35            | -21.64            | 0.90        | Megan Balks                 | Transantarctic Mountains |
| (Bull Pass East)      |           |            |                   |               |               |                            |                    |   |                   |                   |             |                             |                          |
| WV north wall         | -77.57388 | 161.23877  | 50                | 734           | -16.76        | 2011–2017                  | -20.83             | -4.07   | -18.33            | -22.50            | 0.82        | Megan Balks                 | Transantarctic Mountains |
| (Don Juan Pond)       |           |            |                   |               |               |                            |                    |   |                   |                   |             |                             |                          |
| Granite Harbour       | -77.00655 | 162.52561  | 66                | 6             | -14.31        | 2003–2017                  | -18.53             | -4.22   | -15.52            | -20.15            | 0.84        | USDA (Seybold et al., 2010) | Transantarctic Mountains |
| Marble Point          | -77.41955 | 163.68247  | 120               | 47            | -18.15        | 2000–2017                  | -15.99             | 2.16  | -13.67            | -17.83            | 0.65        | Megan Balks                 | Transantarctic Mountains |
| Minna Bluff           | -78.52500 | 166.78240  | 43                | 32            | -16.44        | 2007–2016                  | -16.52             | -0.07   | -10.74            | -19.03            | 1.35        | Megan Balks                 | Transantarctic Mountains |
| Mount Fleming         | -77.54519 | 160.29027  | 22                | 1697          | -23.81        | 2002–2017                  | -23.58             | 0.23  | -19.36            | -25.66            | 1.01        | Megan Balks                 | Transantarctic Mountains |
| Scott Base            | -77.84831 | 166.76058  | 40                | 44            | -17.42        | 2000–2017                  | -16.64             | 0.78  | -10.72            | -18.84            | 1.08        | Megan Balks                 | Transantarctic Mountains |
| Victoria Valley       | -77.33178 | 161.60069  | 30                | 410           | -22.87        | 2000–2017                  | -22.97             | -0.10   | -21.26            | -24.59            | 0.90        | Megan Balks                 | Transantarctic Mountains |
| Wright Valley floor   | -77.51808 | 161.85117  | 75                | NA            | -19.13        | 2000–2017                  | -20.93             | -1.79   | -17.24            | -22.65            | 0.95        | Megan Balks                 | Transantarctic Mountains |
| Marble Point borehole | -77.40732 | 163.72913  | 200               | 85            | -16.90        | 2009–2015                  | -15.96             | 0.95  | -11.46            | -17.72            | 0.83        | Guglielmin et al. (2011)    | Transantarctic Mountains |
| Baker Rocks           | -74.20750 | 164.83361  | 3                 | 11            | -15.60        | 2006–2015                  | -16.52             | -0.92   | -7.11             | -19.39            | 1.59        | Hrbáček et al. (2018)       | Transantarctic Mountains |
| Mount Dolence         | -79.82181 | -83.19714  | 30                | 886           | -18.30        | 2012–2013                  | -20.21             | -1.91   | -13.48            | -22.37            | 1.13        | Schaefer et al. (2017b)     | Ellsworth Mountains      |
| Hope Bay              | -63.40635 | -56.99656  | 80                | NA            | -4.10         | 2010                       | -3.83              | 0.27  | -1.82             | -4.97             | 0.66        | Schaefer et al. (2017a)     | Antarctic Peninsula      |

**Data availability.** The data are available for download at <https://doi.org/10.1594/PANGAEA.902576> (Obu et al., 2019c).

**Author contributions.** JO, SW, GV, AB and AK designed the conceptual framework for the study, and the model was developed and run by SW and JO. Ground validation data were contributed by GV, AA, MB, FH and MR, who also provided interpretation of results on a regional scale. JO wrote the paper, based on input and feedback from all co-authors.

**Competing interests.** The authors declare that they have no conflict of interest.

**Acknowledgements.** This work was funded by the European Space Agency Data User Element GlobPermafrost project in cooperation with ZAMG (grant number 4000116196/15/I-NB) and the Research Council of Norway SatPerm project (grant number 239918). Data storage resources were provided by Norwegian National Infrastructure for Research Data (project NS9079K). The work of Filip Hrbáček was supported by the Ministry of Education Youth and Sports of Czech Republic large infrastructure project LM2015078. Temperature data for Russian stations were obtained with the support from the Russian Antarctic Expedition and government programme AAAA-A18-118013190181-6. The PERMANTAR observatories on the western Antarctic Peninsula have been funded mainly by the Portuguese Foundation for Science and Technology and the Portuguese Polar Program. The Terra and AQUA MODIS LST datasets were acquired from the Level-1 and Atmosphere Archive and Distribution System (LAADS) Distributed Active Archive Center (DAAC), located in the Goddard Space Flight Center in Greenbelt, Maryland (<https://ladsweb.nascom.nasa.gov/>; last access: 23 May 2019). Over the years many people have contributed to installation and maintenance of the McMurdo Dry Valley Soil Climate stations, but special thanks are due to Cathy Seybold, Ron Paetzold and Don Huffman from the USDA; Jackie Aislabie and Fraser Morgan from Landcare Research, New Zealand; and Chris Morcom, Dean Sandwell and Annette Carshalton from the University of Waikato, New Zealand. Antarctica New Zealand provided logistic support for annual station access. The authors also thank Nikita Demidov, Andrey Dolgikh, Elya Zazovskaya, Nikolay Osokin, Dima Fedorov-Davidov, Andrey Ivashchenko, Alexey Lupachev and Nikita Mergelov for borehole data retrieval from the Russian Antarctic stations.

**Financial support.** This research has been supported by the European Space Agency (grant no. 4000116196/15/I-NB), the Research Council of Norway (grant no. 239918), the Norwegian National Infrastructure for Research Data (grant no. NS9079K), the Ministry of Education Youth and Sports of Czech Republic (grant no. LM2015078), and the Russian Antarctic Expedition and Government programme (grant no. AAAA-A18-118013190181-6).

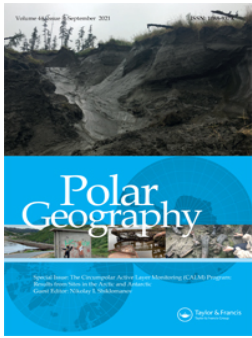
**Review statement.** This paper was edited by Christian Beer and reviewed by Joseph Levy and one anonymous referee.

## References

- Ambrozova, K., Laska, K., Hrbacek, F., Kavan, J., and Ondruch, J.: Air temperature and lapse rate variation in the ice-free and glaciated areas of northern James Ross Island, Antarctic Peninsula, during 2013–2016, *Int. J. Climatol.*, 39, 643–657, <https://doi.org/10.1002/joc.5832>, 2019.
- Beer, C.: Permafrost Sub-grid Heterogeneity of Soil Properties Key for 3-D Soil Processes and Future Climate Projections, *Front. Earth Sci.*, 4, 1–7, <https://doi.org/10.3389/feart.2016.00081>, 2016.
- Bintanja, R. and Reijmer, C. H.: A simple parameterization for snowdrift sublimation over Antarctic snow surfaces, *J. Geophys. Res.-Atmos.*, 106, 31739–31748, <https://doi.org/10.1029/2000JD000107>, 2001.
- Bockheim, J. G., Campbell, I. B., and McLeod, M.: Permafrost distribution and active-layer depths in the McMurdo Dry Valleys, Antarctica, *Permafrost Periglac.*, 18, 217–227, <https://doi.org/10.1002/ppp.588>, 2007.
- Bockheim, J. G., Campbell, I. B., Guglielmin, M., and López-Martínez, J.: Distribution of permafrost types and buried ice in icefree areas of Antarctica, in: 9th International Conference on Permafrost, 28 June–3 July 2008, Proceedings, University of Alaska Press, Fairbanks, USA, 125–130, 2008.
- Bockheim, J. G., Vieira, G., Ramos, M., López-Martínez, J., Serrano, E., Guglielmin, M., Wilhelm, K., and Nieuwendam, A.: Climate warming and permafrost dynamics in the Antarctic Peninsula region, *Global Planet. Change*, 100, 215–223, <https://doi.org/10.1016/j.gloplacha.2012.10.018>, 2013.
- Burton-Johnson, A., Black, M., Fretwell, P. T., and Kaluza-Gilbert, J.: An automated methodology for differentiating rock from snow, clouds and sea in Antarctica from Landsat 8 imagery: a new rock outcrop map and area estimation for the entire Antarctic continent, *The Cryosphere*, 10, 1665–1677, <https://doi.org/10.5194/tc-10-1665-2016>, 2016.
- Danielson, J. J. and Gesch, D. B.: Global multi-resolution terrain elevation data 2010 (GMTED2010), US Geological Survey, Reston, Virginia, USA, 2011.
- Decker, E. R. and Bucher, G. J.: Geothermal studies in Antarctica, *Antarct. J. U. S., United States*, 12:4, available at: <https://www.osti.gov/biblio/6112190> (last access: 30 September 2019), 1977.
- Dee, D. P., Uppala, S. M., Simmons, A. J., Berrisford, P., Poli, P., Kobayashi, S., Andrae, U., Balmaseda, M. A., Balsamo, G., Bauer, P., Bechtold, P., Beljaars, A. C. M., van de Berg, L., Bidlot, J., Bormann, N., Delsol, C., Dragani, R., Fuentes, M., Geer, A. J., Haimberger, L., Healy, S. B., Hersbach, H., Hólm, E. V., Isaksen, I., Kållberg, P., Köhler, M., Matricardi, M., McNally, A. P., Monge-Sanz, B. M., Morcrette, J.-J., Park, B.-K., Peubey, C., de Rosnay, P., Tavolato, C., Thépaut, J.-N., and Vitart, F.: The ERA-Interim reanalysis: configuration and performance of the data assimilation system, *Q. J. Roy. Meteor. Soc.*, 137, 553–597, <https://doi.org/10.1002/qj.828>, 2011.
- de Pablo, M. A., Ramos, M., and Molina, A.: Thermal characterization of the active layer at the Limnopolar Lake CALM-S site on Byers Peninsula (Livingston Island), Antarctica, *Solid Earth*, 5, 721–739, <https://doi.org/10.5194/se-5-721-2014>, 2014.
- de Pablo, M. A., Ramos, M., and Molina, A.: Snow cover evolution, on 2009–2014, at the Limnopolar Lake CALM-S site on Byers Peninsula, Livingston Island, Antarctica, *CATENA*, 149, 538–547, <https://doi.org/10.1016/j.catena.2016.06.002>, 2017.

- Ferreira, A., Vieira, G., Ramos, M., and Nieuwendam, A.: Ground temperature and permafrost distribution in Hurd Peninsula (Livingston Island, Maritime Antarctic): An assessment using freezing indexes and TTOP modelling, *CATENA*, 149, 560–571, <https://doi.org/10.1016/j.catena.2016.08.027>, 2017.
- Fiddes, J. and Gruber, S.: TopoSCALE v.1.0: downscaling gridded climate data in complex terrain, *Geosci. Model Dev.*, 7, 387–405, <https://doi.org/10.5194/gmd-7-387-2014>, 2014.
- Gallée, H.: Simulation of blowing snow over the Antarctic ice sheet, *Ann. Glaciol.*, 26, 203–206, <https://doi.org/10.3189/1998AoS26-1-203-206>, 1998.
- Gisnås, K., Etzelmüller, B., Farbrot, H., Schuler, T. V., and Westermann, S.: CryoGRID 1.0: Permafrost Distribution in Norway estimated by a Spatial Numerical Model, *Permafrost Periglac.*, 24, 2–19, <https://doi.org/10.1002/ppp.1765>, 2013.
- Gisnås, K., Westermann, S., Schuler, T. V., Litherland, T., Isaksen, K., Boike, J., and Etzelmüller, B.: A statistical approach to represent small-scale variability of permafrost temperatures due to snow cover, *The Cryosphere*, 8, 2063–2074, <https://doi.org/10.5194/tc-8-2063-2014>, 2014.
- Gisnås, K., Westermann, S., Schuler, T. V., Melvold, K., and Etzelmüller, B.: Small-scale variation of snow in a regional permafrost model, *The Cryosphere*, 10, 1201–1215, <https://doi.org/10.5194/tc-10-1201-2016>, 2016.
- Greene, S. W., Gressitt, J., Koob, D., Llano, G., Rudolf, E. D., Singer, R., Sreere, W. C., and Ugolini, F. C.: *Terrestrial life of Antarctica*. Antarctic Map Folio Series, Nat. Geogr. Soc., New York, USA, 1967.
- Guglielmin, M.: Ground surface temperature (GST), active layer and permafrost monitoring in continental Antarctica, *Permafrost Periglac.*, 17, 133–143, <https://doi.org/10.1002/ppp.553>, 2006.
- Guglielmin, M.: Advances in permafrost and periglacial research in Antarctica: A review, *Geomorphology*, 155–156, 1–6, <https://doi.org/10.1016/j.geomorph.2011.12.008>, 2012.
- Guglielmin, M., Balks, M. R., Adlam, L. S., and Baio, F.: Permafrost thermal regime from two 30-m deep boreholes in southern Victoria land, Antarctica, *Permafrost Periglac.*, 22, 129–139, <https://doi.org/10.1002/ppp.715>, 2011.
- Guglielmin, M., Worland, M. R., and Cannone, N.: Spatial and temporal variability of ground surface temperature and active layer thickness at the margin of maritime Antarctica, Signy Island, *Geomorphology*, 155–156, 20–33, <https://doi.org/10.1016/j.geomorph.2011.12.016>, 2012.
- Guglielmin, M., Worland, M. R., Baio, F., and Convey, P.: Permafrost and snow monitoring at Rothera Point (Adelaide Island, Maritime Antarctica): Implications for rock weathering in cryotic conditions, *Geomorphology*, 225, 47–56, <https://doi.org/10.1016/j.geomorph.2014.03.051>, 2014.
- Hersbach, H. and Dee, D.: ERA5 reanalysis is in production, *ECMWF newsletter*, 147, 5–6, 2016.
- Hevesi, J. A., Istok, J. D., and Flint, A. L.: Precipitation Estimation in Mountainous Terrain Using Multivariate Geostatistics. Part I: Structural Analysis, *J. Appl. Meteorol.*, 31, 661–676, [https://doi.org/10.1175/1520-0450\(1992\)031<0661:PEIMTU>2.0.CO;2](https://doi.org/10.1175/1520-0450(1992)031<0661:PEIMTU>2.0.CO;2), 1992.
- Hrbáček, F., Láska, K., and Engel, Z.: Effect of Snow Cover on the Active-Layer Thermal Regime – A Case Study from James Ross Island, Antarctic Peninsula, *Permafrost Periglac.*, 27, 307–315, <https://doi.org/10.1002/ppp.1871>, 2016.
- Hrbáček, F., Kňazková, M., Nývt, D., Láska, K., Mueller, C. W., and Ondruch, J.: Active layer monitoring at CALM-S site near J.G. Mendel Station, James Ross Island, eastern Antarctic Peninsula, *Sci. Total Environ.*, 601–602, 987–997, <https://doi.org/10.1016/j.scitotenv.2017.05.266>, 2017a.
- Hrbáček, F., Nývt, D., and Láska, K.: Active layer thermal dynamics at two lithologically different sites on James Ross Island, Eastern Antarctic Peninsula, *CATENA*, 149, 592–602, <https://doi.org/10.1016/j.catena.2016.06.020>, 2017b.
- Hrbáček, F., Vieira, G., Oliva, M., Balks, M., Guglielmin, M., de Pablo, M. Á., Molina, A., Ramos, M., Goyanes, G., Meiklejohn, I., Abramov, A., Demidov, N., Fedorov-Davydov, D., Lupachev, A., Rivkina, E., Láska, K., Kňazková, M., Nývt, D., Raffi, R., Strelin, J., Sone, T., Fukui, K., Dolgikh, A., Zazovskaya, E., Mergelov, N., Osokin, N., and Miamin, V.: Active layer monitoring in Antarctica: an overview of results from 2006 to 2015, *Polar Geogr.*, Taylor & Francis, 1–15, <https://doi.org/10.1080/1088937X.2017.1420105>, 2018.
- Humlum, O., Instanes, A., and Sollid, J. L.: Permafrost in Svalbard: a review of research history, climatic background and engineering challenges, *Polar Res.*, 22, 191–215, <https://doi.org/10.1111/j.1751-8369.2003.tb00107.x>, 2003.
- Kotzé, C. and Meiklejohn, I.: Temporal variability of ground thermal regimes on the northern buttress of the Vesleskarvet nunatak, western Dronning Maud Land, Antarctica, *Antarct. Sci.*, 29, 73–81, <https://doi.org/10.1017/S095410201600047X>, 2017.
- Lacelle, D., Lapalme, C., Davila, A. F., Pollard, W., Marinova, M., Heldmann, J., and McKay, C. P.: Solar Radiation and Air and Ground Temperature Relations in the Cold and Hyper-Arid Quartermain Mountains, McMurdo Dry Valleys of Antarctica, *Permafrost Periglac.*, 27, 163–176, <https://doi.org/10.1002/ppp.1859>, 2016.
- Levy, J.: How big are the McMurdo Dry Valleys? Estimating ice-free area using Landsat image data, *Antarctic Science*, 25, 119–120, <https://doi.org/10.1017/S0954102012000727>, 2013.
- Liston, G. E.: Representing Subgrid Snow Cover Heterogeneities in Regional and Global Models, *J. Climate*, 17, 1381–1397, [https://doi.org/10.1175/1520-0442\(2004\)017<1381:RSSCHI>2.0.CO;2](https://doi.org/10.1175/1520-0442(2004)017<1381:RSSCHI>2.0.CO;2), 2004.
- Obu, J., Westermann, S., Bartsch, A., Berdnikov, N., Christiansen, H. H., Dashtseren, A., Delaloye, R., Elberling, B., Etzelmüller, B., Kholodov, A., Khomutov, A., Kääh, A., Leibman, M. O., Lewkowicz, A. G., Panda, S. K., Romanovsky, V., Way, R. G., Westergaard-Nielsen, A., Wu, T., Yamkhin, J., and Zou, D.: Northern Hemisphere permafrost map based on TTOP modelling for 2000–2016 at 1 km<sup>2</sup> scale, *Earth-Sci. Rev.*, 193, 299–316, <https://doi.org/10.1016/j.earscirev.2019.04.023>, 2019a.
- Obu, J., Westermann, S., Kääh, A., and Bartsch, A.: Ground Temperature Map, 2000–2016, Andes, New Zealand and East African Plateau Permafrost, University of Oslo, <https://doi.org/10.1594/PANGAEA.905512>, 2019b.
- Obu, J., Westermann, S., Kääh, A., and Bartsch, A.: Ground Temperature Map, 2000–2017, Antarctic, University of Oslo, PANGAEA, <https://doi.org/10.1594/PANGAEA.902576>, 2019c.
- Oliva, M., Hrbáček, F., Ruiz-Fernández, J., de Pablo, M. Á., Vieira, G., Ramos, M., and Antoniadou, D.: Active layer dynamics in three topographically distinct lake catchments in Byers Peninsula (Livingston Island, Antarctica), *CATENA*, 149, 548–559, <https://doi.org/10.1016/j.catena.2016.07.011>, 2017.

- Østby, T. I., Schuler, T. V., and Westermann, S.: Severe cloud contamination of MODIS Land Surface Temperatures over an Arctic ice cap, Svalbard, *Remote Sensing of Environment*, 142, 95–102, <https://doi.org/10.1016/j.rse.2013.11.005>, 2014.
- Raffi, R. and Stenni, B.: Isotopic composition and thermal regime of ice wedges in northern Victoria Land, East Antarctica, *Permafrost Periglac.*, 22, 65–83, <https://doi.org/10.1002/ppp.701>, 2011.
- Ramos, M., Vieira, G., de Pablo, M. A., Molina, A., Abramov, A., and Goyanes, G.: Recent shallowing of the thaw depth at Crater Lake, Deception Island, Antarctica (2006–2014), *CATENA*, 149, 519–528, <https://doi.org/10.1016/j.catena.2016.07.019>, 2017.
- Rocha, M. J., Dutra, E., Tomé, R., Vieira, G., Miranda, P., Fragoso, M., and Ramos, M.: ERA-Interim forced H-TESSEL scheme for modeling ground temperatures for Livingston Island (South Shetlands, Antarctic Peninsula), in: *Proceedings of II Iberian Conference of the International Permafrost Association: Periglacial, Environments, Permafrost and Climate Variability: Colección Obras colectivas, Universidad de Alcalá, Sigüenza, Spain, 21–23 June 2009*, 2010.
- Romanovsky, V. E. and Osterkamp, T. E.: Interannual variations of the thermal regime of the active layer and near-surface permafrost in northern Alaska, *Permafrost Periglac.*, 6, 313–335, <https://doi.org/10.1002/ppp.3430060404>, 1995.
- Roth, G., Matsuoka, K., Skoglund, A., Melvær, Y., and Tronstad, S.: Quantarctica: A Unique, Open, Standalone GIS Package for Antarctic Research and Education, in: *EGU General Assembly Conference Abstracts*, 23–28 April 2017, Vienna, Austria, vol. 19, p. 1973, 2017.
- Schaefer, C. E. G. R., Pereira, T. T. C., Almeida, I. C. C., Michel, R. F. M., Corrêa, G. R., Figueiredo, L. P. S., and Ker, J. C.: Penguin activity modify the thermal regime of active layer in Antarctica: A case study from Hope Bay, *CATENA*, 149, 582–591, <https://doi.org/10.1016/j.catena.2016.07.021>, 2017a.
- Schaefer, C. E. G. R., Michel, R. F. M., Delpupo, C., Senra, E. O., Bremer, U. F., and Bockheim, J. G.: Active layer thermal monitoring of a Dry Valley of the Ellsworth Mountains, Continental Antarctica, *CATENA*, 149, 603–615, <https://doi.org/10.1016/j.catena.2016.07.020>, 2017b.
- Seybold, C. A., Balks, M. R., and Harms, D. S.: Characterization of active layer water contents in the McMurdo Sound region, Antarctica, *Antarct. Sci.*, 22, 633–645, <https://doi.org/10.1017/S0954102010000696>, 2010.
- Shiklomanov, N. I.: From Exploration to Systematic Investigation: Development of Geocryology in 19th- and Early-20th-Century Russia, *Phys. Geogr.*, 26, 249–263, <https://doi.org/10.2747/0272-3646.26.4.249>, 2005.
- Smith, M. W. and Riseborough, D. W.: Permafrost monitoring and detection of climate change, *Permafrost Periglac.*, 7, 301–309, [https://doi.org/10.1002/\(SICI\)1099-1530\(199610\)7:4<301::AID-PPP231>3.0.CO;2-R](https://doi.org/10.1002/(SICI)1099-1530(199610)7:4<301::AID-PPP231>3.0.CO;2-R), 1996.
- Smith, M. W. and Riseborough, D. W.: Climate and the limits of permafrost: a zonal analysis, *Permafrost Periglac.*, 13, 1–15, <https://doi.org/10.1002/ppp.410>, 2002.
- Soliman, A., Duguay, C., Saunders, W., and Hachem, S.: Pan-Arctic Land Surface Temperature from MODIS and AATSR: Product Development and Intercomparison, *Remote Sens.*, 4, 3833–3856, <https://doi.org/10.3390/rs4123833>, 2012.
- Vieira, G., Bockheim, J., Guglielmin, M., Balks, M., Abramov, A. A., Boelhouwers, J., Cannone, N., Ganzert, L., Gilichinsky, D. A., Goryachkin, S., López-Martínez, J., Meiklejohn, I., Raffi, R., Ramos, M., Schaefer, C., Serrano, E., Simas, F., Sletten, R., and Wagner, D.: Thermal state of permafrost and active-layer monitoring in the antarctic: Advances during the international polar year 2007–2009, *Permafrost Periglac.*, 21, 182–197, <https://doi.org/10.1002/ppp.685>, 2010.
- Wan, Z.: New refinements and validation of the collection-6 MODIS land-surface temperature/emissivity product, *Remote Sens. Environ.*, 140, 36–45, <https://doi.org/10.1016/j.rse.2013.08.027>, 2014.
- Westermann, S., Langer, M., and Boike, J.: Systematic bias of average winter-time land surface temperatures inferred from MODIS at a site on Svalbard, Norway, *Remote Sens. Environ.*, 118, 162–167, <https://doi.org/10.1016/j.rse.2011.10.025>, 2012.
- Westermann, S., Østby, T. I., Gislås, K., Schuler, T. V., and Etzelmüller, B.: A ground temperature map of the North Atlantic permafrost region based on remote sensing and reanalysis data, *The Cryosphere*, 9, 1303–1319, <https://doi.org/10.5194/tc-9-1303-2015>, 2015.
- Zhang, Y., Olthof, I., Fraser, R., and Wolfe, S. A.: A new approach to mapping permafrost and change incorporating uncertainties in ground conditions and climate projections, *The Cryosphere*, 8, 2177–2194, <https://doi.org/10.5194/tc-8-2177-2014>, 2014.



## Active layer monitoring in Antarctica: an overview of results from 2006 to 2015

Filip Hrbáček, Goncalo Vieira, Marc Oliva, Megan Balks, Mauro Guglielmin, Miguel Ángel de Pablo, Antonio Molina, Miguel Ramos, Gabriel Goyanes, Ian Meiklejohn, Andrey Abramov, Nikita Demidov, Dmitry Fedorov-Davydov, Alexey Lupachev, Elizaveta Rivkina, Kamil Láska, Michaela Kňázková, Daniel Nývlt, Rossana Raffi, Jorge Strelin, Toshio Sone, Kotaro Fukui, Andrey Dolgikh, Elya Zazovskaya, Nikita Mergelov, Nikolay Osokin & Vladislav Miamin

**To cite this article:** Filip Hrbáček, Goncalo Vieira, Marc Oliva, Megan Balks, Mauro Guglielmin, Miguel Ángel de Pablo, Antonio Molina, Miguel Ramos, Gabriel Goyanes, Ian Meiklejohn, Andrey Abramov, Nikita Demidov, Dmitry Fedorov-Davydov, Alexey Lupachev, Elizaveta Rivkina, Kamil Láska, Michaela Kňázková, Daniel Nývlt, Rossana Raffi, Jorge Strelin, Toshio Sone, Kotaro Fukui, Andrey Dolgikh, Elya Zazovskaya, Nikita Mergelov, Nikolay Osokin & Vladislav Miamin (2021) Active layer monitoring in Antarctica: an overview of results from 2006 to 2015, *Polar Geography*, 44:3, 217-231, DOI: [10.1080/1088937X.2017.1420105](https://doi.org/10.1080/1088937X.2017.1420105)

**To link to this article:** <https://doi.org/10.1080/1088937X.2017.1420105>



Published online: 11 Jan 2018.



Submit your article to this journal [↗](#)



Article views: 790



View related articles [↗](#)



View Crossmark data [↗](#)



Citing articles: 11 View citing articles [↗](#)



## Active layer monitoring in Antarctica: an overview of results from 2006 to 2015

Filip Hrbáček<sup>a</sup>, Goncalo Vieira<sup>b</sup>, Marc Oliva<sup>c</sup>, Megan Balks<sup>d</sup>, Mauro Guglielmin<sup>e</sup>, Miguel Ángel de Pablo<sup>f</sup>, Antonio Molina<sup>f</sup>, Miguel Ramos<sup>g</sup>, Gabriel Goyanes<sup>h</sup>, Ian Meiklejohn<sup>i</sup>, Andrey Abramov<sup>j</sup>, Nikita Demidov<sup>j</sup>, Dmitry Fedorov-Davydov<sup>j</sup>, Alexey Lupachev<sup>j</sup>, Elizaveta Rivkina<sup>j</sup>, Kamil Láska<sup>a</sup>, Michaela Křážková<sup>a</sup>, Daniel Nývlt<sup>a</sup>, Rossana Raffi<sup>k</sup>, Jorge Strelin<sup>l</sup>, Toshio Sone<sup>m</sup>, Kotaro Fukui<sup>n</sup>, Andrey Dolgikh<sup>o</sup>, Elya Zazovskaya<sup>o</sup>, Nikita Mergelov<sup>o</sup>, Nikolay Osokin<sup>p</sup> and Vladislav Miamin<sup>q</sup>

<sup>a</sup>Faculty of Science, Department of Geography, Masaryk University, Brno, Czech Republic; <sup>b</sup>CEG/IGOT, Universidade de Lisboa, Lisboa, Portugal; <sup>c</sup>Department of Geography, Universitat de Barcelona, Barcelona, Spain; <sup>d</sup>Faculty of Science and Engineering, University of Waikato, Hamilton, New Zealand; <sup>e</sup>Department of Theoretical and Applied Sciences, Insubria University, Varese, Italy; <sup>f</sup>Department of Geology, Geography and Environment, University of Alcalá, Madrid, Spain; <sup>g</sup>Department of Physics and Mathematics, University of Alcalá, Madrid, Spain; <sup>h</sup>Department of Geology, University of Buenos Aires, Buenos Aires, Argentina; <sup>i</sup>Department of Geography, Rhodes University, Grahamstown, South Africa; <sup>j</sup>Soil Cryology Lab, Institute of Physicochemical and Biological Problems in Soil Science, Moscow, Russia; <sup>k</sup>Department of Earth Sciences, Sapienza University of Rome, Rome, Italy; <sup>l</sup>Ciencias Exactas Físicas y Naturales Universidad de Córdoba, Córdoba, Argentina; <sup>m</sup>Institute of Low Temperature Science, Hokkaido University, Sapporo, Japan; <sup>n</sup>National Institute of Polar Research, Tachikawa, Japan; <sup>o</sup>Department of Soil Geography and Evolution, Institute of Geography, Russian Academy of Sciences, Moscow, Russia; <sup>p</sup>Department of Glaciology, Institute of Geography, Russian Academy of Sciences, Moscow, Russia; <sup>q</sup>Department of Biology, Scientific and Practical Center for Bioresources, National Academy of Sciences of Belarus, Minsk, Belarus

### ABSTRACT

Monitoring of active layer thawing depth and active layer thickness (ALT), using mechanical pronging and continuous temperature data logging, has been undertaken under the Circumpolar Active Layer Monitoring – South (CALM-S) program at a range of sites across Antarctica. The objective of this study was to summarize key data from sites in different Antarctic regions from 2006 to 2015 to review the state of the active layer in Antarctica and the effectiveness of the CALM-S program. The data from 16 sites involving 8 CALM-S and another 8 boreholes across the Antarctic have been used in the study. Probing for thaw depth, while giving information on local spatial variability, often underestimates the maximum ALT of Antarctic soils compared to that determined using continuous temperature monitoring. The differences are likely to be caused by stones limiting probe penetration and the timing of probing not coinciding with the timing of maximum thaw, which varies between seasons. The information on the active layer depth is still sparse in many regions and the monitoring needs to be extended and continued to provide a better understanding of both spatial and temporal variability in Antarctic soil thermal properties.

### ARTICLE HISTORY

Received 22 May 2017  
Accepted 18 December 2017

### KEYWORDS

CALM-S; active layer thickness; ground temperature; Antarctica; active layer monitoring; climate

## Introduction

Antarctica is the coldest continent on Earth and contains about 90% of the World's ice. Apparently, less than 25% (ca. 3.5 mil km<sup>2</sup>) of Antarctica has sub-glacial permafrost

(Bockheim, 1995), and only about 30,900 km<sup>2</sup> of Antarctica comprises ice-free land (Burton-Johnson, Black, Fretwell, & Kaluza-Gilbert, 2016), which is mostly distributed around the continent margins and in nunataks. The largest ice-free areas are located in Victoria Land and the Transantarctic Mountains (about 19,750 km<sup>2</sup>). East Antarctica has about 6930 km<sup>2</sup> of ice-free land, including the Vestfold Hills (about 2750 km<sup>2</sup>), Queen Maud Land (about 2430 km<sup>2</sup>), Enderby Land (about 1140 km<sup>2</sup>) and Wilkes Land (about 400 km<sup>2</sup>). Western Antarctica includes three ice-free regions, the Antarctic Peninsula (about 3800 km<sup>2</sup>), the Ellsworth Mountains (about 380 km<sup>2</sup>) and Marie Byrd Land (about 210 km<sup>2</sup>). Ice-free areas are the unique environments in Antarctica where the active layer can be monitored. Active layer research in Antarctic ice-free areas includes a range of environments with varying topography, geology and climate. Thus, the study of active layer properties in different regions is important to understand the main driving factors affecting local thermal regimes and active layer thickness (ALT).

Significant advances in active layer monitoring have been made since the International Polar Year (IPY, 2007–2009), during which the number of temperature monitoring boreholes in Antarctica increased from 24 to 73 (Vieira et al., 2010). Now there are almost 100 Antarctic ground temperature monitoring sites included in the Global Terrestrial Network for Permafrost (GTN-P) database. The highest densities of boreholes are in the Antarctic Peninsula region and in the Dry Valleys in Victoria Land.

The number of studies on active layer dynamics in the Antarctic increased since 2010 and most of them have focused on characterization of the active layer thermal regime in boreholes located in soils or sediments (e.g. Bockheim, 2015; de Pablo, Ramos, & Molina, 2014; Kotzé & Meiklejohn, 2017; Schaefer et al., 2017) as well as on their climate control (Guglielmin & Cannone, 2012; Lacelle et al., 2016). Important progress has been made in understanding the effect of snow on active layer dynamics, mainly in the Antarctic Peninsula region (e.g. Guglielmin, Worland, Baio, & Convey, 2014; Hrbáček, Láška, & Engel, 2016; de Pablo, Ramos, & Molina, 2017; Oliva, Hrbáček, et al., 2017; Ferreira, Vieira, Ramos, & Nieuwendam, 2017). Other recent studies have focused on the effects of vegetation (Guglielmin, Dalle Fratte, & Cannone, 2014; Michel et al., 2012), lithological or ground thermal properties (Goyanes, Vieira, Caselli, Mora, et al., 2014; Hrbáček, Kňázková, et al., 2017; Hrbáček, Nývt, & Láška, 2017), the active layer thermal regime and thickness, and the thermal regime in the deep boreholes in bedrock (Correia, Vieira, & Ramos, 2012; Guglielmin, Balks, Adlam, & Baio, 2011; Guglielmin, Worland, et al., 2014). The procedures for monitoring active layer dynamics, included in the Circumpolar Active Layer Monitoring (CALM) protocol, were standardized for Arctic regions by Brown, Hinkel, and Nelson (2000). Guglielmin (2006) implemented the CALM protocol in Antarctica and defined its southern form (CALM-S), which he adapted for Antarctic conditions. The CALM-S approach has been applied in various regions across Antarctica (e.g. Guglielmin, Worland, & Cannone, 2012; de Pablo et al., 2013; Guglielmin & Cannone, 2012; Ramos et al., 2017; Hrbáček, Kňázková, et al., 2017). Currently, around 15 CALM-S sites are estimated to be active in Antarctica according to the GTN-P database.

Despite the increase in CALM-S sites, recent studies focused primarily on only one or two sites and a regional perspective on the variability of active layer properties across Antarctica is still lacking. Regional synthesis is mainly limited to the Antarctic Peninsula region (e.g. Bockheim et al., 2013) and the McMurdo Dry Valleys (e.g. Adlam, Balks, Seybold, & Campbell, 2010), while the only overview for Antarctica has been conducted after the International Polar Year in 2007–2009 (Vieira et al., 2010). This work showed the gradient of ground

temperature and ALT from the warmest areas in Antarctic Peninsula (ALT of 0.3–4 m) to the coldest areas in mountainous regions of Eastern Antarctica and Victoria Land (ALT of 0.1–0.5 m).

The main objective of this paper is to present an updated overview of the current state, the active layer at selected CALM-S sites and selected active layer boreholes for three sectors of Antarctica. The assessment focuses on mean annual air and ground temperatures (MAAT and MAGT), thaw depth and ALT as key variables of the active layer thermal state. The selected sites explore the potential importance of the growing dataset to understanding permafrost and climate effects in the ice-free regions of Antarctica. The strengths and weaknesses of the current data collection efforts are assessed and areas for future development are considered.

## Methodology

### *CALM-S sites*

In this study, MAAT and MAGT probed active layer thaw depth (referred to here as ‘thaw depth’), thermally defined ALT and ground temperatures were studied at eight CALM-S sites in Antarctica and additionally in eight boreholes. The CALM-S sites reported in this study are located in the Antarctica Peninsula region (five), and on the coastal fringe of Eastern Antarctica (three) (Table 1 and Figure 1). The boreholes used in this study are representative of ice-free regions in Antarctica where CALM-S sites could not be established due to lithological terrain properties containing a large volume of coarse fraction impeding active layer probing. Areas with continuous temperature monitoring, rather than probing for thaw depth, include the McMurdo dry valleys (four) Eastern Antarctica (three) and the Antarctic Peninsula (one) (Table 1 and Figure 1).

The original CALM protocol, which focused on understanding local thaw depth variability (Brown et al., 2000), was modified to better suit Antarctic conditions for Circumpolar Active Layer Monitoring – South (CALM-S). The main difference was enabling probing in smaller, or irregular, grids instead of the standard 100 × 100 m grid as coarse and rocky terrain is difficult to effectively probe for depth to ice cement (Guglielmin, 2006) and some Dry Valley sites do not have sufficient moisture to form ice cement. Prevailing ground properties of coarse and rocky texture in Antarctica often prevent active layer probing and make this method possible to apply in some areas only. Other limitations of CALM-S probing measurements in Antarctica are also related to climate and logistic constraints, which may prevent grid measurement at, or close to, the date of maximum ALT during the thawing seasons (Guglielmin, 2006). Therefore, the active layer thaw depth measured, by probing, annually at around the same date, was used as a representative approach.

MAAT and MAGT data cover the period from 2006 to 2015; however, at several sites, the period is shorter or not continuous (Table 1).

### *Active layer thermal and thickness monitoring*

Monitoring of ground temperatures in Antarctica has been undertaken both in shallow (e.g. Guglielmin & Cannone, 2012; Guglielmin, 2006; Guglielmin, Dalle Fratte, et al., 2014; Goyanes, Vieira, Caselli, Cardoso, et al., 2014; Goyanes, Vieira, Caselli, Mora, et al., 2014; de Pablo et al., 2014) and deep boreholes (e.g. Bockheim et al., 2013; Correia et al., 2012;

**Table 1.** Summary of CALM-S sites and boreholes in Antarctica selected for this study.

| Region              | Locality            | Site             | Period                 | CALM-S | Cont. | Lat.   | Long.  | Altitude (m asl.) | Borehole (m)     |
|---------------------|---------------------|------------------|------------------------|--------|-------|--------|--------|-------------------|------------------|
| Antarctic Peninsula | Deception Island    | Collado Irizar   | 2009–2015              | Yes    | Yes   | –62.98 | –60.67 | 130               | 1.6              |
|                     | Deception Island    | Crater Lake      | 2006–2015              | Yes    | Yes   | –62.98 | –60.72 | 85                | 4.5              |
|                     | Livingston Island   | Limnopolar Lake  | 2009–2015              | Yes    | No    | –62.65 | –60.11 | 80                | 1.3              |
|                     | King George Island  | Bellingshausen   | 2006–2015 <sup>a</sup> | Yes    | No    | –62.19 | –58.98 | 18                | 9.5 <sup>b</sup> |
|                     | James Ross Island   | J. G. Mendel     | 2012–2015              | Yes    | Yes   | –63.8  | –57.88 | 10                | 2.0              |
|                     | James Ross Island   | Rink Point       | 2006–2014              | No     | Yes   | –63.90 | –58.22 | 400               | 1.0              |
| East Antarctica     | Enderby Land        | Molodyozhnaya    | 2008–2015              | Yes    | No    | –67.66 | –45.86 | 26                | 1.0 <sup>b</sup> |
|                     | Queen Maud Land     | Novolazarevskaya | 2010–2015 <sup>a</sup> | Yes    | No    | –70.46 | 11.47  | 94                | 3.0 <sup>b</sup> |
|                     | Queen Maud Land     | Vesleskarvet     | 2009–2014              | No     | No    | –71.69 | –2.84  | 805               | 0.6              |
|                     | Queen Maud Land     | Flårjuven        | 2008–2015              | No     | No    | –72.01 | –3.39  | 1220              | 0.6              |
|                     | Quenn Maud Land     | Trol             | 2007–2015              | No     | No    | –72.01 | 2.53   | 1320              | 2.0              |
|                     | Vestfold Hills      | Progress         | 2008–2015              | Yes    | No    | –69.24 | 76.2   | 90                | 3.2              |
| Victoria Land       | McMurdo             | Scott Base       | 2006–2015              | No     | No    | –77.85 | 166.76 | 38                | 1.2              |
|                     | McMurdo Dry Valleys | Wright Valley    | 2006–2015              | No     | Yes   | –77.52 | 161.87 | 150               | 1.2              |
|                     | McMurdo Dry Valleys | Mount Fleming    | 2006–2015              | No     | No    | –77.55 | 160.29 | 1700              | 1.0              |
|                     | Wood Bay            | Baker Rocks      | 2006–2015              | No     | Yes   | –74.21 | 164.83 | 11                | 1.6              |

Note: Cont., continuous temperature data series in period 2006–2015; NA, not available.

<sup>a</sup>Data of MAAT was completed from READER database.

<sup>b</sup>Outside CALM-S grid, drilled in bedrock

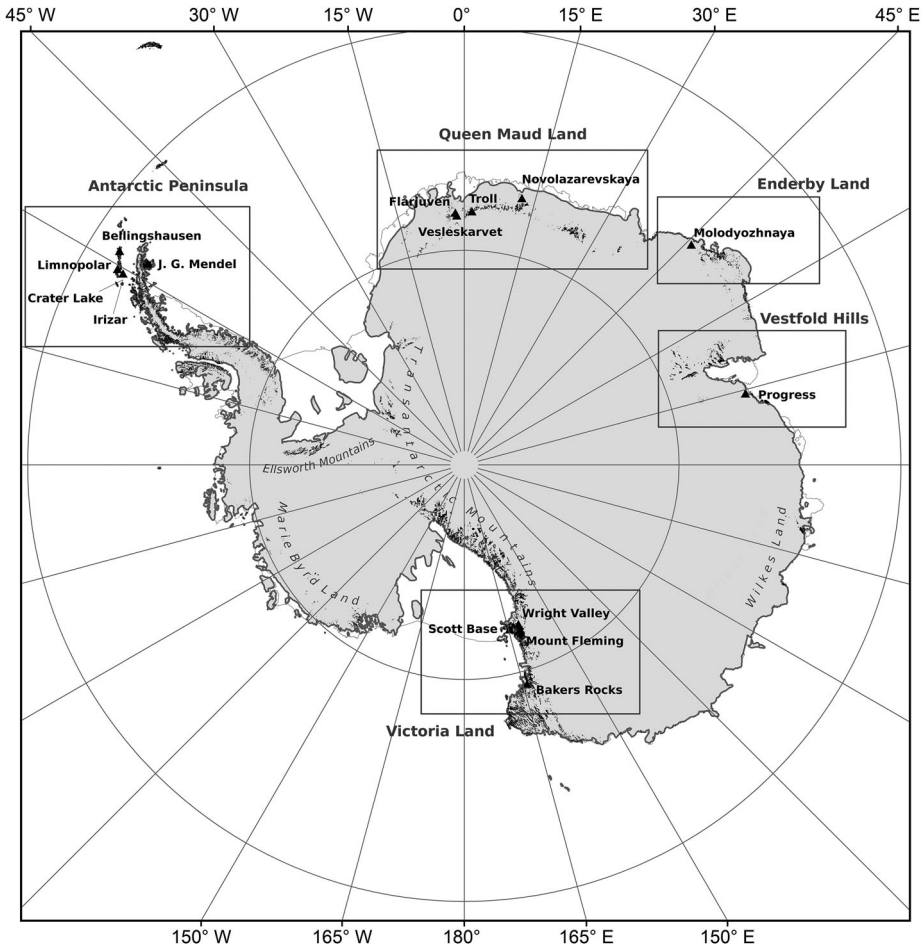


**Figure 1.** Localization of study sites across Antarctica continent. The ice-free regions are marked with black, the glaciers by gray color.

Guglielmin et al., 2011, 2014; Ramos, Hassler, Vieira, Hauck, & Gruber, 2009) or using sensors directly placed in the soil profile (e.g. Adlam et al., 2010; Raffi & Stenni, 2011; Michel et al., 2012; Hrbáček, Láška, et al., 2016; Kotzé & Meiklejohn, 2017). Near-surface ground temperature data are available from the majority of the study sites (Table 2). One of the main inconsistencies is in the position of the near-surface thermistor. Despite the effort carried out by the ‘Antarctic Permafrost, Soils and Periglacial Environments’ (ANTPAS) group, which was approved as a core project of International Permafrost Association for Antarctic research, the proposed protocols for ground thermal monitoring have not been fully implemented yet. Currently, there are differences between sites with regard to the sensor depths in the ground as well as the height of air temperature measurement, accuracy of thermistors and measurement intervals. The near-surface thermistor is recommended to be placed at 2 cm (Guglielmin, 2006); however, it has been placed at depths of between 1 and 5 cm. Also, given the uneven nature of many Antarctic surface pavements, accurate determination of shallow depths is difficult. Similarly, the position of thermistors in the lower parts of profiles, or boreholes depth used, tends to be specific for each site depending on variables such as the ALT, soil texture or drill depth.

**Table 2.** Characteristics of MAAT and MAGT (2–5 cm depth) and mean probed thaw depth (MPTD) and mean active layer thickness (MALT) in the different study sites during the period 2006–2015.

| Region              | Locality           | Site                 | Period    | MAAT  | MAGT  | MPTD | MALT                             |
|---------------------|--------------------|----------------------|-----------|-------|-------|------|----------------------------------|
| Antarctic Peninsula | Deception Island   | Collado Irizar       | 2009–2015 | −3.1  | −2.2  | 54   | 85                               |
|                     | Deception Island   | Crater Lake          | 2006–2015 | −2.8  | −1.6  | 29   | 45                               |
|                     | Livingston Island  | Limnopolar Lake      | 2009–2015 | −2.5  | −0.7  | 30   | >130                             |
|                     | King George Island | Bellingshausen       | 2006–2015 | −2.3  | −0.6  | 60   | 300 <sup>a</sup>                 |
|                     | James Ross Island  | Johann Gregor Mendel | 2012–2015 | −7.0  | −5.7  | 74   | 60 <sup>b</sup> –85 <sup>c</sup> |
|                     | James Ross Island  | Rink Point           | 2006–2014 | −8.2  | −7.0  | NA   | 60                               |
| East Antarctica     | Enderby Land       | Molodyozhnaya        | 2008–2015 | −11.0 | NA    | 65   | >100 <sup>a</sup>                |
|                     | Queen Maud Land    | Novolazarevskaya     | 2010–2015 | −10.3 | −10.1 | 73   | 100 <sup>a</sup>                 |
|                     | Queen Maud Land    | Vesleskarvet         | 2009–2014 | −15.9 | −16.1 | NA   | 16                               |
|                     | Queen Maud Land    | Flärjuven            | 2008–2015 | −17.9 | −17.5 | NA   | 23                               |
|                     | Queen Maud Land    | Troll                | 2007–2015 | −17.8 | −17.4 | NA   | 17                               |
|                     | Vestfold Hills     | Progress             | 2008–2015 | −10.0 | −9.4  | 80   | 80                               |
| Victoria Land       | McMurdo            | Scott Base           | 2006–2015 | −17.8 | −16.1 | NA   | 37                               |
|                     | McMurdo            | Wright Valley        | 2006–2015 | −19.1 | −18.7 | NA   | 51                               |
|                     | McMurdo            | Mount Fleming        | 2006–2015 | −24.0 | −23.3 | NA   | 7                                |
|                     | Wood Bay           | Baker Rocks          | 2006–2015 | −15.7 | −15.6 | NA   | 40                               |

Note: NA, not available.

<sup>a</sup>Borehole outside CALM-S in bedrock.

<sup>b</sup>Johann Gregor Mendel – profile 1.

<sup>c</sup>Johann Gregor Mendel – profile 2.

## Data

In this study, we examine MAAT and MAGT recorded during the period 2005–2016. To obtain the most consistent datasets, MAAT from several localities included in the Reference Antarctic Data for Environmental Research database (READER, 2017) were used to cover the whole period 2006–2015 (Table 1).

Active layer thaw depth measurements were obtained from eight sites, including the CALM-S grid. Thawing depth represents the mean value from all probed measurements within each CALM-S site. On every site, probing was undertaken during the first half of February each year. No CALM-S sites were not analyzed in higher elevated areas of Eastern Antarctica and area of Victoria Land.

For all study sites, the ALT was numerically determined as the maximum annual depth of the 0°C isotherm using interpolation of maximum seasonal ground temperatures from the two deepest temperature measurements following Guglielmin (2006), the annual variability was analyzed in sites without the CALM-S grid.

## Results

### Northern Antarctic Peninsula

The north-western part of the Antarctic Peninsula region is the warmest part of Antarctica. The MAAT in this region varied between −2.0°C and −3.0°C for the period 2006–2015. In the colder north-eastern Antarctic Peninsula, represented by two sites on James Ross Island, the MAAT ranged around −7°C to −8 °C (Figure 2). Considerably higher MAAT in the western part of Antarctic Peninsula resulted in near-surface MAGT close to 0°C in King George (−0.6°C) and Livingston islands (−0.7°C), and lower in Deception Island (−1.6°C to −2.2°C).

The mean thaw depth at CALM-S sites in the western Antarctic Peninsula varied from 29 cm on Deception Island – Crater Lake (2006–2016) to 60 cm on King George Island –

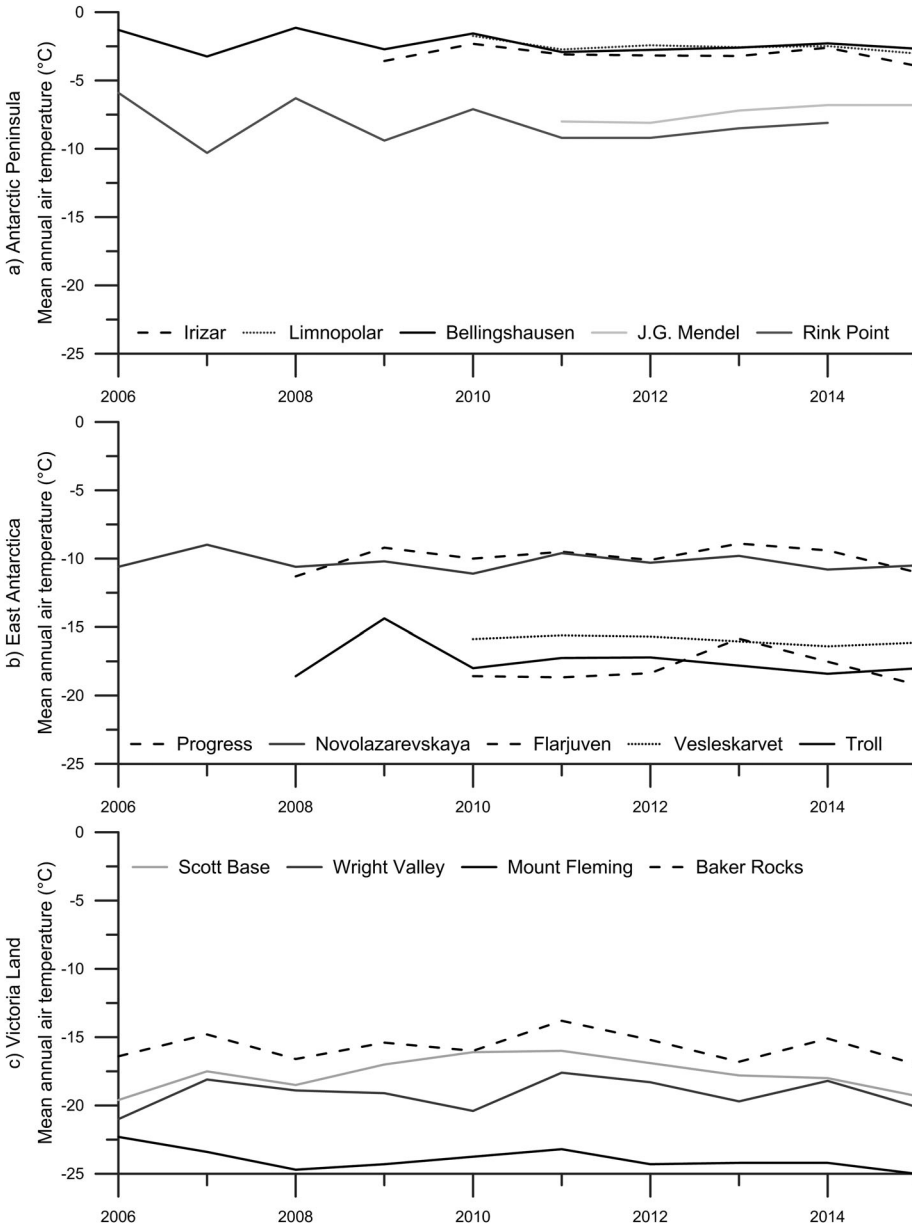


**Figure 2.** MAAT in particular regions of Antarctica.

Bellingshausen (2008–2016) (Table 2). The annual maximum mean active layer depth ranged from 36 cm on Deception Island – Crater Lake (2006) to 86 cm on King George Island (2009). In 2009, the greatest thaw depths were observed, on Deception Island, at Irizar (67 cm) and at Livingston Island (47 cm). At all sites in the western Antarctic Peninsula, a progressive decrease in ALT started in 2009 and persisted until 2015 (Figure 3). The only CALM-S site in the eastern Antarctica Peninsula is located on James Ross Island, where measurements started in 2014. Mean thaw depth for the period 2014–2016 reported 74 cm, varying between 66 cm (2014) and 78 cm (2015) (Figure 3).

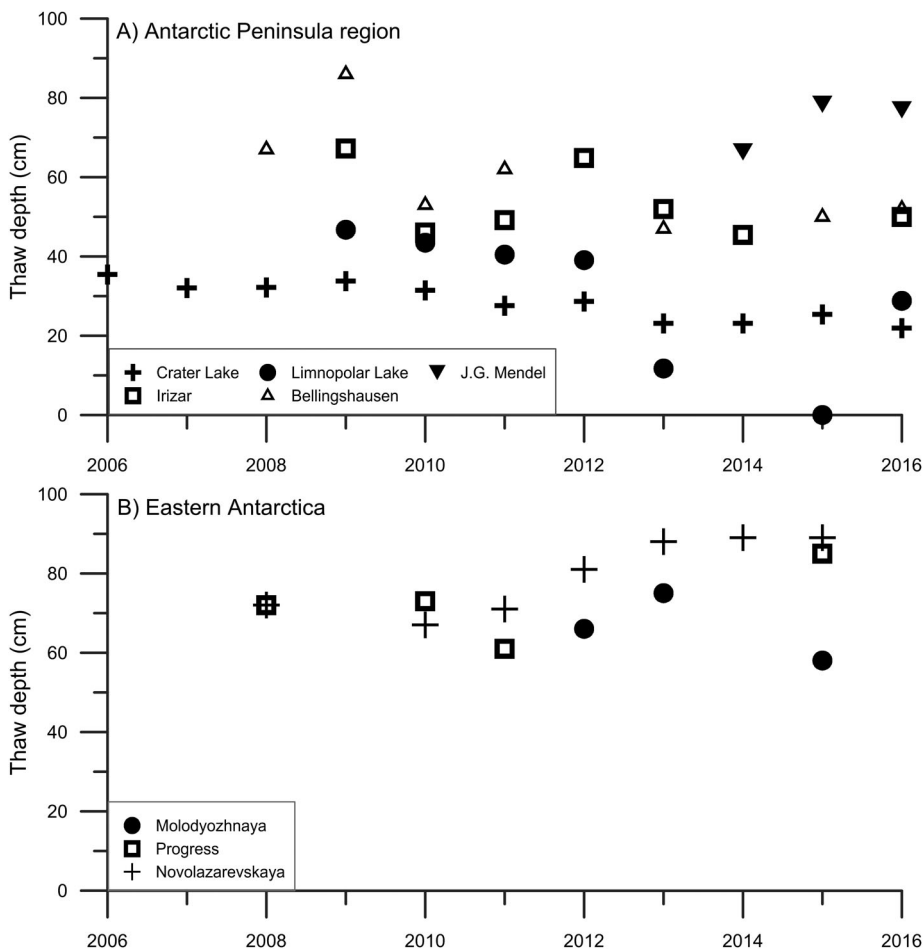


**Figure 3.** Active layer thaw depth measured on CALM-S sites in Antarctic Peninsula and Eastern Antarctica regions.

In the South Shetlands, the ALT regularly exceeded 130 cm at the Limnopolar site (Livingston Island) during the period 2009–2016 (Table 2). The deepest ALT observed in the vicinity of Bellingshausen was 300 cm; however, the borehole is located in bedrock. Deception Island's lower ALTs are attributed to porous pumice lapilli cover in Crater Lake (40–50 cm) and to mixed volcanic ash and pyroclastic deposits, without the lapilli cover at Irizar (70 cm). Despite cooler MAAT on the eastern side of the Antarctic Peninsula, the ALT on James Ross Island was similar to values of Deception Island ranging from 60 to 85 cm in two ground temperature measurement profiles located at the CALM-S J.G. Mendel site. An ALT between 40 and 75 cm was observed at the higher altitude Rink Point site (400 m, Table 2).

### **Eastern Antarctica**

Eastern Antarctica represents the largest part of the continent and therefore a large variability can be expected in this region in terms of air and ground temperatures. Two main ice-free environments are found within this region: (a) the low-altitude coastal areas and (b) the

interior with high mountains and plateaus. The MAAT in maritime environments in Eastern Antarctica varied between  $-11^{\circ}\text{C}$  and  $-9^{\circ}\text{C}$  for the period 2006–2015, while at higher altitudes it ranged from  $-18^{\circ}\text{C}$  to  $-16^{\circ}\text{C}$  (Figure 2). The MAGT showed similar values as MAAT in coastal zones (ci.  $-10^{\circ}\text{C}$ ), while it decreased to  $-17.5^{\circ}\text{C}$  to  $-16^{\circ}\text{C}$  in higher areas.

Thaw depth measurements from the three CALM-S sites located in the coastal zone in Enderby Land, Vestfold Hills and Queen Maud Land (Table 1 and Figure 1) show discontinuous data for the period 2008–2015 (Figure 2). Mean thaw depth varied between 58 and 75 cm in Molodyozhnaya (2012–2015), while slightly thicker mean thaw depths were recorded during four seasons between 2008 and 2015 in Progress (61–85 cm, Figure 3). The only continuous measurement of thaw depth is from Novolazarevskaya, where mean thaw depth reached 81 cm, ranging from 67 to 89 cm (2010–2015). At this site, thaw depth gradually increased from 2010 (67 cm) to 2013 (89 cm) (Figure 3).

Shallow borehole temperatures from the low-altitude coastal regions showed that the ALT regularly exceeded 100 cm at the Molodyozhnaya and Progress stations, with a maximum depth exceeding 120–130 cm. A thinner ALT of around 70–90 cm was observed in Novolazarevskaya. A much thinner active layer was observed at the high altitude sites of Queen Maud Land, where the mean ALT varied from 10 to 17 cm at Vesleskarvet to 13–26 cm at Flårjuven (Figure 4 and Table 2).

### **Victoria Land**

The Dry Valleys in Victoria Land are the largest continuous ice-free area in Antarctica. Although the region includes both coastal and mountain environments, the climate is dry polar-continental. In the Dry Valleys region, air temperature was measured along a transect from near sea level at Scott Base to 1700 m altitude at Mount Fleming. MAAT for the period 2006–2015 decreased with altitude from  $-17.8^{\circ}\text{C}$  at Scott Base to  $-24.0^{\circ}\text{C}$  at Mount Fleming (Table 2). A higher MAAT of  $-15.7^{\circ}\text{C}$  was observed at about  $3.3^{\circ}$  latitude further north, near the coast of Wood Bay, at Baker Rocks (11 m altitude, Figure 2). The MAGT was  $1.6^{\circ}\text{C}$  higher than MAAT on Scott Base, while in other sites varied between  $0.1^{\circ}\text{C}$  (Bakers Rocks) and  $0.7^{\circ}\text{C}$  (Mount Fleming).

Mean ALT in the Dry Valleys varied between 7 cm (Mount Fleming) and 51 cm (Wright Valley). ALT did not follow the same pattern as MAAT and it did not correlate strictly with elevation. In general, ALT varied between 34 and 39 cm at low-altitude Scott Base, 44 and 56 cm at Wright Valley and 3–16 cm at the highest altitude Mount Fleming (Figure 4). The ALT at Baker Rocks in Victoria Land was between 40 and 50 cm (Table 2).

## **Discussion**

### **Climate**

Air temperatures showed significant regional differences within the study areas. In the western Antarctic Peninsula region, Vestfold Hills and northern Victoria Land, a slight air temperature cooling was detected, while at other sites in Victoria Land and East Antarctica the air temperature was more irregular, showing no strong overall trend of warming or cooling during the study period (Figure 2). The Antarctic Peninsula region has been reported as the most rapidly warming part of Antarctica (e.g. Turner et al., 2005, 2014), but cooling has been reported since 2000 (Turner et al., 2016). Relatively stable air temperature conditions during the past 20 years were reported in Victoria Land (Guglielmin & Cannone,

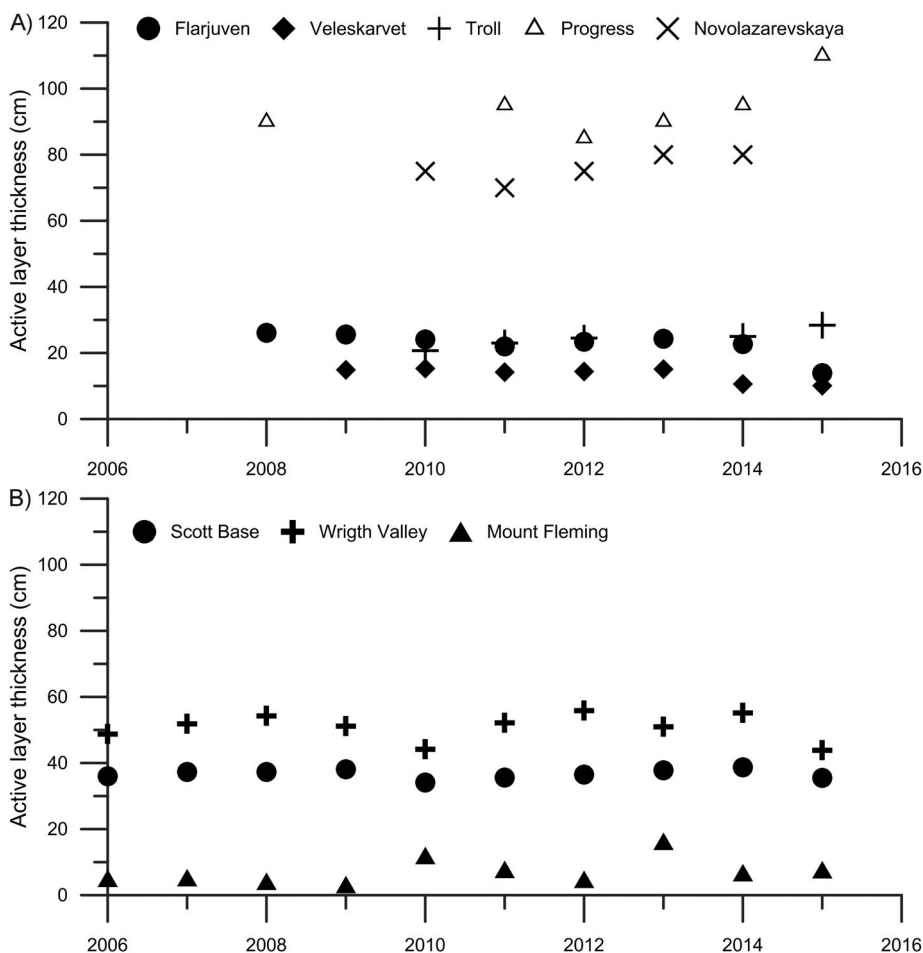


**Figure 4.** ALT in sites in Eastern Antarctica (A) and Victoria Land (B).

2012). MAGTs from 2006 to 2015 showed a spatial pattern similar to the ones identified by Vieira et al. (2010), with temperatures close to  $0^{\circ}\text{C}$  (approximately  $-0.5^{\circ}\text{C}$  to  $-2.5^{\circ}\text{C}$ ) in north-western Antarctic Peninsula to values below  $-17^{\circ}\text{C}$  in high altitude environments in Eastern Antarctica and Victoria Land.

### **Variability of thaw depth probing on CALM-S sites**

Monitored thaw depths on CALM-S sites showed large differences between the studied localities. Some of the thinnest thaw depths ( $<50$  cm) were observed in the western Antarctic Peninsula region (Table 2), although it is the warmest area in Antarctica (Turner et al., 2014). Significantly, thicker thaw depths were observed in the colder regions of the eastern Antarctic Peninsula and the coastal zone of East Antarctica. The general pattern suggests that factors other than regional climate should be considered when examining the ground thermal regime (e.g. Hrbáček, 2016). Between 2009 and 2014, substantial active layer thinning was observed at all sites in the western Antarctic Peninsula. The thinning was attributed to climate cooling in the region (Oliva, Navarro, et al., 2017; Turner et al., 2016) and changes in snow cover

accumulation, as well as snow persistence during the summer, reducing active layer thaw (de Pablo et al., 2017). In contrast, pronounced active layer thickening between 2010 and 2013 was recorded at Novolazarevskaya in coastal East Antarctica (Figure 3).

The ALT data (Table 2) show that the mean thaw depths measured in CALM-S sites were smaller than the ALT at the same sites. There are two possible explanations for these differences. One of the most important factors causing lower reported thawing depth, compared to ALT, has been the date of probing, which is generally not coincident with the maximum thaw depth. For instance, measurements in the South Shetland Islands have generally been undertaken during the first week of February (e.g. de Pablo et al., 2013; Ramos et al., 2017) while the maximum ALT usually occurs in late February or March in this area (e.g. de Pablo et al., 2014; Goyanes, Vieira, Caselli, Cardoso, et al., 2014; Oliva, Hrbacek, et al., 2017). The most pronounced differences between thaw depth and ALT have been observed at Livingston Island (CALM-S Limnopolar), where the mean thaw depth calculated from all thaw depth measurements was less than 50 cm, while the ALT exceeded 130 cm in every year (de Pablo et al., 2013, 2014).

Other factors influencing mean thaw depths are specific for individual sites and frequently related to the fact that the reported depth is an average from the measurements within the CALM.grid. Snow, vegetation cover and soil thermal properties are the most important factors causing local decreasing of the ALT. Irregular snow deposition and seasonal duration reduces thaw depth in parts of the grid with snow cover during summer (e.g. de Pablo et al., 2013; Guglielmin, 2006). Moreover, snow cover duration was prolonged in the South Shetland Islands during the summers 2013–2016 and correlated with pronounced thinning of thaw depth (de Pablo et al., 2017; Ramos et al., 2017) and has even prevented probing the whole CALM grid and even delayed the measures. Studies on vegetation covering the CALM-S sites are limited to northern Victoria Land, where vegetation, when present, shows an insulating effect (Guglielmin, Worland, et al., 2014). On bare ground and snow-free areas, thaw depth differences within a study site are mainly related to lithological variability of the ground (Hrbáček, Nývlt, & Láska, 2017).

Thaw depth measurements showed that probing is a useful and simple tool to study spatial variability of thaw depth (e.g. Vieira et al., 2010; de Pablo et al., 2013; Ramos et al., 2017). Moreover, as Hrbáček, Kňázková, et al. (2017) showed, multiple measurements during summer and potential calculation of the maximum thaw depth according to thawing propagation of the 0°C isotherm, as recommended by Brown et al. (2000), could provide a means to minimize the differences between mean values of probed thaw depth and maximum ALT. Multiple measurements could be important due to the considerable interannual variability of the date of maximum ALT in Antarctica, which can vary by several weeks (e.g. Adlam et al., 2010; de Pablo et al., 2014; Hrbáček, Nývlt, et al., 2017).

### **ALT variability**

Unlike thaw depth, the ALT, measured using temperature data, was greatest in the western Antarctic Peninsula region. Our results are consistent with other observations from the South Shetland Islands, with the ALT usually exceeding 100 cm in loamy soils (e.g. de Pablo et al., 2013; Michel et al., 2012; Oliva, Navarro, et al., 2017). However at Deception Island, where the ALT is impacted by the porous nature of the pyroclastic volcanic material and high soil moisture, which increases the amount of heat necessary for water phase change, the ALT reached only 30–50 cm at Crater Lake under pumice lapilli (Ramos et al., 2017) and

50–70 cm at the Irizar site under finer tephra (Goyanes, Vieira, Caselli, Cardoso, et al., 2014). The deepest ALT (>300 cm) was observed in bedrock in the vicinity of Bellingshausen site, which corresponds to other observations in bedrock in other sites across western Antarctic Peninsula region where the ALT usually exceeded 150 cm (Ramos and Vieira, 2009; Correia et al., 2012; Guglielmin, Worland, et al., 2014). In the eastern Antarctic Peninsula and coastal Eastern Antarctica, where MAAT ranged between  $-7^{\circ}\text{C}$  and  $-10^{\circ}\text{C}$  at sea level, the active layer has been generally thinner, with 50–100 cm (Bockheim et al., 2013; Hrbáček, Láska, et al., 2016; Hrbáček, Kňázková, et al., 2017). Maximum ALT in both the eastern Antarctic Peninsula and East Antarctica usually reached between 100 and 120 cm (e.g. Bockheim, 2015; Hrbáček, Kňázková, et al., 2017; Mergelov, 2014).

Generally, the thinnest ALT in Antarctica was observed in the high altitude areas of Eastern Antarctica in Queen Maud Land where ALT reached about 15–25 cm (e.g. Kotzé & Meiklejohn, 2017) and in Victoria Land with mean ALT of around 30 cm, rarely exceeding 50 cm. Of all the study sites reported here, the minimum ALT was observed at the highest altitude monitoring site, Mount Fleming, in the Dry Valleys region, where the ALT varied between 2 and 15 cm during the period 1999–2006 (Adlam et al., 2010) and between 3 and 16 cm between 2006 and 2015. Due to the low air temperatures during summer and lack of vegetation or snow cover, an important factor affecting ALT in the cold environment of Victoria Land is varying solar radiation, which was found to be an important influence on active layer summer thawing (Adlam et al., 2010; Guglielmin, Worland, et al., 2014).

## Conclusions

In this work, we examine MAAT and MAGT, ALT and thawing depth in multiple sites across Maritime and Continental Antarctica between 2006 and 2015. This synthesis provides the first characterization of the state of the active layer state in Antarctica since the International Polar Year 2007–2009. The most detailed and consistent information on active layer thermal regime, thickness and thaw depth is from the Antarctic Peninsula and Victoria Land, two climatically contrasting regions of Antarctica. Data from coastal and mountainous parts of Eastern Antarctica are still limited to a few sites and time series are frequently discontinuous.

The monitored sites cover a range of environments from maritime, low-altitude sites on the Antarctic Peninsula, to higher altitude continental sites in the McMurdo Dry Valleys in Victoria Land. MAAT ranged from  $-2.5^{\circ}\text{C}$  to  $-24.0^{\circ}\text{C}$  and active layer depths in soil from 7 cm to more than 130 cm. There was a marked interannual variability, with further monitoring still needed to identify trends.

The CALM-S protocol for grid probing to determine depth of thaw and active layer measurements using temperature data logging has generated an important dataset that allowed to better characterize the ground thermal regime and thaw depth variability in Antarctica. CALM-S grids provide spatially distributed thaw depth measures and thus provide a solid approach reflecting soil heterogeneity, water content changes and topography. In some areas, there were large differences between the probed thaw depth and thermally defined ALT inferred from ground temperature measurements in boreholes. Probing generally underestimated the maximum ALT, likely due to stones impeding probing, or to the timing of probing not coinciding with the time of maximum thaw.

For a better understanding of active layer spatial variability in Antarctica, more detailed studies from individual CALM-S sites are needed. To date, research on thaw depth spatial

distribution has been published from only four sites in the Antarctic Peninsula and the South Orkneys and from one site in Victoria Land. This number is clearly insufficient considering that the total number of CALM-S sites was reported as 28 in Vieira et al. (2010), although the total number of currently active sites is likely to be around 15. As such, one of the main efforts of ANTPAS should be coordinating observations and urge results to be published, especially those from outside the Antarctic Peninsula and Victoria Land. Improving and standardization of measurement methods are also needed at some sites. Repeated probing, in combination with multiple temperature-depth monitoring, inside CALM-S grids will significantly improve the results from CALM-S sites and their potential to serve the wider science community and stakeholders.

## Acknowledgements

Antarctica NZ provides logistic support for the McMurdo Dry Valley sites with collaborative support from Landcare Research and the United States Department of Agriculture. Logistical support was provided by the Directorate Antarctica and Islands, Department of Environmental Affairs (South Africa). The research work of J. Strelin, T. Sone and K. Fukui in Rink Point, James Ross Island was carried out under the Instituto Antártico Argentino-UNC-CICTERRA Agreements and the Joint Research Program of the Institute of Low Temperature Science, Hokkaido University. Special words of thanks go to Mr S. Sega for his active participation in the field investigations, and Dr R. Bono for field maintenance of the thermometric station.

## Disclosure statement

No potential conflict of interest was reported by the authors.

## Funding

The research was supported by the Masaryk University project MUNI/A/1315/2015: Integrated research of environmental changes in the landscape sphere. The work was also supported by the Ministry of Education Youth and Sports (MEYS) large infrastructure project LM2015078 'Czech Polar Research Infrastructure'. G. Vieira contribution has been supported by the Portuguese Polar Program and the Fundação para a Ciência e a Tecnologia. Marc Oliva is supported by the Ramón y Cajal Program of the Spanish Ministry of Economy and Competitiveness (RYC-2015-17597). Monitoring stations at Livingston and Deception islands have been supported in the last decade by different projects funded by the Government of Spain, including projects PERMASNOW (CTM2014-52021-R), ANTARPERMA (CTM2011-15565-E), PERMAPLANET (CTM2009-10165) and PERMAMODEL (POL-2006/01918), with the collaboration of Portuguese, Russian, Swiss and Czech researchers. Research and data processing at Bellingshausen, Novolazarevskaya, Molodyozhnaya and Progress stations were supported by the Russian Science Foundation, Project No. 14-27-00133; Russian Fund for Basic Research, Project No. 16-04-01050; Russian Antarctic expedition (logistical support) and UAF (data loggers for ground temperature). The work of I. Meiklejohn is based on the research supported by the National Research Foundation (South Africa). The research of R. Raffi was funded by the Italian Antarctic National Research Program (PNRA). This research was promoted within the SCAR/IPA ANTPAS Expert Group.

## References

Adlam, L. S., Balks, M. R., Seybold, C. A., & Campbell, D. I. (2010). Temporal and spatial variation in active layer depth in the McMurdo Sound region, Antarctica. *Antarctic Science*, 22(1), 45–52.

- Bockheim, J. (1995). Permafrost distribution in the southern circumpolar region and its relation to the environment: A review and recommendations for further research. *Permafrost and Periglacial Processes*, 6, 27–45.
- Bockheim, J. G. (2015). *The soils of Antarctica* (pp. 322). Cham: Springer International.
- Bockheim, J., Vieira, G., Ramos, M., López-Martínez, J., Serrano, E., Guglielmin, M., ... Nieuwendam, A. (2013). Climate warming and permafrost dynamics in the Antarctic Peninsula region. *Global and Planetary Change*, 100, 215–223.
- Brown, J., Hinkel, K. M., & Nelson, F. E. (2000). The Circumpolar Active Layer Monitoring (CALM) program: Research designs and initial results. *Polar Geography*, 24(3), 166–258.
- Burton-Johnson, A., Black, M., Fretwell, P. T., & Kaluza-Gilbert, J., 2016. An automated methodology for differentiating rock from snow, clouds and sea in Antarctica from Landsat 8 imagery: A new rock outcrop map and area estimation for the entire Antarctic continent. *The Cryosphere*, 10(4), 1665–1677.
- Correia, A., Vieira, G., & Ramos, M. (2012). Thermal conductivity and thermal diffusivity of cores from a 26 meter deep borehole drilled in Livingston Island, Maritime Antarctic. *Geomorphology*, 155–156, 7–11.
- de Pablo, M. A., Blanco, J. J., Molina, A., Ramos, M., Quesada, A., & Vieira, G. (2013). Interannual active layer variability at the Limnopolar Lake CALM site on Byers Peninsula, Livingston Island, Antarctica. *Antarctic Science*, 25, 167–180.
- de Pablo, M. A., Ramos, M., & Molina, A. (2014). Thermal characterization of the active layer at the Limnopolar Lake CALM-S site on Byers Peninsula (Livingston Island), Antarctica. *Solid Earth*, 5, 721–739.
- de Pablo, M. A., Ramos, M., & Molina, A. (2017). Snow Cover Evolution, on 2009–2014, at the Limnopolar Lake CALM-S site on Byers Peninsula, Livingston Island, Antarctica. *CATENA*, 149 (2), 538–547.
- Ferreira, A., Vieira, G., Ramos, M., & Nieuwendam, A. (2017). Ground temperature and permafrost distribution in Hurd Peninsula (Livingston Island, Maritime Antarctic): An assessment using freezing indexes and TTOP modelling. *Catena*, 149(2), 560–571.
- Global Terrestrial Network for Permafrost (GTN-P). Retrieved from <https://gtnp.arcticportal.org/>.
- Goyanes, G., Vieira, G., Caselli, A., Cardoso, M., Marmy, A., Santos, F., ... Hauck, C. (2014). Geothermal anomalies, permafrost and geomorphological dynamics (Deception Island, Antarctica). *Geomorphology*, 225, 57–68.
- Goyanes, G., Vieira, G., Caselli, A., Mora, C., Ramos, M., de Pablo, M. A., ... Oliva, M. (2014). Régimen térmico y variabilidad espacial de la capa activa en isla Decepción, Antártida. *Revista de la Asociación Geológica Argentina*, 71(1), 112–124.
- Guglielmin, M. (2006). Ground surface temperature (GST), active layer, and permafrost monitoring in continental Antarctica. *Permafrost and Periglacial Processes*, 17, 133–143.
- Guglielmin, M., Balks, M. R., Adlam, L. S., & Baio, F. (2011). Permafrost thermal regime from two 30-m deep boreholes in Southern Victoria Land, Antarctica. *Permafrost and Periglacial Processes*, 22, 129–139.
- Guglielmin, M., & Cannone, N. (2012). A permafrost warming in a cooling Antarctica? *Climatic Change*, 111, 177–195. doi:10.1007/s10584-011-0137-2.
- Guglielmin, M., Dalle Fratte, M., & Cannone, N. (2014). Permafrost warming and vegetation changes in continental Antarctica. *Environmental Research Letters*, 9. doi:10.1088/1748-9326/9/4/045001
- Guglielmin, M., Worland, M. R., Baio, F., & Convey, P. (2014). Permafrost and snow monitoring at Rothera Point (Adelaide Island, Maritime Antarctica): Implications for rock weathering in cryotic conditions. *Geomorphology*, 225, 47–56.
- Guglielmin, M., Worland, M. R., & Cannone, N. (2012). Spatial and temporal variability of ground surface temperature and active layer thickness at the margin of Maritime Antarctica, Signy Island. *Geomorphology*, 155–156, 20–33.
- Hrbáček, F. (2016). Active layer thermal regime in two climatically contrasted sites of the Antarctic Peninsula region. *Cuadernos de Investigacion Geografica*, 42(2), 469–488.
- Hrbáček, F., Kňázková, M., Nývlt, D., Láška, K., Mueller, C. W., & Ondruch, J. (2017). Active layer monitoring at CALM-S site near J.G.Mendel Station, James Ross Island, Eastern Antarctic Peninsula. *Science of the Total Environment*, 601–602, 987–997.

- Hrbáček, F., Láska, K., & Engel, Z. (2016). Effect of snow cover on the active-layer thermal regime – A case study from James Ross Island, Antarctic Peninsula. *Permafrost and Periglacial Processes*, 27(3), 307–315.
- Hrbáček, F., Nývlt, D., & Láska, K. (2017). Active layer thermal dynamics at two lithologically different sites on James Ross Island, Eastern Antarctic Peninsula. *Catena*, 149, 592–602.
- Kotzé, C., & Meiklejohn, I. (2017). Temporal variability of ground thermal regimes on the northern buttress of the vesleskarvet nunatak, western Dronning Maud Land, Antarctica. *Antarctic Science*, 29(1), 73–81.
- Lacelle, D., Lapalme, C., Davila, A. F., Pollard, W., Marinova, M., Heldmann, J., & McKay, C. P. (2016). Solar radiation and air and ground temperature relations in the cold and hyper-arid Quartermain mountains, McMurdo dry valleys of Antarctica. *Permafrost and Periglacial Processes*, 27, 163–176.
- Mergelov, N. S. (2014). Soils of wet valleys in the Larsemann Hills and Vestfold Hills oases (Princess Elizabeth Land, East Antarctica). *Eurasian Soil Science*, 47 (9), 845–862.
- Michel, R. F. M., Schaefer, C. E. G. R., Poelking, E. L., Simas, F. N. B., Fernandes Filho, E. I., & Bockheim, J. G. (2012). Active layer temperature in two Cryosols from King George Island, Maritime Antarctica. *Geomorphology*, 155–156, 12–19.
- Oliva, M., Hrbáček, F., Ruiz-Fernández, J., de Pablo, M. Á., Vieira, G., Ramos, M., & Antoniadis, D. (2017). Active layer dynamics in three topographically distinct lake catchments in Byers Peninsula (Livingston Island, Antarctica). *CATENA*, 149(2), 548–559.
- Oliva, M., Navarro, F., Hrbáček, F., Hernández, A., Nývlt, D., Pereira, P., ... Trigo, R. (2017). Recent regional climate cooling on the Antarctic Peninsula and associated impacts on the cryosphere. *Science of the Total Environment*, 580, 210–223.
- Raffi, R., & Stenni, B. (2011). Isotopic composition and thermal regime of ice wedges in Northern Victoria Land, East Antarctica. *Permafrost and Periglacial Processes*, 22(1), 65–83.
- Ramos, M., Hassler, A., Vieira, G., Hauck, C., & Gruber, S. (2009). Drilling and installation of boreholes for permafrost thermal monitoring on Livingston Island in the maritime Antarctic. *Permafrost and Periglacial Processes*, 20, 57–64. doi:10.1002/ppp.635.
- Ramos, M., & Vieira, G. (2009). Evaluation of the ground surface Enthalpy balance from bedrock temperatures (Livingston Island, Maritime Antarctic). *The Cryosphere*, 3, 133–145.
- Ramos, M., Vieira, G., de Pablo, M. A., Molina, A., Abramov, A., & Goyanes, G. (2017). Recent shallowing of the thaw depth at Crater Lake, Deception Island, Antarctica (2006–2014). *Catena*, 149(2), 519–528.
- Schaefer, C. E. G. R., Michel, R. F. M., Delpupo, C., Senra, E. O., Bremer, U. F., & Bockheim, J. G. (2017). Active layer thermal monitoring of a dry valley of the Ellsworth Mountains, Continental Antarctica. *CATENA*, 149, 603–615.
- Turner, J., Barrand, N. E., Bracegirdle, T. J., Convey, P., Hodgson, D. A., Jarvis, M., ... Klepikov, A. V. (2014). Antarctic climate change and the environment – An update. *Polar Record*, 50(254), 237–259.
- Turner, J., Colwell, S. R., Marshall, G. J., Lachlan-Cope, T. A., Carleton, A. M., Jones, P. D., ... Iagovkina, S. (2005). Antarctic climate change during the last 50 years. *International Journal of Climatology*, 25, 279–294.
- Turner, J., Lu, H., White, I., King, J. C., Phillips, T., Scott Hosking, J., ... Deb, P. (2016). Absence of 21st century warming on Antarctic Peninsula consistent with natural variability. *Nature*, 535, 411–415.
- Vieira, G., Bockheim, J., Guglielmin, M., Balks, M., Abramov, A. A., Boelhouwers, J., ... Wagner, D. (2010). Thermal state of permafrost and active-layer monitoring in the Antarctic: Advances during the International Polar Year 2007–2008. *Permafrost and Periglacial Processes*, 21, 182–197.

Contents lists available at [ScienceDirect](https://www.sciencedirect.com)

## Earth-Science Reviews

journal homepage: [www.elsevier.com/locate/earscirev](https://www.elsevier.com/locate/earscirev)

## Active layer and permafrost thermal regimes in the ice-free areas of Antarctica

Filip Hrbáček<sup>a,\*</sup>, Marc Oliva<sup>b</sup>, Christel Hansen<sup>c</sup>, Megan Balks<sup>d</sup>, Tanya Ann O'Neill<sup>d</sup>, Miguel Angel de Pablo<sup>e</sup>, Stefano Ponti<sup>f</sup>, Miguel Ramos<sup>g</sup>, Gonçalo Vieira<sup>h</sup>, Andrey Abramov<sup>i</sup>, Lucia Kaplan Pastřířková<sup>a</sup>, Mauro Guglielmin<sup>f</sup>, Gabriel Goyanes<sup>h</sup>, Marcio Rocha Francelino<sup>j</sup>, Carlos Schaefer<sup>j</sup>, Denis Lacelle<sup>k</sup>

<sup>a</sup> Department of Geography, Faculty of Science, Masaryk University, Kotlářská 2, 611 37, Brno, Czech Republic

<sup>b</sup> Department of Geography, Universitat de Barcelona, C/Montalegre 6-8, 3r, 08001 Barcelona, Spain

<sup>c</sup> Department of Geography, Geoinformatics and Meteorology, University of Pretoria, Private Bag X20, Hatfield 0028, South Africa

<sup>d</sup> School of Sciences - Te Aka Mātūatua, The University of Waikato, Gate 1, Knighton Road, Hamilton 3240, New Zealand

<sup>e</sup> Unidad de Geología, Departamento de Geología, Geografía y Medio Ambiente, Universidad de Alcalá, Ctra. A-II Km 33, 6. 28805, Alcalá de Henares, Spain

<sup>f</sup> University Insubria, Department of Theoretical and Applied Sciences, Via J.H. Dunant, 21100, Varese, Italy

<sup>g</sup> Physics and Mathematics department, Universidad de Alcalá, Calle el Escorial, 19-21, 28805 Alcalá de Henares, Madrid, Španělsko

<sup>h</sup> Centro de Estudos Geográficos, IGOT - Universidade de Lisboa, Rua Branca Edmée Marques, 1600-276 Lisboa, Portugal

<sup>i</sup> Soil cryology department, Institute of Physicochemical and biological problems in soil science, Russian Academy of Science, Pushchino, Russia

<sup>j</sup> Department of Soils of the Federal University of Viçosa, 36570, Viçosa, Brazil

<sup>k</sup> Department of Geography, Environment and Geomatics, University of Ottawa, Ontario, ON, K1N 6N5, Canada

## ARTICLE INFO

## Keywords:

Ground thermal regime  
Active layer thickness  
Climate change  
Antarctic ice-free environment  
Cryosols  
Gelisols  
Permafrost

## ABSTRACT

Ice-free areas occupy <0.5% of Antarctica and are unevenly distributed across the continent. Terrestrial ecosystem dynamics in ice free areas are strongly influenced by permafrost and the associated active layer. These features are the least studied component of the cryosphere in Antarctica, with sparse data from permanent study sites mainly providing information related to the ground thermal regime and active layer thickness (ALT). One of the most important results of the International Polar Year (IPY, 2007/08) was an increase in ground thermal regime monitoring sites, and consequently our knowledge of Antarctic permafrost dynamics. Now, 15 years after the IPY, we provide the first comprehensive summary of the state of permafrost across Antarctica, including the sub-Antarctic Islands, with analyses of spatial and temporal patterns of the dominant external factors (climate, lithology, biota, and hydric regime) on the ground thermal regime and active layer thickness. The mean annual ground temperatures of the active layer and uppermost part of the permafrost in Antarctica remain just below 0 °C in the warmest parts of the Antarctic Peninsula, and were below –20 °C in mountainous regions of the continent. The ALT varies between a few cm in the coldest, mountainous, parts of the Transantarctic Mountains up to >5 m in bedrock sites in the Antarctic Peninsula. The deepest and most variable ALTs (ca. 40 to >500 cm) were found in the Antarctic Peninsula, whereas the maximum ALT generally did not exceed 90 cm in Victoria Land and East Antarctica. Notably, found that the mean annual near-surface temperature follows the latitudinal gradient of –0.9 °C/deg. ( $R^2 = 0.9$ ) and the active layer thickness 3.7 cm/deg. ( $R^2 = 0.64$ ). The continuous permafrost occurs in the vast majority of the ice-free areas in Antarctica. The modelling of temperature on the top of the permafrost indicates also the permafrost presence in South Orkneys and South Georgia. The only areas where deep boreholes and geophysical surveys indicates discontinuous or sporadic permafrost are South Shetlands and Western Antarctic Peninsula.

\* Corresponding author.

E-mail address: [hrbacekfilip@gmail.com](mailto:hrbacekfilip@gmail.com) (F. Hrbáček).

<https://doi.org/10.1016/j.earscirev.2023.104458>

Received 13 October 2022; Received in revised form 14 May 2023; Accepted 22 May 2023

Available online 29 May 2023

0012-8252/© 2023 Elsevier B.V. All rights reserved.

## 1. Introduction

The Antarctic ice-free environments constitute one of the rarest terrestrial ecosystems on Earth. The total ice-free surface in Antarctica is estimated to extend from ca. 45,000 to 70,000 km<sup>2</sup> (Vieira et al., 2010; Terauds and Lee, 2016; Lee et al., 2017; Brooks et al., 2019; Gerrish et al., 2020), which represents less than 0.5% of the surface of the Antarctic continent. The ice-free areas consist of a mosaic of surfaces varying from very small rocky outcrops (< 0.1 km<sup>2</sup>) and nunataks, up to large oases (> 100 km<sup>2</sup>) distributed along the coastlines and isolated areas in the interior of the continent. The relief of the ice-free areas has been formed over time scales ranging from millions of years, to the accelerated glacial retreat detected in some areas over the last few decades. As a result, the ice-free environments have been shaped by a combination of glacial, periglacial, paraglacial, and other geomorphic processes, producing a variety of landforms (e.g. Ruiz-Fernández et al., 2019; Oliva and Ruiz-Fernández, 2020).

Permafrost and seasonally thawed active layer are key elements of the cryosphere in Antarctic ice-free environments (Ugolini and Bockheim, 2008). The presence or absence of permafrost is of importance for geomorphological, soil, hydrological, and edaphic processes, and terrestrial ecosystem dynamics in Antarctica (e.g. Guglielmin et al., 2014a). Therefore, the thickness of the active layer, or permafrost presence, are key descriptors of Antarctic terrestrial environments. As active layer thickness (ALT) and the distribution of permafrost are sensitive to climate variability, warming, as recorded for the Antarctic Peninsula over the second half of the 20th century (Turner et al., 2020), may lead to a deepening of the active layer and permafrost degradation that, in turn, triggers changes in soil thermal and hydrological regimes. Furthermore, shifts in temperature and moisture regimes affect the abundance of biota (e.g. Convey and Peck, 2019). Permafrost underlies most of the Antarctic continent. The vast majority comprises subglacial permafrost, in both non-cryotic and cryotic forms, below cold- and warm-based glaciers (e.g. Dawson et al., 2022). However, it is unclear whether permafrost is present below subglacial lakes (Dawson et al., 2022), and the extent of submarine permafrost, which has been reported in some areas in Antarctica (e.g.; Guglielmin et al., 2014b) is also poorly understood. In ice-free terrain, permafrost is mostly continuous and absent only in coastal fringes of the western Antarctic Peninsula (Bockheim et al., 2013).

Major progress in Antarctic active layer and permafrost research began during the International Polar Year in 2007/08, when more than 50 new boreholes shallower than 2 m were drilled across the Antarctic continent (Vieira et al., 2010). Since then, the main research topics have aimed at characterizing the ground thermal regime and active layer thickness under the effect of different factors including; atmospheric temperature (e.g. Adlam et al., 2010; Lacelle et al., 2016), snow cover (e.g., Guglielmin et al., 2014b; de Pablo et al., 2017; Ramos et al., 2020; Farzamián et al., 2020; Hrbáček et al., 2021a), lithological conditions (Hrbáček et al., 2017a, 2017b), topography (Carshalton et al., 2022; Chaves et al., 2017; Ferreira et al., 2017; Francellino et al., 2011; Goyanes et al., 2014; Oliva et al., 2017a; Vieira and Ramos, 2003) or vegetation (Michel et al., 2012; Vieira et al., 2014; Hrbáček et al., 2020a; Cannone et al., 2021). Insights into spatial variability of the active layer mostly come from the monitoring sites of the Circumpolar Active Layer Monitoring – South (CALM-S) programme (Brown et al., 2000; Guglielmin, 2006). Only a few CALM-S sites have been installed in Antarctica due to the hard ground surface conditions (i.e. mostly bedrock, frost-shattering deposits or stony tills) that prevent mechanical probing or other means of spatial measurement of ALT (Guglielmin, 2006; Vieira et al., 2010; de Pablo et al., 2013, 2014, 2018; Guglielmin et al., 2014a; Ramos et al., 2017; Hrbáček et al., 2017a, 2021a, 2021b). Less attention has been given to the thermal state of the deeper permafrost layers. Due to logistical and technical constraints, only a few boreholes have been drilled to reach the depth of zero annual amplitude, typically 10–20 m (Biskaborn et al., 2019).

The harsh climate, environmental conditions, and remoteness of Antarctica, and the technical and logistical difficulties, limit active layer and permafrost research. Thus publications are often fragmented covering short-time, or limited spatial scales. Therefore, we provide a synthesis of the literature on topics related to the active layer thermal regime, active layer thickness, and the permafrost thermal regime, over the last decade, across Antarctica. Particularly, we set three major objectives, which allow us to comprehensively describe the spatial-temporal patterns of the active layer and permafrost in Antarctica:

- 1) Provide a synthesis of the main results describing active layer and permafrost thermal dynamics in Antarctica.
- 2) Assess the spatial variability of the Antarctic active layer and permafrost thermal regime.
- 3) Determine the role of the major parameters driving the thermal state of the active layer and permafrost.

## 2. Methods

### 2.1. Geographical analysis

The area of interest of this review includes the Antarctic continent and the surrounding sub-Antarctic Islands. We defined four main regions and twelve sub-regions based on the geographical and climatic conditions (Table 1). A description of each area is provided in the Results section. To determine the total area of each ice-free region, we followed Brooks et al. (2019) and used the combination of most recent data of automatically derived rock outcrops for Antarctica from Landsat-8 in high resolution and vector polygons of rock outcrops derived in the period 1960s to 2019 in high resolution (Antarctic Digital Database; Gerrish et al., 2020). The total extension of polygons of Antarctic ice-free area including South Orkneys is 52,720 km<sup>2</sup>. Note, that the selected resolution significantly affects the total extension. For example, the ice-free areas on medium resolution cover more than 70,000 km<sup>2</sup> and was used for example by Terauds and Lee et al. (2016) or Lee et al. (2017).

The lack of widespread monitoring sites across the continent determined slightly different regionalization to that used in other studies such as widely used Antarctic Conservation Biogeographic Regions (ACBRs) by Terauds and Lee (2016). Some of ACBRs were not included in this study due absence of data, except those modelled at continental scale by Obu et al. (2020). The reference MAAT for each region was derived from the READER database.

### 2.2. Literature synthesis

For each region (Table 1), we provided a synthesis of the scientific literature focusing on the active layer and permafrost thermal regime and/or thickness published since 2011 (Fig. 1). This year was selected as it follows the first synthesis by Vieira et al. (2010) who summarized the progress of active layer and permafrost research during the International Polar Year (2007–2008), including data from previous years. The particular datasets are then analysed for the period from 2006 which serves as a starting point for multiple measurements or experiments including most of the CALM-S sites (Hrbáček et al., 2021b) and, therefore, represents an important milestone for active layer and permafrost research in Antarctica.

Our aim was to extract the following parameters provided in the literature:

- Study period, number of monitoring sites, and depth of installations
- Mean annual air temperature (MAAT)
- Mean annual near-surface ground temperature (MAGT; depths varied between 2 and 10 cm)
- Mean annual temperature on the top of the permafrost table (MAPT). Particular depths are variable for every locality.

**Table 1**  
Overview of study areas.

| Region                                     | Sub-region               | Ice-free area (km <sup>2</sup> ) | ACBR <sup>1</sup> | MAAT <sup>2</sup> (°C) | Reference station |
|--|--------------------------|----------------------------------|-------------------|------------------------|-------------------|
| Antarctic Peninsula                        | South Shetlands          | 572                              | 3                 | −2.1                   | Bellingshausen    |
|  | Western AP               | 9000                             | 3,4,15            | −2.7                   | Faraday           |
|  | Eastern AP               |                                  | 1                 | −8.0                   | Marambio          |
| West Antarctica                            | Ellsworth Mountains      | 2140                             | 11                | n/a                    | n/a               |
|  | Other regions            | 776                              | 12                | −12.4*                 | Russkaya          |
| East Antarctica                            | Queen Maud Land          | 4485                             | 6                 | −10.1                  | Novolazarevskaya  |
|  | other regions            | 9100                             | 5, 7              | −11.1                  | Mawson            |
| Victoria Land and Transantarctic Mountains | McMurdo Dry Valleys      |                                  | 9                 | −15.8                  | McMurdo           |
|  | North Victoria Land      | 26,480                           | 8                 |                        |                   |
|  | Transantarctic Mountains |                                  |                   |                        |                   |
| Sub-Antarctic Islands                      | South Orkneys            | 167                              | 2                 | −3.1                   | Orcadas           |
|  | Other Islands            | n/a                              | n/a               | 0–9                    | Marion Island     |

<sup>1</sup> Antarctic Conservation Biogeographic Regions defined by [Terauds and Lee \(2016\)](#).

<sup>2</sup> Mean Annual Air Temperature \*1980–1990.

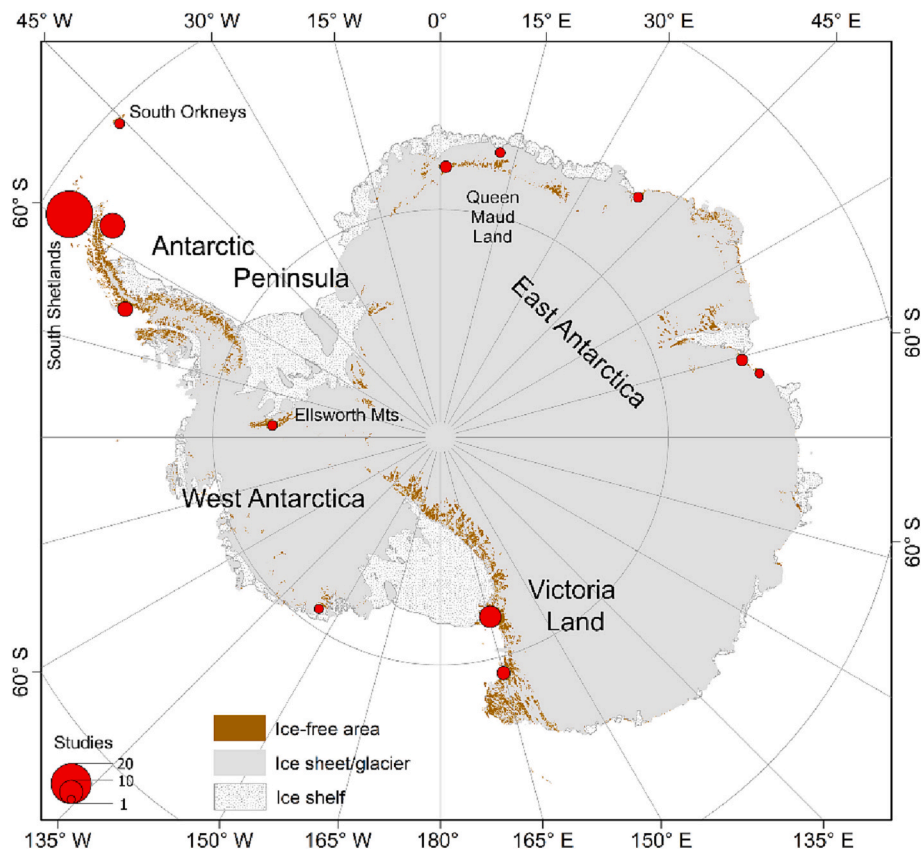


**Fig. 1.** The spatial distribution, and the number, of studies focused on active layer, or permafrost, thermal regime conducted in Antarctica since 2011.

- Active layer thickness (ALT) defined as a maximum annual depth of the interpolated 0 °C isotherm
- Mean value of mechanically measured active layer thickness on CALM-S sites
- The annual sum of near-surface freezing (FDD) and thawing (TDD) degree day indices
- Freezing and thawing n-factors calculated as a ratio between air and near-surface degree days

These parameters are widely used in permafrost research in Arctic, Antarctic and Alpine environments and are described in detail in the Glossary of Permafrost and Related Ground-Ice Terms ([Harris et al., 1988](#)).

We summarized the results in [Tables 1 to 8](#), and datasets providing MAGT, MAPT and ALT for at least 3 consecutive years were displayed as

plots. Data variability within each Antarctic region was also evaluated. Finally, using available datasets, we estimated the trend of MAGT for the South Shetlands, Eastern Antarctic Peninsula, East Antarctica and Victoria Land. As the data miss the full temporal overlap, we set year 2011 when the highest data overlay was available as the baseline year for calculation of temperature anomalies. It allows a regional comparison of annual temperature change from sites with heterogeneous climate conditions. The temporal variability of ALT datasets long at least 7 years were then analysed individually for each of the study sites. The resulting trends were investigated using Mann-Kendal statistics with Sen's slope to estimate the trends in the MAKESENS application ([Salmi et al., 2002](#)).

**Table 2**  
Selected characteristics of the sites in the South Shetland Island region.

| Area               | Study site                                       | Study period   | Profiles | Profile Depth (cm) | MAAT <sup>1</sup> (°C) | MASGT <sup>2</sup> (°C) | MAPT <sup>3</sup> (°C) | ALT (cm)           | TDD (°C.day)  | FDD (°C.day)    | thawing n-factor | freezing n-factor | Reference   |
|--------------------|--|----------------|----------|--------------------|------------------------|-------------------------|------------------------|--------------------|---------------|-----------------|------------------|-------------------|---|
| King George Island | Fildes Peninsula (Brazilian sites)               | 2008–2012      | 1        | 85                 | –2                     | –1.2 (–0.3 to –1.7)     | –1.1                   | 89 to 102.5        | ca 200 to 250 | –527 to –819    |                  |                   | Michel et al., 2012, 2014   |
|                    | Fildes Peninsula (Bellingshausen)                | 2008–2016      | 1        | 500                | –2.3                   | –0.6                    | –0.7                   | 60* / 300          |               |                 |                  |                   | Obu et al., 2020; Osokin et al., 2020, Hrbáček et al., 2021a, 2021b |
|                    | Lion Rumps                                       | 4/2009–1/2011  | 2        | 80                 | –3                     | –0.9 to –1.9            | –0.9 to –1.8           | 120 to 147         |               |                 |                  | ca 0.4 to 1       | Almeida et al., 2014  |
|                    | Low Head   | 3/2011–12/2015 | 1        | 100                | –3.1                   | –1.5                    | –1.5                   | 98 to 106          | 282 to 438    | –715 to –1061   |                  |                   | Almeida et al., 2017  |
|                    | Potter Peninsula                                 | 2/2008–1/2009  | 1        | 90                 |                        | –0.9                    | –0.9                   | 92                 | 281           | –532            |                  |                   | Michel et al., 2012   |
|                    | Keller Peninsula                                 | 2011–2014      | 2        | 80                 | –2.9 to –4.8           | –1.7 to –2.8            |                        |                    |               |                 |                  |                   | Chaves et al., 2017   |
| Livingston Island  | Keller Peninsula                                 | 12/10–1/11     | 5        | 30                 |                        |                         |                        | 45 to 70           |               |                 |                  |                   | Lee et al., 2016  |
|                    | Limnopolare Lake                                 | 2009–2018      | 1        | 130                | –1.7 to –3.2           | –0.3 to –1.4            |                        | 50*/150            | 36 to 290     | –261 to –664    |                  |                   | de Pablo et al., 2013, 2014, 2016, 2018                             |
|                    | Domo, Escondido and Cerro Negro Lakes            | 2/2014–1/2015  | 3        | 80                 | –2.6 to –2.7           | –0.7 to –1.3            |                        | 85 to 115          | 76 to 134     | –311 to –577    | –                | 0.11 to 0.64      | Hrbáček et al., 2016a, Oliva et al., 2017a, 2017b                   |
|                    | Rotsch Glacier Transect                          | 2/2017–2/2019  | 10       | 40                 | –2.1                   | 0 to –1.3               |                        | 102                | 183 to 321    | –241 to –682    | 1.5 to 2.63      | 0.27 to 0.76      | Hrbáček et al., 2020b   |
|                    |  | 1/2015         | 1 (5)    | 40                 |                        |                         |                        | 90 to 150          |               |                 |                  |                   | Correia et al., 2017  |
|                    | Mount Reina Sofia (PG1, PG2)                     | 2008–2015      | 2        | 110; 25 m          | –2.9 to –6.5           |                         |                        | 20 to 500          |               |                 |                  |                   |   |
| Deception Island   | Hurd Peninsula (PAP, CALM, SH, CR, MET, INC, NI) | 2007; 2009     | 7        | 400 to 800         |                        | –0.8 to –1.8            |                        | 100 to >600        | 145 to 318    | –294 to –1042   | 0.76 to 10.95    | 0.43 to 0.80      | Ferreira et al., 2017   |
|                    | Port Foster                                      | 2011           | 2        | 80                 | –2.6                   | 0 to –1                 |                        |                    |               |                 |                  |                   | Goyanes et al., 2014  |
| Other areas        | Crater Lake CALM-S                               | 2006–2014      | 1        | 100 to 450         | –3                     | –1.7                    |                        | 23–36 <sup>1</sup> |               |                 |                  |                   | Ramos et al., 2017  |
|                    | Coppermine Peninsula (Robert Island)             | 2014–2016      | 2        |                    |                        | ca –1.5 to –2           |                        |                    | ca 10 to 70   | ca –500 to –700 |                  |                   | Thomazini et al., 2020  |

<sup>1</sup> Mean annual air temperature.

<sup>2</sup> Mean annual near-surface ground temperature.

<sup>3</sup> Mean annual temperature of the permafrost table.

\* Probing measurement.

**Table 3**  
Selected characteristics of sites in the Western Antarctic Peninsula region.

| Area       | Study site     | Study period  | Profiles | Profile Depth (cm) | MAAT <sup>1</sup> (°C) | MASGT <sup>2</sup> (°C) | MAPT <sup>3</sup> (°C) | ALT (cm)     | TDD (°C·day) | FDD (°C·day)   | thawing n-factor | freezing n-factor | Reference   |
|------------|----------------|---------------|----------|--------------------|------------------------|-------------------------|------------------------|--------------|--------------|----------------|------------------|-------------------|---|
| Western AP | Amesler Island |               | 8        | 160 to 1400        |                        |                         | −0.7 to −1.9           | ca 1 to 17*  | 186 to 307   |                |                  |                   | Wilhelm et al., 2015; Wilhelm and Bockheim, 2016, 2017; Uxa, 2016 |
|            | Rothera        | 2/2009–2/2012 | 3        | 30 m               | −3                     | −2.7 to −4.6            | −1.5 to −4.8           | 65 to 140 cm | 186 to 618   | −1143 to −1731 |                  |                   | Guglielmin et al., 2014b  |
|            | Cierva Cove    |               | 1        | 160                |                        |                         |                        |              |              |                |                  |                   | Wilhelm and Bockheim, 2017  |

<sup>1</sup> Mean annual air temperature.

<sup>2</sup> Mean annual near-surface ground temperature.

<sup>3</sup> Mean annual temperature of the permafrost table.

### 3. Results

#### 3.1. Antarctic Peninsula region

The Antarctic Peninsula region (AP) forms the northernmost tip of the Antarctica continent. The region, including the neighbouring sub-Antarctic islands (SAI), is located south of South America, between latitude 60°S and 75 and longitude 44°W to 75°W. The AP region, including the SAI, exceeds 540,000 km<sup>2</sup>, of which only ca. 9500 km<sup>2</sup> constitute ice-free terrain (Table 1). Considering the geographical diversity of the AP, we set three major sub-regions – South Shetland Islands (SSI) Western Antarctic Peninsula (Western AP), and Eastern Antarctic Peninsula (Eastern AP).

##### 3.1.1. South Shetland Islands

The SSI constitute an archipelago extending over 3687 km<sup>2</sup> in the NW sector of the Antarctic Peninsula. Located at latitudes 61–63°S and longitudes 54–62°W, the SSI run SSW–NNE, parallel to the Antarctic Peninsula, at a distance of 100–120 km. The SSI archipelago is located in a tectonically active zone with several active volcanoes (e.g. Penguin and Deception islands).

During the last glacial cycle, a large ice cap extended from the Antarctic Peninsula and covered the SSI. Post-Last Glacial Maximum warming favoured the shrinking of the ice sheet, and from ~15 to 10 ka a single ice cap, disconnected from the continent, covered the SSI archipelago (Ó Cofaigh et al., 2014). Subsequently, as temperatures increased, at the onset of the Holocene, glacial masses were limited to the respective islands. Holocene glacial shrinking has exposed the land surface on the margins of some of the islands (Oliva et al., 2019), which are still heavily glaciated (between 85 and 100% of the total island surface covered by ice).

The SSI record the highest mean annual air temperatures of Antarctica, with values of ~−2 °C at sea level (e.g. Turner et al., 2020) and an annual precipitation between 500 and 800 mm (Bañón et al., 2013). Snow cover generally persists on the ground for 8–9 months per year. The archipelago is composed of Late Palaeozoic to Quaternary sedimentary, metamorphic, plutonic and volcanic rocks (López-Martínez et al., 2016). The scarce ice-free areas in the SSI archipelago are affected by active periglacial dynamics, with intense frost weathering (Simas et al., 2008; López-Martínez et al., 2012). Vegetation cover is scarce and mostly composed of mosses and grasses along the Holocene marine terraces with abundant lichens on relatively flat areas near lakes and ponds (Ruiz-Fernández et al., 2017).

**3.1.1.1. King George Island.** King George Island is the largest island in the SSI archipelago with an area of 1124 km<sup>2</sup>. The ice-free surfaces occupy ca. 190 km<sup>2</sup> of the island, mainly concentrated in several peninsulas, including; Fildes (30 km<sup>2</sup>), Keller (10 km<sup>2</sup>) and Barton

peninsulas (10 km<sup>2</sup>). The deglaciation of Maxwell Bay (south of Fildes Peninsula) began between 17 and 14 ka cal BP and was fastest between 7 and 6 ka (Yoon et al., 1997; Simms et al., 2011; Oliva et al., 2023). The deglaciation of the smaller peninsulas began around 8 ka cal BP (Barton Peninsula; Oliva et al., 2019). The topography of the ice-free areas is dominated by volcanic outcrops reaching ca. 120 to 150 m a.s.l. surrounded by a relatively flat area. The current MAAT on King George Islands is around −2.1 °C (Tables 1, 2), with a recent warming rate of 0.13 °C/decade over the period 1968–2015 (Oliva et al., 2017b). The annual precipitation is around 500–1000 mm, with prevailing winter snowfall and rainfall during the summer season (van Wessem et al., 2016). The vegetation forms relatively large patches of mosses or lichens in poorly drained areas. Two vascular plant species also occur in lower altitude areas (e.g. Cannone et al., 2016).

Although King George Island includes the greatest number of human infrastructures in Antarctica, research on active layer and permafrost dynamics is incipient and has mainly focused on soil biogeochemical conditions (e.g. Bockheim, 2015; Boy et al., 2016; Prater et al., 2021). The only known long-term monitoring study of active layer and permafrost temperatures, including the only CALM-S grid, has operated near Bellingshausen station since 2006 (Vieira et al., 2010; Osokin et al., 2020; Hrbáček et al., 2021b). Data from other parts of the King George Islands are fragmented with several studies describing the short-term variability of the active layer thermal regime and ALT on several peninsulas in the southern part of the island.

The MAGT near Bellingshausen Station, which has the longest record on Fildes Peninsula (2006–2015), was −0.6 °C (Hrbáček et al., 2021b). The thaw depth varied between 75 and 115 cm (Osokin et al., 2020), and the ALT commonly exceeded 300 cm in bedrock conditions (Hrbáček et al., 2021b). Michel et al. (2012, 2014) reported that ALT, on soils covered by vegetation, ranged between 89 and 102 cm (Fig. 2) and the TDD were between 200 and 400 °C·day, whereas FDD ranged from −527 to −819 °C·day (Table 2). The MAPT is around −1.5 °C.

Data from the Barton and Potter peninsulas are restricted to a short-term monitoring of active layer thermal regime and ALT. The ALT in the vicinity of King Sejong station, near to sea level on Barton Peninsula, varied between 41 and 70 cm in the summer of 2011 (Lee et al., 2016). One year of monitoring on Potter Peninsula showed MAGT of −0.7 °C and an ALT of 92 cm in summer 2008 (Michel et al., 2012).

Chaves et al. (2017) reported that the thermal regime of patterned-ground soils on the Keller Peninsula varied across the patterned ground features. The stony garlands along the edge of the striations had more rock fragments and were more susceptible to energy variations at the surface, resulting in faster thawing/freezing, with a thicker active layer, than the moss-covered polygon centre. Yet, the mean daily soil temperature was −2.1 °C, both at the border and between the polygon centre. The ALT of the patterned-ground soil was 75 cm at the polygon border, and 64 cm at the center, where temperatures remained below

**Table 4**  
Selected characteristics of sites in the Eastern Antarctic Peninsula region.

| Area                             | Study site                 | Study period    | Profiles | Profile Depth (cm) | MAAT <sup>1</sup> (°C) | MASGT <sup>2</sup> (°C) | MAPT <sup>3</sup> (°C) | ALT (cm)      | TDD (°C.day)     | FDD (°C.day)           | thawing n-factor    | freezing n-factor   | Reference  |
|----------------------------------|----------------------------|-----------------|----------|--------------------|------------------------|-------------------------|------------------------|---------------|------------------|------------------------|---------------------|---------------------|--|
| James Ross Island                | J.G.Mendel                 | 2011–2021       | 1        | 200                | -6.7                   | -5.4 (-3.4 to -6.8)     | -5.6 (-4.4 to -6.3)    | 60 (50 to 67) | 471 (379 to 603) | -2450* (-1783 to 2812) |                     |                     | Hrbáček et al., 2016b, 2017a, 2019, Hrbáček et al., 2021a, 2021b, Kaplan Pastříková et al., 2023 |
|                                  |                            |                 |          |                    | same as above          | -4.9 to -5.6            | -5.2 to -5.8           | 82 to 90      | 416 to 502       | -2230 to -2510         | 3.57 to 4.86        | 0.85 to 0.9         | Hrbáček et al., 2017b, 2021a, 2021b  |
|                                  | Berry Hill slopes          | 2011–2015       | 1        | 90                 | -6.6 to -7.6           | -5.7 to -7.0            | -5.6 to -6.6           | 85 to 89      | 300 to 382       | -2444 to -2810         | 2.4 to 4.4          | 0.91 to 0.97        | Hrbáček et al., 2017b, 2019  |
|                                  |                            |                 |          |                    | -7.3                   | -6.1 (-3.8 to -8.2)     | -6.3 to -7.4           | 38 to 68      | 370 (386 to 432) | -1745 to -3116         | 2.35 (1.59 to 3.21) | 0.93 (0.71 to 1.03) | Hrbáček et al., 2016a, 2017b, 2019, Hrbáček and Uxa, 2020, Knazková et al., 2020                 |
| Trinity Peninsula Seymour Island | Abernethy Flats            | 2006–2015; 2017 | 1        | 75                 | -8.1                   | -5.4 to -8.2            | -7.4                   |               |                  |                        |                     |                     |  |
|                                  |                            |                 |          |                    |                        | -6.7                    | -                      | -             | 152 to 509       | -2768                  | -                   | -                   | Knazková et al., 2020  |
|                                  |                            |                 |          |                    |                        | -3.5 to -5.5            | -                      | 61 to 64      | 396 to 409       | -1718 to -2425         | 1.64 to 1.91        | 0.85 to 0.94        |  |
| Trinity Peninsula Seymour Island | Cape Lachman - bare ground | 3/2015–2/2017   | 1        | 50                 | -4.3 to -7.2           | -4.4 to -6.7            | -                      |               |                  |                        |                     |                     |  |
|                                  |                            |                 |          |                    |                        | -4.1 to -5.6            | -4.1 to -5.3           | 50            | 172 to 195       | 2641                   | 0.69 to 0.95        | 0.93 to 0.99        | Hrbáček et al., 2020a  |
| Trinity Peninsula Seymour Island | Hope Bay                   | 2/2009–2/2011   | 2        | 80                 | -10.3                  | -4.1 to -5.6            | -4.1 to -5.3           | 73 to 128     |                  |                        |                     |                     | Schaefer et al., 2017a, 2017b  |
|                                  |                            |                 |          |                    |                        | -8.7                    | -8.3                   | 100           |                  | -2985                  |                     |                     | Gjorup et al., 2020  |

<sup>1</sup> Mean annual air temperature.

<sup>2</sup> Mean annual near-surface ground temperature.

<sup>3</sup> Mean annual temperature of the permafrost table.

**Table 5**  
Selected characteristics of the sites in West Antarctica region.

| Area                | Study site          | Study period | Profiles | Profile Depth (cm) | MAAT <sup>1</sup> (°C) | MASGT <sup>2</sup> (°C) | MAPT <sup>3</sup> (°C) | ALT (cm) | TDD (°C.day) | FDD (°C.day)      | thawing n-factor | freezing n-factor  | Reference                        |
|---------------------|---------------------|--------------|----------|--------------------|------------------------|-------------------------|------------------------|----------|--------------|-------------------|------------------|--------------------|----------------------------------|
| Ellsworth Mountains | Ellsworth Mountains | 2012–2013    | 2        | 30                 | -19.8                  | -18.2 to -18.4          | -18.3                  | 47–48    | ca 40 to 150 | ca -6500 to -7000 |                  | 0.93–0.94          | Schaefer et al., 2017a, 2017b    |
|                     |                     |              |          |                    |                        | -20.3                   | -19.3                  | 10 to 45 |              |                   |                  | McKay et al., 2019 |                                  |
| Marie Byrd Land     | Russkaya            | 2008/2013    | 1        | 10 to 20           | -10.4                  |                         |                        | 10 to 20 |              |                   |                  |                    | Bockheim, 2015; Obu et al., 2020 |
|                     |                     |              |          |                    |                        |                         |                        |          |              |                   |                  |                    |                                  |

<sup>1</sup> Mean annual air temperature.

<sup>2</sup> Mean annual near-surface ground temperature.

<sup>3</sup> Mean annual temperature of the permafrost table.

**Table 6**  
Selected characteristics of the sites in East Antarctica region.

| Area            | Study site                               | Study period | Profiles             | Profile Depth (cm) | MAAT <sup>1</sup> (°C)            | MASGT <sup>2</sup> (°C) | MAPT <sup>3</sup> (°C) | ALT (cm)             | TDD (°C·day) | FDD (°C·day)                                  | thawing n-factor | freezing n-factor | Reference  |
|-----------------|--|--------------|----------------------|--------------------|-----------------------------------|-------------------------|------------------------|----------------------|--------------|---|------------------|-------------------|--|
| Queen Maud Land | Vesleskarvet nunatak                     | 2009–2012    | 1 (20 sample points) |                    | *-2.2 to -27.8 (= -15)? (Setting) |                         |                        |                      |              |   |                  |                   | Hansen et al., 2013                                      |
|                 | Vesleskarvet nunatak                     | 2009–2013    | 1                    | 60 cm              | -15.9 to -18.5                    | -16.1                   |                        | 14 to 20 cm          |              | -5448 to -5983 (near-surface); -6404 to -7214 |                  | 1.00–1.02         | Kotzé and Meikjejohn, 2017, Hrbáček et al., 2021a, 2021b |
|                 | Flarjuven                                | 2008–2015    | 1                    | 60 cm              | -17.9                             | -17.5                   |                        | 23 (13 to 26)        |              |   |                  |                   | Hrbáček et al., 2021a, 2021b                             |
| Prydz Bay       | Troll                                    | 2007–2015    | 1                    | 200 cm             | -17.4                             | -17.4                   |                        | 13 (10 to 15)        |              |   |                  |                   | Hrbáček et al., 2021a, 2021b                             |
|                 | Novolazarevskaya                         |              | 1                    |                    | -10.3                             | -10.1                   |                        | 100 cm               |              |   |                  |                   | Hrbáček et al., 2021a, 2021b                             |
| Enderby Land    | Vestfold Hills and Larsemann Hills oases | 1/2010       | 4                    |                    | *-9.8 to -10.2 (Objects)          | -8.4                    |                        | 83 ± 14 cm (max 110) |              |   |                  |                   | Mergelov, 2014   |
|                 | Molodyozhnaya                            | 2008–2015    | 1                    | 100 cm             | -11                               |                         |                        | 65 to >100 cm        |              |   |                  |                   | Hrbáček et al., 2021a, 2021b                             |

<sup>1</sup> Mean annual air temperature.<sup>2</sup> Mean annual near-surface ground temperature.<sup>3</sup> Mean annual temperature of the permafrost table.

0 °C at 80 cm depth (Fig. 2).

The Krakow Peninsula contains several small ice-free areas. Short-term active layer monitoring results were reported from Lions Rump (Almeida et al., 2014), whereas five-year results are available from a nearby site at Low Head (Almeida et al., 2017). Both areas are located in the eastern part of the Krakow Peninsula. At Lions Rump there was no gradient of MAGT between the surface and the top of the permafrost table. Depending on the site conditions, observed mean annual temperatures varied between -0.9 °C (moss-covered site) and -2.0 °C (lichen-covered site) in 2009/2010, with a relatively thick active layer of about 120–150 cm (Almeida et al., 2014). A similar thermal regime pattern was observed in Low Head. The MAGT did not show any depth gradient and was -1.5 °C at both 1 and 100 cm depths (Fig. 2). The annual sum of TDD ranged between 280 and 440 °C·day, whereas the FDD were -700 to -1100 °C·day at a depth of 1 cm. The ALT was between 98 and 106 cm (Table 2).

Overall, the ground thermal regime on King George Island over recent years correlates well with the evolution of air temperatures on the island (e.g. Michel et al., 2014; Almeida et al., 2017). The role of the factors such as vegetation, snow cover, or lithological variability has not yet been studied in detail. Although the area is considered to be in bordering conditions for continuous permafrost conditions (Bockheim et al., 2013), there are currently no reports suggesting the absence of permafrost at specific sites on King George Island. Indeed, modelled temperatures at the top of the permafrost, using Cryogrid 1 model, of less than 0 °C suggest continuous permafrost conditions on the entire island (Obu et al., 2020).

**3.1.1.2. Livingston Island.** Livingston is an elongated island running west-east for approximately 72 km along the 62°35' S parallel. Livingston Island has an irregular coastline, with several peninsulas and with the relief passing from the low-lying platform of Byers Peninsula, in the west, to the very rugged Friesland mountains that rise up to 1700 m in the eastern limit of the island. Byers is the largest ice-free area of the SSI, while Hurd Peninsula, closer to the Friesland range also has several ice-free areas. Elsewhere, ice-free terrains occur in small peninsulas around the island (e.g. Elephant Point, Hannah Point, Cape Shirreff and Barnard Point), or in small nunataks. Livingston Island is glaciated in over 90% (Recondo et al., 2022) of its area and dominated in the west by the Rotch Dome, and in the east by the glaciated peaks of the Frieslands, with small steep valley glaciers flowing directly into the sea.

**3.1.1.3. Byers Peninsula.** Byers Peninsula is 9 to 18 km long (84.7 km<sup>2</sup>) and formed after the last deglaciation in the Holocene (e.g., Oliva et al., 2016), starting about 5000–4000 years BP (Björck et al., 1996). Byers Peninsula is of high geomorphological, periglacial, and ecological interest and has been specially protected by the Antarctic Treaty since 1966 (Quesada et al., 2009), allowing a wide variety of research activities (Benayas et al., 2013), including active layer permafrost research. The climate of Byers Peninsula is classified as wet oceanic with MAAT around -2.8 °C. Temperatures range between -25 °C in winter and +10 °C in summer (e.g. Bañón et al., 2013), and annual precipitation, mainly as snow, is about 500–800 mm, with snow persisting on the ground surface between 8 and 9 months per year (Bañón et al., 2013; Navarro et al., 2013).

The central spine of the Byers Peninsula is characterized by a smooth, slightly wavy, platform, of about 70–100 m in elevation, with shallow basins, where lakes and ponds are located, and low mounds (Thomson and López-Martínez, 1996). A few small hills (up to 140 m a.s.l.) of eroded volcanic edifices protrude from the platform, which is characterized by Jurassic and Early Cretaceous sediments and volcanic and volcanoclastic materials (e.g., Smellie et al., 1980, 1984; López-Martínez et al., 2012; Hathway and Lomas, 1998). The coast is marked by wide present-day beaches, with 7 levels of terraces that formed during Holocene deglaciation (Oliva et al., 2016). The soils of Byers Peninsula

**Table 7**  
Selected characteristics of the sites in Victoria Land region.

| Area                     | Study site  | Study period       | Profiles | Profile Depth (cm) | MAAT <sup>1</sup> (°C)   | MASGT <sup>2</sup> (°C) | MAPT <sup>3</sup> (°C) | ALT (cm)                          | TDD (°C.day)        | FDD (°C.day)            | thawing n-factor | freezing n-factor    | Reference  |
|--------------------------|---|--------------------|----------|--------------------|--------------------------|-------------------------|------------------------|-----------------------------------|---------------------|-------------------------|------------------|----------------------|--|
| Dry Valleys              | Granite Harbour   | 2003–2018          | 1        | 90                 | −16 (−14.8 to −17.8)     | −14 (−13.1 to −16.3)    | −14 (−12.9 to −14.5)   | 89 cm (82 to >90 cm)              |                     |                         |                  |                      | Adlam et al., 2010; Seybold et al., 2010; Hrbáček et al., 2021a, 2021b; Carshalton et al., 2022                          |
|                          | Marble Point  | 1999–2018          | 1        | 120                | −18 (−16.0 to −18.7)     | −17                     |                        | 49 cm                             |                     |                         |                  |                      | Adlam et al., 2010; Seybold et al., 2010; Guglielmin et al., 2011; Hrbáček et al., 2021a, 2021b; Carshalton et al., 2022 |
|                          | Minna Bluff   | 2003–2018          | 1        | 107                | −16                      | −17                     |                        | 23 cm                             |                     |                         |                  |                      | Adlam et al., 2010; Seybold et al., 2010; Hrbáček et al., 2021a, 2021b; Carshalton et al., 2022                          |
|                          | Mt Fleming  | 2002–2018          | 1        | 60                 | −23                      | −24                     |                        | 7 cm                              |                     |                         |                  |                      | Adlam et al., 2010; Seybold et al., 2010; Hrbáček et al., 2021a, 2021b; Carshalton et al., 2022                          |
|                          | Bull Pass East (Wright Valley – North)                            | 2012–2018          | 1        | 120                | –                        | –                       |                        |                                   |                     |                         |                  |                      | Adlam et al., 2010; Seybold et al., 2010; Hrbáček et al., 2021a, 2021b; Carshalton et al., 2022                          |
|                          | Wright Valley – South wall  | 2011–2018          | 1        | 120                | −17                      | −17                     |                        |                                   |                     |                         |                  |                      | Adlam et al., 2010; Seybold et al., 2010; Hrbáček et al., 2021a, 2021b; Carshalton et al., 2022                          |
|                          | Wright Valley (floor)   | 1999–2018          | 1        | 120                | −19                      | −19                     |                        | 49 cm                             |                     |                         |                  |                      | Adlam et al., 2010; Seybold et al., 2010; Guglielmin et al., 2011; Hrbáček et al., 2021a, 2021b; Carshalton et al., 2022 |
|                          | Scott Base  | 1999–2018          | 1        | 120                | −17                      | −16                     |                        |                                   |                     |                         |                  |                      | Adlam et al., 2010; Seybold et al., 2010; Hrbáček et al., 2021a, 2021b; Carshalton et al., 2022                          |
|                          | Victoria Valley   | 1999–2018          | 1        | 120                | −23                      | −23                     |                        |                                   |                     |                         |                  |                      | Adlam et al., 2010; Seybold et al., 2010; Hrbáček et al., 2021a, 2021b; Carshalton et al., 2022                          |
|                          | Beacon Valley   | 2001–2012          | 1        |                    | −21.6 ± 0.7              | −21.4 ± 0.8             |                        |                                   |                     |                         |                  |                      | Lacelle et al., 2016; Liu et al., 2018   |
| University Valley        | 2015–2016   | 1                  |          |                    | ca. −23 °C               |                         |                        |                                   |                     |                         |                  | Lacelle et al., 2016 |  |
| Wormherder Creek wetland | 2010–2012   | 1                  |          | −23.4 ± 8.3 °C     | −26 ± 10.6 °C (2010)     |                         |                        |                                   |                     |                         |                  | Fisher et al., 2016  |  |
| Taylor Valley            |   |                    | 1        |                    | −18 (Doran et al., 2002) |                         |                        | ~10–60 cm (Bockheim et al., 2007) |                     |                         |                  |                      | Levy et al., 2011  |
| Northern Victoria Land   | Boulder Clay  | 1997–2012          | 1        |                    | −13.8 (−12.7 to −15.3)   | −16.1 (−14.6 to −18.4)  |                        | 24.5 (6 to 30 cm)                 |                     |                         |                  |                      | Guglielmin et al., 2012; Cannone et al., 2021  |
|                          | Prior Island, Boulder Clay MZS, Edmonson Point, Apostrophe Island | 2000 (2002) - 2013 | 4        |                    | −12.5 to −15.3           | −0.3 to 7.8             |                        | 2 to 18 cm (max 23 to 92 cm)      | 39 to 370.1         |                         |                  |                      | Guglielmin et al., 2014a, 2014b  |
|                          | Edmonson Point  | 2015–2016          | 1 (3)    |                    | −16.4 to −16.6           | −13.5 to −15.8          |                        | 23 to 40 cm                       | 110.8 to 702.6 (GT) | −5164.5 to −5940.2 (GT) | 10.83 to 52.23   | 0.92 to 0.99         | Hrbáček et al., 2020a  |

<sup>1</sup> Mean annual air temperature.

<sup>2</sup> Mean annual near-surface ground temperature.

<sup>3</sup> Mean annual temperature of the permafrost table.

**Table 8**  
Selected characteristics of the sites in Sub-Antarctic Islands region.

| Area         | Study site           | Study period             | Profiles | Profile Depth (cm) | MAAT <sup>1</sup> (°C) | MASGT <sup>2</sup> (°C) | MAPT <sup>3</sup> (°C) | ALT (cm)   | TDD (°C-day) | FDD (°C-day)   | thawing n-factor | freezing n-factor | Reference  |
|--------------|----------------------|--------------------------|----------|--------------------|------------------------|-------------------------|------------------------|------------|--------------|----------------|------------------|-------------------|--|
| Signy Island | BG1                  | 2006–2009, 3/2015–2/2017 | 1        | 250                | –3.4 to –4.2           | –1.9 to –2.9            |                        | 124 to 185 | 231 to 538   | –1074 to –1453 | 2.16 to 2.29     | 0.77 to 0.78      | Guglielmin et al., 2012; Hrbáček et al., 2020a     |
|              | BG2                  | 2006–2009                | 1        | 90                 |                        | –2.0 to –2.5            |                        | 83 to 163  | 125 to 385   | –877 to –1190  |                  |                   | Guglielmin et al., 2012                            |
|              | Andreeva             | 2006–2009                | 1        | 90                 |                        | –1.6 to –2.5            |                        | 95 to 108  | 215 to 449   | –900 to –1333  |                  |                   | Guglielmin et al., 2012                            |
|              | Santonnia            | 2006–2009, 3/2015–2/2017 | 1        | 60                 |                        | –1.7 to –3.0            |                        | 55 to 123  | 29 to 413    | –770 to –1162  | 0.29 to 0.55     | 0.54 to 0.69      | Guglielmin et al., 2012; Hrbáček et al., 2020a     |
|              | Marion Island (PEIs) | 2015                     | 2        | –                  | 0.5–5.5                | 0.6–4.6                 |                        | none       | 392 to 499   | –95 to –195    |                  |                   | Nel et al., 2021; Hansen, 2018 for MASGT, TDD, FDD |
|              | Campbell Islands     | 2015; 2017               | –        | –                  | 3.8 to 6               |                         |                        | none       |              |                |                  |                   | Forre et al., 2016                                 |
|              | Crozet Islands       | 2007                     | –        | –                  | 3 to 8                 |                         |                        | none       |              |                |                  |                   | Quilty, 2007                                       |
|              | Kerguelen Island     | 2006                     | –        | –                  | 2 to 9                 |                         |                        | none       |              |                |                  |                   | Leihy et al., 2018                                 |

<sup>1</sup> Mean annual air temperature.

<sup>2</sup> Mean annual near-surface ground temperature.

<sup>3</sup> Mean annual temperature of the permafrost table.

are coarse-grained with a sandy silty matrix (Navas et al., 2008; Moura et al., 2012). The vegetation, classified as open tundra, is scarce and consists of patches of mosses and lichens, as well as the only two autochthonous vascular plants in Antarctica, *Deschampsia antarctica* and *Colobanthis quitensis* (e.g.; Serrano, 2003; Vera, 2011).

Prior to the IPY (2007/08) research on permafrost and frozen ground in Byers Peninsula consisted of geomorphological mapping revealing a wide variety of periglacial landforms associated with the presence of continuous permafrost, an active layer, and freeze-thaw processes (Serrano et al., 1996; López-Martínez et al., 1996, López-Martínez et al., 2012). Permafrost was also detected in the coastal Holocene terraces (Serrano et al., 1996, 2003), confirming its major role in groundwater dynamics (Cuchi et al., 2004).

In 2009, during the IPY, a TSP (Thermal State of Permafrost) and a CALM site (Limnopolare Lake CALM site A-25) were established at the Limnopolare Lake watershed for continuous temperature monitoring of the active layer and ALT measurement by mechanical probing within 100 × 100 grid (de Pablo et al., 2013, 2014, 2016, 2017, 2018, 2020). The TSP station consists of two shallow boreholes (80 and 130 cm deep) and includes devices to measure air and ground surface temperatures, as well as a snow pole to derive snow cover (de Pablo et al., 2016). Other sites for ground temperature measurements in Byers Peninsula do not provide continuous data as they were installed for the purpose of short-term monitoring. Three shallow boreholes (80 cm) are located near to lakes Domo, Escondido and Cerro Negro (Hrbáček et al., 2016a; Oliva et al., 2017a), and 9 shallow measurement pits (10 cm) were installed in a transect from Rotch Dome towards the sea (Hrbáček et al., 2020b).

Existing shallow TSP boreholes in Limnopolare Lake do not reach the permafrost table but only the active layer. Permafrost was calculated to exist at less than 1.5 m deep based on the ground temperatures at the boreholes (de Pablo et al., 2013, 2014). The temperature, estimated for 10 shallow boreholes along a transect from Roch Dome Glacier, at the top of the permafrost ranged between –0.7 °C and –1.2 °C (Hrbáček et al., 2020b). The measured surface offset was 1.7 °C, revealing the presence of a surficial isolator. In the absence of vegetation, snow/ice is the unique possible insulation source. The presence of a zero curtain period, in the thermal signal measured at the ground surface, suggests that an ice layer formed at the base of the snow cover, during the melt period. The zero-curtain period had high interannual variability; from 30 to 90 days (de Pablo et al., 2014). Based on the ground temperatures, the annual ground thermal regime could be divided into thaw and freeze seasons (de Pablo et al., 2014). Thawing seasons ranged from 60 to 90 days while freezing periods extended from 270 to 300 days (de Pablo et al., 2014). Mean GST varied by about –1 °C with thermal amplitudes of about 15 °C (de Pablo et al., 2014).

The thaw depth measured at the CALM site decreased between 2009 and 2015, increasing again in 2016 (de Pablo et al., 2018), related to an increase in snow depth in that period (de Pablo et al., 2016, 2018, 2020). The thaw depths represent the mean value from the CALM-S site measured, usually, in early February. Therefore, the mean thaw depth was lower than the maximum ALTs, which reached about 150 cm (Fig. 2, Table 2). The difference is due to the measuring date in early February, established by logistic constraints, which is earlier than the timing of maximum thaw that usually occurs during March in this region (de Pablo et al., 2014). The ALTs at the other sites on Byers Peninsula were estimated to be ca. 85 to 115 cm (Oliva et al., 2017a; Hrbáček et al., 2020a).

Reported reduction in the freezing n-factor is likely to be due to increasing insulation of the ground surface from atmospheric conditions (de Pablo et al., 2017) due to snow cover. However, a reported reduction in snow-free days (2009 and 2015 period), limited the period in which the ground could have /thawed during the summer, or freeze during the early freeze season (de Pablo et al., 2017), reducing ground surface FDD from –670 °C day in 2011 to –230 °C day in 2013 (Table 2). Meanwhile air FDD where quite stable at about –1000 °C day (de Pablo et al., 2017, 2018). Although snow cover seems to play an important role due to

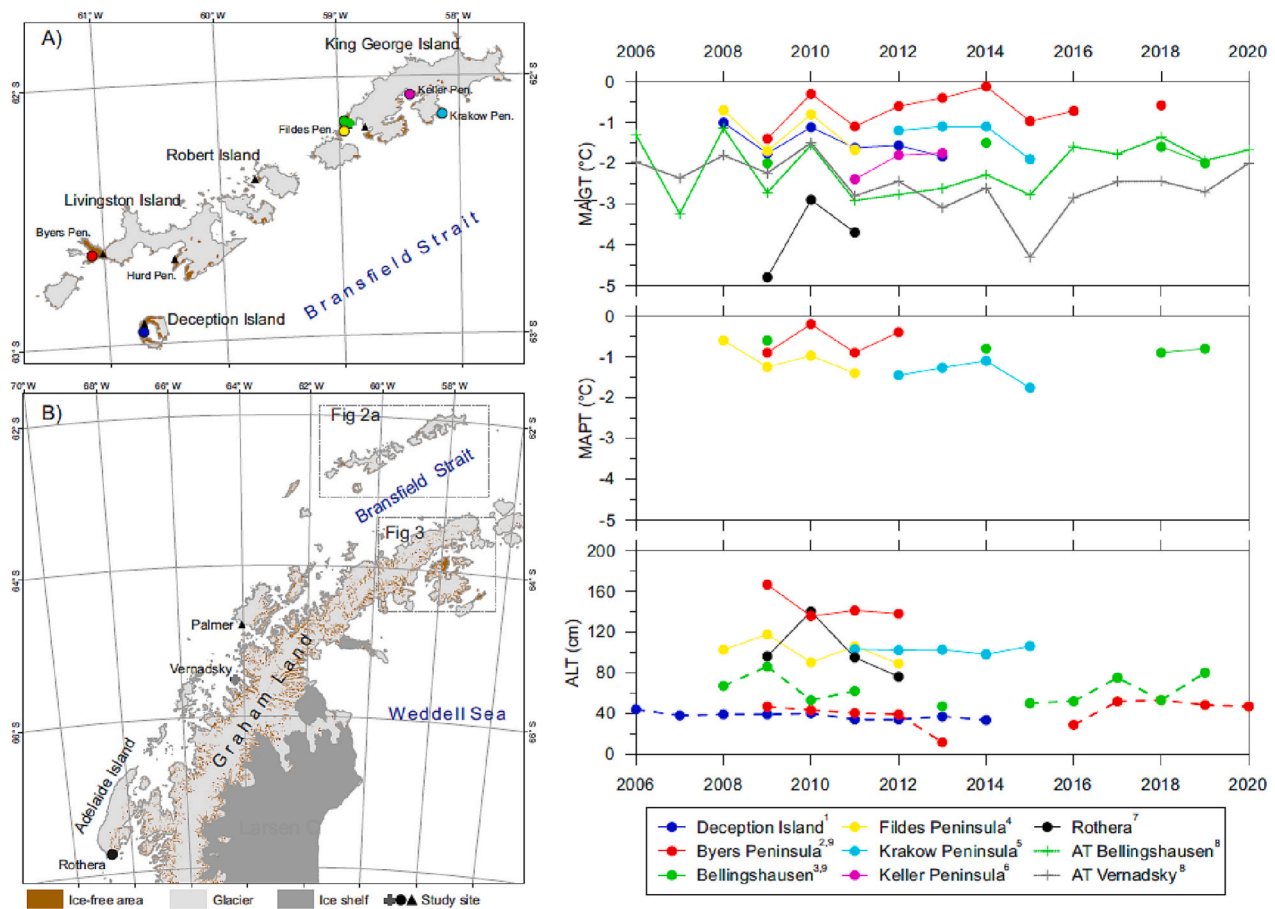


**Fig. 2.** The variability of mean annual near-surface ground temperature (MAGT), mean annual temperature, the permafrost table (MAPT), and active layer thickness (ALT) in selected sites of the South Shetland Islands and Western Antarctic Peninsula. Dashed line in the lowest figure indicate ALTs measured by mechanical probing. The data were extracted from studies by <sup>1</sup>Ramos et al., 2017; <sup>2</sup>de Pablo et al., 2014, 2018; <sup>3</sup>Hrbáček et al., 2021b; <sup>4</sup>Michel et al., 2014; <sup>5</sup>Almeida et al., 2017; <sup>6</sup>Chaves et al., 2017; <sup>7</sup>Guglielmin et al., 2014a, 2014b; <sup>8</sup>READER database, <sup>9</sup>CALM database. Black triangles indicate the position of other study sites in the region.

differential snow accumulation on the wavy relief of the peninsula central plateau (de Pablo et al., 2017), other factors such as the groundwater flow (Cuchi et al., 2004; de Pablo et al., 2013, 2014, 2018), and lithological conditions (e.g., Serrano et al., 1996; López-Martínez et al., 1996) have not yet been studied in this ice-free area, the largest of the SSI.

**3.1.1.4. Hurd Peninsula.** Hurd Peninsula is a small, rugged, elongated area, ca. 8 km long and 1 to 4 km wide that divides South Bay from False Bay on the southern coast of Livingston Island. Most of the peninsula is glaciated, with the Hurd Peninsula ice cap that drains through several small lobes, and with several small ice-free areas that run from sea-level to 407 m a.s.l. at Moores Peak. The bedrock is mainly composed of the Myers Bluff Formation, a turbidite sequence with alternating layers of low-grade metamorphism, claystone, and fine sandstone, with a diorite batholite in the northern sector (Pimpirev et al., 2006). Mean annual air temperatures in Hurd Peninsula are about  $-1.2$  °C at sea level (Bañon and Vasallo, 2015), and  $-4.2$  °C at 275 m in Reina Sofia Peak (Ferreira et al., 2017).

Active layer and permafrost monitoring commenced in Hurd Peninsula in the 1990's near the Spanish Station Juan Carlos I. In 2000 two shallow (70 cm) boreholes were installed with continuous temperature monitoring. During the IPY 2007–08, two deep boreholes (15 and 25 m) were drilled in the Reina Sofia Peak area (Ramos and Vieira, 2009) and three new boreholes, ranging from 4 to 8 m deep, were installed across an altitudinal gradient near the Bulgarian Station St Kliment Ohridski (Vieira et al., 2010; Ferreira et al., 2017).

Permafrost in Hurd Peninsula is absent at low elevations, except in ice-cored moraines or rock-glaciers (Hauck et al., 2007). However, boreholes drilled in bedrock had a thick active layer ( $> 5$  m), and suggest that the boundary of the continuous permafrost zone may be located above ca. 150 m a.s.l. (Ferreira et al., 2017). The shallow boreholes drilled in diamicton, below 150 m a.s.l., did not have permafrost, which suggests that there is a narrow belt of discontinuous permafrost between sea-level and ca. 150 m a.s.l.

The permafrost temperature at 25 m depth in the Permamodel-Gulbenkian 1 borehole varied between  $-2.0$  and  $-1.7$  °C from 2009 to 2015, with no clear trend (Biskaborn et al., 2019). The active layer at Reina Sofia Peak, in a diamicton, was ca. 76 cm in 2009 and only 26 cm in 2015. At Reina Sofia, in 2008 and 2009 FDD ranged from  $-1042$  to  $-811$  °C·day and the TDD ranged from 49 and 145 °C·days (Ferreira et al., 2017). The N-Factor ranged from 0.53 to 0.57 in those same years. Papagal, located at 152 m a.s.l., had 214 TDD °C·day and  $-783$  FDD °C·day in 2009, with a higher freezing n-factor than Reina Sofia (0.7) (Ferreira et al., 2017, Table 2). The snow cover, mainly controlled by topography, rather than elevation, was considered the main controlling factor on the ground thermal regime (Ferreira et al., 2017). Recently, Ramos et al. (2020) have shown that the increase in snow cover thickness between 2009 and 2015 at the borehole Permamodel-Gulbenkian-2, led to the full disappearance of the active layer and to the aggradation of permafrost. However, wind-exposed boreholes in bedrock at Hurd Peninsula at Papagal and CALM Ohridski had an ALT exceeding 5 m, (Ferreira et al., 2017). Like other boreholes in the Antarctic Peninsula region, there was a general decrease in active layer thickness from 2009 to 2015 that was associated with a longer occurrence of snow

persistence in the summer season after 2009 (Oliva et al., 2017a, de Pablo et al., 2020, Ramos et al., 2020).

**3.1.1.5. Deception Island.** Deception Island is a composite volcano with a well-defined main cone ca. 14 km in diameter in its subaerial part and a collapse caldera of ca.  $8.5 \times 10$  km, which is open to the sea in a 500 m breach in the SE coast. The main crater rim rises to 539 m a.s.l. at Mount Pond, with most of the rim more than 250 m a.s.l. Several glaciers are present along the rim, with the ones on the eastern side of the island flowing down to the sea-level, either to the caldera or to the outer coast. The glacier-free area is dominated by lava flows, interbedded with ash and pyroclastic deposits, both from the pre and post-caldera stages (López-Martínez and Serrano, 2002). The inner part of the rim has been affected by several volcanic eruptions, including recent ones in 1967, 1969, and 1970 (Ortiz et al., 1997). The eruptions generated large volumes of lapilli and ash that cover large areas of the island, some burying glaciers and snow patches. The island's substrate is poorly consolidated and, under the effects of the Maritime Antarctic climate, with high snow accumulation and summer temperatures favouring snowmelt and rain events, is prone to water erosion. Vegetation cover only occurs in small, localized, patches, and the lack thereof exposes the islands' soils to severe wind erosion, generating lag surfaces mainly on ridges and convex surfaces (Vieira et al., 2008). Several localities of Deception Island have high geothermal anomalies, with ground temperatures of up to about 90 °C (e.g. Cerro Caliente) and fumaroles or geothermally heated caldera waters occur at several sites. Goyanes et al. (2014) have shown that geothermal anomalies may have a local effect, for example; in the alluvial fan close to the Argentinean station, over about 100 m laterally, ground temperatures pass from a stable +10 °C all year-round, to permafrost.

Most of Deception Island shows the presence of permafrost, except at the beaches, where the influence of sea-water plays a role in warming the terrain. Permafrost and active layer monitoring was initiated in the 1990's with the installation of active layer sensors at various sites, with research focussing on the energy exchange between the soil and the atmosphere (Ramos and Aguirre-Puente, 1994). The initial activities did not include continuous monitoring, as observations were focussed on characterizing the freezing and/or thawing seasons. However, monitoring was conducted at Cerro JB in the vicinity of the Spanish Station Gabriel de Castilla and in Cerro Caliente (Ramos et al., 2007).

In 2006 a CALM-S site was installed on a small plateau in the western rim of Crater Lake (Hauck et al., 2007; Ramos et al., 2010). Continuous monitoring includes a CALM-S grid, 3 permafrost boreholes, a snow-meteorological station (de Pablo et al., 2016), several shallow boreholes, and an automatic electrical resistivity tomography monitoring system (Farzamian et al., 2020). In 2009 the Irizar CALM-S site was established at the crater rim close to Vapour Col in order to obtain data from a wind-exposed site, since Crater Lake is sheltered from the west-winds. Crater Lake comprises a soil characterized by a thick lapilli cover, which generates high insulation, and thus a shallow active layer. Irizar has a lag-surface with a more permeable soil, which results in a thicker active layer. Both CALM-S grids have continuous monitoring of active layer and permafrost temperature, and are probed once per year, generally in early February, for active layer thickness in  $100 \times 100$  m grids. Shallow boreholes located outside the two CALM-S grids were installed at the Chilean Refuge in 2010, close to the Argentinean Station in 2011, and at Fumarole Bay in 2012.

The mean annual air temperature at Crater Lake from January 2009 to January 2014 was  $-3.0$  °C. At the Crater Lake CALM-S site, permafrost occurs beneath a shallow active layer of 25 to 40 cm (Fig. 2) and is from 2.5 to 5 m thick, with temperatures from  $-0.3$  to  $-0.9$  °C (Vieira et al., 2008; Ramos et al., 2017; de Pablo et al., 2020). Crater Lake had a decreasing thaw depth from 2006 to 2014 following several years of longer lasting snow cover (Ramos et al., 2017), with de Pablo et al. (2020) reporting that the decline continued until 2016. The studies

indicate that snow cover plays a major role in the shallowing of the active layer and that it may even decouple ground cooling from the slight atmospheric warming (de Pablo et al., 2020).

The Irizar CALM-S site is located in a wind-exposed setting and recorded a MAAT from  $-2.0$  to  $-3.9$  °C with an active layer, varying from 40 to ca. 100 cm. The thicker active layer at Irizar may be a result of the lack of the lapilli cover that insulates the ground at Crater Lake.

**3.1.1.6. Other areas.** Beyond the monitoring on King George Island, Livingston Island, and Deception Island, little information on active layer or permafrost is available in the region. Bockheim et al. (2013) mention the ALT on Half Moon Island (10–50 cm) and Elephant Island (15–110 cm). Thomazini et al. (2020) provided 2-years of MAGT data from Copermine Peninsula (Robert Island) revealing annual temperatures around  $-1.5$  and  $-2.0$  °C (Table 2), but did not report data on ALT dynamics.

### 3.1.2. Western Antarctic Peninsula

The Western Antarctic Peninsula (Western AP) is located between latitude  $63^\circ\text{S}$  and  $73^\circ\text{S}$ , and longitude  $57^\circ\text{W}$  and  $68^\circ\text{W}$ . The area faces the Bellingshausen sea and is punctuated by islands, promontories, and small peninsulas, which include a complex network of straits, bays, and passages between the islands and the continental mainland. The climate of the Western AP is influenced by wet polar-maritime climates, with MAAT between  $-2$  °C ( $65^\circ\text{S}$ ) and  $-9$  °C ( $70^\circ\text{S}$ ) (Cook and Vaughan, 2010). Annual precipitation is estimated at 500 to 2000 mm in the Western AP and the northern AP (van Wessem et al., 2016). Warming has been occurring with an overall MAAT increase of  $0.8$ – $3.0$  °C between 1950 and 2015 (Oliva et al., 2017b; Turner et al., 2020). The Antarctic Peninsula Ice Sheet retreated from the western continental shelf break relatively rapidly after 18 ka BP, firstly in the north and subsequently the lift-off of grounded ice progressed southwards (Ó Cofaigh et al., 2014). The vegetation of the Western AP includes both the Antarctic herb tundra formation and the Antarctic non-vascular cryptogam tundra formation (Colesie et al., 2023).

Permafrost distribution in the Western AP is mostly discontinuous, with maximum estimated thicknesses around 150 m (Bockheim et al., 2013; Guglielmin et al., 2014a, 2014b). The ALT is highly variable, ranging between 30 and 500 cm (Vieira et al., 2010; Bockheim et al., 2013). Even though several research stations are located in the Western AP, few works focused on the active layer, or permafrost, have been published until recently.

**3.1.2.1. Rothera Point.** Rothera Point is a rocky promontory with an ice-free area of ca.  $1000 \times 250$  m. ( $67.57$  S,  $68.12$  W,  $10$ – $110$  m a.s.l.) located in Adelaide Island in Marguerite Bay, south-Western AP. Marguerite Bay has a cold dry maritime climate with a MAAT of  $-4.2$  °C and mean annual precipitation of about 500 mm (Turner et al., 2020). The bedrock is homogeneous, composed of diorite and granodiorite of mid-Cretaceous to early Tertiary age (Dewar, 1970). The deglaciation age of the Rothera Point area is still not well known, although Emslie (2001) estimated that deglaciation occurred about 6 ka BP. Permafrost is continuous here and ranges between 112 and 157 m in depth with an active layer ranging between 76 and 140 cm (Guglielmin et al., 2014b). Rock surfaces are generally covered by sporadic mosses, as well as diversity of epilithic lichens, that can strongly influence weathering processes (e.g.; Guglielmin et al., 2012).

The borehole site is located on a bedrock knob close to the “Memorial”, on one of the highest summits of Rothera Point, about 100 m a.s.l. Guglielmin et al. (2014b) reported that the MAAT of Rothera Point varied between  $-2.7$  (2010) and  $-4.6$  °C (2009), which was similar to the MAGT ( $-2.9$  °C in 2010 and  $-4.8$  °C in 2009, Fig. 2, Table 3). According to Biskaborn et al. (2019), the permafrost temperature at the depth of zero annual amplitude decreased slightly from 2014 to 2016 representing, at least for that period, the only site in Antarctica with a

decreasing pattern of permafrost temperature. The near-surface TDD varied between 363 (2011) and 186 °C·day (2009), while FDD were lowest in 2009 (−1731 °C·day) and greatest in 2010 (−1371 °C·day). The recorded n-factor for thawing was between 2.34 (2010) and 2.69 (2011). The active layer thickness and thermal conditions are under a strong influence of winter snow cover. At Rothera, the thick cover of winter snow (> 1 m) leads to ground temperature cooling.

**3.1.2.2. Palmer archipelago and Danco Coast.** This sub-region consists of several islands of the Palmer Archipelago and the coastal area of the Antarctic Peninsula called Danco Coast between 64° and 66°S and 60° to 65°W. This sub-region represents the most rapidly warming area of the Antarctic Peninsula with a warming rate around +0.5 °C/decade during the last several decades (Turner et al., 2020). Currently, the MAAT is around −1.5 to −2.5 °C. Active layer and permafrost research in this area has been undertaken in the vicinity of Palmer station (Anvers and Amsler Islands) and Primavera station (Cierva Cove).

The area is expected to be in the discontinuous to sporadic permafrost zone (Bockheim et al., 2013), however, Obu et al. (2020), using Cryogrid-1, modelled negative permafrost table temperatures in the entire sub-region. The near-surface temperature on Amsler Island correlates well with both air temperature and solar radiation (Wilhelm and Bockheim, 2017). Modelling of ALT by Wilhelm et al. (2015) suggested maximum depths exceeding 15 m (Table 3), however these results were contradicted by Uxa (2016) who proposed that modelled active several meters should be several meter thinner if the volumetric latent heat of phase change is considered correctly. Ground thermal data showed the active layer is thicker than 180 cm in all areas including Cierva Cove (Wilhelm and Bockheim, 2016).

### 3.1.3. Eastern Antarctic Peninsula

The Eastern AP, located between latitude 63°S and 75°S, and longitude 55°W and 65°W is bordered by the mountain ridges of the Antarctic Peninsula, with maximum elevations exceeding 3000 m a.s.l. on its western fringe, and the Weddell Sea on the eastern side.

Most of the Eastern AP (> 99%) is currently covered by the Antarctic Peninsula ice sheet and smaller local glaciers. Glacial shrinking in the Eastern AP began at 18.5 ka BP, and the ice-free exposure of the lowlands occurred between 13 and 11 ka BP (e.g. Oliva and Ruiz-Fernández, 2020). Since the Early Holocene, prevailing climate conditions have driven minor glacial advances and retreats. In response to the recent warming trends, several ice-shelves broke up and glacier extension diminished (Cook and Vaughan, 2010). Currently, the Eastern AP includes a few relatively large ice-free areas in the northern sector, such as James Ross Island (ca. 500 km<sup>2</sup> of total ice-free surface extent), Seymour Island (ca. 80 km<sup>2</sup>), or Vega Island (ca. 70 km<sup>2</sup>). The ice-free areas south of 65°S are comparatively smaller (< 5 km<sup>2</sup>) and mostly correspond to nunataks. The subglacial volcanic activity during the Late Cenozoic favoured the formation of volcanic mesas, which are widespread landform features (e.g. Davies et al., 2013; Ruiz-Fernández et al., 2019).

The climate of the Eastern AP is defined as semi-arid polar continental, with the highest MAAT of ca. −5.0 °C at sea level in the northern part of the Trinity Peninsula and decreasing towards southern parts of the region following latitudinal gradients of ca. 0.9 °C/deg. until values of ca. −17.0 °C at sea level at 75°S (e.g.; Cook and Vaughan, 2010). The Eastern AP's climate is strongly affected by the orographic barrier, formed by the mountain range along the Antarctic Peninsula, resulting in relatively low precipitation, mostly snow, estimated as 100 to 700 mm. Higher precipitation is modelled in the northern Eastern AP and in the mountainous parts of the Eastern AP (van Wessem et al., 2016). Strong warming of ca. 1.5–2.0 °C has occurred over the last 40 years in the region (Oliva et al., 2017b; Turner et al., 2020).

Terrestrial ecosystems in the northern Eastern AP are, together with the Western AP, some of the most dynamically changing parts of Antarctica in response to the MAAT increase. The entire area of the

Eastern AP is underlain by continuous permafrost (Bockheim et al., 2013; Obu et al., 2020) with the modelled temperatures on the top of the permafrost between −3.0 °C in the northern tip of Trinity Peninsula and ca. −20 °C in the mountainous areas around latitude 75°S. Geomorphological dynamics of the ice-free terrain is driven by periglacial processes and paraglacial dynamics in the recently exposed areas (Davies et al., 2013; Ruiz-Fernández et al., 2019). Unlike Western AP, the vegetation of the Eastern AP has lower diversity with no vascular plants though patches of mosses, lichens, and biotic crusts occur (Peat et al., 2009).

**3.1.3.1. James Ross Island, Ulu Peninsula.** Permafrost research in the northern Eastern AP has largely been constrained by logistic complexity. To date, the main area for permafrost research has been the ice-free area of Ulu Peninsula (312 km<sup>2</sup>), northern James Ross Island, with only a few studies in other areas. Intense geological and paleontological surveying has been undertaken in Eastern AP (e.g. Nelson, 1975; Olivero et al., 1986), whereas research focused on permafrost and active layer dynamics are recent and scarce.

The first pre-IPY permafrost research was limited to geophysical surveying, and geothermal gradient studies that estimated permafrost thicknesses varying between 6 and 67 m on the marine terraces of the Ulu Peninsula (Fukuda et al., 1992; Borzotta and Trombotto, 2004). Mori et al. (2006) also monitored ALT on Rink Point mesa on the SW section of Ulu Peninsula showing an annual ALT of between 60 and 80 cm. Since the IPY, research into the active layer and permafrost have been carried out more systematically in the northern part of Ulu Peninsula (e.g. Hrbáček et al., 2019; Hrbáček and Uxa, 2020). Here, ground temperatures are monitored in a network of >15 sites with shallow profiles providing continuous records with depths varying from 5 cm to 75–200 cm. Additionally, 3 CALM-S sites of sizes 50 to 50 up to 70 to 80 m have been operating since 2014, with annual probing of thaw depth.

The MAAT near Johan Gregor Mendel station (10 m a.s.l.) on the northern coast of Ulu Peninsula was −6.6 °C (2004–2020), varying from −4.0 to −9.0 °C (Kaplan Pastríková et al., 2023). The modelled annual precipitation ranges between 300 and 700 mm (van Wessem et al., 2016) mostly in the form of snowfall in winter. MAGT in the low-lying areas below 60 m a.s.l. is around −6.0 °C, ranging from −4 to −8 °C, whereas MAGT in the topmost part of the permafrost is around −6.5 °C with a relatively low annual variability (between −5.5 and −7.5 °C). Mean ALT values vary between 55 and 85 cm. Depending on summer climate conditions, ALT can range from 35 to 125 cm (Table 4, Fig. 3). There are noboreholes in the region providing data from depths >2 m.

The thawing season usually extends 100–120 days between late-November and early-March, associated with prevailing positive mean daily near-surface temperatures (Hrbáček et al., 2019). The total sum of TDD has a long-term mean of 300 to 400 °C·day ranging from 150 to 600 °C·day. By contrast, freezing seasons are much longer than thawing seasons with a mean duration of 240–270 days depending on annual climate conditions. The ground remains completely frozen during the winter months and does not even thaw during events with positive air temperatures (e.g. Hrbáček et al., 2019). The seasonal sum of FDD shows a mean of ca. −2600 °C·day, although it is highly variable between −1700 and −3500 °C (Table 4).

The ground thermal regime on Ulu Peninsula correlates well ( $r > 0.75$ ) with the air temperature (Hrbáček et al., 2016b, 2017b; Hrbáček et al., 2020a; Hrbáček and Uxa, 2020) and incoming radiation (Hrbáček et al., 2020a, 2020b). The ALT distribution is strongly related to local lithology and vegetation. In contrast, the effect on the ground thermal regime and ALT of snow cover is considered to be less important than lithology and vegetation (e.g. Hrbáček et al., 2019).

Lithological conditions are considered the most important factor driving differences in ALT on Ulu Peninsula. The major part of the area is formed by coarser volcanic materials and finer Cretaceous sediments.

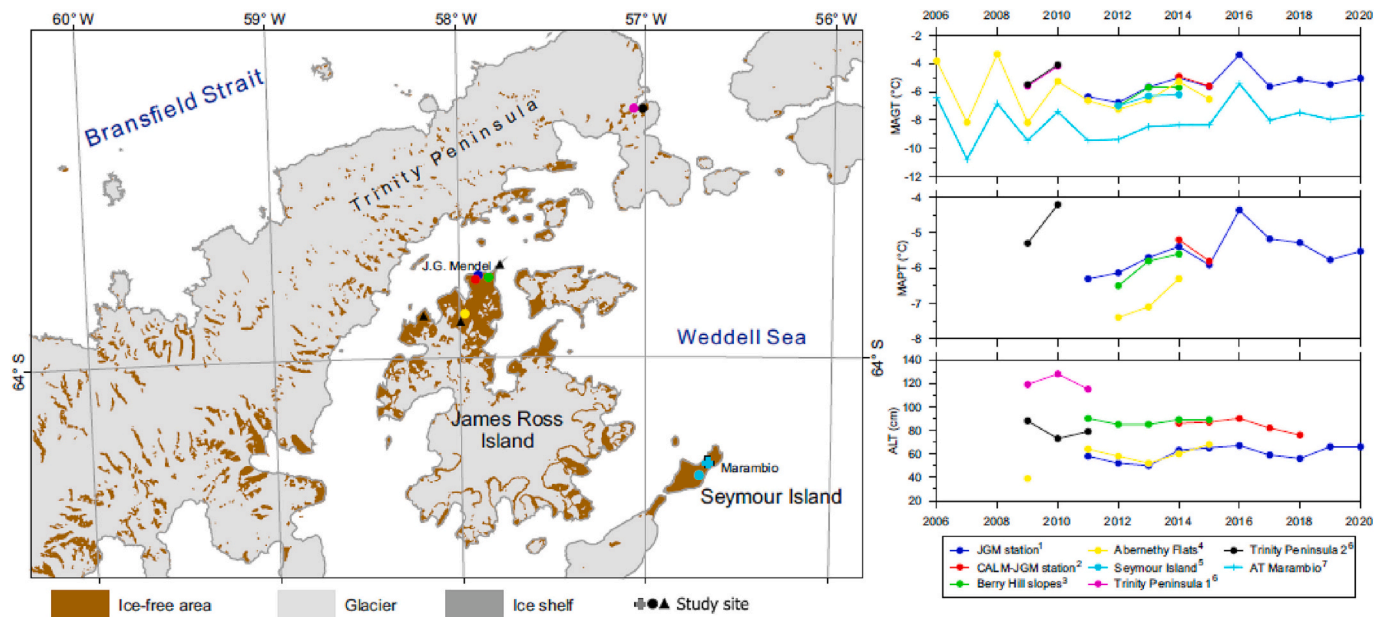


Fig. 3. The variability of mean annual near-surface ground temperature (MAGT), mean annual temperature, the permafrost table (MAPT), and active layer thickness (ALT) in selected sites of Eastern Antarctic Peninsula. The data were extracted from studies by<sup>1</sup>Pastirikova et al., in review;<sup>2</sup>Hrbáček et al., 2017a, 2021a; <sup>3</sup>Hrbáček et al., 2017b, 2019; <sup>4</sup>Hrbáček and Uxa, 2020; <sup>5</sup>Gjorup et al., 2020; <sup>6</sup>Schaefer et al., 2017a, 2017b; <sup>7</sup>READER database. The black triangles indicate the position of other study sites in the region.

The differences in geological composition and ground texture result in highly variable ground thermal properties (i.e. conductivity, capacity and diffusivity). An example of the lithological effects on the spatial distribution of ALT and ground thermal regime was observed on CALM-S JGM, where thermal conductivity was almost three times higher in Cretaceous sediments than in Holocene marine terrace sediments. As a result, the active layer was ca. 50 cm thicker in the Cretaceous terrain (Hrbáček et al., 2017b; Hrbáček et al., 2021b).

Vegetation exerts a weak influence on the ground thermal regime and ALT, at small-scales, as dense patches of mosses or lichens occur only in small (<100 m<sup>2</sup>) niches. Vegetation is an efficient insulator causing 1.1–1.4 °C lower MAGT and a 10–15 cm thinner ALT in moss-covered areas than in bare ground sites (Hrbáček et al., 2020a, 2020b).

The limited effect of snow cover on the ground thermal regime is caused by its irregular accumulations during the winter. The maximum snow depth on flat surfaces can reach 30 to 50 cm in short-term events (<2 days), but it is rapidly redistributed by the strong winds which results in thin snowpacks (< 20 cm) that persist only for a few weeks (Hrbáček et al., 2016a, 2016b; Kňázková et al., 2020). Such snow packs were found to be insufficient to be an effective insulation layer, which was confirmed by the freezing n-factor values of 0.9–1.0 suggesting strong interface between atmosphere and ground surface (Table 4). In specific cases where micro relief favours snow accumulations, snow depths >70 cm may persist most of the winter season and create an efficient insulation layer.

**3.1.3.2. Other parts of Eastern AP.** Previous work on the active layer and permafrost in other sectors of the Eastern AP are limited to soil research studies conducted at Hope Bay (Trinity Peninsula) and on Seymour Island (Bockheim, 2015). Short records from Hope Bay (2009–2011) revealed MAGT between –3.5 °C and –6.0 °C and ALT between 73 and 128 cm (Fig. 3, Table 4). The inter-site differences in ground thermal parameters in Hope Bay were caused by a different stage of ornithogenic activity and the presence of vegetation patches having an insulation effect on the ground thermal regime, causing active layer thinning (Schaefer et al., 2017a). An even shorter dataset from one site in Seymour Island (3/2011–1/2012) revealed very cold conditions during winter with FDD dropping to –3300 °C-day, and an ALT

estimated at 100 cm (Gjorup et al., 2020).

### 3.2. West Antarctica

The West Antarctica region comprises Ellsworth Land, Marie Byrd Land and Edward VII Land. The ice-free areas are limited mostly to mountainous ridges. The most prominent are in the Ellsworth Mountains where the highest point in Antarctica, Vinson Massif (4892 m a.s.l.) is located. Active layer and permafrost research in the West Antarctica region is mostly limited to the Ellsworth Mountains (Schaefer et al., 2017a, 2017b; McKay et al., 2019). The only brief results from the coastal part of Marie Byrd Land report a mean annual permafrost temperature of –10.3 °C (2008–2013) in the vicinity of Ruskaya station (Bockheim, 2015; Obu et al., 2020).

### 3.3. Ellsworth Mountains

The Ellsworth mountains are located around 77° to 88.5°S and 78° to 87°W. The mountain ridge, ca. 350 km long and 48 km wide is formed over two major areas, Sentinel range and Heritage range, which are bisected by the Minnesota Glacier. The prevailing geology consists of marble (late Precambrian), sedimentary rocks (late Cambrian), quartzite (upper Cambrian to Devonian) and marine and terrestrial layers (Permian) (Webers et al., 1992). The ice-free areas are underlain by ice-cemented or dry permafrost and vegetation is scarce (Bockheim, 2015). The climate of Ellsworth Mountains is cold and dry with MAAT ranging from –15 °C in the coastal zone down to –35 °C on the high-elevation polar plateau. The annual precipitation is estimated to about 150–175 mm (Bromwich et al., 2004).

The only two studies in the region are from the Mount Dolence area in the Heritage Range. Schaefer et al. (2017a, 2017b) reported a mean annual ground temperature of between –18.1 °C and –18.3 °C in the period 2012/2013 in two sites at 850 and 886 m elevation. The active layer was thawed only in December and January and the TDD was 50 to 150 °C-day. The ALT was estimated to be 47 and 48 cm (Table 5). However, the results should be considered with caution as the mean daily ground temperature at the depth of 30 cm did not exceed 0 °C. The ALT in the region is affected by the depth at where the ice table in dry

permafrost is present. McKay et al. (2019) observed the depth of the ice table to be between 10 and 45 cm in four sites elevated between 690 and 835 m.

### 3.4. East Antarctica

East Antarctica (EA) represents a large area in the coastal zone between 20°W and 170°E longitudinally and 65–75°S latitudinally. The ice-free areas in EA comprise ca. 10,900 km<sup>2</sup>, and are fragmented into separate nunataks of alpine character forming small ridges penetrating the inland ice sheet. The largest ice-free areas are mountain ridges in Queen Maud Land (ca. 3500 km<sup>2</sup>) and MacRobertson Land (ca. 5000 km<sup>2</sup>). In spite of the presence of several research stations in the area, studies of the active layer and permafrost are scarce.

#### 3.4.1. Queen Maud Land

Queen Maud Land lies between 20°W and 45°E. The coastline extends to 75°S at the western side, but the main part is generally about 70°S. Deglaciation of coastal oases started about 50–35 ka BP according to exposure ages and lacustrine deposits (Altmaier et al., 2011; Abramov et al., 2011). The bedrock geology of Queen Maud Land is dominated by Precambrian gneiss, formed 1 to 1.2 Ga ago, before the creation of the supercontinent Gondwana (Barrett, 1971). The climate follows both altitudinal and latitudinal gradients. The highest MAAT is in the coastal zone at 70°S (ca. −10 °C at Novolazarevskaya station in Schirmacher Hills), whereas the MAAT <15 °C are typical for the areas around 75°S (Halley research station) and mountainous areas around 1000 m a.s.l. (Kotzé and Meiklejohn, 2017). Precipitation is in the range 200–400 mm per year (Bromwich et al., 2004). No significant changes in the MAAT in the region were observed during the observational period (Turner et al., 2020).

There are two major ice-free areas with available permafrost data in Queen Maud Land – the system of nunataks near SANAE VI and Troll stations (Basen, Flårjuven, Grunehogna, Robertsollen, Schumacherfjellet, Slettfjell, Troll, Valterkulen and Vesleskarvetwith and Schirmacher Hills). The longest monitoring records are from the Basen (since 2004) and Troll (since 2007) nunataks. Overall, Queen Maud Land has a total of 10 profiles on 8 nunataks (Troll, Flårjuven, Valterkulen, Slettfjell, Schumacherfjellet, Grunehogna, Robertsollen and Vesleskarvet). Boreholes were installed on the Fossilryggen and Svea

nunataks, however, these are inactive (Vieira et al., 2010). According to recent measurements, the MAATs ranged from −14 to −18 °C and ALTs range from 16 to 58 cm (Kotzé and Meiklejohn, 2017, Fig. 4, Table 6).

The Schirmacher Hills is located in the coastal area of Queen Maud Land. The oasis is 18 km long and from 0.6 to 3.5 km wide, with an elevation ranging from 10 to 226 m a.s.l. The Schirmacher Hills stretch along the slope of the continental ice shelf. In the north the oasis borders the Lazarev Ice Shelf, which separates it from the sea. Sediments in large lake depressions have been radiocarbon dated at 18–30 ka. However, soil development suggests that geomorphic surfaces are only several thousand years old. Moraine deposits dated back at 145–80 ka show evidence of past phases with larger glacial systems. Minor warming and cooling events during the current interglacial period, from 13 ka to 3 ka, have been revealed by dating sediments from dry lake beds and shallow lakes in Schirmacher Oasis. The recession of ice began in the Early Holocene and had three phases, with the main phase recorded at 6.7–2.2 ka BP (Dharwadkar et al., 2018).

The first permafrost investigations were undertaken in the vicinity of Novolazarevskaya station (Schirmacher Oasis) in 1979 finding the active layer depth in the range of 8 cm for icy algae-rich deposits and 70 cm for fine-grained dry sediments. The first site for active layer monitoring (CALM-S) was established in 2008, and boreholes for ground temperature monitoring were installed in 2009 (Abramov et al., 2011). According to recent measurements, the MAGTs in the Schirmacher Oasis are around −9 °C and ALTs are 30–120 cm (Table 6). Modelling estimated the MAGT on the top of the permafrost within the range of −8 to −10 °C (Obu et al., 2020).

#### 3.4.2. Other parts of EA

The remaining parts of EA where some active layer and permafrost monitoring is available are Enderby Land, Princess Elizabeth Land and Wilkes Land. Deglaciation began around 30 ka in the Bunge Hills in Wilkes Land (Gore et al., 2001; Mackintosh et al., 2014), and commenced around 6 to 9 ka BP in Enderby Land (White and Fink, 2014). The geology of the majority of the area is defined by Precambrian schists, quartzites and meta-sedimentary rocks, comprising mainly granulite facies orthogenesis (Tucker et al., 2020). The MAAT of the coastal area is stable between −9 and −11 °C without any trend detected over the last 60 years (Turner et al., 2020). Precipitation oscillated between 200 and 800 mm yr<sup>-1</sup> (Bromwich et al., 2011).

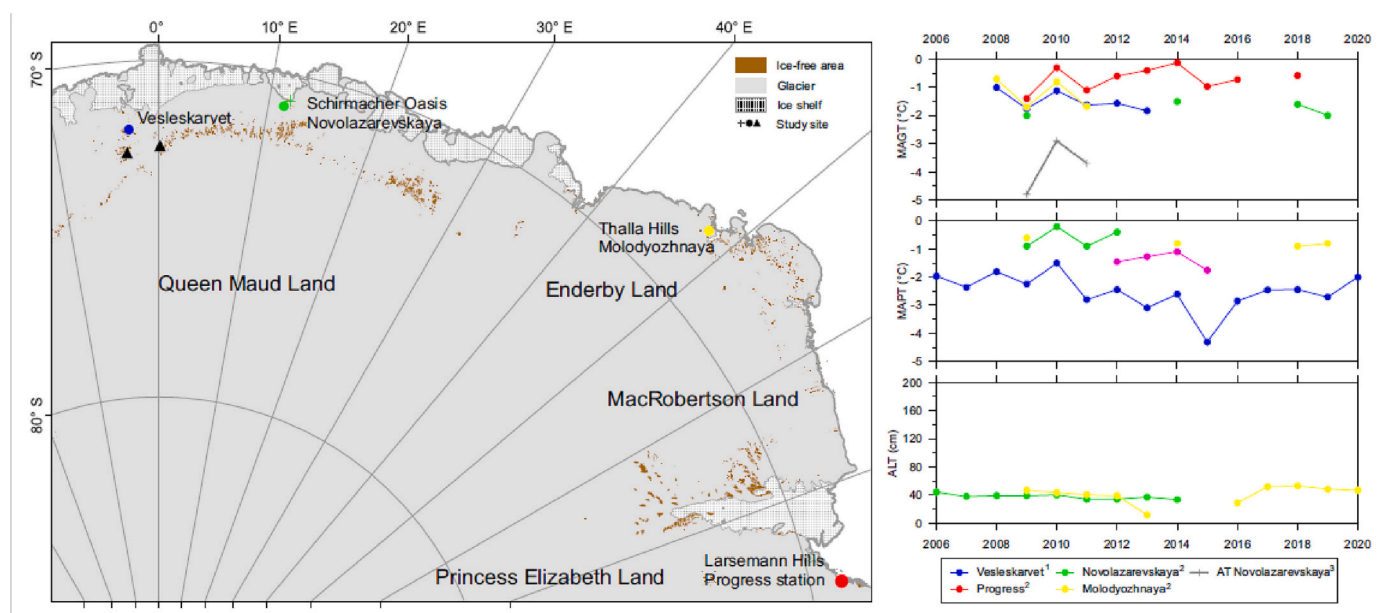


Fig. 4. The variability of mean annual near-surface ground temperature (MAGT), mean annual temperature, the permafrost table (MAPT), and active layer thickness (ALT) in selected sites of East Antarctica. The data were extracted from studies by <sup>1</sup>Kotzé and Meiklejohn, 2017; <sup>2</sup>Hrbáček et al., 2021b; <sup>3</sup>REAEDER database.

Vegetation cover in ice-free areas is sparse and consists of lichens, mosses, and algae.

Permafrost and active layer monitoring have mostly been undertaken in the vicinity of Russian research stations Molodezhnaya in Thalla Hills (Enderby Land); Progress II station in Larseman Hills (Princess Elizabeth Land), and Mirny station in Bunger Hills (Wilkes Land). The first Soviet Antarctic expedition (1956–57) brought permafrost scientists near Mirny station, who installed boreholes for ground temperature measurements and studied ALT in a variety of landscape settings. Shallow (1 m) boreholes for ground temperature and sites for ALT measurements were later (1993–94) organised at Syowa (Sawagaki, 1995), and from 2007 at Molodezhnaya (Abramov et al., 2011).

MAGT is around  $-9\text{ }^{\circ}\text{C}$  and ALT ranges from 60 to 80 cm (more than 100 cm for bedrock) near Molodezhnaya station. At Progress Station, ALT varies from 60 to 85 cm (Hrbáček et al., 2021b). Modelling of the topmost part of the permafrost revealed the highest temperatures between  $-6$  to  $-8\text{ }^{\circ}\text{C}$  in the coastal areas, decreasing to  $-20\text{ }^{\circ}\text{C}$  in the Prince Charles Mountains and Mawson Escarpment in MacRobertson Land (Obu et al., 2020; Table 6).

### 3.5. Victoria Land

#### 3.5.1. Ross Sea region and Transantarctic Mountains

The Ross Sea region (RSR) lies directly south of New Zealand and stretches from latitude  $70^{\circ}\text{S}$  to  $90^{\circ}\text{S}$ , and from longitude  $150^{\circ}\text{E}$  through  $180^{\circ}$  to  $150^{\circ}\text{W}$ . Ice-free areas with soil development cover an estimated area of  $18,480\text{ km}^2$  (e.g. ACBR10, Terauds and Lee, 2016), and soils occur in small pockets along the coastal margins, in the McMurdo Dry Valleys (MDVs) as well as in isolated areas in the Transantarctic Mountains (TAM) further south (Balks and O'Neill, 2016). The MDVs are the largest ice-free expanse in Antarctica, and depending on the portion of ice-free area considered, size estimates range from 2000 to  $15,000\text{ km}^2$  (Levy, 2013).

Basement rocks of the MDVs are mainly Precambrian to Ordovician schists, gneiss, marble, and granites (Isaac et al., 1996) overlain by a range of rock types dominated in many areas by Devonian to Triassic quartz sandstones (Isaac et al., 1996). Ross Island comprises mainly basaltic materials with shallow soils formed on regolith such as glacial till or colluvium that strongly reflect the parent rocks due to the relatively limited weathering that occurs (Campbell and Claridge, 1987).

During the last glacial maximum (LGM), the West Antarctic Ice Sheet (WAIS) expanded into the Ross Sea Embayment and terminated close to the continental shelf edge (Shipp et al., 1999; Denton and Hughes, 2000). Recent modelling by Lowry et al. (2019) show the earliest retreat of the WAIS in the Ross Sea Embayment during the Early Holocene, which was characterized by rapid terrestrial ice sheet thinning.

The timing of various glacial advances and retreats strongly influences soil development. Salt horizons, soil color, the amount of clay present, and the extent of staining, exfoliation, cavernous weathering, and ventifaction of surficial materials are distinctive indicators of age difference in many RSR soil sequences (Bockheim, 1997). The youngest soils are generally found on deposits closest to glaciers and on young features such as beaches, sand dunes, or stream deposits. The oldest, most strongly weathered, soils are often found on high, upland surfaces (Campbell and Claridge, 1987; Bockheim and McLeod, 2008; Bockheim, 2010), which have escaped the erosive effects of subsequent glacial fluctuations.

The MDV landscape has generally been considered stable over periods extending for millennia (Denton et al., 1993; Marchant and Head, 2007), particularly at higher elevations where soil temperatures remain below  $0\text{ }^{\circ}\text{C}$ , thus slowing weathering and geomorphic processes. However, recent observations in the coastal thaw zone by Fountain et al. (2014), Balks and O'Neill (2016) and Levy et al. (2018) describe short-lived erosion and depositional events, occurrence of stream erosion and incision, and melting of massive ice during summers that experienced above average incoming solar radiation. Future changes to soil-

permafrost environments in the RSR are most likely to occur in areas of low elevation and in warm coastal zones and may be a result of warmer than average summers, higher than average snowfall, or human disturbances. In areas of ice-cemented (as opposed to dry-) permafrost such changes may lead to melting of ground ice and thermokarst erosion or subsidence (Fountain et al., 2014; Balks and O'Neill, 2016; Levy et al., 2018).

Mean annual air temperatures across latitudinal and altitudinal gradients from Cape Hallett ( $72^{\circ}\text{S}$ ) to Darwin Glacier ( $79.5^{\circ}\text{S}$ ), and from sea level to the edge of the Polar Plateau, over the period 2000 to 2018, ranged from  $-15\text{ }^{\circ}\text{C}$  at Cape Hallett (2 m a.s.l.) to  $-25\text{ }^{\circ}\text{C}$  at Mt. Fleming at the head of the Wright Valley (1700 m a.s.l.) (Seybold et al., 2009). In the inland MDVs snowfall occurs with no strong seasonal pattern (Fountain et al., 2010). Precipitation is higher in coastal areas with snow accumulating on the ground surface over winter, and following summer snowfall events. On the mid-valley floors precipitation is lowest with a mean annual precipitation of 45 mm recorded at Vanda Station over two years (Campbell and Claridge, 1987) and Fountain et al. (2010) report annual precipitation ranging from 3 to 50 mm in the MDVs. Snowfall is higher at the coastal ends of the valleys and at higher altitudes. In summer snowfall often sublimates within an hour of falling on the valley floors, and within a day or two at higher altitudes (Balks and O'Neill, 2016). Climate data in Antarctica is limited, however continuously monitored soil climate data, since 1999 shows some between-season variability but no significant trends of warming or cooling (Carshalton et al., 2022) (Table 7).

In the MDVs there are no vascular plants, but where conditions are favourable (soil pH and salinity, available water, and shelter from the wind), algal crusts, mosses, lichen, and endolithic communities have been reported (Friedmann, 1982; Gilichinsky et al., 2007; Goordial et al., 2016).

Environmental parameters (pH, water activity) drive abundance, community structure and diversity of variable biological communities (Adams et al., 2006; Aislabie et al., 2006, 2008, 2011; Barrett et al., 2006; Chong et al., 2012; Hopkins et al., 2006; O'Neill et al., 2013; Yergeau et al., 2007). Lee et al. (2012) showed that soils from four geographically disparate dry valleys comprised structurally and phylogenetically distinct communities. In coastal areas (e.g. Capes Royds, Bird, and Hallett) penguin colonies provide high inputs of nutrients forming ornithogenic soils and distinct biological communities (Speir and Cowling, 1984).

The MDVs are one of the most studied permafrost regions in Antarctica (Bockheim et al., 2007; Adlam et al., 2010; Seybold et al., 2010; Levy, 2013; Obu et al., 2020). A soil-permafrost climate network has been maintained since 1999 (Carshalton et al., 2022). The network, comprising nine automated soil climate stations and two borehole sites, provides both a latitudinal and altitudinal gradient across the RSR. The coastal group includes Minna Bluff ( $78^{\circ}30'41.6''\text{S}$ ) (colder, windier, and some distance from the open sea), Scott Base, Marble Point, and Granite Harbour ( $77^{\circ}00'23.7''\text{S}$ ). The Granite Harbour site is not typical of the wider area, but was selected to capture a unique warm wet environment that has unusually lush biological growth. To complement the coastal latitudinal group, the network includes an altitudinal group ranging from Marble Point (60 m a.s.l.) through Wright Valley floor (160 m a.s.l.) and Victoria Valley (410 m a.s.l.) to Mt. Fleming (1697 m a.s.l.) which includes the dry valley floor environment through to the edge of the polar plateau. To capture the valley walls, and intermediate altitude, particularly to support climate modelling efforts, soil climate stations were installed on a terrace above Don Juan Pond (728 m a.s.l.) and on the high Wright Valley wall east of the entrance to Bull Pass (known as Bull Pass East, 832 m a.s.l.). Two 30 m deep boreholes are located in bedrock, one at Marble Point to capture the coastal environment and one on the floor of the Wright Valley (Guglielmin et al., 2011) to capture the more extreme dry climate. Overall, the network captures the range of soil, active layer, and permafrost environments in the McMurdo Dry Valleys region.

Each soil climate station includes an MRC temperature probe, 3-in-1 soil moisture probes which also measure temperature, and Campbell 107 temperature probes, giving at least 15 temperature measurements in the top 1.2 m. Atmospheric conditions (measured 1.5 m above the ground surface) include incoming solar radiation with a pyranometer, wind speed and direction, relative humidity, and air temperature, and sensors are connected to Campbell Scientific data loggers (ranging from CR10X to CR1000X). Measurements of atmospheric variables are made at 10-s intervals, and soil measurements at 20-min intervals, averaged hourly. The data are included in Adlam et al. (2010), Seybold et al. (2010), Vieira et al. (2010), Guglielmin et al. (2011), Balks and O'Neill (2016), Hrbáček et al. (2021b), and Obu et al. (2020).

Another soil climate monitoring network (LTER, Long Term Ecological Research Project) has also operated, since 1994, in the McMurdo Dry Valleys. Systematic soil measurement in the LTER network started in 1999 in the southern part of the RSR (Taylor Valley, Beacon Valley, University Valley). The longest published record (1999–2010) was provided from Beacon Valley by Lacelle et al. (2016); (Fig. 5). Data from the LTER network are not further discussed here, however are summarized in Table 7.

The air, ground and permafrost temperatures all decrease with increasing elevation and latitude (Adlam et al., 2010). Within the data set (gathered between 2006 and 2019) MAAT ranged from  $-14.8\text{ }^{\circ}\text{C}$  at Granite Harbour (5 m a.s.l.) to  $-25.1\text{ }^{\circ}\text{C}$  at Mt. Fleming (1697 m a.s.l.). The MAGT ranged from  $-13.1\text{ }^{\circ}\text{C}$  at Granite Harbour to  $-24.6\text{ }^{\circ}\text{C}$  at Mt. Fleming. The mean annual temperature in the uppermost part of the permafrost ranged from  $-12.9\text{ }^{\circ}\text{C}$  at Granite Harbour to  $-24.2\text{ }^{\circ}\text{C}$  at Mt. Fleming (Fig. 5, Table 7) All sites show interannual variability in MAAT and MAGT (both near surface and at the top of the permafrost). The inter-annual variability was lower at higher altitude sites such as Mt.

Fleming than at the lower altitude coastal sites such as Marble Point (50 m a.s.l.) (Fig. 5).

ALT ranged from 3.4 cm at Mt. Fleming to greater than 90 cm at Granite Harbour (Fig. 5, Table 7), and generally decreased with increasing altitude and latitude. At Granite Harbour, where a large amount of meltwater flows through the soil profile, conducting heat to depth, the maximum thaw depth exceeds the depth of the temperature sensors. At all other sites, the deepest sensors are within the permafrost, at depths of greater than about 50 cm. The ALT at the soil climate station sites showed large variability both in space and in time, reflecting differences in soil characteristics, permafrost types, annual variability in snow cover, and responding sensitively to climate variability (Balks and O'Neill, 2016; Hrbáček et al., 2021b; Seybold et al., 2010); however, no significant trends of increase or decrease in ALT, MAGT (near-surface or at the top of the permafrost) were observed between 2006 and 2019.

The three Wright Valley sites (Bull Pass, Bull Pass East and Don Juan Pond) have dry permafrost (Anhyorthels) while the remaining six sites have ice-cemented permafrost (Haploorthels or Haploturbels) (Carshalton et al., 2022). The coastal sites (Scott Base, Marble Point, Minna Bluff, and Granite Harbour) receive higher snowfall, resulting in some liquid moisture for short periods during snowmelt. The Victoria Valley site is relatively close to Lake Victoria and has moisture mainly derived from groundwater, whereas the predominant source of water at Mt. Fleming is windblown snow carried from the nearby margin of the Polar Plateau. Seybold et al. (2010) described the moisture regime of seven of the sites. There were no clear differences between ALT at ice-cemented sites compared to those with dry permafrost. Substantive vegetation is lacking at all sites and, therefore, would have no influence on the ground thermal regime and ALT.

Numerous studies into the thermal properties of MDV soils, the role

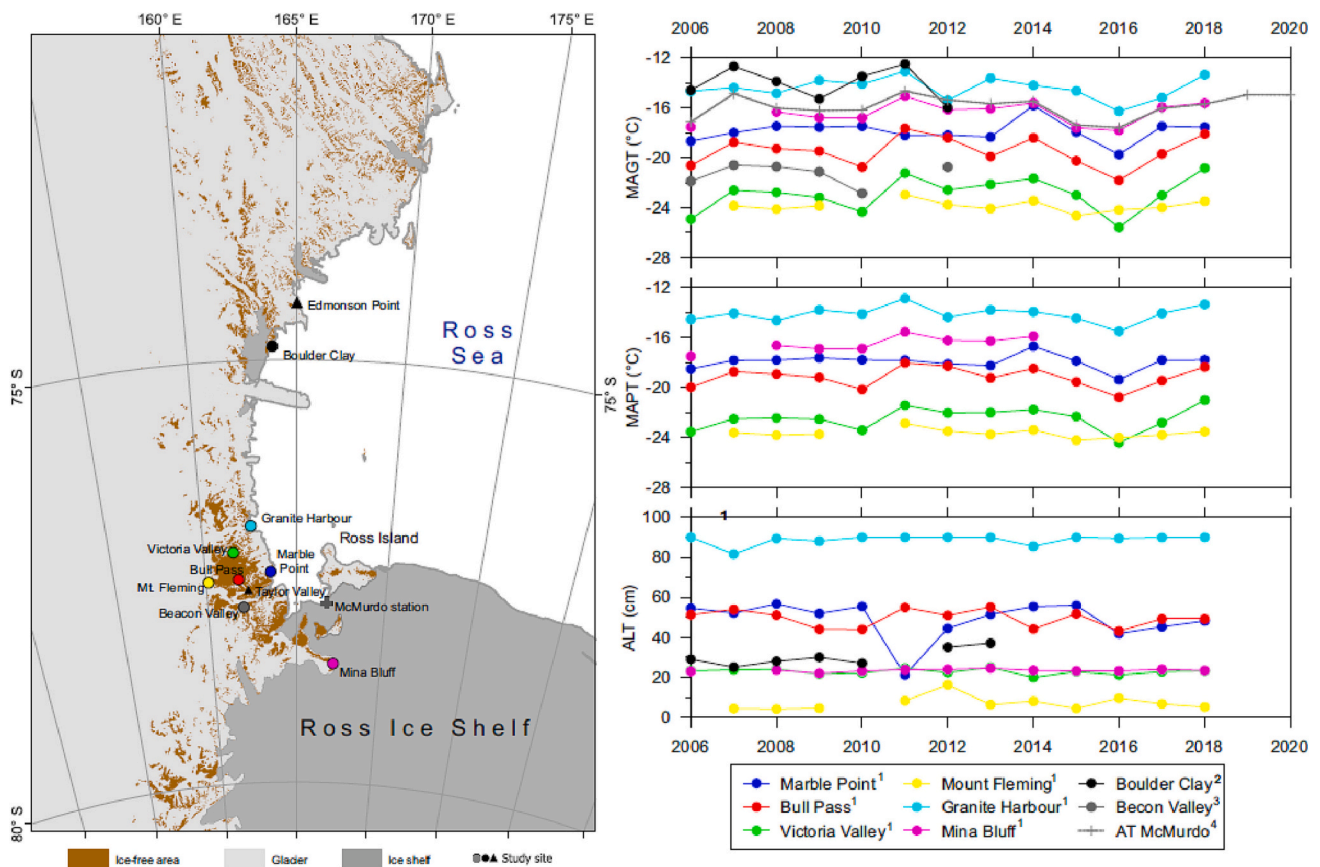


Fig. 5. The variability of mean annual near-surface ground temperature (MAGT), mean annual temperature on the permafrost table (MAPT) and active layer thickness (ALT) in the selected sites of Victoria Land. The data were extracted from studies <sup>1</sup>Carshalton et al., 2022; <sup>2</sup>Cannone et al., 2021; <sup>3</sup>Lacelle et al., 2016; <sup>4</sup>READER database. Black triangle indicate the position of other study sites in the region.

of soil moisture on ALT, short-term ground temperature monitoring, modelling of the subsurface thermal regime, and research into the impacts of climate change on soil thermal regimes and associated soil ecosystems have been undertaken in the RSR (e.g. Andriuzzi et al., 2018; Fisher et al., 2016; Fountain et al., 2016; Lacelle et al., 2016; Lapalme et al., 2017; Liu et al., 2018; Wlostowski et al., 2018). In a study conducted over a two-year period along moisture gradients associated with fluvial features in the Taylor Valley, MDVs, Wlostowski et al. (2018) showed that the rate and sensitivity of soil freeze/thaw processes was related to soil moisture content in the active layer; with wetter soils freezing less frequently and more gradually than dry soils. Wlostowski et al. (2018) concluded that if predicted increases in moisture and temperature occur in the MDVs, soil ecosystems (especially nematode diversity and abundances) will be impacted (Chapman and Walsh, 2007; Walsh, 2009). Similarly long-term observations by the MDV Long Term Ecological Research (LTER) project showed shifts in the dominant nematode species in the Taylor Valley resulting from fluctuations in ice-melt associated with warmer summers and more frequent discrete warming events since the 2000s (Andriuzzi et al., 2018).

### 3.5.2. Northern Victoria Land

Northern Victoria Land is part of the Ross Sea Sector, and was glaciated probably until 12,000 yrs. BP (Forte et al., 2016). It consists of an undulating upland rising to elevations exceeding 1000 m a.s.l., and in one case (Tarn Flat) descending below sea level. The bedrock is composed of Harbour Castle granite, Wilson Terrane meta-granite and high-grade metamorphics, and small areas of meta-sedimentary rocks, all Ordovician in age or older (Pour et al., 2018). Several large glaciers cut through the Trans-Antarctic Mountains (i.e. Reeves, Priestley and Campbell), and there are many smaller ones together with numerous cirque glaciers and snowbanks. The coasts of North Victoria Land consist of a sequence of cliffed headlands and beaches, several of which are raised beaches (i.e. Ponti and Guglielmin, 2021a).

The climate of the area surrounding the Italian Antarctic Research Station 'Mario Zucchelli' is characterized by a mean annual air temperature of  $-14.1\text{ }^{\circ}\text{C}$  (Ponti et al., 2021), and is persistently dominated by strong Katabatic winds. The annual net precipitation, usually in the form of snow, ranges between 50 and 250 mm yr<sup>-1</sup> (Bromwich et al., 2011). The climatic trend is towards a slight increase of MAAT (Cannone et al., 2021) and permafrost is continuous everywhere with a trend of increasing ALT (Guglielmin et al., 2014a; Cannone et al., 2021).

The geomorphological processes of northern Victoria Land are mostly related to wind or salt weathering (Ponti and Guglielmin, 2021) and thermal-contraction cracking polygons (French and Guglielmin, 1999) that may develop ice wedges (Raffi and Stenni, 2011). It is common to find perennially frozen lakes with frost mounds (Ponti et al., 2021) and also active rock glaciers (Guglielmin et al., 2018). Freeze-thaw and mass-wasting (solifluction) processes are limited because of the lack of moisture and the shallow active layer (French and Guglielmin, 1999). The vegetation of Victoria Land is composed exclusively of cryptogams and includes four main vegetation types, dominated by (a) mosses, (b) mosses encrusted by epiphytic lichens, (c) macrolichens, and (d) scattered epilithic lichens and mosses (Cannone and Seppelt, 2008).

**3.5.2.1. Boulder Clay.** Boulder Clay ( $74.74^{\circ}\text{S}$ ,  $164.03^{\circ}\text{E}$ , 205 m a.s.l.) is an ice-free area located at the Northern Foothills about 6 km south of the Italian station on a gentle slope ( $5^{\circ}$ ) with south-eastern exposure. The area consists of glacial ablation-sublimation till overlaying a body of a "dead" glacier ice. The till matrix is generally silty sand with confined zones of clayey silt (Guglielmin et al., 1997). The climate is characterized by a MAAT of  $-14.1\text{ }^{\circ}\text{C}$  (Ponti et al., 2021).

Despite the low precipitation, areas of snow accumulation are formed by strong wind drift (Guglielmin et al., 2014a). Permafrost is continuous and estimated to be 420–900 m thick (Guglielmin, 2006). The ALT ranges between 23 and 92 cm with a thickening trend of  $+0.3$

cm to 1.1 cm per year at different sites during the period 2000–2013 (Guglielmin et al., 2014b; Cannone et al., 2021). The Boulder Clay site is the first CALM-S grid in Antarctica with temperature data from a 3.6 m deep borehole since 1996 (Guglielmin, 2006).

The MAAT ranged between  $-12.5$  and  $-16.0\text{ }^{\circ}\text{C}$ , while the MAGT was between  $-14.6$  and  $-16.7\text{ }^{\circ}\text{C}$ . Surface annual TDD varied considerably, ranging from 90 to 195  $^{\circ}\text{C}\cdot\text{day}$ . Consequently, the ALT recorded at the borehole site ranged between 25 and 37 cm (Guglielmin and Cannone, 2012; Cannone et al., 2021) (Table 7). Incoming radiation, rather than air temperature, is considered the principal driver of AL thickening (Guglielmin and Cannone, 2012).

**3.5.2.2. Edmonson Point.** Edmonson Point ( $74.33^{\circ}\text{S}$ ,  $165.13^{\circ}\text{E}$ , 50 m a.s.l.) is a small ice-free oasis, located in Wood Bay on the west coast of the Ross Sea, of about 1.8 km<sup>2</sup>. Here, the volcanic activity of Mt. Melbourne produced a dark substrate composed of basaltic lavas, scoria, pumice, and tuff (Smykla et al., 2015). Periglacial processes include frost cracking of finer deposits (French and Guglielmin, 1999) and the influence of oceanic flooding on permafrost has been demonstrated (Ponti and Guglielmin, 2021).

The MAAT in the Edmonson Point is around  $-16.5\text{ }^{\circ}\text{C}$ . The innermost area is sheltered from local katabatic winds and in summer easterly winds. Permafrost is continuous everywhere (Obu et al., 2020), and the active layer thickness ranges between 23 and 55 cm at vegetation covered and bare ground sites, respectively (Cannone and Guglielmin, 2009; Hrbáček et al., 2020a, 2020b). MAGT varied between  $-11.4$  and  $-14.7\text{ }^{\circ}\text{C}$ . Surface TDD varied from 534 to 804  $^{\circ}\text{C}\cdot\text{day year}^{-1}$ , producing an n-factor for thawing of between 40.4 and 101. Surface FDD range between  $-4982$  and  $-5940\text{ }^{\circ}\text{C}\cdot\text{day year}^{-1}$ , producing an n-factor for freezing of between 0.9 and 0.99 (Table 7).

## 3.6. Sub-Antarctic Islands

The sub-Antarctic islands encompass several islands that generally include the Antipodes, Auckland, Bounty, Bouvet, Campbell, Crozet, Heard and McDonald, Kerguelen, Macquarie, Prince Edward, South Georgia, South Sandwich, and Snares Islands, located between 40 and 60°S, near the Antarctic Polar Frontal Zone. These islands are further classified according to oceanographic, climate, and floristic data (van de Vijver and Beyens, 1999). They are largely of volcanic origin of varying ages, with some still active (e.g., Hodgson et al., 2014), ranging from volcanic cones, vents, and basal shelf volcanoes (Hodgson et al., 2014), to granite remnants (McGlone, 2002), and uplifted basaltic oceanic crust (Quilty, 2007). Most of the islands are characterized by maritime climates that are moist, cool, mostly cloudy, with strong prevailing westerly winds, brought about by eastward moving cyclonic depressions (e.g.; Hall, 2002; McGlone, 2002; Hodgson et al., 2014; Graham et al., 2017). Annual precipitation varies, ranging from 700 mm for Crozet to 2400 mm for the Prince Edward Islands (e.g.; le Roux and McGeoch, 2008), with those located above the Antarctic Convergence receiving less snowfall (Hall, 2002). Modelled MAAT ranges from  $-9$  to  $-2\text{ }^{\circ}\text{C}$  for South Georgia, to  $+2$  to  $+8\text{ }^{\circ}\text{C}$  for the Antipodes and  $+11\text{ }^{\circ}\text{C}$  for Snares Island; the MAAT for most islands is near  $0\text{ }^{\circ}\text{C}$  (Leihy et al., 2018).

### 3.6.1. South Orkneys

Unlike the other sub-Antarctic Islands, continuous research activities are carried out on the South Orkneys, in Signy Island ( $60^{\circ}43'\text{S}$ ,  $45^{\circ}38'\text{W}$ ). Deglaciation of the area started around 6.6 ka cal BP (Jones et al., 2000) and continues nowadays, as thinning rates of 1 m per year have been measured over the last 20 years (Favero-Longo et al., 2012). The ice-free area of the island covers about 10 km<sup>2</sup> and is composed quartz-mica-schist bedrock, moraine sediments, scree slopes, beaches and alluvial deposits (Matthews and Maling, 1967). A cold oceanic climate dominates with MAAT of around  $-3.5\text{ }^{\circ}\text{C}$ , an annual precipitation of around 400 mm, primarily in the form of summer rain

(Guglielmin et al., 2012). The warming trend of MAAT is  $+0.13$  °C/decade during the period 1960–2009 (Oliva et al., 2017b). Precipitation shows also a slight increase in recent decades (Cannone et al., 2016). Vegetation on Signy Island is composed of both the Antarctic herb tundra formation, as well as the more common Antarctic nonvascular cryptogam tundra formation (Gimingham and Smith, 1970). Present-day geomorphological processes in Signy Island are characterized mainly by periglacial dynamics, including the development of low-centred sorted circles, sorted stripes, and stone-banked lobes, and widespread solifluction processes. One active rock glacier has been described in the island (Guglielmin et al., 2008).

MAGT ranges between  $-1.9$  and  $-2.9$  °C on bare ground and between  $-2.0$  and  $-3.0$  °C for vegetation (Fig. 6). The annual TDD varies between 230 and 540 °C·day in bare ground, and between 100 and 300 °C·day under vegetation carpets (Guglielmin et al., 2012; Hrbáček et al., 2020a). The presence of vegetation strongly affects ALT, which can range from 40 cm to  $>3$  m (Guglielmin et al., 2008; Guglielmin and Cannone, 2012). The shallowest ALT sites are on vegetated surfaces that retain more water (wet mosses), while sites with thicker ALT were found

under bare ground where water is more easily drained (Guglielmin and Cannone, 2012; Hrbáček et al., 2020a) (Table 8).

### 3.6.2. Other areas

The remaining Sub-Antarctic islands have distinct periglacial environments and periglacial landforms, such as sorted and non-sorted patterned ground, protalus ramparts, and stone-banked lobes are common (e.g., Hedding, 2008; Hansen, 2018). However, ground temperature monitoring is largely absent and MAGT on the top of the permafrost table was modelled by the Cryogrid 1 model (Obu et al., 2020), for the South Sandwich Islands, ice free areas of Heard Island, higher elevations of Kerguelen Islands, and South Georgia. Permafrost is absent on the Crozet Islands (Obu et al., 2020), the Prince Edward Islands (Nel et al., 2021), and Macquarie Island (Hodgson et al., 2014).

Investigations by Nel et al. (2021) indicate that Marion Island, of the Prince Edward Islands, may be used as a proxy in evaluating regional climatic trends within the Southern Ocean. Marion Island is characterized by ubiquitous, high-frequency low-intensity, diurnal frost cycles throughout the year (Hansen, 2018), like the Auckland, Campbell, and

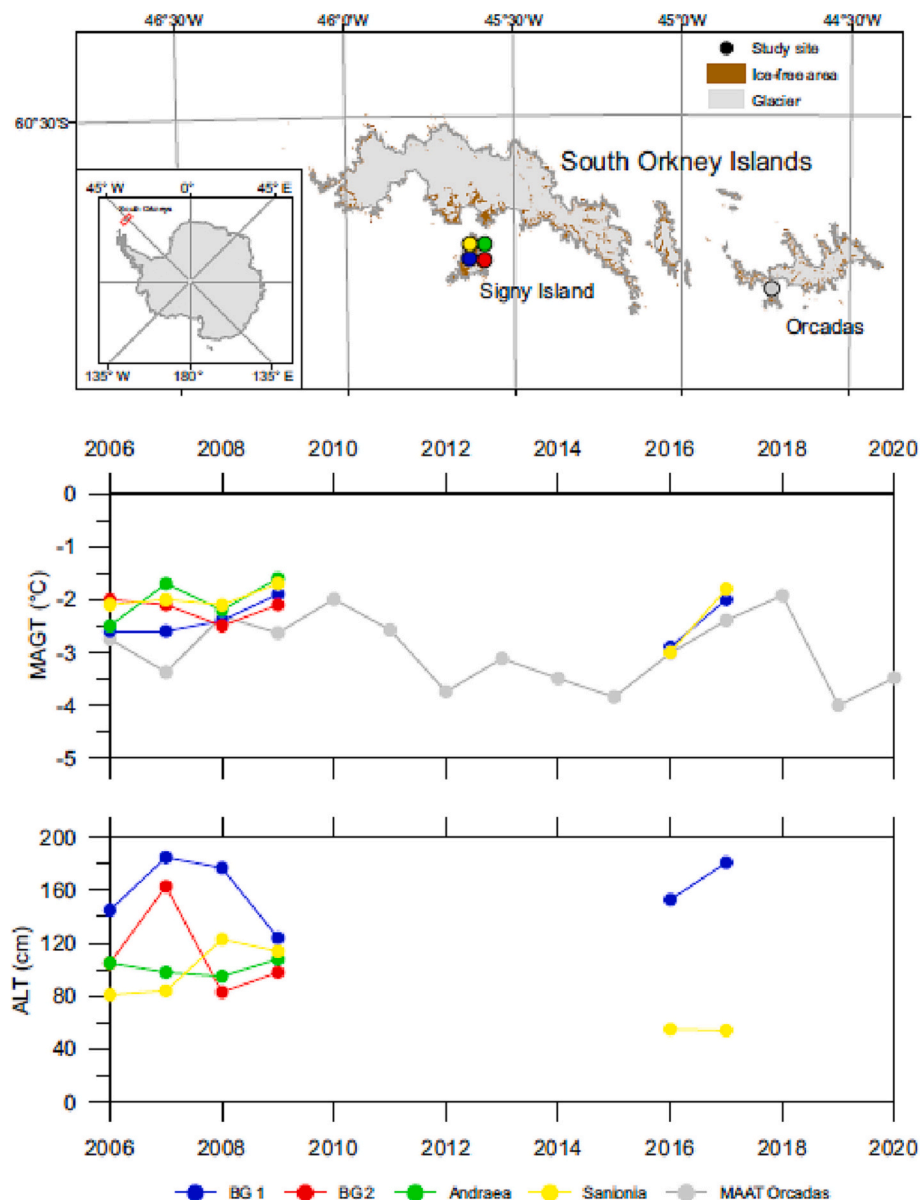


Fig. 6. The variability of mean annual near-surface ground temperature (MAGT) and active layer thickness (ALT) in selected sites of the Sub-Antarctic Islands. The data were extracted from studies by <sup>1</sup>Guglielmin et al., 2012; <sup>2</sup>Hrbáček et al., 2020a; <sup>3</sup>READER database.

Macquarie Islands (McGlone, 2002), with no evidence of permafrost, nor of seasonal freezing at lower elevations (Nel et al., 2021). Ground frost yields the lateral and vertical movement of particles within the soil column (Nel et al., 2021), and subsequent sorting of the ground (Hansen, 2018). MAGT ranges from 1 to 5 °C (Nel et al., 2021), MAAT from 1 to 6 °C (Hansen, 2018) at elevations ranging from 800 to 100 m a.s.l. Annual TDD are 392 °C-day at higher elevation, and 499 °C-day at lower elevation (Table 8). The annual FDD are −195 °C-day at higher, and −95 °C-day at lower elevations (Hansen, 2018). While the majority of the sub-Antarctic islands do not exhibit permafrost, all are undergoing rapid change leading to glacial retreat, reduction of ground ice and snow, changes in frost processes, as well as far-reaching effects on local fauna and flora.

#### 4. Discussion

Permafrost in Antarctica is widespread in ice-free regions and is only absent near sea level in some areas across the South Shetland Islands and Western Antarctic Peninsula (Bockheim et al., 2013, Correia et al., 2017; Ferreira et al., 2017), as well as sub-Antarctic islands north of 60°S, where patchy permafrost occurs only in elevated areas (Obu et al., 2020). Permafrost thickness naturally ranges from a few meters on the warmest Antarctic part in the West Antarctic Peninsula (Bockheim et al., 2013), up to almost 1000 m estimated in the cold conditions of the McMurdo Dry Valleys (Decker and Bucher, 1977). The regional variability of permafrost thickness is mainly affected by geothermal heat-flow (Borzotta and Trombotto, 2004) in areas under active tectonic and volcanic processes (e.g., Burton-Johnson et al., 2020).

##### 4.1. Active layer and permafrost thermal regime

The vast surface of the Antarctic continent, as well as the range of climatic, topographical, and lithological settings, makes it challenging to infer regional characteristics of spatial patterns of the active layer in terms of thermal regime, thickness, or spatio-temporal dynamics. The MAGT is strongly driven by latitude ( $R^2 = 0.9$ ), showing a cooling trend of ca. 0.9 °C/deg. (Fig. 7). The Antarctic Peninsula is the only area where strong temperature asymmetry can be found at the same latitude, with up to 5 °C difference between the western and eastern sides (Cook and Vaughan, 2010). The most of the study sites are elevated lower than 300 m a.s.l. The only area with clearly defined altitude trend is McMurdo Dry Valleys (MDV) where the elevations cover range from sea level up to 1700 m a.s.l. resulting into the lapse rate of MAGT of ca 0.6 °C/100 m (Adlam et al., 2010; Carshalton et al., 2022).

Data reveals (non-significant) warming trends in mean annual near-

surface temperatures (Fig. 8) in the South Shetlands (SSI; 0.028 °C/year), Eastern Antarctic Peninsula (AP; 0.11 °C/year) and Victoria Land (VL; 0.027 °C/year), and a cooling (non-significant) trend was only detected in East Antarctica (EA; −0.062 °C/year). However, the trend analysis of MAAT revealed that all of the Antarctic regions experienced (non-significant) warming during the period 2006–2020 (Fig. 8). The results from AP region show that the initial cooling observed at the beginning of the 21st century (e.g. Turner et al., 2016; Oliva et al., 2017b) has already shifted to a regional warming pattern, following the warming occurred in this region since 1950s (e.g. Turner et al., 2020). This trend change was discussed by Kaplan Pastřířiková et al. (2023), who detected the temperature trend change from cooling to warming around 2012–2014 on James Ross Island. Results from VL are in accordance with Cannone et al. (2021) observing slight warming in several sites in the period 2003–2013. The recent ground temperature trends in Antarctica reaching similar values between 0.3 and 1.0 °C/decade as was observed since 1990s in the Arctic regions (Smith et al., 2022) or.

Data for permafrost temperatures are restricted to several sites located in Western AP, EA and VL (Biskaborn et al., 2019) where there are boreholes that are deep enough to reach the depth of zero annual amplitude. Its depth varies from around 10 to 20 m in Antarctica (Vieira et al., 2010). Biskaborn et al., 2019 reported a non-significant warming trend of  $0.37 \pm 0.1$  °C in the period 2008–2016 for six of the sites (three in Western AP, one in EA, two in VL) involved to the study. The permafrost temperature varied from −1.5 °C in the SSI up to ca. −19 °C in VL (Fig. 9) The variability of annual ground temperatures in the depths above the depth of zero annual amplitude is significantly greater in the colder regions of EA and VL than SSI (Fig. 9). Nevertheless, the mean annual ground temperature exhibits only small offset between surface and the deep part of profile suggesting high thermal stability of the first tens meter of permafrost. Notably, data from some of some boreholes deeper than 5 m suggest that permafrost is absent, which is the case of lower elevated parts on Hurd Peninsula on Livingston Island (Ferreira et al., 2017) and Palmer station in Western AP (Wilhelm et al., 2015).

##### 4.2. Spatio-temporal distribution of active layer thickness

The ALT in Antarctica has higher regional variability than MAGT (Fig. 7). When considering the low-elevation (< 100 m a.s.l.) non-bedrock sites, the active layer follows the latitudinal gradient by thinning of 3.7 cm/deg. ( $R^2 = 0.64$ ;  $p < 0.05$ ). Similarly, to the latitudinal pattern, we found a strong and significant relationship ( $R^2 = 0.6$ ;  $p < 0.01$ ) between the MAGT and ALT at the continental scale (Fig. 7c). The highest variability of ALT is in the warmest sites of SSI and South

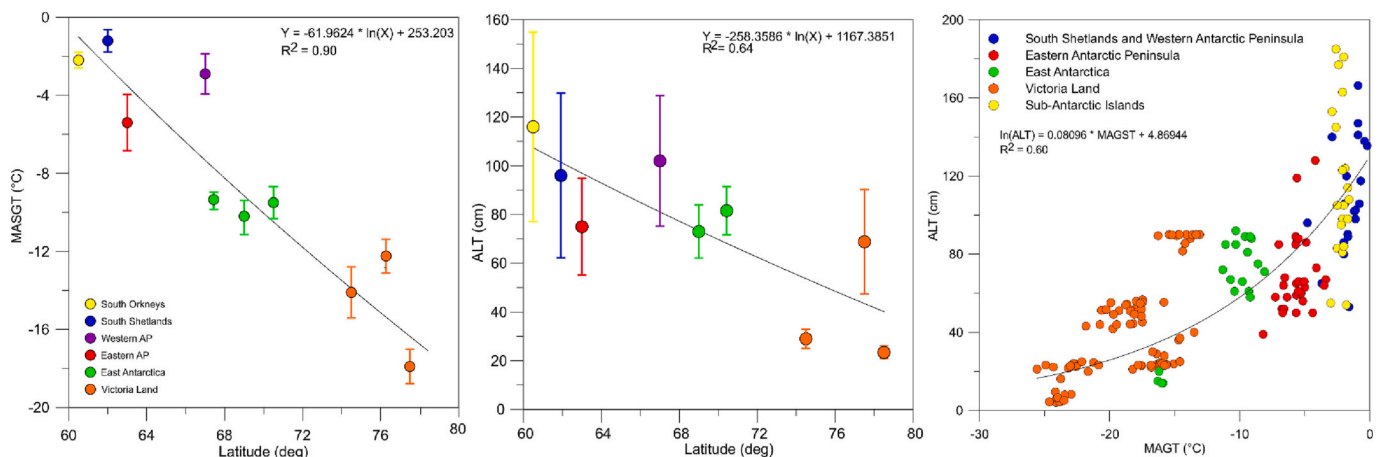
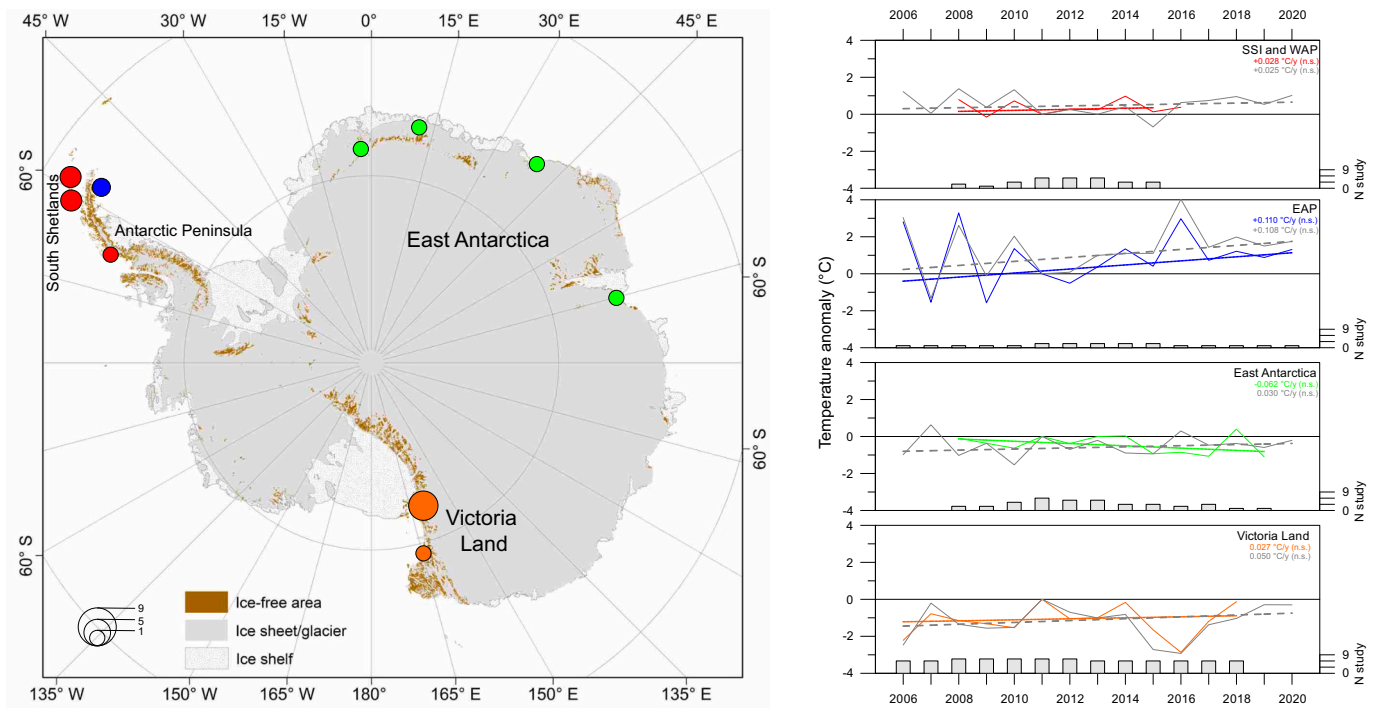
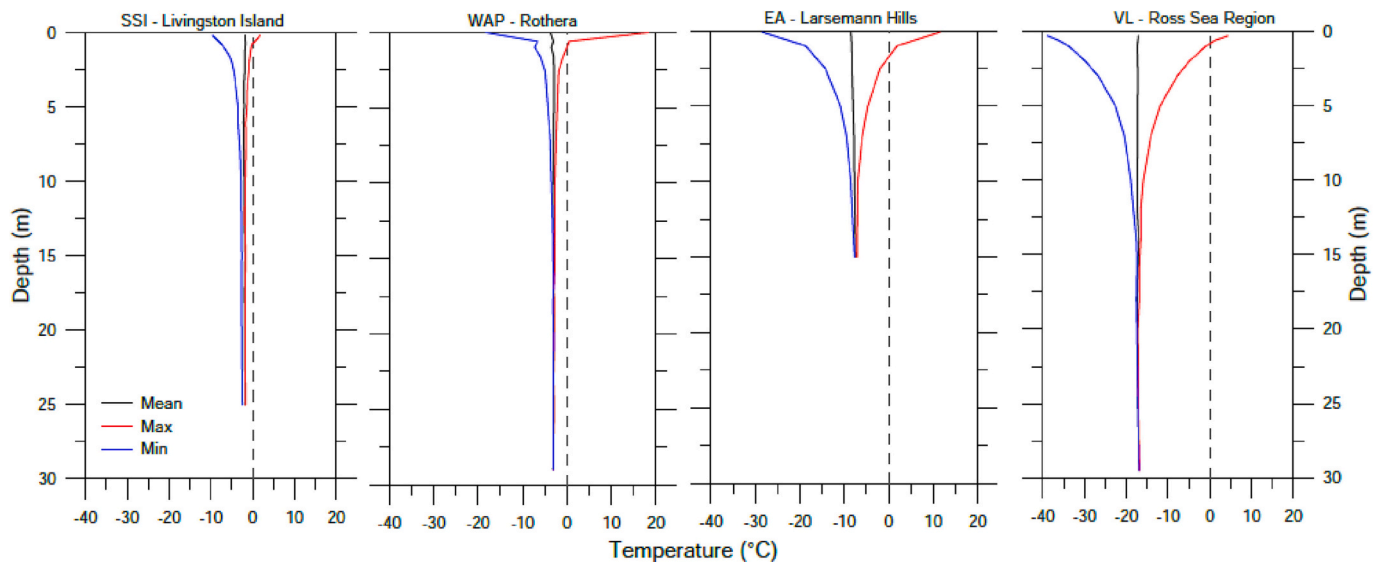


Fig. 7. The relationships between latitude and mean annual near-surface ground temperature and active layer thickness. The bars express standard deviation for each of the study region. The data in right figure represents individual years and was extracted from the studies presented in Tables 2-7.



**Fig. 8.** Variability of annual temperature anomalies of near-surface ground temperature (color lines) and air temperature (grey lines) calculated for the regions of Antarctica. The dashed lines indicate the trends; the color labels distinguish between trends for near-surface and air temperatures (grey), n.s. express that the trend is not statistically significant, box plots indicate the number of studies used for anomaly calculation for individual years, the locations of the datasets are indicated on the map.



**Fig. 9.** Differences in the temperature profile on selected deep boreholes between South Shetlands (SSI; mean data from the period 2008 – 2016; Ramos, unpublished data) Western Antarctic Peninsula (WAP; mean data from the period 2009–2011; Guglielmin et al., 2014b), East Antarctica (EA, mean data from the period 2013 – 2019; Abramov, unpublished data) and Victoria Land (VL, data from year 2009; Guglielmin et al., 2011).

Orkneys where the local conditions clearly have a stronger effect than the temperature. The overall span of ALT observed in Antarctica is from 3 cm in the coldest parts of VL (Adlam et al., 2010; Carshalton et al., 2022) up to more than 500 cm in the bedrock sites in SSI and Western AP (Bockheim et al., 2013; Ferreira et al., 2017).

In general, high intersite variability of ALT in order of tens of centimetres is typical for each of the Antarctic regions (Fig. 7). Such a variability is mostly associated with specific in-situ factors such as local climate patterns and snow, lithology, topography, biota, and the hydric

regime. The particular role of these factors is discussed in detail section 4.3. As in the case of near-surface ground temperature, the altitudinal gradient of ALT was identified in MDV region to be ca. 2.5 cm/100 m for the altitudes between 50 and 1700 m a.s.l. (Adlam et al., 2010; Carshalton et al., 2022).

Overall, the ALT on selected sites providing at least 7 years of data from different regions of Antarctica (Table 9) reaches comparable values of variation index as observed in sites across Arctic (e.g; Christiansen, 2004; Shur et al., 2005; Smith et al., 2009) over similarly long

**Table 9**  
The temporal variability of active layer thickness (ALT) on the selected sites.

| Site description  | Monitoring period | Mean ALT             | Variation index* | Trend                   |
|---|-------------------|----------------------|------------------|-------------------------|
| Eastern Antarctic Peninsula; James Ross Island, Johann Gregor Mendel <sup>1</sup> | 10 years          | 60 cm                | 11%              | +1.2 cm/yr (2011–2020)  |
| South Shetlands, Deception Island, CALM-S Crater Lake <sup>2</sup>                | 9 years           | 37.5 cm <sup>†</sup> | 17%              | −1 cm/yr (2006–2014)    |
| South Shetlands, Livingston Island, Linnopolar Lake <sup>3</sup>                  | 12 years          | 41 cm <sup>†</sup>   | 29%              | +0.4 cm/yr (2009–2020)  |
| South Shetlands, King George Island, CALM-S Bellingshausen <sup>4</sup>           | 10 years          | 62.5 cm <sup>†</sup> | 37%              | 0 cm/yr (2008–2019)     |
| East Antarctica, Schirmacher Oasis <sup>4</sup>                                   | 9 years           | 82 cm <sup>†</sup>   | 12%              | +2.7 cm/yr (2009–2018)  |
| Victoria Land, Ross Sea region, Marble Point <sup>5</sup>                         | 13 years          | 49 cm                | 16%              | −0.5 cm/yr (2006–2018)  |
| Victoria Land, Ross Sea region, Victoria Valley <sup>5</sup>                      | 13 years          | 23 cm                | 9%               | −0.05 cm/yr (2006–2018) |
| Victoria Land, Ross Sea Region, Bull Pass <sup>5</sup>                            | 13 years          | 49 cm                | 11%              | −0.17 cm/yr (2006–2018) |
| Victoria Land, Ross Sea Region, Mina Bluff <sup>5</sup>                           | 12 years          | 23 cm                | 5%               | +0.04 cm/yr (2006–2018) |
| Victoria Land, Northern Victoria Boulder Clay <sup>6</sup>                        | 7 years           | 30 cm                | 22%              | +1.75 cm/yr (2006–2013) |

\* Calculated using equation in Hinkel and Nelson (2003) (mean ALT – max ALT) / mean ALT.

<sup>†</sup> Active layer measured by mechanical probing <sup>1</sup> Kaplan Pastřířková et al., 2023; <sup>2</sup> Ramos et al. (2017); <sup>3</sup> de Pablo et al. (2018) and CALM site (2022); <sup>4</sup> Hrbáček et al. (2021a, 2021b) and CALM site (2022); <sup>5</sup> Carshalton et al. (2022); <sup>6</sup> Cannone et al. (2021).

monitoring periods. However, unlike the sites in the northern hemisphere, there is not a clear thickening or thinning trend of ALT in Antarctica. The active layer thinning was observed on several sites in AP and SSI in the period 2006 to 2015 (de Pablo et al., 2017, 2020; Ramos et al., 2017; Hrbáček and Uxa, 2020) and was associated to regional temperature cooling in the beginning of 21st century (Turner et al., 2016; Oliva et al., 2017b). The most recent results, however, indicated that the cooling and thinning was turned to warming and thickening around 2013–2015 (Kaplan Pastřířková et al., 2023). The results from the network in Ross Sea Region indicates overall stable conditions during the period 2000–2018 (Carshalton et al., 2022), whereas Cannone et al. (2021) found slight active layer thickening in the sites of Northern VL. When comparing to region in the northern hemisphere where the rapid active layer thickening is observed over last few decades (e.g. Xu and Wu, 2021; Strand et al., 2021, Blunden and Boyer, 2022; Smith et al., 2022) the ALT in Antarctica appear to be relatively stable in the last two decades. Our results show that the trends on the selected study sites were both thinning and thickening, but mostly statistically non-significant (Table 9).

The thaw depth variability is well documented by CALM-S sites or similar experiments using probing for the active layer measurement. The thaw depth measurement in the SSI region exhibited much lower values than ALT and range from 12 to 53 cm and 23 to 36 cm on Livingston Island (de Pablo et al., 2014, 2017) and Deception Island (Ramos et al., 2017), respectively. Here, the observed lower thaw depth values are influenced by logistic constraints (Guglielmin, 2006) and do not report the maximum values but the values typical for the certain period of the year. Thawing depths ranging from ca. 50 to 120 cm were observed on CALM-S on James Ross Island in Eastern AP (Hrbáček et al., 2017a, 2017b, 2021a). Relatively high thaw depth variability (ca. 75 to 105 cm)

was also reported by Mergelov (2014) from the transect in Larsemann Oasis in EA. In these sites the difference between probing depth and thermally derived ALT is small as the measurement timing was close to the natural seasonal ALT maximum (Hrbáček et al., 2017a). Even though the CALM-S grids provide important data on spatiotemporal dynamics of ALT, probe-based data has to be considered with the caution because in Antarctica stony soil materials may limit probe penetration and logistic constraints often prevent measurements at the time of maximum thaw when the active layer is the deepest (Guglielmin, 2006). Therefore, it is necessary to support thaw depths from probing with continuous temperature logging to accurately define the ALT.

#### 4.3. Factors affecting active layer thermal regime and thickness in Antarctica

##### 4.3.1. Climate

Air temperature is generally the most important parameter driving variability of the ground thermal regime worldwide (e.g. Lembrechts et al., 2022). Usually, near-surface ground temperature exhibits a high correlation with air temperature ( $r > 0.7$ ) at daily, seasonal and annual time scales, which has been reported in all Antarctic regions (e.g. Michel et al., 2012; Lacelle et al., 2016; Kotzé and Meiklejohn, 2017; Hrbáček et al., 2020a). The only moderate correlations were reported for winter seasons when the surface was covered by thick snowpack (e.g. Guglielmin et al., 2012; Hrbáček et al., 2020a) or the site was densely vegetated (Cannone and Guglielmin, 2009).

With regards to ALT, the most important controlling factor on James Ross Island corresponds to air temperatures during the summer, whereas only medium and non-significant correlation was found against winter temperatures (Hrbáček and Uxa, 2020). Adlam et al. (2010) found, that 73% of ALT variability in the MDV can be explained by mean summer air temperature, mean winter air temperature, total summer solar radiation and mean and summer wind speed whereas the summer air temperature itself explained only 15%.

The most pronounced effect of solar radiation on the active layer thermal regime was reported in the MDV and VL sites (Guglielmin and Cannone, 2012). The near-surface temperature in these regions exhibits higher correlations ( $> 0.9$ ) than in other locations AP, EA and sub-Antarctic regions, where it shows weak to moderate correlation (0.3 to 0.6; Lacelle et al., 2016; Kotzé and Meiklejohn, 2017; Hrbáček et al., 2020a). The intensive incoming radiation can effectively warm the surface to temperatures  $>30$  °C, especially in areas of dark coloured volcanic soils. As a result, unusually high seasonal rates of near-surface TDD exceeding even 800 °C-days and thawing n-factor value  $>40$  were observed (Cannone and Guglielmin, 2009; Hrbáček et al., 2020a). Even though such TDD represent the highest values reported in Antarctica, the ALT was only reported between 40 and 60 cm. Many of the MDV soils have extremely low moisture contents, thus relatively low thermal conductivity.

Snow cover seasonal duration and thickness is also an important factor affecting active layer dynamics in Antarctica. Areas with a relatively thick ( $> 40$  cm) and long-lasting snow cover during winter months had higher ground temperatures and deeper active layers during summer compared to snow-free sites (de Pablo et al., 2014, 2017; Oliva et al., 2017a). Therefore, snow is a potential factor triggering permafrost degradation, especially in the warmest regions with MAAT close to 0 °C (Hrbáček et al., 2020b). As well as the insulating effect of snow, other scenarios were reported. A thick winter snowpack exceeding 1 m was recognized to cause permafrost cooling (Guglielmin et al., 2014b). The presence of snow during the summer months may reduce (Hrbáček et al., 2021a), or prevent, active layer thawing (Guglielmin et al., 2014a). The persistent presence of snow cover, exceeding 1 m, for a few years may promote permafrost aggradation and temporal disappearance of the active layer, as was observed in the SSI (Ramos et al., 2020). Long-lying snow patches also favour the presence or absence of the vegetation cover in ice-free areas as snow-melt supplies water and nutrients, enhancing

soil formation and vegetation growth, and, may therefore, modify ALT distribution and thickness at a very local scale (Guglielmin et al., 2014b).

#### 4.3.2. Lithology and geomorphology

Besides climate, the specific local factors related to lithology or geomorphology, including soil texture, also play a role in active layer dynamics as they may affect soil thermal properties and/or moisture content. The effect of lithology has been studied in detail on James Ross Island, where ALT differences reached up to 40 cm across a short transect across two lithological units with large differences in soil thermal conductivity (Hrbáček et al., 2017a, 2017b, 2021a, 2021b). Certain lithological types, such as coarse-grained volcanic sediments, and varying albedo may explain ALTs that vary from regional averages. For example, the variable lithology on Deception Island is associated with ALTs in a range from between 30 and 40 cm (Ramos et al., 2017) up to 100 cm (Goyanes et al., 2014), whereas ALTs exceed 100 cm in neighbouring sites of the SSI (de Pablo et al., 2017; Ferreira et al., 2017; Oliva et al., 2017b).

The most pronounced effect of lithology is related to observations in bedrock drilled boreholes, where the active layer is typically tens to hundreds of centimetres thicker than in loose material in the same areas. Such differences can be related to the higher thermal conductivity of bedrock. Reported thermal conductivity observed in bedrock sites across Antarctica varied between 2.6 and 4.3  $\text{W m}^{-1} \text{K}^{-1}$  (Guglielmin et al., 2011; Correia et al., 2012; Wilhelm et al., 2015). In contrast, the thermal conductivity of soil or sediments was mainly lower than 1.0  $\text{W m}^{-1} \text{K}^{-1}$  (Hrbáček et al., 2017b; Kaplan Pastřířková et al., 2023) and even lower values, to 0.3  $\text{W m}^{-1} \text{K}^{-1}$  were detected in very dry and porous soils (Liu et al., 2018). Higher thermal conductivities in bedrock potentially create favourable conditions for rapid thawing and deepening of the active layer.

The geomorphological context may also explain local differences in active layer and permafrost characteristics (temperatures, thickness, distribution). The topographical setting and specific geomorphological features can, for example, significantly affect the redistribution of snow cover. Snow can accumulate in topographical depressions and around natural obstacles (Oliva et al., 2017b; Kňazková et al., 2020), and is also blown away from wind-exposed surfaces (Oliva et al., 2017b; Kavan et al., 2020). Landscape features, such as ice-cored moraines, can favour the development of a permafrost layer, even down to sea level in the SSI, where permafrost is generally absent at low altitudes (Oliva and Ruiz-Fernández, 2020; Correia et al., 2017; Ferreira et al., 2017).

#### 4.3.3. Biota

In contrast to the Arctic or Alpine regions, vegetation is scarce or absent in most areas in Antarctica. Ice-free terrain corresponds mostly to bare ground. However, areas of dense vegetation cover have lower ground temperatures and thinner active layers than areas where vegetation is absent (Cannone and Guglielmin, 2009; Michel et al., 2012; Hrbáček et al., 2020a). The most apparent effect of moss carpets has been reported from Signy Island in sub-Antarctica, where the moss communities generally form thicker carpets, working as effective insulators. The active layer under such conditions can be >100 cm thicker in bare ground conditions than under mosses (Hrbáček et al., 2020a). We may anticipate that the predicted “greening” of the warmest part of the AP will lead to the expansion of new vegetation communities (e.g. Siegert et al., 2019), which will potentially insulate the ground, and thus slow the impact of warming air temperatures on the soil thermal regime.

#### 4.3.4. Hydric regime

Soil moisture is one of the most crucial parameters affecting the Antarctic environment in terms of biological (e.g. Convey and Peck, 2019), geomorphological (Levy et al., 2011) or soil (e.g. Kennedy, 1993; Ugolini and Bockheim, 2008) evolution. Soil moisture contents also impact greatly on soil thermal conductivity and heat capacity, and thus

ALT thickness. However, data on the temporal or spatial variability of soil moisture are almost missing from most of the continent. In the MDV there has been research focusing mostly on defining dry vs. ice-cemented permafrost starting in the 1970s/80s (e.g., Campbell et al., 1994, 1997; Campbell and Claridge, 2006; Seybold et al., 2010). The phenomenon called “water tracks” have been shown to have a role in soil moisture spatial variability, and subsurface flow which impact on the soil’s physical and biogeochemical properties and thermal regime (Levy et al., 2011; Wlostowski et al., 2018). Information on soil moisture from other regions is scarce and often only descriptive, providing data on differences in water content between sites with varying lithologies and soil texture (Hrbáček et al., 2017a, 2017b), or a contrast between vegetated and bare ground conditions (Cannone and Guglielmin, 2009; Almeida et al., 2014; Hrbáček et al., 2020a). Antarctic soil gravimetric soil moisture contents can vary within a wide range from very dry conditions <5% (Mergelov et al., 2020) up to fully saturated soils with moisture content around 45–50% and to even greater than 100% where there are ice lenses.

#### 4.4. Surface and thermal offset

The studied sites in Antarctica exhibited low thermal offsets mostly ranging from 0 to 3 °C (Table 10). Such values are lower than reported offsets summarized for Arctic tundra biomes, where they generally exceed 5 °C (Lembrechts et al., 2022). In the AP, we can clearly distinguish the offset differences between sites where prevails the effect of: 1) bare ground sites where the surface offset was generally positive 2) snow, that usually leads to increasing of the thermal offset with the only exception of Rothera where thick snow layer cooled the surface resulting in a negative thermal offset (Guglielmin et al., 2014b); 3) vegetation, where surfaces were cooler than adjacent bare-ground sites (e.g. Hrbáček et al., 2021a, 2021b) resulting in lower values thermal offset; (Table 10)

In EA and the MDV, where the majority of study sites are bare ground, the major factor causing offset differences is presumably soil water content. The higher offset (+1 to +3 °C) is typical at sites with higher contents (e.g. Lacelle et al., 2016) whereas even negative offset can occur on the sites with negligible moisture (Seybold et al., 2010). Similarly, a negative thermal offset was reported by Kotzé and Meiklejohn (2017) from the cold-dry area in EA.

The variation of thermal offsets is generally very low with the mean values between −0.2 °C and +0.2 °C. Some year-to-year variability of thermal offset was observed for example on James Ross Island and MDV region where the it usually ranges from −1.0 to +0.5 °C (e.g.; Lacelle et al., 2016; Kaplan Pastřířková et al., 2023). The offset between the temperature on the top of the permafrost and the depth of zero annual amplitude was the highest on Larsemann Hills in EA (0.9 °C) whereas it was close to 0 °C in the remaining sites (Fig. 9).

## 5. Research opportunities

### 5.1. Monitoring site density and data availability

Sites for monitoring the active layer and the topmost permafrost remain scarce in Antarctica. Vieira et al. (2010) estimated the total number of boreholes to 73 mostly located in the AP and MDV. In this overview, we identified more than 80 profiles deeper than 50 cm or reaching the permafrost table (Tables 2–6) providing temperature data for the active layer and the topmost permafrost. Yet, we expect the number of all boreholes installed in Antarctica is much higher, but unevenly concentrated within a few areas of interest. Similarly, the CALM-S sites are unevenly distributed across the continent. Even though there are 28 sites registered in Antarctica, data from only 9 sites has been shared from 2017 to 2022 in CALM-S database. Overall, increasing data availability and regional coverage is crucial for more comprehensive and reliable results of long-term active layer and permafrost changes.

**Table 10**

The mean values of the surface and thermal offset for the Antarctic region. The threshold of 10% moisture (Seybold et al., 2010) was used for the definition of dry vs. wet sites for the Victoria Land region. N/A reports the non-available information.

| Area           | Surface offset |            |             | Thermal offset |              |              |
|----------------|----------------|------------|-------------|----------------|--------------|--------------|
|                | Bare ground    | Snow       | Vegetation  | Bare ground    | Snow         | Vegetation   |
| SSI and WAP    | 1.29 ± 0.36    | 2.0 ± 0.33 | 0.81 ± 0.4  | +0.02 ± 0.16   | +0.25 ± 0.17 | +0.16 ± 0.26 |
| EAP            | 1.08 ± 0.6     | N/A        | 0.2 ± 0.42  | −0.10 ± 0.42   | N/A          | N/A          |
| EA             | −0.3 ± 0.1     | N/A        | N/A         | N/A            | N/A          | N/A          |
| VL (dry sites) | 0.23 ± 1.13    | N/A        | N/A         | −0.15 ± 0.34   | N/A          | N/A          |
| VL (wet sites) | 1.67 ± 0.65    | N/A        | 1.3 ± 1.0   | −0.22 ± 0.45   | N/A          | N/A          |
| sub-Antar      | 1.41 ± 0.56    | N/A        | 1.63 ± 0.68 | N/A            | N/A          | N/A          |

Another challenge for active layer research relies on establishing a denser network for continuous monitoring of soil moisture. Despite the well-known importance of soil moisture, systematic measurements or observations have been carried out only in the MDV to date with only few case studies in Antarctic Peninsula region (e.g. Michel et al., 2012; Thomazini et al., 2020).

Finally, probably the biggest challenges related to monitoring site density relies on installing new deep boreholes, reaching at least the depth of zero annual temperature amplitude (likely to be 10–20 m deep) which is crucial for determining long-term changes in the permafrost (Biskaborn et al., 2019). Only a few boreholes are active in the SSI, Western AP regions and MDV and VL, which is insufficient to provide representative results for Antarctica.

## 5.2. Modelling approaches

According to recent predictions by Lee et al. (2017), the ice-free surfaces in Antarctica might increase by ca. 25% (17,000 km<sup>2</sup>) by 2100. The vast majority of the potentially newly exposed area is likely to be located in the AP, where the ice-free surfaces may double their extent. The newly deglaciated areas will, therefore, provide a research challenge in terms of their geo-ecological development including active layer and permafrost related topics. The connection between different land-systems should be further addressed in future studies. The cold/warm-based (or polythermal) character of glaciers in some of the warmest regions in Antarctica (i.e.; SSI, Western AP, South Orkneys) may explain the presence or absence of permafrost once glaciers retreat. However, permafrost may form in some proglacial environments following deglaciation, as MAAT in glacier margins may range between −2 to −4 °C.

A more complex evaluation of the driving factors' that influence active layer temperature and thickness, and their mutual complementarity has not yet been sufficiently investigated. Notably, published studies often have spatial (one or two sites) and temporal limitations (less than five years long datasets). Some recent reports evaluating longer-term observations have, so far, shown opposing trends of the active layer and uppermost permafrost cooling in the AP (Ramos et al., 2017; Hrbáček and Uxa, 2020) compared to a general warming trend of the permafrost at a depth of zero annual amplitude (Biskaborn et al., 2019) observed over the similar study period (2006–2015). The mismatch may be because decadal datasets are insufficient to provide statistically significant trends (Hrbáček and Uxa, 2020), and there is also, generally, large diversity between the ice-free surfaces of Antarctica.

One possible solution for dataset spatial and temporal extension could be the implementation of high-resolution permafrost models. Several studies have only used the TTOP (Temperature at the Top of Permafrost) or derived Cryogrid-1 models for modelling the permafrost temperature (Ferreira et al., 2017; Hrbáček et al., 2020b; Obu et al., 2020; Kaplan Pastříková et al., 2023). The models of Gold and Lachenbruch; Stefan; and Kudryavtsev have been used to estimate the active layer thickness (Guglielmin and Cannone, 2012; Wilhelm et al., 2015; Uxa, 2016; Hrbáček and Uxa, 2020; Hrbáček et al., 2020a; Kaplan

Pastříková et al., 2023) or ground thermal regime (Liu et al., 2018; Wlostowski et al., 2018). The models reproduce active layer and permafrost conditions at various temporal (e.g. Liu et al., 2018; Hrbáček and Uxa, 2020) and spatial scales (Obu et al., 2020). A possible reason for limited modelling within permafrost research might be a prevailing lack of knowledge of soil physical properties, particularly, soil moisture and thermal properties (thermal conductivity and heat capacity) represent the key input parameters for all of the above modelling approaches, and their precise assessment is crucial for accurate results (Hrbáček and Uxa, 2020).

## 5.3. Geophysical surveying

Geophysical surveying might be a key tool for identifying the permafrost presence, spatial distribution, or thickness, especially in areas with transition conditions between continuous – discontinuous or sporadic permafrost zones. Until now, only a few studies using different techniques have been undertaken. An electrical resistivity tomography survey revealed patches of thin sporadic permafrost on Livingston Island (Correia et al., 2017) and Deception Island (Goyanes et al., 2014). Further, detailed, automatic electrical resistivity tomography surveying of the active layer in Deception Island is planned to explore the spatial-temporal evolution over one year (Farzaman et al., 2020). Similarly, scarce is surveying with ground-penetrating radar, which was used for the detection of ALT spatial variability on James Ross Island (Hrbáček et al., 2021a), permafrost occurrence on SSI (Hauck et al., 2007), and the subsurface structures, including active layer and ground ice in MDV (Campbell et al., 2018).

## 6. Conclusions

In spite of some flaws, there has been obvious progress in permafrost and active layer research in Antarctica since the International Polar Year in 2007/08. This overview evaluated the current state of the research and discussed challenges for future research. On-going research is important to determine medium term (decadal) changes and to help better predict what changes may occur in the longer-term. In regions such as the South Shetland or sub-Antarctic Islands, where the mean annual temperature is close to 0 °C, small changes in climate may lead to marked changes in soil processes as the balance between liquid water and ice within the soil changes. However, in regions where MAATs are markedly below 0 °C, and where presence of liquid water is scarce, such as the McMurdo Dry Valleys, changes are likely to be less marked.

The mean annual, near-surface, ground temperature ranges from around −1 to −3 °C in the South Shetlands up to temperatures between −14 °C and −24 °C in Victoria Land. The latitudinal gradient for the sites near to sea level is 0.9 °C/deg. In the McMurdo Dry Valleys area, we also observed an altitudinal gradient of near-surface ground temperature of 0.6 °C/100 m. Even though we identified many parameters which have a clear impact on the active layer thermal regime, the differences in surface and thermal offsets for the sites under the influence of variable factors was relatively low. Similarly, to near-surface, the permafrost temperature ranges from ca. −1.5 °C in the South Shetlands to ca. −19 °C

in the McMurdo Dry Valleys. Notably, the thermal offset between the top of the permafrost table and the depth of zero annual amplitude was not for any of the studied sites.

The active layer thickness was spatially variable and sensitive to local driving factors like air temperature, global radiation, snow occurrence, topography, lithology, soil moisture or vegetation. The highest spatial variability of active layer thickness was in the South Shetlands and Antarctic Peninsula regions (ca. 45 to >500 cm) and the lowest is in Victoria Land (ca. 5 to 90 cm). The index of active layer thickness variation was between 9 and 37% on the sites with long term monitoring. When considering the low elevation sites, we identified a mean latitudinal gradient of 3.7 cm/deg. In the McMurdo Dry Valleys, the altitudinal gradient was reported as reaching 2.5 cm/100 m.

Our study also reveals some challenges for future research. There is a lack of results allowing more detailed evaluation of long-term variability of the ground thermal regime. Such results are limited only to a few regions, which currently prevents reliable analysis for the entire continent from being undertaken. Further, very little is known about soil moisture, which should be, especially in harsh conditions of Antarctica, one of the most important parameters influencing the soil thermal regime, active layer thickness, ground thermal parameters, and vegetation distribution. Due to general remoteness of the individual study areas in Antarctica, we should emphasize that international cooperation is necessary for further successful progress in active layer and permafrost research in Antarctica.

#### Declaration of Competing Interest

The authors declare that they have no known competing financial interests or personal relationships that could have appeared to influence the work reported in this paper.

#### Data availability

Data will be made available on request.

#### Acknowledgements

FH and LKP acknowledge Czech Scientific Foundation project (GM22-28659M), Masaryk University internal project (MUNI/A/1323/2022) and Czech Antarctic Research Programme funded by MEYS of Czech Republic. MO acknowledges support from the project NUNANTAR (Fundação para a Ciência e Tecnologia of Portugal; 02/SAICT/2017 - 32002) and the research groups ANTALP (Antarctic, Arctic, Alpine Environments; 2017-SGR-1102) funded by the Agència de Gestió d'Ajuts Universitaris i de Recerca of the Government of Catalonia. TO'N acknowledge ongoing technical and dataset support of Dr. Cathy Seybold of the USDA. Over the years many people have contributed to installation and maintenance of the McMurdo Dry Valley Soil Climate stations, but special thanks are due to Cathy Seybold, Ron Paetzold, Deb Harms and Don Huffman from the USDA; Jackie Aislabie and Fraser Morgan from Landcare Research, New Zealand; Chris Morcom, Dean Sandwell from the University of Waikato, New Zealand; and Pete Wilson from the University of Canterbury. Antarctica New Zealand provided logistic support for annual station access. MG and SP wish to thank PNRA (Programma Nazionale di Ricerca in Antartica) for the logistical and financial support in Continental Antarctica, Antarctic Peninsula and in Signy Island. They want also to thank British Antarctic Survey and in particular the Met Group in Rothera Island and the Station Leader in Signy for their logistical support and to download the data. Finally we want to thank Pete Convey, Nicoletta Cannone, Francesco Malfasi for their support in AP and Signy and Riccardo Bono at Mario Zucchelli Station.

#### References

- Abramov, A.A., Sletten, R.S., Rivkina, E.M., Mironov, V.A., Gilichinsky, D.A., 2011. Geocryological conditions of Antarctica. *Earth's 15* (3), 3–19.
- Adams, B.J., Bardgett, R.D., Ayres, E., Wall, D.H., Aislabie, J., Bamforth, S., Bargagli, R., Cary, C., Cavacini, P., Connell, L., Convey, P., Fell, J.W., Frati, F., Hogg, I.D., Newsham, K.K., O'Donnell, A., Russell, N., Seppelt, R.D., Stevens, M.I., 2006. Diversity and distribution of Victoria Land biota. *Soil Biol. Biochem.* 38 (10), 3003–3018. <https://doi.org/10.1016/j.soilbio.2006.04.030>.
- Adlam, L.S., Balks, M.R., Seybold, C.A., Campbell, D.I., 2010. Temporal and spatial variation in active layer depth in the McMurdo Sound Region, Antarctica. *Antarct. Sci.* 22 (1), 45–52. <https://doi.org/10.1017/S0954102009990460>.
- Aislabie, J.M., Chhour, K.L., Saul, D.J., Miyauchi, S., Ayton, J., Paetzold, R.F., Balks, M.R., 2006. Dominant bacteria in soils of Marble point and Wright valley, Victoria land, Antarctica. *Soil Biol. Biochem.* 38 (10), 3041–3056.
- Aislabie, J.M., Jordan, S., Barker, G.M., 2008. Relation between soil classification and bacterial diversity in soils of the Ross Sea region, Antarctica. *Geoderma* 144 (1–2), 9–20.
- Aislabie, J., McLeod, M., Ryburn, J., McGill, A., Thornburrow, D., 2011. Soil type influences the leaching of microbial indicators under natural rainfall following application of dairy shed effluent. *Soil Res.* 49 (3), 270. <https://doi.org/10.1071/SR10147>.
- Almeida, I., Schaefer, C.E.G.R., Fernandes, R.B.A., Pereira, T.T.C., Nieuwendam, A., Pereira, A.B., 2014. Active layer thermal regime at different vegetation covers at Lions Rump, King George Island, Maritime Antarctica. *Geomorphology* 225, 36–46.
- Almeida, I.C.C., Schaefer, C.E.G.R., Michel, R.F.M., Fernandes, R.B.A., Pereira, T.T.C., Andrade, A.M., Francelino, M.R., Elpidio, I., Filho, F., Bockheim, J.G., 2017. Long term active layer monitoring at a warm-based glacier front from maritime Antarctica. *Catena* 149 (2), 572–581.
- Altmaier, M., Hoppers, U., Delisle, G., Merchel, S., Ott, U., 2011. Glaciation history of Queen Maud Land (Antarctica) reconstructed from in-situ produced cosmogenic <sup>10</sup>Be, <sup>26</sup>Al and <sup>21</sup>Ne. *Polar Sci.* 4 (1), 42–61. <https://doi.org/10.1016/j.polar.2010.01.001>.
- Andriuzzi, W.S., Adams, B.J., Barrett, J.E., Virginia, R.A., Wall, D.H., 2018. Observed trends of soil fauna in the Antarctic Dry Valleys: early signs of shifts predicted under climate change. *Ecology* 99 (2), 312–321.
- Balks, M.R., O'Neill, T.A., 2016. Soil and permafrost in the Ross Sea region of Antarctica: stable or dynamic? *Cuadernos Investig. Geogr.* 42 (2), 415–434. <https://doi.org/10.18172/cig.2923>.
- Bañón, M., Vasallo, F., 2015. Aemet en la Antártida. *Climatología y meteorología sinóptica en las estaciones meteorológicas en las estaciones meteorológicas españolas en la Antártida*. AEMET Min. Madrid, 150 pp.
- Bañón, M., Justel, A., Velázquez, A., Quesada, A., 2013. Regional weather survey in Byers Peninsula, Livingston Island, South Shetland Islands, Antarctica. *Antarct. Sci.* 25, 146–156. <https://doi.org/10.1017/S0954102012001046>.
- Barrett, P.J., 1971. *Geologic Maps of Antarctica*, by Campbell Craddock. ARCTIC 24.
- Barrett, J.E., Virginia, R.A., Hopkins, D.W., Aislabie, J., Bargagli, R., Bockheim, J.G., Wallenstein, M.D., 2006. Terrestrial ecosystem processes of Victoria land, Antarctica. *Soil Biol. Biochem.* 38 (10), 3019–3034.
- Benayas, J., Pertierra, L., Tejedo, P., Lara, F., Bermudez, O., Hughes, K.A., Quesada, A., 2013. A review of scientific research trends within ASPA no. 126 Byers Peninsula, South Shetland Islands, Antarctica. *Antarct. Sci.* 25 (2), 128–145. <https://doi.org/10.1017/S0954102012001058>.
- Biskaborn, B.K., Smith, S.L., Noetzi, J., Matthes, H., Vieira, G., Streletskiy, D.A., Schoeneich, P., Romanovsky, V.E., Lewkowicz, A.G., Abramov, A., Allard, M., Boike, J., Cable, W.L., Christiansen, H.H., Delaloye, R., Diekmann, B., Drozdov, D., Etzelmüller, B., Grosse, G., Guglielmin, M., Ingeman-Nielsen, T., Isaksen, K., Ishikawa, M., Johansson, M., Johannsson, H., Joo, A., Kaverin, D., Kholodov, A., Konstantinov, P., Kröger, T., Lambiel, C., Lanckman, J.P., Luo, D., Malkova, G., Meiklejohn, I., Moskalenko, N., Oliva, M., Phillips, M., Ramos, M., Sannel, A.B.K., Sergeev, D., Seybold, C., Skryabin, P., Vasiliev, A., Wu, Q., Yoshikawa, K., Zheleznyak, M., Lantuit, H., 2019. Permafrost is warming at a global scale. *Nat. Commun.* 10, 1–11. <https://doi.org/10.1038/s41467-018-08240-4>.
- Björck, S., Olsson, S., Ellis-Evans, C., Håkansson, H., Humlum, O., de Lirio, J.M., 1996. Late Holocene palaeoclimatic records from lake sediments on James Ross Island, Antarctica. *Palaeogeogr. Palaeoclimatol. Palaeoecol.* 121 (3–4), 195–220. [https://doi.org/10.1016/0031-0182\(95\)00086-0](https://doi.org/10.1016/0031-0182(95)00086-0).
- Blunden, J., Boyer, T. (Eds.), 2022. State of The Climate 2021. *Bulletin of American Meteorological Society*, pp. S1–S465. [https://journals.ametsoc.org/view/journals/bams/103/8/2022BAMSStateoftheClimate.1.xml?tab\\_body=abstract-display](https://journals.ametsoc.org/view/journals/bams/103/8/2022BAMSStateoftheClimate.1.xml?tab_body=abstract-display).
- Bockheim, J.G., 1997. Properties and classification of cold desert soils from Antarctica. *Soil Sci. Soc. Am. J.* 61 (1), 224–231.
- Bockheim, J.G., 2010. Evolution of desert pavements and the vesicular layer in soils of the Transantarctic Mountains. *Geomorphology* 118 (3–4), 433–443. <https://doi.org/10.1016/j.geomorph.2010.02.012>.
- Bockheim, J.G. (Ed.), 2015. *The Soils of Antarctica*. Springer. <https://doi.org/10.1007/978-3-319-05497-1>, 322 p.
- Bockheim, J.G., McLeod, M., 2008. Soil distribution in the McMurdo Dry Valleys, Antarctica. *Geoderma* 144 (1–2), 43–49. <https://doi.org/10.1016/j.geoderma.2007.10.015>.
- Bockheim, J.G., Campbell, I.B., McLeod, M., 2007. Permafrost distribution and active-layer depths in the McMurdo Dry Valleys, Antarctica. *Permafrost. Periglac. Process.* 18 (3), 217–227. <https://doi.org/10.1002/ppp.588>.
- Bockheim, J., Vieira, G., Ramos, M., López-Martínez, J., Serrano, E., Guglielmin, M., Wilhelm, K., Nieuwendam, A., 2013. Climate warming and permafrost dynamics in

- the Antarctic Peninsula region. *Glob. Planet. Chang.* 100, 215–223. <https://doi.org/10.1016/j.gloplacha.2012.10.018>.
- Borzotta, E., Trombetta, D., 2004. Correlation between frozen ground thickness measured in Antarctica and permafrost thickness estimated on the basis of the heat flow obtained from magnetotelluric soundings. *Cold Reg. Sci. Technol.* 40 (1–2), 81–96. <https://doi.org/10.1016/j.coldregions.2004.06.002>.
- Boy, J., Godoy, R., Shibistova, O., Boy, D., McCulloch, R., Andriano de la Fuente, A., Morales, M.A., Mikutta, R., Guggenberger, G., 2016. Successional patterns along soil development gradients formed by glacier retreat in the Maritime Antarctic, King George Island. *Rev. Chil. Hist. Nat.* 89, 1–17. <https://doi.org/10.1186/s40693-016-0056-8>.
- Bromwich, D.H., Guo, Z., Bai, L., Chen, Q., 2004. Modeled Antarctic Precipitation. Part I: Spatial and Temporal Variability. *J. Clim.* 17, 427–447. [https://doi.org/10.1175/1520-0442\(2004\)017<0427:MAPPIS>2.0.CO;2](https://doi.org/10.1175/1520-0442(2004)017<0427:MAPPIS>2.0.CO;2).
- Bromwich, D.H., Steinhoff, D.F., Simmonds, I., Keay, K., Fogt, R.L., 2011. Climatological aspects of cyclogenesis near Adélie Land Antarctica. *Tellus A* 63 (5), 921. <https://doi.org/10.1111/j.1600-0870.2011.00537.x>.
- Brooks, S.T., Jabour, J., van den Hoff, J., Bergstrom, D.M., 2019. Our footprint on Antarctica competes with nature for rare ice-free land. *Nat. Sustain.* 2 (3), 185–190. <https://doi.org/10.1038/s41893-019-0237-y>.
- Brown, J., Hinkel, K.M., Nelson, F.E., 2000. The Circumpolar active layer monitoring (CALM) program: historical perspectives and initial results. *Polar Geogr.* 24 (3), 165–258.
- Burton-Johnson, A., Dziadek, R., Martin, C., 2020. Review Article: Geothermal heat flow in Antarctica: current and future directions. *The Cryosphere* 14, 3843–3873. <https://doi.org/10.5194/tc-14-3843-2020>.
- CALM site, 2022. Available online: <https://www2.gwu.edu/~calm/>.
- Campbell, I.B., Claridge, G.G.C., 1987. *Antarctica: Soils, Weathering Processes and Environment*. Elsevier, 368 pp.
- Campbell, I.B., Claridge, G.G.C., 2006. Permafrost properties, patterns and processes in the TransAntarctic Mountains Region. *Permafrost Periglacial Process.* 17, 215–232.
- Campbell, I.B., Claridge, G.G.C., Balks, M.R., 1994. The effect of human activities on moisture content of soils and underlying permafrost from the McMurdo Sound region, Antarctica. *Antarct. Sci.* 6, 307–314.
- Campbell, I.B., Claridge, G.G.C., Balks, M.R., Campbell, D.I., 1997. Moisture content in soils of the McMurdo Sound and Dry Valley region of Antarctica. In: Lyons, W.B., Howard-Williams, C., Hawes, I. (Eds.), *Ecosystem Processes in Antarctic Ice-Free Landscapes*. Balkema, Rotterdam, pp. 61–76.
- Cannone, N., Guglielmin, M., 2009. Influence of vegetation on the ground thermal regime in continental Antarctica. *Geoderma* 151 (3–4), 215–223. <https://doi.org/10.1016/j.geoderma.2009.04.007>.
- Cannone, N., Seppelt, R., 2008. A preliminary floristic classification of southern and northern Victoria Land vegetation, continental Antarctica. *Antarct. Sci.* 20 (6), 553–562. <https://doi.org/10.1017/S0954102008001454>.
- Cannone, N., Augusti, A., Malfasi, F., Pallozzi, E., Calfapietra, C., Brugnoli, E., 2016. The interaction of biotic and abiotic factors at multiple spatial scales affects the variability of CO<sub>2</sub> fluxes in polar environments. *Polar Biol.* 39 (9), 1581–1596. <https://doi.org/10.1007/s00300-015-1883-9>.
- Cannone, N., Guglielmin, M., Malfasi, F., Hubberten, H.W., Wagner, D., 2021. Rapid soil and vegetation changes at regional scale in continental Antarctica. *Geoderma* 394, 115017. <https://doi.org/10.1016/j.geoderma.2021.115017>.
- Carshalton, A.G., Balks, M.R., O'Neill, T.A., Bryan, K.R., Seybold, C.A., 2022. Climatic influences on active layer depth between 2000 and 2018 in the McMurdo Dry Valleys, Ross Sea Region, Antarctica. *Geoderma Region.* 29, e00497 <https://doi.org/10.1016/j.geodrs.2022.e00497>.
- Chapman, W.L., Walsh, J.E., 2007. A Synthesis of Antarctic Temperatures. *J. Clim.* 20 (16), 4096–4117. <https://doi.org/10.1175/JCLI4236.1>.
- Chaves, D.A., Lyra, G.B., Francelino, M.R., Silva, L.D.B., Thomazini, A., Schaefer, C.E.G.R., 2017. Active layer and permafrost thermal regime in a patterned ground soil in Maritime Antarctica, and relationship with climate variability models. *Sci. Total Environ.* 584–585, 572–585.
- Chong, C.W., Pearce, D.A., Convey, P., Yew, W.C., Tan, I.K.P., 2012. Patterns in the distribution of soil bacterial 16S rRNA gene sequences from different regions of Antarctica. *Geoderma* 181, 45–55.
- Christiansen, H.H., 2004. Meteorological control on interannual spatial and temporal variations in snow cover and ground thawing in two northeast Greenlandic Circumpolar-Active-Layer-Monitoring (CALM) sites. *Permafrost Periglacial Process.* 15, 155–169. <https://doi.org/10.1002/ppp.489>.
- Colesie, C., Walshaw, C.V., Sancho, L.G., Davey, M.P., Gray, A., 2023. Antarctica's vegetation in a changing climate. *WIREs Clim. Ch.* 14 (1), e810. <https://doi.org/10.1002/wcc.810>.
- Convey, P., Peck, L.S., 2019. Antarctic environmental change and biological responses. *Science Advances* 5 (11), eaaz0888.
- Cook, A.J., Vaughan, D.G., 2010. Overview of areal changes of the ice shelves on the Antarctic Peninsula over the past 50 years. *Cryosphere* 4 (1), 77–98. <https://doi.org/10.5194/tc-4-77-2010>.
- Cuchi, J.J., Durán, J.A., Alfaro, D., Serrano, E., López-Martínez, J., 2004. Discriminación de diferentes tipos de agua en un área con permafrost, Antártida. *Boletín Real Soc. Española Hist. Nat. (Sect. Geol.)* 99 (1–4), 2004.
- Davies, B.J., Glasser, N.F., Carrivick, J.L., Hambrey, M.J., Smellie, J.L., Nývlt, D., 2013. Landscape evolution and ice-sheet behaviour in a semi-arid polar environment: James Ross Island, NE Antarctic Peninsula. *Geol. Soc. Lond., Spec. Publ.* 381 (1), 353–395. <https://doi.org/10.1144/SP381.1>.
- Dawson, E.J., Schroeder, D.M., Chu, W., Mantelli, E., Seroussi, H., 2022. Ice mass loss sensitivity to the Antarctic ice sheet basal thermal state. *Nat. Commun.* 13, 4957.
- Decker, E.R., Bucher, G.J., 1977. Geothermal studies in Antarctica. *Antarct. J. U.S.* 12, 103–104.
- Denton, G.H., Hughes, T.J., 2000. Reconstruction of the Ross ice drainage system, Antarctica, at the last glacial maximum. *Geogr. Ann.* 82 (2–3), 143–166. <https://doi.org/10.1111/j.0435-3676.2000.00120.x>.
- Denton, G.H., Sugden, D.E., Marchant, D.R., Hall, B.L., Wilch, T.I., 1993. East Antarctic Ice Sheet Sensitivity to Pliocene Climatic Change from a Dry Valleys Perspective. *Geogr. Ann.* 75 (4), 155–204. <https://doi.org/10.1080/04353676.1993.11880393>.
- Dewar, G.J., 1970. *The geology of Adelaide Island*. Cambridge, British Antarctic Survey, 66pp. (British Antarctic Survey Scientific Reports, 57).
- Dharwadkar, A., Shukla, S.P., Verma, A., Gajbhiye, D., 2018. Geomorphic evolution of Schirmacher Oasis, central Dronning Maud Land, East Antarctica. *Polar Sci.* 18.
- Emslie, S.D., 2001. Radiocarbon dates from abandoned penguin colonies in the Antarctic Peninsula region. *Antarct. Sci.* 13 (3), 289–295. <https://doi.org/10.1017/S0954102001000414>.
- Farzamian, M., Vieira, G., Monteiro Santos, F.A., Yaghoobi Tabar, B., Hauck, C., Paz, M. C., Bernardo, I., Ramos, M., de Pablo, M.A., 2020. Detailed detection of active layer freeze-thaw dynamics using quasi-continuous electrical resistivity tomography (Deception Island, Antarctica). *Cryosphere* 14 (3), 1105–1120. <https://doi.org/10.5194/tc-14-1105-2020>.
- Favero-Longo, S.E., Worland, M.R., Convey, P., Lewis Smith, R.I., Piervittori, R., Guglielmin, M., Cannone, N., 2012. Primary succession of lichen and bryophyte communities following glacial recession on Signy Island, South Orkney Islands, Maritime Antarctic. *Antarct. Sci.* 24 (4), 323–336. <https://doi.org/10.1017/S0954102012000120>.
- Ferreira, A., Vieira, G., Ramos, M., Nieuwendam, A., 2017. CATENA 149, 560–571. <https://doi.org/10.1016/j.catena.2016.08.027>.
- Fisher, D.A., Laclelle, D., Pollard, W., Davila, A., McKay, C.P., 2016. Ground surface temperature and humidity, ground temperature cycles and the ice table depths in University Valley, McMurdo Dry Valleys of Antarctica. *J. Geophys. Res. Earth Surf.* 121 (11), 2069–2084. <https://doi.org/10.1002/2016JF004054>.
- Forte, E., Dalle Fratte, M., Azzaro, M., Guglielmin, M., 2016. Pressurized brines in continental Antarctica as a possible analogue of Mars. *Sci. Rep.* 6, 33158 (2016). <https://doi.org/10.1038/srep33158>.
- Fountain, A.G., Nylen, T.H., Monaghan, A., Basagic, H.J., Bromwich, D., 2010. Snow in the McMurdo dry valleys, Antarctica. *Int. J. Climatol.* 30 (5), 633–642.
- Fountain, A.G., Levy, J.S., Gooseff, M.N., Van Horn, D., 2014. The McMurdo Dry Valleys: a landscape on the threshold of change. *Geomorphology* 225, 25–35.
- Fountain, A.G., Basagic, H.J., Niebuhr, S., 2016. Glaciers in equilibrium, McMurdo Dry Valleys, Antarctica. *J. Glaciol.* 62 (235), 976–989. <https://doi.org/10.1017/jog.2016.86>.
- Francelino, M.R., Schaefer, C.E.G.R., Simas, F.N.B., Filho, E.I.F., de Souza, J.J.L.L., da Costa, L.M., 2011. Geomorphology and soils distribution under paraglacial conditions in an ice-free area of Admiralty Bay, King George Island, Antarctica. *Catena* 85 (3), 194–204. <https://doi.org/10.1016/j.catena.2010.12.007>.
- French, H.M., Guglielmin, M., 1999. Observations on the ice-marginal, periglacial geomorphology of Terra Nova Bay, Northern Victoria Land, Antarctica. *Permafrost Periglacial Process.* 10 (4), 331–347. [https://doi.org/10.1002/\(SICI\)1099-1530\(199910/12\)10:4<331::AID-PPP328>3.0.CO;2-A](https://doi.org/10.1002/(SICI)1099-1530(199910/12)10:4<331::AID-PPP328>3.0.CO;2-A).
- Friedmann, E.I., 1982. Endolithic microorganisms in the Antarctic cold desert. *Science* 215 (4536), 1045–1053.
- Fukuda, M., Shimokawa, K., Takahashi, N., Sone, T., 1992. Permafrost in Seymour Island and James Ross Island, Antarctic Peninsula region. *Geogr. Rev. Jpn. Ser. A* 65 (2), 124–131.
- Gerrish, L., Fretwell, P., Cooper, P., 2020. High Resolution Vector Polygons of Antarctic Rock Outcrop (7.3) [dataset]. UK Polar Data Centre, Natural Environment Research Council, UK Research and Innovation.
- Gilichinsky, D.A., Nolte, E., Basilyan, A.E., Beer, J., Blinov, A.V., Lazarev, V.E., Khodolov, A.L., Meyer, H., Nikolskiy, P.A., Schirmeister, L., Tumskey, V.E., 2007. Dating of syngenetic ice wedges in permafrost with <sup>36</sup>Cl. *Quat. Sci. Rev.* 26 (11–12), 1547–1556. <https://doi.org/10.1016/j.quascirev.2007.04.004>.
- Gimingham, C.H., Smith, R.L., 1970. Bryophyte and lichen communities in 603 the Maritime Antarctic. In: Holdgate, M.W. (Ed.), *Antarctic Ecology*, vol. 1. Academic Press, London, pp. 752–785.
- Gjorup, D.F., Schaefer, C.E.G.R., Simas, F.N.B., Francelino, M.R., Michel, R.F.M., Bockheim, J.G., 2020. Sulfurization, acid-sulfate soils and active layer monitoring at the semiarid Seymour Island, Antarctica. *Geoderma Region.* 22, e00305 <https://doi.org/10.1016/j.geodrs.2020.e00305>.
- Goordial, J., Raymond-Bouchard, I., Riley, R., Ronholm, J., Shapiro, N., Woyke, T., LaButti, K.M., Tice, H., Amirebrahimi, M., Grigoriev, I.V., Greer, C., Bakermans, C., Whyte, L., 2016. Improved high-quality draft genome sequence of the Eurypsychrophile *Rhodotorula* sp. JG1b, isolated from permafrost in the hyperarid Upper-Elevation McMurdo Dry Valleys, Antarctica. *Genome Announc.* 4 (2) <https://doi.org/10.1128/genomeA.00069-16>.
- Gore, D.B., Rhodes, E.J., Augustinus, P.C., Leishman, M.R., Colhoun, E.A., Rees-Jones, J., 2001. Bunge Hills, East Antarctica: ice free at the last Glacial Maximum. *Geology* 29 (12), 1103. [https://doi.org/10.1130/0091-7613\(2001\)029<1103:BHEAIF>2.0.CO;2](https://doi.org/10.1130/0091-7613(2001)029<1103:BHEAIF>2.0.CO;2).
- Goyanes, G., Vieira, G., Caselli, A., Cardoso, M., Marmy, A., Santos, F., Bernardo, I., Hauck, C., 2014. Local influences of geothermal anomalies on permafrost distribution in an active volcanic island (Deception Island, Antarctica). *Geomorphology* 225, 57–68. <https://doi.org/10.1016/j.geomorph.2014.04.010>.
- Graham, A., Kuhn, G., Meisel, O., et al., 2017. Major advance of South Georgia glaciers during the Antarctic Cold Reversal following extensive sub-Antarctic glaciation. *Nat. Commun.* 8, 14798. <https://doi.org/10.1038/ncomms14798>.

- Guglielmin, M., 2006. Ground surface temperature (GST), active layer, and permafrost monitoring in continental Antarctica. *Permafrost. Periglac. Process.* 17, 133–143. <https://doi.org/10.1002/ppp.553>.
- Guglielmin, M., Cannone, N., 2012. A permafrost warming in a cooling Antarctica? *Clim. Chang.* 111 (2), 177–195. <https://doi.org/10.1007/s10584-011-0137-2>.
- Guglielmin, M., Biasini, A., Smiraglia, C., 1997. The Contribution of Geoelectrical Investigations in the Analysis of Periglacial and Glacial Landforms in Ice Free areas of the Northern Foothills (Northern Victoria Land, Antarctica). *Geogr. Ann. Ser. A Phys. Geogr.* 79A (1–2), 17–24. <https://doi.org/10.1111/1468-0459.00003>.
- Guglielmin, M., Ellis Evans, C.J., Cannone, N., 2008. Active layer thermal regime under different vegetation conditions in permafrost areas. A case study at Signy Island (Maritime Antarctica). *Geoderma* 144 (1–2), 73–85. <https://doi.org/10.1016/j.geoderma.2007.10.010>.
- Guglielmin, M., Balks, M.R., Adlam, L.S., Baio, F., 2011. Permafrost thermal Regime from two 30-m Deep Boreholes in Southern Victoria Land, Antarctica. *Permafrost. Periglac. Process.* 22, 129–139. <https://doi.org/10.1002/ppp.715>.
- Guglielmin, M., Worland, M.R., Convey, P., Cannone, N., 2012. Schmidt Hammer studies in the maritime Antarctic: Application to dating Holocene deglaciation and estimating the effects of macrolichens on rock weathering. *Geomorphology* 155–156, 33–34. <https://doi.org/10.1016/j.geomorph.2011.12.015>.
- Guglielmin, M., Dalle Fratte, M., Cannone, N., 2014a. Permafrost warming and vegetation changes in continental Antarctica. *Environ. Res. Lett.* 9 (4), 045001.
- Guglielmin, M., Worland, M.R., Baio, F., Convey, P., 2014b. Permafrost and snow monitoring at Rothera Point (Adelaide Island, Maritime Antarctica): Implications for rock weathering in cryotic conditions. *Geomorphology* 225, 47–56.
- Guglielmin, M., Ponti, S., Forte, E., 2018. The origins of Antarctic rock glaciers: periglacial or glacial features? *Earth Surf. Process. Landf.* 43 (7), 1390–1402. <https://doi.org/10.1002/esp.4320>.
- Hall, K., 2002. Review of present and Quaternary periglacial processes and landforms of the maritime and sub-Antarctic region. *S. Afr. J. Sci.* 98, 71–81.
- Hansen, C.D., 2018. On High-Altitude and -Latitude Diurnal Frost Environments. Rhodes University.
- Hansen, C.D., Meiklejohn, K.I., Nel, W., Loubser, M.J., Van Der Merwe, B.J., 2013. Aspect-controlled Weathering Observed on a Blockfield in Dronning Maud Land, Antarctica. *Geogr. Ann.: Series A, Phys. Geogr.* 95, 305–313. <https://doi.org/10.1111/geoa.12025>.
- Harris, S.A., French, H.M., Heginbottom, J.A., Johnston, G.H., Ladanyi, B., Segó, D.C., van Everdingen, R.O., 1988. Glossary of Permafrost and Related Ground-Ice Terms. National Research Council of Canada. Associate Committee on Geotechnical Research. <https://doi.org/10.4224/20386561>. Permafrost Subcommittee, 159 p.
- Hathway, B., Lomas, S.A., 1998. The Jurassic–Lower Cretaceous Byers Group, South Shetland Islands, Antarctica: revised stratigraphy and regional correlations. *Cretac. Res.* 19 (1), 43–67. <https://doi.org/10.1006/cres.1997.0095>.
- Hauck, C., Vieira, G., Gruber, S., Blanco, J., Ramos, M., 2007. Geophysical identification of permafrost in Livingston Island, maritime Antarctica. *J. Geophys. Res.* 112 (F2), F02S19. <https://doi.org/10.1029/2006JF000544>.
- Hedding, D.W., 2008. Spatial inventory of landforms in the recently exposed Central Highland of Sub-Antarctic Marion Island. *S. Afr. Geogr. J.* 90 (1), 11–21. <https://doi.org/10.1080/03736245.2008.9725307>.
- Hodgson, D.A., Graham, A.G.C., Roberts, S.J., Bentley, M.J., Cofaigh, C.Ó., Verleyen, E., Vyverman, W., Jomelli, V., Favier, V., Brunstein, D., Verfaillie, D., Colhoun, E.A., Saunders, K.M., Selkirk, P.M., Mackintosh, A., Hedding, D.W., Nel, W., Hall, K., McGlone, M.S., Smith, J.A., 2014. Terrestrial and submarine evidence for the extent and timing of the last Glacial Maximum and the onset of deglaciation on the maritime-Antarctic and sub-Antarctic islands. *Quat. Sci. Rev.* 100, 137–158. <https://doi.org/10.1016/j.quascirev.2013.12.001>.
- Hopkins, D.W., Sparrow, A.D., Novis, P.M., Gregorich, E.G., Elberling, B., Greenfield, L. G., 2006. Controls on the distribution of productivity and organic resources in Antarctic Dry Valley soils. *Proc. R. Soc. B Biol. Sci.* 273 (1602), 2687–2695. <https://doi.org/10.1098/rspb.2006.3595>.
- Hrbáček, F., Uxa, T., 2020. The evolution of a near-surface ground thermal regime and modeled active-layer thickness on James Ross Island, Eastern Antarctic Peninsula, in 2006–2016. *Permafrost. Periglac. Process.* 31 (1), 141–155. <https://doi.org/10.1002/ppp.2018>.
- Hrbáček, F., Oliva, M., Laska, K., Ruiz-Fernández, J., de Pablo, M.A., Vieira, G., Ramos, M., Nývlt, D., 2016a. Active layer thermal regime in two climatically contrasted sites of the Antarctic Peninsula region. *Cuadernos Investig. Geogr.* 42 (2), 457–474. <https://doi.org/10.18172/cig.2915>.
- Hrbáček, F., Laska, K., Engel, Z., 2016b. Effect of snow cover on the active-layer thermal regime - a case study from James Ross Island, Antarctic Peninsula. *Permafrost. Periglac. Process.* 27 (3), 307–315. <https://doi.org/10.1002/ppp.1871>.
- Hrbáček, F., Kňazková, M., Nývlt, D., Laska, K., Mueller, C.W., Ondruch, J., 2017a. Active layer monitoring at CALM-S site near J.G. Mendel station, James Ross Island, eastern Antarctic Peninsula. *Sci. Total Environ.* 601–602, 987–997. <https://doi.org/10.1016/j.scitotenv.2017.05.266>.
- Hrbáček, F., Nývlt, D., Laska, K., 2017b. Active layer thermal dynamics at two lithologically different sites on James Ross Island, Eastern Antarctic Peninsula. *Catena* 149 (2), 592–602.
- Hrbáček, F., Nývlt, D., Laska, K., Kňazková, M., Kampová, B., Engel, Z., Oliva, M., Mueller, C.W., 2019. Permafrost and active layer research on James Ross Island: an overview. *Czech Polar Rep.* 9 (1), 20–36. <https://doi.org/10.5817/CPR2019-1-3>.
- Hrbáček, F., Cannone, N., Kňazková, M., Malfasi, F., Convey, P., Guglielmin, M., 2020a. Effect of climate and moss vegetation on ground surface temperature and the active layer among different biogeographical regions in Antarctica. *Catena* 190, 104562. <https://doi.org/10.1016/j.catena.2020.104562>.
- Hrbáček, F., Oliva, M., Fernández, J.-R., Kňazková, M., de Pablo, M.A., 2020b. Modelling ground thermal regime in bordering (dis)continuous permafrost environments. *Environ. Res.* 181, 108901. <https://doi.org/10.1016/j.envres.2019.108901>.
- Hrbáček, F., Engel, Z., Kňazková, M., Smolíková, J., 2021a. Effect of summer snow cover on the active layer thermal regime and thickness on CALM-S JGM site, James Ross Island, eastern Antarctic Peninsula. *Catena* 207, 105608. <https://doi.org/10.1016/j.catena.2021.105608>.
- Hrbáček, F., Vieira, G., Oliva, M., Balks, M., Guglielmin, M., de Pablo, M.A., Molina, A., Ramos, M., Goyanes, G., Meiklejohn, I., Abramov, A., Demidov, N., Fedorov-Davydov, D., Lupachev, A., Rivkina, E., Laska, K., Kňazková, M., Nývlt, D., Raffi, R., Strelin, J., Sone, T., Fukui, K., Dolgikh, A., Zazovskaya, E., Mergelov, N., Osokin, N., Miamin, V., 2021b. *Polar Geogr.* 44 (3), 217–231. <https://doi.org/10.1080/1088937X.2017.1420105>.
- Isaac, M.J., Chinn, T.J., Edbrooke, S.W., Forsyth, P.J., 1996. *Geology of the Olympus Range Area, Southern Victoria Land, Antarctica*. Institute of Geological and Nuclear Science 1:50 000 geological map 20. Lower Hutt, Institute of Geological & Nuclear Sciences, 1 sheet + 60 p.
- Jones, V.J., Hodgson, D.A., Chepstow-Lusty, A., 2000. Palaeolimnological evidence for marked Holocene environmental changes on Signy Island, Antarctica. *The Holocene* 10 (1), 43–60. <https://doi.org/10.1191/095968300673046662>.
- Kaplan Pastříková, L., Hrbáček, F., Uxa, T., Laska, K., 2023. Permafrost table temperature and active layer thickness variability on James Ross Island, Antarctic Peninsula, in 2004–2021. *Sci. Total Environ.* 869, 161690. <https://doi.org/10.1016/j.scitotenv.2023.161690>.
- Kavan, J., Nývlt, D., Laska, K., Engel, Z., Kňazková, M., 2020. High-latitude dust deposition in snow on the glaciers of James Ross Island, Antarctica. *Earth Surf. Process. Landf.* 45, 1569–1578. <https://doi.org/10.1002/esp.4831>.
- Kennedy, A.D., 1993. Water as a Limiting Factor in the Antarctic Terrestrial Environment: A Biogeographical Synthesis. *Arct. Alp. Res.* 25 (4), 308–315.
- Kňazková, M., Hrbáček, F., Kavan, J., Nývlt, D., 2020. Effect of hyaloclastite breccia boulders on meso-scale periglacial-aeolian landsystem in semi-arid Antarctic environment, James Ross Island, Antarctic Peninsula. *Cuadernos Investig. Geogr.* 46 (1), 7–31. <https://doi.org/10.18172/cig.3800>.
- Kotzé, C., Meiklejohn, I., 2017. Temporal variability of ground thermal regimes on the northern buttress of the Vesleskarvet nunatak, western Dronning Maud Land, Antarctica. *Antarct. Sci.* 29 (1), 73–81. <https://doi.org/10.1017/S095410201600047X>.
- Lacelle, D., Lapalme, C., Davila, A.F., Pollard, W., Marinova, M., Heldmann, J., McKay, C. P., 2016. Solar Radiation and Air and Ground Temperature Relations in the Cold and Hyper-Arid Quartermain Mountains, McMurdo Dry Valleys of Antarctica. *Permafrost. Periglac. Process.* 27 (2), 163–176. <https://doi.org/10.1002/ppp.1859>.
- Lapalme, C.M., Lacelle, D., Pollard, W., Fortier, D., Davila, A., McKay, C.P., 2017. Cryostratigraphy and the Sublimation Nonconformity in Permafrost from an Ultracross Environment, University Valley, McMurdo Dry Valleys of Antarctica. *Permafrost. Periglac. Process.* 28 (4), 649–662. <https://doi.org/10.1002/ppp.1948>.
- Lee, C.K., Barbier, B.A., Bottos, E.M., McDonald, I.R., Cary, S.C., 2012. The Inter-Valley Soil Comparative Survey: the ecology of Dry Valley edaphic microbial communities. *ISME J.* 6 (5), 1046–1057. <https://doi.org/10.1038/ismej.2011.170>.
- Lee, J.Y., Lim, H.S., Yoon, H.I., 2016. Thermal characteristics of soil and water during summer at King Sejong Station, King George Island, Antarctica. *Geosci. J.* 20 (4), 503–516. <https://doi.org/10.1007/s12303-016-0026-9>.
- Lee, J.R., Raymond, B., Bracegirdle, T.J., Chadés, I., Fuller, R.A., Shawn, J.D., Terauds, A., 2017. Climate change drives expansion of Antarctic ice-free habitat. *Nature* 547, 49–54. <https://doi.org/10.1038/nature22996>.
- Leihy, R.I., Duffy, G.A., Nortje, E., Chown, S.L., 2018. Data descriptor: High resolution temperature data for ecological research and management on the Southern Ocean Islands. *Sci. Data* 5, 1–13.
- Lembrechts, J.J., van den Hoogen, J., Aalto, J., Ashcroft, M.B., De Frenne, P., Kempinen, J., Kopecký, M., Luoto, M., Maclean, I.M.D., Crowther, T.W., Bailey, J. J., Haesen, S., Klings, D.H., Niittynen, P., Scheffers, B.R., Van Meerbeek, K., Aartsma, P., Abdalaze, O., Abedi, M., Lenoir, J., 2022. Global maps of soil temperature. *Glob. Change Biol.* 28, 3110–3144. <https://doi.org/10.1111/gcb.16060>.
- Levy, J., 2013. How big are the McMurdo Dry Valleys? Estimating ice-free area using Landsat image data. *Antarct. Sci.* 25 (1), 119–120. <https://doi.org/10.1017/S0954102012000727>.
- Levy, J.S., Fountain, A.G., Obryk, M.K., Telling, J., Glennie, C., Pettersson, R., Gooseff, M., van Horn, D.J., 2018. Decadal topographic change in the McMurdo Dry Valleys of Antarctica: Thermokarst subsidence, glacier thinning, and transfer of water storage from the cryosphere to the hydrosphere. *Geomorphology* 323, 80–97. <https://doi.org/10.1016/j.geomorph.2018.09.012>.
- Liu, L., Sletten, R.S., Hallet, B., Waddington, E.D., 2018. Thermal Regime and Properties of Soils and Ice-Rich Permafrost in Beacon Valley, Antarctica. *J. Geophys. Res. Earth Surf.* 123 (8), 1797–1810. <https://doi.org/10.1029/2017JF004535>.
- López-Martínez, J., Serrano, E., 2002. *Geomorphology of Deception Island*. In: López-Martínez, J., Smellie, J.L., Thomson, J.W., Thomson, M.R.A. (Eds.), *Geology and Geomorphology of Deception Island*: 31–39. BAS Geomap Series, Sheets 6-A and 6-B. British Antarctic Survey, Cambridge.
- López-Martínez, J., Serrano, E., Schmid, T., Mink, S., Linés, C., 2012. Periglacial processes and landforms in the South Shetland Islands (northern Antarctic Peninsula region). *Geomorphology* 155–156, 62–79. <https://doi.org/10.1016/j.geomorph.2011.12.018>.
- López-Martínez, J., Schmid, T., Serrano, E., Mink, S., Nieto, A., Guillaso, S., 2016. Geomorphology and landforms distribution in selected ice-free areas in the South Shetland Islands, Antarctic Northern Peninsula region. *Cuadernos Investig. Geogr.* 42 (2), 435–455. <https://doi.org/10.18172/cig.2965>.

- Lowry, D.P., Gолledge, N.R., Bertler, N.A.N., Jones, R.S., McKay, R., 2019. Deglacial grounding-line retreat in the Ross Embayment, Antarctica, controlled by ocean and atmosphere forcing. *Sci. Adv.* 5 (8) <https://doi.org/10.1126/sciadv.aav8754>.
- Mackintosh, A.N., Verleyen, E., O'Brien, P.E., White, D.A., Jones, R.S., McKay, R., Dunbar, R., Gore, D.B., Fink, D., Post, A.L., Miura, H., Leventer, A., Goodwin, I., Hodgson, D.A., Lilly, K., Crosta, X., Gолledge, N.R., Wagner, B., Berg, S., Masse, G., 2014. Retreat history of the East Antarctic Ice Sheet since the last Glacial Maximum. *Quat. Sci. Rev.* 100, 10–30. <https://doi.org/10.1016/j.quascirev.2013.07.024>.
- Marchant, D.R., Head, J.W., 2007. Antarctic dry valleys: Microclimate zonation, variable geomorphic processes, and implications for assessing climate change on Mars. *Icarus* 192 (1), 187–222. <https://doi.org/10.1016/j.icarus.2007.06.018>.
- Matthews, D.H., Maling, D.H., 1967. The geology of the South Orkney Islands: I Signy Island, Falkland Islands. *Depend. Surv. Sci. Rep.* 25, 32 pp.
- McGlone, M.S., 2002. The late Quaternary peat, vegetation and climate history of the Southern Oceanic Islands of New Zealand. *Quat. Sci. Rev.* 21 (4–6), 683–707. [https://doi.org/10.1016/S0277-3791\(01\)00044-0](https://doi.org/10.1016/S0277-3791(01)00044-0).
- McKay, C., Balaban, E., Abrahams, S., Lewis, N., 2019. Dry permafrost over ice-cemented ground at Elephant Head, Ellsworth Land, Antarctica. *Antarct. Sci.* 31 (5), 263–270. <https://doi.org/10.1017/S0954102019000269>.
- Mergelov, N.S., 2014. Soils of wet valleys in the Larsemann Hills and Vestfold Hills oases (Princess Elizabeth Land, East Antarctica). *Eurasian Soil Sc* 47, 845–862. <https://doi.org/10.1134/S1064229314090099>.
- Mergelov, N., Dolgikh, A., Shorkunov, I., et al., 2020. Hypolithic communities shape soils and organic matter reservoirs in the ice-free landscapes of East Antarctica. *Sci. Rep.* 10, 10277. <https://doi.org/10.1038/s41598-020-67248-3>.
- Michel, R.F.M., Schaefer, C.E.G.R., Poelking, E.L., Simas, F.N.B., Filho, E.I.F., Bockheim, J.G., 2012. Active layer temperature in two Cryosols from King George Island, Maritime Antarctica. *Geomorphology* 155–156, 12–19. <https://doi.org/10.1016/j.geomorph.2011.12.013>.
- Michel, R.F.M., Schaefer, C.E.G.R., Simas, F.N.B., Francelino, M.R., Filho, E.I.F., Lyra, G. B., Bockheim, J.G., 2014. Active-layer thermal monitoring on the Fildes Peninsula, King George Island, maritime Antarctica. *Solid Earth* 5, 1361–1374. <https://doi.org/10.5194/se-5-1361-2014>.
- Mori, J., Sone, T., Strelin, J.A., Torieli, C., Fukui, K., 2006. Characteristics of air and ground temperatures and the reconstruction of active layer thickness on the Rink Plateau, James Ross Island, Antarctic Peninsula. *J. Jpn. Soc. Snow Ice* 68, 287–298 (in Japanese with English abstract. 1–317).
- Moura, P.A., Francelino, M.R., Schaefer, C.E.G.R., Simas, F.N.B., Mendonca, B.A.F., 2012. Distribution and characterization of soils and landform relationships in Byers Peninsula, Livingston Island, Maritime Antarctica. *Geomorphology* 155–156, 45–54. <https://doi.org/10.1016/j.geomorph.2011.12.011>.
- Navarro, F.J., Jonsell, U.Y., Corcuera, M.I., Martín-Español, A., 2013. Decelerated mass loss of Hurd and Johnsons Glaciers, Livingston Island, Antarctic Peninsula. *J. Glaciol.* 59 (213), 115–128. <https://doi.org/10.3189/2013JG12J144>.
- Navas, A., López-Martínez, J., Casas, J., Machín, J., Durán, J.J., Serrano, E., Cuchi, J.-A., Mink, S., 2008. Soil characteristics on varying lithological substrates in the South Shetland Islands, maritime Antarctica. *Geoderma* 144 (1–2), 123–139. <https://doi.org/10.1016/j.geoderma.2007.10.011>.
- Nel, W., Boelhouwers, J.C., Borg, C.-J., Cotrina, J.H., Hansen, C.D., Haussmann, N.S., Hedding, D.W., Meiklejohn, K.I., Nguna, A.A., Rudolph, E.M., Sinuka, S.S., Sumner, P.D., 2021. Earth science research on Marion Island (1996–2020): a synthesis and new findings. *S. Afr. Geogr. J.* 103 (1), 22–42. <https://doi.org/10.1080/03736245.2020.1786445>.
- Nelson, P.H.H., 1975. The James Ross Island Volcanic Group of North-East Graham Land. *Brit. Antarct. Surv. Sci. Rep.* 54 (62 pp.).
- Ó Cofaigh, C., Davies, B.J., Livingstone, S.J., Smith, J.A., Johnson, J.S., Hocking, E.P., Hodgson, D.A., Anderson, J.B., Bentley, M.J., Canals, M., Domack, E., Dowdeswell, J. A., Evans, J., Glasser, N.F., Hillenbrand, C.-D., Larter, R.D., Roberts, S.J., Simms, A.R., 2014. Reconstruction of ice-sheet changes in the Antarctic Peninsula since the last Glacial Maximum. *Quat. Sci. Rev.* 100, 87–110. <https://doi.org/10.1016/j.quascirev.2014.06.023>.
- Obu, J., Westermann, S., Vieira, G., Abramov, A., Balks, M.R., Bartsch, A., Hrbáček, F., Käab, A., Ramos, M., 2020. Pan-Antarctic map of near-surface permafrost temperatures at 1 km<sup>2</sup> scale. *Cryosphere* 14, 497–519. <https://doi.org/10.5194/tc-14-497-2020>.
- Oliva, M., Ruiz-Fernández, J. (Eds.), 2020. *The Past Antarctica, 1<sup>st</sup> edition*. Elsevier. 299 pp.
- Oliva, M., Antoniades, D., Giralt, S., Granados, I., Pla-Rabes, S., Toro, M., Liu, E.J., Sanjurjo, J., Vieira, G., 2016. The Holocene deglaciation of the Byers Peninsula (Livingston Island, Antarctica) based on the dating of lake sedimentary records. *Geomorphology* 261, 89–102. <https://doi.org/10.1016/j.geomorph.2016.02.029>.
- Oliva, M., Hrbáček, F., Ruiz-Fernández, J., de Pablo, M.A., Vieira, G., Ramos, M., Antoniades, D., 2017a. Active layer dynamics in three topographically distinct lake catchments in Byers Peninsula (Livingston Island, Antarctica). *CATENA* 149, 548–559. <https://doi.org/10.1016/j.catena.2016.07.011>.
- Oliva, M., Navarro, F., Hrbáček, F., Hernández, A., Nývlt, D., Perreira, P., Ruiz-Fernández, J., Trigo, R., 2017b. Recent regional climate cooling on the Antarctic Peninsula and associated impacts on the cryosphere. *Sci. Total Environ.* 580, 210–223. <https://doi.org/10.1016/j.scitotenv.2016.12.030>.
- Oliva, M., Antoniades, D., Serrano, E., Giralt, S., Liu, E.J., Granados, I., Pla-Rabes, S., Toro, M., Hong, S.G., Vieira, G., 2019. The deglaciation of Barton Peninsula (King George Island, South Shetland Islands, Antarctica) based on geomorphological evidence and lacustrine records. *Polar Res.* 55 (3), 177–188.
- Oliva, M., Palacios, D., Fernández-Fernández, J.M., Fernandes, M., Schimmelpennig, I., Vieira, G., Antoniades, D., Pérez-Alberti, A., García-Oteyza, J., ASTER Team, 2023. Holocene Deglaciation of the Northern Fildes Peninsula. *Land Degradation & Development*, King George Island, Antarctica. <https://doi.org/10.1002/ldr.4730>.
- Olivero, E., Scasso, R.A., Rinaldi, C.A., 1986. Revision of the Marambio Group, James Ross Island, Antarctica. Instituto Antártico Argentino. *Contribución* 331 (28 pp.).
- O'Neill, T., Balks, M., Stevenson, B., López-Martínez, J., Aislabie, J., Rhodes, P., 2013. The short-term effects of surface soil disturbance on soil bacterial community structure at an experimental site near Scott Base, Antarctica. *Polar Biol.* 36 (7), 985–996. <https://doi.org/10.1007/s00300-013-1322-8>.
- Ortiz, R., García, A., Aparicio, A., Blanco, I., Felpeto, A., Rey, R., Villegas, M., Ibañez, M., Morales, J., Pezzo, E., Olmedillas, J., Astiz, M., Vila, J., Ramos, M., Viramonte, J., Risso, C., Caselli, A., 1997. Monitoring of the volcanic activity of Deception Island, South Shetland islands, Antarctica (1986–1995). In: Ricci, C.A. (Ed.), *The Antarctic Region: Geological Evolution and Processes*. Terra Antarctica Publication, pp. 1071–1076 (ISBN: 88-900221-0-8).
- Osokin, N.I., Sosnovkii, A.V., Mavlyudov, B.R., 2020. Glaciation and Permafrost Dynamics on the Antarctic Peninsula in the 21st Century. *Russ. Meteorol. Hydrol.* 45, 124–131.
- de Pablo, M.A., Blanco, J.J., Molina, A., Ramos, M., Quesada, A., Vieira, G., 2013. Interannual active layer variability at the Limnopolar Lake CALM site on Byers Peninsula, Livingston Island, Antarctica. *Antarct. Sci.* 25 (2), 167–180. <https://doi.org/10.1017/S0954102012000818>.
- de Pablo, M.A., Ramos, M., Molina, A., 2014. Thermal characterization of the active layer at the Limnopolar Lake CALM-S site on Byers Peninsula (Livingston Island), Antarctica. *Solid Earth* 5 (2), 721–739. <https://doi.org/10.5194/se-5-721-2014>.
- de Pablo, M.A., Ramos, M., Molina, A., Vieira, G., Hidalgo, M.A., Prieto, M., Jiménez, J. J., Fernández, S., Recondo, C., Calleja, J.F., Peón, J.J., Mora, C., 2016. Frozen ground and snow cover monitoring in the South Shetland Islands, Antarctica: Instrumentation, effects on ground thermal behaviour and future research. *Cuadernos Investig. Geogr.* 42 (2), 475–495. <https://doi.org/10.18172/cig.2917>.
- de Pablo, M.A., Ramos, M., Molina, A., 2017. Snow cover evolution, on 2009–2014, at the Limnopolar Lake CALM-S site on Byers Peninsula, Livingston Island, Antarctica. *CATENA* 149, 538–547. <https://doi.org/10.1016/j.catena.2016.06.002>.
- de Pablo, M.A., Ramos, M., Molina, A., Prieto, M., 2018. Thaw depth spatial and temporal variability at the Limnopolar Lake CALM-S site, Byers Peninsula, Livingston Island, Antarctica. *Sci. Total Environ.* 615, 814–827. <https://doi.org/10.1016/j.scitotenv.2017.09.284>.
- de Pablo, M.A., Jiménez, J.J., Ramos, M., Prieto, M., Molina, A., Vieira, G., Hidalgo, M. A., Fernández, S., Recondo, C., Calleja, J.F., Peón, J.J., Corbea-Pérez, A., Maior, C.N., Morales, M., Mora, C., 2020. Frozen ground and snow cover monitoring in Livingston and Deception islands, Antarctica: preliminary results of the 2015–2019 PERMANISNOW project. *Cuadernos Investig. Geogr.* 46 (1), 187–222. <https://doi.org/10.18172/cig.4381>.
- Peat, H.J., Clarke, A., Convey, P., 2009. Diversity and biogeography of the Antarctic flora. *J. Biogeogr.* 34 (1), 132–146. <https://doi.org/10.1111/j.1365-2699.2006.01565.x>.
- Pimpirev, C., Stoykova, K., Ivanov, M., Dimov, D., 2006. The sedimentary sequences of Hurd Peninsula, Livingston Island, South Shetland Islands: part of the late Jurassic — Cretaceous depositional history of the Antarctic Peninsula. In: Fütterer, D.K., Damaske, D., Kleinschmidt, G., Miller, H., Tessensohn, F. (Eds.), *Antarctica*. Springer, Berlin, Heidelberg. [https://doi.org/10.1007/3-540-32934-X\\_30](https://doi.org/10.1007/3-540-32934-X_30).
- Ponti, S., Guglielmin, M., 2021. Shore evidences of a high Antarctic Ocean wave event: geomorphology, event reconstruction and coast dynamics through a remote sensing approach. *Remote Sens.* 13 (3), 518. <https://doi.org/10.3390/rs13030518>.
- Ponti, S., Scipinotti, R., Pierattini, S., Guglielmin, M., 2021. The spatio-temporal variability of frost blisters in a perennally Frozen Lake along the Antarctic Coast as indicator of the groundwater supply. *Remote Sens.* 13 (3), 435. <https://doi.org/10.3390/rs13030435>.
- Pour, A.B., Hashim, M., Park, Y., Hong, J.K., 2018. Mapping alteration mineral zones and lithological units in Antarctic regions using spectral bands of ASTER remote sensing data. *Geocarto Int.* 33 (12), 1281–1306. <https://doi.org/10.1080/10106049.2017.1347207>.
- Prater, I., Hrbáček, F., Braun, C., Vidal, A., Meier, L.A., Nývlt, D., Mueller, & C.W., 2021. How vegetation patches drive soil development and organic matter formation on polar islands. *Geoderma Region.* 27, e00429.
- Quesada, A., Camacho, A., Rochera, C., Velázquez, D., 2009. Byers Peninsula: A reference site for coastal, terrestrial and limnetic ecosystem studies in maritime Antarctica. *Polar Sci.* 3 (3), 181–187. <https://doi.org/10.1016/j.polar.2009.05.003>.
- Quilty, P., 2007. Origin and evolution of the sub-Antarctic islands: the foundation. In: *Papers and Proceedings of the Royal Society of Tasmania*, pp. 35–58. <https://doi.org/10.26749/rstpp.141.1.35>.
- Raffi, R., Stenni, B., 2011. Isotopic composition and thermal regime of ice wedges in northern Victoria Land, East Antarctica. *Permafrost. Periglac. Process.* 22 (1), 65–83. <https://doi.org/10.1002/ppp.701>.
- Ramos, M., Aguirre-Puente, J., 1994. Correlation between heat flux on the ground and permafrost thermal regime near the Spanish Antarctic Station. *Ground Freez.* 94, 395–397. Ed. balkema. ISBN: 90 5410 518 6. Libro. HOLLANDA.
- Ramos, M., Vieira, G., 2009. Evaluation of the ground surface Enthalpy balance from bedrock temperatures (Livingston Island, Maritime Antarctic). *Cryosphere* 3 (1), 133–145. <https://doi.org/10.5194/tc-3-133-2009>.
- Ramos, M., Vieira, G., Gruber, S., Blanco, J.J., Hauck, C., Hidalgo, M.A., Tome, D., Neves, M., Trindade, A., 2007. Permafrost and active layer monitoring in the Maritime Antarctic: Preliminary results from CALM sites on Livingston and Deception Islands. In: USGS OF-2007-1047, Short Research Paper 070. U.S. Geological Survey and the National Academies. <https://doi.org/10.3133/ofr2007-1047.srp070>.

- Ramos, M., Vieira, G., Guilichinski, D., de Pablo, M.A., 2010. Nuevas estaciones de medida del régimen térmico del permafrost en el área de "Crater Lake". Isla Decepción (Antártida). Resultados preliminares. In: Blanco, J.J., Ramos, M., de Pablo, M.A. (Eds.), *Proceedings of II Iberian Conference of the International Permafrost Association Periglacial, Environments, Permafrost and Climate Variability*. UAH, pp. 93–109. ISBN: 978-84-9138-885-5. Libro. ESPAÑA.
- Ramos, M., Vieira, G., de Pablo, M.A., Molina, A., Abramov, A., Goyanes, G., 2017. Recent shallowing of the thaw depth at Crater Lake, Deception Island, Antarctica (2006–2014). *Catena* 149 (2), 519–528. <https://doi.org/10.1016/j.catena.2016.07.019>.
- Ramos, M., Vieira, G., de Pablo, M.A., Molina, A., Jimenez, J.J., 2020. Transition from a Subaerial to a Subnival Permafrost Temperature Regime following increased Snow Cover (Livingston Island, Maritime Antarctic). *Atmosphere* 11, 1332. <https://doi.org/10.3390/atmos11121332>.
- Recondo, C., Corbea-Pérez, A., Peón, J., Pendás, E., Ramos, M., Calleja, J.F., de Pablo, M.A., Fernández, S., Corrales, J.A., 2022. Empirical Models for estimating Air Temperature using MODIS Land Surface Temperature (and Spatiotemporal Variables) in the Hurd Peninsula of Livingston Island, Antarctica, between 2000 and 2016. *Remote Sens.* 14 (13), 3206. <https://doi.org/10.3390/rs14133206>.
- le Roux, P.C., McGeoch, M.A., 2008. Changes in climate extremes, variability and signature on sub-Antarctic Marion Island. *Clim. Chang.* 86 (3–4), 309–329. <https://doi.org/10.1007/s10584-007-9259-y>.
- Ruiz-Fernández, J., Oliva, M., García-Hernández, C., 2017. Topographic and geomorphologic controls on the distribution of vegetation formations in Elephant Point (Livingston Island, Maritime Antarctica). *Sci. Total Environ.* 587, 340–349. <https://doi.org/10.1016/j.scitotenv.2017.02.158>.
- Ruiz-Fernández, J., Oliva, M., Nývlt, D., Cannone, N., García-Hernández, C., Guglielmin, M., Hrbáček, F., Roman, M., Fernández, S., López-Martínez, J., Antoniadou, D., 2019. Patterns of spatio-temporal paraglacial response in the Antarctic Peninsula region and associated ecological implications. *Earth-Sci. Rev.* 192, 379–402. <https://doi.org/10.1016/j.earscirev.2019.03.014>.
- Salmi, T., Määttä, A., Anttila, P., Ruoho-Airola, T., Amnell, T., 2002. *Detecting Trends of Annual Values of Atmospheric Pollutants by the Mann-Kendall Test and Sen's Slope Estimates*. Finnish Meteorological Institute, Helsinki.
- Sawagaki, T., 1995. Ground temperature regimes and frost heave activity in the vicinity of Syowa Station, East Antarctica. In: *Proceedings of the NIPR Symposium on Antarctic Geosciences*, 8, pp. 239–249.
- Schaefer, C.E.G.R., Pereira, T.T.C., Almeida, I.C.C., Michel, R.F.M., Corrêa, G.R., Figueiredo, L.P.S., Ker, J.C., 2017a. Penguin activity modify the thermal regime of active layer in Antarctica: A case study from Hope Bay. *CATENA* 149, 582–591. <https://doi.org/10.1016/j.catena.2016.07.021>.
- Schaefer, C.E.G.R., Michel, R.F.M., Delpupo, C., Senra, E.O., Bremer, U.F., Bockheim, J., 2017b. Active layer thermal monitoring of a Dry Valley of the Ellsworth Mountains, Continental Antarctica. *Catena* 149, 603–615.
- Serrano, E., 2003. Natural landscape and geocryological belts on ice free areas of the maritime Antarctica (South Shetland Islands). *AGE Bull.* 35, 5–32.
- Serrano, E., Martínez de Pisón, E., López-Martínez, J., 1996. Periglacial and nival landforms and deposits. In: López-Martínez, J., Thomson, M.R.A., Thomson, J.W. (Eds.), *Geomorphological Map of Byers Peninsula, Livingston Island, BAS GEOMAP Series. British Antarctic Survey, Cambridge*, pp. 28–34. Sheet 5-A, Scale 1:25 000.
- Seybold, C.A., Harms, D.S., Balks, M., Aislabie, J., Paetzold, R.F., Kimble, J., Sletten, R., 2009. Soil climate monitoring project in the Ross Island region of Antarctica. *Soil Surv. Horiz.* 50 (2), 52–57.
- Seybold, C.A., Balks, M.R., Harms, D.S., 2010. Characterization of active layer water contents in the McMurdo Sound region, Antarctica. *Antarct. Sci.* 22 (6), 633–645. <https://doi.org/10.1017/S0954102010000696>.
- Shipp, S.S., Anderson, J.B., Domack, E.W., 1999. Late Pleistocene–Holocene retreat of the West Antarctic Ice-Sheet system in the Ross Sea: Part 1 – Geophysical results. *Geol. Soc. Am. Bull.* 111, 1486–1516.
- Shur, Y., Hinkel, K.M., Nelson, F.E., 2005. The transient layer: implications for geocryology and climate-change science. *Permafrost Periglac. Process.* 16, 5–17. <https://doi.org/10.1002/ppp.518>.
- Siegert, M., Atkinson, A., Banwell, A., Brandon, M., Convey, P., Davies, B., Downie, R., Edwards, T., Hubbard, B., Marshall, G., Rogelj, J., Rumble, J., Stroeve, J., Vaughan, D., 2019. The Antarctic Peninsula under a 1.5°C Global Warming Scenario. *Front. Environ. Sci.* 7 (102) <https://doi.org/10.3389/fenvs.2019.00102>.
- Simas, F.N.B., Schaefer, C.E.G.R., Albuquerque Filho, M.R., Francelino, M.R., Costa, L.M., 2008. Genesis, properties and classification of Cryosols from Admiralty Bay, Maritime Antarctica. *Geoderma* 144 (1–2), 116–122. <https://doi.org/10.1016/j.geoderma.2007.10.019>.
- Simms, A.R., Milliken, K.T., Anderson, J.B., Wellner, J.S., 2011. The marine record of deglaciation of the South Shetland Islands, Antarctica since the last Glacial Maximum. *Quat. Sci. Rev.* 30 (13–14), 1583–1601. <https://doi.org/10.1016/j.quascirev.2011.03.018>.
- Smellie, J.L., Davies, R.E.S., Thomson, M.R.A., 1980. Geology of a Mesozoic intra-arc sequence on Byers Peninsula, Livingston Island, South Shetland Islands. *Brit. Antarct. Surv. Bull.* 50, 55–76.
- Smellie, J.L., Pankhurst, R.J., Thomson, M.R.A., Davies, R.E.S., 1984. The geology of the South Shetland Islands. VI: stratigraphy, geochemistry and evolution. *Brit. Antarct. Surv. Sci. Rep.* 87, 1–85.
- Smith, S.L., O'Neill, H.B., Isaksen, K., Noetzi, J., Romanovsky, V.E., 2022. The changing thermal state of permafrost. *Nat. Rev. Earth Environ.* 3, 10–23. <https://doi.org/10.1038/s43017-021-00240-1>.
- Smith, S.L., Wolfe, S.A., Riseborough, D.W., Nixon, F.M., 2009. Active-layer characteristics and summer climatic indices, Mackenzie Valley, Northwest Territories, Canada. *Permafrost Periglac. Process.* 20, 201–220. <https://doi.org/10.1002/ppp.651>.
- Smykla, J., Drewnik, M., Szarek-Gwiazda, E., Hii, Y.S., Knap, W., Emslie, S.D., 2015. Variation in the characteristics and development of soils at Edmonson Point due to abiotic and biotic factors, northern Victoria Land, Antarctica. *CATENA* 132, 56–67. <https://doi.org/10.1016/j.catena.2015.04.011>.
- Speir, T.W., Cowling, J.C., 1984. Ornithogenic soils of the Cape Bird adielie penguin rookeries, Antarctica. *Polar Biol.* 2 (4), 199–205.
- Strand, S.M., Christiansen, H.H., Johansson, M., Åkerman, J., Humlum, O., 2021. Active layer thickening and controls on interannual variability in the Nordic Arctic compared to the circum-Arctic. *Permafrost Periglac. Process.* 32, 47–58. <https://doi.org/10.1002/ppp.2088>.
- Terauds, A., Lee, J., 2016. Antarctic biogeography revisited: updating the Antarctic Conservation Biogeographic Regions. *Divers. Distrib.* 22 (8), 836–840. <https://doi.org/10.1111/ddi.12453>.
- Thomazini, A., Francelino, M.R., Pereira, A.B., Schünemann, A.L., Mendonça, E.S., Michel, R.F.M., Schaefer, C.E.G.R., 2020. The current response of soil thermal regime and carbon exchange of a paraglacial coastal land system in maritime Antarctica. *Land Degrad. Dev.* 31, 655–666. <https://doi.org/10.1002/ldr.3479>.
- Thomson, M.R.A., López-Martínez, J., 1996. Introduction to the Geology and Geomorphology of Byers Peninsula. In: López-Martínez, J., Thomson, M.R.A., Thomson, J.W. (Eds.), *Geomorphological Map of Byers Peninsula, Livingston Island BAS Geomap Series 5-A. British Ant Surv, Cambridge*, pp. 1–4.
- Tucker, N.M., Hand, M., Clark, C., 2020. The Bunge Hills: 60 years of geological and geophysical research. *Antarct. Sci.* 32 (2), 85–106. <https://doi.org/10.1017/S0954102019000403>.
- Turner, J., Lu, H., White, I., King, J.C., Phillips, T., Scott Hosking, J., Bracegirdle, T.J., Marshall, G.J., Mulvaney, R., Deb, P., 2016. Absence of 21st century warming on Antarctic Peninsula consistent with natural variability. *Nature* 535. <https://doi.org/10.1038/nature18645>.
- Turner, J., Marshall, G., Clem, K., Colwell, S., Phillips, T., Lu, H., 2020. Antarctic temperature variability and change from station data. *Int. J. Climatol.* 40 (6), 2986–3007. <https://doi.org/10.1002/joc.6378>.
- Ugolini, F.C., Bockheim, J.G., 2008. Antarctic soils and soil formation in a changing environment: A review. *Geoderma* 144 (1–2), 1–8. <https://doi.org/10.1016/j.geoderma.2007.10.005>.
- Uxa, T., 2016. Discussion on 'active layer thickness prediction on the Western Antarctic peninsula' by Wilhelm et al. 2015. *Permafrost Periglac. Process.* 28, 493–498.
- Vera, E.I., 2011. Livingstonites Gabriellae gen. et sp. nov., Permineralized Moss (Bryophyta: Bryopsida) from the Aptian Cerro Negro Formation of Livingston Island (South Shetland Islands, Antarctica). *Ameghiniana* 48 (1), 122–128. [https://doi.org/10.5710/AMGH.v48i1\(477\)](https://doi.org/10.5710/AMGH.v48i1(477)).
- Vieira, G., Ramos, M., 2003. Geographic factors and geocryological activity in Livingston Island, Antarctic. Preliminary results. In: Phillips, M., Springman, S.M., Arenson, L. U. (Eds.), *Permafrost. Proceedings of the eight International Conference on Permafrost, 21–25 July 2003, Zurich, Switzerland, Balkema – Swets & Zeitlinger, Lisse*: 1183–1188.
- Vieira, G., López, J., Serrano, E., Ramos, M., Gruber, S., Hauck, C., Blanco, J.J., 2008. Geomorphological observations of permafrost and Ground-Ice Degradation on Deception and Livingston Islands, Maritime Antarctica. In: Kane, Douglas L., Hinkel, Kenneth M. (Eds.), *Proceedings of the Ninth International Conference on Permafrost University of Alaska Fairbanks June 29–July 3, 2008. Institute of Northern Engineering, pp. 1839–1843. NICOP-2008. ISBN: 978-0-980 017 9-2-2*.
- Vieira, G., Bockheim, J., Guglielmin, M., Balks, M., Abramov, A.A., Boelhouwers, J., Cannone, N., Ganzert, L., Gilichinsky, D., Goryachkin, S., López-Martínez, J., Raffi, R., Ramos, M., Schaefer, C., Serrano, E., Simas, F., Sletten, R., Wagner, D., 2010. Thermal state of permafrost and active-layer monitoring in the Antarctic: advances during the international polar year 2007–2008. *Permafrost Periglac. Process.* 21, 182–197.
- Vieira, G., Mora, C., Pina, P., Schaefer, C., 2014. A proxy for snow cover and winter ground surface cooling: mapping *Usnea* sp communities using high resolution remote sensing imagery (Maritime Antarctica). *Geomorphology* 225 (15), 69–75. <https://doi.org/10.1016/j.geomorph.2014.03.049>.
- van de Vijver, B., Beyens, L., 1999. Biogeography and ecology of freshwater diatoms in Subantarctica: a review. *J. Biogeogr.* 26 (5), 993–1000. <https://doi.org/10.1046/j.1365-2699.1999.00358.x>.
- Walsh, J.E., 2009. A comparison of Arctic and Antarctic climate change, present and future. *Antarct. Sci.* 21 (3), 179–188. <https://doi.org/10.1017/S0954102009001874>.
- Webers, G.F., Craddock, C., Spletstoesser, J.F., 1992. Geological history of the Ellsworth Mountains, West Antarctica. In: Webers, G.F., Craddock, C., Spletstoesser, J.F. (Eds.), *Geology and Paleontology of the Ellsworth Mountains*.
- van Wessem, J.M., Ligtenberg, S.R.M., Reijmer, C.H., van de Berg, W.J., van den Broeke, M.R., Barrand, N.E., Thomas, E.R., Turner, J., Wuite, J., Scambos, T.A., van Meijgaard, E., 2016. The modelled surface mass balance of the Antarctic Peninsula at 5.5 km horizontal resolution. *Cryosphere* 10, 271–285. <https://doi.org/10.5194/tc-10-271-2016>.
- White, D.A., Fink, D., 2014. Late Quaternary glacial history constrains glacio-isostatic rebound in Enderby Land, East Antarctica. *J. Geophys. Res. Earth Surf.* 119 (3), 401–413. <https://doi.org/10.1002/2013JF002870>.
- Wilhelm, K., Bockheim, J., 2016. Influence of soil properties on active layer thermal propagation along the western Antarctic Peninsula. *Earth Surf. Process. Landf.* 41 (11), 1550–1563. <https://doi.org/10.1002/esp.3926>.
- Wilhelm, K., Bockheim, J., 2017. Climatic controls on active layer dynamics: Amsler Island, Antarctica. *Antarct. Sci.* 29 (2), 173–182.

- Wilhelm, K.R., Bockheim, J.G., Kung, S., 2015. Active Layer Thickness Prediction on the Western Antarctic Peninsula. *Permafrost. Periglacial Process.* 26 (2), 188–199. <https://doi.org/10.1002/ppp.1845>.
- Wlostowski, A.N., Gooseff, M.N., McKnight, D.M., Lyons, W.B., 2018. Transit Times and Rapid Chemical Equilibrium Explain Chemostasis in Glacial Meltwater Streams in the McMurdo Dry Valleys, Antarctica. *Geophys. Res. Lett.* 45 (24) <https://doi.org/10.1029/2018GL080369>.
- Xu, X., Wu, Q., 2021. Active layer thickness variation on the Qinghai-Tibetan Plateau: Historical and projected trends. *J. Geophys. Res. Atmos.* 126 e2021JD034841. <https://doi.org/10.1029/2021JD034841>.
- Yergeau, E., Newsham, K.K., Pearce, D.A., Kowalchuk, G.A., 2007. Patterns of bacterial diversity across a range of Antarctic terrestrial habitats. *Environ. Microbiol.* 9 (11), 2670–2682.
- Yoon, H.I., Han, M.W., Park, B.K., Oh, J.K., Chang, S.K., 1997. Glaciomarine sedimentation and paleo-glacial setting of Maxwell Bay and its tributary embayment, Marian Cove, South Shetland Island, West Antarctica. *Mar. Geol.* 140, 265–282.
- Levy, J.S., Fountain, A.G., Gooseff, M.N., Welch, K.A., Lyons, W.B., 2011. Water tracks and permafrost in Taylor Valley, Antarctica: Extensive and shallow groundwater connectivity in a cold desert ecosystem. *GSA Bulletin* 123 (11–12), 2295–2311. <https://doi.org/10.1130/B30436.1>.
- Hinkel, K.M., Nelson, F.E., 2003. Spatial and temporal patterns of active layer thickness at Circumpolar Active Layer Monitoring (CALM) sites in northern Alaska, 1995–2000. *J. Geophys. Res.* 108 <https://doi.org/10.1029/2001JD000927>, 81–68.
- López-Martínez, J., Martínez de Pisón, E., Serrano, E., Arche, A., 1996. Geomorphological map of Byers Peninsula, Livingston Island. *Geomap Series. British Antarctic Survey, Cambridge (UK) (Sheet 5-A)*.
- Correia, A., Oliva, M., Ruiz-Fernández, J., 2017. Evaluation of frozen ground conditions along a coastal topographic gradient at Byers Peninsula (Livingston Island, Antarctica) by geophysical and geoecological methods. *Catena* 149 (2), 529–537. <https://doi.org/10.1016/j.catena.2016.08.006>.
- Correia, A., Vieira, G., Ramos, M., 2012. Thermal conductivity and thermal diffusivity of cores from a 26 meter deep borehole drilled in Livingston Island, Maritime Antarctic. *Geomorphology* 155–156, 7–11. <https://doi.org/10.1016/j.geomorph.2011.12.012>.
- Campbell, S., Affleck, R.T., Sinclair, S., 2018. Ground-penetrating radar studies of permafrost, periglacial, and near-surface geology at McMurdo Station, Antarctica. *Cold Reg. Sci. Technol.* 148, 38–49. <https://doi.org/10.1016/j.coldregions.2017.12.008>.